IJCER
ONLINE PEER REVIEWED JOURNAL
International Journal of Computational Engineering research

[Volume 3, Issue 1, January, 2013]

International Journal of Computational Engineering Research (IJCER)

ISSN: 2250-3005

ijceronline@gmail.com **www.ijceronline.com**

IJCER
ONLINE PEER REVIEWED JOURNAL
International Journal of Computational Engineering research

OPEN ACCESS JOURNAL

A broad ranging open access journal Fast and efficient online submission Expert peer review, rapid publication High visibility

2013

About IJCER

International Journal of Computational Engineering Research (IJCER) is an intentional online Journal in English monthly publishing journal. This Journal publish original research work that contributes significantly to further the scientific knowledge in engineering and Technology.

Indexing


IJCER

Editorial Board

CONTENTS :

Exploring the Ethno Medicinal Plant for Bio Remediation

Saravanan P[1], Sathish Kumar S[2], Charles A[3,] Queen Prabha R[4]

[1, ,3,4,]Department of Biotechnology, St. Joseph's College (Autonomous), Trichy-2.
[2]Department of Biotechnology, St. Joseph's College (Autonomous), Trichy-2.

Abstract:

Wild Asparagus racemosus (Asparagaceae) is an important medicinal plant of tropical and subtropical India. Pharmacopoeias and in traditional systems of medicine such as Ayurveda, Unani and Siddha .Asparagus racemosus is mainly known for its phytoestrogenic properties. In Ayurveda, Asparagus racemosus has been described as a rasayana herb and has been used extensively as an adaptogen to increase the non-specific resistance of organisms against a variety of stresses. Besides use in the treatment of diarrhoea and dysentery, the plant also has potent antioxidant, immunostimulant, anti-dyspepsia and antitussive effects. Due to its multiple uses, the demand for Asparagus racemosus is constantly on the rise. The plant is now considered 'endangered' in its natural habitat. Therefore, the need for conservation of this plant is crucial. Keeping in mind the fact that it is the active principle that imparts medicinal value to a plant; consistency in quality and quantity needs to be maintained to ensure uniform drug efficacy. To overcome these prevalent problems, the availability of genetically superior and uniform planting material is essential. Proper agro-techniques and adequate marketing opportunities would encourage cultivation of Asparagus racemosus and thereby contribute to its conservation.

Key Words: Asparagus racemosus, ayurveda, immune stimulant, agro techniques

1. Introduction

Medicinal plants are nature's priceless gift to human. The development in the field of modern medicine temporarily subdued the traditional herbal medicine. India has been known to be rich repository of medicinal plants. In India, ancient drugs have been mentioned in e *Rigveda* (5000 BC) has recorded 67 medicinal plants, *Yajurveda* 81 species, *Atharvaveda* (4500-2500 BC) 290 species, *Charak Samhita* (700 BC) and *Sushrut Samhita* (200 BC) had described properties and uses of 1100 and 1270 species respectively, in compounding of drugs and these are still used in the classical formulations, in the Ayurvedic system of medicine.Among the entire flora, 35,000-70,000 species are used for medicinal purposes. India is two major producers of medicinal plants having more than 40% of global biodiversity. Indian Materia-medica accounts about 3500 medicinal plants. Current trends reveal that, in many countries, a large proportion of the population relies heavily on traditional practitioners and medicinal plants to meet primary health care needs (Agrawal and Jain, 2008) although modern medicine may be available in these countries, herbal medicines have often maintained popularity for historical and cultural reasons. So many details on medicinal plants were depicted in Vedas, about 8,000 herbal remedies have been codified in Ayurveda (Beg and Beg and Ali, 2006) The use of medicinal plants in the treatment of diseases was conceived by tribal people thousands of years ago. Many tribal groups have been using several plant or animal products for medicinal preparations and these medicines are known as ethno medicine.Plants used by primitive people to affect fertility, medicines for obsterics and gynaecological disorders ,plants for anti fertility, conception and abortion , plants used for influenza , leucoderma , rheumatism and leucoderma , plants used for skin diseases.

2. Materials and Methods

Present study is based on the exploring the Wild asparagus (*Asparagus racemosus*) pertinent attention was paid to habit, habitat, distribution pattern, diseases for which plants used, dosages and mode of administration. Wild asparagus (Asparagus racemosus) is a species of asparagus with a long history of use in India and other parts of Asia as a botanical medicine. Many medicinal qualities of wild asparagus have been associated with phytonutrients present in its roots, and especially one type of phytonutrients called saponins. Recent research has shown that the species of asparagus most commonly consumed in the kerala (*Asparagus officinalis*) also contains saponins, not only in its root portion put also in its shoots. Saponins found in common, everyday asparagus include asparanin A, sarsasapogenin, and protodioscin (Caldecott, 2000) Asparagus even contains small amounts of the diosgenin - one of the best-studied saponins that are especially concentrated in yam. Saponins in food have repeatedly been shown to have anti-inflammatory and anti-cancer properties, and their intake has also been associated with improved blood pressure, improved blood sugar regulation, and better control of blood fat levels.

Medicinal principles are present in different parts of the plant like root, stem, leaf or plant exudates. These medicinal principles are separated by different processes; the most common being extraction. Extraction is the separation of the required constituents from plant materials using a solvent.

3. Objective Assessment Of Asparagus Racemosus

Plants possess medicinal value due to the presence of phyto compounds such as phenols, flavanoids, alkaloids, etc also various minerals, vitamins and nutritionally important insoluble fibre. People who consume large amounts of vegetables, fruits and whole grain products are less likely to develop heart disease, cancer, type 2 diabetes and eye disease. Phyto chemicals also appear to kill cancer cells as they arise in the body and particularly help prevent cancer in cells that line the lungs, bladder, cervix, mouth, larynx, throat, oesophagus, stomach, pancreas, colon and rectum. Studies show that some phyto chemicals help preserve memory and prevent ageing-related vision problems like macular degeneration (Indian Express, 2009).

4. Results And Discussion

4.1 Market Survey on availability of *Asparagus Racemosus* Products

Market survey was carried out in supermarkets and ayurvedic shops of Coimbatore district to find out the availing products of Asparagus racemosus.

Table 1 Available Products of Asparagus Racemosus

S.No.	Product Name	Form	Quantity	Cost (Rs.)
1	Abana	Tablet	60 Nos.	560
2	Diabecon	Tablet	60 Nos.	600
3	Evecare	Capsule	30 Nos.	520
4	Shatavari	Capsule	60 Nos.	570
5	Herb powder	Powder	500g	700
6	Shatavari	Tablets	60 Nos.	330
7	Shatavari gulam	Gulam	500g	140
8	Dhanvantharam	Kashayam	200g	94
9	Sowbhagyasundi	Lehyam	250g	89
10	Sukumaran	Lehyam	250g	144
11	Vidaryadi	Lehyam	500g	182
12	Baladhtryadi	Thailam	200ml	137
13	Narayana	Thailam	200ml	131
14	Prabhanjam	Thailam	200ml	76
15	Amrutha prasa ghritham	Gulam	500g	215

Table 1 reveals the products available of *Asparagus racemosus*. Most of these products are a combination of two or more herbs but proportion of Shatavari used is high. Cost of Ayurvedic medicine is comparatively less than the Himalaya products. The selected plant for the research was used only for preparation of medicine, thus it was not found in supermarkets or local shops. Half kilogram of the *Asparagus racemosus* root costs about Rs.10-Rs.50.

4.2 Selection of *Asparagus Racemosus*

The present study is aimed to convert this wide spectrum medicinal plant Asparagus racemosus is underused, posse's high medicinal properties and has strong use in Ayurveda. Other species in this family are Aloe barbadensis (aloe vera), Allium sativum (garlic) and Allium cepha (onion). Asparagus racemosus has various medicinal properties. It is antidiarrheal, antiseptic, antidysenteric, antispasmodic, adaptogenic, antioxytocic, antimicrobial antioxidant and antibacterial.

4.3 Antioxidant activity of *Aspargus racemosus* using different cooking methods

Table II ascribes the antioxidant activity of Asparagus racemosus in different cooking methods.

S.No.	Cooking Methods	Time (mins)	Total Antioxidant Activity (µg/g)
1.	No cooking	-	161.76
2.	Boiling	10	164.47
3.	Steaming	10	168.81
4.	Sautéing (10ml of oil)	10	217.18

Table II ascribes that among the different cooking methods, *Asparagus racemosus* sauted in 10 ml of oil for 10 mins had the highest antioxidant activity (217.8µg/g) since oil has antioxidant properties due to the presence of vitamin E, followed by steamed asparagus (168.81µg/g), boiled asparagus (164.47µg/g) and raw asparagus (161.76µg/g). This reveals that antioxidant activity increases in cooking with oil and steaming.

5. Conclusion

Asparagus racemosus is an herb that grows in varied climatic conditions and in any soil. The plant posses a lot of health benefits as reviewed by ayurvedic doctors. Thus concluding this research by saying that herbs indeed are "curative, preventive, protective and nutritive thus let us join hands to conserve, perpetuate, preserve and nourish it"

BIBLIOGRAPHY

[1]. Agrawal R. K. and Jain P. K. (2008). Asian J. Exp. Science, 22(3):Pp.213- 220.
[2]. Beg M. J., Beg M. Z. and Ali S. J. (2006).Ethnomedicinal studies on Sub-Himalayan forests of North Eastern Uttar Pradesh. P. C. Trivedi. Ethnobotanical approach. Pp.266- 390.
[3]. Caldecott, T. (2000). Shatavari – One hundred roots. Mosby publishing. Pp.2- 4.
[4]. De, K. A. (2000). Recent trends in spices and medicinal plants research. Associated Publishing Company. P. 175.
[5]. Goyal R. K., Singh J. and Lal H. (2003). Asparagus racemosus- An update. Indian Journal of medical sciences. 57(9): Pp.408- 414.
[6]. Krishnaswamy, K. (2008). Traditional Indian Spices and their health significance. Nutritional Abstracts and Reviews. 78(7), P. 868.

An Histogram Based Approach for Content Based Image Mining

[1,]Mr. Ashish Bandre , [2,]Prof. Ramanand Singh , [3,]Prof. S. G. Kerhalkar
[1,2,3,]Electronics & Communication Engg., Oriental Institute of Science & Technology, Bhopal

Abstract

Typical content-based image retrieval (CBIR) system would need to handle the vagueness in the user queries as well as the inherent uncertainty in image representation, similarity measure, and relevance feedback. We discuss how Histogram set theory can be effectively used for this purpose and describe an image retrieval system called HIRST (Histogram image retrieval system) which incorporates many of these ideas. HIRST can handle exemplar-based, graphical-sketch-based, as well as linguistic queries involving region labels, attributes, and spatial relations. HIRST uses Histogram attributed relational graphs (HARGs) to represent images, where each node in the graph represents an image region and each edge represents a relation between two regions. The given query is converted to a FARG, and a low-complexity Histogram graph matching algorithm is used to compare the query graph with the FARGs in the database. The use of an indexing scheme based on a leader clustering algorithm avoids an exhaustive search of the FARG database. We quantify the retrieval performance of the system in terms of several standard measures.

1. Introduction

Retrieval of required-query-similar images from abundantly available / accessible digital images is a challenging need of today. The image retrieval techniques based on visual image content has been in-focus for more than a decade. Many web-search-engines retrieve similar images by searching and matching textual metadata associated with digital images. For better precision of the retrieved resultant images, this type of search requires associating meaningful image-descriptive-text-labels as metadata with all images of the database. Manual image labeling, known as manual image annotation, is practically difficult for exponentially increasing image database. The image search results, appearing on the first page for fired text query rose black, are shown in Figure 1 for leading web search engines Google, Yahoo and AltaVista

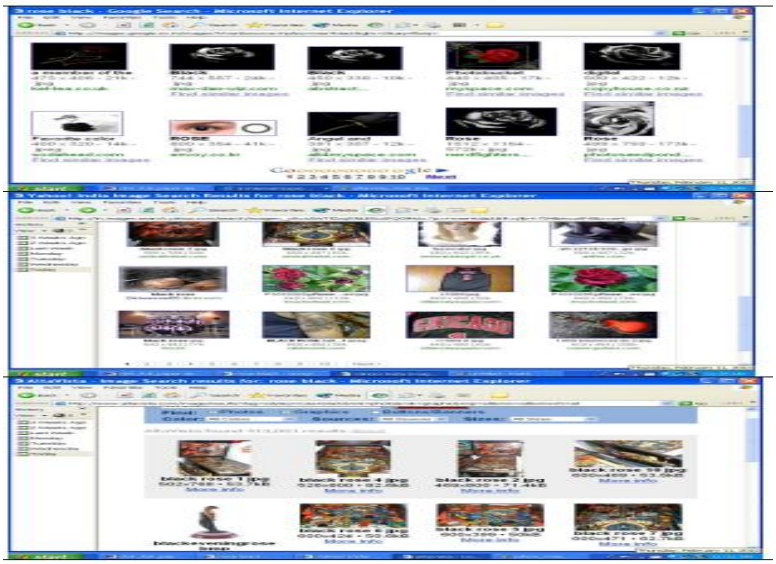

Many resultant images of Figure 1 lack semantic matching with the query, showing vast scope of research leading to improvements in the state-of-art-techniques. The need evolved two solutions – automatic image annotation and content based image retrieval. The content based image retrieval techniques aim to respond to a query image (or sketch) with query-similar resultant images obtained from the image database. The database images are preprocessed for extracting and then storing –indexing corresponding image features. The query image also gets processed for extracting features which are compared with features of database images by applying appropriate similarity measures for retrieving query similar-images.

2. Literature Survey:

The biggest issue for CBIR system is to incorporate versatile techniques so as to process images of diversified characteristics and categories. Many techniques for processing of low level cues are distinguished by the characteristics of domain-images. The performance of these techniques is challenged by various factors like image resolution, intra-image illumination variations, non-homogeneity of intra-region and inter-region textures, multiple and occluded objects etc. The other major difficulty, described as semantic-gap in the literature, is a gap between inferred understanding / semantics by pixel domain processing using low level cues and human perceptions of visual cues of given image. In other words, there exists a gap between mapping of extracted features and human perceived semantics. The dimensionality of the difficulty becomes adverse because of subjectivity in the visually perceived semantics, making image content description a subjective phenomenon of human perception, characterized by human psychology, emotions, and imaginations. The image retrieval system comprises of multiple inter-dependent tasks performed by various phases. Inter-tuning of all these phases of the retrieval system is inevitable for over all good results. The diversity in the images and semantic-gap generally enforce parameter tuning & threshold-value specification suiting to the requirements. For development of a real time CBIR system, feature processing time and query response time should be optimized. A better performance can be achieved if feature-dimensionality and space complexity of the algorithms are optimized. Specific issues, pertaining to application domains are to be addressed for meeting application-specific requirements. Choice of techniques, parameters and threshold-values are many a times application domain specific e.g. a set of techniques and parameters producing good results on an image database of natural images may not produce equally good results for medical or microbiological images.

3. Methodology:

The color histogram for an image is constructed by counting the number of pixels of each color. In project, algorithms follow

(1) Selection of a color space
(2) Quantization of the color space
(3) Computation of histograms.

The approach more frequently adopted for CBIR systems is based on the conventional color histogram (CCH), which contains occurrences of each color obtained counting all image pixels having that color. Each pixel is associated to a specific histogram only on the basis of its own color, and color similarity across different color dissimilarity in the same is not taken into account. Since any pixel in the image can be described by three components in a certain color space histogram, i.e., the distribution of the number of pixels for each quantized color, can be defined for each component. By default the maximum number of colors one can obtain using the histogram function is 256. The conventional color histogram (CCH) of an image indicates the frequency of occurrence of every color in an image. The appealing aspect of the CCH is its simplicity and ease of computation.

4. Data Flow Diagram

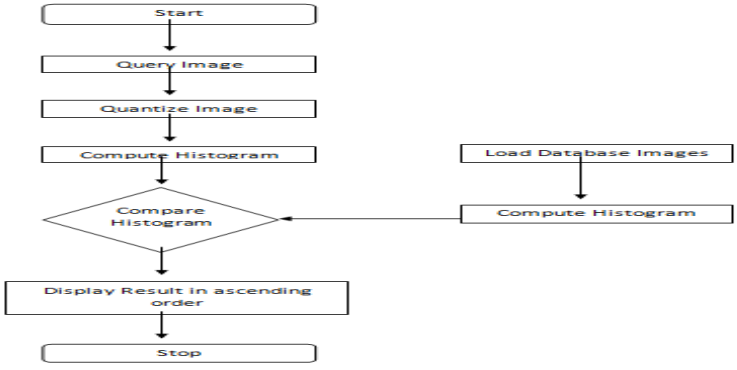

The images data used in the experiment were taken from digital camera & few of the images were downloaded from a web site to create large database.

5. Quantization of the color space

Computing a color histogram for an image, the different color axes are divided into a number of so-called bins. A three dimensional 256x256x256 RGB histogram would therefore contain a total of 16777216 such bins. When indexing the image, the color of each pixel is found, and the corresponding bin's count is incremented by one.

6. Histogram Comparison

In order to compare histograms of two images, we first need to generate specific codes for all histogram bins. In this experiment, (r: 0-255, g: 0-255, b: 0-255) codes were generated for RGB histogram bins. When the images have been quantized into histograms, a method of comparing these is needed. Two Histogram are compared with an Equation

$$L1 = \sum_{i=1}^{n} (Q_i - I_i)$$

Where

Q_i is the value of bin i in the query image.

I_i is the corresponding bin in the database image.

Experiment Result

- **Project GUI**

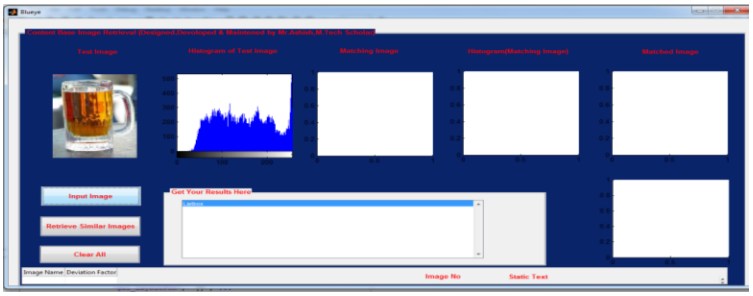

Input Image With Histogram

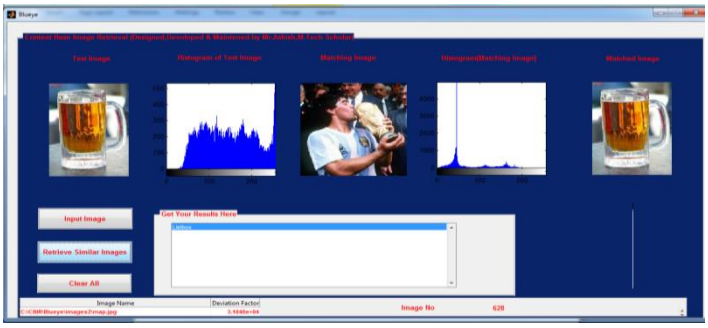

Input Image With Exact Matched

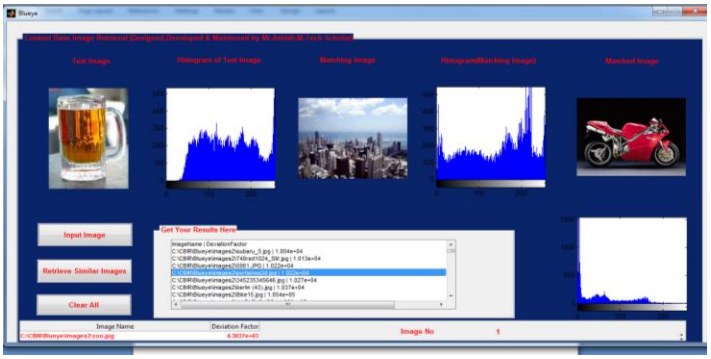

Other Matched Images With respect to input Image

Test	1	2	3	4
Image Type	jpg	jpg	jpg	Jpg
Size	471 X 600	150 X 100	75 X 50	15 X 10
Rotate	No	No	No	No
Image Format	24 Bits RGB	32 Bits RGB	32 Bits RGB	32 Bits RGB
Mining Turn Around time	00:00:14:65	00:00:04:01	00:00:03:02	00:00:03:07
Overall Image Retrieval Time	00:00:53:682	00:00:06:58	00:00:03:95	00:00:03:14
Deviation Factor	0	9.26	11.49	48.52
Overall Mining Precision	100%	100%	100%	100%

Result Analysis with respect to parameters (After Resize the image)

Test	1	2
Image Type	Jpg	jpg
Crop	Yes	Yes
Size	167 X 77	142 x 84
Image Format	32 Bits RGB	32 Bits RGB
Mining Turn Around time	00:00:03:0484	00:00:03:054
Overall Image Retrieval Time	00:00:05:889	00:00:04:67
Deviation Factor	0	0
Overall Mining Precision	100%	100%

Result Analysis with respect to parameters (After Crop the image)

Test	Total Number of Relevant Images	Number of Relevant Images Retrieved	Total Number of Retrieved Images	**Recall**	**Precision**	Result By Srinivasa Kumar [9]	
						Recall	Precision
1	46	42	45	**91.30**	**93.33**	63.04	64.44
2	47	42	46	**89.36**	**91.34**	78.94	68.00
3	45	38	42	**84.44**	**90.37**	66.66	80.00
4	42	35	41	**83.33**	**85.36**	83.33	69.44
5	40	25	35	**59.52**	**71.42**	71.80	65.70

Comparison of Our Method with Shrinivasa Kumar Result

7. Conclusion

The main objective of the image mining is to remove the data loss and extracting the meaningful information to the human expected needs. The images are preprocessed with various techniques and the texture calculation is highly focused. Here, images are clustered based on RGB Components .Histogram is used to compare the images with some threshold constraints. This application can be used in future to classify the medical images in order to diagnose the right disease verified earlier.

8. Future Scope

- This system is useful in future to detect the diseases related with human.
- More effort to be taken to reduce the Image retrieval time of an given input Query Image
- In future this system is also implemented in the field of computer Vision which is concerned with the automated processing of images from the real world to extract and interpret information on a real time basis.
- In future these system is used in Astronomy to the study of celestial objects (such as stars, planets, comets, nebulae, star clusters and galaxies).

References

[1] Ji Zhang Wynne Hsu and Mong Li Lee, "Image Mining: Trends and Developments".

[2] A.Kannan,Dr.V.Mohan and Dr.N.Anbazhagan,"Image clustering and Retrieval using Image Mining Techniques", IEEE International Conference on Computational Intelligence and Computing Research, 2010.

[3] D.S. Zhang and G.Lu, "Content Based Image Retrieval Using Texture Features", In Proc. Of First IEEE Pacific-Rim Conference on Multimedia PCM'2000, pp.392-395.

[4] Yixin Chen, James Z.Wang and Robert Krovetz "Cluster Based Retrieval of Images by Unsupervised Learning". IEEE Transaction on Image Processing, August 2005, Vol 14, pp.1187-1199.

[5] Hewayda M.Lofty, Adel S.Elmaghraby, "CoIRS: Cluster Oriented Image Retrieval System", IEEE conference on tools with Artificial Intelligence, 2004.

[6] M. Datcu and K. Seidel," Image Information Mining: Exploration of Image Content in Large Archives", IEEE Conference on Aerospace, 2000, Vol.3.

[7] Zhang Y.J,"A Survey on evaluation methods for image segmentation," vol.29, no.8, 2000, pp.1335-1346.

[8] Ji Zhang Wynne Hsu Mong Li Lee," Image Mining: Issues, framework and techniques".

[9] Srinivasa Kumar Reddy "Content Based Image Retrieval System", Georgian Electronic Scientific Journal No.5, 2009.

[10] A. Kitamoto "Data Mining for Typhoon Image Collection", In Proceedings of the Second International Workshop on Multimedia Data Mining, August, 2001, San Francisco, CA, USA.

[11] M. Sasikalal and N. Kumaravel "Comparison of Feature Selection Techniques for Detection of Malignant Tumor in Brain Images", IEEE Conference, 11 -13 Dec 2005. Chennai, India.

[12] C.Ordonez and E.Omiecinski,"Discovering Association Rules Based on Image Content" Proceedings of the IEEE Advances in Digital Libraries Conference (ADL'99).

[13] W. Hsu, M. L. Lee and K.G.Goh," Image Mining in IRIS: Integrated Retinal Information System ", In Proceedings of ACM SIGMOD International Conference on the Management of Data, May 2000, Dallas, Texas.

[14] U. M. Fayyad, S. G. Djorgovski, and N.Weir," Automating the Analysis and cataloging of Sky Surveys" Advances in Knowledge Discovery and Data Mining, 1996, 471-493.

[15] O. R. Zaiane and J. W. Han," Mining Multimedia Data", Meeting of Minds, November 1998, pp 83-96, Toronto, Canada.

Ultrasonic Behaviour of Binary Mixtures Containing Stearates and Acetone

[1]r. Kavitha , [2]s. Jayakumar, [3]r. Uma

[1,3.] Research scholar, Department of Chemistry, Pachaiyappa's College, Chennai – 30.
[2]. Assoc Prof., Department of Physics, Vivekananda college, Mylapore, Chennai – 04.

Abstract

The ultrasonic velocity measurements along with density and viscosity in the binary mixtures of zinc stearate - acetone and calcium stearate - acetone at 303 K are studied. It is used to evaluate the different thermo acoustical parameters along with the excess properties. The experimentally determined velocities have been compared with theoretically estimated values obtained using different empirical theories and relations. The results are utilized to compare the relative merits of these theories and relations in terms of percentage of variation.

Keywords: Stearates, stabilizer, solvent, molecular interaction, excess properties.

1. Introduction

Many attempts have been undertaken to assess the association or generally speaking, the structuredness of the solvents [1]. Ion – solvent interaction is always attractive because the solvent molecules can orient their dipoles in the direction which results in minimum potential energy [2]. For many purposes, it is necessary to know the volumes and compressibilities of the solutions relative to their corresponding values at infinite dilution. The determination of such quantities requires the extrapolation of experimental data in very dilute solutions [3]. A stabilizers such as zinc stearate and calcium steartate is highly required in pharmaceutical and PVC industries. The determination of such quantities requires the extrapolation of experimental data in very dilute solutions. Zinc stearate $(C_{18}H_{35}O_2)_2Zn$ and calcium stearate $(C_{17}H_{34}COO)_2Ca$ are the stabilizers used and acetone is used as a solvent. It is the most powerful mold release agent among all metal soaps. It contains no electrolyte and has a hydrophobic effect. Its main application areas are the plastics and rubber industry where it is used as a releasing agent and lubricant which can be easily incorporated. The results have been discussed in terms of molecular interactions. The values of ultrasonic velocity (U), density (ρ) and viscosity (η) for the pure components is given in Table 1. From the experimental values, a few acoustical parameters such as adiabatic compressibility ($ß$), acoustical impedance (Z), molar sound velocity (R), Wada's constant (W), molar volume (V_m), free volume (V_f), intermolecular free length (L_f), internal pressure (π), absorption coefficient (α/f^2) viscous relaxation time (ι), degree of intermolecular attraction (α), excess ultrasonic velocity (U^E), excess adiabatic compressibility ($ß^E$) , excess acoustical impedance (Z^E), excess free length (L_f^E) and excess molar volume (V_m^E) were derived over the entire mole fraction range. Ultrasonic velocities have also been evaluated theoretically with the help of Impedance relation, Nomoto relation, Van Dael & Vangeel relation and Junjie relation. The suitability of these theories and equations were checked by comparing theoretical values of ultrasonic speeds with the values obtained experimentally. Literature survey showed that no measurements have been previously reported for the mixtures reported in this paper.

2. Materials and Methods

The chemicals used were of analytical grade and obtained from E.Merck company. Thermostatically controlled well-stirred water bath whose temperature was maintained to ±0.01 K accuracy was used for all the measurements. Binary mixtures were prepared by weighing in airtight bottles, the possible uncertainty in the concentration is estimated to be less than ±0.0001. Densities of pure components and their mixtures were determined by using a 1 X 10^{-5} m^3 double arm pycnometer. The density values from triplicate replication at the temperature of 303 K were reproducible within ± 2 X 10^{-2} kg m^{-3}. The uncertainty in density and excess molar volume values were found to be ± 4 X 10^{-2} kg m^{-3} and ± 0.001 X 10^{-6} m^3 mol^{-1} respectively. Ostwald's viscometer having capacity of about 15 ml and the capillary having a length of about 90 mm and 0.5 mm internal diameter has been used to measure the flow times of pure liquids and liquid mixtures and it was calibrated with benzene (density ≈ 0.8738 g cm^{-3}) and doubly distilled water (density ≈ 0.9970 g cm^{-3}) at 303 K. The flow time of pure liquids and liquid mixtures were repeated for five times. The uncertainty of viscosity was ± 0.005 X 10^{-3} m Pas. Speed of sound was measured by using a variable path, single crystal interferometer. (United scientific company, India), working at 2 MHz frequency. The interferometer was calibrated using toluene. Measurement of speed of sound through medium was based on the accurate determination of the wavelength of ultrasonic waves of known frequency produced by quartz crystal in the measuring cell. The interferometer cell was filled with the test liquid, and water was circulated around the measuring cell from a thermostat. The uncertainty was estimated to be 0.1ms^{-1}.

The adiabatic compressibility (ßs) was calculated by the equation

$$ß = 1/ \rho U^2 \quad (1)$$

Where ρ is the density of mixture and U is the ultrasonic velocity of the mixture.

The acoustical impedance (Z) was calculated by the equation,

$$Z = \rho U \quad (2)$$

The molar sound velocity (R) was calculated by the equation

$$R = (M_{eff} / \rho) U^{1/3} \quad (3)$$

The molar compressibility or Wada's constant (W), was calculated by the equation

$$W = (M / \rho) ß^{-1/7} \quad (4)$$

The intermolecular free length (L_f) was calculated by the equation

$$L_f = k ß^{½} \quad (5)$$

Where K = 1.98 X 10^{-6}, the Jacobson constant (Jacobson 1952).

The Free volume was calculated by the equation

$$V_f = (M_{eff} U/K\eta)^{3/2} \quad (6)$$

Where K = 4.28 X 10^9 for all liquids which is a temperature independent constant.

The internal pressure was calculated by the equation

$$\pi = \{bRT / (V^2 V_f)^{1/3}\} \quad (7)$$

b is a packing factor, R is a gas constant, V_f is free volume and T is temperature.

The absorption coefficient was calculated by the equation

$$(\alpha/f^2) = (8\pi^2\eta/3\rho U^3) \quad (8)$$

The viscous relaxation time was calculated by the equation

$$\iota = (4\eta/3\rho U^2) \quad (9)$$

The degree of intermolecular attraction (α) was calculated by the equation

$$\alpha = (u^2 / u^2_{im}) - 1 \quad (10)$$

Where $u^2_{im} = 1/ \{(x_1M_1 + x_2M_2)(x_1/M_1u_1^2 + x_2/M_2u_2^2)\}$

The U^E, $ß^E$, Z^E, L_f^E, and V_m^E were derived over the entire mole fraction range by using the general equation

$$A^E = A - (X_i A_1 + (1-X_i) A_2) \quad (11)$$

Where A is the corresponding parameters (U, ß, Z, $L_ß$ and V_m) of binary mixture and A_1 and A_2 are the corresponding pure component values.

The sound velocity can be correlated with the relation called Impedance relation which is represented as

$$U_{IM} = (X_1Z_1 + X_2Z_2) / (X_1\rho_1 + X_2\rho_2) \quad (12)$$

where X, Z, ρ denote the mole fraction, acoustic impedance and density of the component respectively.

Nomoto derived an empirical formula for the sound velocity in binary mixture. It is given by the equation

$$U_{NR} = [R/V]^3 = \left\{ \frac{(X_1R_1 + X_2R_2)}{(X_1V_1 + X_2V_2)} \right\}^3 \quad (13)$$

Where X, R, V denote the mole fraction, molar sound velocity and molar volume at temperature T of the component. The acoustical behaviour of binary mixture was studied in detail by Van deal etal. The expression for sound velocity (U_{IMR}) of binary mixtures can be obtained from equation

$$U_{IMR} = \left\{ \frac{[1/(X_1M_1 + X_2M_2)]}{[X_1/M_1U_1^2 + X_2/M_2U_2^2]} \right\}^{1/2} \quad (14)$$

Where X, M and U are the mole fraction, molecular weight and sound velocity of component.

Junjie derived an empirical formula for the sound velocity in binary mixture. It is given by the equation

$$U_{jun} = \left\{ \frac{(X_1V_1 + X_2V_2)}{(X_1M_1 + X_2M_2)^{1/2}} \left[\frac{X_1V_1}{\rho_{1U1}^2} + \frac{X_2V_2}{\rho_{2U2}^2} \right]^{-1/2} \right\} \quad (15)$$

Where X, V, M, ρ denote the mole fraction, molar volume, molecular weight and density of the components.
The percentage deviation of the experimental velocity from the theoretical value is given by the equation

$$\text{Percentage deviation in velocity} = \frac{U_{Theo} - U_{Expt}}{U_{Theo}} \times 100 \quad (16)$$

3. Results and Discussion

The ultrasonic velocity, density and viscosity data for the pure components at 303 K are given below:

Table 1
Comparison of density, ultrasonic velocity and viscosity data at 303 K

Component	U m/s	ρ Kg/m^3	η X 10^{-1} Nsm^{-2}
Zinc stearate	1404	1133	-
Calcium stearate	1310	1145	-
Acetone	1138	786	3.73

Table 2 gives the measured and acoustic parameters such as ultrasonic velocities (U), density (ρ), viscosity (η), adiabatic compressibility (ß), acoustical impedence (Z), molar sound velocity (R), molar compressibility (W), molar volume (V_m), free volume (V_f), Table 3 gives the thermodynamic properties like intermolecular free length (L_f), internal pressure (π), absorption coefficient (α/f^2), viscous relaxation time (ι), degree of intermolecular attraction (α), Table 4 gives the excess parameters like excess ultrasonic velocity (U^E), excess adiabatic compressibility ($ß^E$) , excess acoustical impedance (Z^E) , excess free length (L_f^E), excess molar volume (V_m^E), Table 5 gives the theoretical values of ultrasonic velocity calculated from Impedance, Nomoto, Van Dael & Vangeel and Junjie's relation along with the experimental ultrasonic velocity and percentage deviation for the binary mixtures zinc stearate - acetone and calcium stearate - acetone over the entire composition range at 303 K.

The ultrasonic velocity values (U) increases linearly with increase in stearate concentration in addition of acetone. Increase in ultrasonic velocity values may be due to decrease in space between chains inside the structure of components, thus it may be attributed to increase in cross linking between chains which consequently cause increase in rigidity of the molecules. When kinetic elements of adjacent chains have high mobility, cross linkages prevent the moving part of adjacent chains increase effectiveness of intermolecular interaction. This may result in a growth in the modulus of elasticity of stearates and ultrasonic velocity with increase in cross linkage factor [4]. In both Zn. St – ACE and Ca. St – ACE systems, aliphatic ketones used are strongly polar molecule with large dipole moment. Specific interaction between polar molecules leads to dipolar alignment forms α multimer and molecular interaction is found to be very less which may be due to the presence of weak dipole – induced dipole interaction between them. It depends upon polarity, increase in polarity due to the high electronegativity increases molecular motion leading to solute – solvent interaction [5]. This also reveals the absence of disruption of like molecular association by the component on one another and absence of strong dipole – dipole interaction between unlike molecules. Comparatively, interaction between aliphatic and aromatic molecules is quite stronger than aliphatic – aliphatic and aromatic – aromatic molecules. The density values (η) increases with increase in stearate concentration predicting the presence of greater molecular interaction between the components. The viscosity values (η) increases with increase in stearate concentration [6].

Table 2 : Measured and acoustic parameters of binary mixtures at 303 K

Conc of stearate	ms^{-1}	Kgm^{-3}	η / 10^{-1} Nsm^{-2}	β / 10^{-10} Kg^{-1}ms^{-2}	Z / 10^6 Kg m^{-2}s^{-1}			V_m / 10^{-1} m^{3}mole^{-1}	V_f / 10^{-7} m^{3}mole^{-1}
				zinc stearate – acetone					
0.01	1172	792.32	2.84	9.19	0.92	0.78	1.44	0.738	4.24
0.02	1176	798.64	2.99	9.05	0.93	0.78	1.44	0.738	3.98
0.03	1184	804.96	3.15	8.86	0.95	0.78	1.45	0.737	3.77
0.04	1188	811.28	3.30	8.73	0.96	0.78	1.45	0.737	3.56
0.05	1200	817.6	3.46	8.49	0.98	0.78	1.45	0.736	3.40
0.06	1372	823.92	3.62	6.45	1.13	0.82	1.51	0.736	3.93
0.07	1404	830.24	3.78	6.11	1.17	0.82	1.52	0.735	3.85
0.08	1406	836.56	3.95	6.05	1.18	0.82	1.52	0.735	3.65

0.09	1408	842.88	4.12	5.98	1.19	0.82	1.53	0.734	3.48
0.1	1412	849.2	4.29	5.91	1.20	0.82	1.53	0.734	3.32
				calcium stearate – acetone					
0.01	1216	792.04	2.97	8.54	0.963	0.79	1.46	0.738	4.19
0.02	1368	798.12	3.12	6.70	1.09	0.82	1.51	0.738	4.69
0.03	1376	804.2	3.27	6.57	1.11	0.82	1.51	0.737	4.44
0.04	1380	810.28	3.43	6.48	1.12	0.82	1.51	0.737	4.20
0.05	1382	816.32	3.59	6.41	1.13	0.82	1.51	0.736	3.98
0.06	1384	822.4	3.75	6.35	1.14	0.82	1.52	0.736	3.77
0.07	1388	828.48	4.05	6.27	1.15	0.82	1.52	0.735	3.41
0.08	1520	834.56	4.21	5.19	1.27	0.84	1.56	0.735	3.72
0.09	1576	840.6	4.38	4.79	1.32	0.85	1.57	0.734	3.74
0.1	1582	846.68	4.96	4.72	1.34	0.85	1.58	0.734	3.15

Table 3 : Thermodynamic parameters of binary mixtures at 303 K

Conc of stearate	$L_f / 10^{-11}$ M	$\pi / 10^6$ atm	$\alpha/f^2 / 10^{-12}$ $m^{-1}s^2$	$\iota / 10^{-10}$ s	$\alpha / 10^{-1}$ m
zinc stearate – acetone					
0.01	6.01	3.81	5.85	3.48	0.676
0.02	5.97	3.89	6.05	3.61	0.820
0.03	5.91	3.97	6.19	3.72	1.04
0.04	5.86	4.04	6.38	3.85	1.18
0.05	5.78	4.11	6.44	3.92	1.48
0.06	5.04	3.92	4.48	3.11	5.11
0.07	4.90	3.95	4.33	3.08	5.92
0.08	4.88	4.02	4.47	3.18	6.06
0.09	4.85	4.09	4.60	3.29	6.21
0.1	4.82	4.15	4.71	3.38	6.40
			calcium stearate – acetone		
0.01	5.80	3.82	5.48	3.38	1.49
0.02	5.13	3.69	4.01	2.78	4.63
0.03	5.08	3.75	4.11	2.87	4.90
0.04	5.05	3.83	4.24	2.96	5.07
0.05	5.02	3.90	4.38	3.07	5.21
0.06	5.00	3.97	4.52	3.17	5.34
0.07	4.97	4.11	4.80	3.38	5.53
0.08	4.52	4.00	3.78	2.91	8.73
0.09	4.34	3.99	3.50	2.80	10.3
0.1	4.31	4.23	3.89	3.12	10.5

Table 4 : Excess parameters of binary mixtures like U^E, $ß^E$, Z^E,L_f^E and v_m^E at 303 K

Conc of stearate	U^E ms^{-1}	$\beta^E / 10^{-10}$ $Kg^{-1}ms^{-2}$	$Z^E / 10^5$ $Kg\ m^{-2}s^{-1}$	L_f^E / 10^{-12} m	$V_m^E / 10^{-3}$ m^3mole^{-1}
			zinc stearate – acetone		
0.01	34	-0.63	0.336	-2.03	-0.412
0.02	38	-0.76	0.437	-2.46	-0.823
0.03	45	-0.95	0.571	-3.08	-1.23
0.04	49	-1.07	0.673	-3.49	-1.64
0.05	61	-1.31	0.841	-4.29	-2.05
0.06	233	-3.35	2.33	-11.7	-2.46
0.07	265	-3.69	2.68	-13.0	-2.87
0.08	266	-3.75	2.78	-13.3	-3.28
0.09	268	-3.80	2.88	-13.5	-3.69
0.1	272	-3.88	2.99	-13.8	-4.09
			calcium stearate – acetone		
0.01	78	-1.28	0.682	-0.420	-0.390
0.02	230	-3.12	1.96	-1.08	-0.781
0.03	238	-3.25	2.11	-1.13	-1.17
0.04	241	-3.33	2.22	-1.16	-1.56
0.05	243	-3.39	2.31	-1.19	-1.95
0.06	245	-3.46	2.41	-1.21	-2.34
0.07	249	-3.53	2.52	-1.24	-2.73
0.08	381	-4.61	3.71	-1.69	-3.12
0.09	437	-5.00	4.26	-1.87	-3.50
0.1	443	-5.07	4.41	-1.90	-3.89

Table 5 Experimental Velocities And Theoretical Velocities Along With The Percentage Deviation Of Binary Mixtures At 303 K

Conc of stearate	Ultrasonic velocity U /ms^{-1}					% Deviation			
	EXPT	Imp	Nom	VDV	Junjie's	Imp	Nom	VDV	Junjie's
					zinc stearate – acetone				
0.01	1172	1138	1139	1134	1138	-2.962	-2.863	-3.327	-2.958
0.02	1176	1139	1141	1131	1139	-3.288	-3.092	-4.018	-3.279
0.03	1184	1139	1142	1127	1139	-3.965	-3.670	-5.064	-3.951
0.04	1188	1139	1143	1123	1139	-4.290	-3.899	-5.756	-4.271
0.05	1200	1139	1145	1120	1140	-5.318	-4.828	-7.163	-5.292
0.06	1372	1140	1146	1116	1140	-20.384	-19.717	-22.908	-20.346
0.07	1404	1140	1147	1113	1140	-23.161	-22.371	-26.166	-23.115
0.08	1406	1140	1149	1109	1141	-23.307	-22.409	-26.736	-23.251
0.09	1408	1141	1150	1106	1141	-23.452	-22.448	-27.304	-23.388
0.1	1412	1141	1151	1103	1141	-23.773	-22.662	-28.052	-23.698
					calcium stearate – acetone				
0.01	1216	1138	1139	1134	1138	-6.837	-6.773	-7.188	-6.847
0.02	1368	1138	1140	1131	1138	-20.172	-20.030	-20.962	-20.194
0.03	1376	1139	1141	1127	1138	-20.855	-20.642	-22.045	-20.887
0.04	1380	1139	1141	1124	1138	-21.187	-20.903	-22.774	-21.228
0.05	1382	1139	1142	1121	1138	-21.343	-20.991	-23.323	-21.393
0.06	1384	1139	1143	1117	1139	-21.499	-21.078	-23.872	-21.557
0.07	1388	1139	1144	1114	1139	-21.831	-21.342	-24.600	-21.896
0.08	1520	1139	1145	1111	1139	-33.396	-32.788	-36.852	-33.475
0.09	1576	1140	1145	1107	1139	-38.288	-37.584	-42.306	-38.377
0.1	1582	1140	1146	1104	1139	-38.792	-38.012	-43.262	-38.889

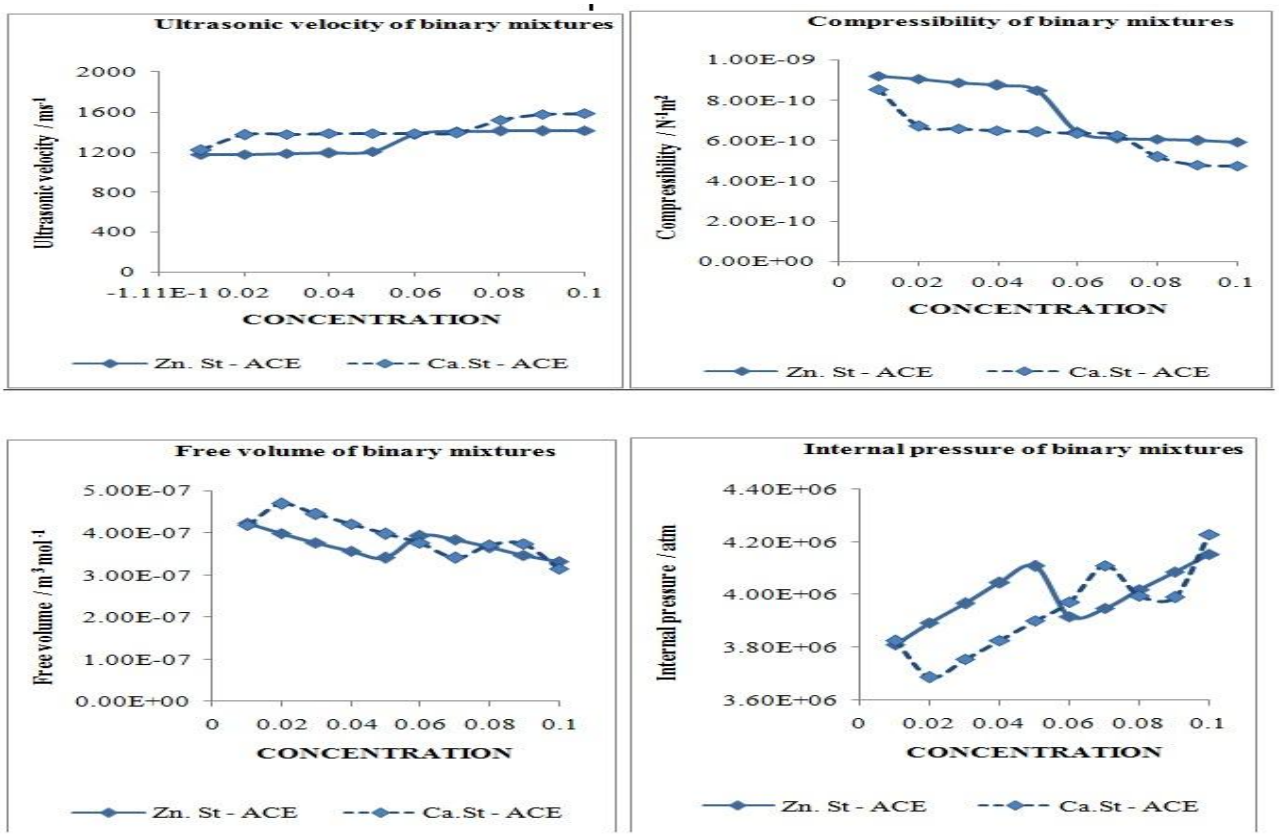

Fig. 1 Computed parameters of Zn. St – ACE and Ca. St – ACE at 303 K

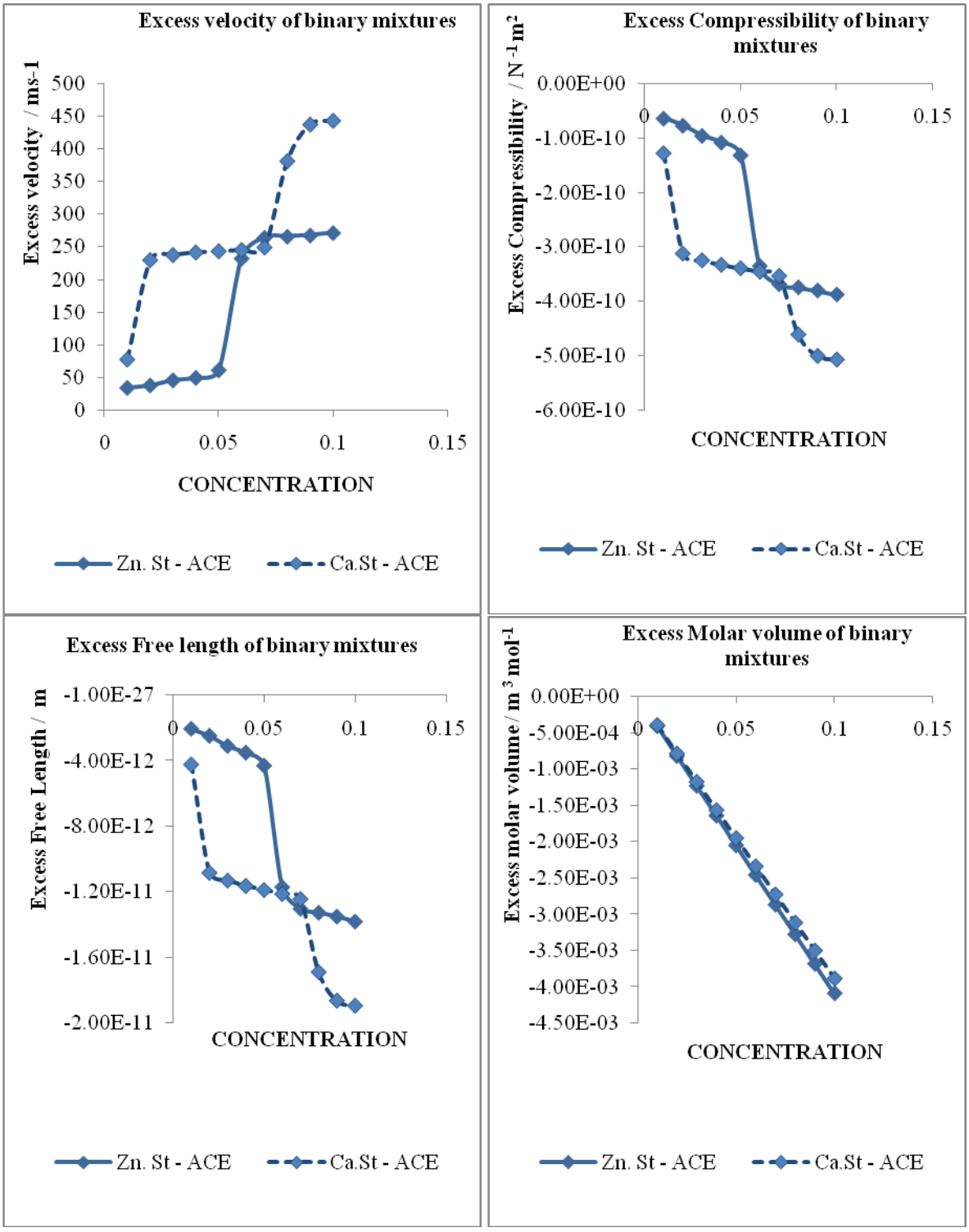

Fig. 2 Excess parameters of Zn. St – ACE and Ca. St – ACE at 303 K

The adiabatic compressibility (β) exhibits an exact reverse trend as that of ultrasonic velocity [7] for both the binary mixtures studied. The available solvent molecules for the next incoming component get decreased and every solvent has a limit for the compression as limiting compressibility value. The compressibility of solvent is greater than that of solution and it decreases with increase in concentration of solution. Solvents examined were chosen to cover a wide range of adiabatic compressibility. In both Zn. St – ACE and Ca. St – ACE systems, non linear decrease trend is observed.

The trend in non linear variation indicates the presence of complex formation which may be due to strong solute – solvent interaction. The disruption of stearates by solvents and weak interaction between unlike molecules leave the binary mixtures more compressible. Acoustic impedance (Z) increases with increase in stearate concentration for Zn. St – ACE and Ca. St – ACE systems. This favours increase in intermolecular distance between stearate and solvent molecules making relatively wider gaps between the molecules and becoming the main cause of impediment in the propagation of ultrasonic waves. It confirms the presence of molecular association between solute – solvent molecules through intermolecular hydrogen bonding [8]. Rao constant (R) and Wada's constant (W) show linear variation and almost it is constant with increase in stearate concentration, indicating the presence of solute – solvent interaction in addition of acetone to stearates . Molar volume (V_m) decreases with increase in stearate concentration. For Ca. St – ACE system, free volume increase and decrease with increase in stearate concentration. Comparatively, Zn. St – ACE system free volume decrease and increase with increase in stearate concentration. The decrease in the free volume also confirms the increasing order of symmetry [9] except for the system, both being aliphatic or aromatic components. The increase in free volume suggests the packing of molecules become looser predicting the presence of weaker interaction among the molecules.

The intermolecular free length (L_f) also follows the same trend as that of adiabatic compressibility in both binary systems. Free length is greater at low stearate concentration which may be due to solvent self association. As solvent density is not affected by association, one can deduce that the distance between the aggregate is greater than between the monomeric solvent molecules [10]. The decrease in free length with increase in ultrasonic velocity along with increase in stearate concentration increases intermolecular force between stearates and solvents. It strengthens the idea of molecular association in each system. The values indicates significant interaction between the components of the mixture through dipole – dipole interaction, dipole – induced dipole, hydrogen bonding etc., The internal pressure (π_i) values suggest the presence of inter – molecular interactions in addition of stearates to solvent. In Zn. St – ACE system, internal pressure increase at low concentration and decrease at high concentration. Comparatively, for Ca. St – ACE system, internal pressure decrease at low concentration and increase at high concentration. Non linear variation with both increased and decreased value suggests the presence of molecular association between unlike molecules. It predicts the existence of greater molecular interaction among the molecules in binary mixture. The absorption coefficient values (α/f^2) shows non linear increase and decrease trend in Zn. St – ACE and Ca. St – ACE systems. The values of relaxation time (τ) shows both increase and decrease data with increase in stearate concentration for Zn. St – ACE and Ca. St – ACE systems, viscous relaxation time increases at low concentration which may be due to increase in frictional resistance force and change in molecular area. As concentration increases, τ value decreases with decrease in available space between the molecules. Interaction parameter values (α) value increases with increase in stearate concentration for Zn. St – ACE and Ca. St – ACE systems, confirms the existence of molecular interaction between them [11].

Excess values may be affected by three factors, first factors explains the specific forces between molecules such as hydrogen bond, charge transfer complex, breaking of hydrogen bond and complexes shows large negative deviation. The second factor deals with the physical intermolecular forces, including electrostatic forces between charged particles and between a permanent dipole and so on induction forces between a permanent dipole and an induced dipole and force of attraction and repulsion between non polar molecules favouring physical intermolecular force shows both positive and negative deviation. The third factor deals with the structural characteristics of the component arising from geometrical fitting of one component into other structure due to the differences in size and shape of the components. The excess velocity shows positive deviations [12] which predict the weak interaction due to dispersion force. It shows non linear variation for Zn. St – ACE and Ca. St – ACE systems. Non linear variation shows specific intermolecular interaction between binary mixtures and the positive values predicts the strong association due to rupture of cohesion and growing adhesion leading to the formation of dipole – induced dipole interaction. The excess compressibility value depends upon two factors ie, first factor is increase in free length which may be due to loss of dipolar association, breaking up of hydrogen bonding, differences in size and shapes of the component. The second factor is the decrease in free length which is due to dipole – dipole interactions, hydrogen bonding association, complex formation, and interstitial accommodation of unlike molecules [13]. The first effect contributes to increase in the spacing between the molecules, such that ultrasound waves cover smaller distances in mixtures than in pure components. This would result in negative deviation of both excess compressibility and free length. The second effect contributes to decrease in the interspace between molecules and ultrasound waves which cover larger distances in the mixtures. This would result in positive deviation in ultrasonic velocity and negative deviation in compressibility and free length. For Zn. St – ACE and Ca. St – ACE systems, non linear trend is observed with respect to stearate concentration. It was reported that the positive deviation in excess impedance indicates the presence of strong interactions between component molecules in the mixture [46]. Excess molar volume shows negative deviation and linear decrease with increase in stearate concentration. Molar volume is slightly greater when calcium stearate is added to acetone than zinc stearate.

The experimental and theoretical velocities calculated by using various empirical relations are presented. The observed deviation of theoretical velocity from the experimental values should be rather treated as evidence of molecular interaction which takes place between stearates and acetone [14]. Deviation is larger in Van Dael and Vangeel relation which is due to the strengthening among unlike molecules. At all concentrations experimental ultrasonic velocity is found to be in good agreement with theoretical Nomoto velocity. It may be due to weak dipolar dispersive interaction between like molecules [56 - 58]. For Zn. St – ACE systems, deviation follows the order $U_{Vdv} > U_{Imp} > U_{Jun} > U_{Nom.}$ However, for Ca. St – ACE systems, deviation follows as $U_{Vdv} > U_{Jun} > U_{Imp} > U_{Nom.}$

4. Conclusion

The present investigation measures ultrasonic velocity, density and viscosity of stearates with acetone at 303 K. It reveals the presence of weak and strong molecular interactions in the binary systems from the acoustic, thermodynamic and excess parameter values. It may be suggested that the strength of interactions between aliphatic molecule and aromatic component will be greater than that of aliphatic – aliphatic and aromatic – aromatic components. Based on the above consideration, Zn. St – ACE and Ca. St – ACE system shows weak dipole – induced dipole interaction. The reason is that, stearate and ketones are aliphatic in nature, so interaction is expected to be very less. Molecular interaction between the stabilizer and solvent used decreases in the order: Ca. St – ACE > Zn. St – ACE From the computed data, standard relations like Impedance relation, Nomoto relation, Van Dael and Vangeel and Junjie relation are calculated. The large deviation of ultrasonic velocity is found in Van Dael & Vangeel and Junjie relation and it is found to be least in Nomoto and Impedance relation.

REFERENCES

[1]. Vasantharani P, Kalaimagal P and Kannappan A N Asian Journal of Applied Sciences 2(1) (2009) 96.
[2]. Jayakumar A, Karunanithi S and Kannappan V Ind. J. Pure Appl. Phys., 34 (1996) 761.
[3]. Srinivasalu U and Naidu P RJ Pure Apl. Ultrason., 17 (1995) 123.
[4]. Ranjan Dey, Anjan Chattopadhyay, Ashish K Sharma, Pandey J D J. Mol. Liq., 147 (2009) 155.
[5]. Muralikrishna P, Ranjith Kum ar B, Sathyanarayana B, Amara Jyothi and Sathyanarayana N Indian Journal of Pure & Applied Physics 47 (2009) 576.
[6]. Viswanathan S and Anand Rao M J. Chem.Eng.Data., 45 (2000) 764. Reddy K S J Chem. Therm., 16 (1984) 943.
[7]. Anuradha S, Prema S and Rajagopal K J. Pure Appl. Ultrason., 27 (2005) 49.
[8]. Jalal Basiri Parsa and Mahboobeh Faraji Journal of Molecular Liquids., 144 (2009) 102.
[9]. R Kavitha, S Jayakumar and R Uma ISST Journal of Applied Chemistry, Vol.1, No.2 (2010) 57.
[10]. R Kavitha, S Jayakumar and R Uma IJESR, Vol.2, Issue 4 (2011) 293.
[11]. R Kavitha, S Jayakumar and R Uma International Journal of Chemistry and Applications, Vol.3, No.1 (2011) 19.
[12]. R Kumar, S Jayakumar and V Kannappan., Indian Journal of Pure & Applied Physics., Vol. 46. March 2008, pp. 169 – 175.
[13]. Ulagendran, R Kumar, S Jayakumar and V Kannappan., Journal of Molecular liquids., 148 (2009) pp. 67 – 72.

"Economic Impact Due To Automobile Air Pollution Linked Diseases In Rewa"

[1,]Priyanka Rai, [2,]R.M.Mishra

[1,2],School of Environmental biology A.P.S.University Rewa(M.P.), 486003 India

Abstract

Nowadays air over major cities throughout the world has become over burdened with gases produced by automobiles. The death rate due to automobiles pollution is increasing rapidly in the metropolitan areas. Every year an estimated 800,000 people die prematurely from illnesses caused by outdoor air pollution worldwide. They compare cost-of-illness (COI) and willingness-to-pay (WTP) estimates of the damages from minor respiratory symptoms associated with air pollution using data from a study in Rewa in 2010-2011. The present study is an attempt to exploit air problems and diseases caused by the automobile air pollution and its cause economic problem by the treatment of disease. We conclude from our results that blood pressure, ENT (Eye, nose and throat), fatigue, gastrointestinal diseases and cancer were highly correlated with lead distribution. We also conclude that the motor vehicles/ automobiles now constitute the main source of air pollution. On the basis of observation Bus stand sites is highly polluted than the Sirmour chauk in which respiratory problem recorded 45.24% at sirmour chauk and 48.73% at Bus stand and expenditure is maximum on Bus stand is 572244 Rs. than the Sirmour chauk 509537 Rs.

Key Words: Urban air pollution, Human health and Economic loss.

1. Introduction

In most countries in Europe, ambient air quality has improved considerably in the last few decades. However, there is a large body of evidence suggesting that exposure to air pollution, even at the levels commonly achieved nowadays in European countries, leads to adverse health effects. In particular, exposure to pollutants such as particulate matter and ozone has been found to be associated with increases in hospital admissions for cardiovascular, respiratory disease, gastrointestinal disease, Skin disease, eye disease, ear disease and mortality in many cities in Europe and other continents. Recent studies have also tried to quantify the health effects caused by ambient air pollution; e.g., within the "Global Burden of Disease" project of the World Health Organization (WHO) it has been estimated that worldwide, close to 6.4 million years of healthy life are lost due to long-term exposure to ambient particulate matter. The World Health Organization (WHO) estimates that every year 800,000 people die prematurely from lung cancer, cardiovascular and respiratory diseases caused by outdoor air pollution. Other adverse health effects include increased incidence of chronic bronchitis and acute respiratory illness, exacerbation of asthma and coronary disease, and impairment of lung Function. This note outlines how cities can estimate health gains to their residents as they take steps to reduce outdoor air pollution. It discusses the types of studies used to quantify the relationships between air pollution and human health. Air quality affects human health. Nearly 1.4 billion urban residents in the world breathe air that fails the WHO air quality standards. At the global level, mortality due to exposure to outdoor air pollution is estimated to range from 200,000 to 570,000. In Indian cities, among the most polluted in the world, available mortality and morbidity statistics indicate that respiratory infections and chronic conditions are widespread. The major source of air pollution in Rewa is vehicular traffic, which emits particulate matter, sulphur dioxide, nitrogen oxides, carbon monoxide, hydrocarbons, etc. Particulate matter, the main atmospheric pollutant, can have severe health effects. Air pollution episodes in Muese Valley (1930),Donora (1948) and the London fog of 1952 resulted in heavy mortality. These events indicate that short term elevated levels of particulate matter and sulphur dioxide can lead to a variety of pulmonary disorders including mortality. Respirable particulate matter (RPM) is a respirable fraction with a diameter of less than the main factors which regulate occupational health status, are:

1. Nature and substance of exposure
2. Intensity or severity of exposure
3. Length of exposure
4. Personal susceptibility

Diesel also produces NO*x* that is easily absorbed in the blood and then reduces the oxygen-carrying capacity of the blood. It makes the lung tissues brittle and leathery and can cause lung cancer and emphysema (severe breathing problems)12. At the ITO Crossing, NO2 is above the standards in one out of every five days13. Even more disturbing is the fact that NO*x* from diesel

once out in the air forms ozone, yet another harmful gas. Adverse effects of air pollutants on human health can be acute or chronic. Acute effect manifests themselves immediately upon short term exposure to high concentrations of air pollutants whereas chronic effects become evident only after continuous exposure to low levels of pollutants. Pollutants can enter the body through a number of ways. They can cause skin and eye irritation; Particulate matter may be swallowed as a result of respiratory cleansing action. However, the primary mode of transfer of pollutants to the human body is through respiratory system. The slow and steady exposure to toxins present in the environment effect the human body and their toxins creep in to body slowly, sometimes causing lethal diseases and even death. The World Bank has estimated that Indians are spending Rs 4550 crores every year on treatment of diseases caused by ambient air pollution. The present study describe the economic impact due to automobile air pollution linked diseases , Rewa is situated on NH-7, traffic pollution is major sources of air pollution which cause human health diseases .

2. Material And Methodology

The questionnaire based survey was conducted in two road, Sirmour chauk and Bus stand for valuation of health cost due to air pollution. Human population was surveyed for the following aspects.

- Human capital (Earnings foregone due to premature death as a result of exposure to air pollution)
- Cost of illness (expenditures in medicines, doctor fees, lost working days and wages, expenditure in transportation and lodging etc.)

The morbidity cost also includes the expenditures associated to persons actually suffering with air pollution oriented chronic diseases, their admission in nursing homes, and other expenditures after their death. The cost of illness is calculated on the basis of lost wages due to lost working days and additional expenditures towards transportation, purchase of medicines, doctor's fees etc.

3. Result And Discussion

Health Impacts

Observation of traffic pollution impact on human health near Sirmour chauk and Bus stand in Rewa city (M.P.) Taple – 1 and Table-2. Represent the air pollution linked diseases in which percentage of persons suffering from respiratory diseases was found to be maximum on Bus stand 48.73% and 45.24% on Sirmour chauk. Most of the respiratory diseases observed under the present study were silicosis, breathlessness, asthma, bronchitis, cough, burning of mouth and throat and lung cancer. cardiovascular diseases 33.34% on sirmour chauk and 35.91% on bus stand. Gastrointestinal diseases is one of the important air pollution oriented diseases which is observed on both side is 43.07 % and 45.10%. sirmour chauk and Bus stand near both side percentage of skin diseases is higher than other air pollution linked diseases which is 47.60 from sirmour chauk and 52.75% from Bus stand .Eye, ear and teeth diseases is also air pollution linked disease in this survey work Percentage of these diseases noted 29.60%,23.83% and 20.73% near Sirmour chauk and 33.24%,31.99% and 25.22% near Bus stand. In this present work we show the percentage of air pollution linked disease is maximum on Bus stand than the Sirmour chauk. Other diseases like malaria, vomiting, anemia, cancer, vitamin deficiency, jaundice, pneumonia etc were reported at both sites. But these are not supposed to be caused by air pollution. Other diseases percentage found at Sirmour chauk 25.08% and at Bus stand 37.17%.Results indicate higher incidence rate of respiratory diseases among the people at Sirmour chauk and Bus stand near road side. Association between air pollution and lung function parameters has already been well documented (Islam and Schlipkoter, 1989;HEI,1995,2000a,2000b; schwela,1996,2000; Schlesinger, 2006;Pope,2000a 2000b; WHO,2000a,2000b). At low level of exposure of SO_2 for 24 hour period (mean annual level below 50 gm) epidemiological studies have demonstrated effect on mortality (total cardiovascular and respiratory) and on hospital emergency admissions for total respiratory causes and chronic pulmonary disease (WHO/EURO, 2000; Schwela, 2000). With respect to morbidity (hospital admission for cardiovascular respiratory diseases) an increase in 502 for long term exposure was significantly associated with an increase in adverse health effects (Schwela,2000). World Health Organization (WHO) estimates that approximately 3 million people die each year due to air pollution in the world (World Bank 2001). According to the WHO, air pollution is responsible for increases in outpatient visits due to respiratory and cardiovascular diseases, hospital admissions and mortality.

Human exposure to TRI emissions and to PM2.5 can be estimated with the intake fraction, defined as the total potential human dose as a function of total exposure relative to the source term (Bennett, McKone et al. 2001). The intake fraction is multiplied by linear dose response and concentration-response functions of human health hazard for TRI and PM2.5 respectively to estimate excess cancer cases and premature mortality (Bennett et al. 2003; Nishioka, Levy et al. 2003). The concentration-response function underlying PM2.5 premature mortality predicts annual adverse outcomes due to respiratory ailments and lung cancer that are specific to an emissions year. Thus, 1998 emissions are

associated with 1998 premature deaths. Mineral silicate is an unavoidable constituent of limestone from which lime and cement are processes (Gupta 1994), Silica is not considered carcinogenic, although the risk of lung cancer increases with silica exposure (Cherry et al. 1998).Air pollution's impact on health is very complex as there are many different sources. The individual effects vary from one to another, and it is especially harmful to the young children and the elderly, and those with existing respiratory problems. Children are at risk because their lungs are not fully developed; they breath faster, and they spend lots of time outdoors.

Table -1 Incidence of automobile air pollution oriented diseases among the people near sirmour chauck in Rewa City (M.P.)

S.NO.	Diseases	Male			Female			Total %
		Child	Adult	Old	Child	Adult	Old	
1	Respiratory	6.81	11.81	8.21	5.54	7.54	5.33	45.24
2	Cardiovascular	3.47	6.81	5.00	4.80	7.41	5.85	33.34
3	gastrointestinal	4.61	7.30	9.75	5.12	7.39	8.90	43.07
4	Skin	6.98	7.87	10.32	4.56	9.22	8.65	47.60
5	Eye	3.42	6.8	6.3	2.76	5.98	4.34	29.60
6	ear	2.87	4.43	5.34	2.54	4.89	3.76	23.83
7	Teeth	2.31	4.11	4.96	2.31	3.61	3.43	20.73
8	Other	3.90	3.73	4.68	3.05	5.54	4.18	25.08

Table -2 Incidence of automobile air pollution oriented diseases among the people near Bus stand in Rewa City (M.P.)

S.NO.	Diseases	Male			Female			Total %
		Child	Adult	Old	Child	Adult	Old	
1	Respiratory	7.21	12.43	8.86	6.32	8.41	5.50	48.73
2	Cardiovascular	3.98	6.51	5.69	5.46	8.67	5.60	35.91
3	gastrointestinal	4.98	7.65	8.79	6.22	7.77	9.69	45.10
4	Skin	7.85	6.87	10.90	6.89	9.71	10.53	52.75
5	Eye	5.05	6.67	8.30	2.66	6.58	3.98	33.24
6	ear	3.87	5..43	7.40	2.61	5.70	6.98	31.99
7	Teeth	3.89	7.01	2.43	2.80	5.66	3.43	25.22
8	Other	5.77	5.81	5.79	3.76	7.53	5.51	37.17

Economic Valuation of Health Impacts

Fig1. Represent the air pollution associated health cost of people at both sides (Sirmour chuk and Bus stand) near traffic pollution. A questionnaire based survey was conducted at sides to collect information on the expenditure made by people, as a result of air pollution, towards cost of illness in which expenditures of medicines 195937 Rs. and 216720 Rs. at both side. Medicinal charge is maximum than other charges. Wages charge 168420 Rs. on Sirmour chauk and 192141 Rs. Bus stand . Transport charge noted on both side is 15370 Rs. And 15588 Rs. Whereas doctor fee, bed charge and pathology is noted on Sirmour chauk is 18630 Rs., 13670Rs. and 2950Rs. and on Bus stand is 21330Rs., 13990 and 4760Rs.Accidental charges on both sites is 87980Rs. and 98765Rs.But other's charges which not include in

these charges is noted 6580 on Sirmour chauk and 8950 on Bus stand. Result indicate the total expenditures is 509537Rs. at Sirmour chauk and 572244 noted on Bus stand. On the all observation we can say Bus stand site is more polluted than Sirmour chauk per year. The world Bank (1997) estimated that air pollution cost china's economy more than 7% of GOP in 1995, largely in health damage. Chinese researches using the risk-dollar trade off method to revels the implied value of statistical life (Li. Schwartz and Xu. 1998) , the median value of willingness to pay in a sample of 500 for avoiding a death was US dollar 160,000,612. It is estimated that 251 premature deaths, 7.7 million cases of acute and chronic mobility, and 6,589 person-years of restricted activities would have been avoided if Shijizhuang had met the national ambient air quality standards in 2000. Appling the economic valuation number, this implies US dollar 40 million for premature deaths and US dollar 31 million for morbidity. Using incidence rates and survey data Li et al. (1998) estimated the costs of public health associated with air pollution in Shijiazhuang to be 63 million dollar. However, health cost estimate under present investigation is smaller than those of estimate cost of Li et al.(1998) .

Fig.1-Human health based economic loss due to air pollution at both sites in Rewa,(M.P.)

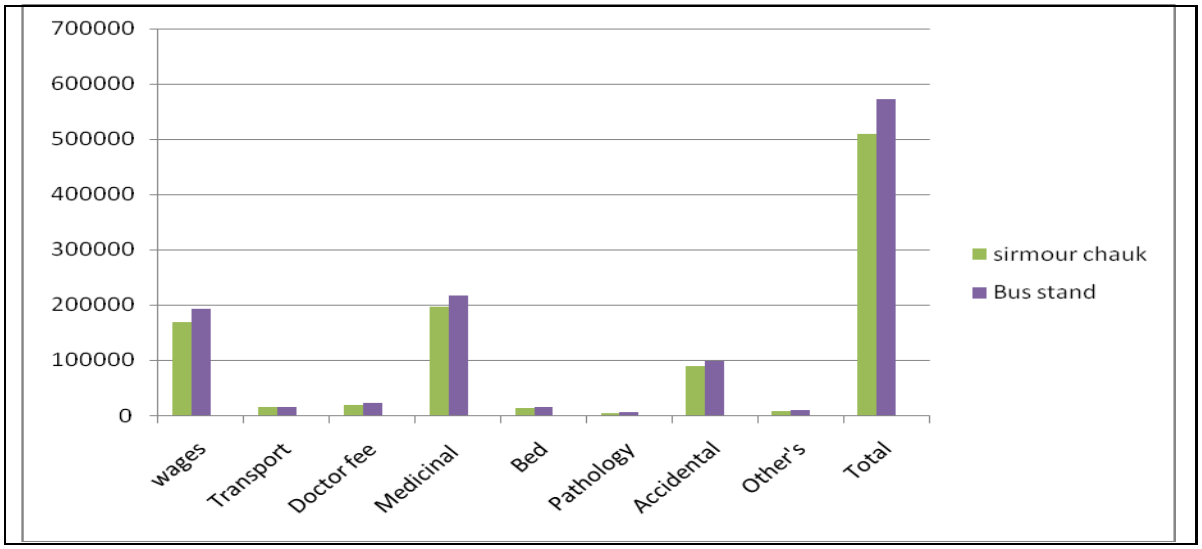

References

[1]. Abbey, D., Nishino, N., Mcdonnell, W., Burchette, R., Knutsen, S., Beeson, W.L., Yang, J.X., 1999. Long-term inhalable particles and other air pollutants related to mortality in nonsmokers. American Journal of Respiratory and Critical Care Medicine 159, 373–382.

[2]. Alberini, A., Cropper, M., Fu, T., Krupnick, A. , Liu, J., Shaw, D. and W. Harrington, W., 1997.Valuing Health Effects of Air Pollution in Developing Countries: The Case of Taiwan. Journal of Environmental Economics and Management 34(2): 107–126.

[3]. Aunan, K., Pan, X.-C., 2004. Exposure-response functions for health effects of ambient air pollution applicable for China—a meta-analysis. Science of the Total Environment 329, 3–16.

[4]. Bennett, D. H., McKone, T. E., et al., 2001. Defining Intake Fraction', Environmental Science and Technology 36: 206A-211A.

[5]. Cropper, M., Simon, N., Alberini A. and Sharma, P.K., 1997. The Health Effects of Air Pollution in Delhi, India. World Bank Policy Research Working Paper 1860. Available <http://econ.worldbank.org/docs/534.pdf>.

[6]. Delucchi, M.A., 2000. Environmental Externalities of motor vehicle use in the US. Journal of Transportation Economics and Policy 34 (2), 135–168.

[7]. Dockery D.W and Pope C.A. III 1994. Acute Respiratory Effects of Particulate Air Pollution, Annual Review of Public Health, v.15, pp: 107-132.

[8]. Dominici, F., Shepard, L., Clyde, M. 2003. Health effects of air pollution: a statistical review. International Statistical Review 71 (2), 243–276.

[9]. Gupta, V.K. Verma, A.K., 1994 Respirable dust exposure in iron and steel industries, Chemical.Environ.Res 3 (1& 2) : 147 – 149.

[10]. HEI, 1995. Particle air pollution and daily mortality. Replication and validation of selected studies; the phase I report of the particles epidemiology evaluation project. Health Effects Institute, Cambridge M.A. USA.

[11]. HEI,2000a. The National Morbidity, Mortality and Air Pollution Study, Part-I: Methods and Methodologic issues; Part-II: Morbidity and Mortality from air pollution in the United States, Research Report 94,June 2000,Health Effects Institute, Cambridge, M.A. USA.

[12]. HEI,2000b. Reanalysis of the Harvard Six cities study and the American cancer society study of particulate air pollution and Mortality, a Special Report of the Health Effects Institute's Reanalysis Project, July 2000. Health Effects Institute, Cambridge,MA,USA.

[13]. HEI, April 2004. Health Effects of Outdoor Air Pollution in Developing Countries of Asia. Special Report 15, Health Effects Institute, Boston, MA.

[14]. Holgate, S., Samet, J., Koren, H., Maynard, R., ed., 1999. Air Pollution and Health. San Diego, California: Academic Press.

[15]. Islam, M.S. and Schlipkoter, H.W,. 1989. Assessment of symptomatic and functional health standard of elderly woman exposed to didderent ambient air qualities. In :Man and his ecosystem (eds. L.J.Brasser and W.C.Mulder). Elsevier Science Publishers. Amserdam. Vol.1:41-44.

[16]. Laden, F., Neas, L.M., Dockery, D.W. , and Schwartz, J., 2000. Association of Fine Particulate Matter from Different Sources with Daily Mortality in Six U.S. Cities. Environmental Health Perspectives 108(10): 941–947.

[17]. Li,J., Schwartz,J. and Xu,X.,1998. Health benefits of air pollution control in Shenyang, China, Research report, School of Public Health, Harvard University.

[18]. Nishioka, Y., Levy, J. , et al., 2003. A Risk-Baed Approach to Human Health Impact Assessment for Input-Output Analysis (Boston, MA: Harvard School of Public Health).

[19]. Pandey, K.D. , Bolt, K., Deichmann, U. , Hamilton, K., Ostro B., and Wheeler, D., 2003 (forthcoming). The Human Cost of Air Pollution: New Estimates for Developing Countries. Washington DC: World Bank.

[20]. Pope, D., Thun, M., Namboodiri, M. , Dockery, D., Evans, J., F. Speizer, F., and Heath., C., 1995. Particulate Air Pollution as a Predictor of Mortality in a Prospective Study of U.S. Adults. American Journal of Respiratory Critical Care Medicine 151(3): 669–674.

[21]. Pope III, C.A., 2000a. Epidemiology of fine particulate air pollution and human health: biologic mechanisms and who's at risk? Environmental Health Perspectives 108 (Supplement 4), 713–723.

[22]. Pope III, C.A., 2000b. Invited commentary: particulate mattermortality exposure-response relations and threshold. American Journal of Epidemiology 152 (5), 407–412.

[23]. Pope III, C.A., Burnett, R.T., Thun, M.J., Calle, E.E., Krewski, D., Ito, K., Thurston, G.D., 2002. Lung cancer, cardiopulmonary mortality, and long-term exposure to fine particulate air pollution. Journal of American Medical Association 287 (9), 1132–1141.

[24]. Samet, J.M., Zeger, S.L., Dominici, F., Curriero, F., Coursac, I., Dockery, D.W., Schwartz, J., Zanobetti, A., 2000. The National Morbidity, Mortality and Air Pollution Study Part II: Morbidity and Mortality From Air Pollution in the United States. Health Effects Institute, Cambridge, MA.

[25]. Samoli, E., et al., 2003. Investigating the dose-response relation between air pollution and total mortality in the APHEA-2 multicity project. Occupational and Environmental Medicine 60 (12), 977–982.

[26]. Schlesinger,R.B., Kunzli, N.,Hidy,G.M.,Gotschi,T. and Jerrett,M., 2006. The health relevance of ambient particulate matter characteristics: coherence of toxicological and epidemiological inferences.Inhal.Toxicol.18:95-125.

[27]. Schwela,D.H.,1996. Exposure to environmental chemicals relevents for respiratory hypersensitivity : global aspects. Toxicology letters 86:131-142.

[28]. Schwela,D.H.,2000. Air pollution and health in urban areas, Reviews on Environmental Health 15:13-42.

[29]. Spix, C., et al. 1998. Short-term effects of air pollution on hospital admissions of respiratory diseases in Europe: a quantitative summary of APHEA study results. Archives of Environmental Health 53 (1), 54–64.

[30]. World Bank,1997. China's Environment in the New Century: Clear water, Blue Skies, The world bank, Washington, DC.

[31]. World Bank, 2001. China: Air,Land and Water, Environmental Priorities for a new Millennium, The World Bank, Washington,DC.

[32]. WHO, 2000a. Guidelines for Air Quality, WHO/SDE/OEH/00.02.World health organization, Geneva, Switzerland, Internet address:http://www.who.int/peh/air/Airquality.htm..

[33]. WHO, 2000b. Guidelines for Air quality http://www.who.int/peh/air/Airqualitygd.htm, World health organization, Geneva.

[34]. World Health Organization Regional Office for Europe. Air Quality guidelines for Europe. 2nd Ed. Copenhagen: World Health Organization Regional office for Europe,2000. (WHO Regional Publications, European Series,91).

[35]. Woodruff, T. J., J. Caldwell, et al., 2000. Estimating Cancer Risk from Outdoor Concentrations of Hazardous Air Pollutants in 1990', Environmental Research 82: 194-206.

An Efficient Memory Architecture For Network Intrusion Detection Systems Using Pattern Partitioning And Parallel String Matching

[1,]T.Aswini Devi, [2,] Mrs. K.Surya Kumari.
[1,2,]M.Tech Project student, Department of ECE, Pragati Engineering College,
Surampalem, Kakinada, A.P, India.

Abstract

Due to the advantages of easy re-configurability and scalability, the memory-based string matching architecture is widely adopted by network intrusion detection systems (NIDS).The ability to inspect both packet headers and payloads to identify attack signatures makes network intrusion detection system (NIDS) a promising approach to protect Internet systems. In this paper, we propose a memory-efficient pattern-matching algorithm which can significantly reduce the memory requirement. Using the pattern dividing, the variety of target pattern lengths can be mitigated, so that memory usage in homogeneous string matchers can be efficient. In order to identify each original long pattern being divided, a two-stage sequential matching scheme is proposed for the successive matches with sub-patterns. We synthesized this design using Quartus II 11.0 version.

Keywords: Computer network security, finite automata,Parallel processing, Deterministic-finite automata (DFA).

1. INTRODUCTION

As Proliferation of Internet applications increases, security becomes a problem within network solutions. Intruders attempt to break into publicly accessible victim systems to misuse the functionality provided. Traditional network based security devices such as firewalls, performing packet filtering on packet headers only, fail to identify attacks that use unsuspicious headers. By inspecting both packet headers and payloads to identify attack signatures, network intrusion detection system (NIDS) is able to discover whether hackers/crackers are attempting to break in or launch a denial of service (DOS) attack.Because most of the known attacks can be represented with strings or combinations of multiple substrings, string matching is one of the key components in NIDS. String matching in NIDS is computationally intensive in that, unlike simple packet classifications, NIDS needs to scan both the headers and the payloads of each incoming packet for thousands of suspicious strings. Worse, the string lengths are variable. As a result, string matching has become the bottleneck in NIDS to address the requirement of constantly increasing capacity. A string matching engine can have multiple string matchers for parallel string matching. Due to the slow speed of the software-based string engine, the hardware-based string matching engine is preferred due to great parallelism for the high-performance IDSs. In particular, the memory-based string matching engine allows on-the-fly update of memory contents for high re-configurability. However, there are several well-known challenges: high throughput, regularity, scalability, and low memory requirements.

Especially, in the memory-based string matching engine, the string matching based on deterministic-finite automaton (DFA) is frequently adopted due to the deterministic transitions between states according to input symbols; state transitions can be performed in a fixed number of cycles, where the throughput can be maintained unchanged. In addition, due to the fixed number of output transitions in a state, regularity can be guaranteed in the DFA-based string matching engine. Scalability can be supported by the homogeneity of multiple string matchers where DFAs are mapped. Because of the deterministic transitions between states, however, memory requirements are proportional to both the number of states and the number of transitions in a state. The total cost of a string matching engine is directly related to memory requirements; therefore, the target pattern information should be compressed. In the traditional Aho-Corasick algorithm and the bit-split DFA-based string matching, common prefixes between target patterns are shared in a DFA.First, the (attack) string patterns are compiled to a finite state machine (FSM) whose output is asserted when any substring of input strings matches the string patterns. Then, the corresponding state table of the FSM is stored in memory. For the pattern identification, a state should contain its own match vector with a set of bits, where each bit represents a matched pattern in the state. Even though the information of shared common infixes was stored in match vectors, the number of shared common infixes was limited by the size of the match vectors. In addition, throughput could decrease due to the modified state transition mechanism. In the memory requirements for match vectors were reduced by relabeling states and eliminating the match vectors of non-output states. By sharing common infixes of target patterns or relabeling states and eliminating the match vectors of non-output states, the memory usage in the match vectors could be efficient The pattern-matching problem considered here is that of searching for occurrences of a pattern string within a larger text string. Stated formally, given a pattern x with length $|x| = m$ and a text y with length $|y| = n$, where $m, n > 0$ and $m \leqslant n$, the task is to determine if x occurs within y. This basic problem is found in many application domains of network intrusion detection systems (NIDS)

2. Pre Design Information

A. Target Patterns

A target pattern and a set of its k sub patterns, which are obtained after dividing the target pattern, are denoted as **P**i and **Q**i={SP_{i1};SP_{i2}; . . . ;SP_{ik}}respectively. The subscript **i** is the index of the target pattern. However, the variety of target pattern lengths is another serious problem in achieving regularity and scalability with low hardware cost. Each pattern consists of multiple character codes, where the number of character codes is defined as the pattern length. According to the rule sets, the distribution of pattern lengths could be different each other. In addition, the variation of pattern lengths in each rule set is irregular. If target patterns are to be mapped onto multiple homogeneous string matchers, memory usage cannot be balanced without considering different pattern lengths.

B. Pattern Dividing

The target pattern has set of k sub-patterns, which are obtained after dividing the target pattern, are denoted as Pi and Qi respectively. A set of k sub-patterns Qi will be called the quotient vector of Pi. The fixed length of k sub-patterns is denoted as f. If the length of a target pattern is shorter than f, the target pattern does not need to be divided, so the pattern is defined as the short pattern. The remnant pattern Ri represents a suffix or residual sub-pattern of the target pattern Pi that succeeds the quotient vector of Pi. The match in a sub-pattern is encoded with a quotient index, which represents the unique index of the sub-pattern match. The remnant pattern Ri should be matched sequentially after the quotient vector Qi is matched.

C. Identification Of Pattern

Consider four target patterns {“abc,” “abcd,” “ac,” “bcd”} are mapped on a DFA, where target pattern lengths range from 2 to 4. The fourth target pattern is a suffix of the second target pattern. If the second target pattern is matched, the fourth target pattern is always matched, but not vice versa. We let a target pattern Pi be a suffix of another target pattern Pj for Pi is not equal to Pj. If different identification indexes are provided for the matches with Pi and Pj, respectively, Pi is explicitly identified when Pj is matched. If only the identification index for Pj is provided, Pi is implicitly identified. In this case, only the target pattern with the longest prefix from the initial state has its own identification index in the implicit identification; therefore, users could detect matches with Pi after analyzing the identification for Pj with extra effort. In addition, a target patternPi can be identified after its quotient vector Qi and its remnant vector Ri are matched in order.

D. Bit- Split Dfa

DFA is an FSM where there is one and only one transition to a next state according to each pair of state and input symbols. DFA can be represented with a five-tuple: a finite set of states (Q), a finite set of input symbols (P), a transition function, an initial state, and a set of output states. The identification index of a target pattern is an individual keyword used to distinguish the target pattern match. The memory requirements of DFA are proportional to the size of Q and P.

3. Proposed Scheme

A. Deterministic Finite Automaton

In automata theory, a branch of theoretical computer science, a deterministic finite automaton (DFA)—also known as deterministic finite state machine—is a finite state machine that accepts/rejects finite strings of symbols and only produces a unique computation (or run) of the automaton for each input string. 'Deterministic' refers to the uniqueness of the computation. In search of simplest models to capture the finite state machines, McCulloch and Pitts were among the first researchers to introduce a concept similar to finite automaton in 1943. The following figure shows the structure of DFA.

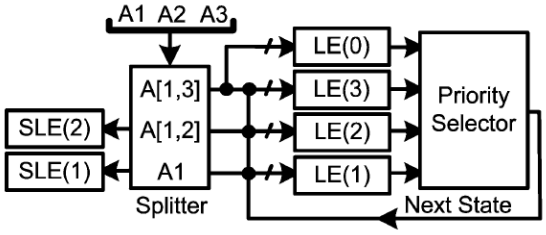

Fig.1. Structure of DFA

In the automaton, there are three states: S0, S1, and S2 (denoted graphically by circles). The automaton takes finite sequence of 0s and 1s as input. For each state, there is a transition arrow leading out to a next state for both 0 and 1. Upon reading a symbol, a DFA jumps deterministically from a state to another by following the transition arrow. For example, if the automaton is currently in state S0 and current input symbol is 1 then it deterministically jumps to state S1. A DFA has a start state (denoted graphically by an arrow coming in from nowhere) where computations begin, and a set of accept states (denoted graphically by a double circle) which help define when a computation is successful.

A DFA representing a regular language can be used either in an accepting mode to validate that an input string is part of the language, or in a generating mode to generate a list of all the strings in the language. In the accept mode an input string is provided which the automaton can read in left to right, one symbol at a time. The computation begins at the start state and proceeds by reading the first symbol from the input string and following the state transition corresponding to that symbol. The system continues reading symbols and following transitions until there are no more symbols in the input, which marks the end of the computation. If after all input symbols have been processed the system is in an accept state then we know that the input string was indeed part of the language, and it is said to be accepted, otherwise it is not part of the language and it is not accepted. The generating mode is similar except that rather than validating an input string its goal is to produce a list of all the strings in the language. Instead of following a single transition out of each state, it follows all of them. In practice this can be accomplished by massive parallelism or through recursion. As before, the computation begins at the start state and then proceeds to follow each available transition, keeping track of which branches it took. Every time the automaton finds itself in an accept state it knows that the sequence of branches it took forms a valid string in the language and it adds that string to the list that it is generating. If the language this automaton describes is infinite (ie contains an infinite number or strings, such as "all the binary string with an even number of 0s) then the computation will never halt.

B. Aho-Corasick Algorithm

Aho-Corasick String Matching Automaton for a given finite set P of patterns is a (deterministic) finite automaton G accepting the set of all words containing a word of P. Transition table is built during the preprocessing part. Where at each state, there is in-formation about where to jump to for each character. It just traverses the string to be matched making transitions, the transition function which tells which state to jump for each character. Whenever we reach a state F, a match is reported by the engine. For simple string matching cases, it does not performs very well but when there are multiple patterns or pattern matching is done at regular expression level, it is one of the best options for pattern matching. Aho-Corasick Matching, implementation first forms a combined DFA for all patterns. Since this is preprocessed during the initialization part, there is no overhead of DFA formation for each pattern and also no (individual or set of) patterns traversal. And for each new character we have to just take one step. But the memory overheads are huge. Also, the state holding at each step is huge because there are multiple copies of active DFA's since a new DFA gets activated at each new character input other than the existing DFA's. Of course some go out also but difference is huge. But power of the algorithm is, it is unaffected by the variance in size of the patterns and worse and average case performance is same.The enhanced design on Aho-Corasick uses an optimized vector storage design for storing the transition table. This memory efficient variant uses sparse matrix storage to reduce the memory requirements and further improve performance on large pattern groups.

Sparse-Row format

Vector: 0 0 0 2 4 0 0 0 6 0 7 0 0 0 0 0 0

Sparse-Row Storage: 8 4 2 5 4 9 7 11 7

Now for each DFA state rather than having a 256-size vector of which most are 0 values, we use sparse matrices to present the transition element and the corresponding value. Cleary since we cannot have O(1) transition time in this implementation, since we need to traverse this new vector to find the transition element. The memory requirements go down by four times which is quite significant.

C. Fsm Tiles

In a string matcher, several homogeneous FSM tiles take n bits as an input at every cycle. In the state of each FSM tile, the pattern identification information is stored as a partial match vector (PMV), where the ith bit indicates whether the ith pattern is matched or not in the state. A pattern can be identified with a full match vector (FMV), which is obtained with the logical AND operation of PMVs in all FSM tiles.

The different types of FSM tiles in can be adopted. The number in the angle brackets describes the field width.

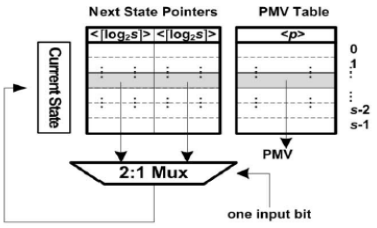

Fig.2a.

Every state can indicate its PMV. A difference of the FSM tile in Fig. 2a is that the FSM memory for storing next-state pointers can be separated from the PMV table. As shown in Fig.2b,

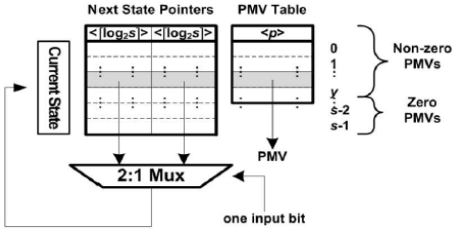

Fig.2b.

If there is no need to have PMVs in several states, the memory allocation for the states is not required; only several PMVs are stored in a PMV table. The stored PMVs are defined as nonzero PMVs; the PMVs to be reduced are defined as zero PMVs. When many PMVs can be shared between multiple states, the FSM tile type in Fig. 2c is beneficial by

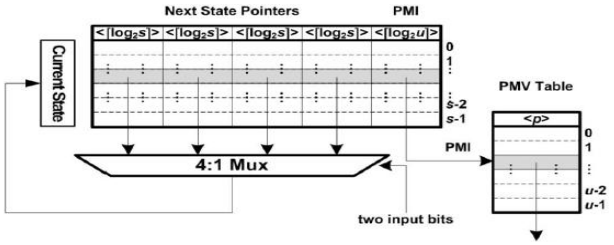

Fig.2

A pattern match index (PMI) in each state indicates a unique PMV for the state. By adopting a separate PMV table, the memory requirements for storing repeated PMVs can be eliminated.

D.Pattern Mapping And Partitioning

The pattern mapping for a string matcher, where sorted patterns ST and string matcher parameter M are given. Initially, for loop checks whether all FSM tiles can be built when the number of mapped patterns is maximum. A variable denotes the number of mapped patterns in each turn. With front patterns from the given sorted patterns, mapped t, a procedure Build tries is called to obtain the tries for FSM tiles in a string matcher. Then, if the largest number of states in tries is greater than the maximum number of states in an FSM tile, next iteration is continued by reducing by one; otherwise, the loop is broken after obtaining the mappable patterns, mapped t. The unmapped patterns are returned by a procedure Remove. After exiting for loop, a procedure Add failing pointer is called to add failing pointers from each state to the longest suffix state. Finally, for the mapped patterns mapped t, the contents of the PMVs are obtained by calling a procedure called Set PMV s.

Pattern Mapping Algorithm:

```
procedure PM(sorted patterns ST, string matcher M)
  t   ST
  for   =p(M) to 1 do
    mapped_t   front(   t)
    tries   Build_tries(mapped_t)
    if max(Num_states(tries) > s(M) then
      continue
    else
      Remove(mapped_t, t)
      break
    end if
  end for
  dfas   Add_failing_pointer(tries,mapped_t)
  fsms   Set_PMV s(dfas, mapped_t)
  return fsms and t
  end procedure
```

Pattern Partitioning Algorithm:

Procedure PP denotes the pattern partitioning with patterns T and string matcher parameter M. First, patterns are sorted lexicographically to increase the number of shared common prefixes. Then, a procedure PM, which denotes the pattern mapping, is called for obtaining the FSM tile contents for a string matcher. Then, the unmapped patterns are returned. The obtained FSM tile contents are stored in *vec_fsms*. The pattern mapping is repeated until there are no unmapped patterns.

```
Procedure PP(patterns T, string matcher M)
    t   Sort(T)
```

While t **do**
fsms, t PM(t,M)
vec_ fsms= vec_ fsms+ fsms
end while
return *vec_fsms*
end procedure

The pattern mapping algorithm shows the constant time complexity. Therefore, the time complexity for partitioning total patterns can be O(T), where T denotes the number of patterns. On the other hand, the time complexity of pattern sorting can be O (T.log2T). However, due to the large constant factor of the pattern mapping, if T is not sufficiently large, the pattern sorting will not be dominant.

4. Results

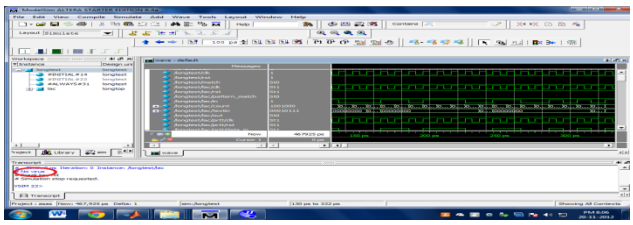

Fig.3.a. Window showing No Virus

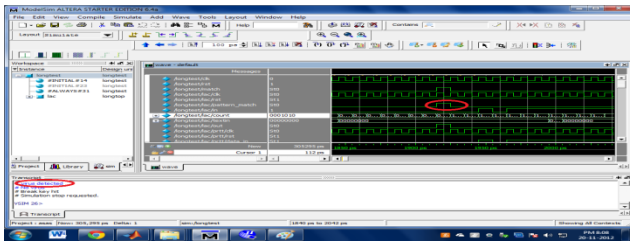

Fig.3.b. Window showing Detected Virus

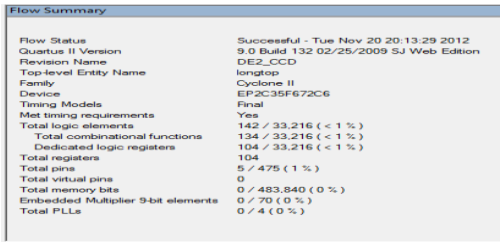

Fig.3.c. Area used by Existing System

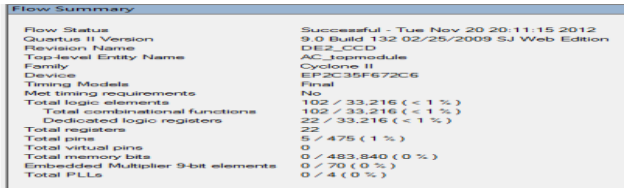

Fig.3.d. Area Used by Proposed System

Extensive verification of the circuit design is performed using the Verilog and then synthesized by the Quatrus II 9.0 to demonstrate the feasibility of the proposed architecture design for Intrusion Detection Systems.

5. Conclusion

The proposed DFA-based parallel string matching scheme minimizes total memory requirements. The problem of various pattern lengths can be mitigated by dividing long target patterns into sub-patterns with a fixed length. The memory-efficient bit-split FSM architectures can reduce the total memory requirements. Considering the reduced memory requirements for the real rule sets, it is concluded that the proposed string matching scheme is useful for reducing total memory requirements of parallel string matching engines.

References:

[1] Snort-the de Facto Standard for Intrusion Detection/Prevention, [Online]. Available: www.snort.org

[2] S. Antonatos, K. G. Anagnostakis, and E. P. Markatos, "Generating realistic workloads for network intrusion detection systems," presented at the Proc. ACM Workshop on Software and Performance, Redwood Shores, CA, 2004.

[3] S. Iyer, A. Awadallah, and N. McKeown, "Analysis of a packet switch with memories running slower than the line rate," in Proc. IEEE INFOCOM, Mar. 2000, pp. 529–537.

[4] Embedded Memory, [Online]. Available: http://www.ti.com/research/ docs/cmosmemory.shtml

[5] G. Navarro and M. Raffinot, Flexible Pattern Matching in Strings-Practical On-Line Search Algorithms for Texts and Biological Sequences. Cambridge, U.K.: Cambridge Univ. Press, 2002.

[6] C. J. Coit, S. Staniford, and J. McAlerney, "Towards faster string matching for intrusion detection or exceeding the speed of snort," in Proc. DARPA Information Survivability Conf. Exposition (DISCEX II'01), 2001, pp. 367–373.

[7] M. Fisk and G. Varghese, "Fast content-based packet handling for intrusion detection," UCSD, UCSD Tech. Rep. CS2001–0670, 2001.

[8] K. G. Anagnostakis, E. P. Markatos, S. Antonatos, and M. Polychronakis, "E XB: A domain-specific string matching algorithm for intrusion detection," presented at the 18th IFIP Int. Information Security Conf., Athens, Greece, 2003.

[9] R. T. Liu, N. F. Huang, C. H. Chen, and C. N. Kao, "A fast string-match algorithm for network processor-based network intrusion detection system," ACM Trans. Embedded Comput. Syst., vol. 3, pp. 614–633, 2004.

[10] J. Moscola, J. Lockwood, R. P. Loui, and M. Pachos, "Implementation of a content-scanning module for an Internet firewall," in Proc. 11th Annu. IEEE Symp. Field-Programmable Custom Comput. Mach., Napa, CA, Apr. 2003, pp. 31–38.

Cost- Benefit Analysis of Wastewater Recycling Plant for Textile Wet Processing

[1,]Prof. Mahesh B. Chougule, [2,]Dr. (Capt.) Nitin P. Sonaje

[1,] Associate Professor in Civil Engineering Textile and Engineering Institute, Ichalkaranji, Maharashtra

[2,] Registrar, Solapur University, Solapur, Maharashtra

Abstract

Water has been a cheaper commodity for a very long period and never accounted for in processing cost. Now it becomes scarce and a priced commodity and the costs for water and its treatment to make it suitable for processing have escalated to the newer heights necessitating its inclusion in production costs. Water conservation techniques must be instigated in the textile industries. The industries must take initiatives to implement water management practices. Also it is necessary to encourage industries for investment in various water recycling methods. Treated wastewater from city wastewater plant is disposed either on land or in river. This water causes various land pollution problems and water pollution. This treated waste water can be used in textile wet processing by retreating it. The treatment plant comprises water storage tank, Oil and gas removal trap, Slow sand filter, Granular Activated carbon unit (GAC), Chlorination unit, two stage ion exchange unit with strong acid cation exchange resin SAC) and strong base anion exchange resin (SBA). This paper focuses on cost benefit analysis of wastewater recycling plant for textile wet processing

Keywords: Wastewater recycling, textile wet processing, GAC technology, strong acid cation exchange resin, strong base anion exchange resin, cost benefit analysis

1. Introduction

Water usage in textile industry and importance of water recycling:

There are many sources of water, the most common being: Surface sources, such as rivers, Deep wells and shallow wells, Municipal or public water systems, Reclaimed waste streams. (Smith and Rucker, 1987) The textile industry in India has been pioneer industry. Indian textile industry is the 2nd largest in the world. Overall India is world's 8th largest economy and among the 10 industrialized countries (Patel, 2004). If global break up of fresh water is seen then from 100 % of freshwater, 20 % is being used by the industries which are responsible for large production of effluents (Himesh, 2001). The rapid growth in population and particularly in urbanization has resulted in sharp increase in generation of these two wastes. In India alone 19000 million liters of sewage is generated every day of which more than 25% is attributed to class I cities. Out of this quantity of sewage 13000 million liters per day (MLD) is collected out of which at the most half is treated to some extent. In terms of nutrients and water availability, economic value of this quantity of domestic sewage has been estimated as Rs. One crore per day. As regards industrial wastewater generation, the same is estimated 10000 MLD, 40% is from small scale industries (Patankar, 2006). Wastewater reclamation and reuse is one element of water resources development and management which provides an innovative and alternative option for agriculture, municipalities and industries (Al-Sulaimi and Asano, 2000). The availability of alternative water sources such as reclaimed municipal waste water or recycled process water can foster more efficient water use practices that translate in to significant cost savings in industries (Tchobanoglous, 1998).

2. Materials and Methods

Pilot treatment plant was prepared and treatment was given to treated municipal wastewater. Units in recycling plant comprises Municipal treated water storage tank, Oil & Grease removal unit, Slow Sand filter (SSF), Granular Activated Carbon filter (GAC), Chlorination unit Cationic Exchange Resin (SAC) and Anionic Exchange Resin (SBA).

Details of Pilot treatment plant:

1. Municipal treated water storage tank: To store the treated wastewater for further treatments. Also acts as a sedimentation tank.

2. Oil & Grease removal unit: Oil & Grease can be removed with this unit .

3. Slow Sand filter (SSF): Slow sand filter is provided with various layers of sand of different particle size.

4. Granular Activated Carbon filter (GAC): Through this the color and odor from the wastewater is removed.

5. Chlorination unit: This is carried out to disinfect the sewage. For this sodium hypochlorite solution (22 gpl) with various dosages was used.

6. Cationic Exchange Resin (SAC): Here cations like Na^{+} Mg^{++}, Ca^{++} etc was exchanged with H^{+} ions. The cationic exchange resin used was strong acid type. It is a premium quality strong acid cation exchange resin containing nuclear sulphonic acid groups having high exchange capacity, combined with excellent physical and chemical stability and operating characteristics. It

is ideally suited for use in a wide range of pH and temperature conditions. It is supplied in hydrogen form for two stages and mixed bed demineralization and in sodium form for softening. It is also used for de-alkalization and chemical processing.

7. Anionic Exchange Resin (SBA): Here anions like $S04^{--}$, $CO3^{--}$, Cl^{-} etc was exchanged with OH^{-} ions. The anionic exchange rein used was strong base type. It is a strong base anion exchange resin based on polystyrene matrix, containing quaternary Ammonium group. It has excellent chemical and operating characteristics along with excellent physical properties due to its crack-free nature. It has a good operating capacity for weak acids like silicic and carbonic along with strong mineral acids, when used in water treatment along with strong acid cation exchange resin. It is ideally suited for use in a wide range of pH and temperatures. It is supplied as moist spherical bead in the chloride form with a particle size distribution to provide good kinetics and minimum pressure drop. Figure 2.1 shows Pilot treatment plant.

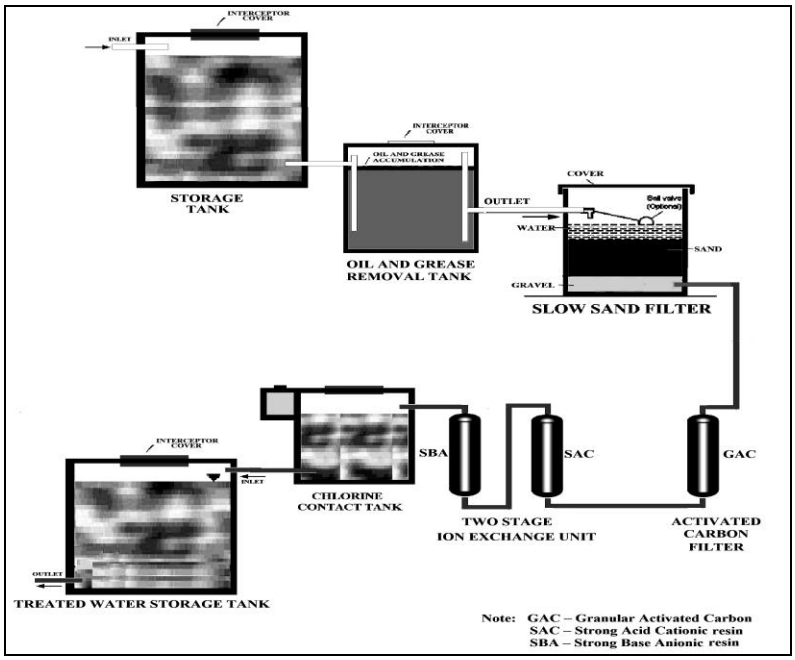

Figure 2.1 Pilot Treatment Plant

Figure 2.2 Photograph of Pilot Treatment Plant

3. Treatment Of Wastewater:

Wastewater was treated to fulfil the requirements of cotton textile wet processing. Following norms were target to treat the wastewater. Shown in table 3.1

Table 3.1 Targeted values of various parameters

Sr. No.	Parameter	Expected treatment quality
1	Total Dissolved Solids (TDS)	400 mg/l
2	Hardness	Less than 70 mg/l
3	Oil and Grease	Less than 1 mg/l
4	Most Probable Number (MPN)/100 ml	Nil
5	Colour	Nil
6	Odour	Nil

3.1 Testing and analysis of wastewater using pilot treatment plant:

Details of TDS, Hardness and oil and Grease inlet and outlet of plant are shown in table 3.2, 3.3 and 3.4

Table 3.2 Total Dissolved Solids (TDS)

Sr. No.	Day	Inlet (mg/l)	Outlet (mg/l)
1	1	930	412
2	2	911	421
3	3	845	423
4	4	865	457
5	5	765	402
6	6	865	438
7	7	852	423

Table 3.3 Hardness

Sr. No.	Day	Inlet (mg/l)	Outlet (mg/l)
1	1	427	31
2	2	413	31
3	3	392	24
4	4	342	24
5	5	368	15
6	6	425	22
7	7	433	18

Table 3.4 Oil and Grease

Sr. No.	Day	Inlet (mg/l)	Outlet (mg/l)
1	1	12	0
2	2	25	0
3	3	25	0
4	4	24	0
5	5	18	0
6	6	31	0
7	7	23	0

3.2 Chlorination:

Optimum chlorine dosage was found with various trials of NaOCl. Following table shows various dosages and corresponding Most probable number (MPN/100 ml). Chlorine contact time was kept 30 minutes. Residual chlorine was measured for every dosage found between 0.2 to 0.3 mg/l.

4. Cost-Benefit analysis of the plant:

Hardness of wastewater = 450 mg/l as $CaCo_3$

Calculation of major costs on maintenance of Cationic Exchange Resin (SAC), Anionic Exchange Resin (SBA) and Chlorination unit is carried out as under.

4.1 Cationic Exchange Resin (SAC):

Total treatment capacity of resin = 1.8 to1.2 meq/ml
Considering 60% operating capacity of resin,
Operating capacity of resin used = 1.08 meq/ml = 1080 meq/l
Hardness concentration of wastewater can worked out in meq/l by using formula weight of $CaCo_3$
1 ppm as $CaCo_3$ = 0.02 meq/l or
One equivalent of calcium carbonate = (40 + 12 +3*16) / 2 = 50 mg /eq = 50 mg/ meq
Hardness concentration in meq/l = 450/ 50 = 9 meq/l
Quantity of water treated by one liter resin = 1080/9 = 120 liters.
Regeneration with 60 gm HCL /liter of resin = 120 liters of water.
HCL / liter = 60/ 120 = 0.5 gm/liter
Commercial rate of HCL Rs. 5/- per kg
Cost per liter = 5/1000*0.5 = Rs. 0.0025 / liter of water

4.2 Strong base anion exchange resin (SBA):

Total treatment capacity of resin = 1.3 meq/ml
Considering 60% operating capacity of resin,
Operating capacity of resin used = 0.78 meq/ml = 780 meq/l
Quantity of water treated with one liter resin = 780/9 = 86.67 liter
Regenerating with NaOH and considering 30gms NaOH / liter
Quantity of NaOH/liter = 30/86.67 = 0.346 gm/liter
Commercial cost of NaOH = Rs. 40/- per kg.
Cost per liter = 40/1000*0.346 = Rs. 0.01384 /liter of water

4.3 Chlorine treatment:

Chlorination charges can be worked out as below,
Commercial cost of Chlorine = Rs. 10/- per kg = Rs. 10/1000 gms
Dosages of Chlorine = 1 ppm per liter of water
Cost of chlorination = 10/1000*0.0001 = Rs. 0.00001 / liter of water
Water to be treated 18 MLD = 18000 m^3/day = 900 m^3/hour
Plant working hours = 20 Hours/day

4.4 Electricity charges:

Gravity and continuous flow plant, Feed flow pump 150 HP, anion cation plant pumps (2 nos.) of 75 HP and considering other electricity charges of the plant = 50 HP
Total electricity consumption = 350 HP
Rs. 5/- Kwh * 0.746 Kwh/hp * 350 * 20 hrs/day = Rs . 26110 = 00
Amp. Drawn 0.75 %. Therefore Cost/day = Rs. 26110 * 0.75 = Rs. 19582.50
Cost per liter = Rs. 19582.50 / 18000000 = Rs. 0.001088/ liter of water

4.5 Maintenance charges of plant:

Maintenance charges for pumps in plant, blowers in degasifiers & other charges. Considering Rs. 500/day.
Cost per liter of water = Rs. 500 / 180000000 = Rs. 0.00002778/ liter of water

4.6 Depreciation costs:

Continuous Automation Control by Instrumentation, Regeneration - flow 0.5 Hrs/Hr each 2 sets of Anion + Cation beds. Sand + Carbon Filters of Capacity of 15 m^3 each, chlorinator- one, Oil-grease Removing Tanks- 2 Nos, Centrifugal Pumps -0=250, 125 liters/sec. Initial cost of plant can be estimated as Rs.40000000/-
Calculating depreciation Rs. 40000000/ (5*365) = Rs. 21917.80 /day
Depreciation cost /liter = Rs. 21917.80 /180000000= Rs. 0.001218/liter

4.7 Staff salaries:

Workers Rs. 150/ day, plant supervisor Rs.250/day, Manager = Rs. 350/ day
Total salary Rs. 1500/ day
Cost of salary worked out per liter of water = Rs. 1500/ 180000000 = Rs. 0.0000833 /liter

4.8 Miscellaneous charges:

Office stationary, testing, printing charges etc. considering Rs. 100/ day

Cost per liter = Rs. 100/ 180000000 = Rs. 0.0000055/liter of water

4.9 Cost-benefit considerations:

Total cost of water per liter can be worked out by addition of all above parameters,

Overall cost = Rs. 0.0025 + Rs. 0.01384 + Rs. 0.00001 + Rs. 0.001088 + Rs. 0.00002778 +

Rs. 0.001218 + Rs. 0.0000833 + Rs. 0.0000055 = 0.01877258/liter of water

Overall cost = 18.77 per 1000 liter of water with TDS less than 400 mg/liter.

With profit overall sale cost of water = Rs. 20.00 per 1000 liter of water

This water cost can be reduced if we get income by selling Oil & Grease & Value added Products which are manufactured from drained TDS of recycling plant. At present Textile industry is purchasing water at Rs. 22 to 25 per 1000 liter of water with TDS more than 1200 mg/liter.

Profit per 1000 liter (1 m^3) = Rs.20.00 – Rs.18.77 = Rs. 1.23

Daily profit = 18000 m^3 * 1.23 = Rs. 22140/-

Annual profit = Rs. 22140 * 365 days = Rs. 80, 81,100/-

5. Conclusion:

Recycled wastewater is having many benefits. This benefit analysis can be carried out as economical benefits and societal benefits.

1. Quality of fabric will enhanced with recycled water .At present textile industries are purchasing water of TDS 900 to 1200 mg/l which leads fabric production with less quality.
2. Textile industry facing strong water crisis. These industries are purchasing water at higher cost. Such water recycling projects may give economical solution to the industries.
3. Disposing wastewater on land or any water body may cause harmful environmental effects. The treated wastewater which would have been wasted can be utilized with effective and economical technology.
4. Improvement in fabric rewashing system so that there is economy in water usage in textile industry.
5. There is dye saving in wet processing which is additional benefit to industry.
6. K/s values of dyed fabric found significantly improved.
7. Washing and rubbing fatness of fabric observed with both ISO-105 and AATCC methods are satisfactory.

References:

[1] Asano, T. , Reclaimed wastewater as a water resource proceeding of the workshop on wastewater reclamation and reuse, Editor Asano, T. and Al-Sulaimi, J. Arab school of science and technology. 1-20, 2000.

[2] Himesh, S., "Ground water pollution", Volume 80, N0.11, Current Science, India, 2001.

[3] Patankar S.N., National workshop on Dream of green city at Pune, India. City sewerage and solid waste management, 1-8, 2006.

[4] Patel, B., Indian Textile Industry Database-2004, Komal Publications, North Gujarat, India, 1-4, 2004.

[5] Smith, B., Rucker, J., Water and Textile Wet Processing-Part I, American Dyestuff Reporter, 15-23, 1987.

[6] Tchobanoglous, G., and Burton F.L. , Metcalf and Eddy Inc. "Waste water disposal – Treatment, Disposal and Reuse" Tata McGraw-Hill Edition, New York, 1137,740, 314,1998.

[7] http://users.tinyonline.co.uk/chrisshort/waterhard.htm

[8] http://dardel.info/IX/capacity.html

[9] http://www.lenntech.com/calculators/exchange/ion-exchange.htm

[10] Peavy S.H., Rowe D.R. and Tchobanoglous, G., Environmental Engineering, McGraw Hill International Editions, Singapore 24-25,1985.

A Novel Approach to Improve Detection Rate and Search Efficiency of NIDS

Prof. (Mrs) Manisha R. Patil[1], Mrs. Madhuri D. Patil[2]

[1] Professor, Department of Computer Engineering, Smt. Kashibai Navale College of Engineering, Pune, India
[2] Student, Department of Computer Engineering, Smt. Kashibai Navale College of Engineering, Pune, India

Abstract

Signature based Network Intrusion Detection System (NIDS) applies a set of rules to identify the traffic and classify known attacks by comparing with the signature. As the detection rate and speed of searching for signature in NIDS have two main aspects, this paper gives data mining approve to improve on detection rate and we use an algorithm to use the known signature to find the signature of the related attack quickly.

Keywords: Classification, Signature Based NIDS, Association Rule Mining, Data Mining, Apriori Algorithm, Network Intrusion Detection.

1. INTRODUCTION

Information is an important asset in an organization which has large amount of personal and critical data with it. Protecting that information from attacks should be the main goal when security is concerned. Intrusion Detection System (IDS) are software or tools that monitor events that take place in a computer or a network, looking for evidence of intrusion [1] .The process of monitoring the events occurring in a computer system or network and analyzing them for sign of intrusions is known as Intrusion Detection System (IDS) [3]. Network Intrusion Detection Systems just analyze the traffic on network and sets alarm for the attack detection, there are two type of NIDS that are anomaly based NIDS and Signature base NIDS. Anomaly based NIDS tries to determine whether deviation from the established normal usage patterns can be flagged as intrusion The normal usage patterns are constructed from the statistical measures of the system features, for example, the CPU and I/O activities by a particular user or program[3]. The behavior of the user is observed and any deviation from the constructed normal behavior is detected as intrusion and signature based NIDS tries to flag intrusion by comparing signatures of attacks with the incoming packets on network [2]. There are two advantages of signature based NIDS. The first is it detects attack without generating overwhelming number of false alarms. The second is that it can quickly diagnose the use of specific attack tool [2] and on other side disadvantage of signature based NIDS is it can only detect known attacks. But in most of the networks signature based NIDS are preferred. The main two problems with signature based NIDS are its detection rate and signature search is time consuming and error prone work. To solve first problem till now data mining is used with GP (genetic programming) to improve on detection rate, in this paper we are going to propose purely a data mining concept to improve on detection rate and second problem was solved until Signature Apriori [5] was proposed. But the signature Apriori waste much time for generate the unnecessary candidate item sets and scan the database .If the size of database is large, the Signature Apriori will be not effective in the signature search . In this system, we used Modified Signature Apriori algorithm to search for the attack quickly.

2. Classification Algorithm

In NIDS the attacks are detected same way as how the classification works. In order to classify the network attacks, we used a well classification algorithm that is C4.5 which is one of old and comparatively good algorithm. Dataset input to C4.5 algorithm is KDD99 which contains attack records with 41 attributes for each connection record plus one class label. The raw data was processed into connection records, which consist of about five million connection records [6] [7]. C4.5 finds the gain ratio of the attributes and uses an attribute for classification whose gain ration is highest. Gain ratio is calculated as (1)

$$\text{SplitInfo}_A(D) = -\sum_{j=1}^{v} \frac{|D_j|}{|D|} \times \log_2\left(\frac{|D_j|}{|D|}\right) \qquad (1)$$

This value represents the potential information generated by splitting the training data set, D, into v partitions, corresponding to the v outcomes of a test on attribute A. Note that, for each outcome, it considers the number of records having that outcome with respect to the total number of records in D. It differs from information gain, which measures the information with respect to classification that is acquired based on the same partitioning. The gain ratio is defined as: The expected information needed to classify a record in D is given by

$$Info(D) = -\sum_{i=1}^{m} pi \log_2(p_i) \qquad (2)$$

Where pi is the probability that an arbitrary record in D belongs to class Ci and is estimated by $|C_{i,D}|/|D|$.

A log function to the base 2 is used, because the information is encoded in bits. Info(D) is just the average amount of information needed to identify the class label of a tuple in D. Note that, at this point, the information we have is based solely on the proportions of tuples of each class. Info(D) is also known as the entropy of D.

$$\text{InfoA(D)} = \sum_{j=1}^{v} \frac{|D_j|}{|D|} \times \text{Info}(D_j) \qquad (3)$$

$$\text{Gain (A)} = \text{Info(D)} - \text{Info}_A\text{(D)} \qquad (4)$$

$$\text{GainRatio (A)} = \frac{\text{Gain(A)}}{\text{SplitInfo(A)}} \qquad (5)$$

In this way the detection of attacks is done and these attacks are represented as decision tree.

3. Ensemble Algorithm

The decision tree is given as text file to the ensemble algorithm. The Adaboost algorithm is one of the good ensemble algorithm but there are two drawbacks with this algorithm. (1) AdaBoost cannot be used in the boosting by filtering framework, and (2) AdaBoost does not seem to be noise resistant. In order to solve them, there is a new boosting algorithm MadaBoost by modifying the weighting system of AdaBoost [5]. So the ensemble algorithm used in this system is Mdaboost. This algorithm improves the accuracy of the classification of attack records and with this improvement in classification will automatically improve the detection rate of NIDS.

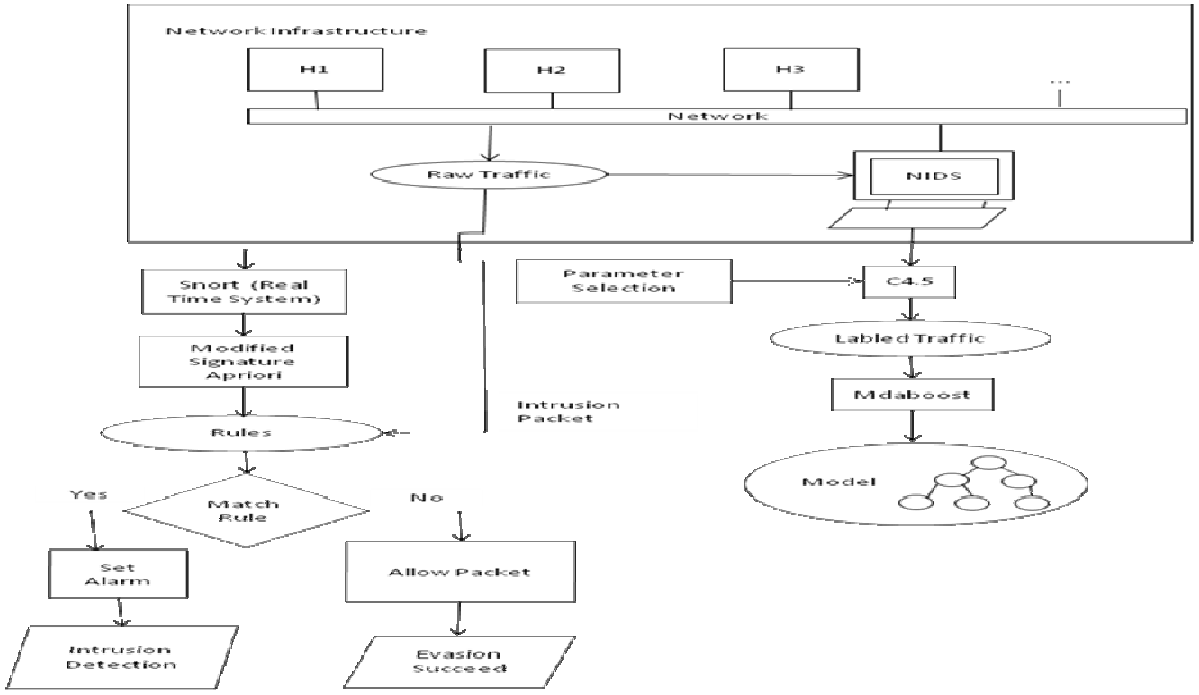

4. Signature Apriori Algorithm

The concept of Signature Apriori is based on Apriori algorithm [8]. The Apriori algorithm is an algorithm for mining frequent itemsets. This algorithm uses the prior knowledge of frequent itemset properties. Apriori employs an iterative approach, where k-itemsets are used to explore (k+1)-itemsets. First, the set of frequent 1-itemsets is found.

This set is denoted as L1. L1 is used to find L2, the frequent 2-itemsets, which is used to find L3 and so on, until no more frequent k- itemsets can be found. The finding of each LK requires one full scan of the database.

5. Modified Signature Apriori Algorithm

The steps of how to find out frequent k-item sets will be as follow. At the first step, all of the frequent items will be found. And then we use a simple way to scan the database in order to find the frequency of occurrence of each item, and decide which one meets the minimum support. Secondly, we generate the candidate n-item sets by checking all of the possible combinations of the frequent items with already known signatures, if they meet the minimum support requirement. Then, append this n-itemsets from right. We can first append the backward, until the minimum support is unsatisfied. Then, we append forward, and stop when the same condition occurred. Finally, the maximum length of frequent-item set can be mined by our method. A simple way to find frequent item set is we read one transaction each time from database and then count the support of each different item. If an item occurs twice in the same transaction, the support count of this item will increase once. Repeat until no transactions available in database. Finally, we will check all items in candidate 1-itemset and append the item that meet the minimum support into L1. After all frequent items have been mined; we will stop generating all possible candidate 2-itemsets we generate the candidate itemsets only related the known signatures. Then, all of the frequent items will be concatenated to the known signature and put them into candidate n itemsets. After that, check all item sets in the candidate n-itemset. Then, add the itemsets that meet the minimum support into L1. The improvement in the algorithm is we know that Ci+1 is generated from Li* Li. Clearly, a Ci'generated from Ci * Ci, instead of from Li* Li, will have a greater size than | Ci | where Ci is generated from Li* Li. However, if | Ci'| is not much larger than | Ci |, we may save one round of database scan. This technique is called scan-reduction [9].

Next, we take an example below to show how the proposed algorithm works. We assume that the transactions in the database are {{A B C D E F G Q}, {M N A B C D E F G}, {J A B C D E F G}, {P Q I}}. The attack signature we have already known is {C D E}. Let the minimum support be 0.7. Applying the proposed algorithm, we can firstly get the frequent items L1= {A B C D E F G}. In order to find out the derived attack signature we expanded the known signature by each frequent item, and we then we have Cn= {{C D E A}, {C D E B}, {C D E C}, {C D E D}, {C D E E}, {C D E F}, {C D E G}} at the first stage. After we have Cn candidate itemsets, we scan the database to find out the Ln={C D E F}. Then we let the Ln be the new attack signature that we have already known. Repeating the step until the minimal support is no longer satisfied. We win get the Ln = {C D E F G} in this example. Next, we expand the Ln in the inversed direction. Finally, we will get the possibility attack signature Ln = {A B C D E F G} [2].

REFERENCES

[1] R. Bace and P. Mell, "NIST Special Publication on Intrusion Detection Systems", 800-31, 2001

[2] Yang,X.R.,Song,Q.B.and Shen, J.Y,"Implementation Of Sequence Patterns Mining In Network Intrusion Detection System", in Proceeding of ICII,2001. Pp.323- 326.

[3] Hu Zhengbing,Li Zhitang, "A Novel Network Intrusion Detection System(NIDS) Based on Signatures Search of Data Mining",10-16,2008

[4] S. Peddabachigari, A. Ajith, C. Grosan, and J. Thomas, "Modeling intrusion detection system using hybrid intelligent systems," Journal in Network Computer Applications, vol. 30, no. 1, pp. 114-132, 2007.

[5] Carlos Domingo, Osamu Watanabe "MadaBoost: A Modification of AdaBoost" Thirteenth Annual Conference on Computational Learning Theory Pages: 180-189 Year of Publication: 2000 ISBN:1-55860-703-X

[6] Han, H., Lu, Lu, X.L., and Ren, L.Y.,"Using Data Mining to Discover Signatures in Network-Based intrusion detection", in Proceeding of IEEE Computer Graphics and Applications,2002. pp.212-217

[7] MIT Lincoln Laboratory. http://www.ll.mit.edu/IST/ideval/

[8] KDD cup 99 Intrusion detection data set. Web site of the data set is as bellow http://kdd.ics.uci.edu/databases/kddcup99/kddcup.data_10_percent.gz

[9] Rakesh, A., and Srikant, R.,"Fast Algorithm For Mining Association Rules", in Proceeding of the 20th international Conference on VLDB, 1994

[10] Park, J.S., Chen, M.S., and Yu, P.S., "Using a Hash – Based Method With Transaction Trimming For Mining Association Rules", Knowledge and Data Engineering, IEEE Transaction, 1997

Application of Ellipse for Horizontal Alignment

[1]Farzin Maniei, Siamak Ardekani[2]

[1]Department of civil Engineering, The University of Texas at Arlington, Box 19308, Arlington,
[2]Department of civil Engineering, The University of Texas at Arlington, Box 19308, Arlington,

Abstract:

In highway design, horizontal curves provide directional transition for roadways. Three categories of horizontal curves are simple circular curves, compound circular curves, and spiral circular curves. Compound and spiral curves, as alternatives to a simple circular curve, are often more costly since they are longer in length and require additional right-of-way; with cost differences amplified at higher design speeds. This study presents calculations associated with using a single elliptical arc in lieu of compound or spiral curves in situations where the use of simple circular curves is not prudent due to driver safety and comfort considerations. The study presents an approach to analytically determine the most suitable substitute elliptical curve for a given design speed and intersection angle. Computational algorithms are also provided to stakeout the elliptical curve. These include algorithms to determine the best fit elliptical arc with the minimum arc length and minimum right-of-way; and algorithms to compute chord lengths and deflection angles and the associated station numbers for points along the elliptical curve. These algorithms are applied to an example problem in which elliptical results are compared to the equivalent circular curve and spiral-circular curve results.

Keywords: Horizontal alignment, elliptical curve, circular curve, spiral curve

I. Introduction

In highway design, a change in the direction of the roadway is achieved by a circular or a compound circular curve connecting the two straight sections of the roadway known as tangents. A common horizontal alignment treatment is a compound curve. It consists of a circular curve and two transition curves, one at each end of the circular curve. The transition curves are either circles of larger radii or spiral curves. In some cases no transition curves are needed when the design speeds or degrees of curvature are fairly low. In such cases, the horizontal alignment could be a single circular curve.

The most important factor in designing horizontal curves is the design speed. When a vehicle negotiates a horizontal curve, it experiences a lateral force known as the centrifugal force. This force, which is due to the change in the direction of the velocity vector, pushes the vehicle outward from the center of curvature. The vehicle is also subjected to an inward radial force, the centripetal force. In fact, the centripetal force is always directed orthogonal to the velocity vector, towards the instantaneous center of curvature. At high speeds, the centripetal force acting inward may not be large enough to balance the centrifugal force acting outward. To mitigate this problem, a lateral roadway angle, known as the superelevation angle e(or banking angle) is provided (Garber and Hoel, 2002, p. 70). To keep these forces in balance, the minimum required radius is then given by the following equation:

$$R = \frac{v^2}{g(e + f_{side})}. \qquad (1)$$

Where R is the minimum radius, is the design speed, e is the superelevation angle in radians, f_{side} is the coefficient of side friction, and **g** is the acceleration of gravity.

1.1 Spiral Transitions

On simple circular curves, as the vehicle enters the horizontal curve with a velocity, the centrifugal force jumps from zero on the tangent section to mv^2/R on the curve. A transition curve such as a larger radius circle or a spiral helps moderate this sudden increase in force, thus making the alignment smoother and safer. Spiral is a particularly good transition curve as its radius decreases gradually along its length (the curvature changes linearly in length), from an infinite radius (zero

curvature) at the tangent to spiral to the design radius at the spiral to circular point. The minimum length of spiral recommended by AASHTO for a horizontal curve of radius is given by:

$$l_s = \frac{3.15\,V^3}{R.C} \tag{2}$$

Where

l_s = minimum length of transition spiral (ft)
V = design speed (mph)
R = radius of curvature (ft)
C = rate of change of centripetal acceleration (ft/sec^3).

The use of transition curves such as the spiral, although yielding smoother alignments, often results in longer roadway lengths and greater right-of-way requirements. In addition the stake-out computations are considerably more involved than using simple circular curves.

II. Approach

2.1 Use of Ellipses as Horizontal Curves

In this section, the application of ellipses as horizontal alignment curves is examined. This includes a general discussion of properties of ellipse followed by a procedure for finding an appropriate elliptical curve that could provide a smooth and safe transition from the PC to PT. The associated chord length and deflection angle calculations for an elliptical arc are also presented.

Geometrically, an ellipse is the set of points in a plane for which the sum of distances from two points F_1 and F_2 is constant (See Figure 2). These two fixed points are called the **foci**. One of the Kepler's laws is that the orbits of the planets in the solar system are ellipses with the sun at one focus.

In order to obtain the simplest equation for an ellipse, we place the foci on the x-axis at points $(-c, 0)$ and $(c, 0)$ so that the origin, which is called the **center** of ellipse, is halfway between F_1 and F_2 (Figure 1). Let the sum of the distances from a point on the ellipse to the foci be $2a > 0$. Let us also suppose that P(x, y) is any point on the ellipse. According to the definition of the ellipse, we will have:

$$|PF_1| + |PF_2| = 2a \tag{3}$$

that is,

$$\sqrt{(x+c)^2 + y^2} + \sqrt{(x-c)^2 + y^2} = 2a\,. \tag{4}$$

Or,

$$(a^2 - c^2)x^2 + a^2y^2 = a^2(a^2 - c^2)\,. \tag{5}$$

In the triangle F_1F_2P (Figure 1), it can be seen that $2c < 2a$, so $c < a$ and therefore $a^2 - c^2 > 0$. For convenience, let $b^2 = a^2 - c^2$. Then the equation of the ellipse becomes

$$b^2x^2 + a^2y^2 = a^2b^2\,. \tag{6}$$

Or by dividing both sides by a^2b^2,

$$\frac{x^2}{a^2} + \frac{y^2}{b^2} = 1\,. \tag{7}$$

Since $b^2 = a^2 - c^2 < a^2$, it follows that $b < a$. The x-intercepts are found by setting $y = 0$. Then $x^2/a^2 = 1$, or $x^2 = a^2$, so $x = \pm a$. The corresponding points $(a, 0)$ and $(-a, 0)$ are called the **vertices** of the ellipse and the line segment joining the vertices is called the **major axis**. To find the y-intercepts, we set $x = 0$ and obtain $y^2 = b^2$, so $y = \pm b$. Equation 7 is

unchanged if x is replaced by $-x$ or y is replaced by $-y$, so the ellipse is symmetric about both axes. Notice that if the foci coincide, then $c = 0$ and $a = b$ and the ellipse becomes a circle with radius $r = a = b$.

In mathematics, there is a parameter for every conic section called **eccentricity** (Larson et al., 2010, p. 701). Eccentricity defines how much the conic section deviates from being a circle. As a conic section, ellipse has its own eccentricity τ which is calculated as,

$$\tau = \frac{c}{a}, \tag{8}$$

in which:

τ = eccentricity,
a = length of major axis,
$c = \sqrt{a^2 - b^2}$.

In most mathematics literature, the eccentricity is denoted by **e** or $\boldsymbol{\varepsilon}$. In this text, we use τ to denote the eccentricity in order to avoid confusion with the superelevation angle, e.

2.2 Circular Curve, Design Speed, and Superelevation

As discussed earlier, the relation between the radius of the circular curve, the design speed, and the superelevation is governed by Eq. 1. Therefore, the desired elliptical curve should as a minimum satisfy the minimum radius required by AASHTO, as per Eq. 1. This establishes one of the constraints for finding an appropriate elliptical curve. Before considering this and other constraints, however, we should determine what constitutes a "radius" for an ellipse. To achieve this, we would utilize the polar coordinate system.

In the polar coordinate system, there are two common equations to describe an ellipse depending on where the origin of the polar coordinates is assumed to be. If, as shown in Figure 2, the origin is placed at the center of the ellipse and the angular coordinate θ is measured from the major axis, then the ellipse's equation will be:

$$r(\theta) = \frac{ab}{\sqrt{\left(b\cos(\theta)\right)^2 + (a\ \sin(\theta))^2}}. \tag{9}$$

On the other hand, if the origin of polar coordinates is located at a focus (Figure 3) and the angular coordinate θ is still measured from the major axis, then the ellipse's equation will be:

$$r(\theta) = \frac{a(1-\tau^2)}{1 \pm \tau\cos(\theta)} \tag{10}$$

Where the sign in the denominator is negative if the reference direction is from $\theta = 0$ towards the center.

From the astronomical point of view, Kepler's laws established that the orbits of planets in a solar system are ellipses with a sun at one focus. Thus, the ellipse's polar Eq. 10, in which the origin of the polar coordinates is assumed at one focus, will be helpful to obtain the desired elliptical arc.

Figure 3 shows that the minimum radius of the desired ellipse with respect to the focus F_2 is $a - c$. Since $= a\tau$, then we have: $a - c = a(1 - \tau)$. On the other hand, the minimum radius should not be smaller than the minimum radius R_{min} recommended by AASHTO (Eq. 1). Thus, we have:

$$a(1-\tau) \geq R_{min}\ . \tag{11}$$

Since we are looking for an elliptical curve to connect the PC to PT, it would be an arc of an ellipse that satisfies the equality below as a constraint:

$$a(1-\tau) = \mathrm{R}_{\min} \ . \tag{12}$$

Therefore, we should first find an appropriate ellipse and then identify the desired arc to be used as a highway curve. In our design problem, as in most highway horizontal alignment problems, the known parameters are the location of PI, the angle , and the design speed, V_d. Based on the known design speed, we can determine a value for R_{min} . With R_{min} known,

we now need to identify an equivalent elliptical arc. In Eq. 12, we have two unknown variables (a and τ) relating to the ellipse. Using numeric methods, we can find all pairs of (a, τ) which satisfy our constraint by inserting acceptable values for τ and solving the equation for a. The eccentricity of ellipse, τ ranges from 0 to 1. To make a finite set of values for τ, we should consider only one or two decimal points depending on the level of accuracy required.

By having the major axis a and the eccentricity τ, the equivalent ellipse can be easily identified as,

$$b = a\sqrt{1-\tau^2}. \tag{13}$$

Other than the minimum radius requirement, another design constraint requires that the arc of the ellipse be tangent to the lines connecting the PI to the PT and the PC. A third constraint is an aesthetic consideration. According to AASHTO, symmetric designs enhance the aesthetics of highway curves. Therefore, a symmetric arc of the ellipse is desirable to meet the aesthetics requirement. Note that since the desired arc should be symmetrical and be of minimum possible length, the arc must be symmetric with respect to the ellipse's major axis (and not the minor axis).

Let us assume a hypothetical ellipse in the Cartesian coordinate system with the center at the origin and the focus on the y-axis (Fig. 4). Suppose that the desired arc is the smallest arc between points A = PT = (x_1, y_1) and B = PC = (x_2, y_2). Since the arc is symmetric with respect to the major axis, we have $x_1 = -x_2$, and $y_1 = y_2$.

Let us also assume that the slope of the tangent line at points and are m_1 and m_2, respectively. So, $m_1 = -m_2$.

As shown in Figure 4, the long chord for the desired arc of the ellipse and the tangent lines form an isosceles triangle. Therefore,

$$m_1 = \tan\left(180 - \frac{\Delta}{2}\right), \tag{14}$$

and

$$m_2 = -\tan\left(180 - \frac{\Delta}{2}\right). \tag{15}$$

On the other hand, the equation of the ellipse in the Cartesian coordinate system is:

$$\frac{x^2}{b^2} + \frac{y^2}{a^2} = 1. \tag{16}$$

By taking the derivative of Eq. 16, the slope of the tangent line at any point on the ellipse is obtained, namely,

$$\frac{dy}{dx} = \frac{-a^2 x}{b^2 y}. \tag{17}$$

Eq. 17 can be re-written as:

$$y = \pm\frac{a}{b}\sqrt{b^2 - x^2}\ . \tag{18}$$

By combining Eqs.17 and 18, we obtain:

$$\frac{dy}{dx} = \frac{-ax}{b\sqrt{b^2 - x^2}}. \tag{19}$$

Therefore,

$$m_1 = \frac{-ax_1}{b\sqrt{b^2 - {x_1}^2}}, \tag{20}$$

and

$$x_1 = \frac{m_1 . b^2}{\sqrt{a^2 + {m_1}^2 . b^2}}, \tag{21}$$

$$y_1 = \frac{a}{b}\sqrt{b^2 - x_1^2}\,. \tag{22}$$

By the same token, the location of point $B = (x_2, y_2)$ is determined to be:

$$x_2 = -x_1 = \frac{-m_1.b^2}{\sqrt{a^2 + {m_1}^2.b^2}} \tag{23}$$

and

$$y_2 = y_1. \tag{24}$$

Consequently, any desired arc of the ellipse can be found by having the slope (direction) of the tangent lines and the intersection angle between them.

2.3 Length of the Arc of an Ellipse

To minimize the right-of-way, a minimum-length arc is desired that meets all three constraints discussed earlier. In the previous section, a method was introduced to identify an arc that only satisfies the tangent lines constraint. After this, the resulting arc should be checked to ensure it is the minimum-length arc.

To find the length of an ellipse arc, the polar coordinate system is again useful. The length of an ellipse arc between 0 and θ can be found from the following integration (Larson et al., 2010, p. 704):

$$E(\theta, \tau) = a\int_0^{\theta} \sqrt{1 - (\tau)^2 sin^2 t}\;\; dt \tag{25}$$

in which,

a: is the length of the major axis of the ellipse;
τ: is the eccentricity of the ellipse; and
$E(\theta, \tau)$: is the length of the arc of an ellipse with eccentricity of τ, between 0 and θ.

To be able to use this integration, we need to know the coordinates of points A and B in the polar coordinate system. Since $A = (x_1, y_1)$ and $B = (x_2, y_2)$, the polar coordinates of points A and B can be obtained to be:

$$\theta_1 = \tan^{-1}\left(\frac{y_1}{x_1}\right),\; r_1 = \sqrt{x_1^2 + y_1^2}\;; \tag{26}$$

and

$$\theta_2 = \tan^{-1}\left(\frac{y_2}{x_2}\right),\; r_2 = \sqrt{x_2^2 + y_2^2}\,. \tag{27}$$

Now, let us define the length of the arc as:

$$l_{a,\tau}(\theta_1, \theta_2) = E(\theta_2, \tau) - E(\theta_1, \tau) \tag{28}$$

in which,

θ_1 = the angle at which the ellipse arc starts;
θ_2 = the angle at which the ellipse arc ends; and
$l_{a,\tau}(\theta_1, \theta_2)$ = is the length of the arc starting at angle θ_1 and ending at θ_2 on an ellipse with major axis a and the eccentricity of τ.

2.4 Area of an Elliptical Sector and the Right-Of-Way

As discussed earlier, there are two ellipse sectors commonly used. One is defined with respect to the center of the ellipse and the other with respect to a focus. The ellipse's equation with respect to the focus is used here to calculate the area of the sector (Figure 5), as follows:

$$A_{E,\tau}(\theta_1, \theta_2) = \int_{\theta_1}^{\theta_2} \frac{1}{2} r^2(\theta)\;\; d\theta \;=\; \int_{\theta_1}^{\theta_2} \frac{a^2(1-\tau^2)^2}{2[1 \pm \tau\cos\theta]^2}\;\; d\theta\,. \tag{29}$$

Let us assume that the right-of-way width is 100 ft., 50 ft. on each side of the centerline. In Figure 6, the shaded strip shows the right-of-way associated with an elliptical arc. The right-of-way can be accordingly calculated as:

$$ROW = \int_{\theta_1}^{\theta_2} \frac{1}{2}(r(\theta)+50)^2 d\theta \; - \int_{\theta_1}^{\theta_2} \frac{1}{2}(r(\theta)-50)^2 d\theta \,. \tag{30}$$

2.5 Chord Length and Deflection Angle Calculations

Assuming that the desired arc of an ellipse connecting the PC to PT is identified, the next step is the calculation of the chord lengths and deflection angles. In Figure 7, the chord length l_c and the deflection angle δ are schematically shown. Using the polar equation with respect to the center of the ellipse, we know that:

$$r(\theta) = \frac{ab}{\sqrt{(b\cos\theta)^2 + (a\sin\theta)^2}} \,. \tag{31}$$

As shown in Figure 7, OB, BD, and DO form the triangle OBD. The length of OB and DO can be calculated by inserting θ_1 and θ_2 in the polar equation of the ellipse. Let us suppose that the deflection angles need to be calculated in decrement of α from θ_2 to θ_1. Therefore, the angle between OB and DO is α, as shown in Figure 7. Thus, the length of chord l_c can be obtained by applying the law of cosines:

$$l_c^2 = r(\theta_2)^2 + r(\theta_1)^2 - 2\, r(\theta_2)\, r(\theta_1)\, \cos(\alpha), \tag{32}$$

Now, we need to find the deflection angle, δ. According to the law of sines, in the triangle OBD we have:

$$\frac{\sin(\gamma)}{r(\theta_2)} = \frac{\sin(\alpha)}{l_c} \,. \tag{33}$$

Then:

$$\gamma = \sin^{-1}\left(\frac{r(\theta_2)\sin(\alpha)}{l_c}\right) \tag{34}$$

In Figure 7, we also have:

$$\varphi = 180° - \theta_1 \tag{35}$$

On the other hand, in the triangle BDE:

$$\begin{aligned} \beta &= 180° - \gamma - \varphi \\ &= 180° - \gamma - (180° - \theta_1) = \theta_1 - \gamma \,. \end{aligned} \tag{36}$$

Then,

$$\delta = B_1 - \beta = \frac{\Delta}{2} - (\theta_1 - \gamma) = \frac{\Delta}{2} - \theta_1 + \gamma. \tag{37}$$

2.6 Station Number Calculations for PC and PT

Referring to Figure 7, the locations of points A (PT) and B (PC) are known. Based on definition, the intersection of the tangent lines at points A and B will be the location of the PI. The equations of tangent lines are:

$$\text{Tangent Line at A: } y = y_1 + m_1(x - x_1), \tag{38}$$

and

$$\text{Tangent Line at B: } y = y_2 + m_2(x - x_2) \,. \tag{39}$$

By solving Eqs.38 and 39 simultaneously, the location of the PI can be determined.
Note that x_1, x_2, y_1, y_2, m_1, and m_2 are all known.

Then:

$$x^* = \frac{y_1 - y_2 + m_1 x_1 - m_2 x_2}{m_1 - m_2} \tag{40}$$

And since $m_1 = -m_2$:

$$x^* = \frac{y_1 - y_2 + m_1(x_1 + x_2)}{2m_1} \,, \tag{41}$$

and

$$y^* = y_1 + m_1(x^* - x_1). \tag{42}$$

Therefore, the length of tangent T is:

$$T = \sqrt{(y^* - y_1)^2 + (x^* - x_1)^2}\,. \tag{43}$$

Given the tangent length T above, the length of the elliptical arc $l_{a\,elp}$ can be calculated as:

$$\begin{aligned} l_{a\,elp} &= E(\theta_2, \tau) - E(\theta_1, \tau) \\ &= a\left(\int_0^{\theta_2} \sqrt{1 - (\tau)^2 sin^2 t}\;\; dt \;- \int_0^{\theta_1} \sqrt{1 - (\tau)^2 sin^2 t}\;\; dt\right). \end{aligned} \tag{44}$$

Therefore, the stations numbers for the PC and the PT can be determined to be:

$$Sta.@\,\mathbf{PC} = \; Sta.@\,\mathbf{PI} - \mathbf{T} \tag{45}$$

and

$$Sta.@\,\mathbf{PT} = \; Sta.@\,\mathbf{PC} + \; \boldsymbol{l_{a_{elp}}}. \tag{46}$$

2.7 Finding the Minimum Arc of Ellipse from the PC to PT

As discussed earlier, the angle Δ, the design speed design, V_d , and the location of the PI are typically known. Given that, the following steps could then be followed to find the desired arc of ellipse connecting the PC to the PT:

Algorithm (A)

0. Angle Δ, design speed V_d, and location of PI are given.
1. According to the design speed V_d , the value of R_{min} for V_d is known.
2. Start with eccentricity τ of 0.1.
3. Find the major axis a by inserting the value of τ into
$$a = \frac{R_{min}}{1 - \tau}. \tag{47}$$
4. Calculate the minor axis b:
$$b = a\sqrt{1 - \tau^2}\,. \tag{48}$$
5. Find the slope of the tangent line at point A, m_1:
$$m_1 = \tan\left(180 - \frac{\Delta}{2}\right) \tag{49}$$
6. Find the slope of the tangent line at point B, m_2:
$$m_2 = -m_1. \tag{50}$$
7. Find the x-coordinate of point A, x_1:
$$x_1 = \frac{m_1\, b^2}{\sqrt{a^2 + m_1^{\,2}\, b^2}} \tag{51}$$
8. Find the y-coordinate of point A, y_1:
$$y_1 = \frac{a}{b}\sqrt{b^2 - x_1^2}\,. \tag{52}$$

9. Determine $\theta_1 = \tan^{-1}\left(\frac{y_1}{x_1}\right)$.
10. Determine $\theta_2 = \tan^{-1}\left(\frac{y_2}{x_2}\right)$.
11. Calculate the length of the elliptical arc,

$$l_{a,\tau}(\theta_1, \theta_2) = E(\theta_2, \tau) - E(\theta_1, \tau) \tag{53}$$

in which

$$E(\theta, \tau) = a\int_0^{\theta} \sqrt{1 - (\tau)^2 sin^2 t}\ \ dt \tag{54}$$

12. Calculate the area of the piece of ellipse, $A_{E,\tau}(\theta_1, \theta_2)$:

$$A_{E,\tau}(\theta_1, \theta_2) = \frac{1}{2}\int_{\theta_1}^{\theta_2} \left[\left(\frac{a(1-\tau^2)}{1 \pm \tau\cos(\theta)} + 50\right)^2 - \left(\frac{a(1-\tau^2)}{1 \pm \tau\cos(\theta)} - 50\right)^2\right].d\theta. \tag{55}$$

13. Repeat the preceding steps for a new eccentricity τ with increments of 0.1 until the current τ is 0.9.
14. Compare the length of the arc and the area of the piece of ellipse gained for each value of eccentricity τ, and pick the eccentricity τ with the minimum length of arc and area. This is the desired minimum-length elliptical arc to be used.

2.8 Calculating Chords Length and Deflection Angles

After the desired elliptical arc is determined, chord lengths and deflection angles should be calculated in order to stake out the elliptical arc, as follows:

Algorithm (B)

0. θ_1 and θ_2 are obtained in steps 9 and 10 above
1. Degree of curvature is:

$$D = \frac{(\theta_2 - \theta_1) \times 100}{l_{a,\tau}(\theta_1, \theta_2)}. \tag{56}$$

2. If $\frac{(\theta_2 - \theta_1)}{D}$ is an integer, then

$$N = \frac{(\theta_2 - \theta_1)}{D}\ ; \tag{57}$$

else

$$N = \left\lceil \frac{(\theta_2 - \theta_1)}{D} \right\rceil. \tag{58}$$

3. Let $i = 1$.
4. $\alpha = i \times D$
5. Calculate $\theta^* = \theta_2 - \alpha$.
6. Find the length of chord by applying the equation below:

$$(l_c)_i = \sqrt{r(\theta_2)^2 + r(\theta^*)^2 - 2\, r(\theta_2)\, r(\theta^*) \cos(\alpha)} \tag{59}$$

in which

$$r(\theta) = \frac{ab}{\sqrt{(a\cos\theta)^2 + (b\sin\theta)^2}}. \tag{60}$$

7. Find γ:

$$\gamma = \sin^{-1}\left(\frac{r(\theta_2)\,\sin(\alpha)}{l_c}\right). \tag{61}$$

8. Find deflection angle, δ_i:

$$\delta_i = \frac{\Delta}{2} - \theta^* + \gamma\,. \tag{62}$$

9. $i = i + 1$.
10. Go to step 4 and repeat until $i = N$.
11. Now, we have the deflection angle and the corresponding chord length for any station along the elliptical arc.

III. An Application Example and Its Results

Let us assume that it is desired to connect the PC to PT through an elliptical arc such that $\Delta = 120°$, $R_{min} = 1000$ ft, and the Sta. # at PI $= 40 + 40$. First, the arc of ellipse should be found so that it satisfies the initial constraints. Applying the algorithm (A) yields the results tabulated in Table 1. Comparing the length of the arc and the right-of-way area, the ellipse with $\tau = 0.1$ provides the minimum length and the minimum right-of-way. Therefore, the desired ellipse is an ellipse with major axis a of 1111.1 ft. and minor axis b of 1105.5 ft. Using the algorithm (B), chord lengths and deflection angles can be obtained, as shown in Table 2.

3.1 The Equivalent Circular Curve Solution

Again, let us assume that it is desired to connect the PC to PT, but this time through a circular curve such that $\Delta = 120°$, $R_{min} = 1000$ ft, and $Sta.\#\ at$ PI $= 40 + 40.0$.
Accordingly, the length of the tangent T is:

$$T = R\tan\left(\frac{\Delta}{2}\right) = 1000\ \tan\left(\frac{120°}{2}\right) = 1732.1 \text{ ft.} \tag{63}$$

On the other hand, the length of arc l_a is:

$$l_a = \frac{\pi}{180}\ \Delta\ R = \frac{\pi}{180}\ \text{x}\ 120\ \text{x}\ 1000 = 2094.4 \text{ ft.} \tag{64}$$

Given the above, the locations of the PC and PT along with the deflection angles and chord lengths for the stations in between can be determined using the conventional circular curve relations.

Note that in highway design, the length of horizontal alignment and its associated right-of-way are two significant variables in evaluating alternative designs. According to the results obtained for the circular versus the elliptical approach, the right-of-way for circular curve connecting A to D, shown Figure 8, is:

$$ROW_{Circular} = (\overline{AB} \times 100) + \frac{\Delta\,\pi}{360} \times [(r_{\overline{BC}} + 50)^2 - (r_{\overline{BC}} - 50)^2] + (\overline{CD} \times 100) \tag{65}$$

where,

$$\overline{\text{AB}} = \overline{\text{CD}} = \frac{\text{LC}_\text{E} - \text{LC}_\text{C}}{2} \times \frac{1}{\cos\left(\frac{\Delta}{2}\right)} = \frac{1913 - 1732}{2} \times \frac{1}{\cos\left(\frac{120}{2}\right)} = \frac{181}{2} \times 2 = 181 \text{ ft.} \tag{66}$$

Then,

$$ROW_{Circular} = (181 \times 100) + \frac{\pi}{3} \times [(1000 + 50)^2 - (1000 - 50)^2] + (181 \times 100) = 24{,}5633 \text{ sq. ft.} = 5.64 \text{ acres.} \tag{67}$$

The roadway length from A to D through circular curve can be computed as:

$$L_{ABCD} = L_{AB} + L_{BC} + L_{CD} = \overline{\text{AB}} + l_{a\,Circular} + \overline{\text{CD}} = 181 + 2094.3 + 181 = 2{,}456.3 \text{ ft.} \tag{68}$$

Table 3 is a comparison of the ROW requirements for the simple circular versus the elliptical curves depicted in Figure 8 above. As shown, the elliptical curve is 137 ft. shorter in length than the equivalent simple circular curve. Another possible advantage of the elliptical alternative, not apparent in Figure 8 or in Table 3, is that the transition from the normal crown to the fully superelevated cross-section and back can be achieved more gradually through the entire length of the

elliptical arc. This provides for a smoother cross-sectional transition. However, the circular curve needs a somewhat smaller right of way, 0.17 acres less than the elliptical curve in this example.

3.2 Comparing the Spiral-Circular Curve Results to the Elliptical Curve Results

In Figure 9, both the elliptical curve and the equivalent spiral-circular curve are shown. The moderately thick curves are the spiral curves and the thin curve in the middle is the circular curve. The thick curve is the elliptical curve. The right-of-way and the length of the spiral-circular curve can be computed as follows:

$$\begin{aligned} ROW_{\text{Spiral }-\text{Circular}} &= (\overline{AB} \times 100) \\ &+ \frac{\Delta_C \pi}{360} \times [(r_{\widehat{BC}} + 50)^2 - (r_{\widehat{BC}} - 50)^2] \\ &+ \frac{2\theta_s \pi}{360} \times [(r_{B-\overline{S.C.}} + 50)^2 - (r_{B-\overline{S.C.}} - 50)^2] \\ &+ (\overline{CD} \times 100) \end{aligned} \tag{69}$$

where,

$$\overline{\text{AB}} = \overline{\text{CD}} = \frac{\text{LC}_\text{E} - \text{LC}_{\text{S.C.}}}{2} \times \frac{1}{\cos\left(\frac{\Delta}{2}\right)} = \frac{1913.2 - 1865.6}{2} \times \frac{1}{\cos\left(\frac{120}{2}\right)} = 47.6 \text{ ft.} \tag{70}$$

Then,

$$ROW_{\text{Spiral }-\text{Circular}} = 32{,}119 \text{ sq. ft.} = 5.33 \text{ acres.} \tag{71}$$

Length of roadway from A to D through spiral-circular curve is:

$$\begin{aligned} L_{ABCD} &= L_{AB} + L_{B-S.C.} + L_{BC} + L_{S.C.-C} + L_{CD} = \overline{\text{AB}} + l_s + l_{a\,Circular} + l_s + \overline{\text{CD}} \\ &= 47.6 + 263 + 1{,}831.1 + 263 + 47.6 = 2{,}452.3 \text{ ft.} \end{aligned} \tag{72}$$

A comparison of the length and ROW requirements for these two curves is also shown in Table 3 above. It can be noted in Table 3 that the elliptical curve is 133 ft. shorter than its equivalent spiral-circular curve. However, the spiral-circular curve needs a slightly smaller right of way, 0.48 acres less than the elliptical curve for this specific example.

IV. Conclusions and Recommendations

Based on the results presented, elliptical curves can be used as viable horizontal transition curves in lieu of simple circular or spiral-circular curves. A possible advantage in using elliptical curves is that elliptical curves can shorten the length of the roadway as shown in the application example while providing a smoother transition in terms of more gradual increase in centrifugal forces. Another possible advantage is that the transition from the normal crown to the fully superelevated cross-section and back to the normal crown can be achieved more gradually through the entire length of the elliptical arc. Therefore, it can also provide a smoother cross-sectional transition and one that is likely more aesthetically pleasing.

As a result, elliptical curves should be considered as an alternative design for horizontal alignments. For instance, for each specific horizontal alignment problem with a given intersection angle and design speed V_d, alternative calculations for simple circular, spiral-circular, compound circular, and elliptical curves can be conducted. Then, the results for each alternative should be compared with respect to the arc length and ROW requirements to optimize the design.

In terms of calculations, the key equation to find the elliptical arc length is an elliptic integral, known as complete elliptic integral of the second kind. This integral should be numerically estimated for each feasible ellipse satisfying the intersection angle and the design speed. Therefore, it is recommended to develop a software to find the most suitable elliptical curve for any given and V_d. Also, elliptical calculations as an alternative design to circular, circular compound, or spiral-circular alignments should be incorporated in highway design software packages such as Geopak (Bentley Systems, 2012) and Microstation (Bentley Systems, 2012). There may also be geometric and aesthetics benefits in using elliptical arcs for reverse curves; an aspect that can be investigated as an extension of this work.

Another computational aspect not addressed here is the sight distance computations associated with tall roadside objects that may interfere with driver's line of sight. In circular curves, this is typically addressed by computing the middle ordinate distance from the driving edge of the road, which establishes a buffer area on the inside of the circular curve to be

kept free of potential line of sight obstructions. If an elliptical arc is used instead, equivalent calculations would be necessary. However, in lieu of conducting those computations, the equivalent circular middle ordinate will be a conservative and safe value to use.

Regarding environmental issues, using elliptical curves has the potential to reduce air pollutants as well. Elliptical curves can shorten the length of the roadway as well as provide a smoother transition from the normal crown to the fully superelevated cross-section and back. Both of these properties could reduce vehicular fuel consumption. During a roadway's design life, an elliptical curve can therefore save road users a significant amount of fuel. Less fuel consumption also typically results in less air pollution. In addition, in the case of asphalt pavements, the shorter length of the roadway will decrease solar radiation absorbed by the asphalt surface. Therefore, elliptical curves can be more environmentally beneficial as they have the potential to substantially reduce air pollution and solar radiation absorbed by the asphalt surface over the design life of the roadway. Another possible extension of this work could be a user-cost study of elliptical versus the more conventional horizontal alignments. The user cost could be quantified in terms of fuel consumption and air pollutants over the design life of a project and be utilized in evaluation of alternative designs.

References

[1]. American Association of State Highway and Transportation Officials, (2004). A policy on
[2]. geometric design of highways and streets. (4th ed.). Washington, DC: American Association of State Highway and Transportation Officials.
[3]. Banks, J. H. (2002). Introduction to Transportation Engineering. Geometric Design (pp. 63-110). McGraw Hill.
[4]. Bentley Systems (2012). Geopak civil engineering suite V8i [computer software]. PA: Exton.
[5]. Bentley Systems (2012). Microstation [computer software]. PA: Exton.
[6]. Garber, N. J., & Hoel, L. A. (2002).Traffic and highway engineering. (3rd ed.). Pacific Grove, CA: Brooks/Cole.
[7]. Grant, I. S., & Phillips, W. R. (2001). The elements of physics. Gravity and orbital motion (chap. 5). Oxford University Press.
[8]. Larson, R., & Edwards, B. H. (2010). Calculus. (9th ed.). Belmont, CA: Brooks/Cole.
[9]. Rogers, M. (2003). Highway engineering. (1st ed.). Padstow, Cornwall, UK: TJ International Ltd.

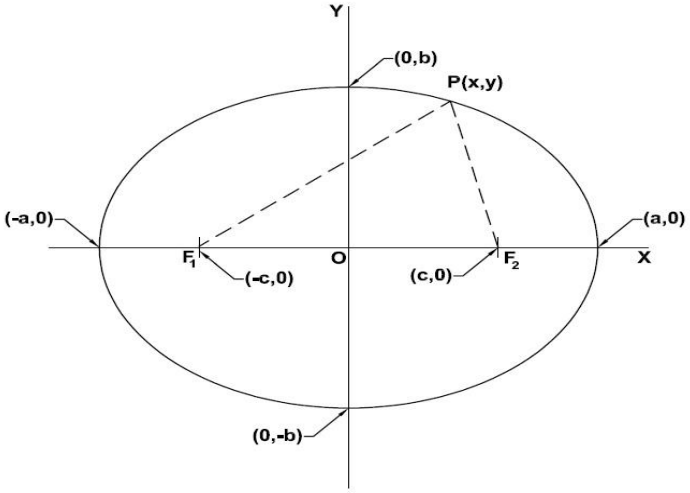

Figure 1. Cartesian components of a point on ellipse with the center at the origin.

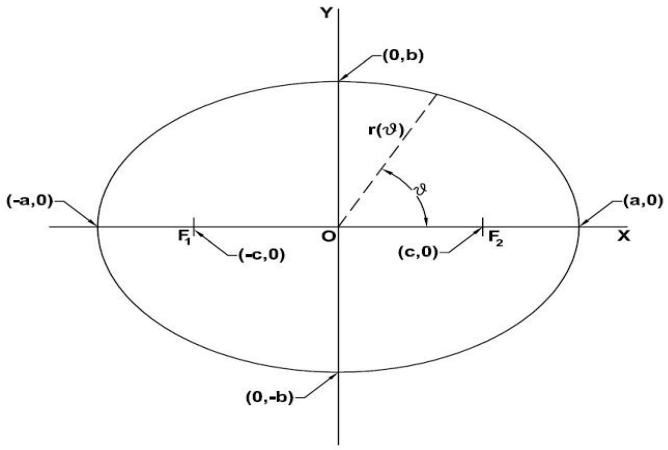

Figure 2. Polar Coordinate System with Origin at Center of the Ellipse.

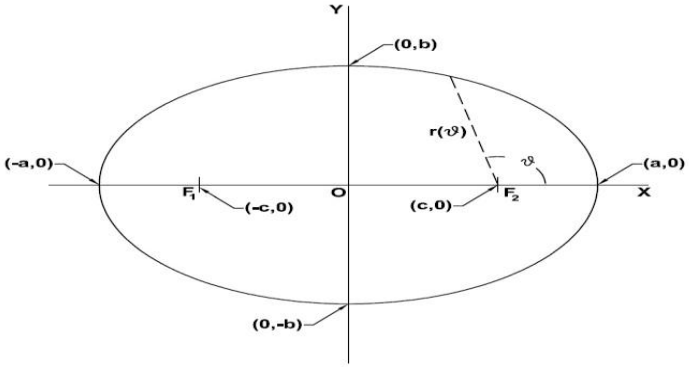

Figure 3. Polar Coordinate System with Origin at a Focus of the Ellipse.

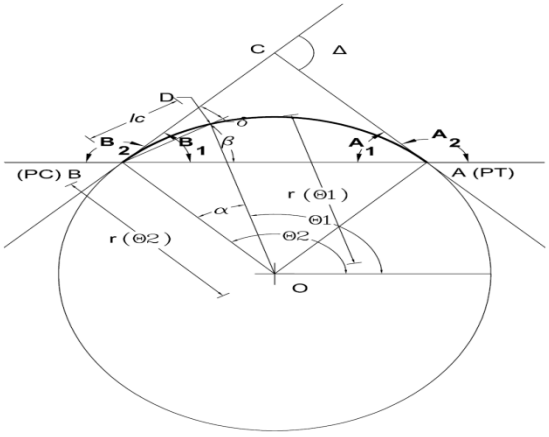

Figure 4. An arc of ellipse needed to connect PC to PT.

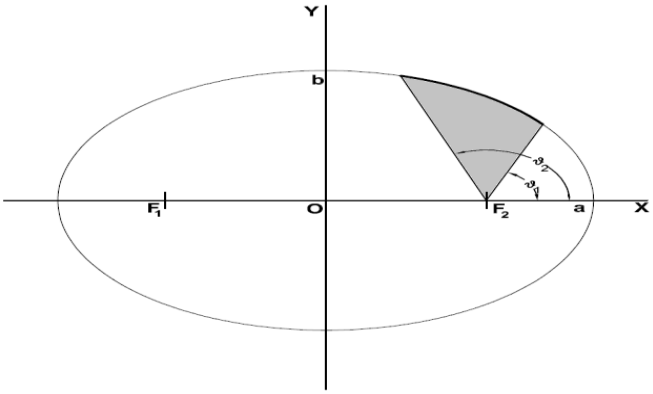

Figure 5. Sector of ellipse with respect to the focus.

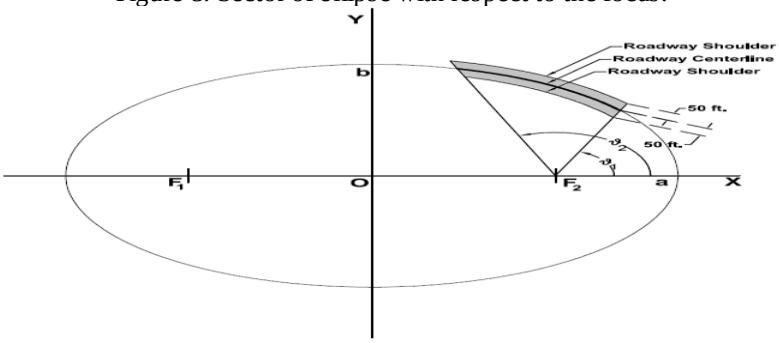

Figure 6. Elliptical Arc Right-Of-Way.

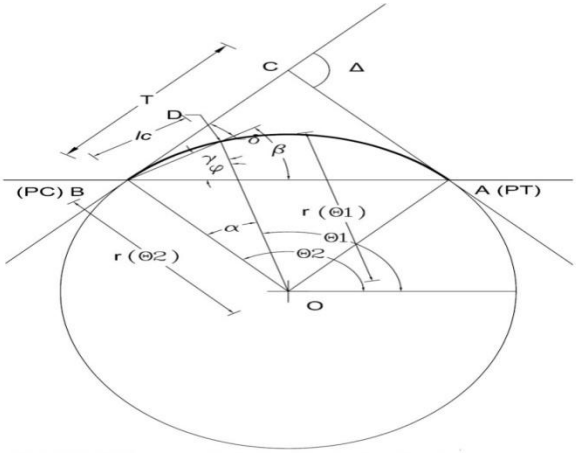

Figure 7. Diagram of an Elliptical Arc.

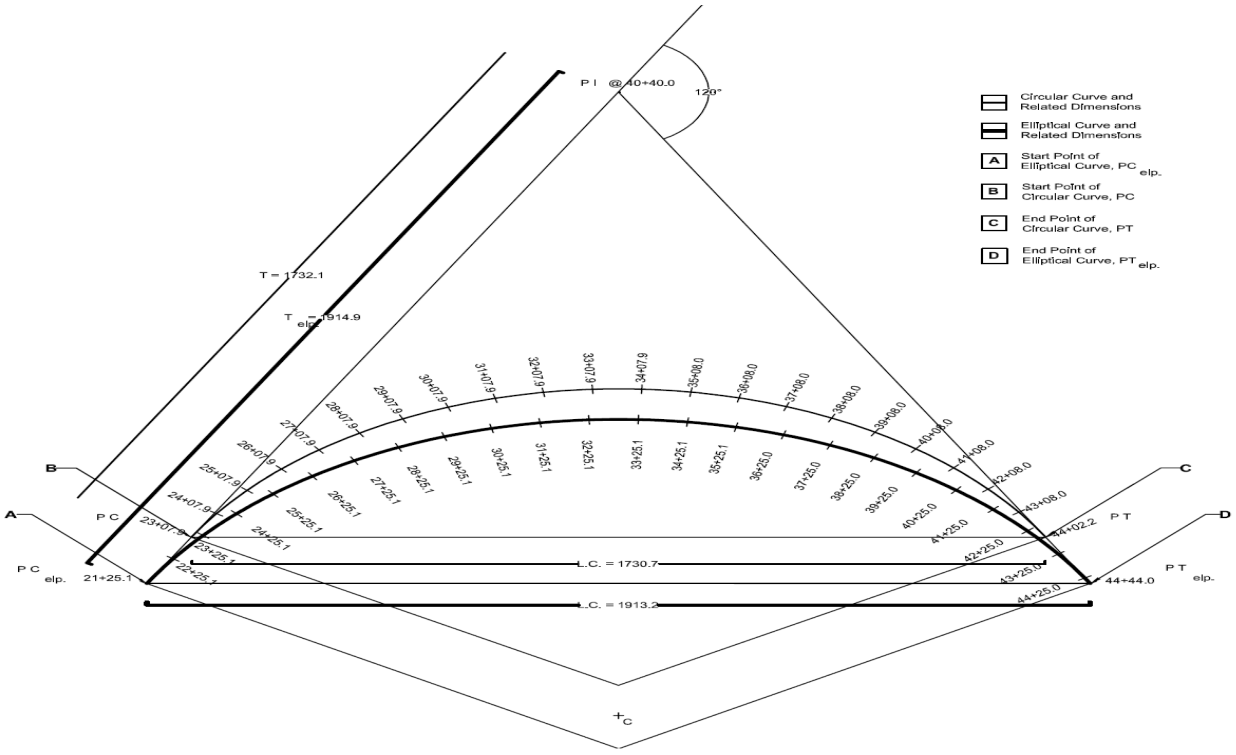

Figure 8. Final Profile: Elliptical curve vs. circular curve.

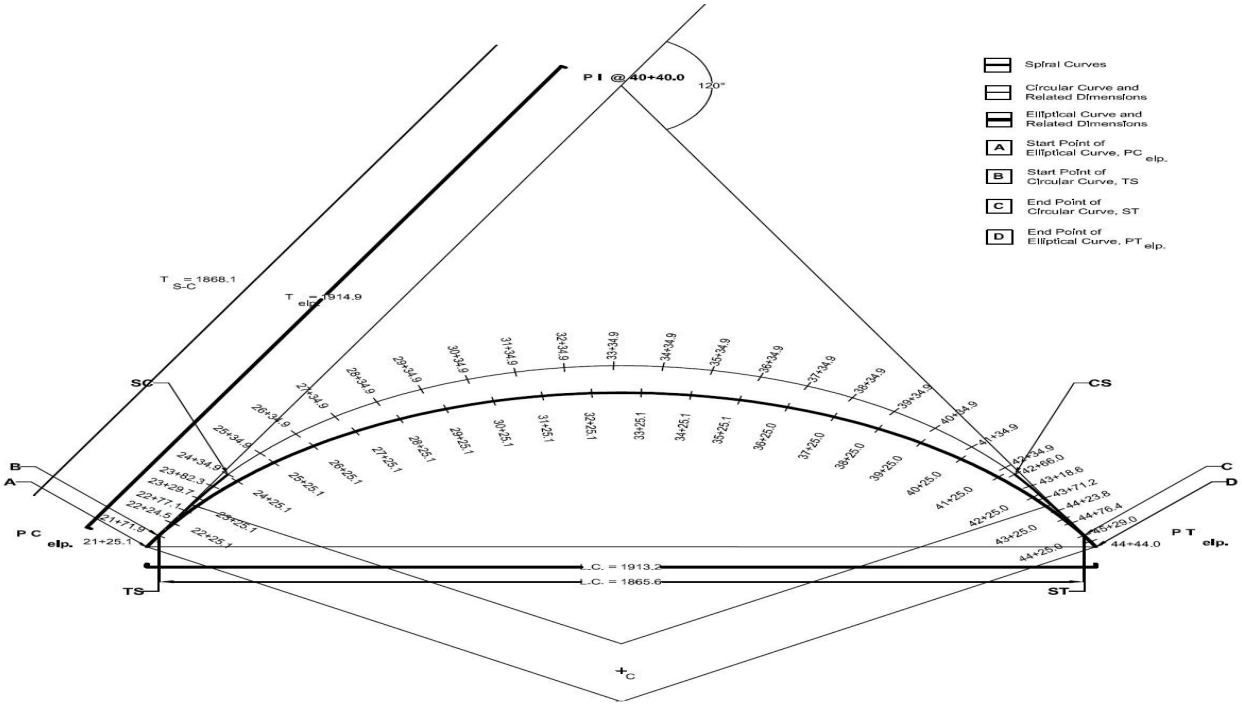

Figure 9. Final Profile. Elliptical curve vs. spiral-circular curve.

Table 1. Determining the Most Suitable Elliptical Arc

Eccentricity ε	R_{min}	a (ft.)	b (ft.)	Δ (deg.)	Slope m_1	Point A x_1 (ft.)	Point A y_1 (ft.)	Point B x_2 (ft.)	Point B y_2 (ft.)	θ_1 (deg.)	θ_2 (deg.)	$l_{a,\tau}(\theta_1,\theta_2)$ (ft.)	ROW) (Sq.ft.)
0.1	1000	1111.1	1105.5	120	-1.734	956.5	557.1	-956.5	557.1	30.22	149.78	2318.9	252,894
0.2	1000	1250.0	1224.7	120	-1.734	1055	635.2	-1055	635.2	31.06	148.94	2570.2	308,832
0.3	1000	1428.6	1362.8	120	-1.734	1166	739.3	-1166	739.3	32.37	147.63	2869.8	385,238
0.4	1000	1666.7	1527.5	120	-1.734	1293	887.3	-1293	887.3	34.46	145.54	3219.2	492,565
0.5	1000	2000.0	1732.1	120	-1.734	1442	1108	-1442	1108	37.54	142.46	3636.5	652,790
0.6	1000	2500.0	2000.0	120	-1.734	1622	1462	-1622	1462	42.04	137.96	4131.2	909,085
0.7	1000	3333.3	2380.5	120	-1.734	1852	2094	-1852	2094	48.52	131.48	4734.7	1,369,860
0.8	1000	5000.0	3000.0	120	-1.734	2163	3466	-2163	3466	58.04	121.96	5467.8	2,366,885
0.9	1000	10000.0	4358.9	120	-1.734	2628	7976	-2628	7976	71.8	108.20	6283.4	5,593,074

Table 2. Chord Lengths and Deflection Angles for Staking Out the Elliptical Arc

	Station Number	θ^* (deg.)	$r(\theta^*)$ (ft.)	Deflection Angle (deg.) δ	Chord Length (ft.) l_c	Arc Length (ft.) $l_{a,\tau}(\theta^*,\theta_2)$
Sta. # @ PC	21+25.1	149.80	1106.9	0	0.0	0.0
	22+25.1	144.64	1107.4	2.52	99.6	100.0
	23+25.1	139.49	1107.9	5.09	199.1	200.0
	24+25.1	134.33	1108.4	7.66	298.2	300.0
	25+25.1	129.17	1108.9	10.24	396.7	400.0
	26+25.1	124.02	1109.4	12.82	494.5	500.0
	27+25.1	118.86	1109.8	15.41	591.3	600.0
	28+25.1	113.70	1110.2	17.99	686.9	700.0
	29+25.1	108.55	1110.5	20.58	781.2	800.0
	30+25.1	103.39	1110.8	23.18	873.8	900.0
	31+25.1	98.23	1111.0	25.77	964.7	1000.0
	32+25.1	93.08	1111.1	28.37	1053.6	1100.0
	33+25.1	87.92	1111.1	30.96	1140.4	1200.0
	34+25.1	82.76	1111.0	33.56	1224.8	1300.0
	35+25.1	77.60	1110.9	36.16	1306.6	1400.0
	36+25.0	72.45	1110.6	38.76	1385.7	1499.9
	37+25.0	67.29	1110.3	41.36	1462.0	1599.9
	38+25.0	62.13	1109.9	43.96	1535.2	1699.9
	39+25.0	56.98	1109.4	46.55	1605.3	1799.9

	40+25.0	51.82	1109.0	49.15	1672.1	1899.9
	41+25.0	46.66	1108.5	51.74	1735.4	1999.9
	42+25.0	41.51	1108.0	54.33	1795.2	2099.9
	43+25.0	36.35	1107.5	56.92	1851.3	2199.9
	44+25.0	31.19	1107.0	59.50	1903.7	2299.9
Sta. # @ PT	44+44.0	30.22	1106.9	59.99	1913.2	2318.9

Table 3. A Comparison of Arc Length and ROW Requirements for the Three Alternative Curves

	Simple Circular Curve	Spiral-Circular Curve	Elliptical Curve
Length	2456 ft.	2452 ft.	2319 ft.
Right-Of-Way	5.64 acres	5.33 acres	5.81 acres

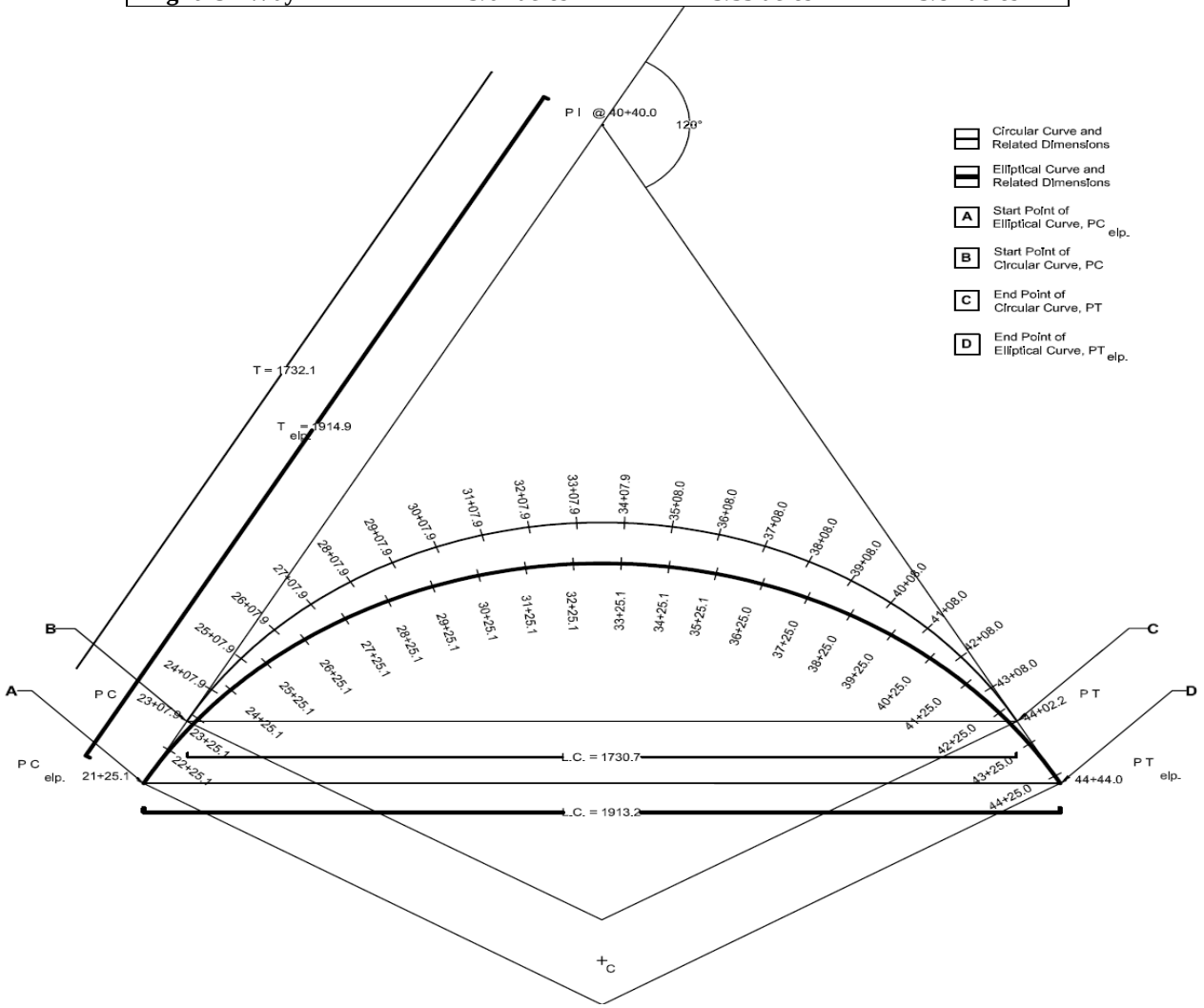

Figure 8. Final Profile: Elliptical curve vs. circular curve.

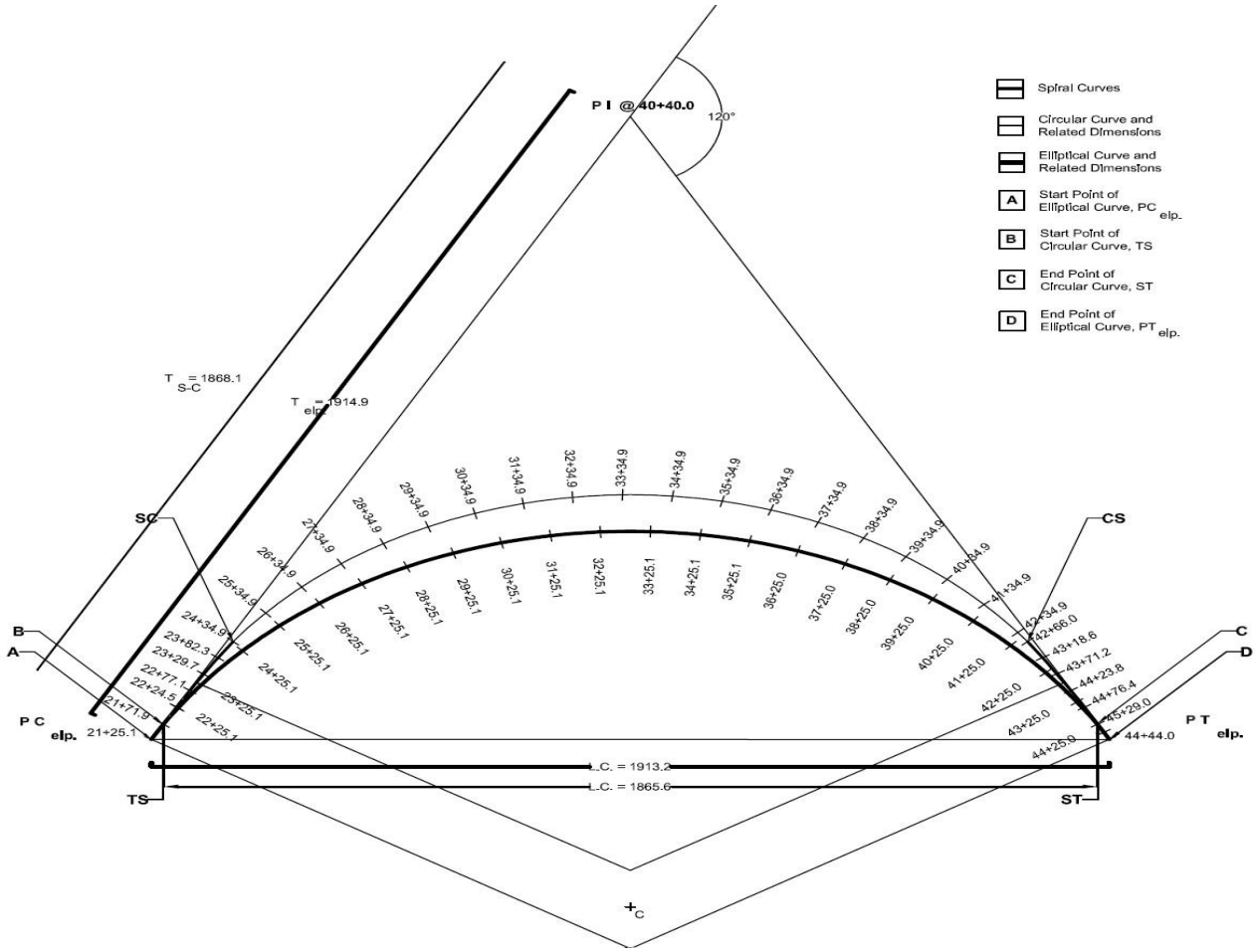

Figure 9. Final Profile. Elliptical curve vs. spiral-circular curve.

Face Feature Recognition System Considering Central Moments

[1]Sundos A. Hameed Al_azawi, [2]Jamila H.Al-A'meri
[1]Al-Mustainsiriyah University, College of Sciences,
[2]Computer sciences Dep. Baghdad, Iraq.

Abstract

Shape Features is used in pattern recognition because of their discrimination power and robustness. These features can also be normalized by Central moment. In this work, Faces Features Recognition System considering central moment (FFRS) is including three steps, first step, some image processing techniques worked together for shape features extraction step, step two, extract features of shape (face image) using central moment, third step is recognition of face features by comparing between an input test face features from the input image and an face features which stored in the features database.

Keyword: Recognition, detection, face feature, moment, image preprocessing, feature database, and central moment.

I. Introduction

To interpret images of faces, it is important to have a model of how the face can appear. Faces can vary widely, but the changes can be broken down into two parts: changes in shape and changes in the texture (patterns of pixel values) across the face. Both shape and texture can vary because of differences between individuals and due to changes in expression, viewpoint, and lighting conditions. One major task of pattern recognition, image processing: is to segment image into homogenous regions, in the several methods for segmentation are distinguished. Common methods are threshold, detection of discontinuities, region growing and merging and clustering techniques [1][2][3].

In recent years face recognition has received substantial attention from researchers in biometrics, pattern recognition, and computer vision communities [4], Computer face recognition promises to be a powerful tool, just like fingerprint scans. Automated face recognition is an interesting computer vision problem with many commercial and law enforcement applications. The biggest motivation for using shape is that it provides additional features in an image to be used by a pattern recognition system [5].

In image processing, image moment is a certain particular weighted average (moment) of the image intensities of pixels, or a function of such moments, usually chosen to have some attractive property or interpretation [1]. Simple properties of the image which are found via image moments include area; Hu [6] has used the moments for character recognition. In our proposed paper, used the boundary description to represented the data obtained from the segment process (black /white pixels) for the gray image and will use the one simple techniques and the task at same time, a technique detect edges to get an image with boundary, then extract a face features after process an image by some preprocessing techniques like enhancement, thinning and limitation for B/W image. The shape features of face image are depending on central moment values for objects of B/W face image result.

Pre-Processing Operations

For extract shape features, color face image must be preprocessed. The preprocessing of the image is done in some techniques: Before convert a gray face image to binary image (B/W), gray face image was enhance to reduce the noise, last operation in this stage is thinned the edge of B/W object to a width of one-pixel (these operations are necessary to simplify the subsequent structural analysis of the image for the extraction of the face shape).

For primary face image, segment the image into small and large regions (objects) such as eyes, nose, and mouth. From the face images, the face is the greatest part of the image, and hence the small object results from Pre-Processing Operations. So, the facial feature objects (eyes, nose, and mouth) are determined.

Shape Feature Extraction

In shape feature extraction stage, the approach is followed using binary image (black and white pixels) and shape information for each face objects (tow eyes, nose , and mouth) extracted by central moments.

There are several types of invariance. For example, if an object may occur in an arbitrary location in an image, then one needs the moments to be invariant to location. For binary connected components, this can be achieved simply by using the central moments [7].

Central Moment has been used as features for image processing, shape recognition and classification. Moments can provide characteristics of an object that uniquely represent its shape. Shape recognition is performed by classification in the multidimensional moment invariant feature space [1][8].

II. Central Moment

Moments are the statistical expectation of certain power functions of a random variable. There are two ways of viewing moments, one based on statistics and one based on arbitrary functions such as f(x) in one dimension or f(x, y) two dimension. As a result moments can be defined in more than one ways [1][4].Central moments are defined as [1][5]:

$$\mu_{pq} = \int_{-\infty}^{\infty}\int (x-\bar{x})^p (y-\bar{y})^q f(x,y)dxdy \ldots\ldots (1)$$

Where, *p* and *q* are the components of the centered, and $\bar{x} = {}^{M_{10}}/_{M_{00}}$, $\bar{Y} = {}^{M_{01}}/_{M_{00}}$.

If *f*(x, y) is a digital image, then the previous eq. (1) becomes:

$$\mu_{pq} = \sum\sum (x-\bar{x})^p (y-\tilde{y})^q f(x,y) \ldots\ldots (2)$$

The central moments of order up to 3 are [1]:

$\mu_{00} = M_{00}$, $\mu_{01} = 0$, $\mu_{10} = 0$, $\mu_{11} = M_{11} - \tilde{x} M_{01} = M_{11} - \tilde{y} M_{10}$, $\mu_{20} = M_{20} - \tilde{x} M_{10}$,$\mu_{02} = M_{02} - \tilde{y} M_{01}$,$\mu_{21} = M_{21} - 2\tilde{x} M_{11} - \tilde{y} M_{20} + 2(\tilde{x})^2 M_{01}$,$\mu_{12} = M_{12} - 2\tilde{y} M_{11} - \tilde{x} M_{02} + 2(\tilde{y})^2 M_{10}$,$\mu_{30} = M_{30} - 3\tilde{x} M_{20} + 2(\tilde{x})^2 M_{10}$, $\mu_{03} = M_{03} - 3\tilde{y} M_{02} + 2(\tilde{y})^2 M_{01}$

It can be shown that:

$$\mu_{pq} = \sum_{p}^{m}\sum_{q}^{n} (-\bar{x})^{(p-m)} (-\tilde{y})^{(q-n)} M_{mn} \ldots\ldots (3)$$

Shape Features

A set of seven invariant moments can be derived from moments in subsection (1) (eqs. 1,2 and 3), which are Shape Features uses to recognition an face image input.

$\partial_1 = \eta_{20} + \eta_{02}$

$\partial_2 = (\eta_{20} + \eta_{02})^2 + 4\eta^2_{11}$

$\partial_3 = (\eta_{30} + 3\eta_{12})^2 + (3\eta_{21} + \eta_{03})^2$

$\partial_4 = (\eta_{30} + \eta_{12})^2 + (\eta_{12} + \eta_{03})^2$

$\partial_5 = (\eta_{30} + 3\eta_{12})(\eta_{30} + \eta_{12})[(\eta_{30} + \eta_{12})^2 - 3(\eta_{21} + \eta_{03})^2] + (3\eta_{21} - \eta_{03})(\eta_{21} + \eta_{03})$

$\partial_6 = (\eta_{20} + \eta_{02})[(\eta_{30} + \eta_{12})^2 - 3(\eta_{21} + \eta_{03})^2] + 4\eta_{11}(\eta_{30} + \eta_{12})(\eta_{21} + \eta_{03})$

$\partial_7 = (3\eta_{21} - 3\eta_{03})(\eta_{30} + \eta_{12})[(\eta_{30} + \eta_{12})^2 - 3(\eta_{21} + \eta_{03})^2] + (3\eta_{12} - \eta_{03})(\eta_{21} + \eta_{03})[3(\eta_{30} + \eta_{12})^2 - (\eta_{21} + \eta_{03})^2]$

III. Face Features Extraction

After applied shape features extraction steps on the input face image, we define Maximum Four Objects, Right Eye, Left Eye, Nose, and Mouth, in the Face Image Input, for each objects we define a set of seven central moments (subsection2). So 28 moment values have been extracted using Face features algorithm (algorithm1).

Algorithm1: Face Features Extraction
Step 1: Input gray face image.
Step 2: Preprocessing of image that result from Step2. By:
a. Convert Gray Image to Binary Image,
b. Segment Binary image using thresholding technique,
c. Thinning its boundary and limitation for largest objects (in this case : Left eye, Right eye, Nose, and mouth)which result from the thinning, and
d. Smoothing the result thinning object images.

Step 3: Compute The seven Moments values (shape features) , in our case, we have an image include four object(step 2), so we can get seven moment values for each object, that mean we have (7 * 4)= 28 moment values for each input image (7 for each object(tow eyes, nose, and mouth)).
Step4: Saved all moment values (28 features value) for all objects from face images testing in Database system to use it in Recognition system for this research.

Face Features Recognition System (FFRS)

The proposed system including two main algorithms: Face Features algorithm (algorithm 1), and Face Recognition algorithm (algorithm 2).

Face Recognition algorithm:

In the Face Recognition system was show in Figure3, each new gray face image including for the system to recognition it, will be applied first in the algorithm (1) to get their 28 features moment and there threshold to compare its features with features for different images of gray face stored in our database system.

Algorithm 2: Face Recognition

Step 1: Input a new gray face image.
Step 2: applied Algorithm (1), to get 28 Features for new face image input.
Step 3: Compare the 28 Features from step2 within each 14 Features from our database by:

$$F = \sum_{i=1}^{28} (F_i p / F_i db) \times 3.57$$

Where: F is the summation of ((F_i p / F_i db) * 3.57), it will between (3.57*28 %) and (100%), 3.57 is the average of (100/28) for 28 features.
(F_i p) is the feature gets it from new person face image; (F_i db) is any feature gets it from our database.
Step 4: we get the rate of $F \geq 80\%$, to say what one features from database is same of features get it newly from new face input to recognition it.
Step 5: for step 3, if the result is more than one face image features have same rate value ($F \geq 80\%$), the Maximum value is the nearest features back in to test person face image.

Implementation and Results

Among the 30 images, 10 images are used to train, and another 10 are used to test. The results of shape feature extract, is the basic step in this work and the task to identify and distinguish between face images were entered and stored in database, then compared between the entrance is a newly characterized to any image data back, this process is the discrimination and that will be apply to the face image only to find out of the image of face back to the input image data that was already stored in the database. In the recognition step, the data will be comparing with the specification of the face image and what had been extracted based on the covariance matrix, considering the features that were stored in images database.

The experiment is calculated under the conditions: All of the test images have same size, only the frontal view of the face image is analyzer throughout this system.

For one face images named Face4, Figure 1 show an objects result from shape features application from algorithm1, were subfigure (e) content four facial features (right eye, left eye, nose, and mouth).

a b c

d e

Fig1: Shape features for Face2: (a) gray Face1 image, (b) enhance image, (c) threshold segment, (d) thinning, (e) four features object detect.

Fig2 show some gray face images saved in our database system, every one of this image have a name Face1, Face2, etc., Face1 in fig1 is one of these images.

Fig3, illustrated the another test face image for recognition it with database images. After we find 28 features moment by applied algorithm1, we saved this features by named Face 21, then made a comparison between 28 features of Face21 test image and 28 features for each face in database system.

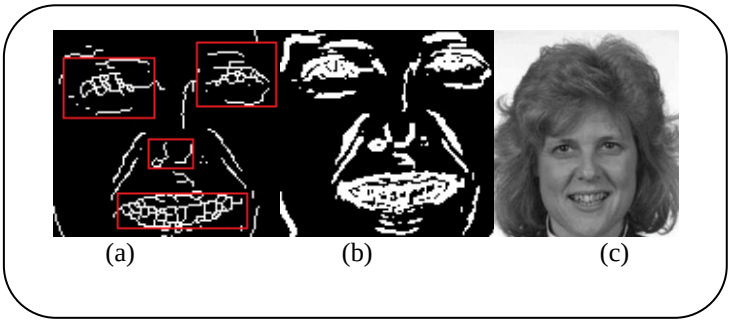

(a) (b) (c)

Fig3: Test face image for recognition steps: (a) Origin Gray face, (b) threshold segment, thinning and four object detect (two eyes, nose, and mouth).

Table1 including all the features for test Face21 image. Each face image test has 28 features, and it will be saved in the database system to recognition level, where Face21, is the name of test face image for recognition steps, F1, F2, F3,…, F14 are the features for tow eyes objects (left and right eye), F15.F16, F17,…,F21 are the features for nose object, and F22,F23,F24, …, F28 are the features for mouth object.

In compare step from Algorithm2 when compare test Face21 features (Table1) with features of 30 gray face images saved in database system, we find another face image have same rate value (F) which is suggested in our recognition method, named Face10 and its moment features show in Table2, this image have same value of ratio 80.023 %.

Table1: Moment Features for test Face21 image.

Right eye	F1	F2	F3	F4	F5	F6	F7
	0.92770	1.86422	2.48800	398765	3.81953	4.39213	4.01208
Left eye	F8	F9	F10	F11	F12	F13	F14
	1.56432	3.45981	5.10086	6.01256	8.01736	8.01123	9.12043
Nose	F15	F16	F17	F18	F19	F20	F21
	0.76543	111347	2.33410	2.00237	3.05432	3.09873	3.03670
Mouth	F22	F23	F24	F25	F26	F27	F28
	1.84397	3.94329	5.67023	5.87209	8.09648	7.04328	7.95437

Table2: Moment Features for Face10 image

Right eye	F1	F2	F3	F4	F5	F6	F7
	1.01521	1.75422	2.47860	3.86420	3.86297	4.19642	4.00247
Left eye	F8	F9	F10	F11	F12	F13	F14
	1.55397	3.57102	5.10982	6.00532	8.10953	8.27631	8.95021
Nose	F15	F16	F17	F18	F19	F20	F21
	0.84320	1.15072	2.45903	3.01094	3.16832	3.05503	3.00589
Mouth	F22	F23	F24	F25	F26	F27	F28
	2.06591	3.79541	4.95621	5.90742	8.10653	7.11091	7.86021

The result compare steps for this tow face image (Face21 and Face10) are clear in Figs (4,5,6, and 7), were Fig4 show the compare result for left eyes from Face21 and Face10, Fig5 show the compare result for right eyes from Face21 and Face10, Fig6 show the compare result for nose from Face21 and Face10, and Fig7 show the compare result for mouth from Face21 and Face10.

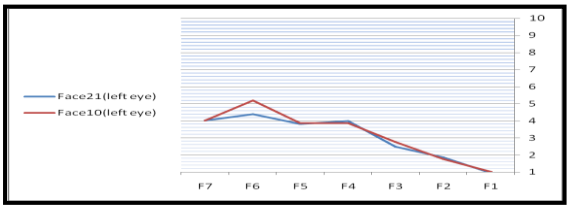

Fig4: Compare result for left eyes from Face21 and Face10

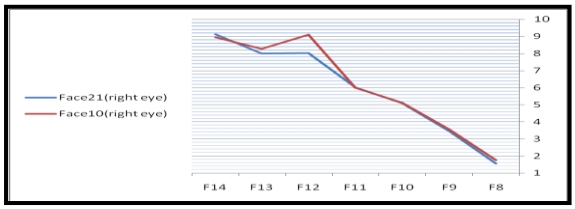

Fig5: Compare result for right eyes from Face21 and Face10

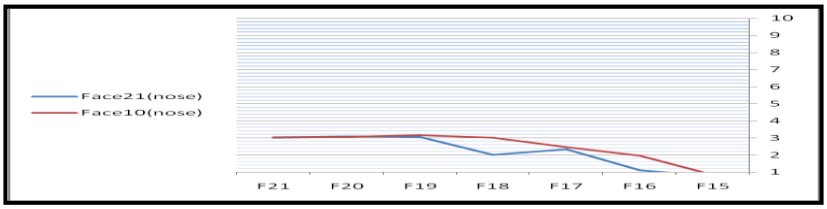

Fig6: Compare result for nose from Face21 and Face10

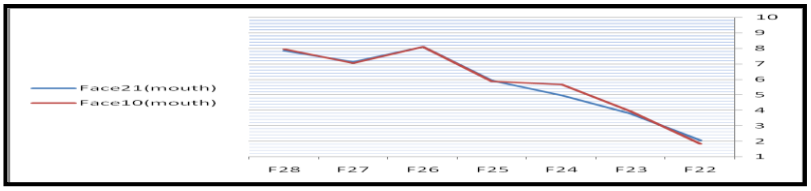

Fig7: Compare result for mouth from Face21 and Face10

IV. Conclusion

This work presented a method for the recognition of human faces in gray images using a object of facial parts (eyes, nose, and mouth) and moment values for these parts. For face recognition these moments can also be. In our proposed paper for Face Recognition based Moment method by using central moment in object of facial parts. First some image processing technique was used together to work for best result of this parts.

Recognition step doing by comparing input 28 features for test gray face image with 28 features for each Faces features saved in database. The image has Maximum rate value it is the true recognized faces back for test face of input image.

References

[1]. Gonzalez R. C., and Woods E., "Digital image Processing",Addison-Wesley Publishing Company, 2004.
[2]. Umbaugh S.E., "Computer Vision and Image Processing", Prentice- Hall, 1998.
[3]. Richard O. Duda, Peter E. Hart, David G. Stork, Pattern classification (2nd edition), Wiley, New York, ISBN 0-71-05669-3, 2001.
[4]. W. Zhao, R. Chellappa, A. Rosenfeld, and P.J. Phillips, "Face recognition: A literature survey," CVL Technical Report, University of Maryland, 2000.
[5]. S. Gong, S.J. McKenna, and A. Psarrou, Dynamic Vision: from Images to Face Recognition,Imperial College Press and World Scientific Publishing, 2000.
[6]. "Facial Recognition Applications" .Animetrics. http://www.Animetrics.com/technology / f rapplications.html. Retrieved, 2008.
[7]. B. K. Low, and E. Hjelmxas, "Face Detection: A Survey", Academic
[8]. Press, computer vision and Image Understanding, 83, 2001, pp. 236–274.
[9]. N. Jaisankar, "Performance comparison of face and fingerprint biometrics for Person Identification", Science Academy Transactions on Computer and Communication Networks, Vol. 1, No. 1, 2011.

Prediction of Weld Width of Shielded Metal Arc Weld under Magnetic Field using Artificial Neural Networks

R.P. Singh[1], R.C. Gupta [2] and S.C. Sarkar [3]

[1]Mechanical Engineering Department, I.E.T., G.L.A. University Mathura, (U.P.)
[2]Mechanical Engineering Department, I.E.T., Lucknow, (U.P)
[3]Mechanical Engineering Department, Kumaon Engineering College, Dwarahat, (Uttarakhand)

I. Abstract:

The prediction of the optimal weld bead width is an important aspect in shielded metal arc welding (SMAW) process as it is related to the strength of the weld. This paper focuses on investigation of the development of the simple and accurate model for prediction of weld bead width of butt joint of SMAW process. Artificial neural networks technique was used to train a program in C++ with the help of sufficient number of welding data sets having input variables current, voltage, speed of welding and external magnetic field and output variable weld bead width. These variables were obtained after welding mild steel plates using SMAW process. The welding set-up was mounted on a lathe machine. In this paper, the effect of a longitudinal magnetic field generated by bar magnets on the weld bead width was experimentally investigated. Using the experimental data a multi-layer feed forward artificial neural network with back propagation algorithm was modeled to predict the effects of welding input process parameters on weld width accurately. It was found that welding voltage, arc current, welding speed and external magnetic field have the large significant effects on weld bead width. It has been realized that with the use of the properly trained program, the prediction of optimal weld bead width becomes much simpler to even a novice user who has no prior knowledge of the SMAW process and optimization techniques.

Keywords: Artificial Neural Network, Back Propagation, External Magnetic Field, Hidden Layer, Input Process Parameters, Shielded Metal Arc Welding, Weld Bead Width.

II. Introduction:

Welding is a process of joining different materials. It is more economical and is a much faster process compared to both casting and riveting [1]. The weld bead width is the maximum width of the weld metal deposited. It influences the flux consumption rate and chemistry of the weld metal and hence determines the mechanical properties of the weld [2]. SMAW input process parameters like welding current, welding speed; open circuit voltage and external magnetic field are highly influencing the quality of weld joints. The applications of magnetic field in welding processes have drawn much attention of researchers [3]. However, the effect of external magnetic field on quality of weld is still lack of understanding. Selection of process parameters has great influence on the quality of a welded connection. A precise means of selection of the process variables and control of weld bead shape has become essential because mechanical strength of weld is influenced not only by the composition of the metal, but also by the weld bead shape. The weld bead width is an important factor of the shape of the weld. The weld quality can be achieved by meeting quality requirements such as bead geometry which is highly influenced by various process parameters involved in the process. Inadequate weld bead dimensions will contribute to failure of the welded structure [4]. Among all the welding processes, SMAW is very important. The advantages of this method are that it is the simplest of the all arc welding processes. The equipment is often small in size and can be easily shifted from one place to the other. Cost of the equipment is very less. This process finds a number of applications because of the availability of a wide variety of electrodes which makes it possible to weld a number of metals and their alloys. The welding of the joints may be carried out in any position with highest weld quality and therefore the joints which are difficult to be welded because of their position by automatic welding machines can be easily welded by shielded metal arc welding. Both alternating and direct current power sources could be used effectively. Power sources for this type of welding could be plugged into domestic single phase electric supply, which makes it popular with fabrications of smaller sizes [5]. However, non equilibrium heating and cooling of the weld pool can produce micro-structural changes which may greatly affect mechanical properties of weld metal. To get the desired weld quality in SMAW process, it is essential to know interrelationships between process parameters and bead geometry as a welding quality. Many efforts have been done to develop the analytical and numerical models to study these relationships, but it was not an easy task because there were some unknown, nonlinear process parameters. For this reason, it is good for solving this problem by the experimental models. One of the experimental models is artificial neural networks technique that can be utilized to establish the empirical models for various arc welding processes. Investigation into the relationship between the welding process parameters and bead geometry began in the mid 1900's and regression analysis was applied to welding geometry research [6]. Many efforts have been carried out for the development of various algorithms

in the modeling of arc welding process. In the early days, arc welding was carried out manually and the weld quality was totally controlled by the welder ability. Mc Glone and Chadwick have reported a mathematical analysis correlating process variables and bead geometry for the submerged arc welding of square edge close butts. Chandel first applied this technique to the GMA welding process and investigated relationship between process variables and bead geometry [7]. These results showed that arc current has the greatest influence on bead geometry, and that mathematical models derived from experimental results can be used to predict bead width accurately. Nearly 90% of welding in world is carried out by one or the other arc welding process; therefore it is imperative to discuss the effects of welding parameters on the weldability of the materials during the arc welding. Mild steel was selected for work-pieces to be welded because it is the most common form of steel as its price is relatively low while it provides material properties which are acceptable for many applications.

III. Experiment Work

To investigate the weldment characteristics weld beads were obtained by welding two mild steel flat plates of 150 mm x 50 mm x 5 mm dimensions in butt position using mild steel electrodes of 3.15 mm diameter. A manual welding machine was used to weld the plates. A lathe machine was used to provide uniform speed of welding, to support electrode holder and bar magnet. The work piece was kept on cross slide with some arrangement. Work-piece moves with cross slide. Bar magnet was connected with tailstock with a wooden structure Since the weldment characteristics depend on welding current, welding voltage, speed of welding and magnetic field, we select different set of values of these inputs [8]. Welding currents were chosen as 90, 95,100, 105 and 110 A, arc voltages were chosen as 20, 21, 22,23 and 24V, the welding speeds were chosen as 40, 60 and 80 mm/min and external magnetic field strengths were used as 0, 20,40, 60 and 80 Gauss for the experiments. Current was measured with a clamp meter, voltage was measured with a multi meter and magnetic field was measured with a Gauss meter. To study the bead geometry, each bead was sectioned transversely at two points one near the start (leaving 2 cm from the start) and the other near the end (leaving 2 cm from the end). To get the microstructure, these sectioned beads were ground with emery belt grinder having 0, 2, 3 grade emery papers then polished with a double disk polishing machine. Etching was done with a mixture of 2% nitric acid and 98% ethyl alcohol solution. To measure the bead height and bead width of each sample a digital slide caliper was used. The average values of bead height, bead width and depth of penetration were measured. Eighteen sets of values out of twenty five such sets obtained were used for training a network based on back propagation algorithm. Remaining seven sets of the values were used for prediction. These data sets are shown in table-1. A program of back propagation neural network in C++ was used for training and prediction [9]. In this program one input layer having four neurons, two hidden layers, both having five neurons and one output layer having three neurons, were used.

Table 1 Data for training and prediction

	Serial Number	Current (A)	Voltage (V)	Welding Speed (mm/min)	Magnetic Field (Gauss)	Weld idth(mm)
Data for Training	1	90	24	40	0	6.95
	2	90	24	40	20	6.94
	3	90	24	40	40	6.96
	4	90	24	40	60	6.99
	5	90	24	40	80	7.03
	6	95	20	60	60	6.01
	7	95	21	60	60	6.08
	8	95	22	60	60	6.10
	9	95	23	60	60	6.15
	10	95	24	60	60	6.25
	11	100	22	40	40	5.94
	12	100	22	60	40	5.90
	13	100	22	80	40	5.86
	14	90	20	80	20	5.91
	15	95	20	80	20	5.92
	16	100	20	80	20	5.94
	17	105	20	80	20	5.95
	18	110	20	80	20	5.97
Data for Prediction	1	90	23	40	0	6.92
	2	95	22	60	40	6.05
	3	95	21	80	60	6.04
	4	100	24	40	40	6.99
	5	105	21	60	40	5.98
	6	105	22	60	20	5.96
	7	110	21	60	20	5.97

Table 2 Measured and predicted values with percentage error

S.N.	Current (A)	Voltage (V)	Welding Speed (mm/min)	Magnetic Field (Gauss)	Weld Width (mm) Measured	Weld Width (mm) Predicted	Error in Weld Width % age
1	90	23	40	0	6.92	6.54	-5.49
2	95	22	60	40	6.05	6.42	+6.12
3	95	21	80	60	6.04	6.44	+6.62
4	100	24	40	40	6.99	6.58	-5.87
5	105	21	60	40	5.98	6.41	+7.20
6	105	22	60	20	5.96	6.40	+7.38
7	110	21	60	20	5.97	6.39	+7.04

Figure 1 Real experimental set-up on a lathe machine

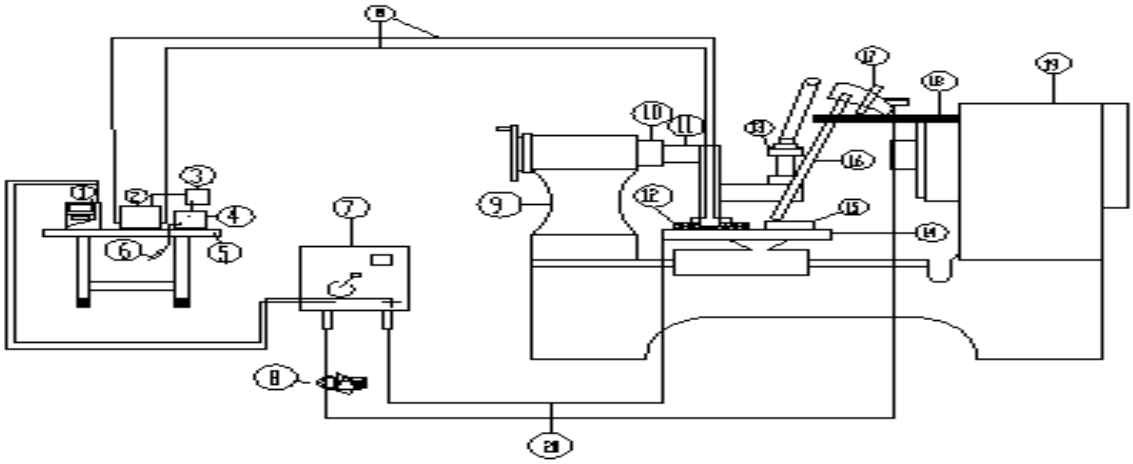

1. Multi-meter 2. Battery Eliminator 3. Electric Board 4. Gauss Meter 5. Table,
6. Measuring Prob 7. Transformer Welding Set 8. Clamp meter 9. Tail Stock 10. Sleeve
11. Link (Wood) 12. Solenoid 13. Tool post 14. Iron sheet 15. Workpiece
16. Electrode 17. Electrode Holder 18. Metal Strip Connected with head stock
19. Head stock 20. Connecting Wires

Figure 2 Experimental set-up (Line Diagram)

IV. Methodology of Artificial Neural Network Modeling

Most of the industrial processes are non-linear, complex and more input variables are involving in processes. The mathematical models are not giving closer approach to describe the behavior of the processes. ANNs are easy to understand, cost effective and have the capability to learn from examples and have found in many industrial application. ANN model has been developed for general application consisting of the following steps: (i) Database collection, (ii) pre-processing of input/output data, (iii) design and training of neural network, (iv) testing of trained network, (v) post processing and (vi) use trained network for prediction [10]. The arrangement of neurons into layer and the connection pattern within and between the layers are called as network architecture. The architecture is consisted of three parts: (i) Input layer receives the welding parameters, (ii) Hidden layers considered as black boxes and (iii) Output layer obtaining the values of bead geometry. The performance of the neural networks depends upon, the number of hidden layers and number of neurons in the hidden layers. Hence, optimum structure is obtained by changing number of hidden layers and neurons by making many attempts. The appropriate neural networks structure was chosen by the trial and error method. Feed forward artificial neural network structure was established by keeping four neurons in the input layer, two hidden layers having five neurons in each and one neurons in output layer using C++. It was trained with help of back propagation (BP) algorithm. BP is essentially stochastic approximation to nonlinear regression. Several researchers were used BP to model welding processes and predict welding parameters using Neural network. The designed neural networks structure was 4-5-5-1 (3 neurons in input layer, 5 neurons in both hidden layers and 1 neuron in output layer). Proposed feed forward neural network architecture is shown in figure-3. Non-linearity and input-output mapping are the useful complement in neural networks. Hence, it has been adapted to model the input-output relation of non-linearity and interconnected system.

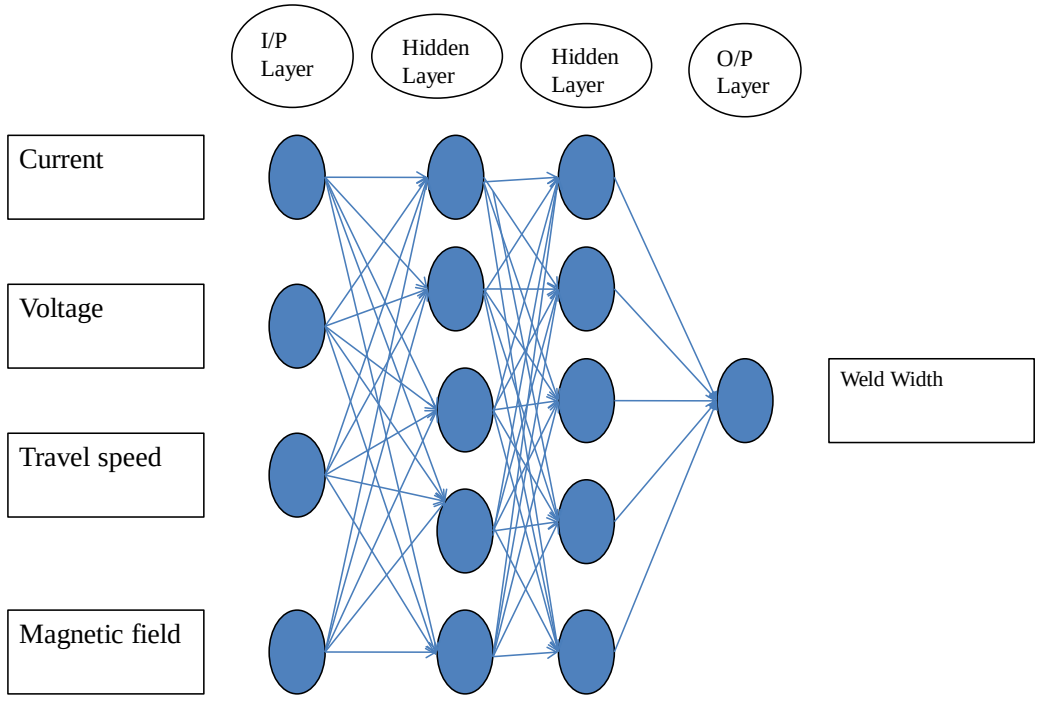

Figure 3 Feed-forward neural network (4-5-5-1) architecture

V. Results and Discussion

Table-2 depicted, the measured weld bead width, from the experiment and predicted output values using artificial neural feed forward network. The measured and predicted output values are close to each other. The aim of this paper shows the possibility of the use of neural network to predict the weld width accurately.

Weld Width

The weld width of the welded joints was almost unaffected if the magnetic field was changed from 0 to 20 gauss or from 20 to 40 gauss. If the field was increased from 40 gauss to 60 gauss, the weld width increased from 6.97 mm to 6.99 mm. and if it was increased from 60 gauss to 80 gauss, the weld width increased from 6.99 mm to 7.03 mm. If the speed of welding was increased from 40 mm/min to 60 mm/ min, the weld width decreased from 5.94 mm to 5.90 mm, and if it was increased from 60 mm/min to 80 mm/min, the weld width of the weld decreased from 5.90 mm to 5.86 mm. The effect of voltage was positive for weld width i.e. if voltage was increased from 20 V to 24 V, the weld width increased from 6.01 mm to 6.25 mm. The increment in current increased the weld width for all the investigated values. If the current was increased from 90 A to 110 A the weld width increased from 5.91 mm to 5.97 mm. The variation of weld width with magnetic field, voltage, welding speed and current were shown in figures 4, 5, 6 and 7 respectively.

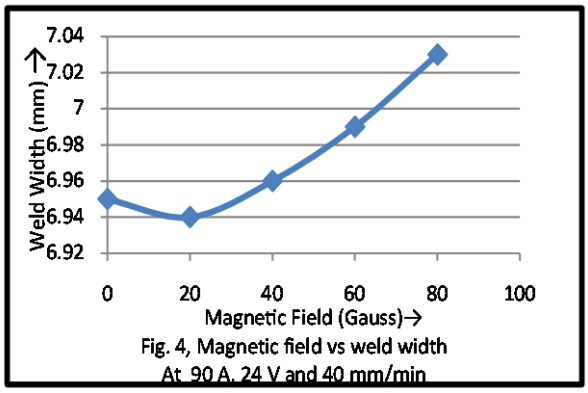

Fig. 4, Magnetic field vs weld width
At 90 A, 24 V and 40 mm/min

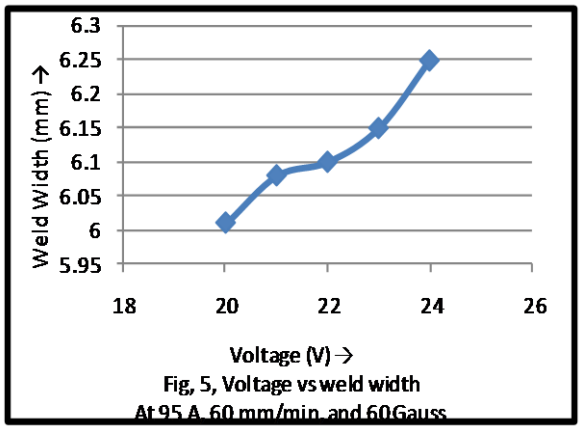

Fig, 5, Voltage vs weld width
At 95 A, 60 mm/min, and 60Gauss

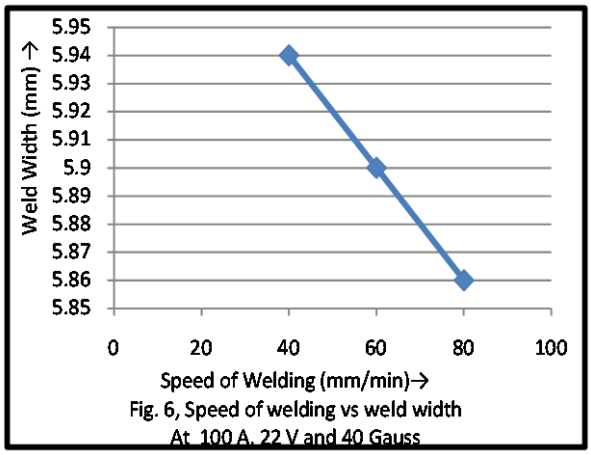

Fig. 6, Speed of welding vs weld width
At 100 A, 22 V and 40 Gauss

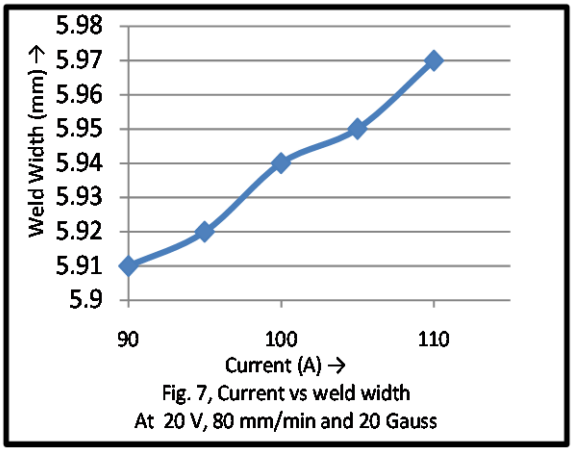

Fig. 7, Current vs weld width
At 20 V, 80 mm/min and 20 Gauss

Prediction of Weld Width using Artificial Neural Networks

The developed neural network architecture was trained with help of back propagation algorithm using 18 data sets. The developed network was tested out of 7 datasets. The training data sets and testing data sets are shown in table-1. The testing data were not used for training the network. The % age error was calculated between the experimental and predicted values as shown in figure-2. The %age error is ranging between -5.87 to 7.38. The other predictions are in between the above ranges and hence are very close to the practical values, which indicate the super predicting capacity of the artificial neural network model.

VI. Discussion

In this investigation, an attempt was made to find out the best set of values of current, voltage, speed of welding and external magnetic field to produce the best quality of weld in respect of weld width. Shielded metal arc welding is a universally used process for joining several metals. Generally in this process speed of welding and feed rate of electrode both are controlled manually but in the present work the speed of welding was controlled with the help of cross slide of a lathe machine hence only feed rate of electrode was controlled manually which ensures better weld quality. In the present work external magnetic field was utilized to distribute the electrode metal and heat produced to larger area of weld which improves several mechanical properties of the weld. The welding process is a very complicated process in which no mathematical accurate relationship among different parameters can be developed. In present work back propagation artificial neural network was used efficiently in which random weights were assigned to co-relate different parameters which were rectified during several iterations of training. Finally the improved weights were used for prediction which provided the results very near to the experimental values.

VII. 6. Conclusion

The experimental analysis confirms that, artificial neural networks are power tools for analysis and modeling. Results revealed that an artificial neural network is one of the alternatives methods to predict the weld width. Hence it can be proposed for real time work environment. Based on the experimental work and the neural network modeling the following conclusions are drawn:

(1) A strong joint of mild steel is found to be produced in this work by using the SMAW technique.
(2) If amperage is increased, weld width generally increases.
(3) If voltage of the arc is increased, weld width generally increases.
(4) If travel speed is increased weld width generally decreases.
(5) If magnetic field is increased weld width, generally increases.
(6) Artificial neural networks based approaches can be used successfully for predicting the output parameters like weld width of weld as shown in table 2. However the error is rather high as in some cases in predicting weld width it is more than 7 percent. Increasing the number of hidden layers and iterations can minimize this error.

References

[1] W.D. Collister. Material Science and Engineering, An Introduction, John Wiley and Sons, Inc., New York, USA, 1997.
[2] S.V. Nadkarni. Modern Arc Welding Technology, Oxford & IBH Publishing Co. Pvt. Ltd., 1988.
[3] M.I. Khan and A.K. Gupta. A study of Hard Facing under Magnetic Field, ASME Conference, I.I.T. Delhi, 174-176, 1989.
[4] W. Robert Messler. Principles of Welding Processes, Physics, Chemistry and Metallurgy, Wiley, VCH Verlag Gmbh and Co. KgaA Weinheim, 2004.
[5] Chien-Yi Lee. A study of an Automatic Welding System, Dissertation of Ph.D., Institute of Mechanical Engineering at National Central University. Jhongli City, Taoyuan County, Taiwan, Republic of China, 2007.
[6] Parikshit Dutta and Dilip Kumar Pratihar. Modeling of TIG Welding Process Using Conventional Regression Analysis and Neural Network Based Approaches, Journal of Materials Processing Technology 184: 56-68, Elsevier, 2007 .
[7] R.P. Singh and R.C. Gupta. Application of Artificial Neural Network to Analyze and Predict the Mechanical Properties of Shielded Metal Arc Welded Joints under the Influence of External Magnetic Field, International Journal of Engineering Research & Technology (IJERT), Vol. 8, Issue 1, 1-12, , October, 2012.
[8] R.P. Singh and R.C. Gupta. Prediction of Weld Bead Geometry in Shielded Metal Arc Welding under External Magnetic Field using Artificial Neural Networks , International Journal of Manufacturing Technology and Research, Vol. 8 number 1, 9-15, 2012.
[9] Rajasekaran and G.A. Vijayalakshmi. Neural Networks, Fuzzy Logic and Genetic Algorithms Synthesis and Applications. Prentice Hall of India, 2003.
[10] Alvin Ramsey. Assessment of Modeling Abilities of Neural Networks, Dissertation, Massachusetts Institute of Technology, 1994.

Author

Rudra pratap Singh received the B.E. degree in Mechanical Engineering from MMMEC Gorakhpur in 1992 and the M.Tech. degree in mechanical Engineering in 2009 from UPTU Lucknow. During 1992 to 1999 he worked in Jindal Group as a quality control engineer, from 1999 to till date he is working in GLA group (now GLA University) Mathura as a faculty in Mechanical Engineering Department. He is pursuing Ph. D. (Registered in, March, 2010) from Uttarakhand Technical University, Dehradun. He has published seven papers in international journals and three papers in national conferences

The Gracefulness of the Merging Graph N ** C_4 with Dotnet Framework

Solairaju[1], N. Abdul Ali[2] and R.M. Karthikkeyan[3]

[1-2]: P.G. & Research Department of Mathematics, Jamal Mohamed College, Trichy – 20.

[3:] M.Phil Scholar, Jamal Mohamed College, Trichy – 20.

Abstract:

There are many graceful graph from standers path, circuit, wheel etc .In this paper a new class of graceful graphs related to c_4 [circuits with 4 vertices] is obtained .

Keyword: - path limit, 'n' - copies of c_4

I. Introduction:

Most graph labeling methods trace their origin to one introduced by Rosa [2] or one given Graham and Sloane [1]. Rosa defined a function f, a β-valuation of a graph with q edges if f is an injective map from the vertices of G to the set {0, 1, 2 ,…,q} such that when each edge xy is assigned the label $|f(x)-f(y)|$, the resulting edge labels are distinct.

A. Solairaju and K. Chitra [3] first introduced the concept of edge-odd graceful labeling of graphs, and edge-odd graceful graphs.

A. Solairaju and others [5,6,7,8,9] proved the results that(1) the Gracefulness of a spanning tree of the graph of Cartesian product of P_m and C_n,was obtained (2) the Gracefulness of a spanning tree of the graph of cartesian product of S_m and S_n, was obtained (3) edge-odd Gracefulness of a spanning tree of Cartesian product of P_2 and C_n was obtained (4) Even - edge Gracefulness of the Graphs was obtained (5) ladder P_2 x P_n is even-edge graceful, and (6) the even-edge gracefulness of P_n o nC_5 is obtained.(8) Gracefulness of Tp-tree with five levels obtained by java programming,(9) Gracefulness of $^nc_4$ Merging with paths,(10) A new class of graceful trees and (11) Gracefulness of $P_K \circ 2_{c_k}$, is obtained. (12, 13, 14) Used for dot net framework 3.5.

Section I: Preliminaries

Definition 1.1:

Let G = (V,E) be a simple graph with p vertices and q edges.

A map f :V(G) → {0,1,2,…,q} is called a graceful labeling if

(i) f is one – to – one

(ii) The edges receive all the labels (numbers) from 1 to q where the label of an edge is the absolute value of the difference between the vertex labels at its ends.

A graph having a graceful labeling is called a graceful graph.

Example 1.1: The graph 6 Δ P_5 is a graceful graph.

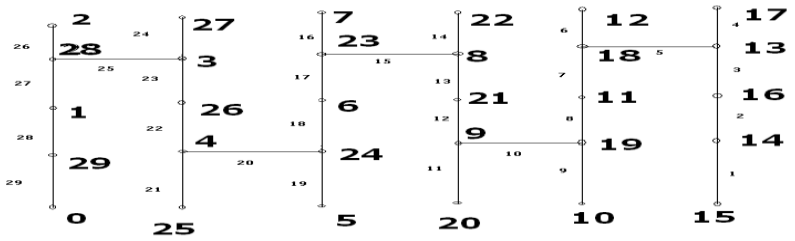

Theorem: The gracefulness of the merging graph n ** c_4 generalization:

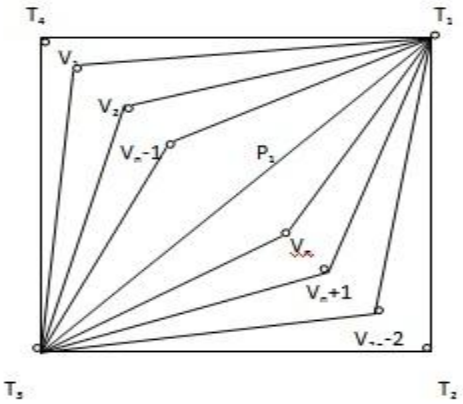

P_2 = Path of length 1,

N = Number of square.

C_4 = Cycle of 4 vertices

q = Number of edges

f (T_1) = 0,
f (T_2) = q,
f (T_3) = 1,
f (T_4) = q-2
f (v_1) = q - 4
f (v_n) = 3.

$$f(v_i) = \begin{cases} f(vi-1)-4, & for \quad i = 2,3,\ldots\ldots(n-1), \\ f(vi-1)+4, & for \quad i = n+1, n+2, \ldots 2(n-1) \end{cases}$$

Example 1.1 :

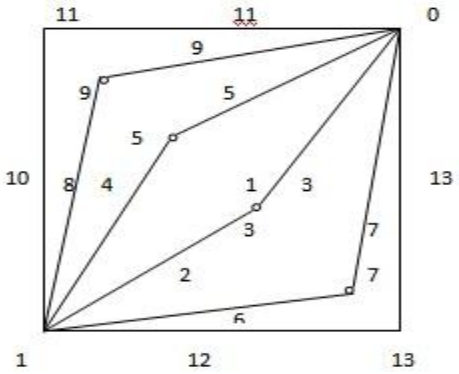

Algorithm for THE GRACEFULNESS OF THE MERGING GRAPH n ** C4 in Dotnet Language

```
using System;
using System.Collections.Generic;
using System.ComponentModel;
using System.Data;
using System.Drawing;
using System.Linq;
using System.Text;
using System.Windows.Forms;
```

```
namespace Class
{
   public partial class Form1 : Form
   {
      public Form1()
      {
         InitializeComponent();
      }
      int StartX = 5;
      int StartY = 5;
      int Width = 500;
      int Height = 500;
      private void btnLine_Click(object sender, EventArgs e)
      {
         // Declare edges and center point
         int edges =Convert.ToInt32( textBox1.Text);
         int center = Width / 2;
         int newedge = (1 + 4 * edges);
         label2.Text = "No of Edges :" + newedge.ToString();
         // Set Graphics Tool
         Graphics g;
         g = this.CreateGraphics();
         g.Clear(Color.White);
         SolidBrush myBrush = new SolidBrush(Color.Black);
         Font font = new Font("Times New Roman", 12.0f);
         Pen myPen = new Pen(Color.Red);
         myPen.Width = 2;

         // Draw center line and Rectangle
         g.DrawLine(myPen, Width, StartX, StartY, Height);
         g.DrawRectangle(myPen, StartX, StartY, Width, Height);
         //draw Inner Rectangle lines
         int nval = (center / edges);
          int sample=center;
          int sample1 = center;
         for (int i = 0; i < edges-1; i++)
         {
            sample = sample + nval;
            sample1 = sample1 - nval;

            g.DrawLine(myPen, sample, sample, StartY, Height);
            g.DrawLine(myPen, Width, StartX, sample, sample);

            g.DrawLine(myPen, sample1, sample1, StartY, Height);
            g.DrawLine(myPen, Width, StartX, sample1, sample1);

         }

        // Find Edges Values
         int q = (1+4*Convert.ToInt32(textBox1.Text));
         int T1 = 0;
         int T2 = q;
         int T3 = 1;
         int T4 = q - 2;
         int P1 = 1;
```

```
        g.DrawString(T1.ToString(), font, myBrush, Width, StartY);
        g.DrawString(T2.ToString(), font, myBrush, Height, Width);
        g.DrawString(T3.ToString(), font, myBrush, StartX, Width);
        g.DrawString(T4.ToString(), font, myBrush, StartX, StartY);
        g.DrawString(P1.ToString(), font, myBrush, center, center);
        g.DrawString(Convert.ToString(T4 - T1), font, myBrush, Width - center, StartY);
        g.DrawString(Convert.ToString(T2 - T1), font, myBrush, Height, Width - center);
        g.DrawString(Convert.ToString(T2 - T3), font, myBrush, Height - center, Width);
        g.DrawString(Convert.ToString(T4 - T3), font, myBrush, StartX, Width - center);
        int v1 = q - 4;
        int vn = 3;
        int incrementvalue = center / edges;
        int addsub = 0;
        int diff = 300;
        for (int j = 0; j < edges-1; j++)
        {
           addsub = addsub + incrementvalue;
           g.DrawString(vn.ToString(), font, myBrush, center+addsub, center+addsub);
            g.DrawString(Convert.ToString(vn - T3), font, myBrush, center +(addsub-100), center +addsub);
           g.DrawString(Convert.ToString(vn - T1), font, myBrush, center+addsub, center +(addsub-100));
           g.DrawString(v1.ToString(), font, myBrush, StartX + addsub, StartY + addsub);
           g.DrawString(Convert.ToString(v1 - T3), font, myBrush, StartY +(addsub-60),StartY+addsub+10);
          g.DrawString(Convert.ToString(v1 - T1), font, myBrush, StartX+addsub+10, StartX+(addsub-60));
           v1 = v1 - 4;
           vn = vn + 4;
        }


      }


   }
}
```

Example 1 : n is Even (n=6) :

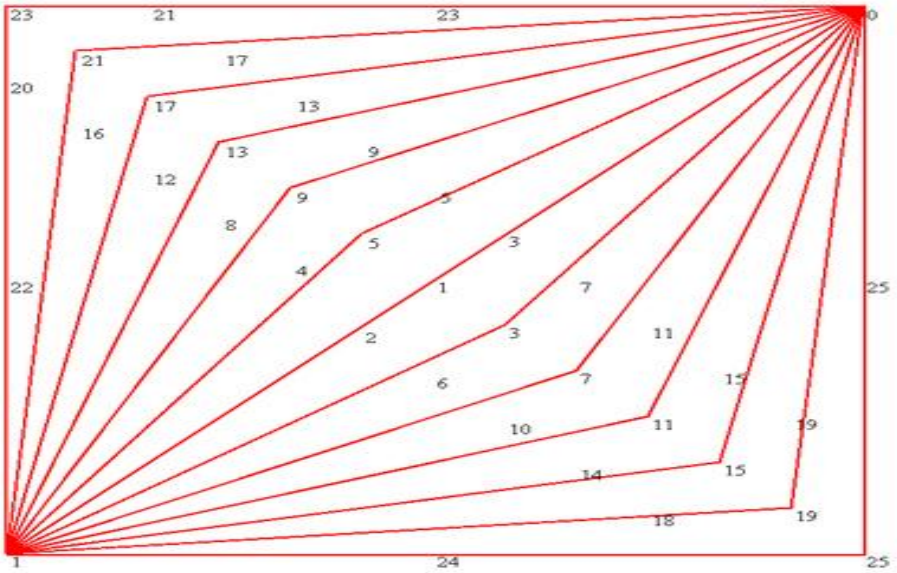

Example 2 : n is Odd (n=5)

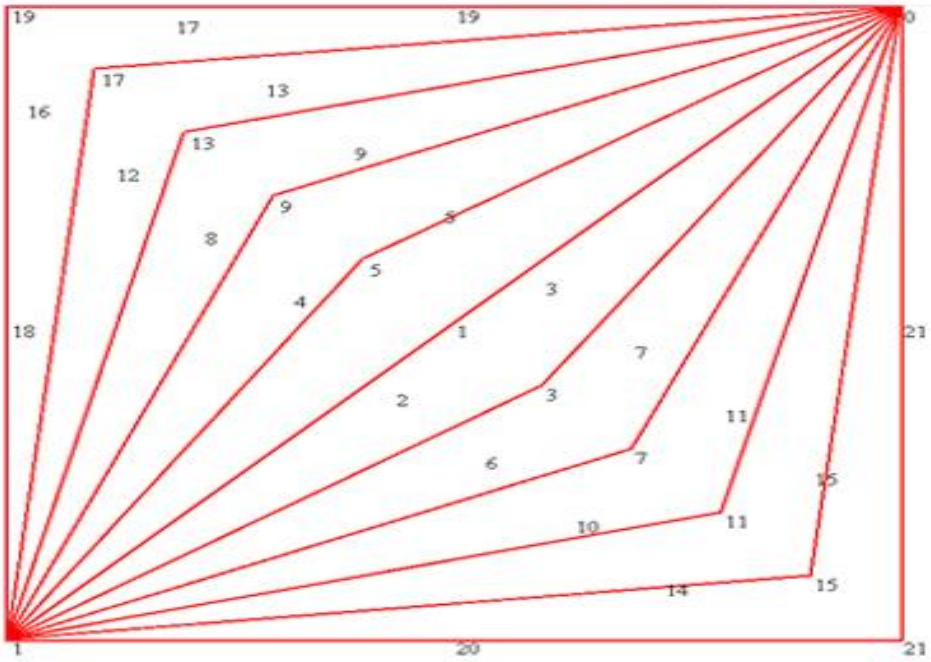

References:

[1]. R. L. Graham and N. J. A. Sloane, On additive bases and harmonious graph, SIAM J. Alg. Discrete Math., 1 (1980) 382 – 404.

[2]. A. Rosa, On certain valuation of the vertices of a graph, Theory of graphs (International

[3]. Synposium,Rome,July 1966),Gordon and Breach, N.Y.and Dunod Paris (1967), 349-355.

[4]. A.Solairaju and K.Chitra Edge-odd graceful labeling of some graphs, Electronics Notes in Discrete Mathematics Volume 33,April 2009,Pages 1.

[5]. A. Solairaju and P.Muruganantham, even-edge gracefulness of ladder, The Global Journal of Applied Mathematics & Mathematical Sciences(GJ-AMMS). Vol.1.No.2, (July-December-2008):pp.149-153.

[6]. A. Solairaju and P.Sarangapani, even-edge gracefulness of P_n o nC_5, Preprint (Accepted for publication in Serials Publishers, New Delhi).

[7]. A.Solairaju, A.Sasikala, C.Vimala Gracefulness of a spanning tree of the graph of product of P_m and C_n, The **Global Journal** of Pure and Applied Mathematics of Mathematical Sciences, Vol. 1, No-2 (July-Dec 2008): pp 133-136.

[8]. A. Solairaju, C.Vimala,A.Sasikala Gracefulness of a spanning tree of the graph of Cartesian product of S_m and S_n, The **Global Journal** of Pure and Applied Mathematics of Mathematical Sciences, Vol. 1, No-2 (July-Dec 2008): pp117-120.

[9]. A. Solairaju, N.Abdul ali , s. Abdul saleem Gracefulness of Tp-tree with five levels obtained by java programming, The International Journel of Scientific and Research Publication (IJSRP), Volume 2,Issue 12,December 2012 Edition [ISSN 2250 – 3153]

[10]. A. Solairaju, N.Abdul ali, Gracefulness of $^{n}c_4$ Merging with paths, International Organization of Scientific Research (IOSR),Volume 4,Issue 4, 20 December 2012.Paper ID:G22078

[11]. A. Solairaju, N.Abdul ali, A new class of gracefull trees. International journal of science & engineering research (IJSER),Volume 4,1st dec 2013.paper ID : I01653

[12]. A. Solairaju, N.Abdul ali, Gracefull ness of $P_K \circ 2_{c_k}$, International Journal of Engineering Research and Technology(IJERT),Volume 1,Issue :10th dec 2012,Paper ID :P12552 [ISSN 2278 – 0181]

[13]. Tbuan thai & hoang Q.Lan,".Net Framework Essentials",O`reilly,2nd Edition 2007.

[14]. D.Nikhil Kothari,",.Net Framework",Addison-Wesley Professional,2008.

[15]. Christian Nagel et al,"Programming in C#",Wrox Publication,2001

A Novel Ultra High Speed D.C Motor Protection Using NI Lab View

Raj Kumar Mishra[1], Dr. S. Chatterji[2], Shimi S.L[3]

[1]*M.E Student, Electrical Engineering Department, NITTTR, Chandigarh, India*
[2]Professor and Head, Electrical Engineering Department, NITTTR, Chandigarh, India
[3]*Assistant Professor, Electrical Engineering Department, NITTTR, Chandigarh, India*

Abstract

This paper presents a novel concept of D.C motor protection using NI Lab VIEW. The researcher has designed highly powerful real time D.C motor protection software by using NI Lab VIEW, which is proficient of protecting D.C motor within fraction of seconds against different types of faults, giving the real time protection, hence giving a brilliant solution to virtual instrument based protection system. Now a days due to increase in complication in motor use, there was a vital necessity of motor protection system which can constantly monitor and control a very large motor system. That is why high speed, high accuracy, real time solutions are required for measuring D.C motor protection. This paper presents a high precision and high fidelity approach based on NI ELVIS Instruments and NI Lab VIEW for monitoring and protection of D.C motors.

Keywords: Lab VIEW, Virtual Instruments, D.C motor protection, D.C motor monitoring, fault analysis

1. INTRODUCTION

D.C Motors are the main building block in different industries. Their malfunction will not only lead to repair or substitution of the motor, but also effect major financial losses due to unpredicted process downtime. Reliable protection of d.c motors is essential for reducing the motor malfunction rate and prolonging a motor's lifetime [1]. Conventional d.c protection techniques are not so efficient as compared to the state-of-the-art of computerized highly efficient NI Lab VIEW based protection system. In this paper the investigator has developed fully computerized d.c motor protection which not only protects the motors against different faults but also shows the type of fault on the front panel. As soon as fault portion is rectified it again starts the proper functioning of motor and protects it against abnormal conditions all the times.

2. NEED AND IMPORTANCE OF NI LABVIEW BASED PROTECTION SYSTEM

To reduce the damage number and the failure rate of motor, improve the reliability of motor operation, intelligent motors monitoring protection system should be developed [2]. As the cost of motors is extremely high, so high fidelity and high performance, fully automatic protection system is required. This said system fulfils all the conditions of excellent protection system at nominal cost [3].

3. DC MOTOR PROTECTION USING NI LABVIEW

The software is divided into following four sections:

(i) Test panel section

This section is the input section. It is shown in Fig.1. In the test panel 10 different types of protection system is given. The basic range is divided in the span of 0-10 units. It can be changed as per requirement from the front panel.

(ii) Preset value section

It is shown in Fig.2. It has also 10 different preset controls corresponding to the test panel. The value of preset control can be changed from the front panel.

(iii) Type of fault section

This section is the indicating system for any type of fault. The faulty section gets red and normal working section is represented by green signal. It is shown in Fig.3

(iv) Waveform section

It is shown in Fig.4. This section shows different values of test panel and preset panel. It also contains on/off switch, motor direction reversal switch etc.

4. CASE STUDY

The benefit and utilization of this software is explained in this case study.

Case 1: Test value is greater than preset value

In this case, the control for which test value is greater than preset value, that type of protection will work and the motor will stop to run. The type of fault section will indicate that control by red colour. As soon as the fault will be rectified it will again become green and motor will start to run.

Case 2: Test value is less than or equal to preset value

This case indicates that there is no fault in any section and all indicators will glow green. This is shown in Fig. 5. In figure .5, all the waveforms are shown in test and preset plot. The motor is also running.

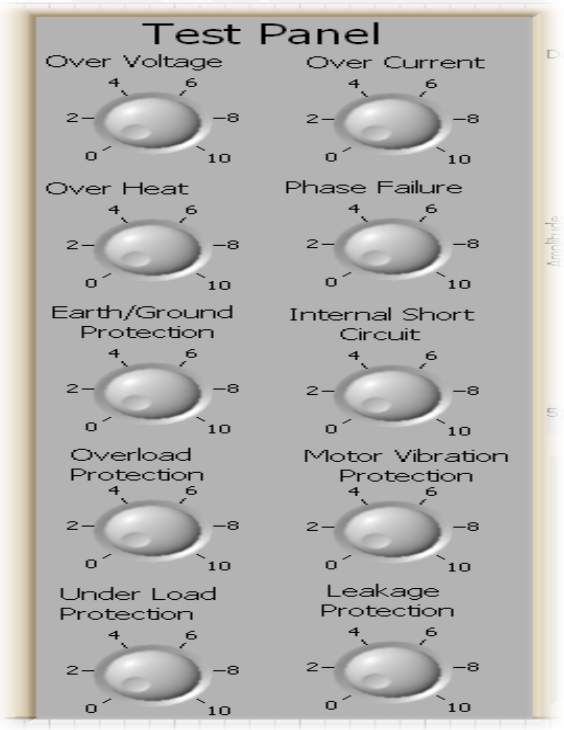

Fig. 1 – Test Panel

The direction of motor can also be changed from the front panel. There is also a provision to control the speed of motor.

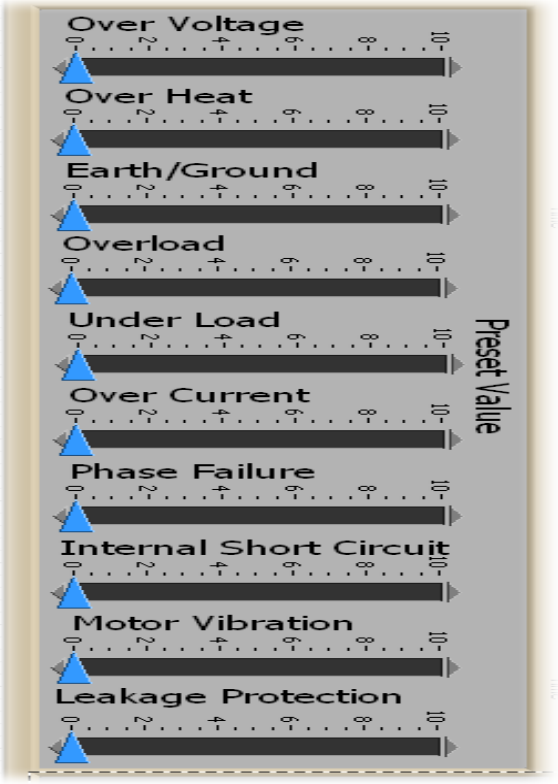

Fig. 2 – Preset value panel

5. HARDWARE AND SOFTWARE INTERFACING

The investigator has successfully tested prototype model of the above software. NI ELVIS and DAQ card and different sensors has been used to acquire different value of test panel. Preset value is set as per the requirement. As soon as the test value acquired from online data is greater than the preset value, the software stops the motor and protects against different type of faults [4], [5], [6].

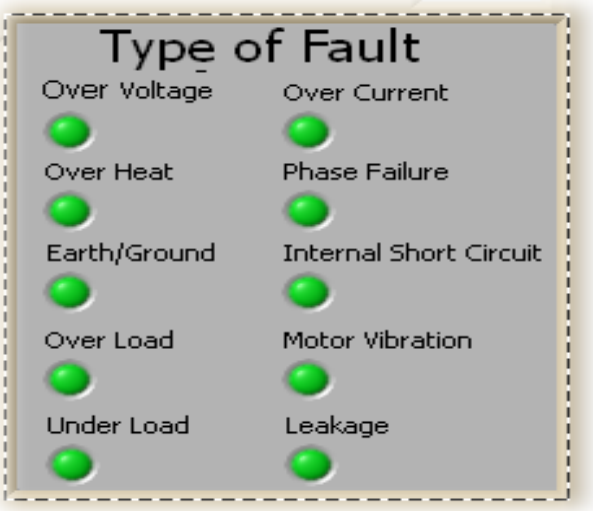

Fig. 3 – Fault monitoring and alarming

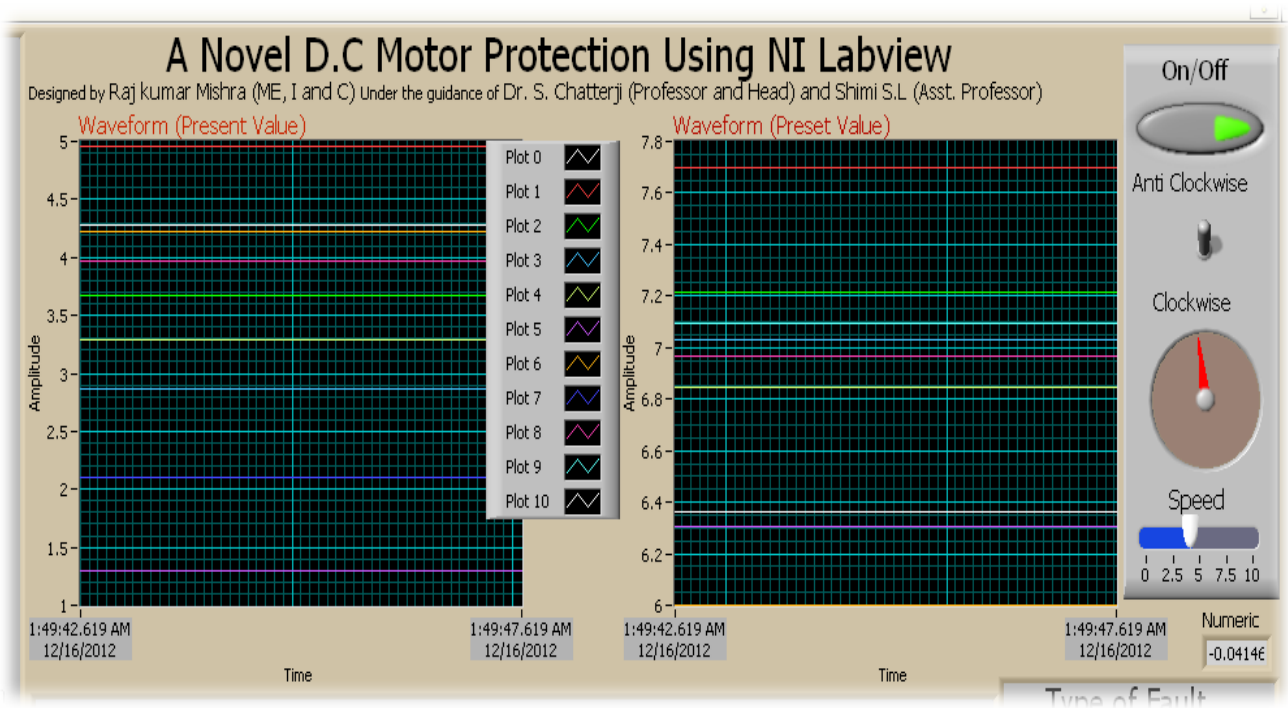

Fig. 4 – Waveforms of test and preset panel

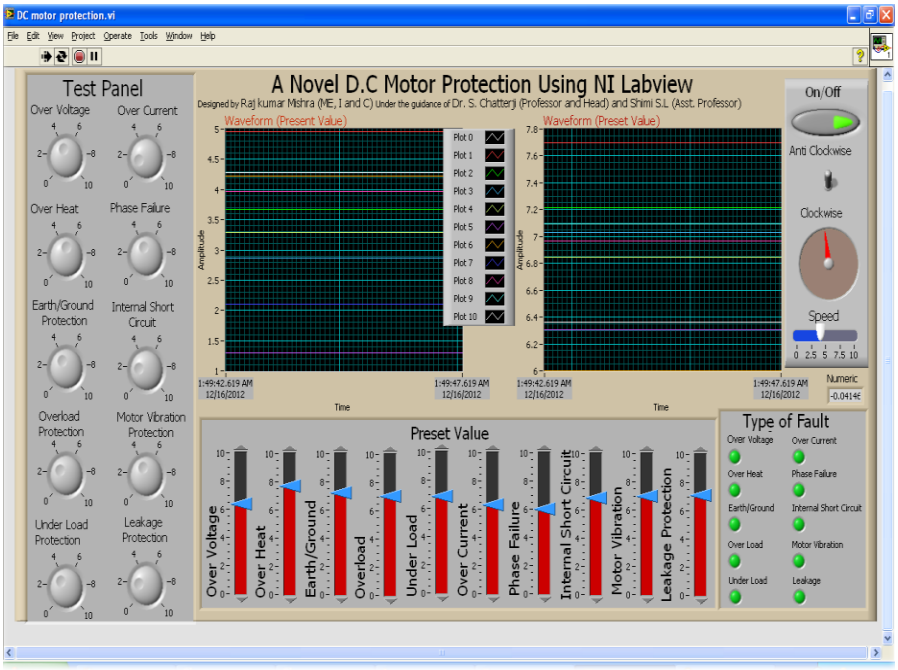

Fig. 5 – Complete functioning software

6. CONCLUSION

The introduction of this software is a revolutionary step in the field of d.c motor protection. Some major points which are very useful regarding this software are:

1. It gives highly accurate result with ultra high speed. So it can be an excellent choice for advance and accurate d.c motor protection.
2. It saves very costly motors. Therefore it can be used in industries very efficiently.
3. Its state of art of protection system makes it exceptionally powerful and very much prominent in the industrial application
4. It can be also used as online monitoring and protection tool.

REFERENCES

[1] Pinjia Zhang, "Active stator winding thermal protection for AC motors ", *IEEE Pulp and Paper Industry Technical Conference.*, 21-26 June, 2009
[2] Gaohua Liao, "Intelligent Monitoring and Overheating Protection System for Motor ", IEEE Conference on *Computing, Control and Industrial Engineering (CCIE)*, 5-6 June 2010
[3] Lin, P.I, "A PC-based measurement and control system for DC motors ", IEEE Conference publication, 7-12 Oct. 1990
[4] Johnson, Gray W., "*LabVIEW Power Programming*", McGraw-Hill Professional Publication, 1998
[5] Riccardo de Asmundis, "*LabVIEW- Modeling, Programming and Simulations*", InTech Publication, 2011
[6] NI Instruments, "*NI ELVIS hardware user manual*" NI Instruments, August 2008

Reengineering of relational Databases to Object Oriented Database

Mr.R.S.Mawale[1], Prof.A.V.Deorankar[2], Prof. P.U. Malve[3]

[1] M.Tech. Scholor, (CSE), Govt. College of Engineering, Amravati, Maharashtra, India
[2] Associate Professor, Dept. of CSE, Govt. College of Engineering, Amravati, Maharashtra, India
[3] Lecturer, Government Polytechnic, Murtizapur , Dept. of Computer Engineering, Maharashtra, India

Abstract:

Many information systems use relational database systems for efficient sharing, storage, and retrieval of large quantities of data. On the other hand, object-oriented programming has been gaining wide acceptance in the programming community as a paradigm for developing complex applications that are easy to extend and maintain. This paper discusses development of an integrated environment which maps a relational schema to an object-oriented schema without the need to modify the existing relational schema and providing a platform for migrating data from relational database to object oriented database.

Keywords: Schema Mapping, RDBMS, OODBMS, Reengineering

1. Introduction

Relational database management systems (RDBMS) provide a variety of tools and services for data management. There are many tools that interface with RDBMSs to enable end-users to carry out reporting, querying, and other data analysis activities easily. On the other hand, object-oriented programming has been gaining wide acceptance in the programming community as a paradigm for developing complex applications that are easy to extend and maintain. Developers typically implement object-oriented applications using object-oriented programming languages such as C# and Java. These applications use a schema made up of object classes and relationships between those object classes. Each object has a set of attributes. The value of an attribute could be another object itself, thus giving rise to complex objects. The main problem arises when the data corresponding to such objects are persistent in a relational database. The problem is due to incompatibility between relations and objects. At first, a solution for this problem may seem to be to use an ODBMS instead of RDBMS. If an ODBMS is managing the persistent data, the objects do not lose their structure after the application stores them in the object database. Moving to an ODBMS might mean throwing away all of the old ("legacy") data and applications. Most users of databases will not accept such a solution. They wish to be able to run their existing applications on existing databases and have access to the same data from object-oriented programs, too. Therefore, we need special techniques to convert the data that is residing in a relational database to a format that is suitable for access and manipulation by object-oriented applications.

2. Literature review

The problem of migrating data is present in almost every application development process, such as data warehousing and application integration. The algorithm implements process of migrating data involves firstly the mapping between the structures of the source and target databases and secondly the migration of the data from the source to the target [3].

The problem is how to effectively migrate existing RDBs, as a source, into OODB/ORDB/XML, as targets, and what is the best way to enrich and maintain RDBs' semantics and constraints in order to meet the characteristics of the three targets? Existing work does not appear to provide a complete solution for more than one target database. We tackle this question by proposing a solution for migrating an RDB into the three targets based on available standards [4].

One general approach to migrate to object technology is to divide the process into two phases, where the first one transforms the relational into an object-oriented schema and the second one migrates the data into the object-oriented database system discussed in [5].

The goal of re-engineering is to mechanically reuse past development efforts particular relational databases (RDBs).in order to reduce maintenance expense and improve software flexibility [4]. The object behavior of eight Java programs including four real-world Java object oriented database management systems and a counterpart of four real-world Java programs are analyzed in [6]. A technique for transferring query optimization techniques, developed for relational databases, into object Databases. This technique for ODMG database schemas defined in ODL and object queries expressed in OQL. The object schema is represented using a logical representation (Datalog) [7].

3. Analysis of problem

Moving to an ODBMS might mean throwing away all of the old ("legacy") data and applications. Most users of databases will not accept such a solution. They wish to be able to run their existing databases and have access to the

same data from object-oriented program.

Thus we need to implement a system that builds an understanding of a given conventional database by taking these characteristics as input and produces the corresponding object-oriented database as output. Finally, we handle the migration of data from the conventional database to the constructed object-oriented database.

The Primary objectives of proposed work are as follows.

1. Study the automatability of the relational-to-OO schema mapping process.
2. Define an interactive process for mapping an existing relational schema to an object-oriented schema.
3. Develop an interactive system to validate proposed work

4. System architecture

The architecture contains two major components needed for fulfilling our aim. The first component deals with mapping the relational schema to an object-oriented schema. The second component deals with the mapping between the relational data and objects.

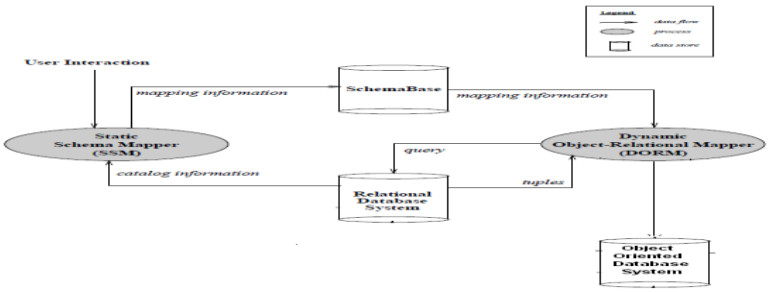

Figure 1. System Architecture

Schema Mapping

The static schema mapping process is a two-phase process. In the first phase, the relational schema is adjusted and transformed into another virtual relational schema that has some specific properties. In the second phase, object-oriented structures are extracted from the virtual relational schema.

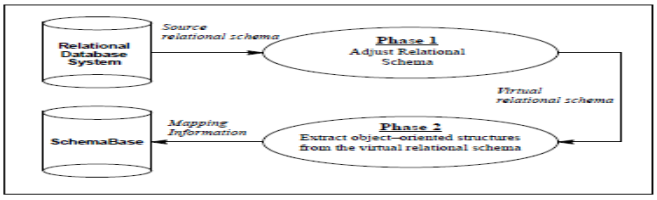

Figure 2.Two Phases of Static Schema Mapping

Phase I: Adjusting the Relational Schema

There are four specific aspects that are addressed during phase one. They are as follows:

Step 1. Eliminate 2NF relations and replace them with new 3NF virtual relations.

Step 2. Create virtual subclass relations for widow super class relations

Step 3. Create virtual superclass relations for orphan subclass relations.

Step 4. Eliminate multi-valued attributes and replace them with new 3NF virtual relations.

Phase II: Generation of the Object Schema

At the end of phase one of the schema mapping process, the relational schema has been adjusted to a form in which schema mapping rules can be applied uniformly.

Step1. Identifying Object Classes:

Those relations that correspond to object- classes must be identified.

Step2. Identifying Relationship:

There are three types of relationships that can be represented in an object model. They are associations, generalizations specializations, and aggregations.

Identifying each of these constructs constitutes a step in the mapping process.

Identifying Associations. Since the object model allows associations to be modeled as classes, we must either establish a simple association between two object classes or identify relationships where the associations are modeled as classes.

Identifying Inheritance. Inheritance structures capture the generalization and specialization relationships between object classes that have been identified so far.

Identifying Aggregation. The aggregation relationship models the composition of one object with other objects. such complex object must be identified. The difference between aggregation and association is that the former involves existence dependence of the sub-object on the whole object. For example, a door object, which is a part-of" of a car object, cannot exist if the car object does not exist. On the other hand, the enrollment of a student in a course is an association rather than an aggregation because the student and course objects can exist independent of each other.

Step 3. Establishing Cardinalities : Establishing the cardinalities of associations is important in order to facilitate the implementation of the object schema in a given programming language (e.g., C#). The different possible cardinalities are one-one, one-many, and many-many.

5. Conclusion

We will implement the architecture having two phases in the data mapping process; one mapping procedure specifies the data mapping between the original relational schema and the adjusted relational schema. The second mapping procedure specifies the data mapping between the adjusted relational schema and the object schema. The data mapping procedures have been specified using relational algebra for each new virtual relation that is created during phase one of the static schema mapping.

References.

[1] Ramanathan, C. Providing object-oriented access to a relational database. In Proceedings of the 32nd ACM annual southeast conference held in Tuscaloosa, Alabama, March, 1994.

[2] Andersson M. Extracting an entity-relationship schema from a relational database through reverse engineering. In Proceedings of the 13th international conference on entity relationship approach held in Manchester, UK, December, 1991

[3] Elton Manoku, Guido Bakema, A fact approach on Data Migration published in Academy of Communication and Information Technology HAN University of Applied Sciences, The Netherlands In June 2006

[4] Abdelsalam Maatuk, Akhtar Ali, and Nick Rossiter , A Framework for Relational Database Migration published in School of Computing, Engineering & Information Sciences Northumbria University, Newcastle upon Tyne, UK in 2001

[5] Andreas Behm, Andreas Geppert, Klaus R. Dittrich2 ,On the migration of relational schemas and data to object-oriented database published in Proceedings of the 5th International Conference on Re-Technologies in Information Systems, Klagenfurt, Austria, December 1997

[6] William J Premerlani, Michael R Blaha, An Approach for Reverse Engineering of Relational Databases published in May 1994 Communications of the ACM

[7] Chia-Tien Dan Lo, Morris Chang, Ophir Frieder and David Grossman, The Object Behavior of Java Object-Oriented Database Management Systems published in the Proceedings of the International Conference on Information Technology: Coding and Computing (ITCC.02) IEEE 2002

[8] John Grant, Jarek Gryz, Jack Minker, and Louiqa Raschid, Logic-Based Query Optimization for Object Databases published in IEEE Transactions on knowledge and data engineering, vol. 12, no. 4, July/August 2000.

Authors Profile:

Mr.R.S.Mawale has received his B.E. degree from Govt. College of Engineering, Amravati, India. He is currently pursing his M.Tech in Computer Science & Engineering from Govt. College of Engineering, Amravati, India. He has published one paper in International Journal.

Prof A.V.Deorankar has received his M.E. degree in Electronics Engineering from Govt. College of Engineering, Amravati, India and pursing his PHD from Computer Science. He has 19 years experience in Teaching in various Government engineering Colleges in Maharashtra. He has published nine papers in national and seven papers in international journals. He has also patent of one paper. His area of research includes Computer network, Web Mining. Currently he is working as an Associate Professor at Govt. college of Engineering, Amravati, Maharashtra, India .

Prof.P.U.Malve has received His M.E.Degree in Information Technology from Sant Gadegebaba Amravati University in 2011. He has published Two papers in National and Three papers in International Journals. He has Five years experience in teaching various Government engineering Colleges & Polytechnics in Maharashtra. His area of research includes Computer Networks, Software Engineering, Network Security He is currently woking as a Lecturer in Department of Computer Engineering, at Government Polytechnic, Murtizapur, Maharashtra India

Hand Palm Vein Authentication by Using Junction Points with Correlation Method

S.Sharavanan[1], Dr.A.Nagappan[2]

[1]*Research Scholar, Vinayaka Missions University, Salem, TN, India*
2Research Guide & Principal, V.M.K.V Engineering College, Salem, TN, India

***Abstract*:**

Hand palm vein authentication is a biometric modality, which can be used to identify a person. In this paper, palm vein authentication by using Junction point with correlation method is proposed. The process of training and testing the palm vein will take less time to produce the output Our proposed method effectively reduce the processing time and increase the accuracy rate.

Keywords— Biometric, Junction point, Hand palm vein, Correlation method.

I. INTRODUCTION

In the digital world, it is very difficult to maintain our personal records and securing data from intruders. Today every person can easily access their information anytime and anyplace. At the same time with the help of modern technology and advanced techniques unauthorized access of other persons is also increased. To overcome these problems highly secured and more accurate hand palm vein authentication is proposed.

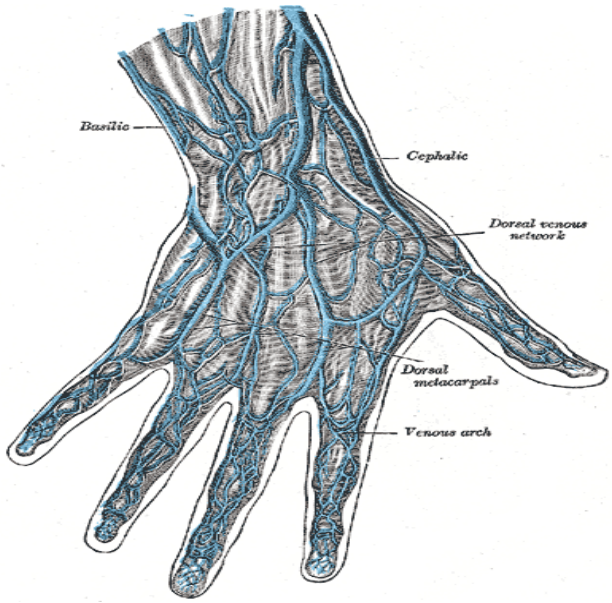

Fig1: Major veins of the hand area (Figure 573 in [15]).

The personal identification system, capturing the palm vein pictures are improved suitably and shared of the quality performance. The palm vein positions are acknowledged and the link positions, which take into their positions and direction of palm veins, are removed to symbolize the merged skin textures. The enthusiasm of the investigation is the link point including the interconnecting spots of the palm vein outline areas are not an aspect in moreover of the two outlines and it presents a new quality aspect that can be performed for detection. Connecting point demonstration significantly diminishes the breathing space have to compared as the frontage of the exhibition [2].

A person has a rest of his/her wrist, and on a quantity of devices, the middle of his/her palm, sensor can produce a infrared light ray from scanner which passes through the palm rest in device with few seconds. Nothing like the skin, through which nearest infrared light ray passes and then take up the junction point line edges of blood cells in the internal surface elegant through the vein, enlightening the blood cells, reason it able to be seen in the scanner. Consequently the infrared ray light are unseen to the sensor which is not perform to take up, blood cells include vein and vessel. Palm vein

image captured by the camera, which take pictures of the light ray range, show as a black set of connections, dazzling the palm layer sample against the lighter backdrop of the palm vein pictures [12].

II. PREVIOUS RESEARCH

Palm Vein substantiation is getting higher and contentious development work in which self-determination groups communicate anxiety in excess of confidentiality and uniqueness concerns. Today [3], biometric acts and policies are being progressed and some other production principles are performed very well.

Identification of a human being through his body involving that the human being body is superficially well-known personality structures of an extraordinarily influential tool for personality administration of Biometric appreciation [4].

Palm vein verification system established as a fresh biometric techniques employing the vein prototypes surrounded by one's palms for delicate recognition. Vein prototypes are dissimilar for each palm vein and for each human being [6] is concealed bottom of the skins exterior position, falsification is tremendously not easy. These exclusive characteristics of palm vein model detection set is separately from preceding appearances of some other methods and enclose led to its embracing the foreign country economical associations as their most recent protection knowledge.

The hypothetical basis and complexities of palm vein identification is exposed at primary level. Then, [8] the doorsill feature extraction process and contraction technique of palm vein figures are intensely deliberated and an innovative doorsill segmentation process and an enhanced provisional contraction techniques are going to be developed. The scheme of palm vein image attributes are removing based on the finishing ends and tripping ends are deliberated in the beginning, and the corresponding techniques based on spaces is used to go with the palm vein images.

Identification systems [9] are offering biometric procedures using extraction of palm vein constructions. For conservative procedures, it is essential to utilize luxurious-quality of figures, which insist of expensive collection of procedures. The implementation way is to making to inexpensive plans are probable. The product of this method is demonstrates that they could be extracted the palm vein arrangements are as profitably as using luxurious quality of figures.

The palm vein authentication system using the palm vein verification tool that uses blood container prototypes as individual categorizing aspects. Achievement of some classification systems are allows as an appliance in open places or in atmospheres [7].

Palm vein verification system consists of miniature Palm vein scanner tools that's very easy to handle and standard to use one and all [11], extremely wonderful and rapid. Just put our palm on the superiority tool of scanner and inside a few instants it interprets your restricted coating samples. A palm vein image is full and palm model is recorded into the file.

III. PROPOSED RESEARCH

In a new palm vein authentication algorithm proposed in the basics of junction points and correlation method. In this method palm vein pictures are captured in accurate manner with the help of vein scanner at the aspect level. The palm vein outlines are removed the joint pixels, which take into their arrangement and direction of the palm veins, which are removed to symbolize the merged skin textures. The enthusiasm of the investigation is the link point including the interconnection spots of the palm vein outline areas are not an aspect in moreover of the two palm vein outlines and it presents a new quality aspect that can be performed for detection. The below algorithm steps operating for our proposed method.

A. Algorithm steps:

Step1: To read the vein Image from scanner

If image name==0

Return

End

Step2: Extracting the inner layer of the palm vein by using segmentation process

Step3: Removing the noise by using wiener function

wiener2 (I, [M N])

I-Input Image

M-Mean

N- Standard Deviation

Step4: To truncate the background portion using Region of Interest
Step5: Picking out the inner layer of vein edges for junction points by applying mallet filter edge
Step6: Applying a mallet filter to a region in an image for detecting the veins
Step7: Identifying the junction points in the palm vein images by using the correlation method
Step8: Palm vein authentication, whether to finding the person is Matching person or non-matching person based junction points

```
c=corr2 (I, img);
If(c==1)
        Msgbox ('Matching')
        Else
        Msgbox ('Non-Matching')
End
```

B. Segmentation

The segmentation technique is widely used to segment the input palm vein image into meaningful regions. Region segmentation algorithm is widely preferred because of its additional flexibility which allows pixels which belong to multiple classes with varying degrees of membership.

This function calculates and plots the intensity values along a line segment or a multiline path in an image. The line segmentation is taken by specifying their coordinates as input arguments.

C. Removing Noises

In this method we are going to reduce the noises by using wiener filters. Filtering is used to remove the unwanted noises in an image. The filtering is a process which is used to remove the noises and improve the quality of the image. This procedure can be applied for all scanning vein images.

D. Image registered and Region of Interest position

Arrange the hand palm veins placed in the slot of screen, figure alignment is required. In the proposed method sample, inflexible check can be much appropriate, because the essential division of the palm captured is exclusive of any get in touch. Hence, a routine non-rigid image registration method is taking up. These model transformation between two figures as close at hand affine, but internationally flat. The representation also clearly demonstrates the limited and general variations in image intensity values. This advanced technique is built upon the discrepancy of multi-scale element, tolerating it to detain both huge and little-size alterations.

The quality level of the combination can be done, matching attains or resolution level with different fusion models. Most of the previous information's on multi-modal alert on merging the results of variety of classifiers at the choice of intensity values. The palm vein are fused at the matching attain range for user identification. The palm vein is extracted the line based on the connecting regions, the system was tested on a database with hand palm vein images. The experimental result gives you an idea about the effectiveness of the method in terms of the detection rate is very close to the maximum level.

E. Junction Point (JP) Detection

The connecting point is meant by the pixel where two or more outlines are meeting and the intersections are used as the prominent skin textures for entity categorization procedures or to get better boundary recognition. In progress intersection of investigation techniques consist of difficulty, which affects a cover in excess of an associate- province of the figure, and dispersal, which increase terrain sequences from pixel-to-pixel based on a rest of regulations. In this technique, the connecting position is described as the joining pixel of the more than three contour sections and a rapid connecting detector is developed. The connecting ends of the palm vein contour sections coupled with their guidelines of palm veins are calculated. Alteration numbers are used to identify the intersection utilities. The boundary detections are slighted using morphological functions. After that, the interior position used is surrounded by the 3x3 neighborhood connection. Here the 3x3 pixel regions are demonstrated as follows:

The crossings point of the P is defined as

$$S=\sum^{8}_{i=1} |f(Zi+1)-f(Zi)|,\ f(Z9)=f(Z1) \qquad (1)$$

Where f (y) is the double value (0 or 1) of point at y. The centre point of Z is measured to be a connection end if Z is an edge point and if S>= 6

F. Cross Correlation on Join Point Extraction

Cross correlation is the best method for calculating the two Join Extractions Point in

$$Rxy=X^i\ u\ Y^i\ u/\sqrt{1}|X^i\ u||Zi||Y^i\ u| \quad (2)$$

The above formula has been explained in the following manner : the values of X variable `are pre-defined and the Y variable is resulted values. If both particular values (i.e.) the value of Rxy is equal to 1, then the particular person is an authorized person. In this proposed work, the resulted value of Rxy is 0.98 which means that the person is an authorized person.

The skin textures of merged palm vein pictorial representations are as a set of connection ends which are belongs to the palm vein contour direction at each texture position.

Whole constraints are as compared with the exterior illustration, e.g. palm vein, or contour image. Given a set Z of joint ends, described as model position, and a reservation position of Q of k joint point n. 24 dot pixels are needed to store the direction. Therefore, the whole images are needed to store for 5n bytes only. The mathematical outputs as of our file demonstrate with the intention of average numbers of joint ends is about 28. The overall necessity is [5x28] =140 bytes.

The verification value of the outline similarities are computed as follows:

$$SS=2/Na+Nb\ \sum^M\ i=1\ \sum^N\ i=1\ La \cap Lb \quad (3)$$

The open database contains palm vein images and the logical operation "AND"`; Na and Nb are the amount of the contour ends in the prototype and the experimental palm vein pictures are correspondingly. SS is connecting between 0 and 1. The contour is symbolized as the finishing end and direction of sequence code in the contour on the end. Suppose the length of a palm line is S, the length of the chain code will be (S±1). Since 3 bit are needed to store a direction code (zero, one, and seven), three± (S-1) bits needed to correspond to the whole chain code. The direction of end pixel one needs two byte to be accumulated. Therefore, total of [3 + 2± (S±1) /8 bytes are needed to store each palm vein line. The mathematical outputs from our file demonstrate that the overall records of palm vein outline are about 37 and the standard distance of the contour is about 21 points. The standard necessity is 37 x [2+3x (21-1)/8] =351.5 bytes.

G. Authentication mechanism

Hand Palm vein verification uses the biometric sample of person palm as own recognition records. A palm has a joint ends and edge detection is more difficult of biometric sample and consequently containing prosperity of make different features for private detection. The hand palm vein is a best part of the human body for this knowledge, its normally does not have hair in the palm which can be a problem for get something on the film biometric sample, and it is less risk to change in a skin color. When the image is captured by using infrared ray in the scanner take up light ray enclose a wavelength absorbs the deoxygenated hemoglobin in the blood flow, during the palm vein testing. Based on this feature, the vein authentication device translates the black lines of the infrared ray image as the junction point sample of the palm, and then matches it with the previously registered junction point value of input and base pattern of the individual. The contour extraction and the joint ends are beginning from left hand side to right hand side. We are going to take the 3, 10 and 27 joint ends in palm vein descriptions correspondingly. Pattern of the feature extraction is a large amount of connecting pixels can be identified in the merged aspect than one in the palm vein only. There are three, ten and twenty seven connecting ends in the palm vein image and merged images recognizing the testing period.

IV. EXPERIMENTAL RESULTS

A. Input image and Segmentation

Get an input image from the scanner and extract the inner layer of the hand palm vein image by using segmentation process. Image creates an graphics object by interpreting each element in a color map.

Wiener de-convolution can be used effectively when the frequency characteristics of the image and additive noise are known, to at least some degree. In the absence of noise, the Wiener filter reduces to the ideal inverse filter. Remove the noise, by using the wiener function.

Fig2: Palm Vein Segmentation

B. Region of Interest (ROI)

Fig3: ROI performance of palm vein image

The registered palm vein image appears ROI with the base image is to truncate the background portion by discarding any areas that would extrapolate beyond the extent of the base image.

C. Intersecting point

Intersecting palm image is pick out the inner layer of vein edges for calculate junction points with correlation method by applying mallet filter edge.

Fig4: Intersecting point of Palm vein images

D. Region growing of palm vein Lines (Mallet filter)

Region growing is the process of applying a filter to a region in an image, where a binary mask defines the region.

E. Junction point identification

Easily identify the junction point in the palm vein image with the identifying the intersect point of two more lines.

An account of connection points stands for chronological pronouncement points in the situation course map based on the chronological data qualified to the condition movement. The sample registered palm vein is accumulating into the folder beside through the individual information of the testing periods.

To select control points in two related images which are used to identify the meeting point in the hand palm vein. Input is the figure that desires to be distorted to transport it into the organizing scheme of the base figure. Input and foundation points of palm vein can also be changeable that embrace grayscale, true color, or binary images, or sequences that recognize files restraining these images. The proposed system of recognized processing period of time in (sec) is less than previous method.

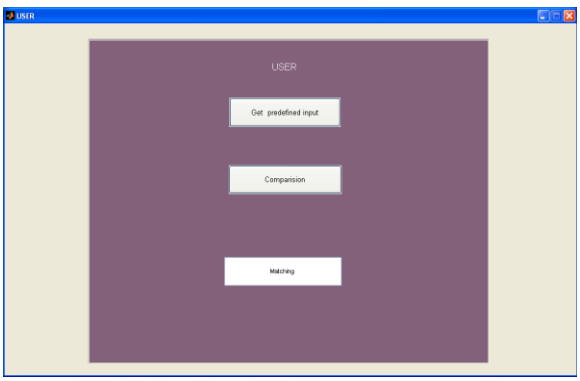

Fig2: Palm vein Verification performance

TABLE1:

THE PERFORMANCE OF EXISTING VS. PROPOSED SYSTEM IN PALM VEIN AUTHENTICATION ACCURACY AND TIMING PERFORMANCE

Performance	Palm image	Process time(sec)	Accuracy
Palm Vein authentication using curve let and neural networks	500	13ms	82%
Palm Vein authentication using line Tracking Algorithm	500	12ms	85%
Palm vein authentication using Gabor filter and SIFT	500	10ms	90%
Proposed	500	8ms	94%

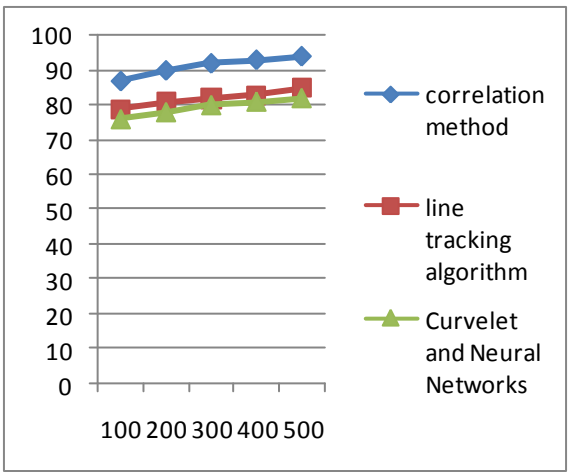

X Axis-Total No of Palm Images Y Axis-Authentication performance in percentage

Fig 3: Graphical representation of Existing vs. Proposed Authentication Performance Results

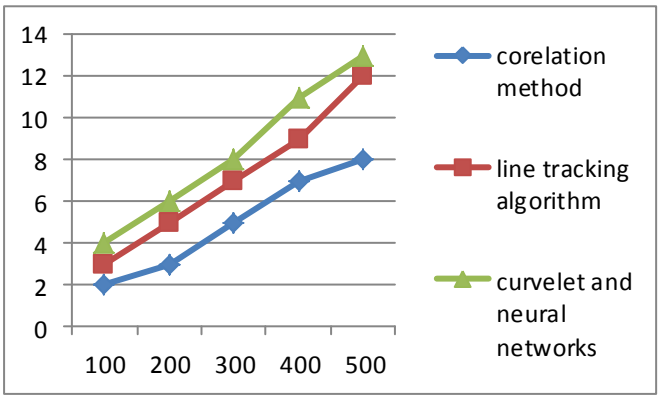

X Axis-Total No of Palm Images Y Axis-Mille seconds

Fig4: Graphical Representation of Existing vs. Proposed Authentication Timing performance in Mille seconds

V. CONCLUSION

The hand Palm vein authentication using junction points with correlation method easily find out the person's authentication. The advantage of the proposed system is less processing time and high accuracy than the existing system

REFERENCES

[1] Anil K. Jain & Arun Ross Sharath Pankanti, "A Prototype Hand Geometry-based Verification System", Washington D.C., pp.166-171, March 22-24, 1999.

[2] Chin-Chuan Hana; Hsu-Liang Chengb, Chih-Lung Linb and Kuo-Chin Fanb, "Personal authentication using palm-vein features", aiwan, Republic of China Received 21 December 2001.

[3] Chih-Lung Lin and Kuo-Chin Fan, Member, "Biometric Verification Using Thermal Images of Palm-Dorsa Vein Patterns", no. 2, February 2004.

[4] Ying-Han Pang, Andrew Teoh Beng Jin, and David Ngo Chek Ling, "Palmprint based Cancelable Biometric Authentication System", World Academy of Science, Engineering and Technology, 9th June, 2005.

[5] Masaki Watanabe, Toshio Endoh, Morito Shiohara, and Shigeru Sasaki, "Palm vein authentication technology and its applications", sept 19-21st, 2005 hyatt Regency crystal-USA.

[6] Ajay Kumar1, David C. M. Wong1, Helen C. Shen1 and Anil K. Jain 2, "Personal Verification using Palmprint and Hand Geometry Biometric", Engineering, Michigan State University, East Lansing, MI 48824.(2007).

[7] Shinichiro Watanabe, Toshiyuki Tanaka and Eizaburo Iwata, "Vein emphasis filter for Biometric Authentication", Sept. 17-20, 2007, Kagawa University, Japan.

[8] Jian-Gang Wang and Wei-Yun Yau, "Andy Suwandy Fusion of Palmprint and Palm Vein Images for Person Recognition Based on "Laplacianpalm" Feature", 1-4244-1180-7/07/$25.00, 2007.

[9] shi zhao, yi-ding wang and yun-hong wang, "biometric, Identification based on low-quality hand vein pattern images", Proceedings of the Seventh International Conference on Machine Learning and Cybernetics, Kunming, 12-15 July 2008.

[10] M.Deepamalar and M.Madheswaran. "An Improved Multimodal Palm Vein Recognition System Using Shape and Texture Features", Vol. 2, No. 3, June, 2010 (1793-8201).

[11] Jiansheng Chen, Yiu-Sang Moon, Ming-Fai Wong and Guangda Su, "Palmprint authentication using a symbolic representation of images", Image and Vision Computing ,28Jan (2010) 343–351.

[12] Ishani Sarkar, Farkhod Alisherov, Tai-hoon Kim, and Debnath Bhattacharyya, "Palm Vein Authentication System: A Review", International Journal of Control and Automation Vol. 3, No. 1, March, 2010.

[13] Aythami Morales, Miguel A. Ferrer and Ajay Kumar, "Improved Palmprint Authentication using Contactless Imaging", 978-1-4244-7580-3/10/$26.00 ©2010 IEEE.

[14] K.krishneswari and S.Arumugam, "Intermodal feature fusion using wavelet for palmprint authentication", Vol. 3 No. 2 Feb 2011.

[15] GRAY, H. Anatomy of the Human Body, 20 ed. Lea and Febiger, 1918. Retrieved from Wikimedia Commons. ix, 11, 13, 14

Solution Of Matrix Game In Intuitionistic Fuzzy Environment

[1]Sibasis Bandyopadhyay, [2]Prasun Kumar Nayak, [3]Madhumangal Pal
[1, 2] Bankura Christian College, Bankura, 722 101, India,
[3] Department of Applied Mathematics with Oceanology and Computer Programming,
Vidyasagar University, Midnapore-721 102, INDIA.

Abstract:
In this paper, an intuitionistic fuzzy matrix game has been considered and its solution method has been proposed using defuzzification method. Score functions have been defined to construct the problem and numerical example has been given in support of the solution method.
Key words: Intuitionistic fuzzy number, score function, matrix game.

1 Introduction

In modern era there are lot of situations in the society where there is a conflicting interest situation and such situation is handled by game theory. But there are lot of cases where the information given are not in precise manner and in such situation we apply fuzzy mathematics to get a solution.Fuzziness in matrix games can appear in so many ways but two classes of fuzziness are very common. These two classes of fuzzy matrix games are referred as matrix games with fuzzy goal [1] and matrix games with fuzzy pay off [2]. But there such situation may exist where the players can estimate the approximate pay-off values with some degree but with a hesitation. These situations are overcome by applying intuitionistic fuzzy (IF) numbers in game theory.. Atanassov[3] first introduced the concept of IF-set where he explained an element of an IF-set in respect of degree of belongingness, degree of non-belongingness and degree of hesitancy. This degree of hesitancy is nothing but the uncertainty in taking a decision by a decision maker(DM).Atanassov [4] first described a game using the IF-set. Li and Nan [5] considered the matrix games with pay-offs as IF-sets. Nayak and Pal [6] considered a bi-matrix game where they used IF-set. In this paper, We have considered a matrix game where the elements of the pay-off matrix are all intuitionistic fuzzy numbers. We have applied score function method to defuzzify such matrix. Two theorems given, establish the reason behind such defuzzification. An example establishes the theory on strong ground. The paper is organized as follow: In section 2 a basic definition of intuitionistic fuzzy set and intuitionistic fuzzy number are given.In section 3 score function is defined and some properties are given thereafter. In section 4 intuitionistic matrix game has been defined.In section 5 Numerical example is given. In section 6 conclusion has been drawn.

2 Intuitionistic Fuzzy Sets

Here we are going to discuss some basic preliminaries, notations and definitions of Intuitionistic fuzzy sets (IFS), in particular the works of Atanassov [3, 7].

Definition 1 Let $X = \{x_1, x_2, \ldots, x_n\}$ be a finite universal set. An Atanassov's intuitionistic fuzzy set (IFS) in a given universal set X is an expression A given by

$$A = \{\langle x_i, \mu_A(x_i), \nu_A(x_i)\rangle : x_i \in X\} \quad (1)$$

where the functions

$$\mu_A : X \to [0,1];\ x_i \in X \to \mu_A(x_i) \in [0,1]$$

and

$$\nu_A : X \to [0,1]; x_i \in X \to \nu_A(x_i) \in [0,1]$$

define the degree of membership and the degree of non-membership of an element $x_i \in X$ to the set $A \subseteq X$, respectively, such that they satisfy the following condition : for every $x_i \in X$

$$0 \le \mu_A(x) + \nu_A(x) \le 1.$$

Let

$$\pi_A(x_i) = 1 - \mu_A(x) - \nu_A(x)$$

which is called the Atanassov's [7] intuitionistic index of an element x_i in the set A. It is the degree of indeterminacy membership of the element x_i to the set A. Obviously,

$$0 \le \pi_A(x_i) \le 1$$

If an Atanassov's IFS C in X has only an element, then C is written as follows

$$C = \{\langle x_k, \mu_C(x_k), \nu_C(x_k)\rangle\}$$

which is usually denoted by $C = \{\langle \mu_C(x_k), \nu_C(x_k)\rangle\}$ for short.

Definition 2 Let A and B be two Atanassov's IFSs in the set X. $A \subset B$ iff
$\mu_A(x_i) \le \mu_B(x_i)$ *and* $\nu_A(x_i) \ge \nu_B(x_i)$; *for any* $x_i \in X$.

Definition 3 Let A and B be two Atanassov's IFSs in the set X. $A = B$ iff
$\mu_A(x_i) = \mu_B(x_i)$ *and* $\nu_A(x_i) = \nu_B(x_i)$; *for any* $x_i \in X$. Namely, $A = B$ iff $A \subset B$ and $B \subset A$.

Definition 4 Let A and B be two Atanassov's IFSs in the set X. The intersection of A and B is defined as follows :

$$A \cap B = \{\langle x_i, \min(\mu_A(x_i), \mu_B(x_i)), \max(\nu_A(x_i), \nu_B(x_i))\rangle \mid x_i \in X\}.$$

Definition 5 (**Intuitionistic Fuzzy Number**): Intuitionistic fuzzy number was introduced by Seikh et al.[8]. An intuitionistic fuzzy number A

1. an intuitionistic fuzzy subset of the real line
2. normal i.e. there exists $x_0 \in \Re$ such that $\mu_A(x_0) = 1$ (so $\nu_A(x_0) = 0$)
3. convex for the membership function μ_A i.e.

$$\mu_A(\lambda x_1 + (1-\lambda x_2)) \ge \min\{\mu_A(x_1), \mu_A(x_2)\}; \forall x_1, x_2 \in \Re, \lambda \in [0,1]$$

4. concave for the non-membership function ν_A i.e.

$$\nu_A(\lambda x_1 + (1-\lambda x_2)) \le \max\{\nu_A(x_1), \nu_A(x_2)\}; \forall x_1, x_2 \in \Re, \lambda \in [0,1].$$

In our discussion we consider an intuitionistic fuzzy number A as (μ_{ij}, ν_{ij}) and the addition and scalar multiplication operations are given as

1. $(\mu_{ij}, \nu_{ij}) + (\mu'_{ij}, \nu'_{ij}) = (\mu_{ij} + \mu'_{ij} - \mu_{ij}\mu'_{ij}, \nu_{ij}\nu'_{ij})$ (2)
2. $k(\mu_{ij}, \nu_{ij}) = (k\mu_{ij}, k\nu_{ij})$ for $0 \le k < 1$ (3)

3 Defuzzification by Score Function

Chen and Tan[9] first defined a score function S as deviation of a membership function μ from non-membership function ν as

$$S_{ij} = \mu_{ij} - \nu_{ij} \qquad (4)$$

Here bigger the value of S represents bigger IFN but when S of two IFN are same then this definition does not work. So, analyzing the deficiency of this score function Hong and Chi[10] have given a precise function as

$$H_{ij} = \mu_{ij} + \nu_{ij} \qquad (5)$$

.

Here also bigger the value of H gives bigger IFN.Now these two scoring functions defined above have fundamental deficiency that they do not involve the uncertainty function π and this seems to be very unrealistic. Liu[11] analyzing the hesitancy degree π modified the definition as

$$S1_{ij} = (\mu_{ij} - \nu_{ij})(1 + \pi_{ij}) \qquad (6)$$

But this is a non-linear function and hence we will introduce a score function,called linearizing score function which is defined as

$$D\{f(\mu_{ij}), g(\nu_{ij})\} = L\{f(\mu_{ij})\} \qquad (7)$$

Where $f(\mu_{ij})$ and $g(\nu_{ij})$ are functions of μ_{ij} and ν_{ij} and the function L gives the linear part of the function f. The arithmetic operations on the function D are given as

1. $D(t_1 + t_2) = D(t_1) + D(t_2)$
2. $kD(t_1) = D(kt_1) \quad where \quad 0 \le k < 1$ (8)

The inequality relation is given as

$$D(t_1) \le D(t_2) \quad iff \quad t_1 \le t_2 \qquad (9)$$

.

4 Intuitionistic matrix game

Let $A_i (i = 1,2,\cdots,m)$ and $B_j (j = 1,2,\cdots,n)$ be pure strategies for players (or DMs) A and B, respectively. If player A adopts the pure strategy A_i (i.e., the row i) and player B adopts pure strategy B_j (i.e., the column j), then the pay-off for player A is expressed with the intuitionistic number (μ_{ij}, ν_{ij}). The intuitionistic pay-off matrix of a matrix game is concisely expressed in the matrix form as

$$B_1 \qquad B_2 \qquad \cdots \qquad B_n$$

$$G = \begin{matrix} A_1 \\ A_2 \\ \vdots \\ A_m \end{matrix} \begin{pmatrix} (\mu_{11}, \nu_{11}) & (\mu_{12}, \nu_{12}) & \cdots (\mu_{1n}, \nu_{1n}] \\ (\mu_{21}, \nu_{21}) & (\mu_{22}, \nu_{22}) & \cdots (\mu_{2n}, \nu_{2n}) \\ \vdots & \vdots & \vdots \\ (\mu_{m1}, \nu_{m1}) & (\mu_{m2}, \nu_{m2}) & \cdots (\mu_{mn}, \nu_{mn}) \end{pmatrix} \qquad (10)$$

which is said to be intuitionistic matrix game .

4.1 Pure strategy

Pure strategy is a decision making rule in which one particular course of action is selected. For fuzzy games the min-max principle is described by Nishizaki [2]. The course of the fuzzy game is determined by the desire of A to maximize his gain and that of restrict his loss to a minimum. Now for IF game,

$$max - min = \bigvee_i \{ \bigwedge_j (\mu_{ij}, \nu_{ij}) \} = \bigwedge_j \{ \bigvee_i (\mu_{ij}, \nu_{ij}) \}. \qquad (11)$$

Based on TIFN order, for such games, we define the concepts of $\min - \max$ equilibrium strategies.

Definition 6 (Saddle Point) : The concept of saddle point in classical form is introduced by Neumann [12]. The $(k,r)th$ position of the pay-off matrix will be called a saddle point, if and only if,

$$(\mu_{kr}, \nu_{kr}) = \bigvee_i \{ \bigwedge_j (\mu_{ij}, \nu_{ij}) \} = \bigwedge_j \{ \bigvee_i (\mu_{ij}, \nu_{ij}) \}. \qquad (12)$$

We call the position (k,r) of entry a saddle point, the entry itself (μ_{kr}, ν_{kr}) ,the value of the game (denoted by V) and the pair of pure strategies leading to it are optimal pure strategies.

Definition 7 (IF expected pay-off): If the mixed strategies $x = (x_1, x_2, \cdots, x_m)$ and $y = (y_1, y_2, \cdots, y_n)$ are proposed by players A and B respectively, then the expected pay-off of the player A by player B is defined by

$$E(x, y) = \sum_{j=1}^{n} \sum_{i=1}^{m} (\mu_{ij}, \nu_{ij}) x_i y_j. \qquad (13)$$

Addition and other composition rules on IF set which we have discussed in section 21 are used in this definition of expected pay-off (13). In such a situation,player A chooses x so as to maximize his expectation and player B chooses y so as to minimize player A's maximum expectation and mathematically we write

$$\min_y \max_x E(x, y) = E(x^*, y^*) = \max_x \min_y E(x, y) \qquad (14)$$

where (x^*, y^*) is called strategic saddle point of the game and $V = E(x^*, y^*)$ is value of the game.

Theorem 1 *If a pay-off matrix with elements as IFN has saddle point* (k,r) *and* t_{kr} *be the value of the game then the pay-off matrix obtained after defuzzification with the help of score function* D *has also saddle point* (k,r) *and* $D(t_{kr})$ *is the value of the game.*

Proof: If (k,r) be the saddle point of the pay-off matrix and t_{kr} be the value of the game then

$$t_{kr} = \bigvee_i \{ \bigwedge_j t_{ij} \} = \bigwedge_j \{ \bigvee_i t_{ij} \}$$

Now using the equations (6) and (1) we get

$$D(t_{kr}) = D(\bigvee_i \{\bigwedge_j t_{ij}\}) = D(\bigwedge_j \{\bigvee_i t_{ij}\})$$

$$\Rightarrow D(t_{kr}) = \bigvee_i D(\{\bigwedge_j t_{ij}\}) = \bigwedge_j D(\{\bigvee_i t_{ij}\})$$

$$\Rightarrow D(t_{kr}) = \bigvee_i \{\bigwedge_j D(t_{ij})\} = \bigwedge_j \{\bigvee_i D(t_{ij})\}$$

Therefore, (k,r) is also the saddle point of the defuzzified pay-off matrix. $D(t_{kr})$ is the value of the game. Hence the theorem.

Theorem 2 *If (x^*, y^*) be the strategic solution of the pay-off matrix with mixed strategies then (x^*, y^*) is also the solution of the pay-off matrix after defuzzification by score function D.*

Proof: Let (x^*, y^*) be the solution of the pay-off matrix then

$$\min_y \max_x E(x,y) = E(x^*, y^*) = \sum_{i=1}^m \sum_{j=1}^n t_{ij} x_{ij}^* y_{ij}^* = \max_x \min_y E(x,y)$$

$$\Rightarrow D(\min_y \max_x E(x,y)) = D(E(x^*, y^*)) = D(\sum_{i=1}^m \sum_{j=1}^n t_{ij} x_{ij}^* y_{ij}^*) = D(\max_x \min_y E(x,y))$$

$$\Rightarrow \min_y \max_x D(E(x,y)) = D(E(x^*, y^*)) = \sum_{i=1}^m \sum_{j=1}^n D(t_{ij}) x_{ij}^* y_{ij}^* = E(D) = \max_x \min_y D(E(x,y)).$$

Therefore, (x^*, y^*) is also a strategic solution of the defuzzified pay-off matrix and value of the game is $V(x^*, y^*) = \sum_{i=1}^m \sum_{j=1}^n t_{ij} x_{ij}^* y_{ij}^*$. Hence the theorem.

5 Numerical example

Let us consider a pay-off matrix with intuitionistic fuzzy elements as

$$\begin{array}{c} \\ A_1 \\ A_2 \end{array} \begin{array}{c} \begin{array}{cc} B_1 & B_2 \end{array} \\ \begin{pmatrix} (0.5,0.25) & (0.45,0.20), \\ (0.4,0.3) & (0.3,0.1) \end{pmatrix}. \end{array}$$

When this matrix gets defuzzified with the given score function then we get the matrix as

$$\begin{array}{c} \\ A_1 \\ A_2 \end{array} \begin{array}{c} \begin{array}{cc} B_1 & B_2 \end{array} \\ \begin{pmatrix} 0.5 & 0.45, \\ 0.4 & 0.3 \end{pmatrix}. \end{array}$$

Since $\bigvee_i \{\bigwedge_j (a_{ij}, b_{ij})\} = 0.45 = \bigwedge_j \{\bigvee_i (a_{ij}, b_{ij})\}$ the saddle point is $(2,1)$ and value of the game is 0.1625.

Hence, saddle point of the original pay-off matrix is $(2,1)$ and value of the game is (0.45,0.2).

Now let us consider the pay-off matrix as

$$\begin{array}{c} \\ A_1 \\ A_2 \end{array} \begin{array}{c} \begin{array}{cc} B_1 & B_2 \end{array} \\ \begin{pmatrix} (0.4,0.3) & (0.45,0.20), \\ (0.5,0.25) & (0.3,0.1) \end{pmatrix}. \end{array}$$

When we defuzzify this matrix using the score function then we get the matrix as

$$\begin{array}{c} \\ A_1 \\ A_2 \end{array} \begin{array}{c} \begin{array}{cc} B_1 & B_2 \end{array} \\ \begin{pmatrix} 0.4 & 0.45, \\ 0.5 & 0.3 \end{pmatrix} \end{array}.$$

Since $\bigvee_i \{\bigwedge_j (a_{ij}, b_{ij})\} = 0.4 \neq 0.45 = \bigwedge_j \{\bigvee_i (a_{ij}, b_{ij})\}$, saddle point does not exits. Since this is a mixed strategy game its solution is obtained as the strategic solution $x^* = (0.8, 0.2), y^* = (0.8, 0.2)$ and value of the game is $(0.388, 0.012)$.

6 Conclusion

In this paper, a matrix game has been considered with pay-off elements as intuitionistic fuzzy numbers. The intuitionistic fuzzy number is considered as a membership and a non-membership function which actually represents the acceptance and rejection degree of a decision maker. The matrix is defuzzified with the help of a score function. It gives a strategic solution and value of the game as an intuitionistic fuzzy number. The example given, establishes the theory on strong ground. It has strong impact on modern socio economic structure where conflicting interests exist. There is a scope to apply other score function for such defuzzification.

References

[1] I.Nishizaki and M.Sakawa,Equilibrium solutions for multiobjective bimatrix games incorporating fuzzy goals, Journal of Optimization Theory and Applications, 86(1995)433-457.

[2] I Nishizaki and M.Sakawa,Max-min Solution for fuzzy multiobjective matrix games, Fuzzy Sets and Systems, 61(1994)265-275

[3] K.Atanassov,Intutionistic fuzzy sets, Fuzzy Sets and Systems, 20(1986)87-96.

[4] K. T. Atanassov, Ideas for intuitionistic fuzzy equations, inequalities and optimization, Notes on Intuitionistic Fuzzy Sets, 1 (1) (1995) 17–24.

[5] D. F. Li and J. X. Nan, A nonlinear programming approach to matrix games with payoffs of Atanassov's intuitionistic fuzzy sets, International Journal of Uncertainty, Fuzziness and Knowledge-Based Systems, 17 (4) (2009) 585–607.

[6] P.K. Nayak and M. Pal, Solution of rectangular fuzzy games, OPSEARCH, 44(3)(2009) 211-226.

[7] K.Atanassov, Intuitionistic fuzzy sets: Theory and Applications, Physica-Verlag, 1999.

[8] M.R.Seikh, M. Pal and P.K.Nayak, Notes On Triangular Intuitionistic Fuzzy Numbers, International Journal Mathematics in Operation Research, (2012).

[9] Chen and Tan,Handling multicriteria fuzzy decision making problems based on vague set theory,Fuzzy Sets and Systems,67(2)(1994)163-172.

[10] Hong and Choi,multicriteria fuzzy decision making problems based on vague set theory,Fuzzy Sets and Systems,144(1)(2000)103-113.

[11] Liu H.W,vague set methods of multicriteria fuzzy decision making,System Engineering, Theory and Practice,5(5)(2004)214-220.

[12] J.V. Neumann and O. Morgenstern, Theory of Games and Economic Behaviour, Princeton University Press, Princeton, New Jersey, (1947).

A Survey on 3d Localization in Wireless Sensor Networks

Shayon Samanta[1,] Prof. Punesh U.Tembhare[2,] Prof. Charan R. Pote[3]
1,2,3,Department of Computer Technology, Rashtrasant Tukadoji Maharaj Nagpur University, Nagpur, (M.H.)

Abstract:
WSN is used in many recent trends in wireless application, where its nodes needed to localize him before sending any data. Nodes are defines their coordinates in localization process, through coordinates they localize himself. There are various algorithm proposed in localization based on 2D works on two plane, it provides accuracy but in real world needed all three planes for correct estimation and more accuracy in localization. The 2D works on flat terrain, we need to deploy WSN in harsh terrain also, so we needed to define algorithm on 3D basis for providing better accuracy and decrease the error of estimation and it provide a real world view. This paper works on localization of node using 3D and its algorithm.

Keywords: Beacon Node, Localization Algorithm, Unknown Nodes, Wireless Sensor Networks.

1. Introduction

Wireless Sensor Network consists of autonomous devices which called as node. Node is used to sense or monitor the environment, where it gathered the data through it, and send to the user through base stations. Its applications used in military as battlefield surveillance, habitat monitoring, environmental monitoring, and health application etc. Sensor network send the data to neighbor node or base station, but before it they need to know their own location, because the data have no meaning without location information from where the data is coming. Nodes are large in numbers it's difficult for base station to calculate the node position, so it need for individual node to send the location information with their collected information, form it provide exact location information to the user. Therefore, node needed to localize himself. The term "Localization" means to find the exact location in any geographical area with the help of references node.

Localization can be done earlier by using manual configuration and by GPS system. In manual configuration localization is done by human interaction and calculation. Where it deploys by using human being and calculation is done through it. But in real world human interaction is not always possible just like in military field, we need airplanes for deployment and the calculation is not always correct. Another is GPS system, which is done by satellite. It is not feasible for all nodes because by using GPS its antenna increases the sensor node size factor, but Sensor nodes are required to be small. The power consumption of GPS will reduce the battery life of the sensor nodes and also reduce the effective lifetime of the entire network; cost factor of GPS is also increases in the network. Also In the presence of dense forests, mountains or other obstacles that block the line-of-sight from GPS satellites, so GPS cannot be implemented. Therefore we need to implement a localization algorithm for every node. Localization algorithm uses the reference node, just as neighbor node and anchor node (which known their position earlier with the help of GPS) for localization. In localization algorithm mostly works on 2-dimensional plane, i.e. x and y plane. In a 2D system, the process of estimation is less complex and requires less energy and time. In 2D plane provide good accuracy is on flat terrains and is difficult to estimate in harsh terrains. It provides accurate distance when more node density and anchor nodes are present. By using 3-dimensional plane added one extra plane called as height i.e. z plane, concept is to it provide more accurate result using height. It can be used in harsh and hilly terrains to provide good accuracy in it. Using 2-dimensional algorithms on a system the position estimate by using point in the plane i.e. x and y plane, where the x and y coordinate are the same as the real position of the surface and altitude is fixed. But when mapping these estimated positions to the real world an error can occur, because it consists of all three planes. Any angle between the reference plane and the ground where it present result may be an error during mapping. By using a localization system for 3D this problem is eliminated completely.

2. Literature Survey

WSN contain few nodes who known there location earlier known as anchor or beacon node through it unknown node known's their position. In their some methods and algorithm are proposed for localization using anchor node.

2.1 Localization Method

In a 2D space, three anchor nodes are uniquely determine a coordinate system. In a 3D space, four anchor nodes are required. In 3D localization same method uses as define in 2D. Range-based and range-free method is defined for localization process. In which range-based provide point-to-point information with reference node. It provides higher accuracy, but it need additional hardware and through it needed continuous update of information. In there it increases size and cost. Range-free

scheme is used where no additional thing needed, node organize by own self. On comparison range-based provide better accuracy, but it is affected by obstacles and through it accuracy is decreases. There are some techniques is present for localization i.e. distance, angle and position techniques. It is done by using anchor or anchor-free scheme. Some range based schemes are ToA, TDoA, AoA, RSSI, lateration, and angulation method is used. Range-free schemes are Hop Count, APIT. Techniques are defines in localization is as follows:

1) Position Computation: Calculation is based on anchor node position from it estimate his own position.

1.1) Lateration: In 2D three or more non collinear anchors node are present whereas in 3D four or more non collinear anchor nodes are present and position calculation is done through this non collinear anchor node and estimate the location using the calculated value.

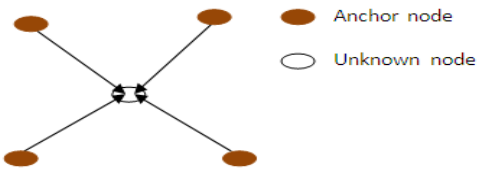

Fig. 1 Lateration techniques in 3D localization using four nodes

2) Angle measurement: Calculation is done using information about angles instead of distance, for determining the position of an object.

2.1) Angle of Arrival (AoA): Nodes uses Omni-direction antenna. It estimate angle with the help of known reference axis and with signal is send to another node.

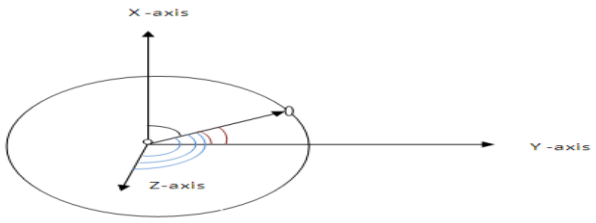

Fig. 2 AoA techniques in 3D localization

3) Distance measurement: It uses the anchor node or position of known node for calculation where it uses three anchor nodes in 2D whereas four anchor nodes in 3D.

1) Received Signal Strength Indicator: RSSI is a measurement of the signal power coming in a received node. It calculates distance using received signal. Advantage is easy to estimate. Main drawback is the power is decrease when the node present at long distance. Power strength is fading in distance. It is also affected from obstacles. Accuracy is affected from it. Good accuracy is in less distance.

2) Time of arrival: This uses a packet for sending from the anchor node to other node. Packet consist of time when it was transmitted, in there the perfect clock synchronization needed between the nodes. The distance formula is calculated between them,

i.e. Distance= speed * time,

Where time is the difference between one node to other node and speed of light is used here because the packet travelled with the speed of light. The advantage of using ToA it is not affected from fading of signal, but if synchronization between the nodes is not their then it cannot be useful.

3) Time different of arrival: In TDoA, distance measurement depends upon the difference in time between two waves, or one wave with two destinations. ToA uses two frequency and estimate distance through it. One is radio frequency another is ultrasonic frequency. If unknown node uses one frequency signal, then source sends same RF signal to two different anchor nodes. These two known nodes calculate the difference of time arrival of the signal and calculate the distance between themselves and source node. Similar process used in ultrasonic frequency. If unknown node use two different signal then two destination

nodes are not required only one destination can calculate distance using two different signals. Node sends RF and ultra sonic signal at same time. But known node will receive these two signals with time difference because speed of RF signal is higher than ultrasound signal and calculate difference of time of two signals receive with time difference between them.

$$\text{Distance} = \Delta t * \Delta S$$

Where, Δt is the difference between sending and receiving signal between two nodes. ΔS difference in two signal received by other node.

$$\Delta S = (s1 * s2)/(s1 - s2)$$

4) Hop Count: It calculates using number of hop receive the signal by the sender. The number of hop receive the signal is calculate the distance between them. Hop counting techniques is used in range-free method.

2.2 Localization Algorithm

For any nodes localization first it is classified into two categories.

1. Centralized localization: In there basically one central base station is present for computation. Disadvantage is overhead increase and cost also increases.

2. Distributed localization: In their computation are done by own self and node communicate with each other to get their position in the network.

There are many algorithms defines in localization process in 2D WSN and few work have done on 3D WSN and we need 3D localization for providing accuracy and improving positioning error in harsh as well as flat terrain areas.

1) New 3-dimensional DV-Hop Localization Algorithm: It expanded the traditional range-free DV-Hop algorithm in to 3D-space. It divide into three steps as follows:

i. Computing the minimum hop counts between the unknown nodes and the beacon nodes: Mobile agent is used for localization, all beacon nodes sent the mobile agent to the other nodes, and mobile nodes recorded the coordinates of the beacon nodes and the number of hops between two nodes. The nodes only saved the mobile agent whose hop counts is the smallest among them, and discarded others.

ii. Calculating the average per-hop distance and measurement error: In it calculated the average per-hop distance of the beacon nodes, and dealt with the measurement error of the beacon nodes. Broadcasted this value in the whole network, the unknown node saved all the average per-hop distance of the beacon nodes which it can receive, and forwarded to the other neighbor of the nodes, then used these average per-hop distances estimate using previously saved hops information to calculate the distance between the beacon nodes.

iii. Calculating the average per-hop distance of the unknown node: If extended the DV-Hop algorithm to the 3-D space simply, then the unknown node will only save the first received average per-hop distance of the beacon node, so that only the information of the most recent beacon node to be used.

2) Novel Centroid Algorithm for 3D: This scheme needs no additional hardware support and can be implemented in a distributed way. This algorithm derives a novel node localization method for 3D WSNs. It uses the developed in earlier implement Centroid algorithm. In there the Centroid theorem uses the coordinate-tetrahedron in the volume-coordinate system which acts as a key component of in estimation. All anchors send their positions information to all unknown nodes within their transmission range. Each unknown node collects all the beacon signals from various reference points after it select randomly four anchor nodes in range to form a series of tetrahedrons. It uses the proposed Centroid theorem of coordinate- tetrahedron in the volume-coordinate system to calculate the barycentre (nodes have non-rotating coordinates and present at the centre of two or more bodies) of each tetrahedron. Then we use the average coordinates of these barycentre as the final estimated position of unknown node.

3) Three-dimensional azimuthally defined area localization algorithm (3D-ADAL): It proposed an algorithm of three-dimensional distributed range-free localization for WSNs, using a mobile beacon (MB) equipped with a rotary and tilting directional antenna. It is a distributed and energy efficient algorithm and contributes to extend the lifetime of the sensor network. Here uses two types of antenna first is omni-directional antenna which is used by unknown node. Second is equipped with a rotary and tilting directional antenna which is present in MB. The mobile beacon is flight over the whole network and broadcast the beacon messages to the sensor nodes during the localization process. Co-ordinates will be considered for the calculation of the sensor nodes position in its horizontal plane (xy-plane) and the z-coordinates of the MB will be used to determining its altitude. In their virtual beacon message is sent by MB. It divides the algorithm into four phases. The sensor nodes integrate all the received information to firstly estimate its xy-coordinates.

i. Initialization phase: In this phase are established important parameters just as antennas.
ii. Latitude and longitude preliminary determination phase: The algorithm is used to accomplish the position estimation in the local *xy*-plane of each sensor node (local horizontal plane of each sensor node).
iii. Altitude preliminary determination phase: The algorithm performs the calculation of the altitude of each sensor node. To accomplish this task, it focuses in the local *yz*-plane (vertical plane) of the mobile beacon. After a sensor node calculates its preliminary *xy*-position, it uses the information of tilt (β) in the data packet to determine its altitude.
iv. Refinement phase: It estimation of the position made in the previous phase was performed and continue the process.

4) The three-dimensional accurate positioning algorithm: It converts the loss of wireless signal strength between unknown node and beacon node to distance first, and then uses the maximum likelihood estimation method to calculate the unknown node's three-dimensional coordinate according to the beacon node's three dimensional coordinates. It depend of five parameters:

i. Parameter matching: For providing positioning accuracy maximally, any two node's parameters need re-matching before positioning.
ii. RSSI ranging: It Convert the RSSI value to distance between unknown and beacon node.
iii. Role switching between beacon node and unknown node under a particular situation: For 3D positioning, unknown node needs to communicate with four adjacent beacon nodes at least. If the four beacon node is not present then positioning is not completed, so the unknown nodes whose coordinates are known can temporarily act as beacon nodes to complete the positioning.
iv. Signal compensating when there are obstacles between wireless nodes: When obstacles are presents the attenuation degree of wireless signal in barrier is not same with that in atmosphere. It does not meet linear relationship with the distance between nodes any longer, so there is need to compensate the wireless signal.
v. Improving energy efficiency to reduce power consumption.

The three-dimensional accurate positioning algorithm based on Initialization and parameter matching in wireless sensor networks.

5) Unitary Matrix Pencil Algorithm for Range-Based 3D Localization: It is a range-based 3D localization methods, it is based on time-of-arrival (TOA) estimation of ultra wideband signal using unitary matrix pencil (UMP) algorithm. This method combines unitary matrix pencil (UMP) algorithm, multilateral localization and three-dimensional Taylor algorithm. UMP algorithm is extended to estimate the time of arrival (TOA) between nodes so as to measure the propagation distance between them. UMP utilizes the centro-hermitian property of a matrix and applies a unitary transformation, which can convert a complex matrix to a real matrix with eigenvectors. This significantly reduces the processing time for real time implementation. As for node position computation algorithm, multilateral localization other than trilateral localization is used here. Taylor algorithm is extended to 3D to solve nonlinear equations. UMP algorithm is extended to the application of UWB wireless sensor network to reduce computational load and improve time resolution. A UMP based TOA estimation algorithm is proposed to measure the distance between two nodes. The estimation results will be used in 3D position computation. In their Channel impulse response (CIR) is modelled is computed and estimated channel and its frequency domain. From it real matrix is constructed and estimation the path delay.

6) Space distance intersection (SDI): It is define as a 3D positioning algorithm. It provides two features:
i. Beacon placement strategy: Here mobile beacon is used. Mobile beacon known there location by GPS. Each beacon contains the mobile beacons current location.
ii. 3D position derivation: This process is done by sensor node itself and it divides it into two phases:
Phase1: Each sensor node measures a set of distances with the help of mobile beacon. This algorithm proposed a range based method, so mobile beacon uses UWB signal it is good for multi-path performance and can provide an excellent time resolution. In there it uses TOA techniques for high precision.
Phase2: sensor node derives it 3D position form node-beacon distance measurements by using algorithm, for that SDI is proposed.

SDI is flexible, effective techniques, where computational and accuracy assessment is used. The control points are present who knows their own coordinates in 3D and it used for finding position of unknown node.

Algorithm proposed in 2D there altitude is fixed, not with actual altitude. Through 3D localization it works with real measurement and the algorithm proposed in 3D are provide the unique features and provide good positing error compare to their earlier methods.

3. Conclusions and Future Work

Localization is very important in WSN, where to increase the usage of WSN not only in plane surface but in all terrain we need the 3D localization to provide better results. Few algorithms is work on 3D, we need to work more for future to provide more accuracy, flexibility and potential of nodes. In future work need to implement new algorithms and this 3D localization concept also be implement in indoor bases.

References

[1] Amitangshu Pal "Localization Algorithms in Wireless Sensor Networks: Current Approaches and Future Challenges", ISSN 1943- 3581, Vol. 2, No. 1, 2010.

[2] Jing WANG1, R. K. GHOSH, Sajal K. DAS," A survey on sensor localization". J Control Theory Appl 2010 8 (1) 2–11.

[3] Samira Afzal, "A Review of Localization Techniques for Wireless Sensor Networks". Text Road Publication ISSN 2090-4304 Journal of Basic and Applied Scientific Research www.textroad.com, 2012-09-27.

[4] Azzedine Boukerche, Horacio A. B. F. Oliveira, Eduardo F. Nakamura, and Antonio A. F. Loureiro, "Localization Systems for Wireless Sensor Networks". IEEE Wireless Communications, December 2007.

[5] Lina M. Pestana Leão de Brito, Laura M. Rodríguez Peralta,"An Analysis of Localization Problems and Solutions in Wireless Sensor Networks". ISSN: 1645-9911 Revista de Estudos Politécnicos Polytechnical Studies Review Vol VI, nº 9, Year 2008.

[6] P.K Singh, Bharat Tripathi, Narendra Pal Singh,"NODE LOCALIZATION IN WIRELESS SENSOR NETWORKS", P.K.Singh et al / (IJCSIT) International Journal of Computer Science and Information Technologies, Vol. 2 (6) , 2568-2572 Year 2011.

[7] Li Wang, Jing Zhang, Dun Cao. "A New 3-dimensional DV-Hop Localization Algorithm". Journal of Computational Information Systems 8: 6 (2012) 2463-2475, March 2012.

[8] Hongyang Chen, Pei Huang, Marcelo Martins, Hing Cheung, and Kaoru Sezaki. "Novel Centroid Localization Algorithm for Three-Dimensional Wireless Sensor Networks". IEEE 978-1-4244-2108-4/2008.

[9] Guerrero E, Wang Hao, Alvarez J, Rivero L," A Three-Dimensional Range-Free Localization Algorithm Based on Mobile Beacons for Wireless Sensor Networks". Vol. 20 No.1 June 2010.

[10] Quan LIU, Ping REN, Zude ZHOU," Three-dimensional Accurate Positioning Algorithm based on Wireless Sensor Networks". Journal of Computers, Vol. 6, No. 12, December 2011.

[11] Chang Liu, Hong Jiang and De-Long Zeng, "Unitary Matrix Pencil Algorithm for Range- Based 3D Localization of Wireless Sensor Network Nodes". Journal of Networks, Vol. 7, No. 9, September 2012.

[12] Q.Shi, H.Huo, T.Fang, and. Li,"A 3D node localization scheme for wireless sensor networks". IEICE Electronics Express, Vol.6, No.3, 167-172, 10-Feb-2009.

[13] me.emu.edu.tr/majid/MENG584/Localization.ppt
Localization *in* Wireless Sensor Networks.

Crosswind Sensitivity of Passenger Cars and the Influence of Chassis

Ram Bansal[1], R. B. Sharma[2]

[1,] Research Scholar, Department of Automobile Engineering,RJIT BSF ACEDEMY Tekanpur
[2,] Hod of Mechanical Engineering department, RJIT BSF ACEDEMY Tekanpur

Abstract:

Results of vehicle crosswind research involving both full-scale driver-vehicle tests and associated analyses are presented. The paper focuses on experimental crosswind testing of several different vehicle configurations and a group of seven drivers. Atest procedure, which utilized wind-generating fans arranged in alternating directions to provide a crosswind "gauntlet", is introduced and described. Driver preferences for certain basic chassis and aerodynamic properties aredemonstrated and linked to elementary system responses measured during the crosswind gauntlet tests. Based on these experimental findings and confirming analytical results, a two-stage vehicle design process is then recommended for predicting and analysing the crosswind sensitivity of a particular vehicle or new design.

Keywords: (A) vehicle dynamics considerations (e.g., weight distribution, tire, and suspension characteristics), (B) vehicle aerodynamic properties, (C) steering system characteristics (most notably steering system compliance, friction and torque assists), and (D) driver closed-loop steering behaviour.

1. Introduction

This paper is based on recent findings from a vehicle aerodynamics research project [1]sponsored by the Chrysler Motors Corporation at the University of Michigan Transportation Research Institute. The general thrust of that research was directed at the crosswind sensitivity of passenger cars, and specifically, the influence and interaction of chassis characteristics. The key elements considered in that study are outlined in Figure 1 and included: (A) vehicle dynamics considerations (e.g., weight distribution, tire, and suspension characteristics), (B) vehicle aerodynamic properties, (C) steering system characteristics (most notably steering system compliance, friction and torque assists), and (D) driver closed-loop steering behaviour and preferences obtained from experimental crosswind tests. This paper focuses on the experimental crosswind testing conducted during the project using several different vehicle configurations and a group of seven drivers. It reports on driver preferences for certain basic chassis and aerodynamic properties and demonstrates a linkage to elementary system responses measured during those crosswind tests.

The paper begins with an examination of previous research findings related tocrosswind sensitivity of passenger cars. A computer model, developed under this research program, is then briefly described. The use of that model at different stages of the research helped to identify and probe certain vehicle-related mechanisms identified as possibly significant contributors to the issue of crosswind sensitivity. As will be seen, the ability of the model to predict basic dynamic behaviour patterns, observed in experimental measurements of driver-vehicle systems operating in crosswinds, is an important factor for recommending it as a tool within the vehicle design process. The basis of the conclusions of this paper, however, rest upon experimental measurements and evaluations of a group of seven test drivers operating seven distinctly different vehicle configurations during nearly identical crosswind conditions. The crosswind tests were conducted using a set of eight fans (arranged in an alternating direction over a length of several hundred feet) to approximate a random-like crosswind "gauntlet" driven repeatedly by each driver.

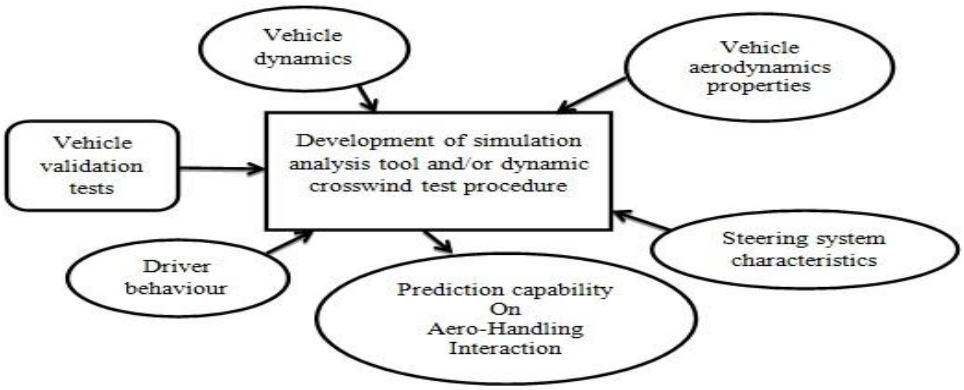

Fig. 1. Key Elements in Vehicle Crosswind Stability.

2. Previous Research

The trends during the last decade or so to lighter, more fuel efficient cars in response to changing energy policies, combined with more recent trends toward higher performance passenger cars, have led to increased interest in aerodynamic styling as a means for providing low drag configurations and for mitigating any high-speed crosswind sensitivities. In many cases, attempts at streamlining passenger cars for minimizing drag have led to unwanted increases in crosswind sensitivity. As noted in such comprehensive texts such as Hucho [2]and Scibor-Rylski [3],this tradeoff was observed as early as **1933** by Kamm [4]out of which arose the well-known truncated rear-end design ("Kamm-back") which helped to offset much of the crosswind susceptibility introduced from streamlining. More recent observations, such as Kohri and Kataoka [5]or Hucho [2],have contributed to improved understandings on the subtle influences relating to A-and C-pillar styling designs and their importance in affecting crosswind sensitivity of passenger cars. Studies such as Noguchi [6]have also noted the importanceof certain suspension properties (e.g., roll steer and lateral force compliances) as elements not to be discounted when considering a vehicle's crosswind sensitivity. Other studies relating to crosswind sensitivity of passenger cars have been compiled in such documents as Kobayashi and Kitoh [7],which was primarily concerned with literature related to the crosswind sensitivity of light weight cars.

Wind Measurement Technology

In addition to the studies cited above, a number of technological advancements in on-board wind measurement capabilities have also occurred in the last two decades which have helped to promote further understanding of the nature of crosswinds acting on vehicles in open areas, as well as in the vicinity of fixed roadway objects and other moving vehicles. Smith in 1972 [8] described a MIRA wind measurement device (utilizing anemometers) and its use in measuring a number of different crosswind profiles. More recently, Tran [9] presented a pressure transducer system for measuring the wind forces and moments acting on a vehicle by recording the pressures at approximately 10 points along the circumference of a vehicle and then combining this information with a uniform flow model. A wind transducer developed by the Chrysler Corporation aerodynamics department utilizing a strain-gauged sphere in combination with an inertial mass compensating accelerometer, is described by Pointer in [10]. This latter device was also used during the crosswind testing described subsequently in this paper.

3. A Driver-Vehicle Crosswind Model

A computer model for predicting the interaction between vehicle and driver during crosswind conditions is introduced and outlined briefly in this section. Its use as an advanced tool that can be used in place of, or in conjunction with, certain types of dynamic random crosswind test procedures is subsequently being recommended as part of a total crosswind sensitivity design process. The model was developed during this research and was used to help identify and separate different mechanisms of the driver-vehicle system contributing significantly to the crosswind sensitivity of the system. Figure 2shows a block diagram outlining the principal components of the crosswind driver/vehicle model. The technical details of the computer model can be found in Sayers et a1 [11].The four primary components of the model are described briefly in the following.

Vehicle Model

The vehicle model is characterized by five degrees of freedom for the sprung mass, constant forward speed, and massless suspension/wheel assemblies. Tire and suspension compliances are also included. Tire lateral force is treated as largely linear except for cornering stiffness dependency on vertical load. The basic dynamics of the vehicle are very similar to that developed by Segel [12].High speed test data, collected during the course of the aerodynamic crosswind stability research program at UMTRI [1],were used to validate the baseline model behaviour through direct comparisons with model predictions. Test track handling measurements and aerodynamic wind tunnel measurements of a baseline passenger car, in several different aerodynamic configurations, were conducted at nominal speeds of 50 and 100 mph to validate the model. As part of the model validation process, a stable platform and a variety of transducers were used to measure all body motions. Steering wheel displacement and torque measurements, front wheel rotations, and other steering system functions (power boost pressures, pitman arm motion, and tie rod forces) were also recorded and utilized in the model validation.

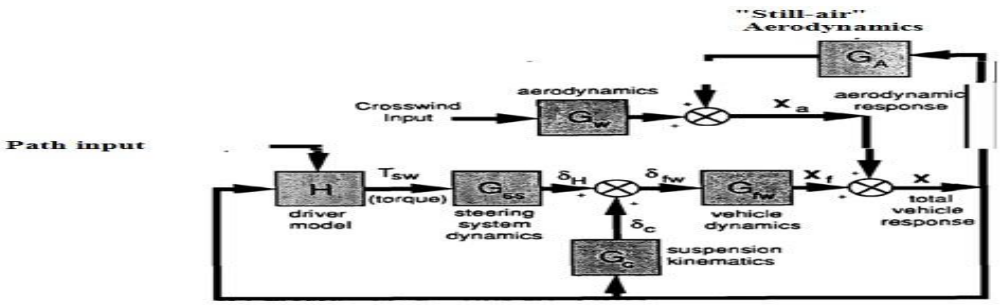

δ_H front wheel angle contribution from steering command and compliance
δ_C front wheel angle contribution from suspension kinematics
δ_{fw} total front wheel steer angle
X_f non-aerodynamic vehicle response

Fig. 2. Chrysler/UMTRI Crosswind Vehicle Model.

4. Experimental Crosswind Measurements

The results of experimental crosswind tests of driver-vehicle systems conducted during the research program are presented in this section. All full-scale testing was performed on the vehicle dynamics facility at the Chrysler Proving Grounds in Chelsea, Michigan. The vehicle crosswind testing results were obtained with the use of eight U.S. Government-owned wind generating fans described in detail by Klein and Jex in [13].

The use of fan-generated crosswinds in this research program was based upon several needs. One need was to obtain crosswinds of sufficient magnitude that the test drivers would be given a definite subjective impression of the different vehicle configurations being driven, and, that would also produce a system response that could be readily measured by on-board instrumentation. Test speeds of 90-100 mph were selected so that the aerodynamic inputs provided by sizeable crosswinds (25 mph or so) would still permit a linear-regime characterization of the vehicle aerodynamics. A second need was to have available a generally repeatable set of crosswind conditions so that different drivers could be exposed to more or less the same crosswind experiences at widely varying times during the test program. And finally, there was the practical need to be able to schedule test drivers on a regular basis and be guaranteed that sufficient crosswind test conditions would be available.

Against this back-drop of perceived needs was the clear observation, wellreported in the literature, that fan-generated crosswinds were generally insufficient for obtaining reliable subjective evaluations from test drivers. Since nearly all of the previous uses of fans for subjective evaluations were for short duration drive-by scenarios, in which drivers attempted to regulate the lateral path in response to a short-term pulse of crosswind, a different approach was considered for this research program. It was decided that the traditional, closely-grouped fan arrangement, which provides a short-duration pulse of crosswind, would be used only to evaluate the passive (non-driver) vehicle response. Anew arrangement of the fans, in the form of a crosswind "gauntlet" course, would be used, instead, to expose the test drivers to the fan-generated crosswinds over a longer period of time for collecting their subjective evaluations.

Test Procedures

Two basic test maneuverers were used to evaluate the response of the various driver-vehicle configurations. The first maneuverer was a fixed steering wheel drive-by of a constant pulse of fan-generated crosswind. It was used to primarily characterize and verify differences in the passive crosswind behaviour of the different vehicle configurations. The second maneuverer, serving to evaluate the active (driver and vehicle) crosswind system behaviour, employed the same fans spread out over a longer distance but arranged in alternating directions. Active steering for path regulation by each driver was required during this latter test. All tests were conducted for vehicle speeds of 90-100 mph. Further descriptions of these two test procedures follow.

***Crosswind** Pulse. This maneuverer was conducted with the eight fan units grouped togetherand facing perpendicular to the test track as seen in Figure 3. Fixed steering wheel drive-by tests were then performed for each vehicle configuration to evaluate their respective passive (no regulatory driver steering) wind behaviour. Each test vehicle was driven in a straight line at 100 mph from the ambient environment past the fans whereupon it encountered an approximately constant 25 mph crosswind for a period of nearly 0.7 seconds. A pulse-like vehicle response due to entering and then exiting the crosswind stream was recorded by on-board instrumentation. The resulting peak yaw rate and lateral acceleration responses observed for each vehicle configuration were then used to confirm that significant and distinctly measurable differences in the vehicle aerodynamic andchassis configurations were

Vehicle trajectory

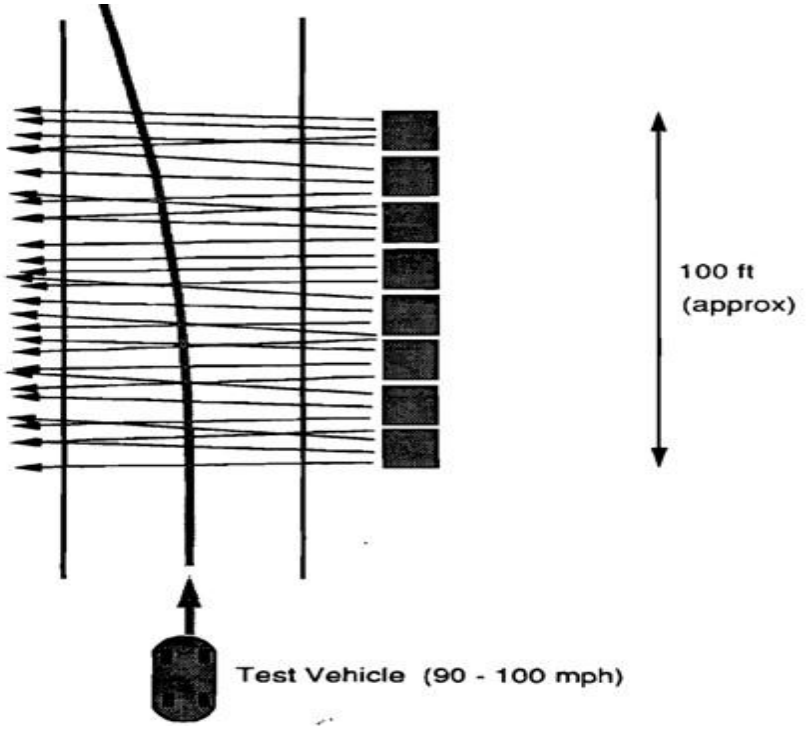

Fig. 3. Crosswind Pulse, Fixed Steering Wheel Test.

present in the passive crosswind behaviour of eachvehicle. (The short duration of the crosswind pulse at these speeds did not permitthe vehicle to fully establish itself in a steady-state turning condition.)

***Crosswind "Gauntlet" Maneuvre.** For this set of tests, the eight fan units were located, in an alternating manner, along opposite sides of a straight-line testcourse (single lane width) and distributed over a longitudinal travel distance of approximately 350 feet. See Figure 4. This arrangement presented the driver-vehicle system with a series of fluctuating pulses of crosswind from one side and then the other in a repeating sequence. The spacing between the fans was approximately 52 feet. Wind output from each fan was set at an approximate level of 25 mph and the test course was driven at speeds of 90 to 100 mph. An inner lane width of approximately 8 to 9 feet was defined by a series of traffic cones along the centre of the course in order to require each driver to regulate the vehicle path (without undue demand) within those bounds during traversal of the crosswind course. All of the subjective evaluations collected during the test program were obtained from this crosswind test procedure.

Impressions of several drivers who drove past the fans in both arrangements(Crosswind Pulse versus the Crosswind Gauntlet) noted significant differences. The closely grouped pulse arrangement had a very small effect on a driver's subjective and objective response as the crosswind pulse was encountered. The primary inputs to the drivers were reported to be sound (from wind noise) and a mild change in direction as the fans were passed. Drivers also commented that the experience was too brief. In contrast, the driving experience through the crosswind gauntlet generally made a much'stronger impression on the test drivers. This was most likely due to the longer length of time of crosswind exposure provided by the gauntlet course and significantly increased driver-vehicle system responses during this test. For the same levels of fan wind output, the gauntlet course produced noticeably amplified system responses compared to those obtained from simple drive-bys of the closely-spaced pulse arrangement. The alternating pulses and their input frequency during the gauntlet test produced a more resonating dynamic response that further contributed to subjective driver impressions. The on-board measurements, as well as simple visual observation of the different vehicle configurations traversing the gauntlet, confirmed the amplifying qualities of the gauntlet test procedure. As an example, in a few of the worst-case vehicle configurations, peak lateral accelerations greater than 0.6g were recorded at the driver head position and more than 0.45g's on the stabilized platform. Levels approximately half these would have been recorded in the crosswind pulse test for the same fan output. Drivers Seven different drivers were utilized in the test program to provide subjective evaluations of each of the vehicle configurations during the crosswind gauntlettests. Objective measurements of the total driver-vehicle system responses werealso collected for four of these test drivers to obtain representative system responses during the gauntlet tests. All of the drivers were males with backgrounds as engineers or technicians ranging in age from 25 to 55. All drivers, but one, were associated to varying degree with the crosswind research program. (Other drivers also participated intermittently during the testing but were not included in these results because of not having driven each of the different vehicle configurations, or, because their chosen speeds fell significantly outside the nominal 90-100 mph range.)

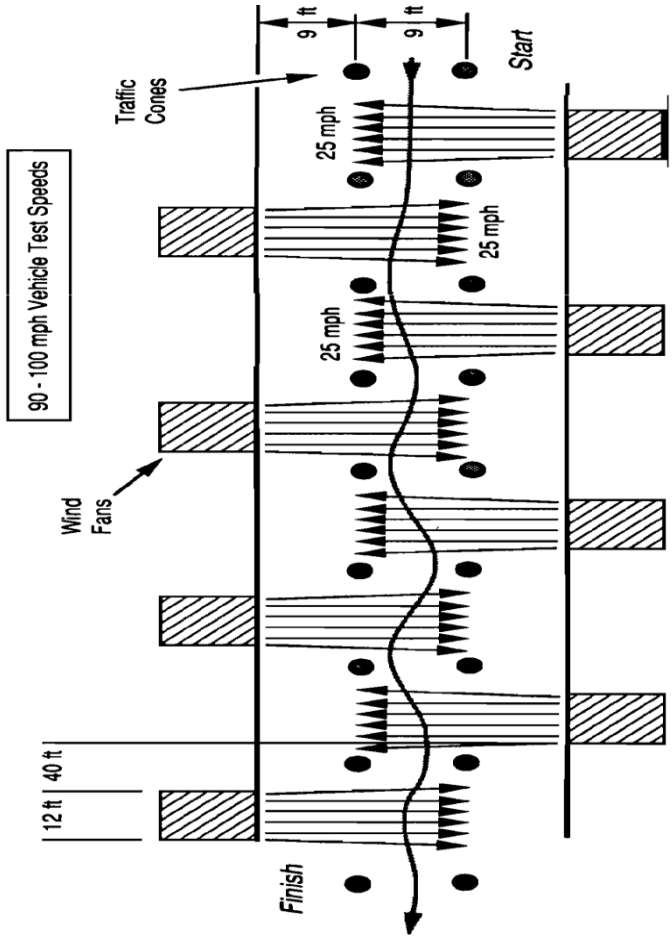

Fig. 4. Crosswind Gauntlet Test Course Used in Study

5. Conclusions

The results of the full-scale driver-vehicle crosswind tests presented above, in combination with static turning analyses of vehicles in constant crosswinds and more complete dynamic crosswind simulations, suggest the following conclusions:

- A vehicle's static turning response due to a constant crosswind input and fixed steering wheel angle is a useful, first-stage predictor of driver's likely subjective evaluation of a vehicle's crosswind sensitivity.
- That same static turning measure will also frequently predict a vehicle's likely ranking of RMS responses obtained during dynamic crosswind maneuvers.
- A more reliable and accurate method for predicting subjective evaluations ofvehicle crosswind sensitivity is with RMS yaw rate values obtained from fullscale testing or comprehensive dynamic simulation of driver-vehicle systems during dynamic, random-like or natural crosswind conditions.
- Increased roll motion due to decreased suspension roll stiffness was associated with lower driver subjective evaluations of vehicle crosswind sensitivity.
- At vehicle speeds of 90-100 mph, variations in fore-aft weight distributionplayed as important a role as comparable variations in aerodynamic canter-of-pressurelocation in influencing both subjective and objective evaluations ofvehicle crosswind sensitivity.
- A two-stage vehicle design process is recommended for analysing the crosswind sensitivity of a potential vehicle or new design: (1) A preliminaryscreening of candidate vehicle designs for crosswind sensitivity, based uponthe simplified statics analysis of Equations (3) or (4),should first be conductedto screen out ineligible candidate designs having unsuitable vehicle properties(e.g., relative locations of mass canter, neutral steer point, and aerodynamicCP that promote high passive crosswind sensitivity). (2) conduct a more in-depthand comprehensive analysis of the "final round" candidate designs usingdynamic analysis (such as the crosswind model described above). The dynamicmodel should employ random-like, natural crosswind inputs to examine likelydriver-vehicle responses to systematic variations of vehicle chassis properties(suspension, steering system, and weight distributions particularly) and differentaerodynamic designs. RMS values of system responses (e.g., yaw rate) can beused to evaluate the influence of alternate designs.

- The dynamic crosswind model developed under this work can be used to further explain and analyse the crosswind sensitivity of driver-vehicle systems in a dynamic context, particularly for driving scenarios involving active driver steering control during representative random crosswind conditions. Its use as a tool to systematically examine the influences of vehicle sub-components on crosswind stability is especially useful.
- Further man-machine research into likely driver preferences regarding body roll motion and driver-cantered motion experiences deriving from aerodynamic crosswind forces and moments is recommended.
- Re-examination by other parties of the crosswind gauntlet test procedure (orsimilar procedures) utilizing wind-generating fans is also recommended. Basedon the experiences reported here, this type of crosswind test procedure appearsto offer significant promise for collecting driver-based subjective data of vehiclecrosswind sensitivities. Whether such procedures can effectively replacenatural crosswind testing as a reliable method for collecting driver subjectiveinformation remains to be seen.

References:

[1]. Vehicle Crosswind Stability. Chrysler Challenge Fund Project - #2000533, UMTRI, Sponsored by the Chrysler Motors Corporation, 1987-1990.
[2]. W. Hucho, **Aerodynamics of Road Vehicles.** Butterworths, 1987.
[3]. A. J. Scibor-Rylski, **Road Vehicle Aerodynamics.** Revised by D.M. Sykes ed. Wiley, New York, 1984.
[4]. W. Kamm, Anforderungen an Kraftwagen bei Dauerfahrten. ZVDI. vol77, 1933.
[5]. I. Kohri and T. Kataoka, Research on Improvement of Cross-Wind Properties of Passenger Cars. **JSAEReview,** Vol. 10, No. 3, 1989. pp. 46-51.
[6]. H. Noguchi, Crosswind Stability and Suspension Properties. MIRA Translation by G. Wood, Rept No. Translation 2/87. 1987.
[7]. T. Kobayashi and K. Kitoh, Cross-Wind Effects and the Dynamics of Light Cars. **Int. J. of Vehicle Design.** Vol. No. Special Publication SP3, 1983. pp. 142-157.
[8]. J. P. Smith. Wind Gusts Measured on High-Speed Roads. The Motor Industry Research Association, Rept No. 197217, May, 1972.
[9]. V. T. Tran, Determining the Wind Forces and Moments Acting on Vehicles by Means of Pressure Transducers. SAE Paper No. 900313, 1990.
[10]. J. D. Pointer, On-Road Calibration of the Dynamic Pressure Vector System. 10/17/88. Memorandum to G. Romberg. Chrysler Motors Corporation. 1988.
[11]. M. Sayers, C. C. MacAdam and Y. Guy, Chrysler/UMTRI Wind-Steer Vehicle Simulation. User's Manual, Version 1.0, vols I and 11, Report No. UMTRI-89-811-2, 1989.
[12]. L. Segel, On the Lateral Stability and Control of the Automobile as Influenced by the Dynamics of the Steering System. **Journal Engineering for Industry,** Vol. **66,** No. 8, 1966. pp.
[13]. R. H. Klein and H. R. Jex, Development and Calibration of an Aerodynamic Disturbance Test Facility. SAE Paper No. 800143, 1980.

Comparison of Imputation Techniques after Classifying the Dataset Using Knn Classifier for the Imputation of Missing Data

Ms.R.Malarvizhi[1], Dr. Antony Selvadoss Thanamani[2]

[1]Research Scholar ,Research Department of Computer Science, NGM College, 90 Palghat Road,Pollachi, ,Bharathiyar.
[2]Professor and HOD, Research Department of Computer Science, NGM College 90 Palghat Road, Pollachi Bharathiyar University, Coimbatore.

Abstract:

Missing data has to be imputed by using the techniques available. In this paper four imputation techniques are compared in the datasets grouped by using k-nn classifier. The results are compared in terms of percentage of accuracy. The imputation techniques Mean Substitution and Standard Deviation show better results than Linear Regression and Median Substitution.

Keywords: Mean Substitution, Median Substitution, Linear Regression, Standard Deviation, k-nn Classifier.

1. Introduction

Missing Data Imputation involves imputation of missing data from the available data. Improper imputation produces bias result. Therefore proper attention is needed to impute the missing values. Imputation techniques help to impute the missing value. The accuracy can be measured in terms of percentage. Pre-processing has to be done before imputing the values using imputation techniques. kNN classifier helps to classify the datasets into several groups by using the given training dataset. The imputation techniques are separately imputed in each dataset and checked for accuracy. The results are then compared.

2. Missing Data Mechanisms

In statistical analysis, data-values in a data set are missing completely at random (MCAR) if the events that lead to any particular data-item being missing are independent both of observable variables and of unobservable parameters of interest. Missing at random (MAR) is the alternative, suggesting that what caused the data to be missing does not depend upon the missing data itself. Not missing at random (NMAR) is data that is missing for a specific reason.

3. Imputation Methods

Imputation is the process of replacing imputed values from the available data. There are some supervised and unsupervised imputation techniques. The imputation techniques like Listwise Deletion and Pairwise Deletion deletes the entire row. The motivation of this paper is to impute missing values rather than deletion. In this paper, unsupervised imputation techniques are used and the results are compared in terms of percentage of accuracy.

3.1. Mean Substitution

Mean Substitution substitutes the mean value of data available. It can be calculated from the available data. Mean can be calculated by using the formula

$$\bar{X} = \frac{\Sigma X}{N}$$

Where:

$\bar{X}$ is the symbol for the mean.
Σ is the symbol for summation.
X is the symbol for the scores.
N is the symbol for the number of scores.

3.2. Median Substitution

Median Substitution is calculated by grouping up of data and finding average for the data. Median can be calculated by using the formula

Median =L+h/f(n/2-c)

where
L is the lower class boundary of median class
h is the size of median class i.e. difference between upper and lower class boundaries of median class
f is the frequency of median class

c is previous cumulative frequency of the median class
n/2 is total no. of observations divided by 2

3.3. Standard Deviation

The standard deviation measures the spread of the data about the mean value. It is useful in comparing sets of data which may have the same mean but a different range. The Standard Deviation is given by the formula

$$s_N = \sqrt{\frac{1}{N}\sum_{i=1}^{N}(x_i - \overline{x})^2}.$$

where $\{x_1, x_2, \ldots, x_N\}$ are the observed values of the sample items and $\overline{x}$ is the mean value of these observations, while the denominator N stands for the size of the sample.

3.4. Linear Regression

Linear regression attempts to model the relationship between two variables by fitting a linear equation to observed data. One variable is considered to be an explanatory variable, and the other is considered to be a dependent variable. Linear regression can be calculated by using the formula

$$\boldsymbol{Y = a + bX},$$

where $\boldsymbol{X}$ is the explanatory variable and $\boldsymbol{Y}$ is the dependent variable. The slope of the line is $\boldsymbol{b}$, and $\boldsymbol{a}$ is the intercept.

4. Database and Data Pre-Processing

The dataset consists of 10000 records which is taken from a UK census report conducted in the year 2001. It has 6 variables. The data has to be pre-processed before it is used for experiment. The original dataset is modified by making some data as missed. The missing percentage may vary as 2, 5, 10, 15, and 20 percentages. Next data is classified into several groups. For grouping of data, knn classifier is used. Each group is then separately taken for the experiment. The imputation techniques are implemented one by one and the performance is measured by comparing with original database in terms of accuracy.

5. K-Nearest Neighbor Classifiers

The idea in k-Nearest Neighbor methods is to identify k samples in the training set whose independent variables x are similar to u, and to use these k samples to classify this new sample into a class, v. f is a smooth function, a reasonable idea is to look for samples in our training data that are near it (in terms of the independent variables) and then to compute v from the values of y for these samples. The distance or dissimilarity measure can be computed between samples by measuring distance using Euclidean distance.

The simplest case is k = 1 where we find the sample in the training set that is closest (the nearest neighbor) to u and set v = y where y is the class of the nearest neighbouring sample. In k-NN the nearest k neighbors of u is calculated and then use a majority decision rule to classify the new sample. The advantage is that higher values of k provide smoothing that reduces the risk of over-fitting due to noise in the training data. In typical applications k is in units or tens rather than in hundreds or thousands.

6. Experimental Analysis

In our research the database is grouped into 3, 6 and 9 groups for experiment. The above said imputation techniques are implemented in each group. The missing percentages were 2, 5, 10, 15 and 20. The imputation techniques are Mean Substitution, Median Substitution, Standard Deviation and Linear Regression.

Table 1 describes the percentage of accuracy for various groups. For accuracy each imputed data set is compared with the original dataset. Linear Regression and Mean Substitution shows same result as well as poor result. Median Substitution and Standard Deviation shows same result as well as better result. When the group size is large there is some improvement in the result.

Table 2 describes the overall average of accuracy.

Table 1. Comparison of Imputation Techniques in Groups Classified Using k-NN Classifier

Percentage of Missing	3 GROUPS				6 GROUPS				9 GROUPS			
	Mean Sub	Med Sub	Std Dev	Linear Regress	Mean Sub	Med Sub	Std Dev	Linear Regress	Mean Sub	Med Sub	Std Dev	Linear Regress
2	67	70	70	70	69	71	71	66	71	73	72	67
5	69	72	72	69	75	76	76	75	74	77	77	75
10	66	71	71	66	72	78	78	72	71	80	80	71
15	64	72	72	64	66	77	77	66	66	79	79	66
20	60	72	72	60	55	78	77	56	50	80	80	52

Table 2: Performance of Above Imputation Methods in Terms of Percentage of Accuracy

Percentage of Missing	Mean Substitution	Median Substitution	Standard Deviation	Linear Regression
2	69	71	71	68
5	73	75	75	73
10	70	76	76	70
15	65	76	76	65
20	55	77	76	56
% of Accuracy	66.4	75	74.8	66.4

Figure 1: Comparison of Imputation Methods

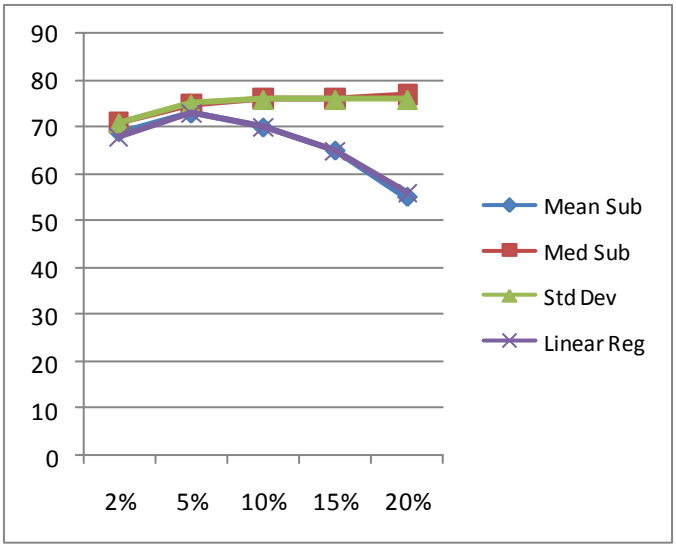

Figure 1 shows the difference graphically.

7. Conclusions and Future Enhancement

In this paper, as the imputation techniques like Median Substitution and Standard deviation shows better result, it can be used for further research. Our research also finds out that when the data gets groups into several sizes, there is some drastic improvement in the accuracy of percentage. In future data algorithms can be generated for grouping of data. After grouping, the two imputation methods can be applied.

References

[1]. Graham, J.W, "Missing Data Analysis: Making it work in the real world. Annual Review of Psychology", 60, 549 – 576 , 2009.

[2]. Jeffrey C.Wayman , "Multiple Imputation For Missing Data : What Is It And How Can I Use It?" , Paper presented at the 2003 Annual Meeting of the American Educational Research Association, Chicago, IL ,pp . 2 -16, 2003.

[3]. A.Rogier T.Donders, Geert J.M.G Vander Heljden, Theo Stijnen, Kernel G.M Moons, "Review: A gentle introduction to imputation of missing values" , Journal of Clinical Epidemiology 59 , pp.1087 – 1091, 2006.

[4]. Kin Wagstaff ,"Clustering with Missing Values : No Imputation Required" -NSF grant IIS-0325329,pp.1-10.

[5]. S.Hichao Zhang , Jilian Zhang, Xiaofeng Zhu, Yongsong Qin,chengqi Zhang , "Missing Value Imputation Based on Data Clustering", Springer-Verlag Berlin, Heidelberg ,2008.

[6]. Richard J.Hathuway , James C.Bezex, Jacalyn M.Huband , "Scalable Visual Assessment of Cluster Tendency for Large Data Sets", Pattern Recognition ,Volume 39, Issue 7,pp,1315-1324- Feb 2006.

[7]. Gabriel L.Scholmer, Sheri Bauman and Noel A.card "Best practices for Missing Data Management in Counseling Psychology", Journal of Counseling Psychology, Vol. 57, No. 1,pp. 1–10,2010.

[8]. R.Kavitha Kumar, Dr.R.M Chandrasekar,"Missing Data Imputation in Cardiac Data Set" ,International Journal on Computer Science and Engineering , Vol.02 , No.05,pp-1836 – 1840 , 2010.

[9]. Jinhai Ma, Noori Aichar –Danesh , Lisa Dolovich, Lahana Thabane , "Imputation Strategies for Missing Binary Outcomes in Cluster Randomized Trials"- BMC Med Res Methodol. 2011; pp- 11: 18. – 2011.

[10]. R.S.Somasundaram , R.Nedunchezhian , "Evaluation of Three Simple Imputation Methods for Enhancing Preprocessing of Data with Missing Values", International Journal of Computer Applications (0975 – 8887) Volume 21 – No.10 ,pp.14-19 ,May 2011.

[11]. K.Raja , G.Tholkappia Arasu , Chitra. S.Nair , "Imputation Framework for Missing Value" , International Journal of Computer Trends and Technology – volume3Issue2 – 2012.

[12]. Paul D. Allison, Statistical Horizons, Haverford, PA, USA," Handling Missing Data by Maximum Likelihood", SAS Global Forum 2012- Statistics and Data Analysis

[13]. BOB L.Wall , Jeff K.Elser – "Imputation of Missing Data for Input to Support Vector Machines" ,

[14]. Ms.R.Malarvizhi, Dr.Antony Selvadoss Thanamani – "K-Nearest Neighbor in Missing Data Imputation", International Journal of Engineering Research and Development, volume 5Issue 1-November - 2012

Bandwidth Enhancement of A 2×2 Triangular Microstrip Patch Antenna Using Triangular Lattice Ebgs in the Ground Plane

Jalaj Sharma[1], Sunil Kumar Singh[2]

[1,2,]Department of Electronics & Communication Jabalpur Engineering College, Jabalpur- 482011, India

Abstract:

Triangular lattice Electromagnetic Band-Gap (EBG) Structure in the ground plane is used in the design of a Triangular Microstrip Patch Antenna (TMPA) Array to improve its bandwidth. The patch elements are equilateral triangular in shape. The Equilateral Triangular Microstrip Patch Antenna (ETMPA) Array design has four patch elements in 2×2 form with ground plane having circular cutouts forming triangular lattice EBG. The ETMPA array with EBG provides better antenna gain and bandwidth. The ETMPA Array with EBG gives an impedance bandwidth of 16.76GHz and a percentage bandwidth of 110% while ETMPA Array gives an impedance bandwidth of 2.46GHz and a percentage bandwidth of 17.7%, thus an increment of approximately 500% in impedance bandwidth is observed. The achieved bandwidth of the ETMPA array with EBG extends from 2.7034GHz to 19.4649GHz. The array gain with EBG structure improved to 14.6dBi which is 9.7dBi for ETMPA array without EBG.

Keywords: ETMPA, ETMPA Array, Electromagnetic Band-Gap (EBG), Impedance Bandwidth, Percentage Bandwidth, Triangular Lattice.

1. Introduction

With the increasing utilization of high performance antennas in the wireless communication applications, the popularity of microstrip patch antenna has increased a lot, though it has limitations like narrow bandwidth, low gain, low efficiency, spurious feed radiations etc. Efforts have been made to improve the performance of the microstrip patch antenna using various techniques. Some of these techniques are to increase the substrate height or using aperture coupled feed etc. These techniques increases the bandwidth of the patch antenna to some extent but also increases the surface waves on the substrate causing distortion in the radiation pattern and reducing the gain and directivity of the patch antenna [6]. Arrays is also one of the solution for increasing the gain and directivity of the antenna, though they also have limitations narrow bandwidth, spurious signal feed radiations, low efficiency etc. To overcome above problems Electromagnetic Band- Gap (EBG) substrates and materials have attracted much attention of the researchers in microwave and antenna communities. EBG has many applications in the field of microwaves and millimeter waves device development, as well as antenna designing. EBG material, in general, are periodic structures that forbid the propagation of electromagnetic surface waves within a particular frequency band called the band-gap [8]. In this paper we have designed triangular lattice of circular holes in the ground plane to improve the gain and bandwidth of the ETMPA Array. We have used simulating software HFSS v13 for designing the array and simulating the results. HFSS software works on the Finite Element Method (FEM) in which triangular elements are used for surface meshes and tetrahedron elements for volumetric meshes. For achieving maximum band-gap we have used r/a= 0.45 and a/λ_g= 0.5, where r is the radius of circular holes in the ground plane, a is the separation between the holes and λ_g is the guided wavelength [7].

2. Design Of An ETMPA Array

Microstrip Patch Antenna in general have a conducting patch on a grounded microwave dielectric substrate and have attractive features like low profile, light weight, easy fabrication and conformability to mounting hosts [3]. But above all these attractive features microstrip patch antenna have one disadvantage that they provide narrow bandwidth and for practical utilization we need to enhance the bandwidth of the patch antenna. Thus to overcome the above problem we can form an assembly of radiating elements in a specific electrical and geometrical configuration, which is referred to as an *array*. An array may have a number of elements in different geometrical configuration; each element is provided with the same magnitude of electric current and is in same phase. To provide very directive patterns, it is essential that the fields from the elements of array should interfere constructively (add) in a desired direction and interfere destructively in the remaining space [1]. Triangular patch is one of a basic patch geometry used in several applications because of being physically smaller than other patch geometries like rectangular and circular patches. The resonance frequency of a triangular patch can be found using the cavity model, in which the triangle is surrounded by a magnetic wall along the periphery. Corresponding to several modes the resonance frequency of an equilateral triangular patch can be given as [2]:

$$f_r = \frac{2c}{3a\sqrt{\varepsilon_r}}\sqrt{(m^2 + mn + n^2)} \quad (1)$$

Where, c is the velocity of light, a is side length of equilateral triangular patch and ε_r is the dielectric constant of the substrate. In the above equation for better results we change the side length a by the effective side length a_e, hence our expression for resonance frequency for TM_{10} mode will become-

$$f_{10} = \frac{2c}{3a_e\sqrt{\varepsilon_r}} \quad (2)$$

Where effective side length of equilateral triangular patch is given as [2]:

$$a_e = a\left[1 + 2.199\frac{h}{a} - 12.853\frac{h}{a\sqrt{\varepsilon_r}} + 16.436\frac{h}{a\varepsilon_r} + 6.182\left(\frac{h}{a}\right)^2 - 9.802\frac{1}{\sqrt{\varepsilon_r}}\left(\frac{h}{a}\right)^2\right] \quad (3)$$

Where h is height of the substrate. Using equations (2) and (3) we can calculate the side length of the equilateral triangular patch for a given operating frequency.

In the case of conventional microwave antennas, characteristics such as high gain, beam scanning, or steering capability are possible only when discrete radiators are combined to form arrays. The elements of an array may be spatially distributed to form a linear, planar, or volume array. A linear array consists of elements located finite distances apart along a straight line. Similarly, a planar array has elements distributed on a plane and a volume array has elements that are distributed in three dimensions [5, 9]. In the design of an array one of the most essential factor is the feed technique, generally, it is divided in two broad categories, parallel feed technique and series feed technique. In parallel or corporate feed technique there are single input port and multiple feed lines in parallel constituting the output ports. Each of these feed lines is terminated at an individual radiating element. Series feed consists of a continuous transmission line from which small proportion of energy are progressively coupled into the individual element disposed along the line by various means including proximity coupling, direct coupling, probe coupling, or aperture coupling [2]. In designing of an ETMPA Array we have taken parallel feed technique in utilization. The feed is taken such that each element receives equal input impedance. The feed works as the 2:1 power divider, i.e. power is divided equally in both the arms from the common feed [11]. Rogers RT/ Duroid 6010 substrate is used having dielectric constant 10.2 and dielectric loss tangent tan δ= 0.0023 with dimensions equal to $60\times60mm^2$ and thickness of substrate as 2.5mm. The patch element side length is 10.7mm; common feed is of 3mm and arms feed is of 1.5mm. The separation between the patch elements is taken as $0.5\lambda_0$ and operating frequency used is 5.2GHz.

The model of an ETMPA Array designed in HFSS simulating software is shown as below:

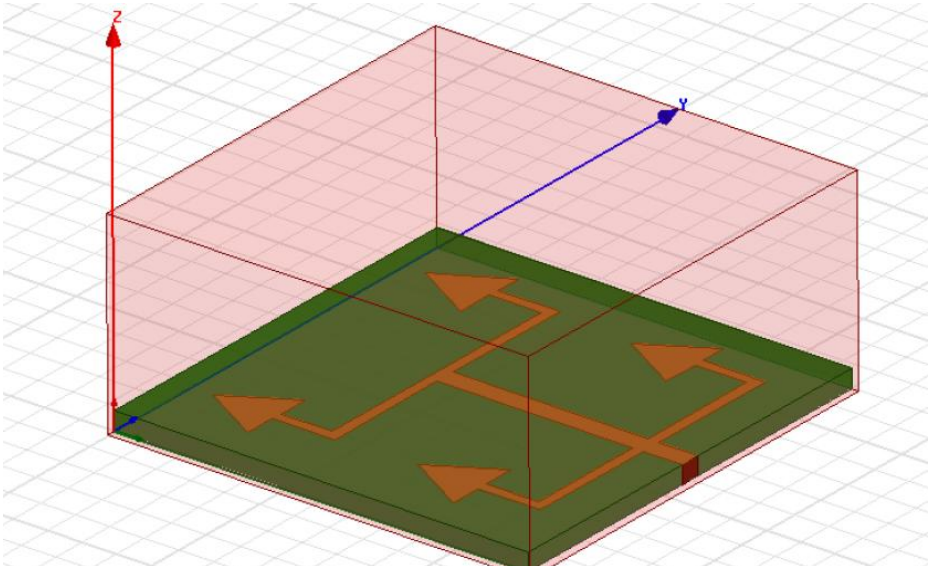

Figure 1: ETMPA array model designed in HFSS

3. Design Of An ETMPA Array Using Triangular Lattice Ebgs In The Ground Plane

Electromagnetic band-gap structures are defined as artificial periodic (or sometimes non-periodic) objects that prevent/assist the propagation of electromagnetic waves in a specified band of frequency for all incident angles and all polarization states. EBG structures are usually realized by periodic arrangement of dielectric materials and metallic conductors [4]. The 2-D EBG surfaces have the advantages of low profile, light weight, and low fabrication cost. Surface waves are by-products in many antenna designs. Directing electromagnetic wave propagation along the ground plane instead of radiation into free space, the surface waves reduce the antenna efficiency and gain. The diffraction of surface waves increases the back lobe radiations, which may deteriorate the signal to noise ratio in wireless communication systems such as GPS receivers. The band gap feature of EBG structures has found useful applications in suppressing the surface waves in various antenna designs. When the incident wave is a surface wave the EBG structures show a frequency band gap through which the surface wave cannot propagate for any incident angles and polarization states. Thus reducing the surface waves and increasing the gain and directivity of the antenna design [10].Electromagnetic band-gap substrates (EBGs) have produced a wide variety of design alternatives for researchers working in the area of microwaves and photonics. 2-D EBGs in the ground plane have been introduced by Itoh. Triangular lattice has been chosen because triangular lattice EBGs can give rise to a complete band-gap for both transverse electric (TE) and transverse magnetic (TM) polarizations. It has been observed that for maximum band-gap [7]:

$$\frac{r}{a} = 0.45 \quad \text{and} \quad \frac{a}{\lambda g} = 0.5 \tag{4}$$

Where r is the radius of circular holes in the ground plane, a is the separation between the holes and λ_g is the guided wavelength defined as $\lambda_g = \lambda/\sqrt{\varepsilon_r}$, where λ is free space wavelength and ε_r is the dielectric constant of the substrate.

Using equation (4) the radius of the circular holes in the ground plane is calculated as 4mm and the separation between the holes as 9mm. Hence the HFSS modeled design of the ETMPA Array with triangular lattice EBGs in the ground plane is -

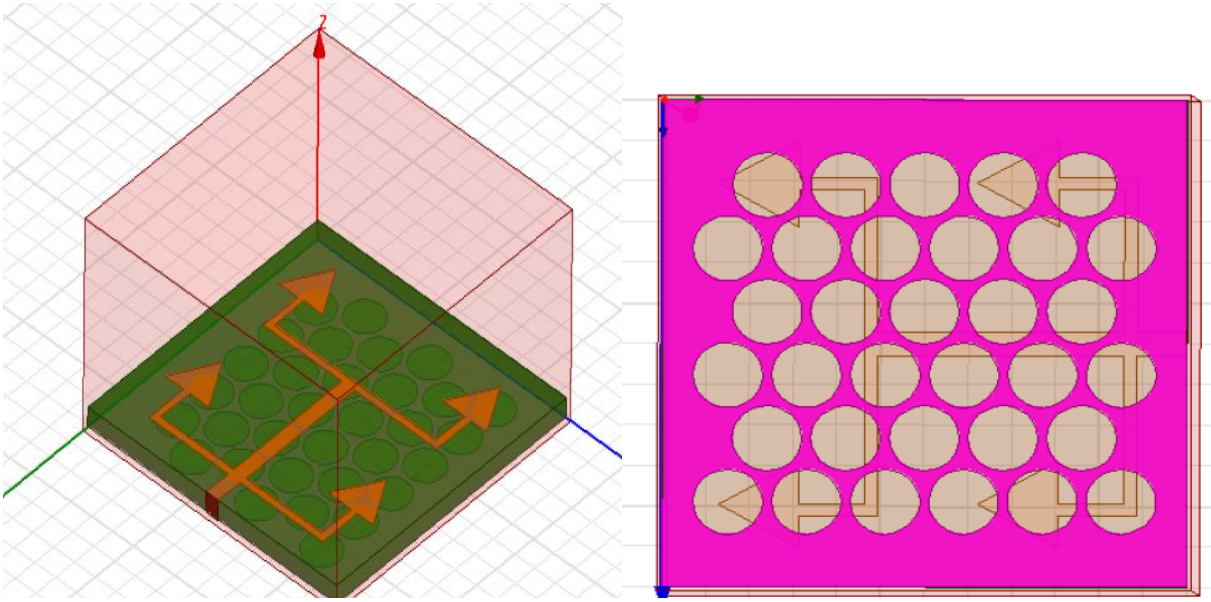

(a) (b)

Figure 2: ETMPA array with triangular lattice EBGs (a) Top view, (b) Back view

4. Simulations And Results

Designing and simulating the 2×2 ETMPA Array using Triangular Lattice EBGs in ground plane in HFSS simulating software, it has been observed that an impedance bandwidth of 16.76GHz is obtained i.e. a percentage bandwidth of 110%, while for ETMPA Array without EBG an impedance bandwidth of 2.46GHz and a percentage bandwidth of 17.7% are obtained. Thus an increment of approximately 500% in impedance bandwidth is observed. The return loss value for the ETMPA Array with EBG is -32.2801 at the resonance frequency of 15.2405GHz. The S parameter results for both the design are shown in figure 3 and VSWR results in figure 4. The VSWR for the ETMPA array with EBG is 1.0499.

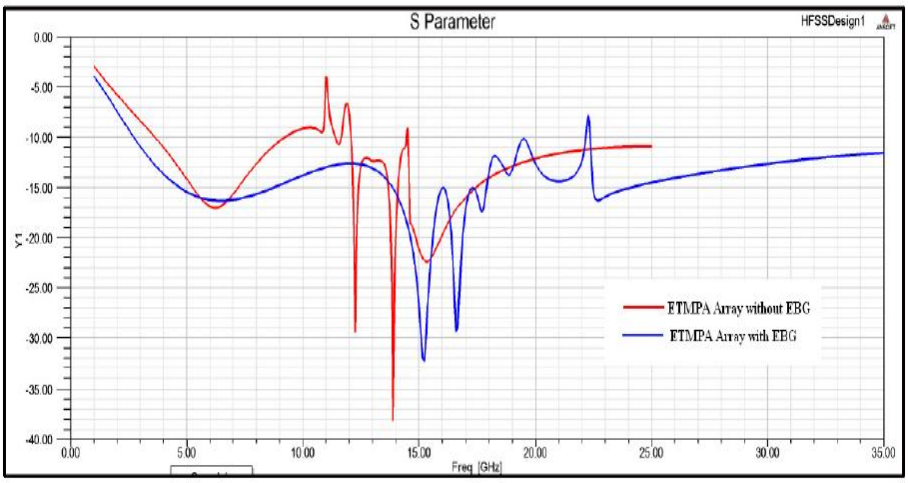

Figure 3: S parameter result for both the designs

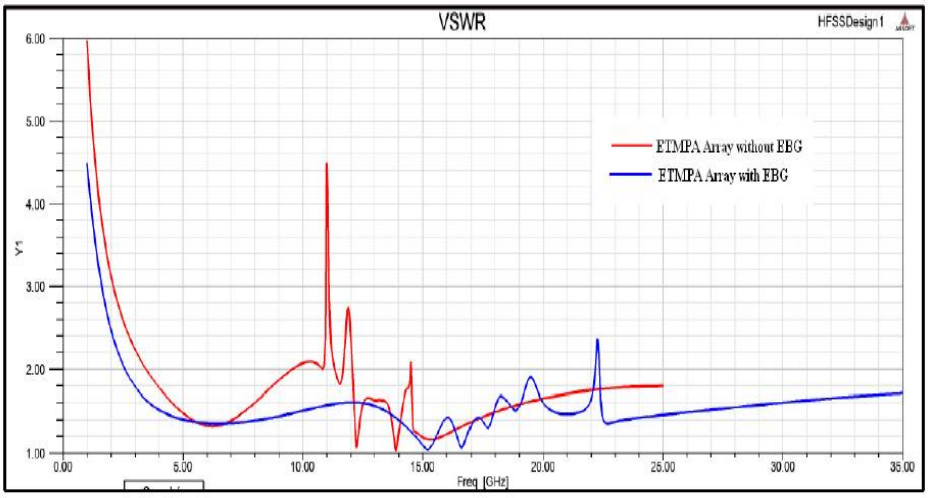

Figure 4: VSWR result for both the designs

ETMPA Array with EBG has a gain of 14.6dBi whereas the gain value of ETMPA Array without EBG is 9.7dBi. The impedance bandwidth and the radiation bandwidth for an ETMPA design are determined using:

$$\text{Impedance Bandwidth} = f_H - f_L \quad (4)$$

And,

$$\text{Percentage Bandwidth} = \frac{f_H - f_L}{f_c} \times 100\% \quad (5)$$

Where f_H and f_L are the start and end point of the S parameter curve where minimum return loss is obtained, however both the frequency point must lie on -10dB line and f_C is the center frequency.

5. Conclusion

From full wave simulations of both the designs i.e. ETMPA Array without EBG and ETMPA Array with triangular lattice EBGs in ground plane for same dielectric constant substrate and same operating frequency, it has been observed that using EBG structure there is an increment of approximately 500% in impedance bandwidth of the array. ETMPA Array with EBG gives an impedance bandwidth of 16.76GHz and a percentage bandwidth of 110%. Its gain has also increased up to 14.6dBi. The results of the ETMPA Array with EBG not only cover the whole Ultra wide band spectrum but also can be used for X band RADAR applications.

References

[1] Constantine A. Balanis, "Antenna Theory, Analysis and Design", Third Edition, John Wiley & Sons, Inc.

[2] Ramesh garg, Prakash Bhartia, Inder Bahl and Apisak Ittipiboon, "Microtrip Design Antenna Handbook", Artech House, Boston London.

[3] Kin-Lu Wong, "Compact and Broadband Microstrip Antennas", John Wiley & Sons, Inc.

[4] Fan Yang and Yahya Rahmat- Samii, "Electromagnetic Band-gap Structures in Antenna Engineering", Cambridge University Press.

[5] Horng-Dean Chen, Chow-Yen-Desmond Sim, Jun-Yi Wu, and Tsung-Wen Chiu, "Broadband High-Gain Microstrip Array Antennas for WiMAX Base Station", IEEE transaction on Antennas and Propagation, Vol 60, No. 8 August 2012.

[6] Dalia Nashaat, Hala A. Elsadek, Esmat A. Abdallah, Magdy F. Iskander and Hadia M. El Hennawy "Ultrawide Bandwidth 2×2 Microstrip Patch Array Antenna Using Electromagnetic Band-gap Structure (EBG)", IEEE Transactions Antennas and Propagation, Vol. 59, N0. 5, May 2011.

[7] Rakhesh Singh Kshetrimayum, Sholampettai Subramanian Karthikeyan and Dipto Dey, "Band-Gap Determination of Triangular Lattice EBGs in Ground Plane", International Journal of Electronics and Communication (AEU), Vol. 63, 2009, 699- 702.

[8] Hossein Sarbandi Farahani, Mehdi Veysi, Manouchehr Kamyab, and Alireza Tadjalli, "Mutual Coupling Reduction in Patch Antenna Arrays using a UC- EBG Superstrate", IEEE Antennas and Wireless Propagation Letters, Vol. 9, 2010.

[9] Aixin Chen, Yanjun Zhang, Zhizhang Chen and Shunfeng Cao, "A Ka Band High Gain Circularly Polarized Microstrip Antenna Array", IEEE Antennas and Wireless Propagation Letters, Vol. 9, 2010.

[10] Ryo Ikeuchi and Akimasa Hirata, "Dipole Antenna above EBG Substrate for local SAR Reduction", IEEE Antennas and Wireless Propagation Letters, Vol. 10, 2011.

[11] Steven Gao, Yi Qin and Alistair Sambell, "Low cost Circularly Polarized Printed Antennas and Array", IEEE Antennas and Propagation Magazine, Vol. 49, No.4, August 2007.

Single Layer Monopole Hexagonal Microstrip Patch Antenna for Direct Broadcast Satellite (DBS) System

Supriya Jana[1], Bipadtaran Sinhamahapatra[2], Sudeshna Dey[3], Arnab Das[4], Bipa Datta[5], Moumita Mukherjee[6], Samiran Chatterjee[7]

[1,2,3,4,5]ECE Department, West Bengal University of Technology, Brainware Group of Institutions, Barasat, West Bengal, India.

[6]Centre for Millimeter wave Semiconductor Devices and Systems, University of Calcutta, West Bengal, India

[^7]University of Kalyani, Kalyani, West Bengal, India.

Abstract:

In recent years, great interest was focused on microstrip antennas for their small volumes, low profiles, excellent integration, low costs and good performance. With the continuous growth of wireless communication service and the constant miniaturization of communication equipment, there are higher and higher demands for the volume of antennas, integration and working band. This paper presents a single layer monopole hexagonal microstrip patch antenna is thoroughly simulated for wireless communications system application which are suitable for the 13.71GHz operations. These systems may include direct broadcast satellite (DBS) system, also known as "Direct-To-Home". DBS systems are commonly referred to as "mini-dish" systems. DBS uses the upper portion of the Ku band. The initial design and optimization of the patch antenna is operating in Ku band (12-18GHz).It has been performed in Zeland IE3D software.

Keywords: Compact, Patch, Slot, Resonant frequency, Bandwidth, DBS System.

1. INTRODUCTION

In recent years, demand for small antennas on wireless communication has increased the interest of research work on compact microstrip antenna design among microwave and wireless engineers [1-6]. Because of their simplicity and compatibility with printed-circuit technology microstrip antennas are widely used in the microwave frequency spectrum. Simply a microstrip antenna is a rectangular or other shape, patch of metal on top of a grounded dielectric substrate. Microstrip patch antennas are attractive in antenna applications for many reasons. They are easy and cheap to manufacture, lightweight, and planar to list just a few advantages. Also they can be manufactured either as a stand-alone element or as part of an array. However, these advantages are offset by low efficiency and limited bandwidth. In recent years much research and testing has been done to increase both the bandwidth and radiation efficiency of microstrip antennas.

Due to the recent interest in broadband antennas a microstrip patch antenna [7-8] was developed to meet the need for a cheap, low profile, broadband antenna. This antenna could be used in a wide range of applications such as in the communications industry for cell phones or satellite communication. Our aim is to reduce the size of the antenna as well as increase the operating bandwidth. The proposed antenna (substrate with ε_r = 4.4) has a gain of 3.19 dBi and presents a size reduction of 56.55% when compared to a conventional microstrip patch (10mm X 6mm). The simulation has been carried out by IE3D [19] software which uses the MoM method. Due to the small size, low cost and low weight this antenna is a good entrant for the application of X-Band microwave communication and Ku-Band RADAR communication & satellite communication. The X band and Ku-Band defined by an IEEE standard for radio waves and radar engineering with frequencies that ranges from 8.0 to 12.0 GHz and 12.0 to 18.0 GHz respectively[10]. The X band is used for short range tracking, missile guidance, marine, radar and air bone intercept. Especially it is used for radar communication ranges roughly from 8.29 GHz to 11.4 GHz. The Ku band [11-18] is used for high resolution mapping and satellite altimetry. Especially, Ku Band is used for tracking the satellite within the ranges roughly from 12.87 GHz to 14.43 GHz. In this paper the microstrip patch antenna is designed for use in a satellite TV at 13.7173 GHz. The results obtained provide a workable antenna design for incorporation in a satellite TV. We consider the satellite TV has two different bands one is FSS-band and another is DBS-band. The DBS systems can also run on C-band satellites and have been used by some networks in the past to get around legislation by some countries against reception of Ku-band transmissions.

2. ANTENNA DESIGN

The configuration of the conventional printed antenna is shown in Figure 1 with L=6 mm, W=10 mm, substrate (PTFE) thickness h = 1.6 mm, dielectric constant ε_r = 4.4. Coaxial probe-feed (radius=0.5mm) is located at W/2 and L/3. Assuming practical patch width W= 10 mm for efficient radiation and using the equation [6],

$$f_r = \frac{c}{2W} \times \sqrt{\frac{2}{(1+\varepsilon_r)}}$$

Where, c = velocity of light in free space. Using the following equation [9] we determined the practical length L (=6mm).

$$L = L_{eff} - 2\Delta L$$

Where, $\frac{\Delta L}{h} = \left[0.412 \times \frac{(\varepsilon_{reff}+0.3)\times(W/h+0.264)}{(\varepsilon_{reff}-0.258)\times(W/h+0.8)}\right]$

$$\varepsilon_{reff} = \left[\left(\frac{\varepsilon_r+1}{2}\right) + \frac{\varepsilon_r-1}{\left(2\times\sqrt{\left(1+12\times\frac{h}{W}\right)}\right)}\right]$$

and $$L_{eff} = \left[\frac{c}{2\times f_r \times \sqrt{\varepsilon_{eff}}}\right]$$

Where, L_{eff} = Effective length of the patch, $\Delta L/h$ =Normalized extension of the patch length, ε_{reff} = Effective dielectric constant.

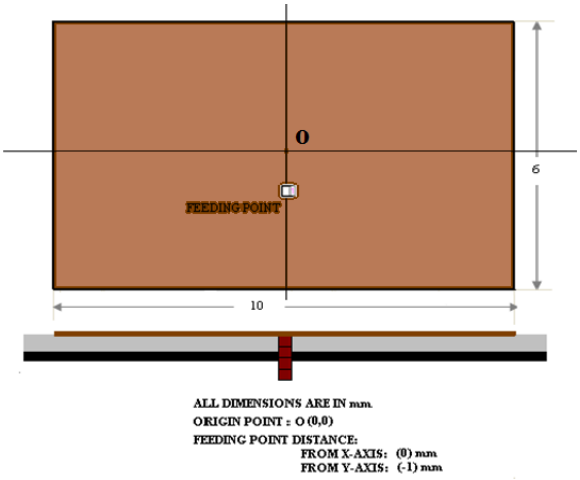

Figure 1: Conventional Antenna configuration

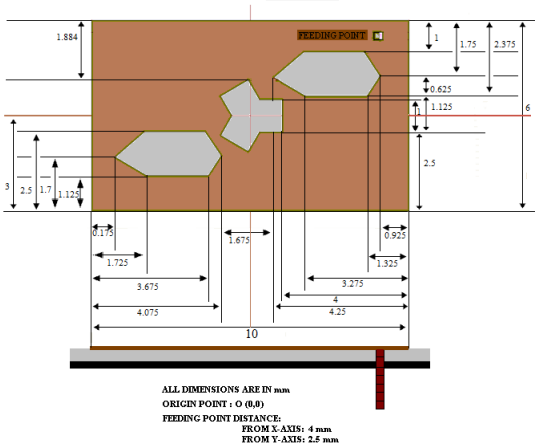

Figure 2: Simulated Antenna configuration

Figure 2 shows the configuration of simulated printed antenna designed with similar PTFE substrate. Two equal slots which are the combinations of two triangular and a rectangular slot at the upper right and lower left corner and the location of coaxial probe-feed (radius=0.5 mm) are shown in the figure 2.

3. Results And Discussion

Simulated (using IE3D [19]) results of return loss in conventional and simulated antenna structures are shown in Figure 3-4. A significant improvement of frequency reduction is achieved in simulated antenna with respect to the conventional antenna structure.

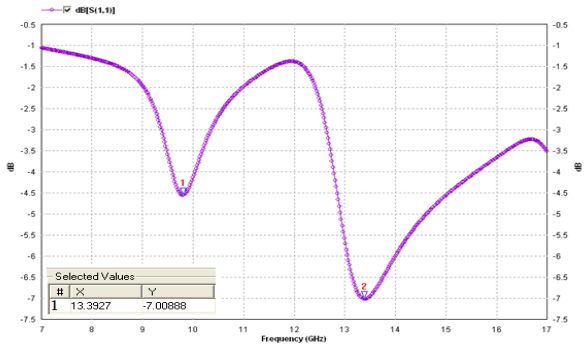

Figure 3: Return Loss vs. Frequency (Conventional Antenna)

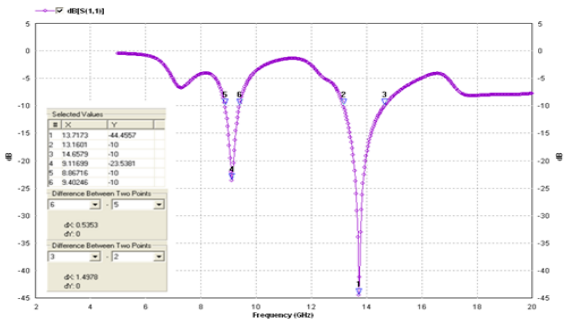

Figure 4: Return Loss vs. Frequency (Slotted Antenna)

In the conventional antenna return loss of about -7.01 dB is obtained at 13.39 GHz. Comparing fig.3 and fig.4 it may be observed that for the conventional antenna (fig.3), there is practically no resonant frequency at around 9.12 GHz with a return loss of around -6 dB. For the simulated antenna there is a resonant frequency at around 9.12 GHz where the return loss is as high as -23.43 dB.

Due to the presence of slots in simulated antenna resonant frequency operation is obtained with large values of frequency ratio. The first and second resonant frequency is obtained at f_1= 9.12 GHz with return loss of about -23.43 dB and at f_2 =

13.71 GHz with return losses -44.457 dB respectively. Corresponding 10dB band width obtained for Antenna 2 at f1, f2 are 535.30 MHz and 1.49 GHz respectively. The simulated E plane and H-plane radiation patterns are shown in Figure 5-16. The simulated E plane radiation pattern of simulated antenna for 9.12GHz is shown in figure 5.

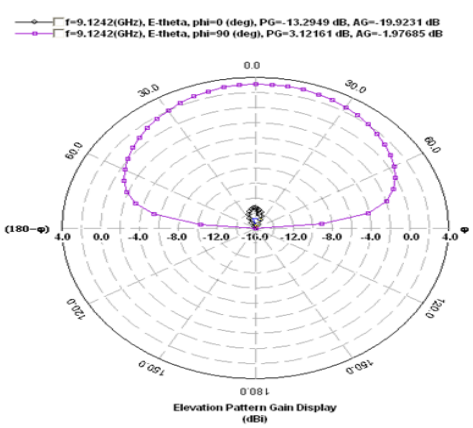

Figure 5: E-Plane Radiation Pattern for Slotted Antenna at 9.1242 GHz

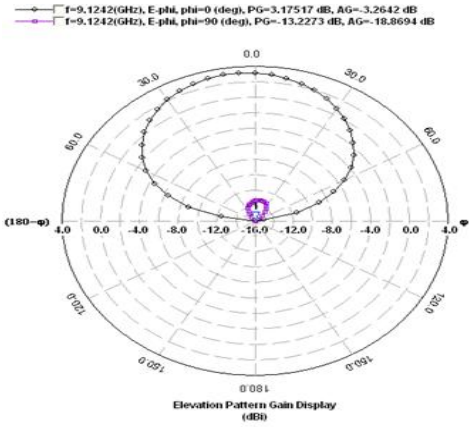

Figure 6: H-Plane Radiation Pattern for slotted Antenna at 9.1242 GHz

The simulated H plane radiation pattern of simulated antenna for 9.12 GHz is shown in figure 6.
The simulated E -plane & H-plane radiation pattern (3D) of simulated antenna for 9.12 GHz is shown in figure 7 & figure 8.

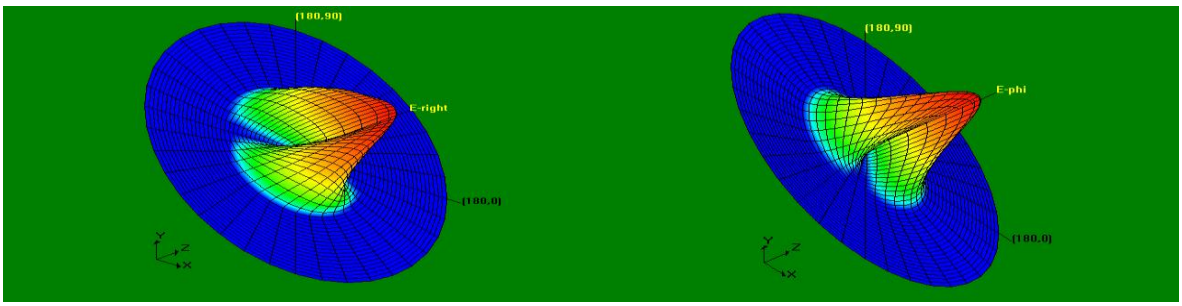

Figure 7: E-Plane Radiation Pattern (3D) for slotted antenna at 9.12GHz

Figure 8: E-Plane Radiation Pattern (3D) for slotted antenna at 9.12 GHz

The simulated E plane radiation pattern of slotted antenna for 13.71 GHz is shown in figure 9. The simulated H plane radiation pattern of slotted antenna for 13.71 GHz is shown in figure10.

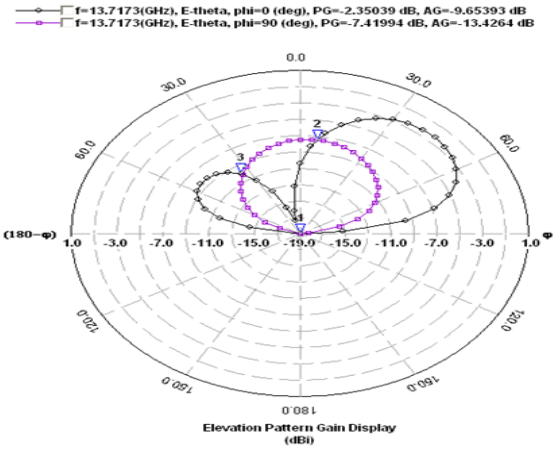

Figure9: E-Plane Radiation Pattern for slotted antenna at 13.71 GHz

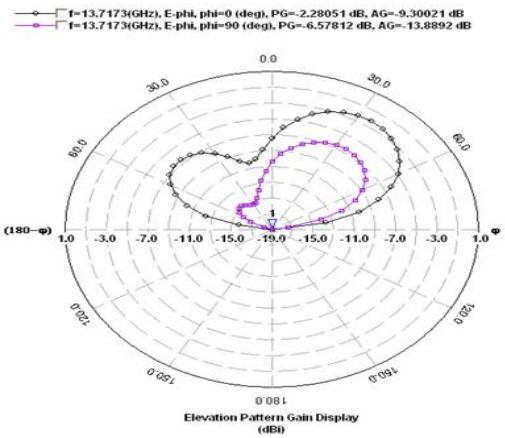

Figure 10: H-Plane Radiation Pattern for slotted antenna at 13.71 GHz

The simulated E -plane & H-plane radiation pattern (3D) of simulated antenna for 13.71 GHz is shown in figure 11 & figure 12.

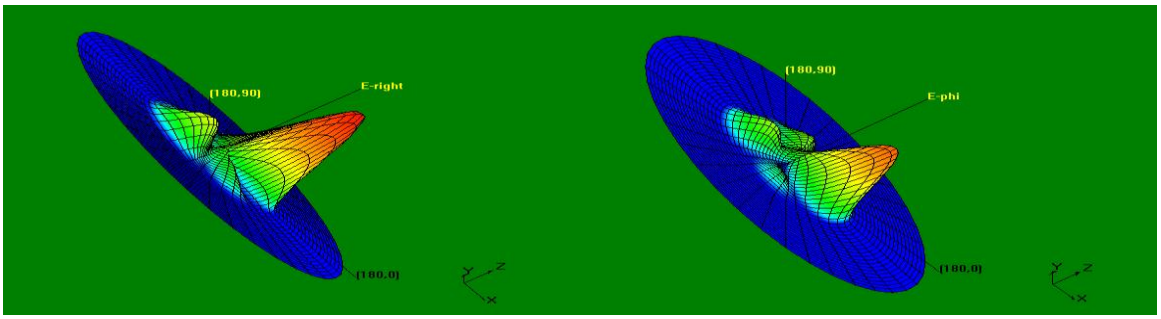

Figure11: E-Plane Radiation Pattern for slotted antenna at 13.71 GHz

Figure 12: H-Plane Radiation Pattern for slotted antenna at 13.71 GHz

The simulated smith chart and VSWR of simulated antenna shown in figure 13 & figure 14.

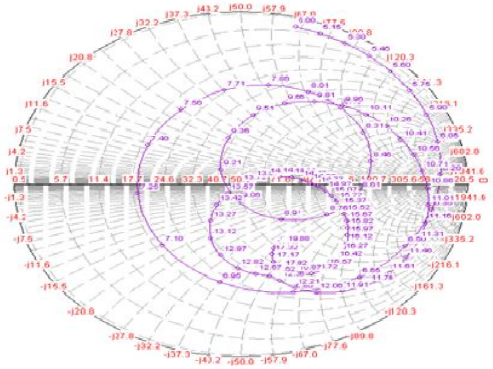

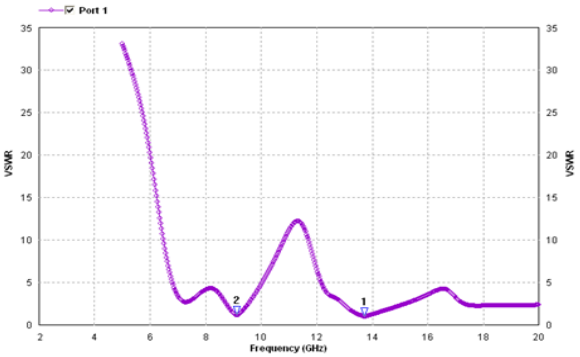

Figure13: Simulated Smith Chart for slotted antenna

Figure 14: Simulated VSWR for slotted antenna

The simulated E -plane & H-plane radiation pattern (2D) of simulated antenna for 13.71 GHz is shown in figure 15 & figure 16.

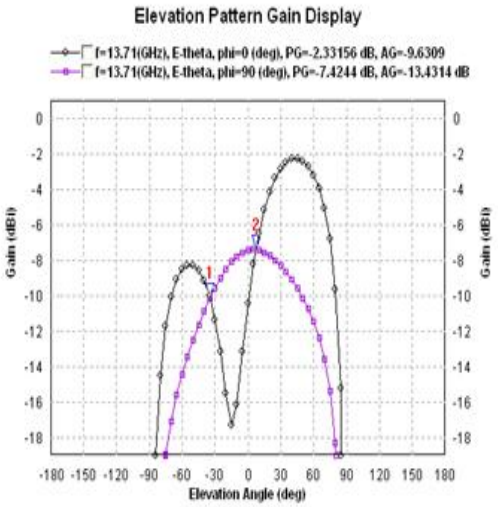

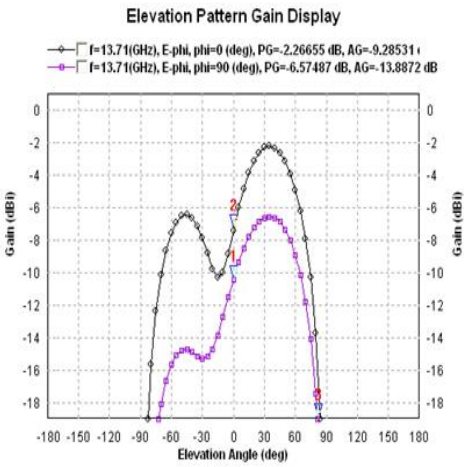

Figure9: E-Plane Radiation Pattern (2D) for slotted antenna at 13.71 GHz

Figure 10: H-Plane Radiation Pattern (2D) for slotted antenna at 13.71 GH

All the simulated results are summarized in the following Table1 and Table2.

TABLE I: SIMULATED RESULTS FOR ANTENNA 1 AND 2 w.r.t RETURN LOSS

ANTENNA STRUCTURE	RESONANT FREQUENCY (GHz)	RETURN LOSS (dB)	10 DB BANDWIDTH (GHz)
Conventional	f_1= 13.39	-7.00	NA
Slotted	f_1= 9.1242	-23.43	0.5353
	f_2 =13.7173	-44.457	1.4978

TABLE II: SIMULATED RESULTS FOR ANTENNA 1 AND 2 w.r.t RADIATION PATTERN

ANTENNA STRUCTURE	RESONANT FREQUENCY (GHz)	3DB BEAMWIDTH (^{0})	ABSOLUTE GAIN *(dBi)*
Conventional	f_1= 13.39	NA	NA
Slotted	f_1= 9.1242	162.914	3.19137
	f_2 =13.7173	64.47	0.627052
Frequency Ratio for Slotted Antenna			f_2 / f_1 =1.5034

4. CONCLUSION

This paper focused on the simulated design on differentially-driven microstrip antennas. Simulation studies of a single layer monopole hexagonal microstrip patch antenna have been carried out using Method of Moment based software IE3D. Introducing slots at the edge of the patch size reduction of about 56.55% has been achieved. The 3dB beam-width of the radiation patterns are 162.914° (for f_1), 64.47° (for f_2) which is sufficiently broad beam for the applications for which it is intended. The resonant frequency of slotted antenna, presented in the paper, designed for a particular location of feed point (4mm, 2.5mm) considering the centre as the origin. Alteration of the location of the feed point results in narrower 10dB bandwidth and less sharp resonances.

5. ACKNOWLEDGEMENT

M. Mukherjee wishes to acknowledge Defense Research and Development Organization (DRDO, Ministry of Defense), Govt. of India for their financial assistance.

REFERENCES

[1] I.Sarkar, P.P.Sarkar, S.K.Chowdhury "A New Compact Printed Antenna for Mobile Communication", 2009 Loughborough Antennas& Propagation Conference, 16-17 November 2009, pp 109-112.

[2] S. Chatterjee, U. Chakraborty, I.Sarkar, S. K. Chowdhury, and P.P.Sarkar, "A Compact Microstrip Antenna for Mobile Communication", IEEE annual conference. Paper ID: 510

[3] J.-W. Wu, H.-M. Hsiao, J.-H. Lu and S.-H. Chang, "Dual broadband design of rectangular slot antenna for 2.4 and 5 GHz wireless communication", IEE Electron. Lett. Vol. 40 No. 23, 11th November 2004.

[4] U. Chakraborty, S. Chatterjee, S. K. Chowdhury, and P. P. Sarkar, "A comact microstrip patch antenna for wireless communication," Progress In Electromagnetics Research C, Vol. 18, 211-220, 2011 http://www.jpier.org/pierc/pier.php?paper=10101205

[5] Rohit K. Raj, Monoj Joseph, C.K. Anandan, K. Vasudevan, P. Mohanan, " A New Compact Microstrip-Fed Dual-Band Coplaner Antenna for WLAN Applications", IEEE Trans. Antennas Propag., Vol. 54, No. 12, December 2006, pp 3755-3762.

[6] Zhijun Zhang, Magdy F. Iskander, Jean-Christophe Langer, and Jim Mathews, "Dual-Band WLAN Dipole Antenna Using an Internal Matching Circuit", IEEE Trans. Antennas and Propag.,VOL. 53, NO. 5, May 2005, pp 1813-1818.

[7] J. -Y. Jan and L. -C. Tseng, " Small planar monopole Antenna with a shorted parasitic inverted-L wire for Wireless communications in the 2.4, 5.2 and 5.8 GHz. bands" , IEEE Trans. Antennas and Propag., VOL. 52, NO. 7, July 2004, pp -1903-1905.

[8] Samiran Chatterjee, Joydeep Paul, Kalyanbrata Ghosh, P. P. Sarkar and S. K. Chowdhury "A Printed Patch Antenna for

Mobile Communication", Convergence of Optics and Electronics conference, 2011, Paper ID: 15, pp 102-107
[9] C. A. Balanis, "Advanced Engineering Electromagnetics", John Wiley & Sons., New York, 1989.
[10] Bipa Datta, Arnab Das, Samiran Chatterjee, Bipadtaran Sinhamahapatra, Supriya Jana, Moumita Mukherjee, Santosh Kumar Chowdhury, "Design of Compact Patch Antenna for Multi-Band Microwave Communication", National Conference on Sustainable Development through Innovative Research in Science and Technology (Extended Abstracts), Paper ID: 115, pp 155, 2012
[11] Arnab Das, Bipa Datta, Samiran Chatterjee, Bipadtaran Sinhamahapatra, Supriya Jana, Moumita Mukherjee, Santosh Kumar Chowdhury, "Multi-Band Microstrip Slotted Patch Antenna for Application in Microwave Communication," International Journal of Science and Advanced Technology(IJSAT), (ISSN 2221-8386), Vol. 2, Issue-9, 91-95, September 2012.
[12] Bipa Datta, Arnab Das, S.Chatterjee, B. Sinhamahapatra, S. Jana, M. Mukherjee, S. Kr. Chowdhury "Monopole Slotted Patch Antenna for Microwave Communication," International Journal of Scientific and Research Publications (IJSRP), ISSN 2250-3153, Volume 2, Issue 11, November 2012.
[13] Bipa Datta, Arnab Das, S.Chatterjee, M. Mukherjee, S. Kr. Chowdhury"A Monopole Printed Antenna for Tracking the Satellite," International Journal on Electronics & Communication Technology (IJECT), ISSN: 2230-7109 (Online) | ISSN: 2230-9543 (Print), IJECT Vol. 3, Issue 4, Oct - Dec 2012, PP 57-63.
[14] Arnab Das, Bipa Datta, Samiran Chatterjee, Moumita Mukherjee, Santosh Kumar Chowdhury, "A Dual- Band Size Deducted Slotted Patch Antenna for Application in Microwave Communication," International Journal on Electronics & Communication Technology, , ISSN : 2230-7109 (Online) | ISSN : 2230-9543 (Print), IJECT Vol. 3, Issue 4, Oct - Dec 2012, PP 51-56.
[15] Bipa Datta, Arnab Das, Samiran Chatterjee, Moumita Mukherjee, Santosh Kumar Chowdhury, "A Monopole Printed Antenna for Tracking the Satellite," International Journal on Electronics & Communication Technology, , ISSN : 2230-7109 (Online) | ISSN : 2230-9543 (Print), IJECT Vol. 3, Issue 4, Oct - Dec 2012, PP 57-63.
[16] Bipa Datta, Arnab Das, Samiran Chatterjee, Bipadtaran Sinhamahapatra, Supriya Jana, Moumita Mukherjee, Santosh Kumar Chowdhury, "Design of Single layer, Single Feed Slotted Patch Antenna for Microwave Communication", International Symposium on Microwaves-2012 (ISM-12) Paper ID: 106, 2012.
[17] Bipa Datta, Arnab Das, Samiran Chatterjee, Bipadtaran Sinhamahapatra, Supriya Jana, Moumita Mukherjee, Santosh Kumar Chowdhury, "A Compact Multi-resonant Microstrip Antenna", National Conference on Antennas and Propagation Symposium (APSYM-2012), Paper ID: 13102, 2012.
[18] Bipa Datta, Arnab Das, Samiran Chatterjee, Moumita Mukherjee, Santosh Kumar Chowdhury, "Monopole Slotted Patch Antenna for Microwave Communication," International Journal of Scientific and Research Publications (IJSRP) ISSN 2250-3153, Volume 2, Issue 11, November 2012.
[19] Zeland Software Inc. IE3D: MoM-Based EM Simulator. Web: http://www.zeland.com/

Study of Decision Making Process Using Psychology-Oriented Artificial Society Model, Part 2: Analysis of Decision Making Process in Bangladesh Regarding the Acceptance of Nuclear Power Plants

Sarkar Barbaq Quarmal[1], M. Khaled Kamal[2], Shanjida Afroj[3], Nalin Warnajith[4], Md. Ruhul Amin[5], Masanori Itaba[6], Atsushi Minato[7], and Satoru Ozawa[8]

[1, 4, 6, 7, 8] Graduate School of Science & Engineering, Ibaraki University, Hitachi 316-8511, Japan
[2]University of Rajshahi, Rajshahi-6205, Bangladesh, [5]Robert Walters Japan K. K., Tokyo 150-0002, Japan

Abstract:

The decision making process in Bangladesh regarding the acceptance of nuclear power plants has been analyzed on the basis of authors' psychology-oriented artificial society model [1]. The first part of this paper includes the selection of agents for the modeling, and collection of various parameters of Bangladeshi society. In particular, a "keyword analysis method" is proposed to determine the knowledge function of agents. From the keyword analysis of various message data from the agents, it has been found that the knowledge functions of government, general people and mass media have a similar structure which reflects their positive attitude to the problem; only social network media is against the problem. In the latter part, computer simulations are carried out and the knowledge function of each agent is calculated as a function of time. It has been shown from the computational study that the Bangladeshi society, as a whole, will continue to have a positive attitude to the problem in the next six years, and that this trend will not change even in a suppositional case where the effect of social network media is 10 times stronger than that of the present.

Keywords: artificial society model, knowledge, social decision making, message transfer, cognitive psychology

1. Introduction

This is Part 2 of authors' work on "the study of decision making process using psychology-oriented artificial society model". In Part 1 of the work [1], an artificial society model (ASM hereafter) [2] has been proposed which describes knowledge-based decision making processes in society on a given problem. The model consists of a set of agents which represent groups of similar character people in society regarding the problem. The agents are characterized by the extent of knowledge that they have on the problem. The knowledge of an agent is expressed by a mathematical function. Thinking process of the agent is simulated by using a linkage model of cognitive psychology [3]. A message is formed by the agent based on the knowledge function and the decision of the agent on the given problem, which is also expressed mathematically, and is transferred to another agent and modifies the knowledge function of the agent that receives the message. As a result, the model enables to simulate dynamics of decision making processes in society. This paper concerns the application of the ASM to analyze the problem of decision making process in Bangladesh regarding the acceptance of nuclear power plants (NPP hereafter). The aim of this paper is to carry out computer simulations of message exchange processes between agents and to forecast a future trend of Bangladeshi society regarding the acceptance of NPP.

2. NPP Problem in Bangladesh

The Government of Bangladesh has a plan to establish NPP in order to solve the problem of electricity shortage. A bilateral agreement with Russia has already been signed for setting up a two-unit NPP with a capacity of 1,000 megawatts each [4, 5]. Before going into the details of the computational analysis of the social acceptance of NPP, let us have a look over the present situation of Bangladeshi society related to the NPP problem. Bangladesh is a developing third world country. The capacity of the electricity generation plants in operation is not enough to meet the demand even though more than half of the population still does not have electricity at their home. At the end of 2011, electricity generation capacity was about 5200 MW which was short to the demand by roughly 1600 MW, which is shown in Figure 1. Therefore, the people often suffer from the shortage of electricity, especially in hot summer days. The farmers suffer from the problem in irrigation season. The industrial development of Bangladesh is slow due to the electricity shortage problem. The people want to get rid of this problem and the government of Bangladesh is also looking forward to solve this problem to activate further development of the country.

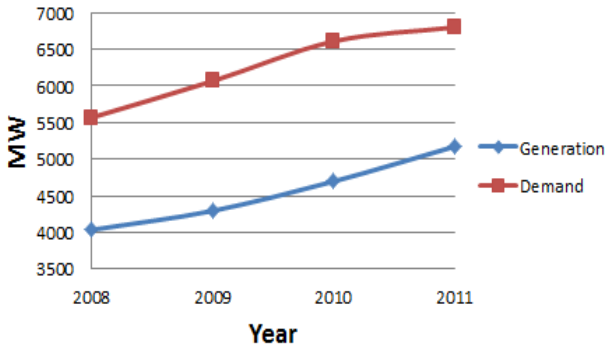

Figure 1: Electricity generation - demand curves in the last four years in Bangladesh (BPDB, Jan 2012).

Bangladesh is now depending on natural gas but the quantity of the possible reserves, which will sustain only for eight to ten years [6], is not enough to support the future energy demand. The government thinks that there is no other way but to depend on NPP. The government believes that NPP will help improving the electricity situation in a short period. When the government announced the NPP project in 2009, the major part of the general people welcomed it. The mass media of Bangladesh has not been negative to the NPP problem. But, when the Fukushima NPP accident happened in Japan on 11th March 2011, the general people in Bangladesh became panicked for fear that the radioactive contamination may reach to Bangladesh. Non-scientific rumors regarding radioactive contamination were spread by the people. The mass media in Bangladesh also played a role in driving the general people into the panic situation. A number of articles which stressed the negative aspects of using nuclear energy were published in most of the newspapers in Bangladesh. The television channels also did the same thing. On the other hand, social networking media, namely community blogs, were against the government's planning itself of producing NPP in Bangladesh. They discussed the negative aspects of using nuclear energy in a country like Bangladesh which is small, densely populated, and technologically non-matured. They urged the government to search for alternative energy sources such as solar energy, wind energy etc.

3. Modeling

In order to apply the psychology-oriented ASM of Part 1 to analyze decision making processes in Bangladesh regarding the acceptance of NPP, the following works are needed:

(1) Selection of agents,
(2) Definition and characterization of channels between agents,
(3) Preparation of knowledge functions of agents.

In the following subsections, these are described in detail.

3.1. Selection of agents

Bangladesh is a developing country in south Asia. By the constitution of Bangladesh, it is a democratic country where the prime minister is the head of the government. Bangladeshi economy is mainly agriculture-based and about two third of the total population are directly involved in agriculture. Table 1 shows some data regarding Bangladesh which portrays the society of Bangladesh.

Table 1: Bangladesh country profile [7-13]

Official name	People's Republic of Bangladesh		
Government	Unitary parliamentary democracy		
Gross national income per capita	$700		
	National	Urban	Rural
Population	150 million	38 million	112 million
Adult literacy	58%	68%	54%
Newspaper readers	40%	50%	36%
Mobile phone users	58%	80%	51%
Internet users	3.7%	10%	1.6%

To model the Bangladeshi society in the framework of ASM, we adopted four agents, i.e., general people (GP), government (GOV), mass media (MM), and social networking media (SNM). Hereafter, these agents are expressed in abbreviation. This model of four agents is very simple and basic. However, it can be the first approximation of the Bangladeshi society, from which we will deduce some valuable results on the problem. The first three agents, GOV, GP, and MM are "automatic choices" regarding this problem. We add here SNM as the fourth agent. The reasons why the first three are the automatic choices and why we need the fourth agent are described in the followings.

(1) The acceptance of NPP has become an issue of GOV for the electricity power supply. It is quite obvious that GOV plays the central role in decision making process regarding such a national problem in a country like Bangladesh.

(2) GP will be benefitted from the NPP by having enough electricity, and they support GOV's planning to produce NPP. On the other hand, GP will have to suffer if anything goes wrong in the NPP. So naturally, GP must take part in the decision making process regarding the establishment of an NPP. Although three-fourth of the population lives in the rural area, history of Bangladesh tells that the mass movements were mostly carried out in the urban centers, mainly at Dhaka, the capital of the country. Therefore, in the first approximation of Bangladesh society, GP is represented by the people in urban area. More detailed modeling which takes into account the negotiations between rural area and urban area will be given in author's next paper.

(3) MM is a very important agent in almost any social issue. It works as the main source of information to GP and ensures constant flow of public information or news about events occurring within the country and in the world. By providing information, MM works as the "agent of social change" and play important role in changing of attitudes, beliefs, and social norms [14-16]. On the other hand, thoughts and opinions from different part of the society on a particular problem are also reflected in MM. In this way MM works as a bridge between different parts of the society. As for the present problem, MM in Bangladesh has apparently positive attitude. Because, GOV and GP are showing positive attitude to the problem and their attitude reflects in MM.

(4) The emergence of SNM is not so old, but, it has already become a notable source of information as well as a popular media to exchange message around the globe. It is said that the SNM played a crucial role in the recent revolutions (the so called "Arab Spring") in Arabic world [17]. Few years ago, such phenomenon was observed in Bangladesh also. Local community blogs played a good role in building mass opinion to initiate the trial procedure of war criminals in the country's liberation war. The popularity and reliability that SNM has gained so quickly is due to its openness. Bangladesh is a democratic country and the MM is enjoying quite a freedom, while in some countries, voice of MM can be suppressed in many ways. However, SNM is free from this problem because it is the Internet-based and no one can completely control the flow of information through the Internet.

3.2. Definition and characterization of channels between agents

In the present study, there are four agents. Therefore, there are ${}_4P_2 = 4 \times 3 = 12$ channels among the agents, i.e., message flows through twelve channels from MM to GP, from GP to MM, from MM to GOV, from GOV to MM etc. But, no evidence has been found regarding direct message exchange between GOV and GP, and that between GOV and SNM in Bangladesh. GOV sends its message through MM. Also, GP send their messages to GOV through MM. Hence, message transfers from GOV to GP, from GP to GOV, from GOV to SNM and from SNM to GOV are excluded in the present model (See Figure 2). Table 2 shows the number of messages regarding NPP problem which are sent from one agent to the other agents per one year in Bangladesh.

Table 2: Number of messages sent by agents per year

To / From	GP	GOV	MM	SNM
GP	-	-	1	2.5
GOV	-	-	1.5	-
MM	3	3	-	3
SNM	3.5	-	3.5	-

In the ASM described in Part 1 [1], each agent has different character in receiving message. Some of them accept it as it is and the others do not. But, in the present study, the agents are assumed to be "simple-minded". Namely, they receive the messages from other agents without filtering. So, no modification has been implemented in the message receiving process of the agents. The parameter, $C_{i,j}(x)$ in Section II D of Part 1 is assumed to unit. Note that the definitions of $C_{i,j}(x)$ in Sections II C and II D are different although the same notation $C_{i,j}(x)$ is used there. In Section II C, it is used to modify conclusion function to produce message function, while in Section II D, it is a factor that represents effectiveness of acceptance of message. The message modification factor $C_{i,j}(x)$ in Section II C is also neglected in this study. Namely agents are assumed to express their idea honestly

as they are. Table 2 shows the channel capacity measured by the number of messages sent by an agent per one year. The messages from one agent do not reach all the members of the other agents. It depends on the "audience rating". For example, in Bangladesh, only about 50% of urban people read newspaper [12]. Therefore, the audience rating coefficient of the channel from MM to GP is 0.5 and the effective channel capacity, i.e., the number of messages from MM to GP is $3 \times 0.5 = 1.5$ per one year. Although the rate of the Internet users in Bangladesh [13] is about 3.7%, it rises to 10% in the urban areas. Therefore, the audience rating coefficient of the channel from SNM and GP is 0.1 and the effective capacity of the channel is $3.5 \times 0.1 = 0.35$. Note the character of GP regarding the social decision making process is estimated by that of GP in urban area (See (2) of Section 3.1). The audience rating coefficients of channels are summarized in Table 3, and the effective capacities of the channels are in Table 4. Thus, we obtain the distribution of channels between agents and their effective channel capacities, which is summarized in Figure 2.

Table 3: "Audience rating" coefficients of channels between agents

To / From	GP	GOV	MM	SNM
GP	-	-	0.08	0.02
GOV	-	-	1	-
MM	0.5	0.2	-	0.07
SNM	0.1	-	0.1	-

Table 4: Effective capacity of channels

To / From	GP	GOV	MM	SNM
GP	-	-	0.08	0.05
GOV	-	-	1.5	-
MM	1.5	0.6	-	0.21
SNM	0.35	-	0.35	-

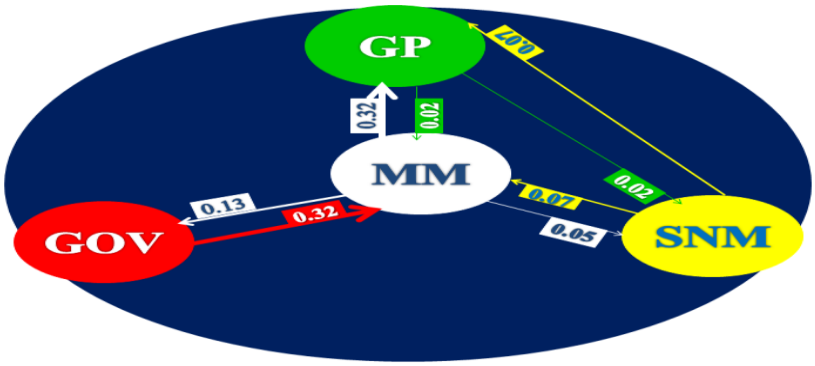

Figure 2: Assignment of channels and their effective channel capacity parameters.

3.3. Preparation of knowledge functions of agents

In the process of the application of the psychology-oriented ASM, preparation of knowledge functions is the most important part of the work. In order to explain how to do it, let us go back to the definition of knowledge function which was described in Section II of Part 1 of this study [1]. Look at Figure 3 of Part 1, where the ensemble of knowledge of an agent is shown. Each of the elements of the knowledge is labeled by an influential parameter, x ($x = 0$ is labeled to the knowledge completely negative to the question; $x = 1$is labeled to the completely positive knowledge; and $0 < x < 1$ correspond to the intermediate). As shown in Figure 4 of Part 1, we can produce the knowledge function of the agent if we arrange a lot of elements of the knowledge against the parameter x. Therefore, the method of obtaining the knowledge function of an agent is composed of the following two steps.

Step 1: Collection of elements of knowledge of an agent regarding a given problem.

Step 2: Labeling a value of influential parameter x to each of the elements of the knowledge.

One problem in Step 1 is that knowledge stored in human brain is not observable directly. But there is a method to guess the knowledge structure of an agent. It is to analyze messages from the agent. Note that message of an agent is formed from the knowledge of the agent (See Figure 2 of Part 1). The messages from an agent are samples of knowledge of the agent. There

would be various methods to analyze messages from agents. The authors propose here "keyword analysis method" to analyze messages from agents.
The keyword analysis method is composed of the following processes.

(1) The problem studied in the ASM is expressed in the form of a question: "Do you support or accept (something: action of the problem) in order to (do something)?" In our case, it becomes "Do you accept construction of NPP in order to solve the problem of shortage in electricity supply in Bangladesh?"
(2) Two kinds of questionnaire surveys are carried out, which correspond to Step 1 and Step2. In the questionnaire of Step 1, the question of (1) is asked to the members of an agent. This question triggers thinking and some ideas related to the question are coming into their mind (See Figure 5 of Part 1). They are requested to write their answers freely in sentences.
(3) These sentences are analyzed by computer and "keywords" are extracted by the software prepared by the authors for this purpose.
(4) These keywords and key phrases (combination of keywords) are tested by inserting them into a format: "Do you think the idea of (keyword/key phrase) leads positive answer to the question?" If the inserted sentence makes sense, it is adopted as a question of the questionnaire in Step 2. The sentence is rewritten without changing its meaning in case the sentence is not fluent even if it makes sense. In such a way, questionnaire format of Step 2 is prepared. The examinees of the questionnaire of Step 2 are requested to answer by "yes" or "no". The frequency of "yes" gives the value of the influence parameter, x.
(5) The number of one keyword counted in Step 1 versus the corresponding influence parameter, x curve gives the knowledge function of the agent.

The questionnaire experiments of Step 1 and Step 2 were carried out between June, 2011 and August, 2011 for GP of Bangladesh. One hundred people of different ages and of different professions were randomly selected and were interviewed with the aid of the questionnaire document of Step 1. Then, "keywords" were extracted by using the software, "Keyword Extractor" developed by authors [18]. They were tested by the method described in the process (4), and the questionnaire document for Step 2 was prepared. The questionnaire experiment of Step 2 was carried out also to one hundred examinees. Table 5 shows the result of the questionnaire experiments. The value of influence parameter, x for each keyword is obtained by dividing the number of "yes" by the number of examinees. By plotting the 2nd column data against the 4th column data, the knowledge function of GP can be obtained.

Table 5: Result of key word analysis for GP

Keyword or key phrase	Number Counted in Step 1	Number of "yes" in Step 2	Value of x
Nuclear waste management	12	8	0.08
Many countries going to stop using nuclear energy	14	16	0.16
Past accidents	23	20	0.20
lack of financial & tech. abilities	20	22	0.22
Radioactivity/health hazard	21	31	0.31
corruption	40	35	0.35
plant safety	45	39	0.39
Safe & clean source of energy	48	49	0.49
Efficient	48	51	0.51
Low cost	46	55	0.55
New employment opportunity	54	65	0.65
National development	63	74	0.74
Solve electricity crisis	68	80	0.80

These keywords were also examined in newspaper articles (the daily "Prothom Alo" [19] published in Bengali and the Daily Star [20] published in English), websites of the governmental organization [21], documents presented by Bangladesh government at International Atomic energy Agency (IAEA) [22] and articles published in social networking blogs ("Somewhereinblog" [23]). And the numbers of appearance of the keywords in these documents were counted. Namely, the 2nd column data were prepared also for GOV, MM and SNM. In such a way, we finally obtained the knowledge functions of the four agents, which has been

shown in Figure 3. Note that the knowledge functions are presented after the normalization. (See Section IIA of Part 1). It is seen from Figure 3 that the knowledge functions of GOV, GP and MM are similar and have a positive attitude to the problem; only SNM is against the problem. This is quite consistent with the description about the present status of Bangladeshi society (See Section 3.1 for the details.) As GP suffer a lot due to the shortage of electricity, GP as well as GOV wants a solution to this problem as soon as possible by any means. Such idea of GOV and GP reflects to MM. Therefore, the knowledge functions of GOV, GP and MM have a positive structure to the problem.

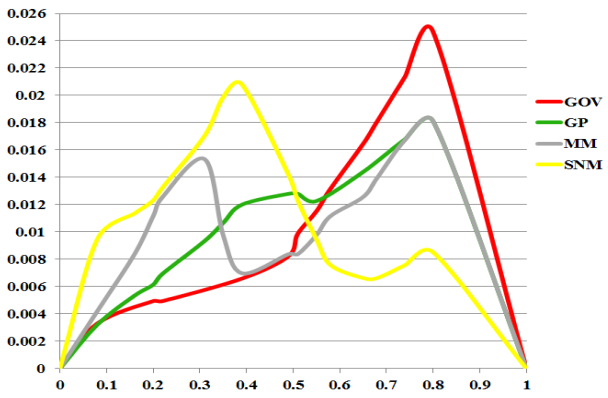

Figure 3: Knowledge Functions of four agents regarding acceptance of NPP in Bangladesh.

4. Computer Simulation

Since the knowledge functions of agents have been obtained in the previous section, the next step is to study how they will change in time. This work is equivalent to forecasting the future Bangladeshi society regarding the acceptance of NPP. The mechanism of the dynamics of the development of knowledge function is given in Part 1 of this work [1]. The decision making process (1) - (3), the message producing process (4), (5), and the knowledge modification process (6) - (8) are included in the present study. (See Section II of Part 1). However, the aging of received knowledge (9) - (11) is neglected here because the dynamics of knowledge function is to be studied for a short period less than six years (Compare the curve (2) to the others in Figure 12 of Part 1). The Figure 4 shows the flow chart of the program for the computer simulation of decision making processes in society. Note that after the calculations of the decision function, the message function and the modified knowledge function, they are always normalized numerically. All the procedures between the channel selection and the knowledge modification are repeated until a maximum number of iterations which corresponds to six years. Programming language C together with a graphics tool, SGL (Simple Graphics Library) [24] has been used in the program code.

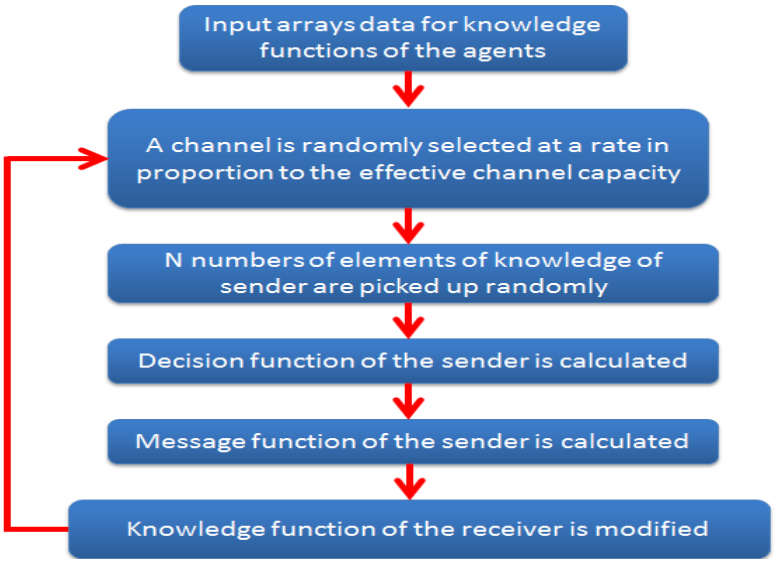

Figure 4: Flowchart of the computer simulation to realize time development of knowledge functions.

4.1. Computer Simulation by Using Real Channel Parameters

Computer simulations have been carried out using the channel parameters shown in Figure 2. Figure 5 shows the time-variation of the shape of the knowledge function of each agent.

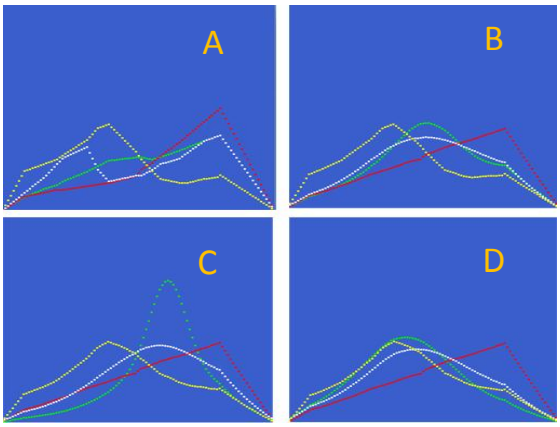

Figure 5: Time variation of the knowledge functions of the agents. (A) at present, (B) after 2 years, (C) after 4 years, and (D) after 6 years. The red, green, white and yellow curves represent knowledge functions of GOV, GP, MM and SNM, respectively.

It is seen from Figure 5 that the shape of knowledge functions of GP and MM changes dynamically in six years, while that of GOV and SNM does not change so much. The reason why the shape of knowledge functions of GP and MM fluctuate so much is that they have a wide structure of knowledge ranging from very positive to very negative to the problem and their conclusions sometimes fluctuate (see Section IIIA of Part 1). The reason why the shape of knowledge functions of GOV and SNM do not fluctuate is understood from the fact that their knowledge structure is sharp and they do not have strong message flows from the other agents. This is related to the strict attitude of the government concerning NPP problem as described in Section III A. The change in attitude of the agents regarding the problem can more clearly be observed if we calculate the center x_c of knowledge which is defined as

$$x_c = \frac{\int_0^1 x\, f(x)\, dx}{\int_0^1 f(x)\, dx} = \int_0^1 x\, f(x) dx.$$

Here, $f(x)$ is knowledge function of an agent. Note the knowledge function is always normalized, i.e., $\int_0^1 f(x)\, dx = 1$.

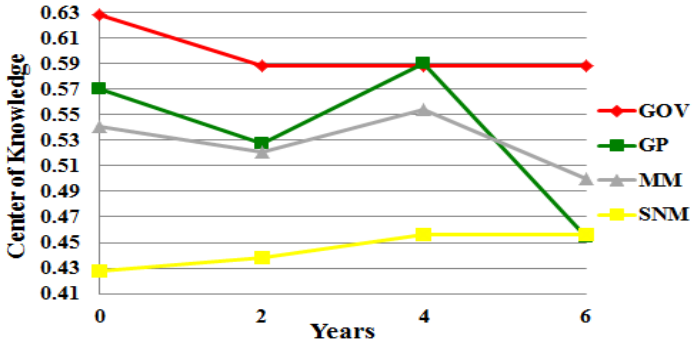

Figure 6: Time variation of center of knowledge of four agents.

The value of center of knowledge can be a measure of "mean attitude" of the agent to the problem. When the value of center of knowledge is higher than 0.5, it represents a positive attitude to the problem. And the values lower than 0.5 represent a negative attitude to the problem. It is seen from Figure 6 that all the agents except SNM usually have a positive attitude to the problem, and GOV is the most positive. It should be noted again that the attitude of GP fluctuates so much. The fluctuations are also seen for MM. The knowledge function of MM has two peaks which correspond to negative and positive groups of knowledge. The wide range of the knowledge distribution produces greater fluctuations in the decision making processes, which, in turn, produce

fluctuations in time variation of their attitude. The fluctuations occur in the real society as well. But we like to discuss here "mean time variation of attitude". So we repeated the same computer simulations only by changing the series of random number and produced thirty samples of time variation of knowledge functions, and then calculated the mean of x_c over the thirty samples. Figure 7 shows the ensemble-averaged time variation of x_c. Small fluctuations of x_c are still observed for GP and MM in Figure 7. The fluctuation becomes smaller if we take ensemble average over much more samples. It is seen from Figure 7 that GOV moves by a small extent to negative direction but its attitude is still most positive to the problem; GP and MM do not change notably; SNM moves to positive direction but its attitude is still the most negative. As a whole, the Bangladeshi society keeps the positive attitude to the problem of the acceptance of NPP. The change in the attitude in six years is negligibly small as far as we discuss the problem on the basis of "ensemble-averaged time variation of attitude". In real society as well as in computer simulations, fluctuations of the attitude always happen. For example, if NPP accident occurs, then the knowledge functions tend to shift to the negative direction. Since we cannot forecast such happenings, we cannot discuss when and how the knowledge function fluctuates. We should note that the thing we can discuss here by this model is only "ensemble-averaged" quantity. This is because the model is based on stochastic processes where the causality is not taken into account. In this sense, the formulation of the present study is similar to that of quantum mechanics, which is stressed in Section III B in Part 1 of this study [1].

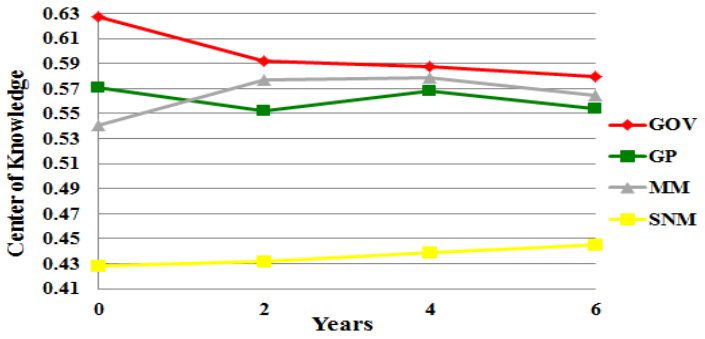

Figure 7: Ensemble-averaged time-variation of center of knowledge of four agents.

3.2. Computer Simulation by Using Suppositional Channel Parameters

As is shown in the previous section, GOV, GP and MM have positive attitude to the acceptance of NPP in Bangladesh. Only SNM has negative attitude to the problem. It has been found from the computer simulation that this situation will not change in next six years. It is because SNM is very weak in Bangladeshi society at present. Now, let us consider a suppositional case where SNM is much stronger than as it is today. For example, we assume that the effective channel capacity is five times larger than it is now, namely, we modify the corresponding values in Table 4 from 0.35 to 1.75. The reason why we consider such suppositional case is that the number of the Internet users is rapidly increasing in Bangladesh [13]. Figure 8 show the result of the computer simulation in which the suppositional parameters are adopted. It is seen from this figure that GOV, GP and MM move much more to the negative direction as compared with the computer simulation with the real parameters (Figure 7). However, as a whole, the Bangladeshi society still remains at positive attitude to the problem even if SNM is five time stronger than the present situation of SNM in Bangladesh. From a similar computer simulation where the effect of SNM is ten times stronger than that of the present, it has been found that the Bangladeshi society will be, as a whole, positive to the problem in the next six years.

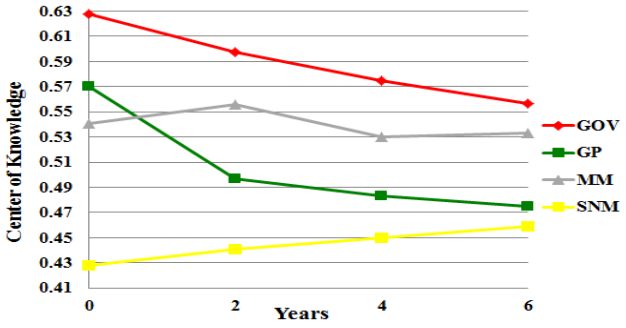

Figure 8: Ensemble-averaged time-variation of center of knowledge in the suppositional case where SNM is five times stronger than present.

5. Conclusion

The psychology-oriented ASM of Part 1 of this study [1] was used to analyze decision making processes in Bangladesh regarding the acceptance of NPP. The four agents, GOV, GP, MM and SNM were selected to model the Bangladeshi society in the framework of the psychology-oriented ASM. Between the agents, the channels were defined and the effective channel capacities were determined from the data in references. The keyword analysis method was proposed to determine the knowledge functions of the agents. This method was applied for the analysis of publications of GOV, questionnaire data of GP, newspaper articles of MM, and blog articles of SNM. It has been found from the analysis that the knowledge functions of GOV, GP and MM have a similar structure which reflects their positive attitude to the problem; only SNM is against the problem. Computer simulations were carried out to forecast the future trend of the acceptance of NPP in Bangladesh. It has been found from the simulations that the structure of knowledge of GP and MM changes dynamically in six years, while that of GOV and SNM does not change so much. The reason for the behavior of GP and MM is that they have a wide structure of knowledge ranging from very positive to very negative to the problem and their conclusions sometimes fluctuate. The reason why GOV and SNM do not fluctuate is that their knowledge structure is sharp and they do not have strong message flows from the other agents. Such fluctuations actually happen in real society. However, we liked to exclude the fluctuations from our discussion because the fluctuation has a stochastic character and it is nonsense to forecast. So, the same computer simulations were repeated only by changing series of random number, and the obtained data were ensemble-averaged over many samples. From the analysis of the ensemble-averaged time-variation of center of knowledge, it has been found that the Bangladeshi society, as a whole, keeps their positive attitude to the problem in the next six years. The computer simulation showed that this trend does not change even in a suppositional case where the effect of SNM is ten times stronger than that of the present.

6. Acknowledgement

One of the authors (Prof. Dr. Satoru Ozawa) expresses sincere thanks to Prof. Dr. Dieter W. Heermann, University of Heidelberg for his interest into this topic. This work was partly supported by the Grants in Aid 20500825, the Grand in Aid 24650124 and the Grants in Aid 24300278, Ministry of Education, Culture Sports, Science and Technology, Japan.

References

[1] **Sarkar Barbaq Quarmal, Masanori Itaba, Atsushi Minato and Satoru Ozawa**, Study of Decision Making Process using Psychology- Oriented Artificial Society Model, Part 1: Proposal of Mathematical Formulation for Computer Simulations of Psychology, Canadian Journal on Artificial Intelligence, Machine Learning and Pattern Recognition Vol. 3 No. 1, pp. 14-23, January 2012

[2] **Epstein, J. M. and Axtell R.,** Growing Artificial Societies: Social Science from the Bottom Up, Brookings Institution Press, Washington DC, U. S. A., (1996)

[3] **Weiner, B.**, A cognitive (attribution)-emotion-action
Model of motivated behavior, Jour. Personality and Social Psychology, Vol. 39(2), pp.186-200, Aug, 1980

[4] **The Daily Star**, 2011 Nov 03;

[5] **The Daily Prothom Alo**, 2011 Nov 03).

[6] Engr. Khondkar Abdus Saleque, How Long Bangladesh Gas Reserve Resource Will Last?, Energy Bangla, 01 February 2012

[7] **Constitution of Bangladesh,** Part 1, Article 1

[8] **Constitution of Bangladesh,** Part V, Chapter 1, Article 66

[9] **Bangladesh Bureau of Statistics (BBS),** Population and Housing Census 2011 (preliminary results), April, 2012

[10] **International Monetary Fund (IMF),** World Economic Outlook Database, April 2012

[11] **Bangladesh Bureau of Statistics (BBS),** The Bangladesh Literacy Survey (2010), June, 2011

[12] **AC Nielsen**, National Media and Demographic Survey 2011

[13] ^ **The World Bank website**, The Internet users (per 100 people), http://data.worldbank.org/indicator/IT.NET.USER.P2

[14] **Harold Lasswell**, "The Structure and Function of Communication in Society", in **Lyman Bryson (1948) (ed.)**, The Communication of Ideas, The Institute for Religious and Social Studies.

[15] **Schramm, W. ve Roberts, D. F. (1971)** The Process and Effects of Mass Communication, Urbana: University of Illinois Press, s. 84-99.

[16] **Wilbur schramm**, Mass Media and National Development: The Role of Information in the Developing Countries, 1964 Stanford University Press, PP. 114

[17] **Kate Taylor**, "Arab Spring really was social media revolution", TG Daily, **September 13, 2011**

[18] ^ **Keyword Extractor,** www.kissel1.base.ibaraki.ac.jp/apps/keywordextractor

[19] The Daily Prothom Alo, issues published between 2009 Jan 01 – 2011 Dec 31

[20] The Daily Star, issues published between 2009 Jan 01 – 2011 Dec 31

[21] ^ **Website of Ministry of Science and Technology, Government of Bangladsh**, Background and Current Status of Rooppur Nuclear Power Plant, http://www.mosict.gov.bd

[22] **Documents presented by Bangladesh government at IAEA,** downloaded from www.IAEA.org

[23] **Somewhereinblog (community blog space, url: www.sowhereinblog.com), articles published between** 2009 Jan 01 – 2011 Dec 31

[24] **Ozawa, S, Joarder, M. A., Dassanayake, G. and Patu V.,** Introduction to C and X Window Programming, Godage International Publishers (Pvt) Ltd., Colombo, Sri Lanka, 2010

Design of Simulink Model for Real Time Video/Image Splitting

[1,] Naveen B.,[2,] Dr. K.R. Nataraj., [3,] Dr. K.R. Rekha
[1,]Department of ECE, Jnana Vikas Institute of Technology, Bangalore.
[2,] Department of ECE, SJB Institute of Technology, Bangalore.
[3,] Department of ECE, SJB Institute of Technology, Bangalore.

Abstract

For split the real time image/video of size P x Q into four image/video blocks. Each splitted image/video blocks are interpolated to the dimension of the original image without blurring and display video/image in four different screens. Video splitting is the process of dividing the video into non overlapping parts. In this paper , techniques for splitting an image are implemented using MATLAB simulink.

Keywords: Image, Video, Splitting, Simulink.

1. Introduction

Video is the technology of electronically capturing, recording, processing, storing, transmitting, and reconstructing a sequence of still images representing scenes in motion. Video Splitting is the process of dividing the video into non overlapping parts. Then row mean and column mean or each part is obtained. By using splitting higher precision and display in different Screen [1,2]. An image is defined as a two dimensional function, *f(x, y),* where *x* and *y* are spatial coordinates, and the amplitude of *f* at any pair of coordinates *(x, y)* is called the intensity or gray level of the image at that point. When *x, y* and the intensity values of *f* are all finite, discrete quantities, we call the image a digital image [3]. Digital image is composed of a finite number of elements, each of which has a particular location and value. These elements are called picture elements, image elements, pels, and pixels. Pixel is a term used most widely to denote the elements of a digital image. Pixels are normally arranged in a two dimensional grid and are often represented using dots or squares. Number of pixels in an image can be called as resolution. Associated with each pixel is a number known as Digital Number or Brightness Value that depicts the average radiance of a relatively small area within a scene. The matrix structure of the digital image is shown in Fig 1.

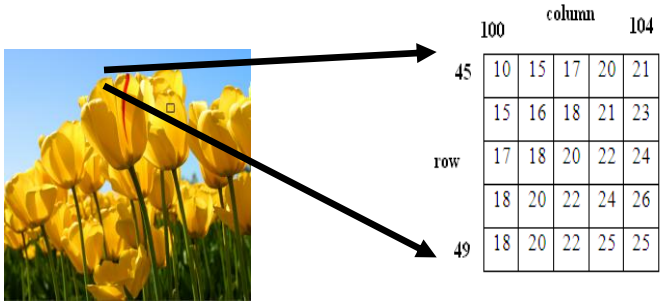

Fig 1: Structure of Digital Image

In Fig 2. These block diagram the input video image with resolution P X Q is applied to the image splitting system. After processing in image splitting system the video image is displayed on the four different LCD screens. Each splitted frame is interpolated to the original input video image resolution. a modified version of classical split and merge algorithm. Instead of performing a regular decomposition of image, it relies on a split at an optimal position that does a good inter region separation [4].The implementation of the algorithm uses an initial image processing to speed up computation. An interpolation algorithm for 3-D reconstruction of magnetic resonance images [5]. This investigation evaluates various interpolation algorithms for generating "missing data between multiple, 2D magnetic resonance image plane. Slices when stacked parallel and displayed, represents a 3D volume of data usually with poorer resolution in the third dimension. Interpolation algorithm have been developed to determine the missing data between the image slices and to compute a 3D volume data array representing equal spatial resolution in three dimension . An enhanced pixel-based video frame interpolation algorithms [6].

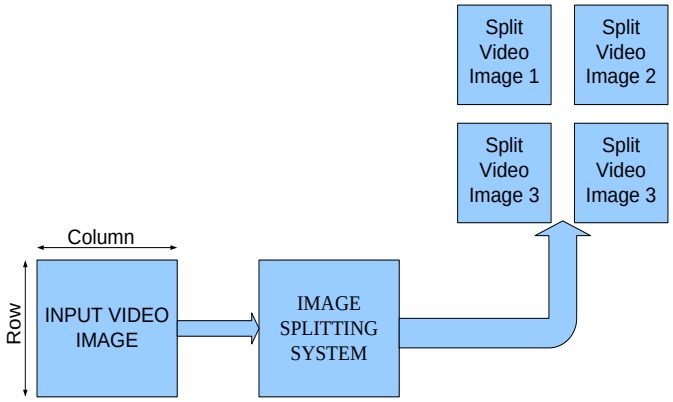

Fig 2: Block Diagram of the Video/Image Splitting

In paper [7] compares three motion compensated interpolation algorithms: adjacent frame motion compensated interpolation (AFI), and wide span motion compensated interpolation (WS-TH) and wide span motion compensated interpolation with spatial hinting. The latter represents an extension to WS-TS by adding spatial hinting to the generation of motion vectors. a design methodology for implementing DSP with Xilinx system generator for Matlab [7]. This methodology aims at improving the efficiency of learning the use of complex designs. This paper is organized as follows. Section 2 gives a Brief overview of the Image/video Splitting. Section 3 presents the Simulink parameters for the Image/video Splitting. Section.4 gives the design of simulink for proposed real time Image/video Splitting. For Simulink results are presented in Section 5. A conclusion and future work is given in Section 6.

2. Proposed Block Diagram Of Image/Video Splitting

The block diagram of the design is as shown in Fig. 3. Video from the web camera at 30 frames per second is applied to the video input block. Resize block enlarge or shrinks image size. Captured video will be in RGB format. It is converted into croma and luma components. Luma represents the brightness in an image and it represents the achromatic image without any color while the croma component represents the color information. Image split block splits the image into number of blocks. Each spitted block is resized using bilinear interpolation technique. The split image is displayed using the video display output block

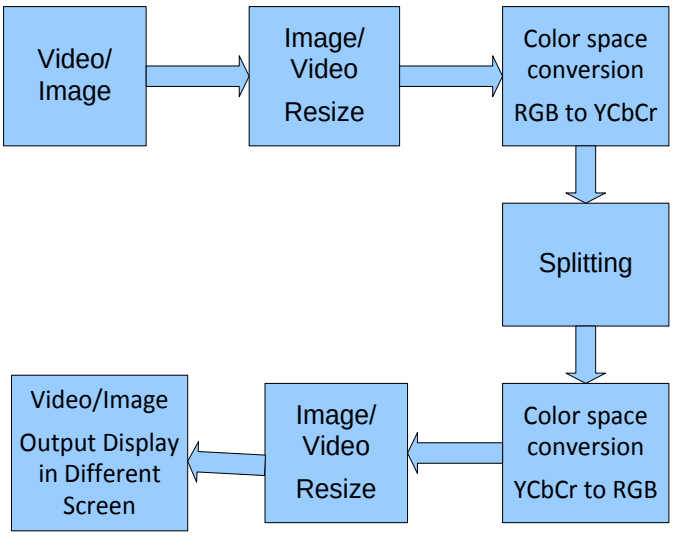

Fig. 3: Block Diagram of Image/video Splitting

3. Simulink Parameters

The Design is carried out using video and image processing blockset in MATLAB simulink version R2007b. here how images are spitted and various parameters required achieving the desired task.

A. Image From File:

Image From camera

Image From camera device is used to import an image from a supported image file. If the image is a M-by-N array, the block outputs a binary or intensity image, where M and N are the number of rows and columns in the image. If the image is a M-by-N-by-P array, the block outputs a color image, where M and N are the number of rows and columns in each color plane, P. For Video and Image Processing Blockset blocks to display video data properly, double- and single-precision floating-point pixel values must be between 0 and 1[2]. Use the Image signal parameter to specify how the block outputs a color video signal.

B. From Video Device:

From Video Device

The From Video Device block allows acquiring image and video data streams from image acquisition devices, such as cameras and frame grabbers, in order to bring the image data into a Simulink model [2]. The block also allows configuring and previewing the acquisition directly from Simulink. The From Video Device block opens, initializes, configures, and controls an acquisition device.The opening, initializing, and configuring occur once, at the start of the model's execution. During the model's run time, the block buffers image data, delivering one image frame for each simulation time step. The block has no input ports. Block can be configured to have either one output port, or three output ports corresponding to the uncompressed color bands, such as red, green, and blue, or Y, C_b, C_r.

C. Resize:

Resize

The Resize block enlarges or shrinks an image by resizing the image along one dimension (row or column). Then, it resizes the image along the other dimension (column or row). If the data type of the input signal is floating point, the output has the same data type. Use the specify parameter to designate the parameters to use to resize the image. Important choices in this block are Output size as a percentage of input size, Number of output columns and preserve aspect ratio, Number of output rows and preserve aspect ratio, Number of output rows and columns. If, for the Specify parameter, we can select Output size as a percentage of input size, the Resize factor in % parameter appears in the dialog box.

D. Color Space Conversion:

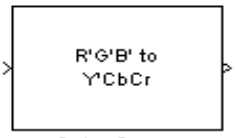

Color Space
Conversion

The R'G'B' to Y'CbCr conversion and the Y'CbCr to R'G'B' conversion are defined by the following equation

$$\begin{bmatrix} Y' \\ Cb \\ Cr \end{bmatrix} = \begin{bmatrix} 16 \\ 128 \\ 128 \end{bmatrix} + A \times \begin{bmatrix} R' \\ G' \\ B' \end{bmatrix}$$

$$\begin{bmatrix} R' \\ G' \\ B' \end{bmatrix} = B \times \left(\begin{bmatrix} Y' \\ Cb \\ Cr \end{bmatrix} - \begin{bmatrix} 16 \\ 128 \\ 128 \end{bmatrix} \right)$$

The values in the A and B matrices are based on your choices for the Use conversion specified by and scanning standard parameters.

Why RGB To YC_bC_r Conversion:

A Bitmap image uses the RGB Planes directly to represent color images. Medical research proved that the human eye has different sensitivity to color and brightness. Thus there came about the transformation of RGB to YC_bC_r. Medical investigation shows that there are rods are 120 million in number and cons are 6-7 million. Rods are much more sensitive than cons. The rods are not sensitive to color, while the cons which provide much of the eyes sensitivity are found to be located close to a central region called the mocula. And another reason is conversion reduces the simulation time in other words increases the data transfer rate. Fig. 4. a, b, c, d shows RGB, Y, C_b, C_r image respectively.

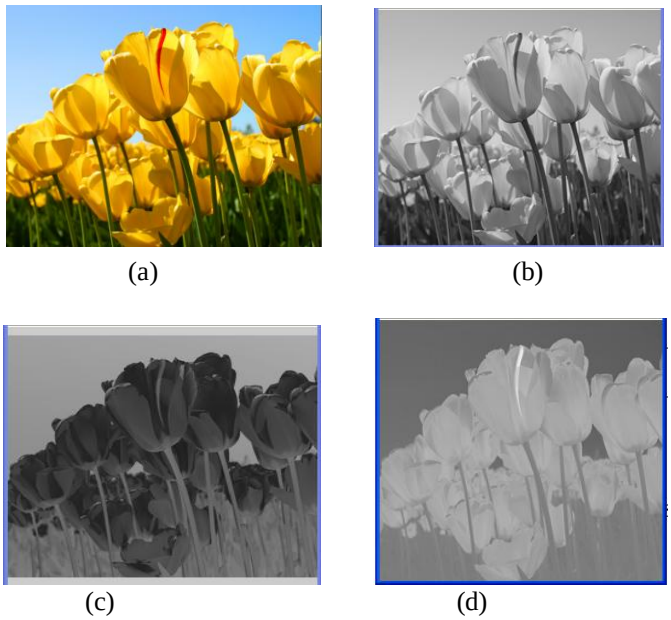

(a) (b)

(c) (d)

Fig 4: Color Representation (a) RGB image (b) Y Component (c) Cb Component (d) Cr Component

E. Matrix Concatenation*:*

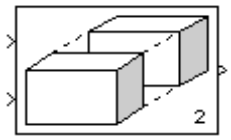

The Concatenate block concatenates the signals at its inputs to create an output signal whose elements reside in contiguous locations in memory. This block operates in either vector or multidimensional array concatenation mode, depending on the setting of its Mode parameter. In either case, the inputs are concatenated from the top to bottom, or left to right, input ports. In vector mode, all input signals must be either vectors or row vectors [1xM matrices] or column vectors [Mx1 matrices] or a combination of vectors and either row or column vectors.

F. Submatrix Selection:

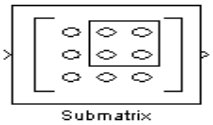

The Submatrix block extracts a contiguous submatrix from the M-by-N input matrix u as shown in Fig.5. The Row span parameter provides three options for specifying the range of rows in u to be retained in submatrix output y:

1. All rows: Specifies that y contains all M rows of 'u'.
2. One row: Specifies that y contains only one row from u. The Starting row parameter is enabled to allow selection of the desired row.
3. Range of rows: Specifies that y contains one or more rows from u. The Row and Ending row parameters are enabled to allow selection of the desired range of rows.

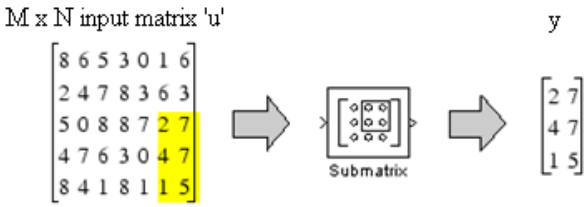

Fig. 5: Submatrix Selection

The Column span parameter contains a corresponding set of three options for specifying the range of columns in u to be retained in submatrix y: All columns, one column, or Range of columns. The One column option enables the Column parameter, and Range of columns options enables the Starting column and Ending column parameters. The output has the same frame status as the input.

G. To Video Display:

To Video Display block sends video data to a DirectX supported video output device or video camera. Alternatively, we can send the video data to a separate monitor or view the data in a window on your own computer screen. For the block to display video data properly, double- and single-precision floating-point pixel values are from 0 to 1. For any other data type, the pixel values must be between the minimum and maximum values supported by their data type. Use the Video output device parameter to specify where we want the video stream to be sent. If On-screen video monitor is selected then video stream is displayed in the To Video Display window when we run the model. This window closes automatically when the simulation stops.

H. UDP Send:

The Send block has only one input port, which receives the uint8 vector that is sent as a UDP packet.IP address to send to specify the IP address to send the packet. IP port to send to specify the port to which to send the packet. Use the following local IP port Set this parameter to -1 (default) to allow the networking stack to automatically determine the local IP port that is used for sending. Otherwise, specify a particular port to send a packet from that port. Sample time You can set this parameter to -1 for an inheritable sample time, but it is recommended that this be set to some specific (large) value to eliminate chances of dropped packets. This is especially true when you are using a small base sample time.

I. UDP Receive:

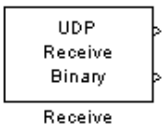

The Receive block has two output ports. The first port is the output of the received data as a vector of uint8 while the second one is a flag indicating whether any new data has been received. This port outputs a value of 1 for the sample when there is new data and a 0 otherwise. The default behaviour of the Receive block is to keep the previous output when there is no new data. You can modify this behaviour by using the second port to flag when there is new data. IP address to receive from can be left with the default value of 0.0.0.0. This accepts all UDP packets from any other computer. If set to a specific IP address, only packets arriving from that IP address are received. IP port to receive from port that the block accepts data from. The other end of the communication sends data to the port specified here. Output port with width of the acceptable packets. You can obtain this when designing the other side (send side) of the communication. Sample time You can set this parameter to -1 for an inheritable sample time, but it is recommended that this be set to some specific (large) value to eliminate chances of dropped packets. This is especially true when you are using a small base sample time.

4. Simulink Design For Real Time Video Image Splitting

The simulink model for splitting the image into four parts is as show in Fig.6. The original real time image in RGB format. Resize block resizes the image to the specified value say 256 x 256.

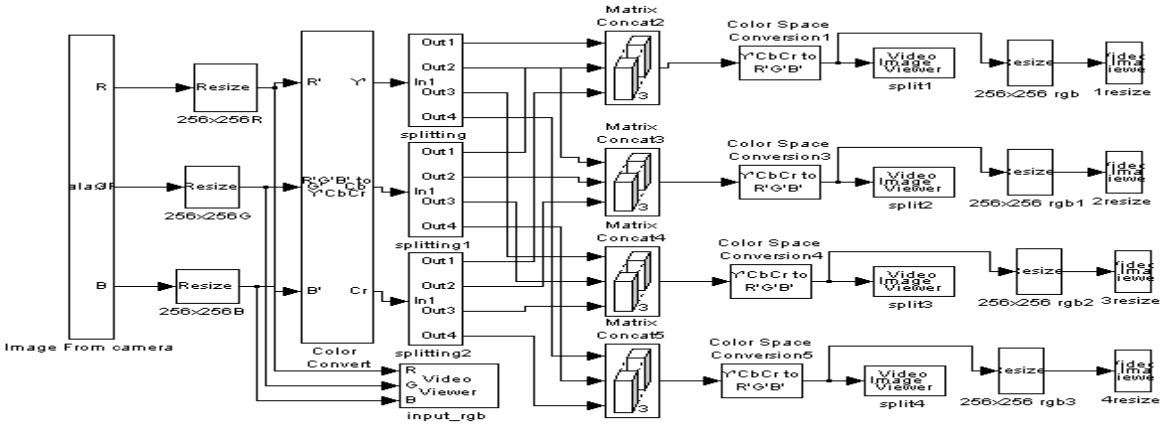

Fig 6 : Simulink Design for Video Image Splitting

Color conversion block converts the input RGB format to YC_bC_r format. Y stands for intensity component (luma). C_b and C_r stands for blue difference and red difference (croma) components respectively. These croma and luma components is applied to the splitting block. Splitting block is a subsystem which is having one input and four outputs. This splitting block consists of submatrix block. Submatric is used to select the image matrix. Each Splitting block contains four outputs of dimension 128 x 128. One output from each splitting block is concatenated.ie first output from splitting block, splitting1 block and splitting2 block respectively. When we do this we will get one entire image. Similarly this procedure is carried out for all the outputs of splitting block. This image is in YC_bC_r format. The image is converted back to RGB format using color conversion block. Splitted bocks are resized to the original dimension of the input image. For resizing we use bicubic interpolation technique. Resized images are displayed using video display blocks.

5. Simulink Model Results

The results of the software reference model are shown below. The input image for the reference model is in RGB format. Its dimension is 256 x 256 shown in Fig. 7.

Fig 7: Input Image(256 x 256)

The input image/video of the software reference model is splitted as shown in Fig.8. Even the splitted image in RGB format and having dimension 128 x 128.

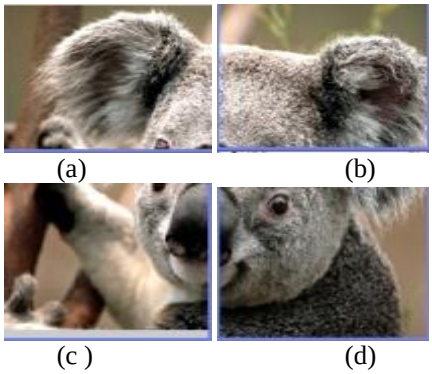

(a) (b)

(c) (d)

Fig 8: Splitted Image 128 x 128

6. Conclusion and Future Work

We proposed Video image splitting, in that first step in this work was to split the image using the Matlab simulink. Simulink design is carried out using the sub matrix block to split the image. Then this splitted image is resized using bilinear interpolation technique. Splitted image is sent to four different pc's by using simulink. In future the design can be extended for eight splitted blocks to different LCD screens to have a closer look of the spot also it can be implemented on system generator and FPGA.

References

[1] Cyril Prassana Raj P, Dr. S.L. Pinjare, and Swamy.T.N, **"FPGA implementation of efficient algorithm of image splitting for video streaming data"**, International Journal of Engineering Research and Applications (IJERA) ISSN: 2248-9622 www.ijera.com Vol. 2, Issue 5, page 1244-1247,October 2012.

[2] Naveen.B, Dr. K.R. Nataraj, and Dr. K .R. Rekha , **"Design and Analysis of Real Time Video/Image Splitting Using Matlab "**, International Conference IRD India at Bangalore, India page 46-48, Dec 2012.

[3] Rafael C. Gonzalez and Richard E. Woods, **"Digital Image Processing"**, Pearson Prentice Hall, 3 Edition, 2008.

[4] Alain Merigot, **"Revisiting image splitting"**, Proc of 12th international conference on image analysis and processing, page 314-319, 2003.

[5] Marco Aurelio, Nunu maganda, **"Real time FPGA based architecture for bi cubic interpolation: an application for digital image scaling"**, Proc of the International conference on reconfigurable computing and FPGAs.

[6] Belgacem Ben Yousef and Jim Bizzochi, **"Enhance Pixel-Based Video Frame Interpolation Algorithms"**, IEEE International symposium on Signal Processing and Information Technology, page 23-28, Dec 2007.

[7] Matthew Own by, Dr Wagdy.H. mhmoud, **"A design methodology for implementing DSP with xilinx system Generator for Matlab"**, processdings of 35th south eastern symposium, Vol 15, page 2226-2238, 2006.

Cascade Reliability for Generalized Exponential Distribution

[1,]T.sumathi UmaMaheswari, [2,]N.Swathi.
[1,2,]Department of Mathematics, Kakatiya University, Warangal, Andhra Pradesh

Abstract

Cascade reliability model is a special type of Stress- Strength model. The n- Cascade system is a hierarchical standby redundancy system, where the standby component taking the place of failed component with decreased value of stress and independently distributed strength. This paper deals with the generalized exponential distribution with cascade system.

Key Words: Stress – Strength model, Cascade system, generalized exponential distribution.

1. Introduction

The two- parameter generalized exponential (GE) distribution has been proposed by the Debasis Kundu and Rameshwar D.Gupta[1]. It has been extensively studied by Gupta and Kundu [2] and Kundu, Gupta and [3]. Note that the generalized exponential distribution is a sub- model of the exponential Weibull distribution introduced by Mudholkar and Srivastava [4] and later studied by Mudholkar, Srivastava and Freimer [5].An n - cascade system is defined as a special type of standby system with n components by Sriwastav et al .,[6]. Cascade redundancy is defined as a hierarchical standby redundancy where a standby component takes the place of a failed component with a changed stress. This changed stress is k times the preceding stress. k is the attenuation factor. Sriwastav and Pandit[6] derived the expressions for reliability of an n-cascade system when stress and strength follow exponential distribution. They computed reliability values for a 2-cascade system with gamma and normal stress and strength distributions. Raghava Char et al [7] studied the reliability of a cascade system with normal stress and strength distribution. T.S.Uma Maheswari et al [9] studied the reliability comparison of n-cascade system with addition of n-strengths system when stress and strength follow exponential distribution.

2. Statistical Model

If the r.v .X denotes the strength and the r.v. Y denotes the stress of the component, then the reliability of the component is given by

$$R = P(X > Y) = \int_{y=0}^{\infty} \left(\int_{x=y}^{\infty} f(x)\,dx \right) g(y)\,dy \qquad (1)$$

Let $X_1, X_2, X_3, \dots, X_n$ be the strengths of the components $C_1, C_2, C_3, \dots, C_n$ as arranged in order of activation respectively. All the X_i's are independently distributed random variables with probability density functions $f_i(x_i); i = 1,2, \dots, n$. Also let Y be the stress acted on the components which is also randomly distributed with the density function $g(y)$

If $< X_1$, the first component C_1 works and hence the system survives. $Y \geq X_1$ leads to the failure of C_1 ; thus the second component in line viz., C_2 ,takes its place and has a strength X_2 ..Although the system has suffered the loss of one component, it survives if $Y < X_2$ and so on . In general, if the $(i-1)^{th}$ component C_{i-1} fails then the i^{th} component C_i , with the strength X_i, gets activated and will be subjected to the stress Y.

The system could survive with a loss of the first $(n-1)$ components if and only if $X_i \leq Y\ ; \forall i = 1,2,3, \dots \dots, n-1 \text{ and } X_n > Y$. The system totally fails if all the components fail when $X_i \leq Y\ ; \forall i = 1,2, \dots \dots n.$ The probability $R(n)$ of the system to survive with the first $(n-1)$ components failed and the n^{th} component active is

$$R(n) = P\left[\left\{ \bigcap_{i=1}^{n-1} (X_i \leq Y) \right\} \cap (X_n > Y) \right] \qquad (3)$$

$R(2), R(3), \dots \dots \dots, R(n)$ are the increments in reliability due to the addition of $2^{nd}, 3^{rd}, \dots \dots, n^{th}$ components respectively.

Then

$$R(n) = P[X_1 \le Y, X_2 \le Y, \dots\dots\dots, X_{n-1} \le Y, X_n > Y] \qquad (4)$$

we can obviously associate the n^{th} component attenuation factor with Y.

Let $g(y)$ and $f_i(x_i)$ be the probability density function of Y and X_i $(i = 1,2, \dots, n)$ respectively.

The equation (4) can now be written as

$$R(n) = \int_0^\infty \left[\int_0^y f_1(x_1)dx_1 \times \int_0^y f_2(x_2)dx_2 \times \dots\dots \int_0^y f_{n-1}(x_{n-1})dx_{n-1} \times \int_y^\infty f_n(x_n)dx_n \right] g(y)dy \qquad (5)$$

(or)

$$\int_0^\infty [F_1(y)F_2(y) \dots\dots\dots F_{n-1}(y)\bar{F}_n(y)]g(y)dy \qquad (6)$$

where $F_i(y) = \int_0^y f_i(x_i)dx_i$ and

$$\bar{F}_i(y) = 1 - F_i(y) \qquad (7)$$

The two- parameter GE distribution has the following density functions

$$f(x;\alpha,\lambda) = \alpha\lambda e^{-\lambda x}\left(1 - e^{-\lambda x}\right)^{\alpha-1};\ for\ x > 0$$

And the distribution function

$$F(x;\alpha,\lambda) = \left(1 - e^{-\lambda x}\right)^{\alpha}\ for\ x > 0$$

$$g(y;\beta,\lambda) = \beta\lambda e^{-\lambda y}\left(1 - e^{-\lambda y}\right)^{\beta-1};\ for\ y > 0$$

$$The\ distribution\ function\ is \quad G(y;\beta,\lambda) = \left(1 - e^{-\lambda y}\right)^{\beta}\ for\ y > 0$$

1 – Cascade system

$$R(1) = P[X > Y]$$

$$= \int_{y=0}^\infty \left(\int_{x=y}^\infty f(x)dx \right) g(y)dy$$

$$= \int_{y=0}^\infty (f_1(x_1)dx_1)g(y)\,dy$$

$$R(1) = \int_{y=0}^\infty \bar{F}_1(y)\,g(y)\,dy$$

$$R(1) = \int_{y=0}^\infty \left(1 - e^{-\lambda y}\right)^{\beta} \alpha\lambda e^{-\lambda y}\left(1 - e^{-\lambda y}\right)^{\alpha-1} dy$$

$$put\ 1-e^{-\lambda y}=t$$

$$\lambda e^{-\lambda y}dy=dt\ and\ y=0\rightarrow t=0\ and\ y=\infty\rightarrow t=1$$

$$R(1)=\frac{\alpha}{\alpha+\beta}$$

2- Cascade system

$$R(2)=P[X_1<Y,X_2>Y]$$

$$R(2)=\int_{y=0}^{\infty}\left(\int_{x_1=0}^{y}(f_1(x_1)dx_1)\right)\left(\int_{x_2=y}^{\infty}(f_2(x_2)dx_2)\right)g(y)dy$$

$$=\int_{y=0}^{\infty}\left(1-e^{-\lambda y}\right)^{\alpha}\left(1-\left(1-e^{-\lambda y}\right)^{\alpha}\right)\beta\lambda e^{-\lambda y}\left(1-e^{-\lambda y}\right)^{\beta-1}dy$$

$$R(2)=\frac{\alpha\beta}{(\alpha+\beta)(2\alpha+\beta)}$$

3- Cascade system

$$R(3)=P[X_1<Y,X_2<Y,X_3>Y]$$

$$=\int_{y=0}^{\infty}\left(\int_{x_1=0}^{y}(f_1(x_1)dx_1)\right)\left(\int_{x_2=0}^{y}(f_2(x_2)dx_2)\right)\left(\int_{x_3=y}^{\infty}(f_3(x_3)dx_3)\right)g(y)\,dy$$

$$=\int_{y=0}^{\infty}\left(1-e^{-\lambda y}\right)^{\alpha}\left(1-e^{-\lambda y}\right)^{\alpha}\left(1-\left(1-e^{-\lambda y}\right)^{\alpha}\right)\beta\lambda e^{-\lambda y}\left(1-e^{-\lambda y}\right)^{\beta-1}dy$$

$$R(3)=\frac{\alpha\beta}{(2\alpha+\beta)(3\alpha+\beta)}$$

In general

$$R(n)=\frac{\alpha\beta}{((n-1)\alpha+\beta)(n\alpha+\beta)}$$

3. Reliability Computations:

Table 1

α	β	R(1)
1	2	0.333333
2	2	0.5
3	2	0.6
4	2	0.666667
5	2	0.714286
6	2	0.75
7	2	0.777778
8	2	0.8
9	2	0.818182
10	2	0.833333
11	2	0.846154

Table 2

α	β	R(1)
5	1	0.833333
5	2	0.714286
5	3	0.625
5	4	0.555556
5	5	0.5
5	6	0.454545
5	7	0.416667
5	8	0.384615
5	9	0.357143
5	10	0.333333
5	11	0.3125

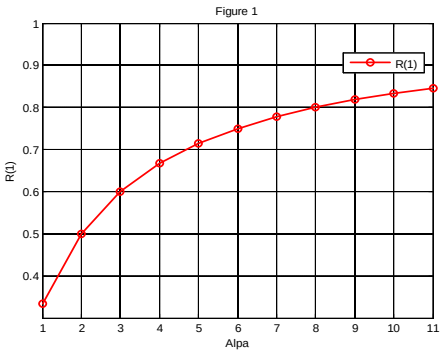

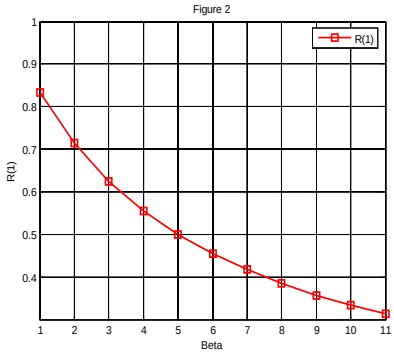

Table 3

α	β	R(2)
1	2	0.166667
2	2	0.166667
3	2	0.15
4	2	0.133333
5	2	0.119048
6	2	0.107143
7	2	0.097222
8	2	0.088889
9	2	0.081818
10	2	0.075758
11	2	0.070513

Table 4

α	β	R(2)
5	1	0.075758
5	2	0.119048
5	3	0.144231
5	4	0.15873
5	5	0.166667
5	6	0.170455
5	7	0.171569
5	8	0.17094
5	9	0.169173
5	10	0.166667
5	11	0.16369

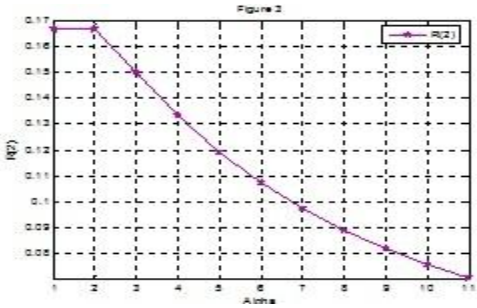

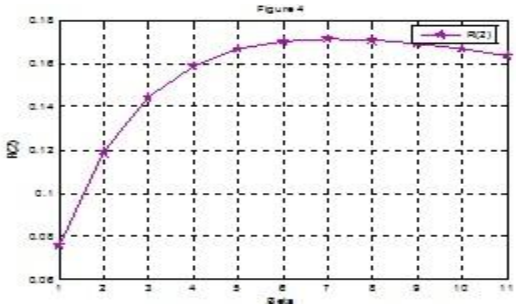

Table 5

α	β	R(3)
1	2	0.1
2	2	0.083333
3	2	0.068182
4	2	0.057143
5	2	0.04902
6	2	0.042857
7	2	0.038043
8	2	0.034188
9	2	0.031034
10	2	0.028409
11	2	0.02619

Table 6

α	β	R(3)
5	1	0.028409
5	2	0.04902
5	3	0.064103
5	4	0.075188
5	5	0.083333
5	6	0.089286
5	7	0.093583
5	8	0.096618
5	9	0.098684
5	10	0.1

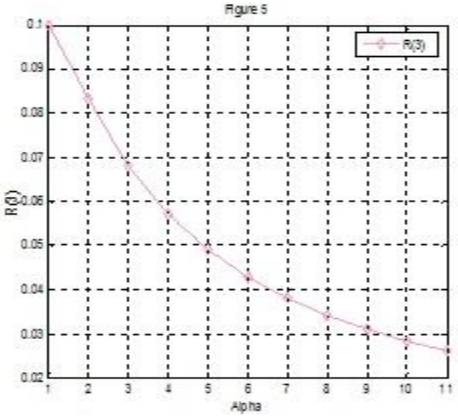

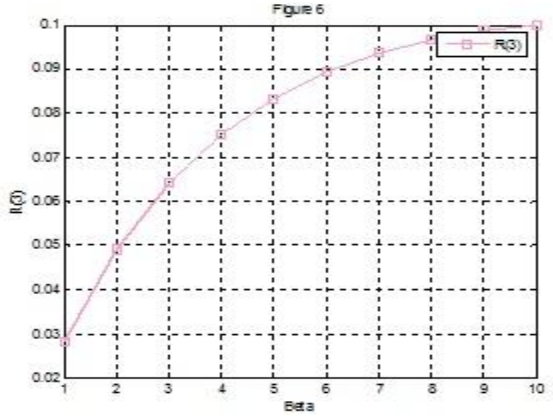

4. Conclusion

The reliability of n- cascade system when stress and strength follow generalized exponential distribution. In this paper we find out the formula for n-cascade system. From computations Reliability increases in 1-cascade system whenever strength parameter α increases and reliability decreases whenever stress parameter β increases and vice-versa for 2-cascade, 3-cascade,---n-cascade system.

References

[1]. Rameshwar D.Gupta & Debasis Kundu (1999): Generalized Exponential Distribution, Austral. & New Zealand J.Statist. 41(2), 173-188.

[2]. Gupta, R.D. &Kundu D. (2001): Generalizes exponential distribution, different method of estimations, Journal of Statistical Computation and Simulation 69, 315-338.

[3]. Gupta, R.D. & Kundu, D. (2002): Generalized exponential distribution, statistical inferences, Journal of Statistical theory and Applications 1, 101-118.

[4]. Govind S. Mudholkar & Srivastava (1996) : Generalization of the weibull distribution with Application to the Analysis of survival data , journal of the Americal Statistical Association , Dec 1996, vol 91, No. 436, 1575- 1583.

[5]. Govind S. Mudholkar , Srivastava and D.K. Freimerm (1995) : The exponential weibull family ; a reanalysis of the bus motor failure data , Technometrics, 37(4), 436- 445

[6]. S.N.Narahari Pandit and G.L.Sriwastav (1975). Studies in Cascade Reliability–I, IEEE Transactions on Reliability , Vol.R-24, No.1, pp.53-57.

[7]. A.C.N.Raghava char, B.Kesava Rao and S.N.Narahari Pandit(Sept.1987).The Reliability of a Cascade system with Normal Stress and Strength distribution, ASR, Vol. No.2, pp. 49-54.

[8]. T.S.Uma Maheswari(1993). Reliability of cascade system with normal stress and exponential strength, Micro Electron Reliability, Pergamon Press, OXFORD, Vol.33, pp: 927-936.

Seismic Damage Prediction of Reinforced Concrete Buildings Using Pushover Analysis

M.Mouzzoun[1], O.Moustachi[2], A.Taleb[3]
[1] PhD student, Mohammadia School of engineers, Rabat, Morocco,
[2] Professor, Mohammadia School of engineers, Rabat, Morocco

Abstract:
This paper investigates the seismic damage of a sex storey reinforced concrete frame building designed according to the Moroccan seismic code RPS2000 [1].The building is residential and has a reinforced concrete frame structural system. In the first time a set of dynamic analysis are carried out to compute dynamic properties of the building (fundamental period, natural frequencies, deformation modes,), in the second time a pushover analysis is carried out.Performances levels are used with the pushover analysis to assess the seismic damage of the building. Three performance levels considered in the present study are immediate occupancy, life safety and collapse prevention.

Keywords: Analysis**,** building, pushover, damage, performance point, reinforced concrete, seismic.

1. Introduction

The earthquakes that occurred recently in the world, Loma Prieta 1989, Northridge 1994, Kobe 1995, Izmit 1999 Bam 2003, El Hoceima 2004 and in other parts of the world has highlighted the seismic vulnerability of existing buildings . In urban areas, this vulnerability, combined with a high concentration of buildings built before the introduction of seismic standards, can cause high seismic risk, even in areas where the seismicity is considered moderate. The pushover analysis is a powerful tool in this area which allows the evaluation of the seismic performance of buildings by estimating damage to structural and non-structural elements caused by a future shaking. Pushover analysis [2, 3, and 4] has been developed over the past twenty years and has become the preferred analysis procedure for design and seismic performance evaluation purposes as the procedure is relatively simple and considers post elastic behaviour.

Pushover analysis is an analysis method in which the structure is subjected to monotonically increasing lateral forces with an invariant height-wise distribution until a target displacement is reached. Pushover analysis consists of a series of sequential elastic analyses, superimposed to approximate a force-displacement curve of the overall structure. A two or three dimensional model which includes bilinear or trilinear load-deformation diagrams of all lateral force resisting elements is first created and gravity loads are applied initially. A predefined lateral load pattern which is distributed along the building height is then applied. The lateral forces are increased until some members yield. The structural model is modified to account for the reduced stiffness of yielded members and lateral forces are again increased until additional members yield. The process is continued until a control displacement at the top of building reaches a certain level of deformation or structure becomes unstable. The roof displacement is plotted with base shear to get the capacity curve (Fig 1).

The pushover analysis is very useful in estimating the following characteristics of a structure.

1) The capacity of the structure as represented by the base shear versus roof- displacement graph
2) Maximum rotation and ductility of critical members load
3) The distribution of plastic hinges at the ultimate load
4) The distribution of damage in the structure, as expressed in the from of load damage indices
5) Determination of the yield lateral resistance of the structure
6) Estimates of inter-story drifts and its distribution along the height

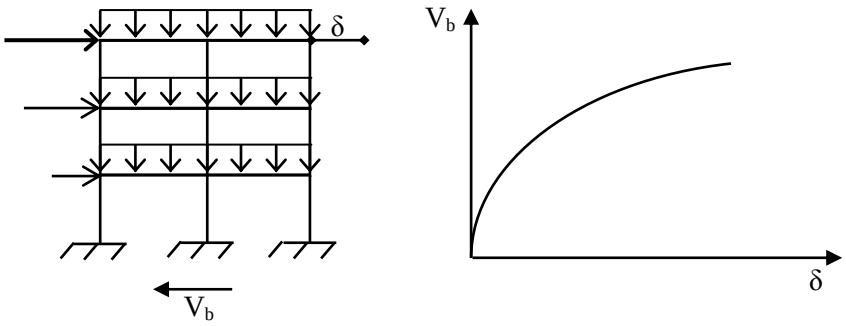

Figure 1. Construction of pushover curve

2. Building performance levels

The seismic performance of buildings [6, 11] is measured by the state of damage under a certain level of seismic hazard. The state of damage is quantified by the drift of the roof and the displacement of the structural elements. Initially, gravity push is carried out using force control method. It is followed by lateral push with displacement control using SAP2000 [10]. For carrying out displacement based pushover analysis, target displacement need to be defined. Pushover analysis gives an insight into the maximum base shear that the structure is capable of resisting. A building performance level is a combination of the performance levels of the structure and the nonstructural components. A performance level describes a limiting damage condition which may be considered satisfactory for a given building with specific ground motion. The performances levels as per FEMA [6], ATC 40 [8] and vision 2000[11] are:

Immediate occupancy IO: damage is relatively limited; the structure retains a significant portion of its original stiffness and most if not all of its strength.

Life safety level LS: substantial damage has occurred to the structure, and it may have lost a significant amount of its original stiffness. However, a substantial margin remains for additional lateral deformation before collapse would occur.
Collapse prevention CP: at this level the building has experienced extreme damage, if laterally deformed beyond this point; the structure can experience instability and collapse.

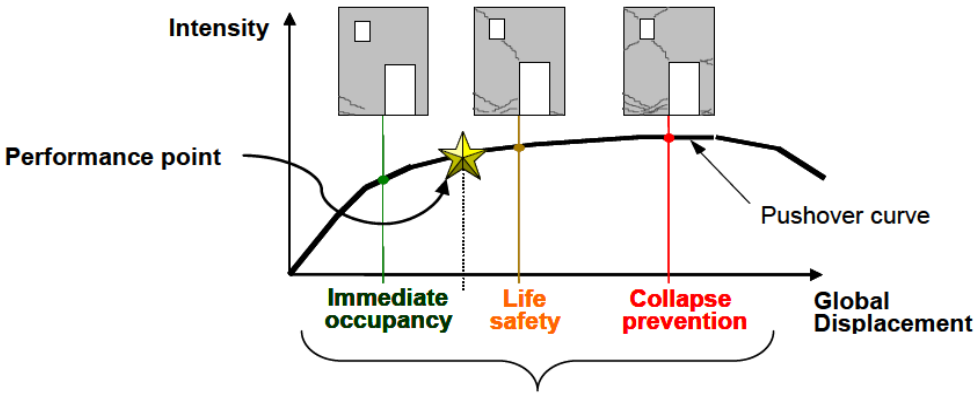

Figure 2. Performance levels described by a pushover curve [6]

3. Case Study

3.1. Building description

The building studied here is a six storey reinforced concrete building, for residential use.The building has 2 spans of 3.50m, and 4 bays of 3.00m. The slab thickness is 12 cm, column section is 35x35cm, and the beam section is 25x35cm.The height of each level is 3m; the building is located in seismic zone 3[1], based on soil type S2[1]. The materials used are fc28=25MPa for concrete and HA500 for longitudinal and shear reinforcement. The building is designed according to the Moroccan seismic code RPS2000 [1].

For the pushover analysis, 3 load cases were considered:

- PUSHGRA – applying the gravity loads.
- PUSHX– applying lateral loads in the X-X direction.
- PUSHY – applying lateral loads in the Y-Y direction

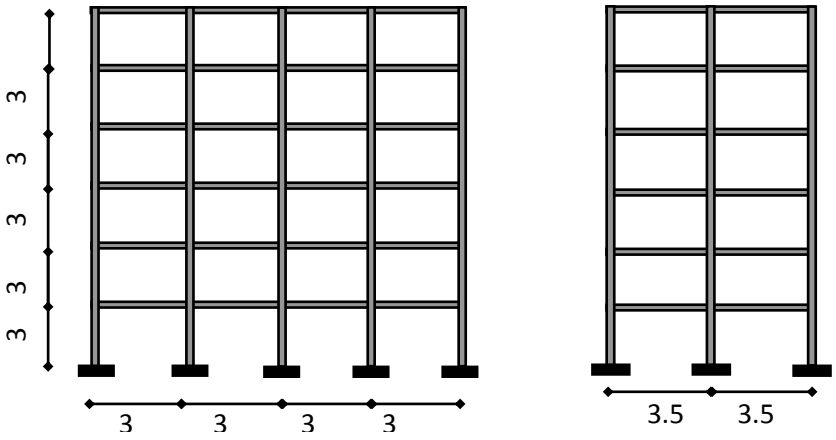

Figure 3.Building elevation

4. Results

4.1 modeling parameters

The structure was analyzed using SAP2000 computer code. The superstructure was modelled as a spatial frame, considered fixed at the base of the ground floor. The reinforced concrete floor has substantial stiffness and resistance to take over the stresses produced by the lateral forces, and due to the regularity and homogeneity of the structure, it can be considered non-deformable in its plan. The beam and column elements are modelled as nonlinear frame elements with lumped plasticity by defining plastic hinges at both ends of beams and columns.

4.2 pushover analysis

Results of the Push-Over analysis are presented in Figures 4, 5, 6 and 7 (push-over curves, in each of the 2 main directions). The performance point at the intersection of the capacity spectrum with the single demand spectrum for different levels of shaking (moderate, severe) has been obtained. Figures 8 and 9 show the floor displacement. Plastic hinge formation for the building mechanisms has been obtained at different displacements levels. The hinging patterns are plotted in figures 10 and 11. Plastic hinges formation starts with beam ends and base columns of lower stories , then propagates to upper stories and continue with yielding of interior intermediate columns in the upper stories.

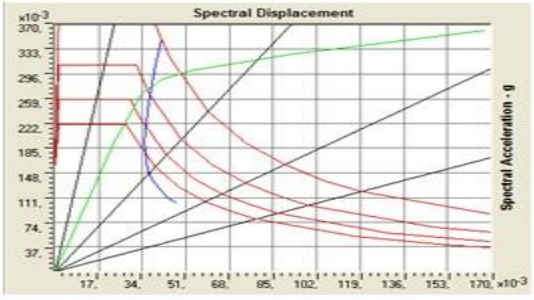

Figure 4. Performance point A=0.16g/X-X

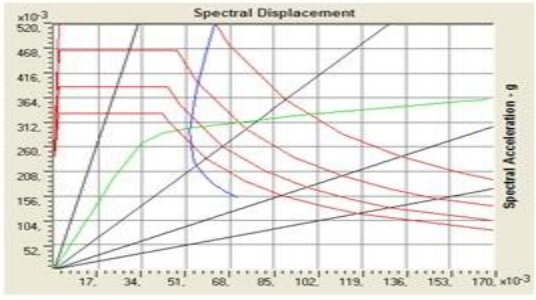

Figure 5. Performance point A=0.24g/X-X

Figure 6.Performance point A=0.16g/Y-Y

Figure 7.Performance point A=0.24g/Y-Y

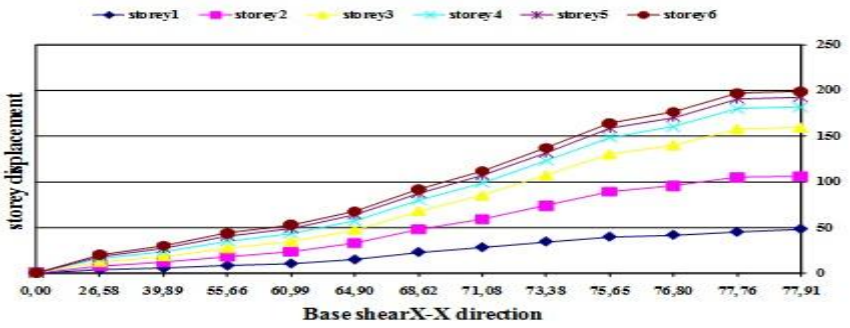

Figure 8.Base shear versus storey displacement X-X direction

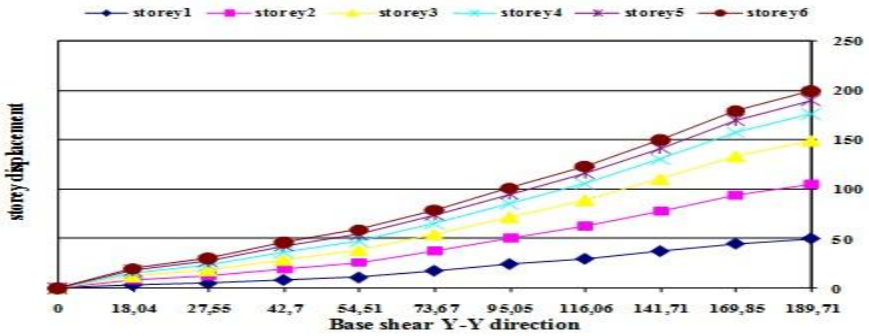

Figure 9.Base shear versus storey displacement Y-Y direction

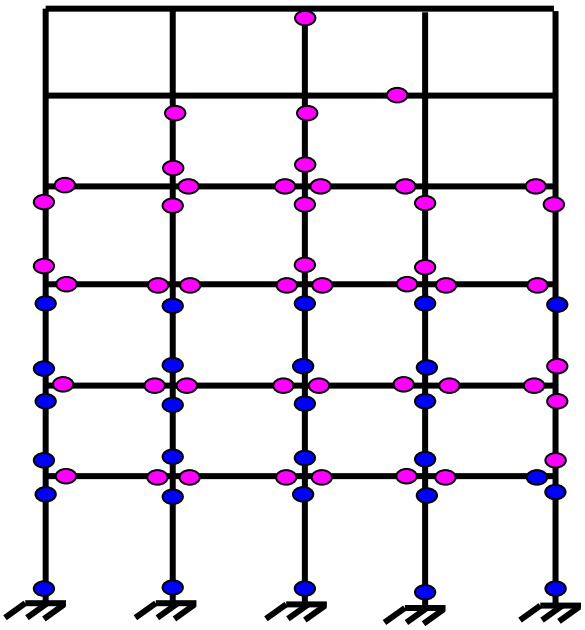

Figure 10. Plastic hinges IO under moderate shaking

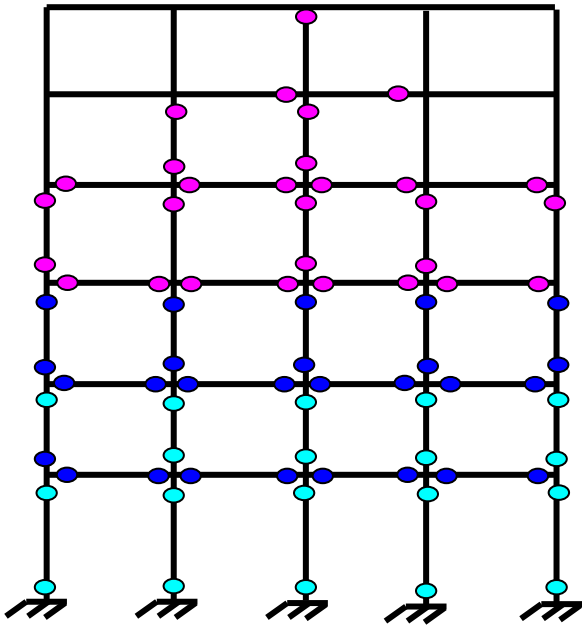

Figure 11. Plastic hinges LS under high shaking

First yield immediate occupation Life Safety Collapse Prevention

5. Conclusion

Under moderate shaking, we see from Figures 4, 6 and 10 that demand curve intersects the capacity curve at event IO (immediate occupation), plastic hinges occurred so the structure remains stable with onset of damage privileges, minor cracking of facades, partitions, and ceilings as well as structural elements, no permanent drift, structure substantially retains original strength and stiffness. Repair lightweight non-structural elements, any repairs to the structural elements are required.

Under high shaking we see from Figures 5, 7 and 11that the demand curve intersects the capacity curve at event LS (life safety), plastic hinges occurred, the structure is damaged, it lost its rigidity and its original strength, Some structural elements and components are severely damaged, but this has not resulted in large falling debris hazards, either within or outside the building. Injuries may occur during the earthquake; however, it is expected that the overall risk of life-threatening injury as a result of structural damage is low. It should be possible to repair the structure; however, for economic reasons this may not be practical. The amount of damage in the buildings is limited and collapse is prevented. Finally the pushover analysis combined with the performance levels is able to evaluate the seismic damage of buildings, to examine the state of the structure under the action of an earthquake and thus provide information on the damage that can be sustained by a structure and the elements that will be affected in a future earthquake.

References

[1] RPS2000, Moroccan Seismic Provisions. Published by Ministry of housing 2000.

[2] M.Priestley, Preliminary development of direct displacement-based design of multidegree of freedom systems, Proceedings 65th Annual Convention, SEAOC, Maui, Hawai, 1996.

[3] A. M .Reinhorn, inelastic analysis techniques in seismic evaluations, Seismic Design methodologies for structures.

[4] H. Krawinkler, Procedure and construction of pushover analysis of seismic performance evaluation engineering structure,
vol: 20, edition: Elsevier science, Department of civil engineering standford university U.S.A 1998.

[5] M. Mouzzoun, O. Moustachi and A.Taleb, fragility curve for seismic vulnerability assessment of reinforced concrete buildings, International Journal of materials and environmental science, Sci. 3 (6) (2012) 1037-1044.

[6] FEMA273 Federal Emergency Management Agency. NEHRP recommended Provisions for Seismic Regulations for New Buildings and Other Structures.

[7] SAP2000, Web tutorial1-quick pushover analysis tutorial (1999).computer and structures, Berkeley, California.

[8] ATC – Seismic Evaluation and Retrofit of Concrete Buildings, Volume 1, ATC-40 Report, Applied Technology Council, Redwood City, California, 1996.

[9] CSI, Analysis Reference Manual for SAP2000, ETABS, and SAFE – Computers and Structures, Inc. Berkeley,California,
USA, October 2005.

[10] CSI, Analysis Reference Manual for SAP2000, ETABS and SAFE – Computers and Structures, Inc. Berkeley, California, USA, October 2005.

[11] Vision 2000 committee, performance based seismic engineering of buildings, structural Engineers Association of California (SEAOC), California.

Implementation of SPI Protocol in FPGA

Veda Patil[1], Vijay Dahake [2], Dharmesh Verma[3], Elton Pinto[4]

[1,2](Electronics & Telecommunication, Rama rao Adik Institute of technology/ Mumbai, India)

[3,4](Electronics & Telecommunication, Society of Applied Microwave Electronics Engineering & Research/Mumbai, India)

Abstract:

In this paper, Serial Peripheral Interface (SPI) protocol is implemented in Field Programmable Gate Array (FPGA). Both the components SPI Master and SPI Slave are implemented using state machine diagram. The coding is done in Very high speed integrated circuits Hardware Descriptive Language (VHDL). The simulated data is shown and Received data is analyzed by receiving an acknowledgment.

Keywords: Clock Phase, Clock Polarity, FPGA, MISO, MOSI, SPI master, SPI Slave, VHDL.

1. Introduction

Serial communication is the process of sending data one bit at a time, sequentially, over a communication channel. Serial communication is used for all long-haul communication and most computer networks, where the cost of cabling and synchronization difficulties makes parallel communication impractical. A serial connection requires fewer interconnecting cables (e.g., wires/fibers) and hence occupies less space. The extra space allows for better isolation of the channel from its surroundings. Serial buses are becoming more common even at shorter distances, as improved signal integrity and transmission speeds in newer serial technologies have begun to outweigh the parallel bus's advantage of simplicity and to outstrip its disadvantages. Serial links can be clocked considerably faster than parallel links in order to achieve a higher data rate. Crosstalk is less of an issue, because there are fewer conductors in proximity. In many cases, serial is a better option because it is cheaper to implement. Many Integrated Circuits have serial interfaces, as opposed to parallel ones, so that they have fewer pins and are therefore less expensive.

2. Serial Peripheral Interface (SPI) Protocol

The SPI bus is a synchronous serial data link standard, named by Motorola that operates in full duplex mode. Devices communicate in master/slave mode where the master device initiates the clock and data frame. Multiple slave devices are allowed with individual slave select (chip select) lines. SPI is often referred to as SSI (Synchronous Serial Interface). The SPI bus interface consists four logic signals namely Serial Clock (SCLK), Master Output Slave In (MOSI), Master In Slave out (MISO) and Slave Select (SS).

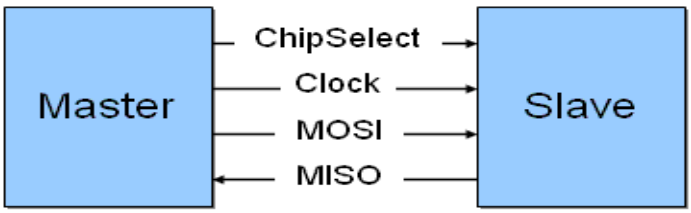

Figure1. SPI Protocol Interface

To begin a communication, the bus master first configures the clock, using a frequency less than or equal to the maximum frequency the slave device supports. Such frequencies are commonly in the range of 1–100 MHz the master then transmits the appropriate chip select bit for the desired chip to logic 0. Logic 0 is transmitted because the chip select line is active low, meaning its off state is logic 1; *on* is asserted with logic 0. If a waiting period is required then the master must wait for at least that period of time before starting to issue clock cycles. Transmissions normally involve two shift registers of some given word size, such as eight bits, one in the master and one in the slave; they are connected in a ring. Data is usually shifted out with the most significant bit first, while shifting a new least significant bit into the same register. After that register has been shifted out, the master and slave have exchanged register values. Then each device takes that value and is written to memory. If there is more data to exchange, the shift registers are loaded with new data and the process repeats. Transmissions may involve any number of clock cycles. When there is no more data to be transmitted, the master stops toggling its clock. Normally, it then deselects the slave.

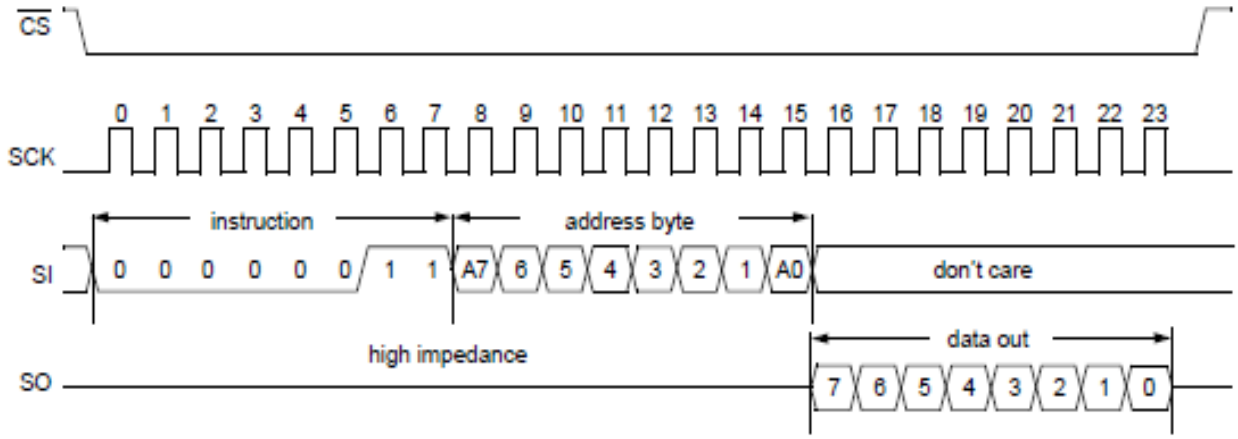

Figure 2. SPI Timing diagram

3. Clock Polarity and Phase

In addition to setting the clock frequency, the master must also configure the clock polarity and phase with respect to the data. The timing applies to both the master and the slave to communicate articulately. The combinations of Clock polarity (CPOL) and Clock Phase (CPHA) give rise to different modes.

Table 1.Different modes of clock

Mode	CPOL	CPHA
0	0	0
1	0	1
2	1	0
3	1	1

Mode 0: CPOL=0 i.e. SCLK is normally low and the first clock edge is a rising edge & CPHA=0, the data is captured on the clock's rising edge (low to high transition) and data is received on the clock's falling edge (high to low clock transition) Mode 1: CPOL=0 i.e. SCLK is normally low and the first clock edge is a rising edge & CPHA=1, data is captured on the clock's falling edge and data is propagated on a rising edge. Mode 2: CPOL=1 i.e. SCLK is normally high and the first clock edge is a falling edge & CPHA=0, data is captured on clock's falling edge and data is received on a rising edge. Mode 3: CPOL=1 i.e. SCLK is normally high and the first clock edge is a falling edge & CPHA=1, data is captured on clock's rising edge and data is received on a falling edge. For all CPOL and CPHA modes, the initial clock value must be stable before the chip select line goes active. The MOSI and MISO signals are usually stable (at their reception points) for the half cycle until the next clock transition. SPI master and slave devices may well sample data at different points in that half cycle. This adds more flexibility to the communication channel between the master and slave.

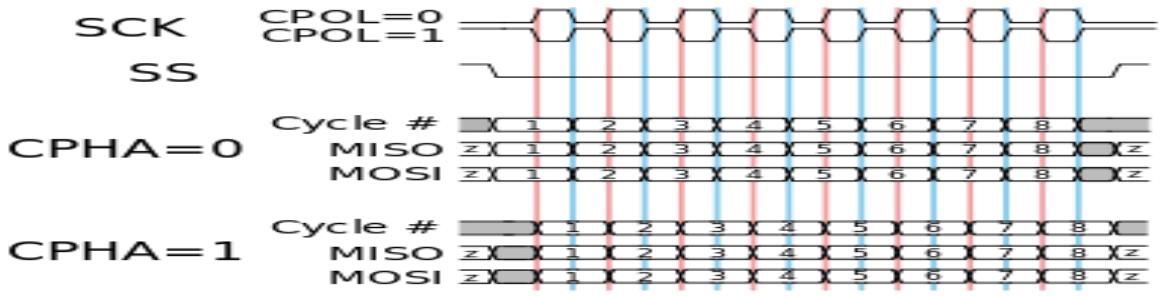

Figure 3. Timing diagram showing clock polarity and clock phase.

4. VHDL Coding And Result

4.1. SPI Master

The number of slaves is declared in the ENTITY by the GENERIC parameter as slaves and the transmit and receive data bus widths are declared by GENERIC parameter d_width. Table below shows different input - output ports which are defined in the code. In the table M specifies the data width and N specifics the number of slaves. The clock and clk_div inputs define the frequency of SCLK (i.e. the SPI data rate). Clock is the system clock used to operate the synchronous logic inside the component. The clk_div integer input allows the user to set the relative speed at which the current transaction occurs. Clk_div is the number of clock periods between SCLK transitions. The enable pin latches in the standard logic values of clk_div, cpol and cpha at the start of each transaction. This allows communication with individual slaves using independent SPI speeds & modes. A low logic level on the busy output port indicates that the component is ready to accept a command. The component latches the settings, address, and data for a transaction on the first rising edge of clock where the enable input is asserted. On the following clock, the component asserts the busy signal and begins performing the transaction. Once complete, the component outputs the received data on the rx_data port. This data remains on the port until the component receives new data from a subsequent transaction. The component sets busy low to notify the user when the data is available, and the component is immediately ready for another instruction .The transition timing diagram is obtained by the simulator is given in the table 2. This SPI master is instantiated with one slaves and eight bit data width. It transmits the data"10110010" to slave 2, which operates in mode 3 (CPOL='1'and CPHA='1').The master receives the"00000000" data.

Table 2. Port descriptions of SPI Master entity

Port	Width	Mode	Data Type	Interface	Description
clock	1	in	standard logic	user logic	System clock.
reset_n	1	in	standard logic	user logic	Asynchronous active low reset.
enable	1	in	standard logic	user logic	H: latches in settings, address, and data to initiate a transaction, L: no transaction is initiated.
cpol	1	in	standard logic	user logic	SPI clock polarity setting.
cpha	1	in	standard logic	user logic	SPI clock phase setting.
cont	1	in	standard logic	user logic	Continuous mode flag.
clk_div	32	in	integer	user logic	Speed setting. The integer input is the number of system clocks per 1/2 period of sclk.
addr	32	in	integer	user logic	Address of target slave. The slaves are assigned addresses starting with 0.
tx_data	M*	in	standard logic vector	user logic	Data to transmit.
miso	1	in	standard logic	slave devices	Master in, slave out data line.
sclk	1	buffer	standard logic	slave devices	SPI clock.
ss_n	N^	buffer	standard logic vector	slave devices	Slave select signals.
mosi	1	out	standard logic	slave devices	Master out, slave in data line.
busy	1	out	standard logic	user logic	Busy / data ready signal.
rx_data	M*	out	standard logic vector	user logic	Data received from target slave.

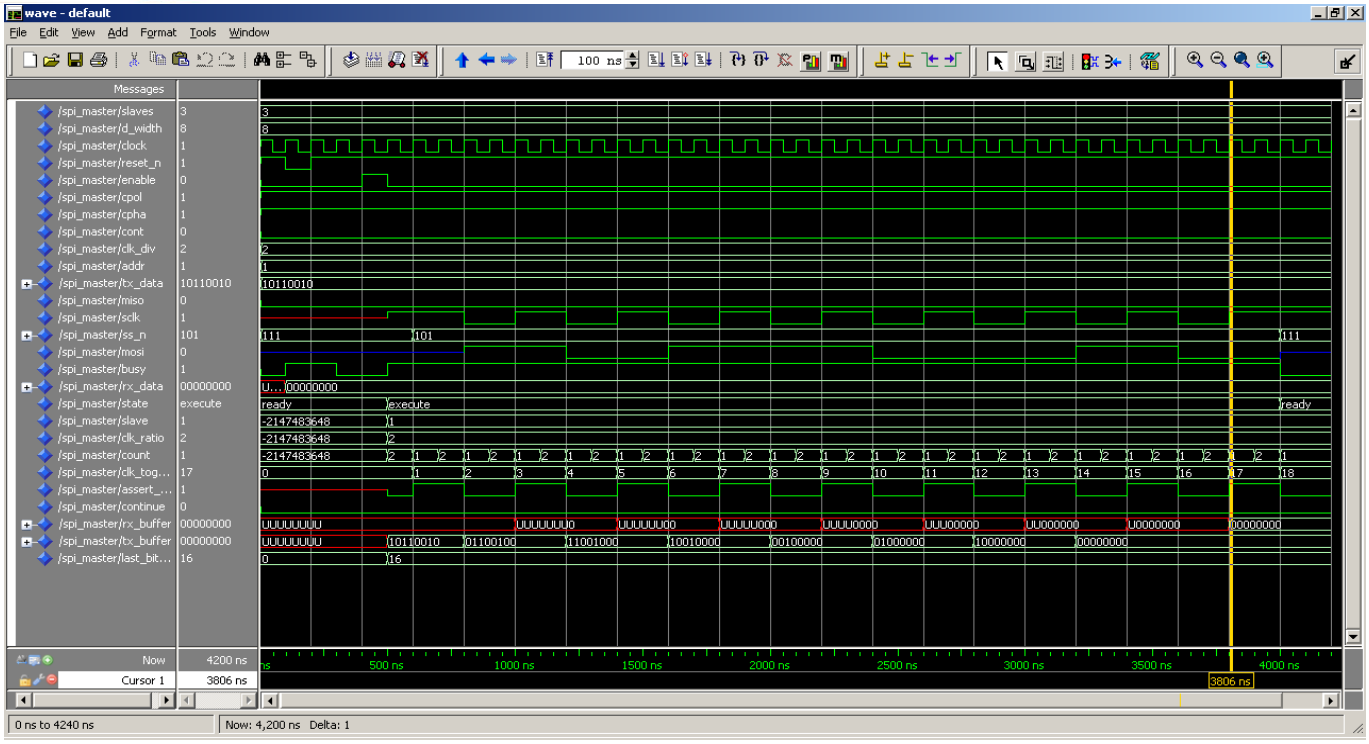

Figure 4. Simulated results of SPI Master

4.2. SPI Slave

The mode that the slave operates in is defined by the GENERIC parameters cpol and cpha. The transmit and receive data bus width are declared by the GENERIC parameter d_width. Each transaction between the SPI slave component and the SPI master must consist of an 8-bit command, followed by a N-bit data transfer. The size N of the data transfer is determined by the GENERIC d_width parameter in the VHDL entity and is set by the user. The receive register is a buffer that holds data received from the master over the MOSI line. For the user logic to access the resulting data, the user must pulse the rx_req input when the component is not performing a transaction. The slave then outputs the receive register contents on the rx_data port. The transmit register is a buffer that holds the data intended to be transmitted by the slave to the master over the MISO line. The user logic fills this register by presenting the data on the tx_load_data port and pulsing the tx_load_en input when the component is not performing a transaction. The status register contains three status bits. The master can read, set, or clear these bits with transactions addressed to this register. During a transaction that reads or writes the status register, the first three data bits sent correspond to trdy, rrdy, and roe, respectively. The slave component ignores the remaining bits sent or received during the transaction. The user logic has access to these bits via the ports bearing their names. The user logic can also set or clear these bits by presenting the desired values on the st_load_trdy, st_load_rrdy, and st_load_roe inputs and pulsing the st_load_en input when the component is not performing a transaction (i.e. the busy output is low). The reset_n input port must have logic high for the SPI slave component to operate. A low signal on this port asynchronously resets the component. During reset, the miso output assumes a high impedance state, and the rx_data output port clears. The transmit, receive, transmit ready, receive ready, and receive overrun error registers all clear.

Figure 5 illustrates a transaction with cpol = 0, cpha = 0, and d_width = 8. The slave is configured to operate in mode 0. While the slave is not busy, the user logic pulses the tx_load_en input while presenting the data "10101010" on the tx_load_data bus. The trdy signal immediately goes high to indicate that new data exists to transmit. The master then initiates the transaction with the command "00000000", instructing the slave to load the subsequent MOSI data into the receive register and output the transmit register's contents to MISO. Once the last data bit is sent, the trdy signal goes low to indicate that the transmit register's current value has been sent to the master. Likewise, when the slave reads the last data bit into the receive register, the rrdy signal asserts to indicate that new data has been received. The user logic then pulses the rx_req input, and the slave responds by outputting the received data "10110001" on the rx_data bus. The rrdy output then deasserts to indicate that the data contained in the receive register has already been read by the user logic.

Table 3. Port descriptions of SPI Slave entity

Port	Width	Mode	Data Type	Interface	Description
sclk	1	in	standard logic	master device	SPI clock.
mosi	1	in	standard logic	master device	Master out, slave in data line.
miso	1	out	standard logic	master device	Master in, slave out data line.
ss_n	1	in	standard logic	master device	Active low slave select signal.
busy	1	out	standard logic	user logic	'1' during transactions with the master device, '0' when available to user logic
reset_n	1	in	standard logic	user logic	Active low asynchronous reset.
tx_load_en	1	in	standard logic	user logic	Latches tx_load_data into the transmit register (the slave must not be busy).
tx_load_data	M*	in	standard logic vector	user logic	Data to be latched into the transmit register.
rx_req	1	in	standard logic	user logic	Requests the last received data from the master (the slave must not be busy).
rx_data	M*	out	standard logic vector	user logic	Presents the last received data from the master when requested.
trdy	1	buffer	standard logic	user logic, master device	Transmit Ready. '1' when the slave has loaded data into the transmit register, but it has not yet been sent.
rrdy	1	buffer	standard logic	user logic, master device	Receive Ready. '1' when the slave has received data from the master, but it has not yet been requested.
roe	1	buffer	standard logic	user logic, master device	Receive Overrun Error. '1' when data received from the master is overwritten by new data from the master before it has been accessed by the user logic.
st_load_en	1	in	standard logic	user logic	Status Load Enable. Latches data into the trdy, rrdy, and roe registers from the user logic (the slave must not be busy).
st_load_trdy	1	in	standard logic	user logic	The trdy value that is latched in by st_load_en.
st_load_rrdy	1	in	standard logic	user logic	The rrdy value that is latched in by st_load_en.
st_load_roe	1	in	standard logic	user logic	The roe value that is latched in by st_load_en.

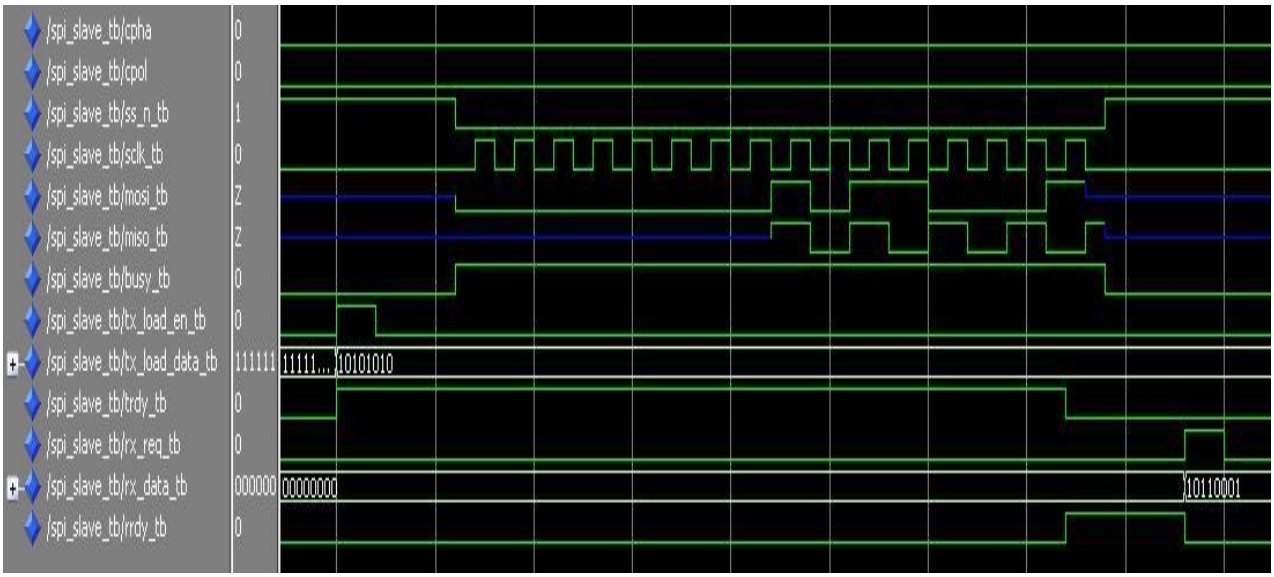

Figure 4. Simulated results of SPI Slave

5. Conclusion

In this paper SPI Master and SPI Slave protocol has been implemented in VHDL. This SPI Master is a flexible programmable logic component that accommodates communication with a variety of slaves via single parallel interface. It allows communication with user specified number of slaves, which may require independent SPI modes, data widths, and serial clock speeds. The VHDL SPI slave offers a user definable mode and data width. It includes status signals for transmit ready, receive ready, and receive overrun error.

References

[1] Motorola MMC 2001 Reference Manual.
[2] Motorola SPI Block Guide V03.06, 2003.
[3] Microchip MCP2510 Application Note AN215.

Packet-Hiding Methods for Preventing Selective Jamming Attacks

[1,]Ashish Kumar, [2,]Sachin Kumar Gupta, [4,]Shubham Singh
[1,2,3,4,]Department of Information Technology , Institute Of Technology And Management , AL-1 Sector-7 Gida , Gorakhpur

Abstract :
The open nature of the wireless medium leaves it vulnerable to intentional interference attacks, typically referred to as jamming. This intentional interference with wireless transmissions can be used as a launch pad for mounting Denial-of-Service attacks on wireless networks. Typically, jamming has been addressed under an external threat model. However, adversaries with internal knowledge of protocol specifications and network secrets can launch low-effort jamming attacks that are difficult to detect and counter. In this work, we address the problem of selective jamming attacks in wireless networks. In these attacks, the adversary is active only for a short period of time, selectively targeting messages of high importance. We illustrate the advantages of selective jamming in terms of network performance degradation and adversary effort by presenting two case studies; a selective attack on TCP and one on routing. We show that selective jamming attacks can be launched by performing real-time packet classification at the physical layer. To mitigate these attacks, we develop three schemes that prevent real-time packet classification by combining cryptographic primitives with physical-layer attributes. We analyze the security of our methods and evaluate their computational and communication overhead.

Keywords – Selective Jamming, Denial of Service, Wireless Network , Packet Classification .

I. INTRODUCTION

Wireless Local Area Networks (WLANs) are becoming an increasingly important technology that is bringing the world closer together. WLANs are used in every area, such as education, agriculture, pharmaceuticals, manufacturing, transportation, military, and research. Therefore, the importance of WLAN security is significant. There are two popular styles of WLANs: client-server networks and ad-hoc networks. The difference between these two networks is that client-server networks use access points or routers to transmit data, but ad-hoc networks do not rely on any pre-existing transmitters. Instead, all the nodes in an ad-hoc network participate in the routing process by forwarding messages to each other. According to The Institute of Electrical and Electronics Engineers (IEEE) 802.11g standards (IEEE Org., 2012), all wireless network nodes transmit data packets in different channels. Since channels in WLANs are defined by frequencies, they are susceptible to malicious jamming attacks. It is easy for attackers to accomplish sending multitudes of useless packets in a specific frequency. Jamming attacks attempt to make the system crash by flooding it with useless traffic, and use all the resources in the network so users in the network cannot connect to the system. It is consistently used by hackers to break network systems, because of ease and security issues. In this thesis, client-server networks and ad-hoc networks were simulated by using the simulation tool OPNET Modeler (OPNET Technologies, Inc., 2012). During the simulation, factors that may influence the result of the simulation were taken into consideration such as the distance, power level, and protocols used in ad-hoc networks.

1.1 Statement Of The Problem

Previous research had found that jammers influence the performance of WLAN networks. However, most research could not demonstrate how different jammers and changed characteristics vary the result of jamming attacks. Jammers disturb networks in different situations in order to achieve various jamming effects. Also, because of the mobility of the WLAN, users cannot be simulated by only using a fixed node or a specific trajectory. Random trajectories in both nodes and jammers have to be considered a real world simulation Scenario. Finally, most esearch used single ad-hoc routing protocols in the network. A comparison of multiple routing protocols needs to be simulated.

1.2 Significance of the Study

It is worth mentioning that the work presented here contributes several issues relevant in the field of jamming attacks in WLAN. First this thesis had provided a better understanding of jamming behavior in WLANs. Multiple experiments had shown a comparison of different jammer performances. Second, this thesis demonstrated the use of different jammers in various environments, including the feasibility of switching channels to avoid jamming attacks. Third, it also provided a way to simulate random trajectory jamming attacks, and used it to simulate and compare the performance of multiple ad-hoc routing protocols.

2. LITERATURE SURVEY

In this Chapter, references of previous research that utilized the concepts in Introduction are introduced. For each of the concepts, an overview of related literature is provided. In section 2.1, WLAN is introduced. Specifically, client-server and ad-hoc networks are explained. In section 2.2, DoS attacks, especially jamming attacks are presented. In Section 2.3, detection methods of jamming attacks are analyzed. Section 2.4 examines the simulation tools that can be used to simulate networks. In section 2.5, the simulation tool OPNET Modeler which is used in this thesis is introduced. Finally, in section 2.6, ad-hoc routing protocols are presented.

WLAN – Client-Server & Ad-Hoc Network.

2.1 WLAN – Client-Server & Ad-Hoc Network

Because WLAN provides users the mobility to move around within a local area without a wire and still connect to the network, it is widely used in many important areas. Banks, governments, corporations, and institutions transmit highly import ant data through WLANs. The security problems of WLANs become important for the users.Most WLANs are based on the IEEE 802.11 standard, which transmits data in different channels based on frequencies. Due to the ease of installation and convenience, WLAN is regularly used in daily life. An introduction of WLANs was done by Gast (2005) and Mark (2005). They presented basic wireless LAN technology, why the technology had emerged, how it works, the architecture of WLANs, and the types of WLANs.Because of the popularity of WLANs, security research must be done in various types of WLANs. Experiments were done by Varadarajan , Kumar, and Reddy (2011) about improving WLAN performance under DoS attacks. DoS attacks on the physical layer were analyzed and expanded to the security of the physical layer of the sensor network model. This research was done by using the ant system. By using Receiver Operating Characteristics (ROC) on nodes, DoS 8 attacks can be predicted by formulating the classification of jammers under various attack scenarios. This approach can help improving detecting DoS atta cks in WLANs.Research in this thesis was focuses on two types of WLANs: client-server and ad-hoc networks.

2.2 Jamming Attacks

The DNS is a hierarchical tree structure whose root node is known as the root domain. A label in a DNS name directly corresponds with a node in the DNS tree structure. A label is an alphanumeric string that uniquely identifies that node from its brothers. Labels are connected together with a dot notation, ".", and a DNS name containing multiple labels represents its path along the tree to the root. Labels are written from left to right. Only one zero length label is allowed and is reserved for the root of the tree. This is commonly referred to as the root zone. Due to the root label being zero length, all FQDNs end in a dot [RFC 1034].A study into DoS attacks and defense was done by Raymond and Midkiff (2008). Since WSNs are used in monitoring medical uses, homeland security, industrial automation, and military applications, security of WSNs must be guaranteed. Defeating many threats of DoS attacks on WSNs can be done by encryption and authentication, but some other techniques still need to be found to prevent from special DoS attacks, especially Denial of Sleep attacks, which are still critical threats in WSNs.

2.3 Detection of Jamming

WLANs are built upon a shared medium that makes it easy to launch jamming attacks. These attacks can be easily accomplished by sending radio frequency signals that do not follow any MAC protocols. Detection of jamming attacks can be done in multiple ways. One of the most efficient ways is to jump channels. Because communication between two legitimate nodes is done through a specific frequency, the frequency can be changed if necessary. While a jammer is attacking the wireless network, there are other effective ways to continue legitimate communication in the network. Engaging the jammer on the jammed channel and continuing communication in another channel was introduced by Beg, Ahsan, and Mohsin (2010). When the nodes detected the jamming in the wireless network, they jumped to another channel to continue legitimate communication. In the experiments, both 10 and 20 nodes experiments were done, and in both scenarios, after channels were jumped, the network resumes communications as normal. In both scenarios, the amount of packets dropped reduced immediately. The research concluded that channel jumping will decrease the throughput of the network. Also, it was easier to detect jamming through intermitted channel jumping. Concluded, channel jumping was a superior method of combating network interference, rather than changing network protocols (Jeung, Jeong, and Lim, 2011).The research concluded that channel jumping will decrease the throughput of the network. Also, it was easier to detect jamming through intermitted channel jumping. Concluded, channel jumping was a superior method of combating network interference, rather than changing network protocols (Jeung, Jeong, and Lim, 2011).In order to prevent from multi-channel jamming attacks, a cross-layer jamming detection method was developed (Chiang and Hu, 2011). Cross-layer jamming detection is a tree-based approach. A jamming detection algorithm was utilized in all legitimate nodes; when the communication process began, all the nodes had the ability to report jamming attacks in differ ent layers, and only the reports which were generated by nodes with jamming detection algorithm were accepted by the system in order to avoid error. Research was also done about multi-channel jamming attacks by Jiang and Xue (2010). The difference from the jamming detection algorithm was that it focused on network restoration and design of traffic rerouting.

2.5 Algorithm

1. Symmetric encryption algorithm
2. Brute force attacks against block encryption algorithms.

We propose a solution based on All-Or- Nothing Transformations (AONT) that introduces a modest communication and computation overhead. Such transformations were originally proposed by Rivest to slow down brute force attacks against block encryption algorithms . An AONT serves as a publicly known and completely invertible pre-processing step to a plaintext before it is passed to an ordinary block encryption algorithm

Algorithm Description

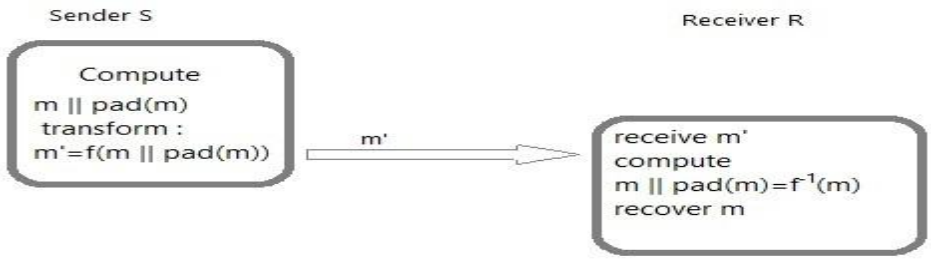

fig-2.5 :The AONT-based Hiding Scheme (AONT-HS)

The Package Transform- In the package transform ,given a message m, and a random key k′, the output pseudo-messages are computed as follows:–

$$m'_i = m_i \oplus E_{k'}(i) \text{ , for } i=1,2,3\ldots\ldots,x$$
$$m'_{x+1} = k' \oplus e_1 \oplus e_2 \oplus e_3 \oplus \ldots\ldots\ldots\ldots \oplus e_x ,$$

Where $e_i = E_{k0}(m'_i \oplus i)$, for i = 1, 2, . . . , x, and k0 is a fixed publicly-known encryption key. With the reception of all pseudo-messages message m is recovered as follows:

$$k' = m'_{x+1} \oplus e_1 \oplus e_2 \oplus e_3 \oplus \ldots\ldots\ldots\ldots \oplus e_x ,$$
$$m_i = m'_i \oplus E_{k'}(i) \text{ , for } i=1,2,3\ldots\ldots,x,$$

Note that if any m'_i is unknown, any value of k′ is possible, because the corresponding e_i is not known. Hence, $E_{k'}(i)$ cannot be recovered for any i, making it infeasible to obtain any of the m_i .

Hiding Sublayer Details- AONT-HS is implemented at the hiding sublayer residing between the MAC and the PHY layers. In the first step, m is padded by applying function pad() to adjust the frame length so that no padding is needed at the PHY layer, and the length of m becomes a multiple of the length of the pseudo-messages m′ i. This will ensure that all bits of the transmitted packet are part of the AONT. In the next step, m||pad(m) is partitioned to x blocks, and the AONT f is applied. Message m′ is delivered to the PHY layer. At the receiver, the inverse transformation f–1 is applied to obtain m||pad(m). The padded bits are removed and the original message m is recovered. The steps of AONT-HS are shown in Fig. 2.5.

3. ARCHITECTURE

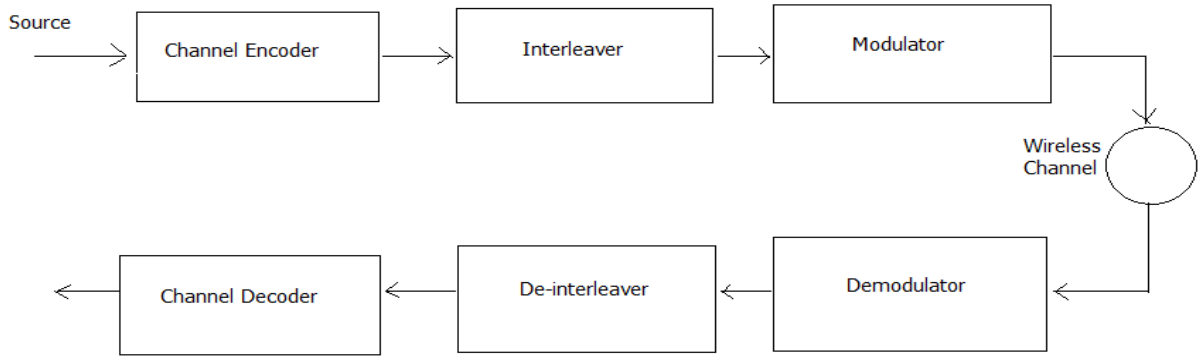

4. PROBLEM FORMULATION

4.1 Existing System

Jamming attacks are much harder to counter and more security problems. They have been shown to actualize severe Denial-of-Service (DoS) attacks against wireless networks. In the simplest form of jamming, the adversary interferes with the reception of messages by transmitting a continuous jamming signal , or several short jamming pulses jamming attacks have been considered under an external threat model, in which the jammer is not part of the network. Under this model, jamming strategies include the continuous or random transmission of highpower interference signals.

4.2 Proposed System

In this paper, we address the problem of jamming under an internal threat model. We consider a sophisticated adversary who is aware of network secrets and the implementation details of network protocols at any layer in the network stack. The adversary exploits his internal knowledge for launching selective jamming attacks in which specific messages of "high importance" are targeted. For example, a jammer can target route-request/route-reply messages at the routing layer to prevent route discovery, or target TCP acknowledgments in a TCP session to severely degrade the throughput of an end-to-end flow.

To launch selective jamming attacks, the adversary must be capable of implementing a "classify-then-jam" strategy before the completion of a wireless transmission. Such strategy can be actualized either by classifying transmitted packets using protocol semantics, or by decoding packets on the fly. In the latter method, the jammer may decode the first few bits of a packet for recovering useful packet identifiers such as packet type, source and destination address. After classification, the adversary must induce a sufficient number of bit errors so that the packet cannot be recovered at the receiver . Selective jamming requires an intimate knowledge of the physical (PHY) layer, as well as of the specifics of upper layers.

5. MODULES

1. Network module
2. Real Time Packet Classification
3. Selective Jamming Module
4. Strong Hiding Commitment Scheme (SHCS)
5. Cryptographic Puzzle Hiding Scheme (CPHS)

Module Descriptions

6. Network module

We address the problem of preventing the jamming node from classifying m in real time, thus mitigating J's ability to perform selective jamming. The network consists of a collection of nodes connected via wireless links. Nodes may communicate directly if they are within communication range, or indirectly via multiple hops. Nodes communicate both in unicast mode and broadcast mode. Communications can be either unencrypted or encrypted. For encrypted broadcast communications, symmetric keys are shared among all intended receivers. These keys are established using pre shared pair wise keys or asymmetric cryptography.

7. Real Time Packet Classification

Consider the generic communication system depicted in Fig. At the PHY layer, a packet m is encoded, interleaved, and modulated before it is transmitted over the wireless channel. At the receiver, the signal is demodulated, deinterleaved, and decoded, to recover the original packet. Moreover, even if the encryption key of a hiding scheme were to remain secret, the static portions of a transmitted packet could potentially lead to packet classification. This is because for computationally-efficient encryption methods such as block encryption, the encryption of a prefix plaintext with the same key yields a static cipher text prefix. Hence, an adversary who is aware of the underlying protocol specifics (structure of the frame) can use the static cipher text portions of a transmitted packet to classify it.

8. Selective Jamming Module

We illustrate the impact of selective jamming attacks on the network performance. implement selective jamming attacks in two multi-hop wireless network scenarios. In the first scenario, the attacker targeted a TCP connection established over a multi-hop wireless route. In the second scenario, the jammer targeted network-layer control messages transmitted during the route establishment process selective jamming would be the encryption of transmitted packets (including headers) with a static key. However, for broadcast communications, this static decryption key must be known to all intended receivers and hence, is susceptible to compromise. An adversary in possession of the decryption key can start decrypting as early as the reception of the first cipher text block.

9. Strong Hiding Commitment Scheme (Shcs)

We propose a strong hiding commitment scheme (SHCS), which is based on symmetric cryptography. Our main motivation is to satisfy the strong hiding property while keeping the computation and communication overhead to a minimum.

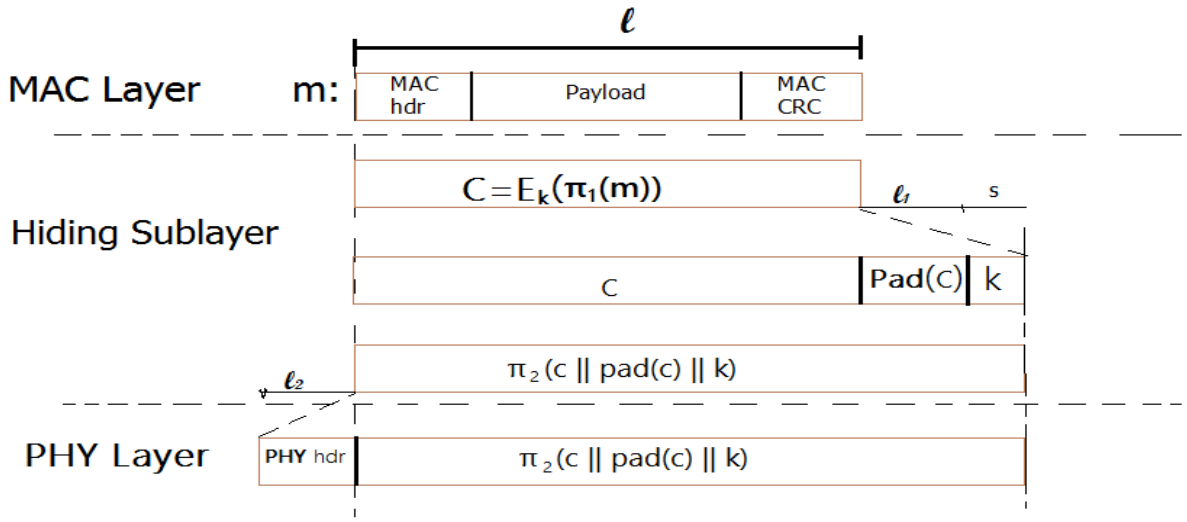

The computation overhead of SHCS is one symmetric encryption at the sender and one symmetric decryption at the receiver. Because the header information is permuted as a trailer and encrypted, all receivers in the vicinity of a sender must receive the entire packet and decrypt it, before the packet type and destination can be determined. However, in wireless protocols such as 802.11, the complete packet is received at the MAC layer before it is decided if the packet must be discarded or be further processed . If some parts of the MAC header are deemed not to be useful information to the jammer, they can remain unencrypted in the header of the packet, thus\ avoiding the decryption operation at the receiver.

10. Cryptographic Puzzle Hiding Scheme (Cphs)

we present a packet hiding scheme based on cryptographic puzzles. The main idea behind such puzzles is to force the recipient of a puzzle execute a pre-defined set of computations before he is able to extract a secret of interest. The time required for obtaining the solution of a puzzle depends on its hardness and the computational ability of the solver. The advantage of the puzzle based scheme is that its security does not rely on the PHY layer parameters. However, it has higher computation and communication overhead We consider several puzzle schemes as the basis for CPHS. For each scheme, we analyze the implementation details which impact security and performance. Cryptographic puzzles are primitives originally suggested by Merkle as a method for establishing a secret over an insecure channel. They find a wide range of applications from preventing DoS attacks to providing broadcast authentication and key escrow schemes.

11. Conclusion

We addressed the problem of selective jamming attacks in wireless networks. We considered an internal adversary model in which the jammer is part of the network under attack, thus being aware of the protocol specifications and shared network secrets. We showed that the jammer can classify transmitted packets in real time by decoding the first few symbols of an ongoing transmission. We evaluated the impact of selective jamming attacks on network protocols such as TCP and routing. Our findings show that a selective jammer can significantly impact performance with very low effort. We developed three schemes that transform a selective jammer to a random one by preventing real-time packet classification. Our schemes combine cryptographic primitives such as commitment schemes, cryptographic puzzles, and all-or-nothing transformations (AONTs) with physical layer characteristics. We analyzed the security of our schemes and quantified their computational and communication overhead.

12. Acknowledgements

This work is supported by BBN Technologies and the Air Force. The authors thank Dan Coffin and Jeff Ward for the many conversations in developing this paper and the helpful comments of the anonymous reviewers. Jesse James is currently with the Air Force.

REFERENCES

Journal Papers:

[1] T. X. Brown, J. E. James, and A. Sethi. Jamming and sensing of encrypted wireless ad hoc networks. In Proceedings of MobiHoc, pages 120–130, 2006..

[2] M. Wilhelm, I. Martinovic, J. Schmitt, and V. Lenders. Reactive jamming in wireless networks: How realistic is the threat? In Proceedings of WiSec, 2011.

[3] W. Xu, W. Trappe, Y. Zhang, and T.Wood. The feasibility of launching and detecting jamming attacks in wireless networks. In Proceedings of MobiHoc, pages 46–57, 2005.

[4] IEEE. IEEE 802.11 standard. http://standards.ieee.org/getieee802/download/802.11-2007.pdf, 2007.

[5] Akyildiz, I. F., Wang, W., & Wang, W. (2005, January). Wireless mesh networks: a survey. Computer Networks Journal, 47(4), 445-487.

[6] D. Stinson. Cryptography: theory and practice. CRC press, 2006.

[7] Eriksson, J. and Koivunen, V.: Identi¯ability, separability, and uniqueness of linear ica models. IEEE Signal Processing Letters, 11(7), July 2004.

[8] P. Tague, M. Li, and R. Poovendran. Mitigation of control channel jamming under node capture attacks. IEEE Transactions on Mobile Computing, 8(9):1221–1234, 2009.

An Approach to Find Maintenance Costs Using Cost Drivers of Cocomo Intermediate Model

C.V.S.R SYAVASYA
[1,]M.Tech, GITAM UNIVERSITY

Abstract:
Maintenance of software under several cost drivers is as sort of assigning a range of ratings instead of a single point rating to get range of estimates. Several parameters come into use like Annual change traffic and development costs in man-months. Software is being used worldwide, in the same way maintenance of software is equally important as of development of software. Here, we have taken particular range values of lines of code to evaluate costs pertaining to development which intern evaluates final maintenance costs. Every multiplier is taken randomly according to characteristics of product and made a product with development costs to obtain maintenance costs of software. This procedure is done for all the three modes namely organic, semidetached and embedded modes in order to obtain comparison statements of results. The main aim to carry out this review is to explore the changes in maintenance of software when new cost drivers are introduced to the product.

Keywords: Eaf, Act, Cocomo, Ks, Sloc, Nnl, Nml, Nol

1.Introduction

As COCOMO is a non-proprietary model, its details are available in the public domain [1], encouraging researchers and practitioners in the software engineering community to independently evaluate the model. There have been many extensions independently reported; use machine learning techniques to generate effort models from the original COCOMO model. Gulezian proposed a calibration method by transforming the model equation into a linear form and estimating the model parameters using standard linear regression techniques.

Source Lines of Code [2]

The COCOMO calculations are based on your estimates of a project's size in Source Lines of Code (SLOC). SLOC is defined such that only Source lines that are DELIVERED as part of the product are included, test drivers and other support software is excluded, SOURCE lines are created by the project staff , code created by applications generators is excluded. The original COCOMO 81 model was defined in terms of Delivered Source Instructions, which are very similar to SLOC. The major difference between DSI and SLOC is that a single Source Line of Code may be several physical lines. For example, an "if-then-else" statement would be counted as one SLOC, but might be counted as several DSI. Glance of cocomo model: The COCOMO cost estimation model is used by thousands of software project managers, and is based on a study of hundreds of software projects. Unlike other cost estimation models, it is an open model, so all of the details are published, including: The underlying cost estimation equations are obtained by software maintenance cost formulated. It is well defined, and because it doesn't rely upon proprietary estimation algorithms, Costar offers these advantages to its users: Its estimates are more objective and repeatable than estimates made by methods relying on proprietary models it can be calibrated to reflect your software development environment, and to produce more accurate estimates Costar is a faithful implementation of this model that is easy to use on small projects, and yet powerful enough to plan and control large projects. Typically, you'll start with only a rough description of the software system that you'll be developing, and you'll use Costar to give you early estimates about the proper schedule and staffing levels. As you refine your knowledge of the problem, and as you design more of the system, you can use Costar to produce more and more refined estimates.Costar allows defining a software structure to meet your needs. Your initial estimate might be made on the basis of a system containing 3,000 lines of code. Your second estimate might be more refined so that you now understand that your system will consist of two subsystems. There are some sizing approaches for estimating the software maintenance efforts such as source lines of code (SLOC). COCOMO is used to compute the effort and calendar time based on the size and several characteristics of the software product.

Effort Adjustment Factor [2]

The Effort Adjustment Factor in the effort equation is simply the product of the effort multipliers corresponding to each of the cost drivers for your project. For example, if your project is rated Very High for Complexity (effort multiplier of 1.34), and Low for Language & Tools Experience (effort multiplier of 1.09),

and all of the other cost drivers are rated to be Nominal (effort multiplier of 1.00), the EAF is the product of 1.34 and 1.09.

2. Cost Drivers

COCOMO II has 17 cost drivers to assess project, development environment, and team to set each cost driver. The cost drivers are multiplicative factors that determine the effort required to complete your software project. For example, if a project will develop software that controls an airplane's flight, you would set the Required Software Reliability (RELY) cost driver to Very High. That rating corresponds to an effort multiplier of 1.26, meaning that your project will require 26% more effort than a typical software project. *Co*nstructive *Co*st *Mo*del is used for estimating costs of software projects [3]. It was created by Barry W. Boehm and published in 1981 using data collected from 63 projects. The quantity of projects studied and the care in its articulation have made the model popular and encouraged its use. The model offers empirical formulas for estimating software costs. We have taken the COCOMO as the starting point for our research. After application of the first version of his model to a wide range of situations, Boehm concluded that coverage for only one mode of developing software was insufficient, so he provided for three modes: organic, semidetached and embedded. In this way, he recognized the influence of various characteristics such as size, communication needs, experience in similar projects, etc. Furthermore, Boehm provides the COCOMO in three versions: basic, intermediate, and detailed. The basic version is useful for quick estimations, although without fine precision. The intermediate version deals with 15 attributes of the project (reliability required, database size, memory restrictions, response time required, etc.), all of whose valuation acts as a multiplying factor in the model.

3. Estimating Maintenance Cost using Cost Model

The first version of COCOMO is COCOMO 81. This model, extensively described The Software Engineering Economics is still an interesting model to understand. The detailed version deals with estimates in each of the phases in the life cycle of the project. The basic version of the model offers the following formulas to calculate the cost of software development measured in *MM* (i.e., man-months):
The COCOMO 81 model is a static model with a hierarchy of three estimation models.

1) Basic Model: It provides a rough estimate of effort based on size and mode of software development.
2) Intermediate Model: It refines the basic model by use of 15 cost drivers-these are subjective attributes. The impact of cost drivers is considered at the project level, Effort is further adjusted to take into account any schedule constraint.
3) Detailed Model: This model further refines the estimation by considering the phase-wise impact of cost-drivers, and the computations in this are for various sub-systems/modules.
   All the three COCOMO 81 models use size as the main input. Another factor used in all three models is the "mode" of project development- the way the project is going to be handled. The three modes considered are:

1) Organic Mode: Project developed by a small, experienced team working in a familiar environment. The team communicates easily. Projects done like these are small or medium sizes with minimal need for innovations. Environment, hardware and tools are stable.
2) Semi-detached Mode: This mode lies between organic and embedded mode.
3) Embedded Mode: Projects developed by large teams where communication is not achieved easily. Projects are medium to large, being developed under tight constraints, possibly with instable hardware and software environment and requiring complex, innovate processing.
   We propose and review under the intermediate model basing on some multipliers taken randomly according to requirement of project.

4. Intermediate Model:

The Intermediate model refines the Basic Model by introducing cost drivers" [3]. It first uses a nominal cost equation for computation and then applies a factor based on the cost driver to it.
Here, cost driver is the product of a *(size^b) implies:

$$\mathbf{MM_{dev} = a * (size^b) * Multiplier}$$

Where MM_{dev} is the development costs in man-months, a and b are factors to calibrate using past data for each development mode.
There are totally 15 multipliers in Intermediate Model which are rated in different value starting from very low to extra high.

5. Results and Discussion:

According to our review done starting from organic mode, where lines of code starting from 80 to 120, where *KS* is an estimate of the delivered program size in thousands of instructions (or roughly, lines of source code).

To estimate the maintenance cost, another parameter is needed: the annual change traffic (*ACT*) which consists of the proportion of original instructions that undergo a change during a year by addition or modification [5].

$$ACT = (NNL + NML)/(NOL) \quad (4)$$

Where:
NNL = number of new lines, *NML* = number of modified lines, and *NOL* = number of original lines

$$MM_{MAIN} = ACT * MM_{DEV}$$

WHERE **ACT = (*NNL + NML)/ (NOL)***
NNL = number of new lines, *NML* = number of modified lines, and *NOL* = number of original lines *and* MM_{DEV}:
AT Organic mode: $MM_{DEV} = 3.2\ KS^{1.05}$ * **Multiplier value**
Semidetached mode: $MM_{DEV} = 3{\cdot}0\ KS^{1.12}$ * **Multiplier value**
Embedded mode: $MM_{DEV} = 2.8\ KS^{1.20}$ * **Multiplier value**

Finding Act Values

Where, KS is thousand source lines of code. Here the range of KS started from 80 to 120 In first step, we have calculated Annual change traffic values and formulated in the form of table as follows: In the below table, Number of lines added is taken (NNL) as 15, Number of lines deleted (NML) as 20, Total Number of original lines (NOL) as 80. Therefore, According to above formula, ACT is resulted as 0.4375. Number of lines added is taken (NNL) as 25, Number of lines deleted (NML) as 30, Total Number of original lines (NOL) as 90. Therefore, According to above formula, ACT is resulted as 0.611. Number of lines added is taken (NNL) as 35, Number of lines deleted (NML) as 40, Total Number of original lines (NOL) as 100. Therefore, According to above formula, ACT is resulted as 0.75. Number of lines added is taken (NNL) as 45, Number of lines deleted (NML) as 50, Total Number of original lines (NOL) as 110. Therefore, According to above formula, ACT is resulted as 0.8636. Number of lines added is taken (NNL) as 55, Number of lines deleted (NML) as 60, Total Number of original lines (NOL) as 120. Therefore, According to above formula, ACT is resulted as 0.9583. Here, the table is shown between the Total Number of lines taken and obtained Annual Change traffic values.

NOL(Original Lines of Code)	ACT
80	0.4375
90	0.611
100	0.75
110	0.8636
120	0.9583

Table1: Value of ACT after Inserting Values in Equation

Finding Multiplier Values

Now, After Annual change traffic values are obtained, we calculate Development costs in man-months. According to formula to calculate development costs in man-months, we first calculate Multipliers, which are used as a product value for all the three modes namely organic, semidetached, embedded modes.
Now, we assign range of cost driver and calculate Multiplier values as follows:

KS(NOL)	MULTIPLIER EQUATION	MULTIPLIER VALUE
80	RELY(LOW) * SCED(HIGH)	0.915
90	DATA(LOW) * TOOL(HIGH)	0.8554
100	CPLX(LOW)*MODP(HIGH)	0.7735
110	TIME(HIGH)*PCAP(VERY HIGH)	0.777
120	STOR(NOMINAL)*ACAP(VERY HIGH)	0.71

Table2: Showing the Results of Multiplier Values

In the above table, we observe that, at Thousand lines of source code (KS) as 80, by taking RELY (Required Software Reliability) as low and SCED (Required Development Schedule) as high, the product of both parameters resulted as 0.915. At thousand lines of code (KS) as 90, by taking DATA (Database size) as low and TOOL (Usage of software tools) as high, the product of both parameters resulted as 0.8554. At thousand lines of code (KS) as 100, by taking CPLX (Project complexity) as low and MODP (Modem programming practices) as

high, the product of both resulted as 0.7735. In the same way, we have calculated for KS 110 and 120 and obtained values are 0.777 and 0.71.

Now, after knowing the Multiplier values from the above table, we calculate Development costs in man-months by using the formula of MM_{DEV} mentioned as equation1:

AT ORGANIC MODE:

By taking KS values ranging from 80 to 120 and a value is 3.2 and b value is 1.05 in intermediate model of organic mode. Initially, at KS as 80 and substituted in organic mode equation and multiplied by Multiplier value of 80, development cost is obtained as 291.61. In this way, remaining values of development costs are obtained and formulated in form of table as follows:

KS VALUE(NOL)	MM_{DEV}(with multipliers)
80	291.61
90	308.51
100	311.60
110	345.96
120	346.37

Table3: Showing the Results of Development Costs for Its Ks Values

Final Maintenance Costs In Man-Months:

Here, we have obtained values of MMdev and ACT. Hence the product of both Development costs in man-months and Annual Change Traffic gives final Maintenance cost in man-months as follows:

KS	MM_{MAIN}(ACT * MM_{DEV})
80	127.57
90	188.49
100	233.7
110	298.77
120	331.92

Table4: Showing Results Of Final Maintenance Cost

Therefore, as thousand lines of code (KS) increases, Maintenance costs in Man-months also increases in organic mode.

In the same way,
At Semi-Detached Mode:

By taking KS values ranging from 80 to 120 and a value is 3.0 and b value is 1.12 in intermediate model of organic mode. After the product made between each value of cost driver to development cost equation, and the obtained result is multiplied to annual change traffic, finally Maintenance cost in man-months is obtained. The values obtained in calculating Maintenance cost in man-months in Organic mode are used here in calculating maintenance cost in man-months in semidetached mode. The purpose of same values imposing on equation of semidetached mode is to make comparisons between Line of code and maintenance cost in man-months.

KS VALUE(NOL)	MM_{MAIN}
80	162.54 (NNL-15,NML-20)
90	242.1 (NNL-25,NML-30)
100	355.8 (NNL-35,NML-40)
110	389.2 (NNL-45,NML-50)
120	435 (NNL-55, NML-60)

TABLE5: Showing the Final Results of Maintenance Costs for Its KS Values

The above table shows that, for each lines of code taken as same in both organic and semidetached modes, Maintenance costs moves from low to high from each KS point of view.
In the same way Embedded mode values are calculated and are observed that, for every KS value increasing, Maintenance cost in man-months is also increasing for all the three modes. Increasing factor is more by introducing cost drivers multipliers in Development costs.

6. Conclusion:

Multiplier factor is used in the equation to get the total cost. The development cost computed uses the same equation as the basic model. Here, we have taken range of values from multipliers and finally maintenance cost is summarised according to each source lines of code. The aim of taking up this task of exploring new results in maintenance costs by introducing new cost driver multipliers is fulfilled by figuring out the result tables and conclusions are made according to the obtained results. We conclude that, as the multiplier is introduced in a project and as lines of code increases, maintenance cost of project also increases. As part of Future work, Estimation can also be done using a range of new cost drivers based on new requirement to get a range of estimations.

References:

1) http://csse.usc.edu/csse/TECHRPTS/PhD_Dissertations/files/Nguyen_Dissertation.pdf
2) http://www.softstarsystems.com/overview.htm
3) "Software Requirements and Estimation" by Swapna Kishore, Rajesh Naik published by TATA McGRAW HILL
4) Pressman RS. Software Engineering A Practitioner's Approach, ch. 20. McGraw-Hill: New York NY, 1992; 677.

Potential of Information and Communication Technology Towards the Success of the Indian IT Software Industry

Sheela Bhatt[1], Dr.S.S.Sarangdevot[2]
[1,] Research Scholar, Suresh Gyan Vihar University, India
[2,]Vice Chancellor, Jrn Rajasthan Vidhyapeeth University, India

Abstract:

India has also embraced ICT tools for strengthening its economic and technical power. The present research explores the potential of ICT towards the Indian IT Software Industry. This paper embraces modern ICT to explore and examines the potential of ICT towards the Indian Software Sector. In particular, it surveys the impact of Information on Communication Technologies with respect to information on the company's framed policies procedures. Further, it also examines its potential towards the Indian IT software and services sector. Only Primary data is used.Two Structured Questionnaire Modules are set. Cluster sampling and Random sampling is used respectively. Sampling frame is South India. Data collection methods are: Mails, Interviews and Schedules for both modules. Source list comprises of important Indian Software Entrepreneurs/Organizations.. A Pilot Testing is undertaken. To meet objectives, hypothesis test is applied. For statistical analysis, multivariate regression, Analysis of Variance and Factor Analysis is used. Test Statistics F or t is also used. For coding and computations, SPSS and Microsoft Office Excel along with embedded Q1Macros 2012 is used.

Keywords: Entrepreneur /Organization, explore, impact, Indian, Information on Communication Technologies, policies and procedures, potential, Software, Industry.

Overview: This paper comprises of seven sections in all. They are respectively: Introduction to ICT; Objectives of Research; Methods and Tools used; Review of Literature ; Meeting the Objectives; Recommendations and Bibliography.

1. Introduction to ICT

ICT or Information and Communication Technologies research and applications include areas such as, ICTs towards education, ICT towards health care, ICT towards Pharmacy, ICT in libraries, ICT in Software and Services, ICT in Child Development, ICT in Women Empowering and ICT towards Gender Divide. Modern ICT can be used to for development in these fields. ICT is embraced by most of the countries today, for most modern economies and development.ICT proves to be an essential tool that empowers the poor by developing skills and strengthening governance. Hence, embracing ICT has become a must for any developing country like India. ManySeminars and conferences related to ICT in various disciplines are conducted in India every year. The Government of India has also realized its importance. The success of ICT–enabled development or e-Development is measured technically and also by its own advancement and development. This paper explores the potential of ICT towards the Indian IT Software Sector, including software services sector.

2. Objectives of Research

2.1 Objective A.

To examine the impact of ICT and its potential towards the Indian Software Sector and explore the role of Information on Communication Technologies with respect to information on the company's framed policies and procedures**.**

2.2 Objective B

To study the potential of ICT towards the Indian IT Software Sector.

3. Methods and Tools Used

3.1. Types of data used

3.1.1. Secondary data. This is used only for review purpose. Secondary data is collected through Websites [1], journals, [2], [3], [4], books, e-books, NASSCOM publications[5], working papers, online libraries / journals [6],[7],[8],[9].

3.1.2. Primary data

Table 1. Details of primary data

	MODULE 1	MODULE 2
Data collection Methods	Mailing Interviews Schedules	Mailing, Interviews, Schedules
Sample size	60 (Out of 75 respondents, only 60 responded).	32
Sampling technique	Cluster Sampling.	Random Sampling
Type of universe	Finite Population	Finite Population
Sampling design	Informal experimental design (Before-and-after without control design) Formal experimental designs	Informal experimental design (Before-and-after without control design) Formal experimental designs
Sampling unit	Bangalore	South India
Source list	Important Indian IT/ Software Companies/Entrepreneurs	Important Indian IT/ Software Companies/Entrepreneurs

To meet objectives only primary data is used. Primary data is collected through two different modules of structured questionnaires. A Pilot Testing of the Questionnaire was conducted and thereafter, the required changes were made in the questionnaire, in an organized way, with the assistant of the respondents. Further details about collection of primary data, the sampling methods, sample size, sampling technique, sampling unit and the source list is as described in Table 1.

3.2. Techniques or tools used

The following other statistical tools are used and multivariate analysis is also done .

KMO and Bartlett's Test.

Important statistical measures like Mean, Mode, Standard deviation, variance, Multiple covariance and Correlation Matrices are used.

Analysis Of Variance.

Regression.

F statistic or **t** statistic is used as test statistic.

3.3. Other materials used

SPSS and Excel is used. Q1 Macros 2012 incorporated/embedded with Microsoft Works (Excel) has also been used for further analysis and computations.

4. Review of Literature

4.1 ICT policies and strategies aimed at implementing the UNMDGS and WSIS objectives

WSIS Follow-up Regional Workshop was conducted at Bangkok during 29-31 May 2006. It throws light on WSIS Plan of Action Objectives and UN Millennium Development Goals.

4.2 Nature of liberalisation, government support or other policy changes required

The development of stronger national and international protection for intelligence for intellectual property rights was also seen as essential to the development of the software industry. Foreign software firms that might send work to India were hesitant to do so if they could not be sure of the protection of their proprietary rights. A comprehensive analysis of the Indian Software industry with special emphasis on the software exports can be summarized as follows: The domestic as well as the

software industry has shown consistently high growth rates in the 90s although our share in the global export market is miniscule. About 73% of our export cargo consists of Professional Services, Consultancy and Training. However, there has been a visible shift of our software exports towards off shore project development, which also includes off shore package development. Indian companies have exported software to more than forty countries but there has been a heavy reliance on the US market. India's software export trade has been characterized contracts, which allocate only the less-skilled coding and testing stages to Indian professionals. Indian software export industry is heavily concentrated. It can be evidenced by the fact that only top 20 of the 400 exporting firms generate 70% of the exports.

4.3 Evidence from Bangalore in India

ICT Sector, Globalization and Urban Economic Growth Evidence from Bangalore, India, is a present working research paper (Working Paper No. 2010/80) by M. R. Narayana. This paper aims at economic analysis of economic globalization and urban growth of Bangalore, the *Silicon Valley of India*, as they are related to ICT sector.

4.4 Lessons from the Indian software sector

Economic Adversity and Entrepreneurship-led Growth Lessons from the Indian Software Sector is a research Paper (Working Paper No. 2010/04) by Suma Athreye. This paper argues that the business models chosen by Indian firms were those that best aligned the country's abundant labour resources and advantages to global demand. The paper also shows that the presence of growth opportunities and the success of firms stimulated institutional evolution to promote entrepreneurial growth.

4.5 National software industry development: considerations for government planners and software development India services

The research paper [10] jointly by Umesh Sehgal, Kuljeet Kaur & Pawan Kumar discusses on National Software Industry Development: Considerations for Government Planners[11]. Webdhoom [12] is a Software development India company who is dedicated to deliver the services as expected with due care and we fill proud our self to deliver the best approach to the customers. The Indian government has given complete support to the IT and ITES industry in India. The Indian government has even permitted 100% foreign equity [13]. From the foregoing analysis, it is clear that software is an area which will work as a catalyst to make India a 'Global IT Super Power' [14] . In India, the IT sector has not only grown in size but also complexity. Indian States resemble little nations. So, it is important to take regular stock of e-Readiness [15].

4.6 Review of Indian software industry

The Indian software industry has a unique distinction in that most of its output is [16] exported**.** Despite the high growth rates, India's share in the world software market is very low, but India still enjoys an advantage over some of the other nations, which are trying to promote software exports. Coupled with the fact that the quality of Indian software is good and manpower cost is relatively low, it provides India a very good opportunity in the world market.

Location of Software Companies and Growth Rate. The industry is mainly concentrated around metros: Mumbai, Bangalore, Delhi, Hyderabad, Chennai, Calcutta, Pune and few other cities. Lately, Hyderabad, Chennai, Pune and Gurgaon and Noida have emerged as fast growing Software cities. At the same time Bangalore and Mumbai continue to attract investment in software sector With the amendments to the copyright Act and its rigorous enforcement, it is expected that in the coming years, piracy would be brought under further control. Also, the government has announced zero import duty on software.

Software Export Industry Growth and Revenue and Future. Interestingly, most of the export is in the form of providing software services, that is developing or helping develop software for organizations overseas. Most of domestic turnover comes through selling of software products developed primarily in other countries. That is, the overseas revenue is earned by providing services while the domestic revenue comes mostly through trading.[17].

Type of Services. On-Site Services, Offshore Services and Offshore Packages.

Software Activity for Domestic Software Export. Professional Services, Products & Packages, Turnkey, Consultancy & Training, Data Processing and Other.

Destination of Indian Software Exports. India exports almost of its total software exports of USA and to Europe. The six OECD countries (USA, Japan, UK, Germany, France and Italy) together have a good percentage of the market share of the world-wide software market. Interestingly, India's exports to these countries are yet higher. In the coming years, India is expected to strike many joint ventures and strategic alliances in Europe. The trade with European nations is growing rapidly.

There have been alliances to create more co-operation between Indian and European software companies [18].

Activity And Structure of Software Exports. There has been a shift towards offshore services in the software export cargo of India. The bulk of Indian software exports have been in the form of professional services. A detailed analysis indicates that majority of software exports are in the areas classified as "customized" or "professional consultancy". However, since last two years, there has been a visible shift towards off shore project development, which also includes offshore package development has increased to over a good extent during the year. Reasons attributed for this growth are increasing number of Software Technology Parks, liberalized economic policy and unnatural visa restrictions by U.S. and some Western European countries The degree of on-site development is still very high. It is expected to decrease further in the coming years with improved data communication links.

5.Meeting the Objectives

5.1. Objective A

To examines the impact of ICT and its potential towards the Indian Software Sector and explores the role of Information on Communication Technologies with respect to Work Culture Satisfaction of the respondents based on information of the company's framed policies and procedures. We now construct a regression model with Work Culture Satisfaction (X24) of the Indian IT Organizations as, the dependent variable. The test checks if the Indian IT Software Entrepreneurs are capable of implementing good policies and procedures so as to result in a good work culture satisfaction.
The independent variables X26, X28, X29,X30, X31 and X32 are respectively; Well informed about company's policies and procedures, Feel free to suggest changes for Dept. Improvement, Receive proper training to perform job effectively, Treated as a Valuable member of Company, Employees problems and complaints are resolved fairly & promptly, Job duties and responsibilities are clearly defined[a] Factor analysis is performed, and the Correlation Matrix of the variables prove to be 0.002.

5.1.1 Test1. We now construct a regression model with Work Culture Satisfaction (X24) of the Indian IT Organizations as, the dependent variable. The test checks if the Indian IT Software Entrepreneurs are capable of implementing good policies and procedures so as to result in a good work culture satisfaction. The independent variables X26, X28, X29, X30, X31 and X32 are respectively; Well informed about company's policies and procedures, Feel free to suggest changes for Dept. Improvement, Receive proper training to perform job effectively, Treated as a Valuable member of Company, Employees problems and complaints are resolved fairly & promptly, Job duties and responsibilities are clearly defined[a]
Factor analysis is performed, and the Correlation Matrix of the variables prove to be 0.002.

5.1.2 KMO and Bartlett's test

Table 2. KMO and Bartlett's test

Kaiser-Meyer-Olkin Measure of Sampling Adequacy.		.721
Bartlett's Test of Sphericity	Approx. Chi-Square	355.367
	df	28
	Sig.	.000

The KMO coefficient is .721, which is a good indicator of acceptance.

5.1.3 Syntax

```
REGRESSION
  /MISSING LISTWISE
  /STATISTICS COEFF OUTS R ANOVA
  /CRITERIA=PIN(.05) POUT(.10)
  /NOORIGIN
  /DEPENDENT X24
  /METHOD=ENTER X26 X28 X29 X30 X31 X32.
```

5.1.4 Output: Regression

Table 3. Variables entered /removed

Model	Variables Entered	Variables Removed	Method

	Well informed about company's policies and procedures, Feel free to suggest changes for Dept. Improvement, Receive proper training to perform job effectively, Treated as a Valuable member of Company, Employees problems and complaints are resolved fairly & promptly, Job duties and responsibilities are clearly defined[a] .	.	Enter

a. All requested variables entered.

Table 4. Model summary

Model	R	R Square	Adjusted R Square	Std. Error of the Estimate
1	.955[a]	.912	.902	.157

Table 5. ANOVA[b]

Model		Sum of Squares	df	Mean Square	F	Sig.
1	Regression	13.623	6	2.271	91.873	.000[a]
	Residual	1.310	53	.025		
	Total	14.933	59			

a. Predictors: (Constant), Well informed about company's policies and procedures, Feel free to suggest changes for Dept. Improvement, Receive proper training to perform job effectively, Treated as a Valuable member of Company, Employees problems and complaints are resolved fairly & promptly, Job duties and responsibilities are clearly defined.
b. Dependent Variable: WORK CULTURE SATISFACTION.

Table 6. Coefficients[a]

Model	Un standardized Coefficients		Standardized Coefficients	t	Sig.
	B	Std. Error	Beta		
1 (Constant)	-.058	.094		-.619	.538
Treated as a Valuable member of Company	.087	.042	.108	2.061	.044
Feel free to suggest changes for Dept. Improvement	-.013	.035	-.016	-.380	.705
Job duties and responsibilities are clearly defined	.521	.087	.565	5.999	.000
Receive proper training to perform job effectively	.015	.050	.019	.305	.761
Employees problems and complaints are resolved fairly & promptly	-.107	.066	-.131	-1.622	.111
Well informed about company's policies and procedures	.456	.080	.495	5.681	.000

a. Dependent Variable: WORK CULTURE SATISFACTION

Result of Test1. The computed value of F is too high compared to the table value of F(6,59)
That is, the Indian IT Entrepreneurs are successful in providing an excellent work culture satisfaction, based on its policies and procedures.

Note. Yet, the required and necessary positive improvements or changes can be studied from the Table 6.

5.2. Objective B

To study potential of ICT towards the Indian IT Software and Services Sector.

5.2.1 Association With Various Stages of Software Development

Table 7. Type of participation of respondents in various stages of software development

Frequency	Team leader	Team member	Programmer	Software engineer
Conceptualization	8	4	4	12
Requirement analysis	0	12	8	8
High level design	8	8	4	8
Low level design	4	12	4	8
Coding	4	4	12	8
Support	4	8	4	12
Other stage	4	4	4	8
Total	32	52	40	64

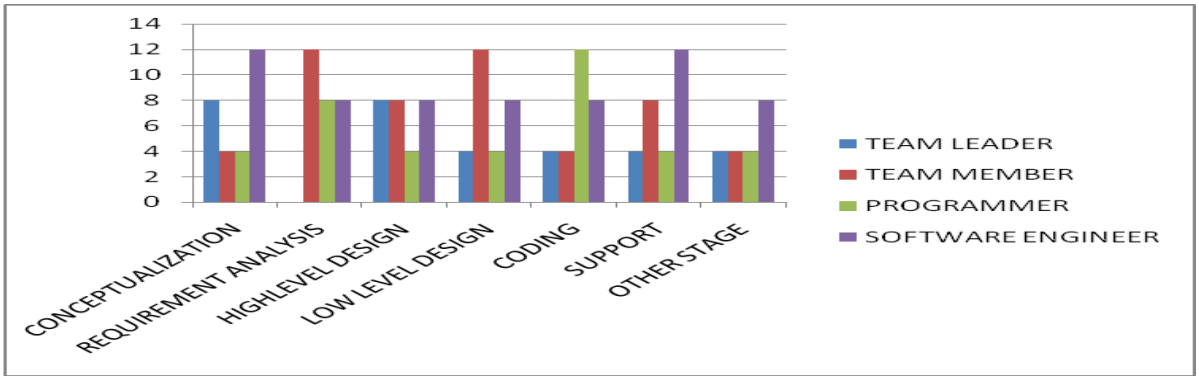

Figure 5. 1 Type of participation of respondents in various stages of software development

Result. Share of the respondents as Software Engineer is Highest (and equal) in Conceptualization and Support Stages; lesser (and equal) in all other stages Share of respondents as Programmer is highest in coding level, lesser in Requirement Analysis. In all other levels this share is equal. It is equal to one- third of coding level contribution. Share of Team members is highest and equal in Requirement Analysis and Low level Design; followed by a lesser contribution but equal in both high level design and support level; equal and yet half of this in other levels. Share of Team Leader is highest and equal in Conceptualization and High Level Design; half of it and equal in other levels.

5.2.2. Partnership with global IT leaders

Table 8. Partnership with global IT leaders

Column1	Frequency
YES	28
NO	4
TOTAL	32

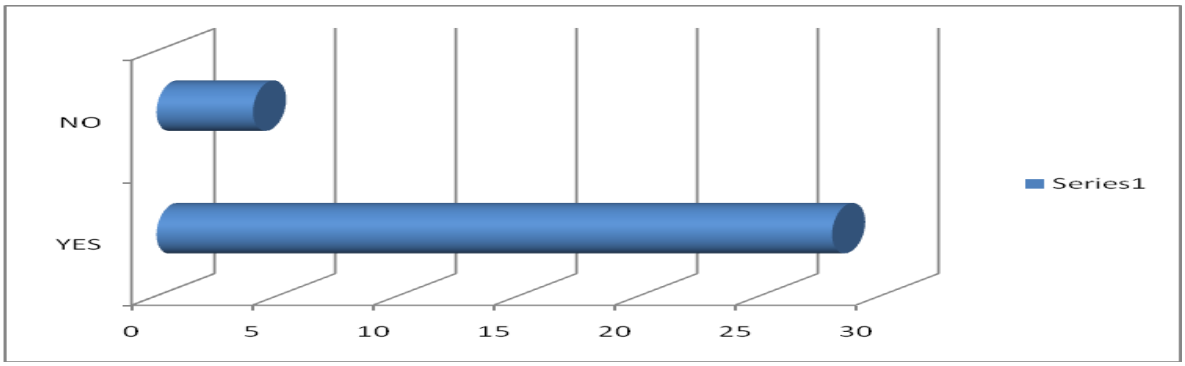

Figure 5. 2 Partnership with global IT leaders

Result. 87. 5% of the Indian IT Companies under this study report to have partnership with Global IT Leaders. This is an excellent indicator of the positive Impact of ICT on the Globalization with Indian IT Software Companies / Entrepreneurs.

5.2.2 Financial Resources

Table 9. Financial resources

Column1	FREQUENCY
Personal funds	8
Equity funds	16
Bank loan	16
Private loan	8
Total	48

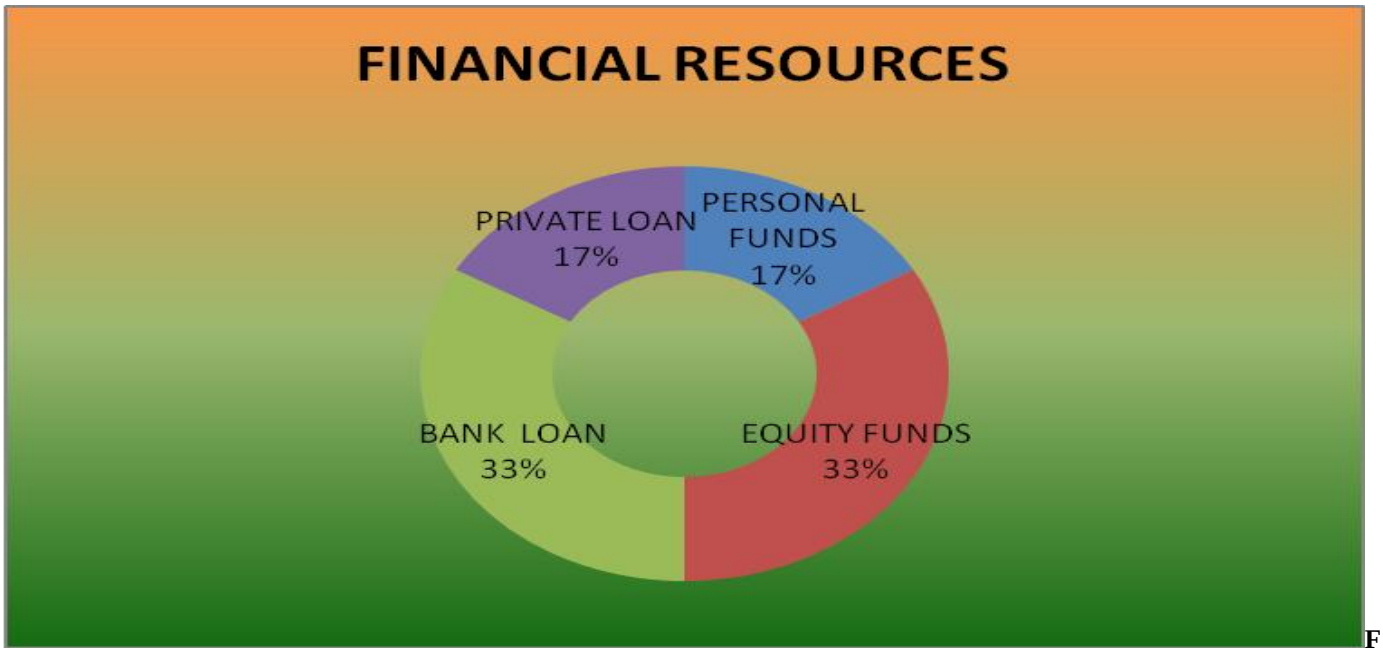

Figure 5.3 Financial resources

Result. Among the financial sources, both Equity Funds and Bank Loans contribute equal share of 33.3% **.**

6. Recommendations

Software reuse and related area is another related demanding research area, which can prove to be fruitful. Structural equation Model can also be used for statistical analysis purpose.

7. Bibliography

[1] http://asia.esevier.com
[2] http://www.indersciencecom
International Journal of Industrial and Systems Engineering 2010 – Vol. 6, No. 3 pp. 225-275, Padmanav Acharya, Biswajit Mahanty.
[3] International Journal of Industrial and Systems Engineering 2010 - Vol. 6, No.3 pp. 255 - 275
[4] Indian Dept. of Electronics annual reports, Dataquest
[5] Heeks, Richard (1996) India's Software Industry - State Policy, liberalisation and industrial development
[6] http://www.man.ac.uk/idpm/isiexpt.htm
[7] http://www.economictimes.com/today/03feat3.htm
[8] http://www.tagish.co.uk/ethos/news/lit1/e8ba.htm
[9] http://www.aiia.com.au
[10] International Journal of Computer Science & Communication Vol. 1, No. 1, January-June 2010, pp. 1-5
[11] Government Public Sector Of Software Development India Outsourcing software development.
[12] http://www.webdhoom.com
[13] Government Public Sector Of Software Development India Outsourcing software development .
[14] Journal of Theoretical and Applied Information Technology Performance, Challenges And Opportunities Of Indian Software Export by Asheref Illiyan
[15] India: E-Readiness Assessment Report 2005
[16] STPI , Government Departments and other Centres:

- Software Technology Parks of India (STPI), Hyderabad
- Department of Information Technology, Govt. of India
- Software Technology Parks of India, HQ, New Delhi
- National Taskforce on Information Technology & Software Development
- National Association of Software and Service Companies (NASSCOM)
- National Informatics Centre (NIC)
- National Centre for Software Technology (NCST)
- Centre for Development of Advanced Computing (CDAC)
- Centre for Materials for Electronics Technology (C-MET)
- Computer Maintenance Corporation Ltd. (CMC)
- ERNET India
- Standardisation, Testing & Quality Certification (STQC)
- MIT Accreditation of Computer Courses (DOEACC)
- IT & Communication Dept., Govt. of AP, AP Technology Services (APTS), Govt. of AP
- AP Online, Govt. of Andhra Pradesh Institute of Electronic Governance HITEC City, Hyderabad
- International Institute of Information Technology (IIIT), Hyderabad
- Hyderabad Software Exporters Association (HYSEA)

[17] http://www.economictimes.com/today/03feat3.htm
[18] http://www.nasscom.org

Synchronization, Anti-Synchronization and Hybrid-Synchronization Of A Double Pendulum Under The Effect Of External Forces

Ayub Khan[1], Priyamvada Tripathi,[2]

[1.] Department Of Mathematics, Zakir Husain Delhi College, University Of Delhi, Delhi–110002, India
[2.] Department Of Mathematics, University Of Delhi, Delhi–110007, India;

Abstract

In the present manuscript, an investigation on synchronization, anti-synchronization and hybrid-synchronization behavior of a double pendulum under the effect of external forces using active control technique based on the Lyapunov stability theory and the Routh-Hurwitz criteria, have been made. The designed controller with a new choice of co-efficient matrix of the error-dynamics are found to be effective in the stabilization of error states at the origin, thereby achieving synchronization between the states variables of two dynamical systems under consideration. Numerical simulations have been presented to illustrate the effectiveness of the proposed control techniques using mathematica.

Keywords: Double Pendulum under the effect of external forces, Lyapunov stability theory and Routh- Hurwitz Criteria, Synchronization, Anti-synchronization and Hybrid- synchronization.

1 Introduction

Classically, synchronization means adjustment of rhythm of self-sustained periodic oscillations due to their weak interaction and this adjustment can be described in terms of phase-locking and frequency entrainment. In the modern context we call such type of objects as rotators and chaotic systems. The history of synchronization actually goes back to the 17th century. In 1673, when the famous Dutch scientist Huygens [1] observed weak synchronization of two double pendulum clocks, which is about two model shape of vibration. He had invented shortly before: “It is quite worth noting that when we suspended two clocks so constructed from two hooks imbedded in the same wooden beam, the motion of each pendulum in opposite swings were so much in agreement and sound of each was always heard simultaneously”. Furthermore he described that if one of the pendulum was disturbed by interference, it would return back to its normal state. This was first discovery of synchronization. After careful observation, finally he found that the cause of this is due to motion of the beam, even though this is hardly perceptible [2].Synchronization of periodic self-sustained oscillators are based on the existence of a special variable, called phase. If the coupled two pendulums have small oscillations with the same initial conditions or the zero initial phase difference, the two pendulums will be synchronized. If the initial phase difference is 180◦, the anti-synchronization of two pendulums can be observed. For a general case, the motion of the two pendulums will be combined by the synchronization and anti-synchronization modes of vibration.The recent progress on the Huygens synchronization was presented in [3].

Chaotic synchronization did not attract much attention until Pecora and Carroll [4] introduced a method to synchronize two identical chaotic systems with different initial conditions in 1990. From then on, enormous studies have been done by researchers on the synchronization of dynamical systems. In 1994, Kapitaniak [5] used continuous control to achieve a synchronization of two chaotic systems. In 1996, Peng et al.[6] presented chaotic synchronization of n-dimensional system. In the past few decades, the concept of synchronization from the traditional point of view has also been extended. In 2002, Boccaletti et al. [7] gave a review on the synchronization of chaotic systems and clarified definitions and concepts of dynamical system synchronization. In 2004, Compos and Urias [8] mathematically described multimodel synchronization with chaos, and introduced a multi-valued synchronized function. In 2005, Chen [9] investigated the synchronization of two different chaotic systems. Such synchronization is based on the error dynamics of the slave and master systems. The active control functions were used to remove non-linear terms, and the Lyapunov function was used to determine the stability of the synchronization. Lu and Cao [10] used the similar technique of Chen [9] to discuss the adaptive complete synchronization of two identical or different chaotic systems with unknown parameters. Thus in the continuation, a wide variety of methods have successfully been applied to achieve synchronization of chaotic systems. These methods including adaptive control [11, 12], backstepping design [13, 14, 15], active control [16, 17, 18] nonlinear control [19, 20, 21, 22] and observer based control method [23, 24]. Using these methods, numerous synchronization problem of well-known chaotic systems such as Lorenz, Chen, L¨u and R¨ossler system have been worked on by many researchers. Recently, Ge et al. [25, 26, 27, 28, 29, 30] also studied

chaotic synchronization of many practical physical systems and obtained interesting results. Among these methods, chaos synchronization using active control has recently been widely accepted because it can be used to synchronize identical as well as non-identical systems. In order to achieve stable synchronization this method has been applied to many practical systems such as the electronic circuits, in which model there is third order "Jerk" equation [31], Lorenz, Chen and Lu system [32], geophysical systems [33], nonlinear equations waves (Lorenz Stenflo system)[34], Van-der Pol-duffing oscillator [35], forced damped pendulum [36], RCL-shunted Josephson function [37], modified projective synchronization [38]. In this paper, we have applied the active control techniques based on Lyapunov stability theory and Routh-Hurwitz criteria to study the synchronization, anti-synchronization and hybrid synchronization behavior of a double pendulum under the effect of external forces. It is well known that double pendulum is a chaotic system, its long term behavior can not be predicted. Slight changes in the initial conditions can result in drastic long term differences. If one starts the system at slightly different angles, perhaps by fraction of a degree, the resulting motion will not look same in the long run. In synchronization, two systems (master and slave) are synchronized and start with different initial conditions. The problem may be treated as the design of control laws for full chaotic slave system using known information of the master system so as to ensure that the controlled receiver synchronizes with the master system. Hence, the slave chaotic system completely traces the dynamics of the master system in the course of time. The aim of this study is to investigate the synchronization, anti-synchronization and hybrid synchronization of a double pendulum under the effect of external forces.

2 Equations of Motion Of Double Pendulum Under The Effect Of External Forces

In the figure given below, a double pendulum consists of two point masses $m1$ and $m2$ connected by massless rods to the pivot point. Let $\ell 1$ and $\ell 2$ are the lengths of rods respectively and $\theta 1$ and $\theta 2$ be the angles that two rods make with the vertical. Let F be the external force exerted on the pivot point by pendulum and ϕ be the angle that F makes with rod $\ell 1$.

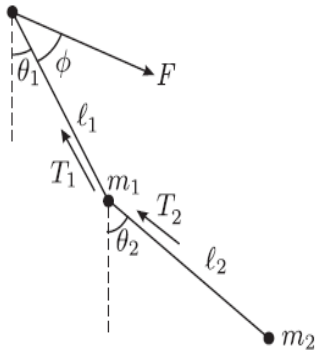

Fig. 1

The equations of motion are [39]:

$$\ddot{\theta}_1 = -\frac{T_1 \sin(\theta_1 - \theta_2) + g m_1 \sin\theta_2 - \ell_1 m_1 \sin(\theta_1 - \theta_2) \cdot \theta_1^2}{\cos(\theta_1 - \theta_2)\ell_1 m_1} \tag{1}$$

$$\ddot{\theta}_2 = -\frac{g m_2 - T_2 \cos\theta_2 + \ell_1 m_2 \cos\theta_1 \cdot \dot{\theta}_1^2 + \ell_1 m_2 \sin\theta_1 \cdot \ddot{\theta}_1 + \ell_2 m_2 \cos\theta_2 \cdot \dot{\theta}_2^2}{\sin\theta_2 \cdot \ell_2 m_2}, \tag{2}$$

where g is the acceleration due to gravity, T_1 and T_2 be the tensions on each rod and are respectively given by

$$T_1 = F\cos(\phi - \theta) - \frac{(m_1\ddot{x}_1 + m_2\ddot{x}_2)}{\sin\theta_1}$$

and

$$T_2 = -\frac{m_2\ddot{x}_2}{\sin\theta_2} + F\cos(\phi - \theta_1)\cos(\theta_1 + \theta_2).$$

3 Synchronization Via Active Control

The systems defined by (1) and (2) can be written as a system of four first order differential equations, the four variables are introduced as below:

$$\begin{cases} x_1 = \theta_1 \\ x_2 = \dot{\theta}_1 \\ x_3 = \theta_2 \\ x_4 = \dot{\theta}_2 \end{cases} \tag{3}$$

Then

$$\begin{aligned} \dot{x}_1 &= x_2, \\ \dot{x}_2 &= -\frac{T_1 \sin(x_1 - x_3) + gm_1 \sin x_3 - l_1 m_1 \sin(x_1 - x_3) \cdot x_2^2}{\cos(x_1 - x_3) l_1 m_1}, \\ \dot{x}_3 &= x_4, \\ \dot{x}_4 &= -\frac{gm_2 - T_2 \cos x_3 + l_1 m_2 \cos x_1 \cdot x_2^2 + l_1 m_2 \sin x_1 \cdot \dot{x}_2 + l_2 m_2 \cos x_3 \cdot x_4^2}{\sin x_3 \cdot m_2 l_2}. \end{aligned}$$

After expanding trigonometrical terms and neglecting higher order terms only (for reducing non-linearity) in the above equations, we get:

$$\begin{cases} \dot{x}_1 = x_2 \\ \dot{x}_2 = -\dfrac{T_1(x_1 - x_3) + gm_1 x_3 - \ell_1 m_1 x_1 x_2^2}{\ell_1 m_1 + \dfrac{(x_1 - x_3)^2}{2} \ell_1 m_1} \\ \dot{x}_3 = x_4 \\ \dot{x}_4 = -\dfrac{gm_2 - T_2\left(1 + \dfrac{x_3^2}{2}\right) + l_1 m_2 x_2^2 + l_1 m_2 x_1 \dot{x}_2 + l_2 m_2\left(x_4^2 + \dfrac{x_4^2 x_3^2}{2}\right)}{l_2 m_2 x_3} \end{cases} \tag{4}$$

Corresponding to the master system (4), the identical slave system is defined as:

$$\begin{cases} \dot{y}_1 = y_2 + u_1(t) \\ \dot{y}_2 = -\dfrac{T_1(y_1 - y_3) + gm_1 y_3 - \ell_1 m_1 y_1 y_2^2}{\ell_1 m_1 + \dfrac{(y_1 - y_3)^2}{2} \ell_1 m_1} + u_2(t) \\ \dot{y}_3 = y_4 + u_3(t) \\ \dot{y}_4 = -\dfrac{gm_2 - T_2\left(1 + \dfrac{y_3^2}{2}\right) + l_1 m_2 y_2^2 + l_1 m_2 y_1 \dot{y}_2 + l_2 m_2\left(y_4^2 + \dfrac{y_4^2 y_3^2}{2}\right)}{l_2 m_2 y_3} \\ \qquad + u_4(t) \end{cases} \tag{5}$$

where $ui(t)$, $i = 1, 2, 3, 4$ are control functions to be determined. Now defining error functions such that in synchronization state $\lim_{t \to \infty} ei(t) \to 0$, $i = 1, 2, 3, 4$.

$$\begin{aligned} e1 &= y1 - x1 \\ e2 &= y2 - x2 \\ e3 &= y3 - x3 \\ e4 &= y4 - x4 \end{aligned}$$

and the error dynamics are expressed as:

$$\begin{cases} \dot{e}_1 = \dot{y}_1 - \dot{x}_1 \\ \dot{e}_2 = \dot{y}_2 - \dot{x}_2 \\ \dot{e}_3 = \dot{y}_3 - \dot{x}_3 \\ \dot{e}_4 = \dot{y}_4 - \dot{x}_4 \end{cases} \tag{6}$$

from equations (4), (5) and (6), we get:

$$\begin{cases} \dot{e}_1(t) = e_2(t) + u_1(t) \\ \dot{e}_2(t) = -\dfrac{T_1(y_1 - y_3) + gm_1y_3 - \ell_1 m_1 y_1 y_2^2}{\ell_1 m_1 + \dfrac{(y_1 - y_3)^2}{2}\ell_1 m_1} \\ \qquad + \dfrac{T_1(x_1 - x_3) + gm_1x_3 - \ell_1 m_1 x_1 x_2^2}{\ell_1 m_1 + \dfrac{(x_1 - x_3)^2}{2}\ell_1 m_1} + u_2(t) \\ \dot{e}_3(t) = e_4(t) + u_3(t) \\ \dot{e}_4(t) = -\dfrac{gm_2 - T_2\left(1 + \dfrac{y_3^2}{2}\right) + \ell_1 m_2 y_2^2 + \ell_1 m_2 y_1 \dot{y}_2 + \ell_2 m_2\left(y_4^2 + \dfrac{y_4^2 y_3^2}{2}\right)}{\ell_2 m_2 y_3} \\ \qquad + \dfrac{gm_2 - T_2(1 + \frac{x_3^2}{2}) + \ell_1 m_2 x_2^2 + \ell_1 m_2 x_1 \dot{x}_2 + \ell_2 m_2\left(x_4^2 + \dfrac{x_4^2 x_3^2}{2}\right)}{\ell_2 m_2 x_3} \\ \qquad + u_4(t). \end{cases} \tag{7}$$

The error dynamical system (7) to be controlled must be a linear system with control inputs. Therefore we redefine the control functions such as to eliminate non-linear terms in $e1(t)$, $e2(t)$, $e3(t)$ and $e4(t)$ of equation (7) as follows:

$$\begin{cases} u_1(t) = v_1(t) \\ u_2(t) = \dfrac{T_1(y_1 - y_3) + gm_1y_3 - \ell_1 m_1 y_1 y_2^2}{\ell_1 m_1 + \dfrac{(y_1 - y_3)^2}{2}\ell_1 m_1} \\ \quad - \dfrac{T_1(x_1 - x_3) + gm_1x_3 - \ell_1 m_1 x_1 x_2^2}{\ell_1 m_1 + \frac{(x_1 - x_3)^2}{2}\ell_1 m_1} + v_2(t) \\ u_3(t) = v_3(t) \\ u_4(t) = \dfrac{gm_2 - T_2\left(1 + \dfrac{y_3^2}{2}\right) + \ell_1 m_2 y_2^2 + \ell_1 m_2 y_1 \dot{y}_2 + \ell_2 m_2\left(y_4^2 + \dfrac{y_4^2 y_3^2}{2}\right)}{\ell_2 m_2 y_3} \\ \quad - \dfrac{gm_2 - T_2\left(1 + \dfrac{x_3^2}{2}\right) + \ell_1 m_2 x_2^2 + \ell_1 m_2 x_1 \dot{x}_2 + \ell_2 m_2\left(x_4^2 + \dfrac{x_4^2 x_3^2}{2}\right)}{\ell_2 m_2 x_3} \\ \quad + v_4(t) \end{cases} \tag{8}$$

using (7) and (8), we have

$$\begin{cases} \dot{e}_1(t) = e_2(t) + v_1(t) \\ \dot{e}_2(t) = v_2(t) \\ \dot{e}_3(t) = e_4(t) + v_3(t) \\ \dot{e}_4(t) = v_4(t) \end{cases} \tag{9}$$

Equation (9) is the error dynamics, which can be interpreted as a control problem where the system to be controlled is a linear system with control inputs $v_1(t)$, $v_2(t)$, $v_3(t)$ and $v_4(t)$. We choose $v_1(t)$, $v_2(t)$, $v_3(t)$, $v_4(t)$ as follows:

$$\begin{pmatrix} v_1(t) \\ v_2(t) \\ v_3(t) \\ v_4(t) \end{pmatrix} = A \begin{pmatrix} e_1(t) \\ e_2(t) \\ e_3(t) \\ e_4(t) \end{pmatrix},$$

where A is a 4×4 constant feedback matrix to be determined. The error dynamical system (9) can be written as:

$$\begin{pmatrix} \dot{e}_1(t) \\ \dot{e}_2(t) \\ \dot{e}_3(t) \\ \dot{e}_4(t) \end{pmatrix} = B \begin{pmatrix} e_1(t) \\ e_2(t) \\ e_3(t) \\ e_4(t) \end{pmatrix}, \tag{10}$$

where B is 4×4 co-efficient matrix. According to the Lyapunov stability theory and Routh-Hurwitz criteria, eigen-values of the co-efficient matrix of error system must be real or complex with negative real parts. We can choose elements of matrix arbitrarily; there are several ways to choose in order to satisfy Lyapunov and Routh-Herwitz criteria. Consequently, for

$$A = \begin{pmatrix} -1 & -1 & 0 & 0 \\ 0 & -2 & 0 & 0 \\ 0 & 0 & -3 & -1 \\ 0 & 0 & 0 & -4 \end{pmatrix}$$

$$B = \begin{pmatrix} -1 & 0 & 0 & 0 \\ 0 & -2 & 0 & 0 \\ 0 & 0 & -3 & 0 \\ 0 & 0 & 0 & -4 \end{pmatrix} \qquad (11)$$

becomes a matrix with eigen values having negative real parts and equation (10) reduces to

$$\left.\begin{aligned} \dot{e}_1(t) &= -e_1(t) \\ \dot{e}_2(t) &= -2e_2(t) \\ \dot{e}_3(t) &= -3e_3(t) \\ \dot{e}_4(t) &= -4e_4(t) \end{aligned}\right\} \qquad (12)$$

Thus, by Lyapunov stability theory, the error dynamical system (12) is stable.

4 . Numerical Simulation For Synchronization

For the parameters involved in system under investigation, $T1 = 1$, $T2 = 2$, $\ell 1 = 1$, $\ell 2 = 2$, $m1 = 1$, $m2 = 1$ and $g = 9.8$m/s2 with the initial conditions for master system and slave system

$[x1(0), x2(0), x3(0), x4(0)] = [3.5, 0.4, -3.5, 0.4]$

And

$[y1(0), y2(0), y3(0), y4(0)] = [1.5, 0.2, -0.5, 0.8]$

respectively. We have simulated the system under consideration using mathematica. Phase portraits and time series analysis of master and slave system are the witness of irregular behavior of system (see figures 2, 3, 4 and 5). For

$[e1(0), e2(0), e3(0), e4(0)] = [-2, 0.2, 3, 0.4]$

convergence diagrams of errors are the witness of achieving synchronization between master and slave systems (see figure 6).

5 Anti-Synchronization Via Active Control

In order to formulate the active controllers for anti-synchronization we need to redefine the error functions as, $e_1(t) = y1 + x1$, $e_2(t) = y2 + x2$, $e_3(t) = y3 + x3$, $e_4(t) = y4 + x4$.

Accordingly, error dynamics are:

$$\dot{e}_1(t) = \dot{y}_1 + \dot{x}_1 \quad \dot{e}_3(t) = \dot{y}_3 + \dot{x}_3$$
$$\dot{e}_2(t) = \dot{y}_2 + \dot{x}_2, \quad \dot{e}_4(t) = \dot{y}_4 + \dot{x}_4$$

from (4) and (5), error dynamics can be written as:

$$\begin{cases} \dot{e}_1(t) = e_2(t) + u_1(t) \\ \dot{e}_2(t) = -\dfrac{T_1(y_1 - y_3) + gm_1y_3 - \ell_1 m_1 y_1 y_2^2}{\ell_1 m_1 + \dfrac{(y_1 - y_3)^2}{2}\ell_1 m_1} \\ \quad -\dfrac{T_1(x_1 - x_3) + gm_1x_3 - \ell_1 m_1 x_1 x_2^2}{\ell_1 m_1 + \dfrac{(x_1 - x_3)^2}{2}\ell_1 m_1} + u_2(t) \\ \dot{e}_3(t) = e_4(t) + u_3(t) \\ \dot{e}_4(t) = -\dfrac{\left[gm_2 - T_2\left(1 + \dfrac{y_3^2}{2}\right) + \ell_1 m_2 y_2^2 + \ell_1 m_2 y_1 \dot{y}_2 + \ell_2 m_2\left(y_4^2 + \dfrac{y_4^2 y_3^2}{2}\right)\right]}{\ell_2 m_2 y_3} \\ \quad -\dfrac{\left[gm_2 - T_2\left(1 + \dfrac{x_3^2}{2}\right) + \ell_1 m_2 x_2^2 + \ell_1 m_2 x_1 \dot{x}_2 + \ell_2 m_2\left(x_4^2 + \dfrac{x_4^2 x_3^2}{2}\right)\right]}{\ell_2 m_2 x_3} \\ \quad + u_4(t). \end{cases} \tag{13}$$

In order to express (13) as only linear terms in $e1(t)$, $e2(t)$, $e2(t)$ and $e4(t)$, we redefine the control functions as follows:

$$\begin{cases} u_1(t) = v_1(t) \\ u_2(t) = \dfrac{T_1(y_1 - y_3) + gm_1y_3 - \ell_1 m_1 y_1 y_2^2}{\ell_1 m_1 + \dfrac{(y_1 - y_3)^2}{2}\ell_1 m_1} \\ \quad + \dfrac{T_1(x_1 - x_3) + gm_1x_3 - \ell_1 m_1 x_1 x_2^2}{\ell_1 m_1 + \dfrac{(x_1 - x_3)^2}{2}\ell_1 m_1} + v_2(t) \\ u_3(t) = v_3(t) \\ u_4(t) = \dfrac{gm_2 - T_2\left(1 + \dfrac{y_3^2}{2}\right) + \ell_1 m_2 y_2^2 + \ell_1 m_2 y_1 \dot{y}_2 + \ell_2 m_2\left(y_4^2 + \dfrac{y_4^2 y_3^2}{2}\right)}{\ell_2 m_2 y_3} \\ \quad + \dfrac{gm_2 - T_2\left(1 + \dfrac{x_3^2}{2}\right) + \ell_1 m_2 x_2^2 + \ell_1 m_2 x_1 \dot{x}_2 + \ell_2 m_2\left(x_4^2 + \dfrac{x_4^2 x_3^2}{2}\right)}{\ell_2 m_2 x_3} \\ \quad + v_4(t). \end{cases} \tag{14}$$

Using (13) and (14), we have

$$\begin{cases} \dot{e}_1(t) = e_2(t) + v_1(t) \\ \dot{e}_2(t) = v_2(t) \\ \dot{e}_3(t) = e_4(t) + v_3(t) \\ \dot{e}_4(t) = v_4(t) \end{cases} \tag{15}$$

Furthermore, as in the previous case we choose $v1(t)$, $v2(t)$, $v3(t)$ and $v4(t)$ as follows:

$$\begin{pmatrix} v_1(t) \\ v_2(t) \\ v_3(t) \\ v_4(t) \end{pmatrix} = A \begin{pmatrix} e_1(t) \\ e_2(t) \\ e_3(t) \\ e_4(t) \end{pmatrix},$$

where A is 4×4 constant matrix to be determined. Equation (15) reduces to

$$\begin{pmatrix} \dot{e}_1(t) \\ \dot{e}_2(t) \\ \dot{e}_3(t) \\ \dot{e}_4(t) \end{pmatrix} = B \begin{pmatrix} e_1(t) \\ e_2(t) \\ e_3(t) \\ e_4(t) \end{pmatrix},$$

where B is given by (11) whose eigen values have negative real parts. Thus by Lyapunov stability theory, the error dynamical system (15) is stable.

6 Numerical Simulation For Anti-Synchronization

For the parameters involved in system under investigation, $T1 = 1$, $T2 = 2$, $\ell 1 = 1$, $\ell 2 = 2$, $m1 = 1$, $m2 = 1$ and $g = 9.8$m/s2 with the initial conditions for master and slave systems

$[x1(0), x2(0), x3(0), x4(0)] = [3.5, 0.4, -3.5, 0.4]$
and

$[y1(0), y2(t), y3(0), y4(0)] = [1.5, 0.2, -0.5, 0.8]$
respectively. We have simulated the system under consideration using mathematica. Phase portraits and time series analysis of master system and slave system are the witness of irregular behavior of system (see figures 2, 3, 4 and 5). For

$[e1(0), e2(0), e3(0), e4(0)] = [5, 0.6, 4.0, 1.2]$

convergence diagram of errors are the witness of achieving anti-synchronization between master and slave system (see figure 7).

7 Hybrid Synchronization Via Active Control

The idea of the hybrid synchronization is to use the output of the master system to control the slave system so that the odd outputs of the two systems are completely synchronized, while the even outputs of the two systems are anti-synchronized so that both complete synchronization and anti-synchronization persist in the synchronization of master and slave systems. In order to formulate the active controllers for "hybrid synchronization" we are redefining the error functions in the following three ways:

$$\begin{array}{lll} e_1 = y_1 - x_1 & e_1 = y_1 - x_1 & e_1 = y_1 - x_1 \\ e_2 = y_2 + x_2 & e_2 = y_2 + x_2 & e_2 = y_2 - x_2 \\ e_3 = y_3 + x_3 & e_3 = y_3 - x_3 & e_3 = y_3 - x_3 \\ e_4 = y_3 + x_4 & e_4 = y_4 + x_4 & e_4 = y_4 + x_4 \\ \text{(I)} & \text{(II)} & \text{(III)} \end{array}$$

Accordingly, the error dynamics are:

$$\begin{array}{lll} \dot{e}_1 = \dot{y}_1 - \dot{x}_1 & \dot{e}_1 = \dot{y}_1 - \dot{x}_1 & \dot{e}_1 = \dot{y}_1 - \dot{x}_1 \\ \dot{e}_2 = \dot{y}_2 + \dot{x}_2 & \dot{e}_2 = \dot{y}_2 + \dot{x}_2 & \dot{e}_2 = \dot{y}_2 - \dot{x}_2 \\ \dot{e}_3 = \dot{y}_3 + \dot{x}_3 & \dot{e}_3 = \dot{y}_3 - \dot{x}_3 & \dot{e}_3 = \dot{y}_3 - \dot{x}_3 \\ \dot{e}_4 = \dot{y}_4 + \dot{x}_4 & \dot{e}_4 = \dot{y}_4 + \dot{x}_4 & \dot{e}_4 = \dot{y}_4 + \dot{x}_4 \\ \text{(I)} & \text{(II)} & \text{(III)} \end{array}$$

Now first we take any one of above equation, let us take (II),

$$\begin{aligned} \dot{e}_1 &= \dot{y}_1 - \dot{x}_1 \\ \dot{e}_2 &= \dot{y}_2 + \dot{x}_2 \\ \dot{e}_3 &= \dot{y}_3 - \dot{x}_3 \\ \dot{e}_4 &= \dot{y}_4 + \dot{x}_4 \end{aligned}$$

from (II), (4) and (5) we have,

$$\begin{cases} \dot{e}_1(t) = e_2(t) + u_1(t) \\ \dot{e}_2(t) = -\dfrac{T_1(y_1 - y_3) + gm_1y_3 - \ell_1 m_1 y_1 y_2^2}{\ell_1 m_1 + \dfrac{(y_1 - y_3)^2}{2}\ell_1 m_1} \\ \qquad -\dfrac{T_1(x_1 - x_3) + gm_1x_3 - \ell_1 m_1 x_1 x_2^2}{\ell_1 m_1 + \dfrac{(x_1 - x_3)^2}{2}\ell_1 m_1} + u_2(t) \\ \dot{e}_3(t) = e_4(t) + u_3(t) \\ \dot{e}_4(t) = \dfrac{-\left[gm_2 - T_2\left(1 + \dfrac{y_3^2}{2}\right) + \ell_1 m_2 y_2^2 + \ell_1 m_2 y_1 \dot{y}_2 + \ell_2 m_2\left(y_4^2 + \dfrac{y_4^2 y_3^2}{2}\right)\right]}{\ell_2 m_2 y_3} \\ \qquad \dfrac{-\left[gm_2 - T_2\left(1 + \dfrac{x_3^2}{2}\right) + \ell_1 m_2 x_2^2 + \ell_1 m_2 x_1 \dot{x}_2 + \ell_2 m_2\left(x_4^2 + \dfrac{x_4^2 x_3^2}{2}\right)\right]}{\ell_2 m_2 x_3} \\ \qquad + u_4(t). \end{cases} \tag{16}$$

The error dynamical system (16) to be controlled must be a linear system with control inputs. Therefore we redefine the control functions such as to eliminate non-linear terms in $e1(t)$, $e2(t)$, $e3(t)$ and $e4(t)$ of (16) as follows:

$$\begin{cases} u_1(t) = v_1(t) \\ u_2(t) = \dfrac{T_1(y_1 - y_3) + gm_1y_3 - \ell_1m_1y_1y_2^2}{\ell_1m_1 + \dfrac{(y_1 - y_3)^2}{2}\ell_1m_1} \\ \quad + \dfrac{T_1(x_1 - x_3) + gm_1x_3 - \ell_1m_1x_1x_2^2}{\ell_1m_1 + \dfrac{(x_1 - x_3)^2}{2}\ell_1m_1} + v_2(t) \\ u_3(t) = v_3(t) \\ u_4(t) = \dfrac{\left[gm_2 - T_2\left(1+\dfrac{y_3^2}{2}\right) + \ell_1m_2y_2^2 + \ell_1m_2y_1\dot{y}_2 + \ell_2m_2\left(y_4^2 + \dfrac{y_4^2y_3^2}{2}\right)\right]}{\ell_2m_2y_3} \\ \quad + \dfrac{\left[gm_2 - T_2\left(1+\dfrac{x_3^2}{2}\right) + \ell_1m_2x_2^2 + \ell_1m_2x_1\dot{x}_2 + \ell_2m_2\left(x_4^2 + \dfrac{x_4^2x_3^2}{2}\right)\right]}{\ell_2m_2x_3} \\ \quad + v_4(t). \end{cases} \tag{17}$$

From (16) and (17), error dynamics are:

$$\begin{cases} \dot{e}_1(t) = e_2(t) + v_1(t) \\ \dot{e}_2(t) = v_2(t) \\ \dot{e}_3(t) = e_4(t) + v_3(t) \\ \dot{e}_4(t) = v_4(t). \end{cases} \tag{18}$$

Similarly, we get same error-dynamical systems in all three cases. Furthermore, as in the above cases we choose $v_1(t)$, $v_2(t)$, $v_3(t)$ and $v_4(t)$ as follows:

$$\begin{pmatrix} v_1(t) \\ v_2(t) \\ v_3(t) \\ v_4(t) \end{pmatrix} = A \begin{pmatrix} e_1(t) \\ e_2(t) \\ e_3(t) \\ e_4(t) \end{pmatrix}$$

and (18) reduces to

$$\begin{pmatrix} \dot{e}_1(t) \\ \dot{e}_2(t) \\ \dot{e}_3(t) \\ \dot{e}_4(t) \end{pmatrix} = B \begin{pmatrix} e_1(t) \\ e_2(t) \\ e_3(t) \\ e_4(t) \end{pmatrix},$$

where B is given by (11), whose eigen-values have negative real parts. Thus, by Lyapunov stability theory, the error dynamical system (18) is stable.

8 Numerical Simulation For Hybrid Synchronization

For the parameters involved in system under investigation, $T1 = 1$, $T2 = 2$, $\ell 1 = 1$, $\ell 2 = 2$, $m1 = 1$, $m2 = 1$ and $g = 9.8 m/s2$ with the initial conditions of master and slave systems

$[x1(0), x2(0), x3(0), x4(0)] = [3.5, 0.4, -3.5, 0.4]$,

and

$[y1(0), y2(0), y3(0), y4(0)] = [1.5, 0.2, -0.5, 0.8]$

respectively.

We have simulated the system under consideration by using mathematica. Phase portraits and time series analysis of master and slave system are the witness of irregulars behavior of the system (see figures 2, 3, 4 and 5) and for

$[e1(0), e2(0), e3(0), e4(0)] = [-2, 0.6, 3, 1.2]$

convergence diagram of errors are the witness of achieving hybrid synchronization between master and slave system (see figure 8). Figures are given below:

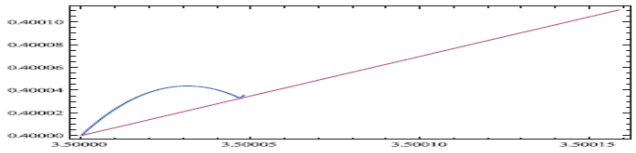

Fig. 2 Phase portrait of master system.

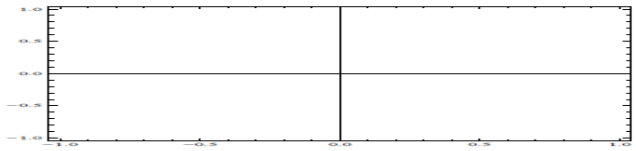

Fig. 3 Phase portrait of slave system.

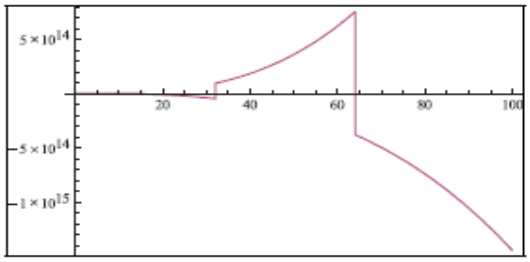

Fig. 4 Time series analysis of $x(t)$

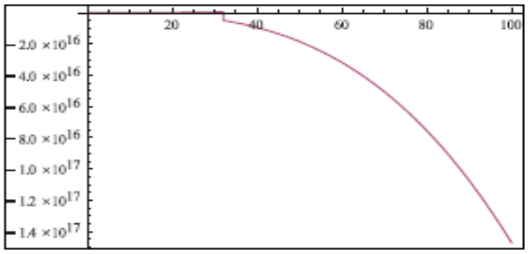

Fig. 5 Time series analysis of $y(t)$

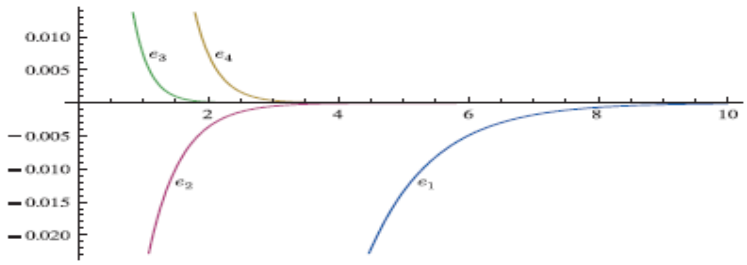

Fig. 6 Convergence of errors e_1, e_2, e_3 and e_4 for synchronization and $t = [0, 10]$

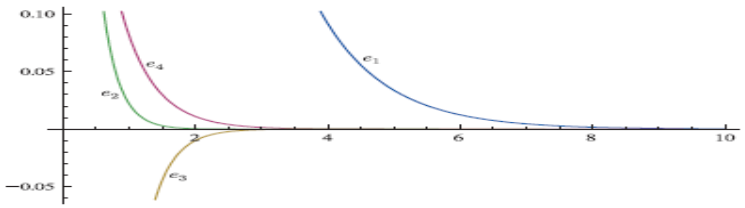

Fig. 7 Convergence of errors e_1, e_2, e_3 and e_4 for anti-synchronization and $t = [0, 10]$

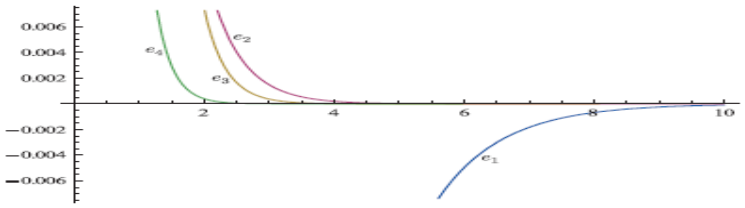

Fig. 8 Convergence of errors e_1, e_2, e_3 and e_4 for hybrid synchronization and $t = [0, 10]$

9 Conclusion

An investigation on synchronization, anti-synchronization and hybrid synchronization of the double pendulum under the effect of external forces via active control technique based on Lyapunov stability theory and Routh-Hurwitz criteria have been made. The results are validated by numerical simulations using mathematica.

References

[1] Huygens (Hugenii) (1986), Horologium Oscillatorium, Apud F. Muguet, Parisiis, France, 1973 (English translation: The pendulum clock, Lowa State University, Ames, 1986).

[2] A. Pikovsky, M. Rosenblum and J. Kurths. Synchronization, Cambridge Nonlinear Science Series, 12, Cambridge Univ. Press, Cambridge, 2001.

[3] G. Leonov, H. Nijmeijer, A. Pogromsky and A. Fradkov, Dynamics and Control of Hybrid Mechanical Systems, World Scientific, Singapore, 2010.

[4] L. M. Pecora and T. L. Carroll. Synchronization in Chaotic Systems. Phys. Rev. Lett. **64** (1990), no. 8, 821–824.

[5] T. Kapitaniak. Synchronization of Chaos Using Continuous Control, Physical Review E **50** (1994), Issue 2, 1642-1644.

[6] J. H. Peng, E. J. Ding, M. Ding and W. Yang. Synchronizing Hyperchaos with a Scalar Transmitted Signal, Physical Review Letters **76** (1996) 904-907.

[7] S. Boccaletti, J. Kurths, G. Osipov, D. L. Valladares and C. S. Zhou. The Synchronization of Chaotic Systems. Phys. Rep. **366** (2002), no. 1-2, 1–101.

[8] E. Campos, J. Ur´ıas and N. F. Rulkov. Multimodal Synchronization of Chaos, Chaos **14** (2004), no. 1, 48–54.

[9] H. K. Chen. Synchronization of Two Different Chaotic Systems: A New System and Each of the Dynamical Systems Lorenz, Chen and L¨u, Chaos Solitons Fractals **25** (2005), no. 5, 1049–1056.

[10] J. Lu and J. Cao. Adaptive Complete Synchronization of Two Identical or Different Chaotic (Hyperchaotic) Systems with Fully Unknown Parameters, Chaos **15** (2005), no. 4, 043901, 10 pp.

[11] S. H. Chen and J. Lu. Synchronization of an Uncertain Unified System via Adaptive Control, Chaos Solitons & Fractals 14(2002), 643–647.

[12] Z. M. Ge and Y. S. Chen. Adaptive Synchronization of Unidirectional and Mutual Coupled Chaotic Systems, Chaos Solitons & Fractals 26(2005), 881–888.

[13] C. Wang and S.S. Ge. Synchronization of Two Uncertain Chaotic Systems via Adaptive Backstepping, Int. J. Bifurcat. Chaos 11(2001), 1743- 1751.

[14] C. Wang and S. S. Ge. Adaptive Synchronization of Uncertain Chaotic Systems via Adaptive Backstepping Design, Chaos Solitons & Fractals 12(2001), 1199–1206.

[15] X. Tan, J. Zhang and Y. Yang. Synchronizing Chaotic Systems Using Backstepping Design, Chaos Solitons & Fractals 16(2003): 37–45.

[16] H. K. Chen. Synchronization of Two Different Chaotic System: A New System and Each of the Dynamical Systems Lorenz, Chen and Lu, Chaos Solitons & Fractals 25(2005), 1049–1056.
[17] M. C. Ho and Y.C. Hung. Synchronization two Different Systems by using Generalized Active Control, Phys. Lett. A 301(2002), 424–428.
[18] M. T. Yassen. Chaos Synchronization Between Two Different Chaotic Systems using Active Control, Chaos Solitons & Fractals 23(2005), 131–140.
[19] J. H. Park. Chaos Synchronization Between Two Different Chaotic Dynamical Systems, Chaos Solitons & Fractals 27(2006), 549–554.
[20] L. Huang, R. Feng and M. Wang. Synchronization of Chaotic Dynamical Systems via Nonlinear Control, Phys. Lett. A 320(2004), 271–275.
[21] H. K. Chen. Global Chaos Synchronization of New Chaotic Systems via Nonlinear Control, Chaos Solitons & Fractals 23(2005), 1245–1251.
[22] J. H. Park. Chaos Synchronization of a Chaotic System via Nonlinear Control, Chaos Solitons & Fractals 25(2005), 549–584.
[23] Z. M. Ge, T.C. Yu and Y.S. Chen. Chaos Synchronization of a Horizontal Platform System, J. Sound Vibrat 268(2003), 731–749.
[24] Gl. Wen and D. Xu. Observer-based Control for Full-state Projective Synchronization of a General Class of Chaotic Maps in Any Dimension, Phys. Lett. A 330(2004), 420–425.
[25] Gl. Wen and D. Xu, Nonlinear Observer Control for Full-state Projective Synchronization in Chaotic Continuous-time Systems, Chaos Solitons & Fractals 26(2005), 71–77.
[26] Z. M. Ge, J.W. Cheng and Y.S. Chen. Chaos Anti-control and Synchronization of Three Time Scales Brushless DC Motor System, Chaos Solitons & Fractals 22(2004), 1165–1182.
[27] Z. M. Ge and H.W. Wu. Chaos Synchronization and Chaos Anti-control of a Suspended Track with Moving Load, J. Sound Vibrat 270(2004), 685–712.
[28] Z. M. Ge and C. C. Chen. Phase Synchronization of Coupled Chaotic Multiple Time Scale Systems, Chaos Solitons & Fractals 20(2004), 639–647.
[29] Z. M. Ge and C.I. Control, Anti-control and Synchronization of Chaos for an Autonomous Rotational -machine System with Time-delay, Chaos Solitons & Fractals 23(2005), 1855–1864.
[30] Z. M. Ge, C.M. Chang and Y.S. Chen. Anti-control of Chaos of Single Time Scale Brushless DC Motors and Chaos Synchronization of Different Order Systems, Chaos Solitons & Fractals 27(2006), 1298-1315.
[31] E. W. Bai and K. E. Lonngren. Synchronization of Two Lorenz Systems Using Active Control, Chaos, Soliton & Fractials **9** (1998), 1555-1561.
[32] H. K. Chen. Synchronization of Two Different Chaotic Systems: A New System and Each of the Dynamical Systems Lorenz, Chen and L¨u, Chaos Solitons Fractals **25** (2005), no. 5, 1049–1056.
[33] U. E. Vincent. Synchronization of Rikitake Chaotic Attractor using Active Control, Physics Letter, Section A, **343** (1-3) (2005), 133–138.
[34] U. E. Vincent. Synchronization of Identical and Non-identical 4-D Chaotic Systems Using Active Control, Chaos Solitons Fractals **37** (2008), no. 4, 1065–1075.
[35] A. N. Njah and U. E. Vincent. Synchronization and Anti-synchronization of Chaos in an Extended Bonhoffer-Van Der Pol Oscillator Using Active Control, Journal of Sound and Vibration **319**(1-2) (2009), 41–49.
[36] A. Ucar, K. E. Lonngren, and E. W. Bai. Synchronization of Chaotic Behavior in Nonlinear Bloch Equations, Phys. Lett. A **314** (2003), no. 1-2, 96–101.
[37] A. Ucar, K. E. Lonngren and E.W. Bai. Chaos Synchronization in RCL-Shunted Josephson Junction via Active Control, Chaos, Solitons & Fractals **31** (1) (2007), 105–111.
[38] H. Zhu and X. Zhang. Modified Projective Synchronization of Different Hyprchaotic Systems, Journal of Information and Computing Science **4** (2009), 33–40.
[39] Chris LeBailly. Synchronization of Chaotic Oscillators, Evanston Township High-School, November 19, 2003.

Dynamic Voltage Restorer (DVR) System for Compensation of Voltage Sags, State-of-the-Art Review

Shazly A. Mohammed[1], Aurelio G. Cerrada[2], Abdel-Moamen M. A[1], and B. Hasanin[3]

1Faculty of Engineering, South Valley University, Electrical Engineering Dep., Qena - Egypt

2Faculty of Electrical and Electronic Engineering, IIT - Comillas Pontifical University, Madrid - Spain

3Dean of Faculty of Engineering, Al-Azhar University, Electrical Engineering Dep., Qena – Egypt

Abstract:

The problem of voltage sags and its severe impact on sensitive loads is well known. To solve this problem, The DVR is a modern and important custom power device for compensation voltage sags in power distribution systems. The Dynamic Voltage Restorer (DVR) is fast, flexible and efficient solution to voltage sag problem. The DVR is a series compensator used to mitigate voltage sags and to restore load voltage to its rated value. In this paper, an overview of the DVR, its functions, configurations, components, operating modes, voltage injection methods and closed-loop control of the DVR output voltage are reviewed along with the device capabilities and limitations.

Keywords: Power Quality, Voltage Sag, Dynamic Voltage Restorer (DVR), Control Strategy, Voltage Source Converter.

1. Introduction

Power quality is a very important issue due to its impact on electricity suppliers, equipment manufactures and customers. "Power quality is described as the variation of voltage, current and frequency in a power system. It refers to a wide variety of electromagnetic phenomena that characterize the voltage and current at a given time and at a given location in the power system" [1], [2]. Both, electric utilities and end users of electrical power are becoming increasingly concerned about the quality of electric power. Sensitive loads such as computers, programmable logic controllers (PLC), variable speed drives (VSD)-etc. need high quality supplies [3], [4]. Power quality is an umbrella concept for multitude of individual types of power system disturbances. Quality of Supply may be categorized as in Figure 1 [5].

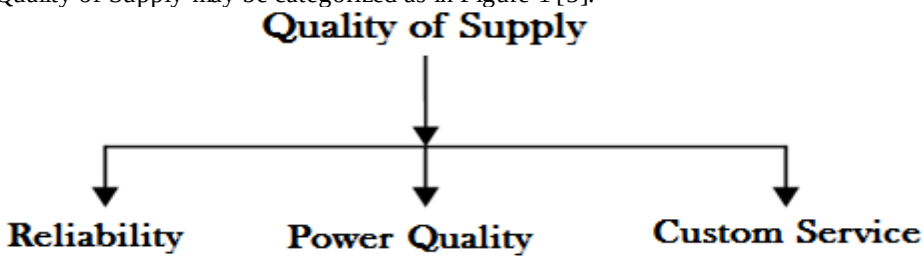

Fig. 1 Quality of Supply Categories

Power distribution systems, should ideally provide their customers with an uninterrupted flow of energy with a smooth sinusoidal voltage at the contracted magnitude level and frequency. However, in practice, power systems, especially distribution systems, have numerous nonlinear loads, which significantly affect the quality of the power supply. As a result of these nonlinear loads, the purity of the supply waveform is lost in many places. This ends up producing many power quality problems [6], [7]. An important percentage of all power quality problems are of the voltage-quality type where what matters is the deviation of the voltage waveform from its ideal form. The best known disturbances of the voltage waveform are voltage sags and swells, harmonics, interharmonics and voltage imbalances. Voltage-quality problems are as follows [8]-[15]:

Voltage Sag: A Voltage Sag is a momentary decrease in the root mean square (RMS) voltage between 0.1 to 0.9 per unit, with a duration ranging from half cycle up to 1 min. It is considered as the most serious problem of power quality. It is caused by faults in the power system or by the starting of large induction motor [13, 22].

Voltage Swell: Voltage swell is defined as an increase in the root mean square (RMS) voltage from 1.1 to 1.8 per unit for duration from 0.5 cycles to 1 min. Voltage swells are not as important as voltage sags because they are less common in distribution systems. The main causes for voltage swell are switching of large capacitors or start/stop of heavy loads [7, 8].

Harmonics: The fundamental frequency of the AC electric power distribution system is 50 Hz. A harmonic frequency is any sinusoidal frequency, which is a multiple of the fundamental frequency. Harmonic frequencies can be even or odd multiples of the sinusoidal fundamental frequency. The main causes for harmonic distortion are rectifiers and all non-linear loads, such as power electronics equipment including VSDs [17].

Voltage transients: They are temporary and undesirable voltages that appear on the power supply line. Transients are high over-voltage disturbances (up to 20kV) that last for a very short time.

Flicker: Oscillation of voltage value, amplitude modulated by a signal with frequency of 0 to 30 Hz. The main causes are frequent start/stop of electric motors (for instance elevators), oscillating loads [17]. Figure 2 shows the sketch of a voltage waveform with physical power- quality problems.

This paper is structured as follows: Section 2 presents solutions to voltage quality problems. Section 3 discusses an overview of the DVR, its functions, configurations, components and operating modes of DVR. Voltage injection methods of DVR are presented in section 4. Section 5 presents closed-loop control of the DVR's output voltage. At the end, some conclusions are given in section 6.

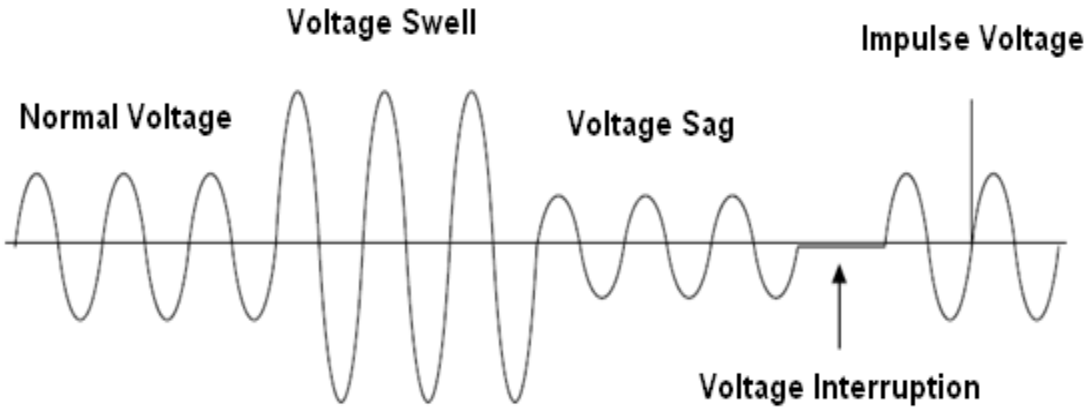

Fig. 2 Regular power- quality problems in power system [16], [17].

2. Solutions to Voltage Quality Problems

There are two approaches to tackle power-quality problems. (a) Actions taken from the customer side or (b) Actions taken from the utility side. The first approach is called "load conditioning", which ensures that the equipment is less sensitive to power disturbances, allowing the operation even under significant voltage distortion. The second approach consists of line-conditioning systems that suppress or counteracts the power system disturbances. Currently, line-conditioning systems are based on pulse width modulation (PWM) converters connected to low-voltage and medium-voltage distribution system in shunt mode or in series. However, with the restructuring of the power sector and with shifting trend towards distributed and dispersed generation, the line-conditioning systems or utility side solutions will play a major role in improving the inherent supply quality [18], [19].Though there are many different methods to mitigate voltage sags and swells, the use of a custom Power device is considered to be the most efficient method. The term custom power refers to the use of power electronics controllers in a distribution system, especially, to deal with various power-quality problems [2].There are many types of Custom Power devices. Some of these devices include: Active Power Filters (APF), Battery Energy Storage Systems (BESS), Distribution STATic synchronous COMpensators (DSTATCOM), Distribution Series Capacitors (DSC), Dynamic Voltage Restorer (DVR), Surge Arresters (SA), Super-conducting Magnetic Energy Systems (SMES), Static Electronic Tap Changers (SETC), Solid-State Transfer Switches (SSTS), Solid State Fault Current Limiter (SSFCL), Static Var Compensator (SVC), Thyristor-Switched Capacitors (TSC), and Uninterruptible Power Supplies (UPS) [7,15,20]. In this paper, an overview of the DVR, its functions, configurations, components, operating modes, voltage injection methods and closed-loop control of the DVR output voltage are reviewed along with the device capabilities and limitations.

3. Dynamic Voltage Restorer (DVR) System

Among the power quality problems (sags, swells, harmonics…) voltage sags are probably the most severe disturbances [7]. In order to overcome these problems the concept of custom power device has become introduced recently. One of those devices is the Dynamic Voltage Restorer (DVR), which is one of the most efficient and modern custom power device used in power distribution networks [7, 31]. A DVR is a series-connected solid-state device that injects voltage into the system in order to regulate the load side voltage. It is normally installed in a distribution system between the supply and a critical load feeder at the so-called point of common coupling (PCC).Its primary function is to rapidly boost up the load-side voltage in the event of a voltage sag in order to avoid any power disruption to that load. There are various circuit topologies and control schemes that can be used to implement a DVR [9, 12, 22].Together with voltage sags and swells compensation, DVR can also have other

features like: line voltage harmonics compensation, reduction of transients in voltage and fault current limitations [8, 27]. Figure 3 shows the location of dynamic voltage restorer (DVR) in an electrical power system.

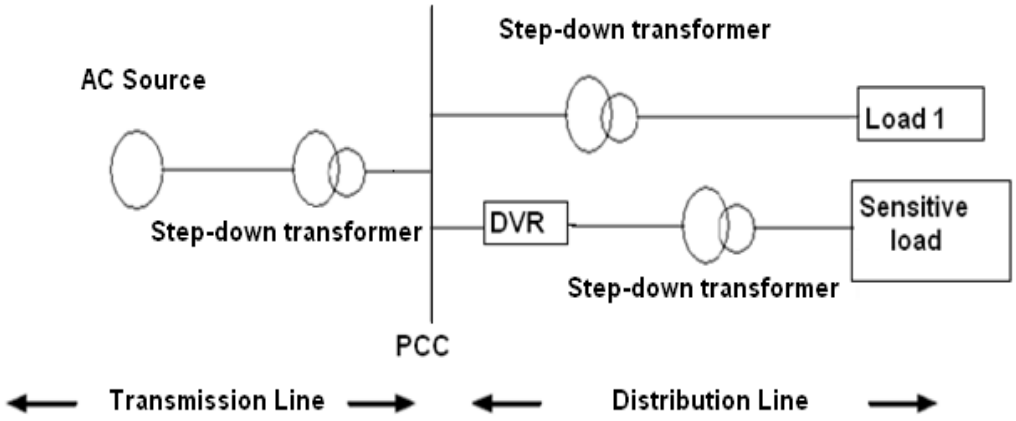

Fig. 3 Location of a dynamic voltage restorer (DVR)

The DVR is a power-electronic-converter-based device capable of protecting sensitive loads from most supply-side disturbances. As shown in Figure 4 the general configuration of the DVR consists of [7, 21, 23, 24, 25]:

3.1. Injection / Booster transformer

The Injection / Booster transformer has two purposes [8, 15, 32]: It connects the DVR to the distribution network via the HV-winding and transforms and couples the injected compensating voltages generated by the voltage source converter (VSC) in series with the incoming supply voltage. In addition, the Injection / Booster transformer serves the purpose of isolating the load from the system (VSC and control mechanism). In [8] a transformer-less DVR based on the multilevel inverter is presented. As a result of employing this inverter, the proposed DVR has lower number of switches in comparison with other multilevel DVR topologies. In [22] transformer-less and Neutral Point Connected DVRs use inductors instead of transformers to inject voltage in the system and are presented as the cheapest solutions. In [33] the proposed transformer-less DVR can satisfactorily mitigate the voltage-sag problems. The design is promising as it points at a less costly restorer of a more compact structure. It also possesses a superior voltage regulation property and has lower losses.

3.2. Harmonic filter

The main task of the harmonic filter is to keep the harmonic voltage content generated by the voltage source converters (VSC) below the permissible level. (i.e. eliminate high-frequency switching harmonics) [23].

3.3. Energy-Storage Unit

It is responsible for the energy storage in DC form. Flywheels, batteries, superconducting magnetic energy storage (SMES) and super capacitors can be used as energy storage devices. It will supply the real-power requirements of the system when DVR is used for compensation [24], [26].

3.4. Voltage Source Converter (VSC)

A voltage-source converter is a power electronic system consisting of switching devices like: Metal Oxide Semiconductor Field Effect Transistor (MOSFET), Gate Turn-Off-Thyristors (GTO), Insulated Gate Bipolar Transistors (IGBT), and Integrated Gate Commutated Thyristors (IGCT), which can generate a sinusoidal voltage at any required frequency, magnitude, and phase angle [23].The output voltage does not need to be of a single frequency. Voltage source converters are widely used in Variable-speed drives (VSD), but can also be used to mitigate voltage dips. The VSC is used to either completely replace the supply voltage or to inject the 'missing voltage'. The 'missing voltage' is the difference between the nominal voltage and the actual one. Normally the VSC is not only used for voltage dip mitigation, but also for other power quality issues, e.g. flicker and harmonics [27, 28].

3.5. Control System

The main purpose of the control system is to maintain a constant voltage magnitude at the point where a sensitive load is connected, under system disturbances. It will also look after the D.C. link voltage using the DC-charging unit [23], [25].

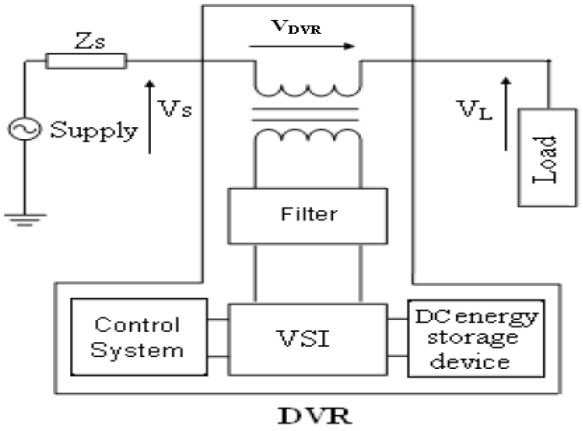

Fig. 4 Dynamic Voltage Restorer (DVR) general configuration

The DVR has three modes of operation which are: protection mode, standby mode (during steady state), and injection/boost mode (during sag) [29].

A- Protection Mode

If the current on the load side exceeds a permissible limit due to a short circuit on the load or large inrush current, the DVR will be isolated from the systems by using the bypass switches as shown in Figure 5, S2 and S3 will open and S1 will be closed to provide an alternative path for the load current.

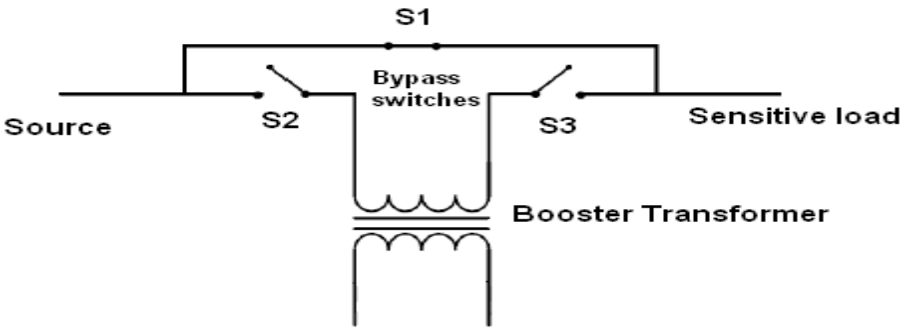

Fig. 5 Protection Mode (creating another path for the load current)

B- Standby Mode: (VDVR = 0)

In the standby mode the booster transformer's low-voltage winding is shorted through the converter as shown in Figure 6. No switching of semiconductors occurs in this mode of operation and the full load current will pass through the transformer primary [15, 23].

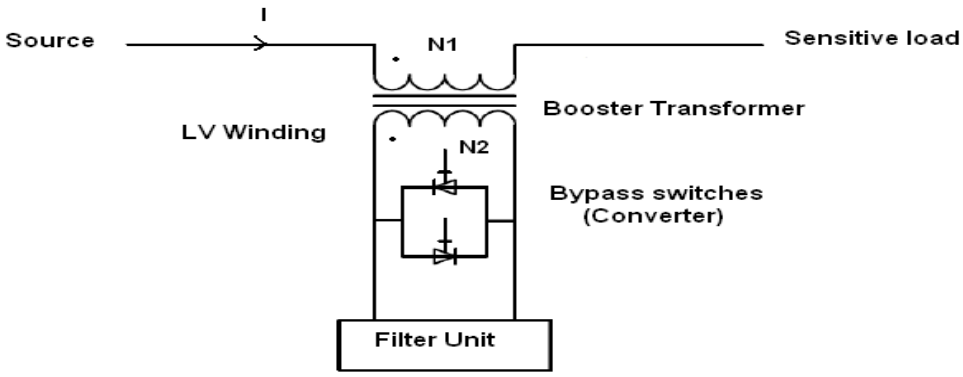

Fig. 6 Standby Mode

C- Injection/Boost Mode: (VDVR≠0)

In the Injection/Boost mode the DVR is injecting a compensating voltage through the booster transformer after the detection of a disturbance in the supply voltage [15, 23].

4. Voltage Injection Methods of DVR

The way in which the dynamic voltage restorer (DVR) is used during the voltage injection mode depends upon several limiting factors such as: DVR power rating, load conditions, and voltage-sag type. For example, some loads are sensitive to phase-angel jumps, some others are sensitive to a change in voltage magnitude and some others are tolerant to all these disturbances. Therefore the control strategies to be applied depend upon the load characteristics [7, 12, 13, 21]. There are four different methods of DVR voltage injection [18, 29]

4.1. Pre-sag/dip compensation method.
4.2. In-phase compensation method.
4.3. In-phase advanced compensation method.
4.4. Voltage tolerance method with minimum energy injection.

4.1. Pre-Sag/Dip Compensation Method (PDC)

The pre-sag method tracks the supply voltage continuously and if it detects any disturbance in that voltage it will inject the difference voltage between the sag or voltage at the PCC and the ideal pre-fault condition. In this way, the load voltage can be restored back to the pre-fault conditions. Compensation of voltage sags in both phase-angle and an amplitude sensitive load has to be achieved by pre-sag compensation method. In this method, the active power injected by the DVR cannot be controlled and it is determined by external conditions such as the type of faults and the load conditions. Figure 7 shows the single-phase vector diagram of this compensation method [7, 21, 30].

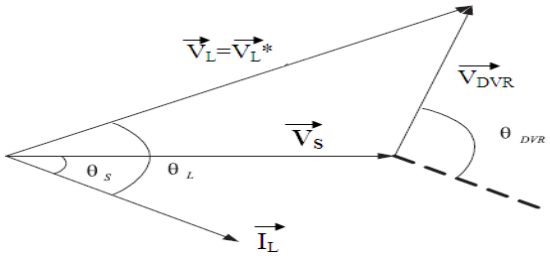

Where $\vec{V}_L^*$ ⟶ Pre-sag voltage

Fig. 7 Single-phase vector diagram of the PDC method

4.2. In-Phase Compensation Method (IPC)

This is the most straight-forward method. In this method the injected voltage is in phase with the PCC voltage regardless of the load current and pre-fault voltage. The phase angles of the pre-sag and load voltage are different but the attention is placed on maintaining a constant voltage magnitude on the load. One of the advantages of this method is that the amplitude of DVR injection voltage is minimum for a certain voltage sag in comparison with other strategies. Practical application of this method is in loads which are not sensitive to phase-angle jumps. Figure 8 shows the single-phase vector diagram of this method [7, 21, 30].

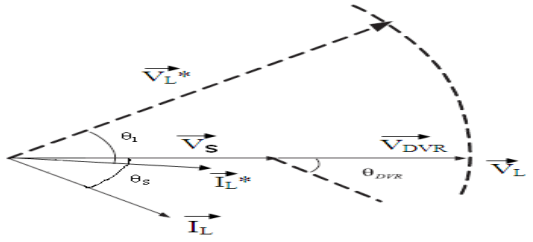

Where $\vec{V}_L^*$ ⟶ Pre-sag voltage, $\vec{I}_L^*$ ⟶ Pre-sag load current, $\theta_1 = \theta_S$

Fig. 8 Single-phase vector diagram of the IPC method

4.3. In-Phase Advanced Compensation Method (IPAC)

In this method the real power spent by DVR is minimized by decreasing the power angle between the sag voltage and the load current [29]. In the two previous cases, namely pre-sag and in-phase compensation, active power is injected into the system by the DVR during disturbances. Morever, the active power supplied is limited to the stored energy in the DC link and this part is one of the most expensive parts of the DVR. The minimization of injected energy is achieved by making the injection voltage phasor perpendicular to the load current phasor. In this method the values of load current and voltage are fixed in the system so one can change only the phase of the sag voltage [7, 21, 29]. In short, IPAC method uses only reactive power and unfortunately, not all the sags can be mitigated without real power, as a consequence, this method is only suitable for a limited sag range.

4.4. Voltage Tolerance Method with Minimum Energy Injection

Generally voltage magnitudes between 90%-110% of the nominal voltage and phase angle variations between 5%-10% of the normal state will not disturb the operation characteristics of loads. This compensation method will maintain the load voltage within the tolerance area with small change of voltage magnitude as shown in Figure 9 [29].

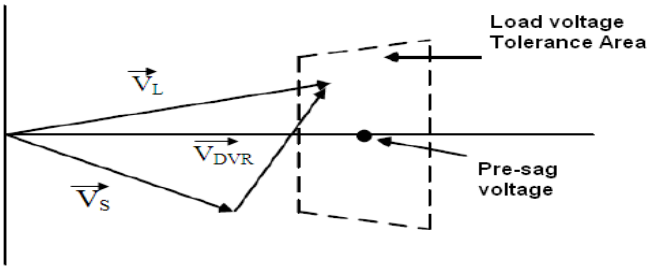

Fig. 9 Voltage tolerance method with minimum energy injection

5. Closed-Loop Control of the DVR's Output Voltage

The control system of a DVR plays an important role, with the requirements of fast response in the face of voltage sags and variations in the connected load. Generally, two control schemes are used in DVR applications, namely, open-loop controller [35] and closed-loop controller [36], [37].In [9] a repetitive controller is used in a DVR system to ameliorate voltage sags, harmonic voltages, and voltage imbalances. It has a wide range of applicability, a fast transient response and ensures zero error in steady state. In [23] the proposed controller combines fuzzy logic with a classical PI controller to adjust the PI gains. Authors report that the main advantage of an adaptive fuzzy PI controller over the classical one (PI) is its ability to compensate notching when the DVR is connected to a weak power system.In [34] the proposed control algorithm based on Space Vector Pulse Width Modulation (SVPWM) technique to generate the pulses for mitigation voltage sags are presented. The simulation and experimental results by using PSCAD / EMTDC showed clearly the performance of the dynamic voltage restorer (DVR) in mitigating voltage sags.In [38] a control method is developed and implemented in order to mitigate voltage sag in distribution systems. The main parts of the controller are the maximum block (Max), filter, lead-lag, PI controller and phase locked loop (PLL). The simulation results showed that the DVR compensates the voltage sag quickly and provides excellent voltage regulation, also better efficiency is achieved by using the proposed control.In [39] a survey on control strategies of Dynamic Voltage Restorer (DVR) is presented. Authors report that the inverter is the core component of DVR, this reference presents the inverter control strategies used in DVR recently, which are linear control and Non-linear control and their types.In [40] a fast repetitive controller based feedback control loop for dynamic voltage restorer (DVR) system is proposed. The Author reports that the fast repetitive controller has fast dynamic response when compared with traditional repetitive controller and Simulation results demonstrated the validity of proposed control system to mitigate voltage sag and maintain load voltage constant.

6. Conclusions

This paper presents power and voltage quality problems such as voltage sage, swells and others. Also an overview of dynamic voltage restorer (DVR) is presented. DVRs are effective recent custom power devices for voltage sags and swells compensation. They inject the appropriate voltage component to correct rapidly any anomaly in the supply voltage to keep the load voltage balanced and constant at the nominal value. The Dynamic Voltage Restorer (DVR) is considered to be an efficient solution due to its relatively low cost and small size, also it has a fast dynamic response.

References

[1] M. Izhwan M, N. Mariun, and M. Amran M. Radzi, "The effect of Power Quality to the industries", The 5th SCORED, Dec. 2007, Malaysia, pp. 1- 4.
[2] R. Ibrahim, A. M. Haidar, M. Zahim "The Effect of DVR Location for Enhancing Voltage Sag" Proceedings of the 9th WSEAS International Conference on A pplications of Electrical Engineering, pp. 92-98.
[3] P. T. Nguyen, Tapan. K. Saha, "Dynamic Voltage Restorer against Balanced and Unbalanced Voltage Sags: Modelling and Simulation," IEEE Power Engineering Society General Meeting, vol. 1, pp. 639-644, June 2004.
[4] E. Babaei, M. F. Kangarlu,"A New Topology for Dynamic Voltage Restorers without dc Link" IEEE Symposium on Industrial Electronics and Applications (ISIEA 2009), October 4-6, 2009, Kuala Lumpur, Malaysia.
[5] V. S. Mallela, P. S. Solanki, and A. Chaturvedi "Role of a Dynamic Voltage Restorer in Mitigation of Power Quality Problems" International Conference on Communication, Computer & Power (ICCCP'05), Feb. 2005, pp. 161- 166.
[6] P. Boonchiam, and N. Mithulananthan "Understanding of Dynamic Voltage Restorers through MATLAB Simulation" Thammasat I nt. J. Sc.Tech., Vol. 11, No. 3, pp. 1-6, July-September 2006.
[7] C. Benachaiba, and B. Ferdi "Voltage quality improvement using DVR", Electrical Power Quality and Utilization, Journal Vol. XIV, No. 1, pp. 39-45, 2008.
[8] M. F. Kangarlu, S. H. Hosseini, A. K. Sadigh "Transformerless DVR topology based on multilevel inverter with reduced number of switches" 1st Power Electronic & Drive Systems & Technologies Conference,IEEE,pp. 371-375,2010.

[9] P. Roncero-Sánchez, E. Acha, J. E. Ortega-Calderon Vicente Feliu, A. García-Cerrada, "A versatile control scheme for a dynamic voltage restorer for power-quality improvement", IEEE Trans., Power Del., vol. 24, no. 1, pp. 277-284, Jan. 2009.

[10] R.Omar, and N.A.Rahim "power quality improvement in low voltage distribution system using dynamic voltage restorer (DVR)" Industrial Electronics and Applications (ICIEA), 2010 the 5th IEEE Conference, pp. 973-978, 2010.

[11] R.Omar, N. A. Rahim, and M. Sulaiman "New control technique applied in dynamic voltage restorer for voltage sag mitigation", American J. of Engineering and Applied Sciences 3 (1): pp.42-48, 2010.

[12] P. R. Sanchez, and E. Acha "Dynamic voltage restorer based on flying capacitor multilevel converters operated by repetitive control", IEEE Transactions on power delivery, Vol.24, No.2, pp. 951-960, April 2009.

[13] R. Amrita, and A. K. Nadir "Modeling & Simulation of dynamic voltage restorer (DVR) for enhancing voltage sag", Sensors & Transducers Journal, Vol. 87, Issue 1, January 2008, pp. 85-93, 2008.

[14] R. Omar, and N. A. Rahim "Modeling and simulation for voltage sags/swells mitigation using dynamic voltage restorer (DVR)", Power Engineering Conference, 2008. AUPEC '08. Dec.2008, pp. 1-5.

[15] M. A. Bhaskar, S. S. Dash, C. Subramani, M. J. Kumar, P. R. Giresh, M. V. Kumar "Voltage quality improvement using DVR", 2010 International Conference on Recent Trends in Information, Telecommunication and Computing, pp. 378-380, IEEE,2010.

[16] Wang Kai, "Analysis of a dynamic voltage regulator", Master of Science Thesis. Stockholm, Sweden 2009, XR-EE-EME 2009:010.

[17] A. Almeida, L. Moreira, J. Delgado, "Power quality problems and new solutions", The electrical and computer engineering,pp. 1-9, 2003.

[18] M. V. Kasuni Perera, "Control of a dynamic voltage restorer to compensate single phase voltage sags" Master of Science Thesis, KTH Electrical Engineering, Stockholm, Sweden, 2007.

[19] Ray Arnold "Solutions to Power Quality Problems" power engineering journal pages: 65-73. 2001.

[20] T. Devaraju, V. C. Veera Reddy, and M. V. Kumar "Role of custom power devices in power quality enhancement: A Review", International Journal of Engineering Science and Technology, Vol.2 (8), 2010, pp. 3628-3634.

[21] C. Benachaiba, and B. Ferdi "Power quality improvement using DVR", American Journal of Applied Sciences 6 (3): 396-400, 2009.

[22] P. G. Gonzalez, and A. G. Cerrada "Analysis of a Neutral-Point-Connected DVR and comparison with a conventional and a Transformer-less DVR", Internal report.

[23] B. Ferdi, C. Benachaiba, S. Dib, R. Dehini "Adaptive PI control of dynamic voltage restorer using fuzzy logic" Journal of Electrical Engineering: Theory and Application (Vol.1-2010/Iss.3),pp. 165-173,2010.

[24] S. K. Gupta, H. P. Tiwari, and R. Pachar, "Estimation of DC voltage storage requirements for dynamic voltage compensation on distribution network using DVR", IACSIT International Journal of Engineering and Technology, Vol. 2, No. 1, February 2010,pp. 124-131.

[25] H. Ezoji, A. sheikholeslami, M. Tabasi,M. M. Saeednia, " Simulation of dynamic voltage restorer using hysteresis voltage control", European Journal of Scientific Research, ISSN 1450-216X Vol.27 No.1 (2009), pp.152-166,2009.

[26] H. P. Tiwari, and S. K. Gupta, "Dynamic voltage restorer against voltage sag", International Journal of Innovation, Management and Technology, Vol. 1, No. 3, pp. 232-237, August 2010.

[27] S. V. Ravi Kumar, and S. Siva Nagaraju, "Simulation of D-statcom and DVR in power systems", ARPN Journal of Engineering and Applied Sciences, Vol.2, No.3, pp. 7-13June 2007.

[28] S. V. Ravi Kumar, and S. Siva Nagaraju, "Power quality improvement using D-Statcom and DVR", International Journal of Electrical and Power Engineering 1(3): pp. 368-376, 2007.

[29] M. Tumay, A. Teke, K. C. Bayindir, M. U. Cuma, "Simulation and modeling of a dynamic voltage restorer", Electrical & Electronics Engineering, pp.1-5, 2006.

[30] A. M. Moreno, D. Oterino, M. Gonzalez, F. A. Olivencia, and Juan J. Gonzalez, "Study of sag compensation with DVR", IEEE MELECON, 2006, May 16-19, pp. 990-993, 2006.

[31] L. Gyugy, C. D. Schaudar, C. W. Edwards, M. Sarkozi, "Apparatus and method for Dynamic Voltage Restoration of utility distribution networks", Westinghouse Electric Corporation, Patent number 5,329,222,Jul.12,1994.

[32] T. Fujii, A. Beer, "Controller for performing a decoupling control of a transformer less reactive series compensator", Patent number US 6,225,791 B1, May 1, 2001.

[33] B. H. Li, S. S. Choi, and D. M. Vilathgamuwa, "Transformer less dynamic voltage restorer", IEE Proceedings-Generation, Transmission and Distribution, Vol. 149, No. 3, pp. 263 – 273,May 2002.

[34] R. Omar, N. A. Rahim, "Implementation and control of a Dynamic Voltage Restorer using Space Vector Pulse Width Modulation (SVPWM) for voltage sag mitigation" IEEE International Conference ,pp. 1- 6, 2009.

[35] C. Zhan, V. K. Ramachandaramurthy, A. Arulampalam, C. Fitzer, S. Kromlidis, M. Barnes, and N. Jenkins, "Dynamic voltage restorer based on voltage-space-vector PWM control," IEEE Trans. Ind. Appl., vol. 37, no. 6, pp. 1855–1863, Nov./Dec. 2001.

[36] J. G. Nielsen, M. J. Newman, H. Nielsen, and F. Blaabjerg, "Control and testing of a dynamic voltage restorer (DVR) at medium voltage level," IEEE Trans. Power Electron., vol. 19, no. 3, pp. 806–813, May 2004.

[37] D. M. Vilathgamuwa, A. A. D. R. Perera, and S. S. Choi, "Performance improvement of the dynamic voltage restorer with closed-loop load voltage and current-mode control," IEEE Transactions on Power Electronics, vol. 17, no. 5, pp. 824–834, September 2002.

[38] A. O. Al-Mathnani, M. A. Hannan, M. A. Al-Dabbagh, M. Mohd Ali, and M. A. Mohamed, "Development of new control strategy for voltage sag mitigation", 2nd IEEE International Conference on Power and Energy (PECon 08), December 1-3, pp. 318 – 323, 2008.

[39] W. Jing, X. Aiqin, S. Yueyue, "A survey on control strategies Of Dynamic Voltage Restorer", 13th IEEE International Conference on harmonics and quality of power, pp. 1 – 5, 2008.

[40] Suxuan Guo, "Fast repetitive controller based low-voltage Dynamic Voltage Restorer for Voltage-Quality Issues in Distribution System", 2010 2nd IEEE International Symposium on Power Electronics for Distributed Generation Systems, pp. 988 – 992, 2010.

Studies on the Dielectric Beheviour of Some Plant Fibers

[1,]Gajendra Nath Sarma,[2,]Manoranjan Talukdar
[1,]Department Of Physics, Hojai College, Hojai, Assam (India), PIN 782435
[2,]Department Of Physics, Bajali College, Pathsala, Assam (India), PIN 781325

Abstract

The dielectric diffractogram of raw and chemically degummed ginger (*Zingiber officinale*), turmeric (*Curcuma longa*) and java galangal (*Alpinia galangal*) fibers are taken at different temperatures and at different frequencies. It is found that the dielectric constants of the plant fibers are changed due to degumming. Also the dielectric constants of the fibers decrease with the increase of frequency at temperature 30^0C. The variation of dielectric constant with change of frequency indicates that the plant fibers are hydrophilic in nature. The hydrophilic nature of the fibers has not been changed due to degumming. The glass transition temperature (T_g) has changed when the fibers are degummed by 2% NaOH. The dielectric loss tangent (tanδ) shows a linear relation with temperature in air and in vacuum. The tanδ changes due to degumming of the fibers at lower temperature but remain almost same at higher temperature. Further, the values of tanδ vary at different medium.

Key Words: Dielectric diffractogram, *Zingiber officinale*, *Curcuma longa*, *Alpinia galangal*, dielectric loss tangent.

1. Introduction:

The cellulose fibers such as ginger, turmeric and java galangal are semicrystalline and hygroscopic in nature. The dielectric properties of these fibers have great importance in textile technology. The dielectric properties of the cellulose materials by capacity measuring method have been reported by various workers[1-4]. The action of absorbed water and influence of gum on the dielectric properties of some cellulose fibers have been studied[5-7]. The dielectric behaviour of ginger, turmeric and java galangal have been observed at room temperature as well as at different temperatures and at different frequencies at which they are quenched and annealed. In present investigation, raw and degummed fibers of ginger, turmeric and java galangal are subjected to dielectric cell arrangement at different temperatures and at audio frequency range 20 Hz – 20 KHz. The measurements were carried out in this range which is a suitable range[8].

2. Sample Preparation:

Ginger (*Zingiber officinale*), turmeric (*Curcuma longa*) and java galangal (*Alpinia galangal*) plants, from the various parts of the chosen area of the north-east region of India, have been collected. The fibers are extracted from the stems of these plants. One part of each of the raw fibers of these plants were immerged in a mixture of Benzene and Alcohol (ratio 1:1) for six hours. These were then washed with distilled water, and then boiled with NaOH solutions at 2% concentration. The fibers were then again washed with distilled water and dried normally (at room temperature). Samples so prepared were then taken into the Dielectric cell arrangement for analysis the dielectric properties.

3. Experimental Arrangement:

The capacity measurement method is a suitable method to study the dielectric properties fibers. The arrangement mainly consisted of a dielectric cell, which is a combination of one outer cylindrical plate and one inner cylinder (both made of copper). They act as the outer and the inner electrodes of the cell. A copper wire was wielded to the plate. The fibers were wounded round the inner cylinder uniformly so as to form a thin layer of thickness of about 0.2 mm. The outer plate was then placed coaxially upon the inner cylinder completely covering the fiber layer. The thickness of the fiber layer was measured directly by a traveling microscope. The cell was mounted inside a glass tube assembly of high temperature resistance with cone socket arrangement. A vacuum arrangement is attached with the glass tube, with the help of a side tube, to study the fibers under vacuum condition. The lower part of the tube assembly with the cell was inserted vertically into a muffled furnace. The cavity dimension of the furnace was 14 cm. in depth and 11 cm in diameter. With the help of copper – constantan thermocouple, the temperature of the dielectric cell was measured. The closed end of the thermocouple of length 20 cm was kept very near to the cell and the open ends of the lead were connected to digital microvoltmeter of the type DMV – 010 (Scientific equipment, Roorkee) having an accuracy of ± 0.01 mV. An LCR bridge (Marconi TF 2700 universal LCR bridge) is used to measure the capacitance directly from 0.5 pfd to 1100 pfd. The frequency of the internal generator was fixed at 1 KHz. For other frequencies, an external audio frequency oscillator was used. This external source with an isolating transformer of type TM 7120 (Marconi) in series was connected to the bridge via a jacket plug.

4. Measurement:

The fibers were wounded round the inner cylinder of the dielectric cell uniformly so as to form a thin layer of thickness of about 0.2 mm. The dimensions of the capacitance cell were measured with the help of the travelling microscope. The values of the capacitance and dielectric loss tangent (tanδ) of the cell with the specimen were recorded directly from the bridge at temperature from 303 K to 573 K under frequency 1 KHz in both air and in vacuum. Also the capacitance and tanδ for the specimen were measured in the frequency range 20 Hz to 20 KHz at room temperature (at 308 K). From the data obtained, the values of dielectric constant and dielectric loss factor in each case were calculated. The formulae used to calculate the dielectric constant and dielectric loss factor are same as used by Talukdar et al[9].

5. Results and Discussion

The variation of dielectric constant with temperature for the three plant fibers viz. ginger, turmeric and java galangal fibers, in air and in vacuum, are shown in fig. 1. The observed values are shown in table1. No first step variation of dielectric curves is attributed in the samples kept in vacuum except a slight decrease is observed initially. This is attributed due to the decrease of water molecules in vacuum. The values of dielectric constant remain almost same in the temperature range 363 – 453 K. The transition up to which these values remain constant corresponds to the glass transition temperature[10] (T_g) of the plant fibers. This is in agreement with the result obtained earlier for some polymers[11]. The variation of dielectric constant with temperature for raw and degummed fibers is given by figure 2. From the figures it is observed that the peak areas of dielectric thermograms of ginger, turmeric and java galangal fibers at dehydrated and decomposition state are decreased remarkably. This may be due to the decrease of water molecules at dehydrated state and change of interfacial polarization effect in decomposition state.

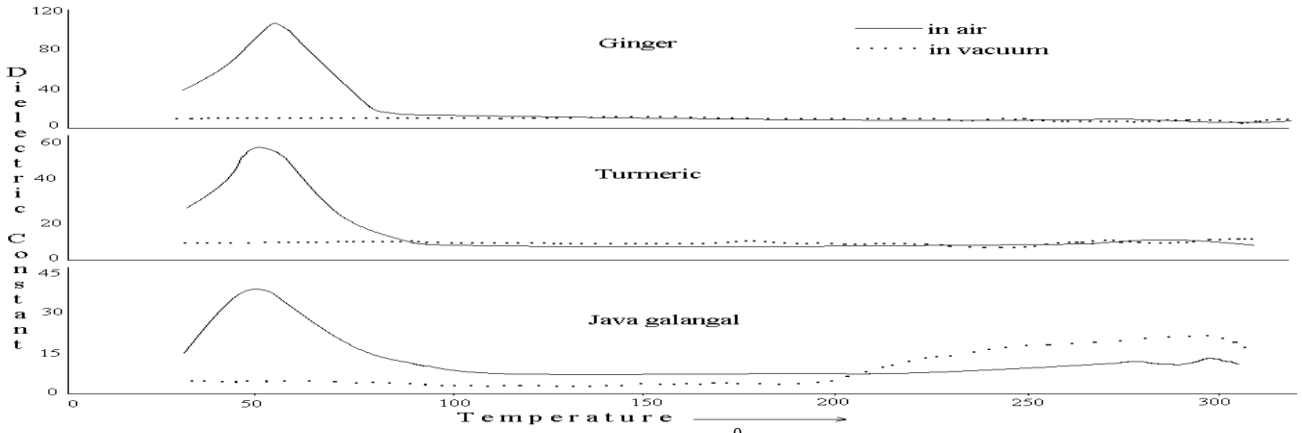

Fig.1-Variation of dielectric constant with temp. (^{0}C) of raw fibers in air & vacuum.

Table 1 - Dielectric constant (ε) of different plant fibers at different temperatures in air and in vacuum at frequency 1 KHz

(Samples : ra – raw in air, rv – raw in vacuum, da – degummed in air)

Temp.(K)	Ginger			Turmeric			Java galangal		
	ra	rv	da	ra	rv	da	ra	rv	da
303	45.83	4.07	44.67	23.54	5.17	17.15	22.78	8.68	7.49
323	80.43	4.07	50.61	36.56	5.17	18.76	38.34	6.17	8.83
423	3.87	4.07	3.95	4.78	5.17	3.89	7.12	4.23	5.27
543	11.78	10.59	11.18	8.13	10.11	4.95	16.43	22.12	8.73

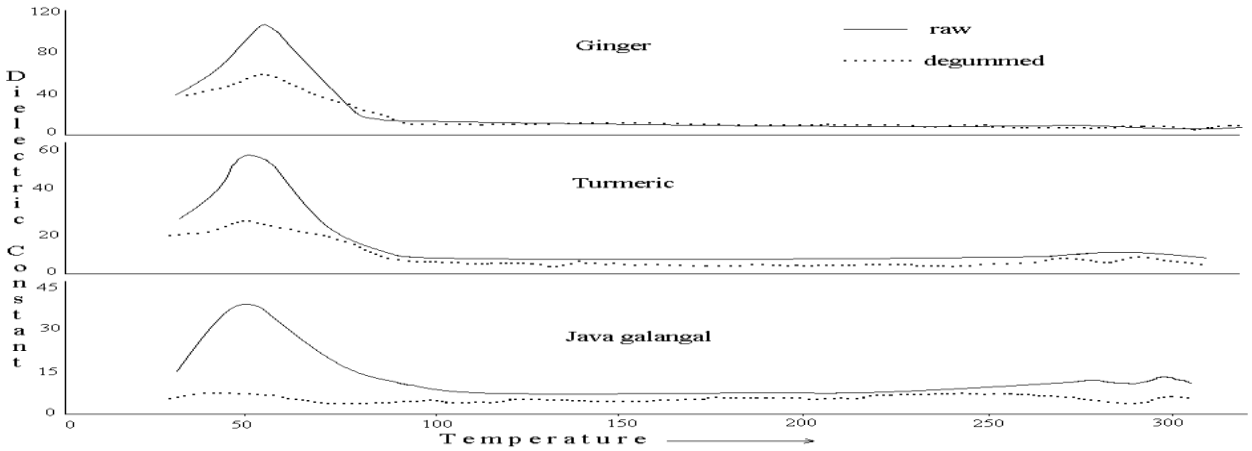

Fig.2- Variation of dielectric constant with temperature (^{0}C) of raw and degummed plant fibers

The variation of dielectric constant with change of frequency for the raw plant fibers are depicted in figure 3, from which it is observed that the dielectric constant of the fibers decreases with increase of frequency at temperature 303 K. This indicates that lower the frequency of the applied alternating field to the fibrous medium, greater is the dielectric constant due to moisture absorption. The same result was observed for polymeric fibers by some workers [12]. Thus it may be inferred that the plant fibers are hydrophilic in nature. The variation of dielectric constant with frequency for degummed plant fibers is found to be same as that for the raw fibers. This indicates that the hydrophilic nature of the fibers has not been changed due to degumming.

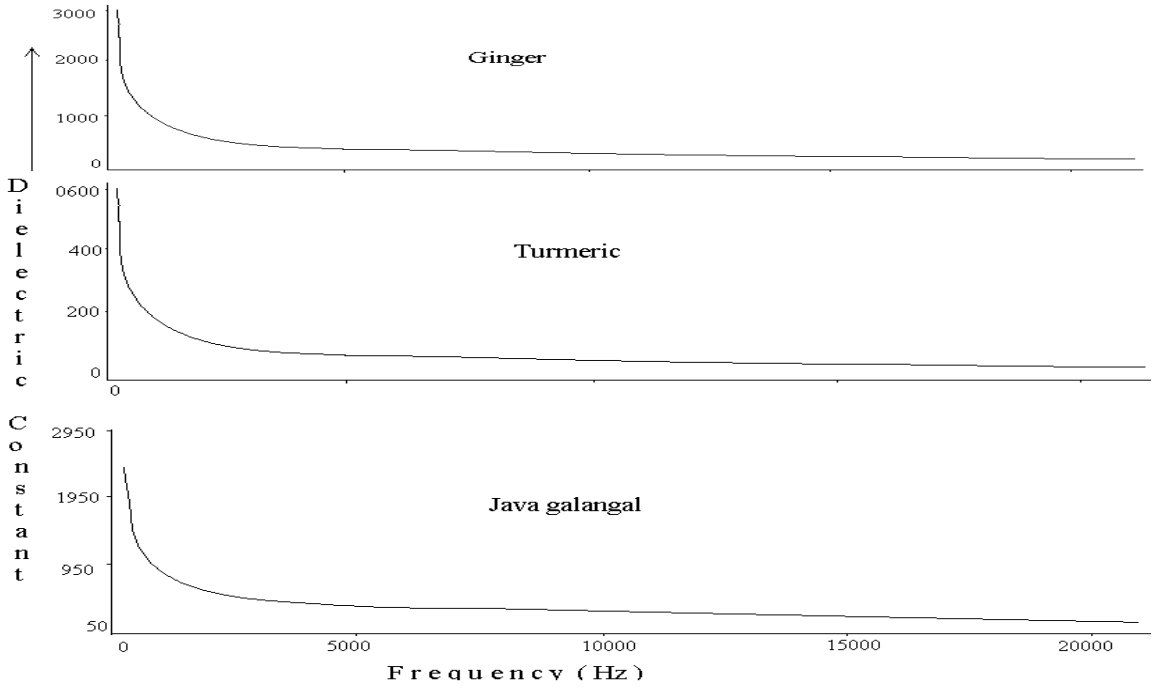

Fig. 3 - Variation of dielectric constant with frequency of some raw plant fibers.

The variation of dielectric constant with frequency for ginger fiber at different temperatures is shown in fig.4. From the figure it is observed that at higher temperature the dielectric constant decreases. This may be due to the change of interfacial polarization. This decrease in values of dielectric constant with increasing frequency at higher temperature may takes place due to influence of interfacial polarization during decomposition stage. Kitamara [13] obtained the same results for some plant fibers.

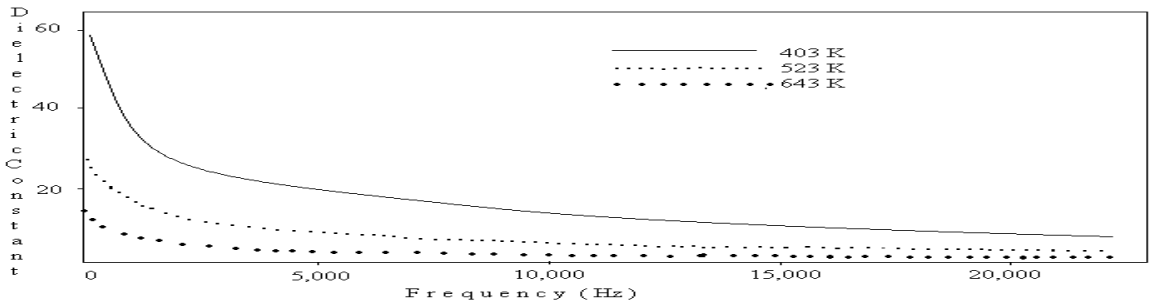

Fig.4 - Variation of dielectric constant with frequency for ginger fiber at different temperatures.

Table 2. Dielectric loss tangent (tan δ) of different raw and degummed fibers at different temperatures at frequency 1 KHz

(Samples : r – raw fibers, d – degummed fibers)

Temp. K	Ginger		Turmeric		Java galangal	
	r	d	r	d	r	d
303	0.12	0.13	0.12	0.12	0.15	0.19
363	2.20	0.21	2.20	2.20	2.24	2.28
423	4.65	4.65	4.65	4.65	4.69	4.83
483	7.16	7.16	7.16	7.16	7.20	7.24
573	10.34	10.34	10.34	10.34	10.39	10.45

In table 2, values of dielectric losses with temperature in air of the three plant raw and degummed fibers are displayed. From the table it is evident that the dielectric loss is gradually increased for all the fibers in the temperature range 303 – 573 K. This variation is due to the fact that due to increase of temperature the rotation of side groups and by segmental mobility of the fibers, which is agreed by I I Perepechko[14]. It is also inferred that the dielectric loss character of the observed plant fibers has not changed due to degumming.

6. Conclusion:

The dielectric constant of raw and degummed plant fibers is found to be different. It is noticed that the glass transition temperature (T_g) has changed when the fibers are degummed. These fibers are hygroscopic and hydrophilic in nature. The dielectric constant is highest for the ginger fiber and lowest for java galangal fiber amongst the observed fibers. The dielectric loss tangent changes due to degumming at lower temperature and remain nearly constant as the temperature rises. Further, the dielectric loss tangent changes its values at different medium, such as air, oxygen and vacuum.

References:

[1]. Bora M N, Saikia D, Saikia R, Talukdar C,1997, High Temp Phy. Vol.29, p.683-688.
[2]. Duswalt A A, 1974 Thermocimica Acta, 8, 57.
[3]. Bora M N, Baruah G C, Talukdar C, 1993, Thermocimica Acta, 218, 435 – 443.
[4]. Bora M N, Talukdar M, Talukdar C, 1999 Indian Journal of Fiber & Textile Research, Vol. 24, p. 172 – 176.
[5]. Physics of dielectric materials, Tareev B, Mir publishers, Moscow, 1978, p. 78.
[6]. An investigation on Thermophysical behaviour of some fibers readily available in the north east region of India by various physical methods, Gauhati University Ph D Thesis, Talukdar C, 1993, p. 67.
[7]. Boruah G C, Talukdar C, Bora M N, Gauhati University J Sci., 30 A, p.45.
[8]. Studies on the thermophysical properties of some organic complexes (fibers) by X-ray diffraction and other physical methods, Baruah G C, Gauhati University Ph.D. Thesis, 1991, p. 88.
[9]. Study of thermophysical and tensile properties of irradiated and chemically treated natural fibers available in north east India, Talukdar M, Gauhati University Ph.D. Thesis, 2003, pp. 46 – 50.
[10]. An introduction to polymer Physics, Perepechko I I, Mir publishers, Moscow, p.83.
[11]. Stetrovskii A P and Tarasova L V, Vysocomom Soedi A.20 (5), 1978, p. 1116.
[12]. Boruah G C, Talukdar C, Bora M N, Gauhati University J Sci., 30 A, p.45 -52.
[13]. Kitamara A I O, Nippon Sanshigaku Xasshi 39 (2), 1970, 119.
[14]. An Introduction to polym Phy, Perepechko I I, Mir publishers, Moscow,1981, p.162.

Numerical Simulation of Flow past a Circular Cylinder with Varying Tunnel Height to Cylinder Diameter at Re 40.

Rajani B.N[1], R.V.P Gowda[2] And P. Ranjan[2]

[1] Computational and Theoretical Fluid Dynamics Department, National Aerospace laboratories, Bangalore 560017, Karnataka, India.

[2] Dept. of Industrial Engineering, Dayananda Sagar College of Engineering, Shavige Malleshwara Hills, Kumaraswamy layout, Bangalore 560078, Karnataka, India.

Abstract:

The current study mainly focuses on the two-dimensional numerical simulation of the unsteady laminar flow past a circular cylinder in a channel, mimicking the effect of the tunnel wall. The computational results obtained using two different flow solution codes are validated against other computational and measurement data available in the literature. The study confirms a decrease in wake length and a shift in flow separation further downstream at smaller gaps between the tunnel walls and cylinder.

Keywords: Cylinder, OpenFOAM, parabolic flow, tunnel, uniform flow, vortices.

1. Introduction

Flow around a circular cylinder is a challenging kaleidoscopic phenomenon. Cross flow normal to the axis of a circular cylinder and the associated problems of heat and mass transport are encountered in a wide variety of engineering applications. In case of cylinders with regular polygonal cross section, the flow usually separates at one or more sharp corners of the cross-section geometry itself, forming a pair of symmetric vortices in the wake on either side of the mid symmetry plane. On the other hand, for a circular cylinder, where the point of flow separation, decided by the nature of the upstream boundary layer, is not fixed, the physics of the flow is much more complex than its relatively simple shape might suggest. Both experimental measurements and numerical computations have confirmed that beyond a critical Reynolds number the flow structure is attributed mainly to the effect of walls on the flow close to the cylinder. The vortices shed from the wall interact with the vortices shed from the cylinder, hence forming a new vortex structure. Due to close proximity of the tunnel walls, the flow velocity above and below the cylinder increases, resulting in change in pressure field around the cylinder. Experimental studies conducted by Buresti *et al* [1] and Price *et al* [2] also provide a great insight into the change in flow around a cylinder near tunnel walls. However, the experiments conducted in this field of study were at high Reynolds numbers, where flow can no longer be considered two dimensional. Recently, in studies conducted by Sahin *et al* [3], finite volume symmetry is lost and the wake becomes unstable leading to the shedding of alternate vortices from the cylinder surface at a definite frequency, well known in literature as the von Karman vortex street. The size and strength of the symmetric pair of vortex and the Reynolds number at which the onset of the wake instability is observed greatly depends on the blockage effect (ratio of the cylinder diameter to tunnel diameter), cylinder aspect ratio, end plate and any other disturbances arising out of the experimental set up.
A brief overview of the flow algorithm employed is presented in Majumdar *et al* [4]. Previously conducted studies, such as Singha *et al* [5] and Zovatto *et al* [6] have shown a significant change in the flow characteristics around a cylinder with close proximity of tunnel walls. In a global point of view, the observation presented in these studies are the same as discussed in this study: A shift in the point of separation downstream and delay in vortex shedding in the proximity of tunnel walls. This change in velocity only formulation was developed in order to study the effects of wall proximity on the flow field around a circular cylinder. Studies of linear stability of the flow were conducted over a range of Reynolds number (0-280) and blockage ratio (0.1-0.9).

Present study emphasizes on two main subjects: understanding the physics of flow around a confined circular cylinder at various values of tunnel height to cylinder diameter aspect ratio *(H/D)* and understanding the use of OpenFOAM as a solver to solve the defined problem. An in house multiblock structured implicit finite volume flow solution algorithm, 3D PURLES, developed at National Aerospace Laboratories, is used to solve the problem initially. The results are thereafter compared with those obtained from OpenFOAM. The conclusion drawn from the study is thus an effective one, supported by two different flow solution codes. The simulations are carried out long enough for the flow characteristics to evolve. Simulations are carried out at Re 40, consistent with the two-dimensionality assumption. Grids of significantly high resolution are generated using an in-house grid generation tool and a third party software, Gridgen. Emphasis is given to the behavior of wake and the separation length over the surface of the cylinder. Significant changes in wake behavior are seen as the tunnel height is reduced. Reduction in wake length for lower *H/D* values is seen along with increase in drag on the cylinder. Several important flow characteristics such as separation point and re-circulation length (wake length) in the steady flow regime are correlated with the input parameters (Re and *H/D*).

2. Problem Statement And Mathematical Formulation.

Numerical simulations of low Reynolds number flow over a circular cylinder placed centrally in a channel with varying height are carried out using a primitive variable based finite volume Navier-Stoke solver, implemented on a structured grid. Figures 1(a) and 1(b) show the schematic diagram of the flow configuration for uniform and parabolic flow profile respectively. The flow simulation is carried out at Re 40, based on the centerline velocity, diameter (D) of the cylinder and normalized tunnel height (*H/D*). The tunnel height to diameter ratio (*H/D*) varies in the range: $30 \geq H/D \geq 2$. Based on the study of previous experiments [4,5], the far field boundary is placed initially at 30 D and grid resolution is fixed at 30 × 30 × 1 to cover the entire domain of the cylinder (azimuthal angle θ varying from 0 to 360 degrees).

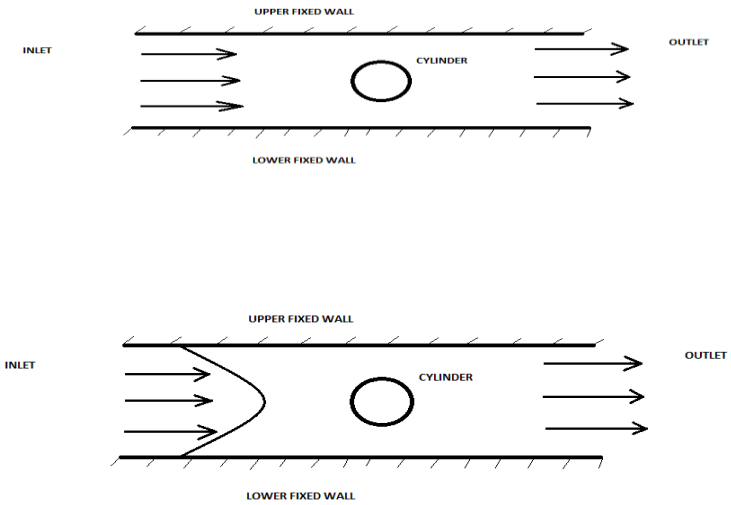

Figure 1: (a) Uniform flow (b) Parabolic flow.

The in house grid generation algorithm involves the solution of the elliptic type differential equations at a coarse level, followed by simple algebraic interpolation from the coarse to a finer level. The coarser grid is primarily generated by solving a system of inverted Poisson equations for a given point distribution at all four boundaries of a two-dimensional computation domain. The control functions in the equations are automatically adjusted in an iterative procedure to achieve boundary-orthogonality and need no ad-hoc adjustment of the problem dependent parameters. Finally, when the desired concentration of grid points is specified at the fine level on one boundary along each direction, the fine level field grid coordinates is obtained by fitting bicubic spline functions passing through the coarse level grid nodes. The Hybrid approach makes a compromise between the simple algebraic and the expensive differential approach and guarantees smooth grid of desired fineness and approximate boundary-orthogonality for a very reasonable computation cost.

The flow computation is carried out using O-topology for the cylinder. Near the cylinder surface, the grid lines are specially stretched along the wall-normal direction in order to have a better resolution of the steep flow variable gradients in the boundary layer. Five different grids are created for previously mentioned cylinder-wall aspect ratios (Table 1). Grid resolution is kept constant for all values of aspect ratios. The grid lines are stretched radially near the cylinder wall to resolve the sharp local gradients of the flow variables.

Table 1: Reynolds numbers and channel heights considered.

Reynolds Number *(Re)*	40	
Normalized cylinder to wall ratio(3D – PURLES)	10,20,30,5 and 2	Uniform and Parabolic
Normalized cylinder to wall ratio(OpenFOAM)	10,20 and 30	Uniform

The numerical solution of the NS equation uses an appropriate mathematical model, which handles the geometrical complexities like arbitrary shaped boundaries as well as the physical complexities like simulating the effect of vortex shedding. In Cartesian coordinates form, the Navier-Stokes equations for a general case are expressed as

$$\frac{\partial(\rho u_i)}{\partial t}+\frac{\partial(\rho u_i u_j)}{\partial x_j}=\frac{\partial(\tau_{ij})}{\partial x_j}+F_i \tag{1}$$

where,

$$\tau_{ij}=-(P+2/3\mu\frac{\partial u_j}{\partial x_i})\delta y+2\mu e_{ij} \tag{2}$$

and

$$e_y=\frac{1}{2}\left(\frac{\partial u_i}{\partial x_j}+\frac{\partial u_j}{\partial x_i}\right) \tag{3}$$

Here j =1, 2, 3 is the summation index of the tensor, τ_{ij} is the stress tensor. δ_{ij} is the Kronecker delta and e_{ij} is the strain rate tensor and μ is the viscosity. With appropriate transformations, the equation is used in 3D-PURLES and OpenFOAM. The equation of continuity becomes

$$\frac{\partial\rho}{\partial t}+\frac{\partial\rho u_i}{\partial x_j}=0 \tag{4}$$

The governing differential equations for the flow are integrated over a finite number of control volumes covering the computation domain formed by the grid generation procedure The grid generation procedure calculates the coordinates of the control volume vertices which are simply joined by linear segments to form the six boundary planes and hence the volume. All the variables are stored at the geometric center *P* of the control volume. The six neighboring control volume centers are denoted by *N*, *S*, *E*, *W*, *T* and *B* for the north, south, east, west, top and bottom neighbors respectively. The face center points n, s, e, w, t and b are located at the intersection of the lines joining the midpoint of the opposite edges, e.g. ne and se are the middle points of the edge forming the east edge with 'e' at its center. These points specified on edges are used for locating the variables and their gradients on the control volume faces. The Cartesian velocities at the control volume faces of control volume are computed and finally the total convective mass fluxes at the cell faces are stored.

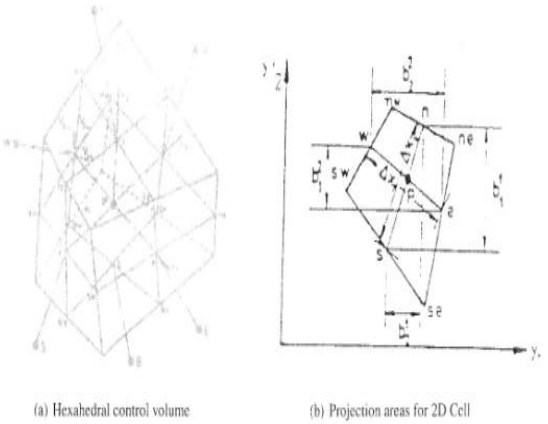

(a) Hexahedral control volume (b) Projection areas for 2D Cell

Figure 2: (a) Hexahedral Control volume (b) Projection areas for 2D Cell.

The most important geometrical parameters required in the present formulation are the metric coefficients β^i_j, which may always be expressed in terms of the projection area of the control volume, faces as follows:

$$\beta^i_i = b^i_j\Delta_i /(\Delta x_1\Delta x_2\Delta x_3) \tag{5}$$

where the areas b^i_j for the control volume around *P* are shown in Figure 2(b) for a two dimensional situation on y_1 – $y_2$plane. The other geometrical quantities of interest are the normal distance of a near boundary node from the boundary surface, the volume and the projection of boundary face areas on the Cartesian reference planes. The calculation of these quantities however involves only some simple arithmetic operations In addition to the discretised governing equations, the complete specification of the mathematical problem requires the incorporation of proper boundary conditions for all the variables. The appropriate boundary conditions used for the present multiblock computation are shown in Figure 3.

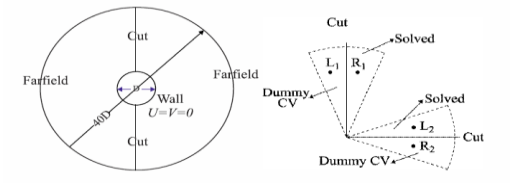

Figure 3: Boundary conditions for a typical two block computation of flow past a cylinder.

The two dimensional flow equations are discretised and solved as follows: Time accurate computations are carried out using the central difference scheme (CDS) for spatial discretization of convective flux coupled to deferred correction procedure (i.e. combining 10% of Upwind fluxes 90% of CDS fluxes) and a second order accurate scheme for temporal discretization. In OpenFOAM, the SimpleFOAM solver is used to solve the problem in steady state conditions. The scheme used is same as that in 3D-PURLES. The convergence criterion (CC) is fixed to be about 10^{-5} for the continuity and momentum equations, for both 3D-PURLES and OpenFOAM.

3. Results.

3.1 Flow at Reynolds number 40: Uniform flow profile.

Simulations are carried out using 3D-PURLES and OpenFOAM with uniform profile ($u_{in}=u_0$) at the inlet as shown in figure 1.The unconfined flow at *Re* 40 is approaching transition but in the steady, attached wake regime. The bounded flows also belong to the same flow regime. Figures 4 and 5 show the streamlines of the flows for various channel heights. Changes in wake length are observed with the changing tunnel height to cylinder diameter (*H/D*) ratio. For a smaller value of *H/D*, the wake is attached to the cylinder and has a shorter length as compared to that for a higher *H/D*. The kinetic energy of the fluid near the cylinder increases and separation point behind the cylinder moves downstream on the cylinder for a small *H/D*. Consequently, the normalized wake length (L_w) behind the cylinder becomes smaller. Figure 6 shows the movement of the separation points in terms of the angle measured clockwise from the forward stagnation point as the channel height varies.

According to [5], location of the separation point at Re 45 is analytically given by

$$\theta = 147.3(H/D)^{-0.07}, \qquad (6)$$

where, θ is the azimuth angle measured in clockwise direction. The relation holds valid for a lower Reynolds number 40 to a considerable extent. Figure 7 shows the corresponding variation in wake length obtained for the present computation. The length of the wake increases almost linearly up to a certain limit as the channel height varies. In the present simulations, the non-dimensional wake length is observed to increase from about 1.39 and 2.51 at *H/D* = 10 to about 2.30 and 2.62 at *H/D* = 30 in OpenFOAM and 3D PURLES respectively. Significant decrease in the size of the two counter rotating vortices with decrease in *H/D* is observed in Figures 4 and 5.The wake vortices are strengthened but confined in a short region. The lift and drag coefficients attain constant values quite rapidly after the initial transients settle down. Figure 8 shows lift coefficient remains fixed at zero for all the configurations confirming the symmetric nature of the flows. The vorticity in the flow at different H/D values also shows the symmetric nature of flow. The drag coefficients attain a high value of 2.01 and 1.97 at *H/D* = 10, but significantly reduce to 1.58 and 1.60 at H/D = 30, based on the results obtained from 3D PURLES and OpenFOAM respectively.

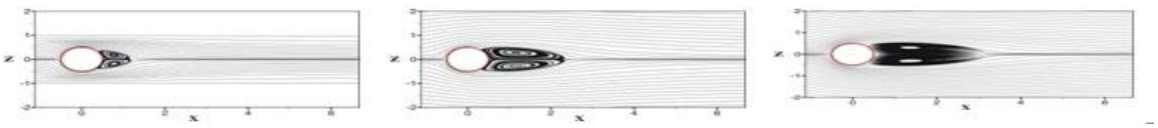

H/D=2 H/D=5 H/D=10

Figure 4: Velocity contours at Re 40 obtained using 3D-PURLES.

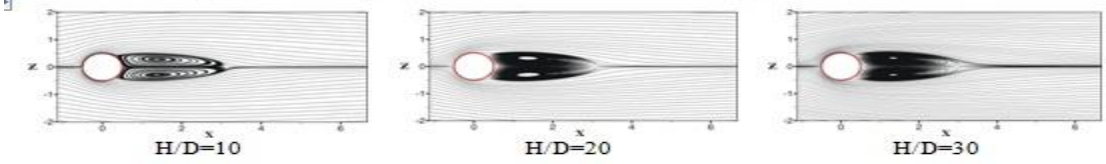

Figure 5: Velocity contours at Re 40 obtained using OpenFOAM.

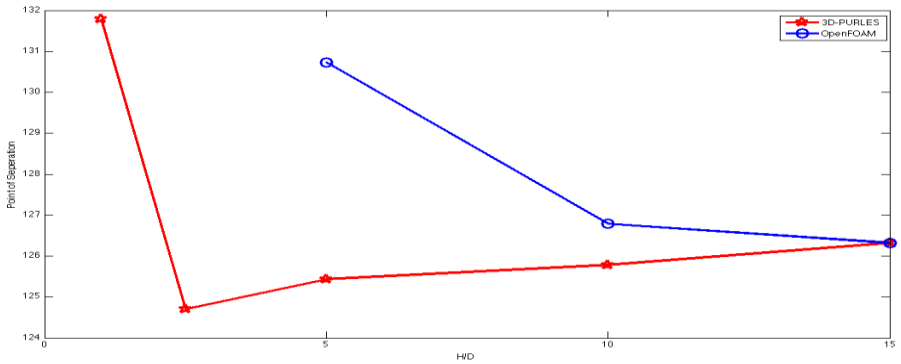

Figure 6: Plot of Point of Separation vs. H/D using 3D PURLES and OpenFOAM.

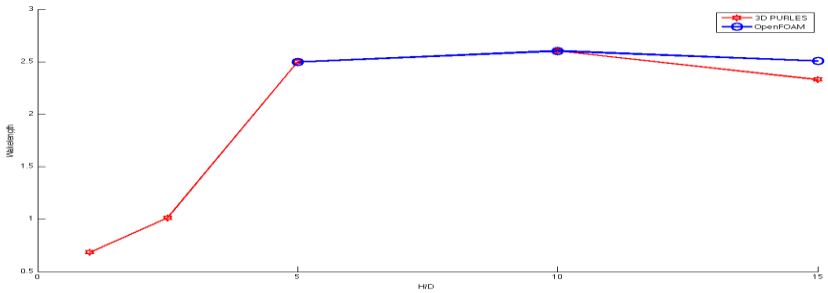

Figure 7: Wake length with H/D; Re = 40 for uniform inlet profile: 3D-PURLES and OpenFOAM.

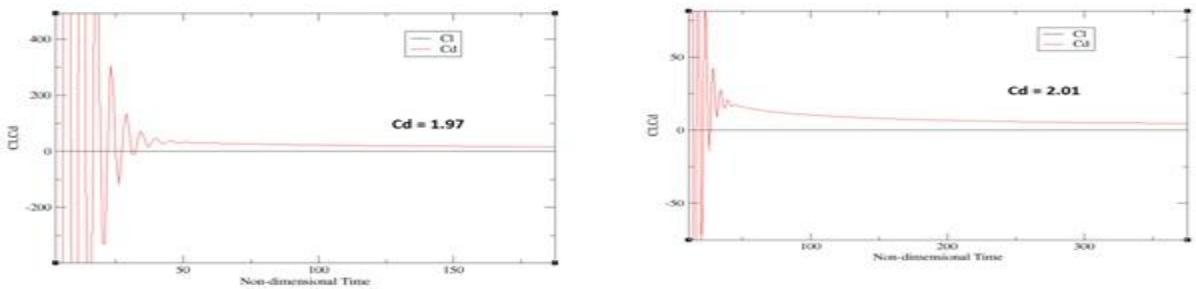

Figure 8: (a)Cl and Cd vs. Non-dimensional time for H/D = 10 at Re 40 using 3D-PURLES.
(b)Cl and Cd vs. Non-dimensional time for H/D = 10 at Re 40 using OpenFOAM.

The vortex strengths in the boundary layers increase and the re-circulation zone attached behind cylinder shortens for H/D up to 8 [5] and then increases for *H/D* = 10 and so on. This causes increased pressure on the front face and a larger drag coefficient at small channel heights. The kinetic energy of the flow decreases with the increase in *H/D*, causing the boundary layer to shift upstream on the cylinder. The flow separation is observed upstream on the cylinder, causing an increase in wake length.

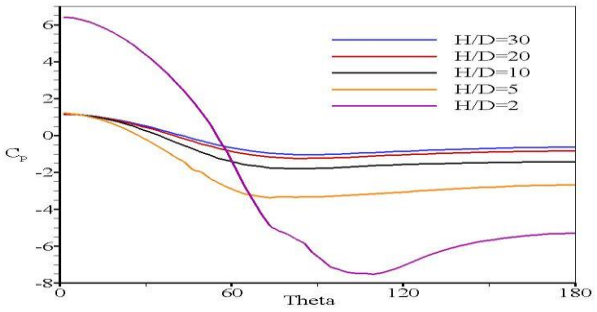

Figure 9: Pressure distribution on the cylinder surface for various channel heights at Re 40 obtained using 3D-PURLES.

The pressure distribution on the cylinder surface for various channel heights is presented in Figure 9, where non-dimensional surface pressure, C_p is plotted against angle measured clockwise from the forward stagnation point. The figure clearly shows considerable increased pressure on the front face when the channel height is small. The pressure falls very fast between *H/D* = 30 and 10. The results show that the wall proximity effects are most significant for normalized channel height *H/D*<20. Above this value, the blockage effect on pressure and drag become relatively less effective.

3.2 Flows at Reynolds number 40: Parabolic flow profile.

In the present section, simulations have been carried out with a parabolic flow profile ($u_{in}=u_0[1-4(y/H)^2]$) at the inlet as shown in figure 1(b).The observed flow and wake characteristics are different from those of the uniform flow profile to a significant extent. with H/D =2 as the lowest and H/D = 30 as the highest. Figure 10 shows the streamlines of the flows for various channel heights using 3D-PURLES. At a low value of *H/D* =2, the pair of symmetric vortices are compressed and wake length is shorter when compared to the case of uniform flow profile for the same value of *H/D*. An increase in wake length is observed as the walls mover farther away. However the non-dimensional wake length for a parabolic inlet profile is shorter by a significant extent when compared to wake length of uniform flow profile for similar *H/D* values. The difference between the wake lengths tend to vanish for a value of *H/D* greater than 10.

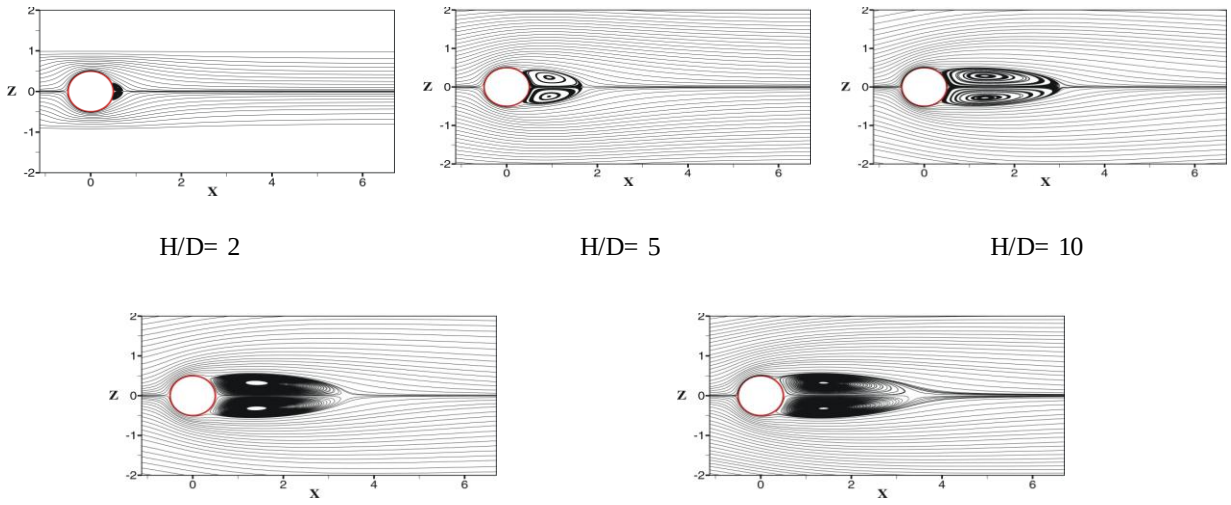

H/D= 2 H/D= 5 H/D= 10

H/D= 20 H/D= 30

Figure 10: Velocity contours at Re 40 obtained using 3D-PURLES

The pressure distribution on the cylinder surface for various channel heights is presented in Figure 11, where non-dimensional surface pressure, C_p is plotted against angle measured clockwise from the forward stagnation point

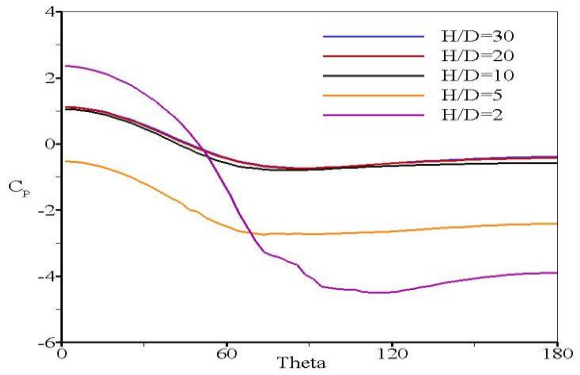

Figure 11: Pressure distribution on the cylinder surface for various channel heights at Re40 obtained using 3D-PURLES.

A short non-dimensional wake length of 0.21 and a high drag coefficient of 2.32 is observed at *H/D*= 2. At a higher value of *H/D* = 30, the flow around the cylinder behaves as an unconfined flow, resulting in an increased wake length of 2.77 and a reduced drag coefficient 1.62. The reasons for such variation between uniform and parabolic flow in terms of wake length and drag coefficient are unknown to the author and need to be investigated.

4. Conclusion.

The flow past a circular cylinder symmetrically in a channel is simulated with a primitive variable based second order accurate, structured grid, finite column collocated Navier-Stokes solvers (3D PURLES and OpenFOAM). The cylinder diameter based Reynolds number is 40 with the normalized channel height H/D varying from 10 to 30. Wall proximity is found to have considerable influence on the location of the separation points and length of the closed re-circulating zones in both cases i.e., Uniform flow profile and Parabolic flow profiles. The separation points are found to move rearward resulting in a shorter wake with decreasing channel height only up to a certain limit. Beyond *H/D* = 9, the wake length increases as the walls go farther. The coefficients of drag and lift keep changing based on wall proximity. The value of Cd increases as the walls come closer. Being a steady case and of a non rotating cylinder, the value of Cl is almost zero. The change in the flow structure is mainly attributed to the high energy fluid passing above and below the cylinder due to blockage effect and interacting of tunnel wall vortices with the cylinder vortices. In the end, the computational results obtained from 3D-PURLES and OpenFOAM are comparable to a significant extent.

References

[1] Buresti, G., Lanciotti, A., Vortex shedding from smooth and roughened cylinders in cross-flow near a plane surface. The Aeronautical Quarterly 30(1979), pp305-321.

[2] Price,S.J., Summer, D., Smith, J.G., Leong, K., Paidoussiss,M.P.,Flow visualization around a circular cylinder near to a plane wall. In proceedings of the Seventh International Conference on Flow-Induced Vibration.,(2000),pp105-114.

[3] Sahin, M., Owens, R.G., A numerical investigation of wall effects up to high blockage ratios on two-dimensional flow past a confined circular cylinder.,16(2004), pp1305-1320

[4] Majumdar, S., Pressure based finite volume method for computation of viscous flows, Computational and Theoretical Fluid dynamics Division, National Aerospace Laboratories, Bangalore.

[5] Singha, S and Sinhamahapatra, K.P, Flow past a circular cylinder between parallel walls at low Reynolds numbers, J.Ocean engineering, 37(2010), pp.757-769

[6] Zovatto, L., Pedrizzetti, G.,. Flow about a circular cylinder between parallel walls. Journal of Fluid Mechanics 440(2001), pp.1-25.

Behaviour of Reinforced Concrete Slab Subjected To Fire

Mr. C Sangluaia [1], Mr. M K Haridharan[2], Dr. C Natarajan[3], Dr. A. Rajaraman[4]

[1] M Tech Scholar, National Institute of Technology, Thiruchirappalli, India ,
[2]PhD Scholar, National Institute of Technology, Thiruchirappalli, India,
[3]Professor, National Institute of Technology, Thiruchirappalli, India
[4]Former Visiting Professor, Indian Institute of Technology, Madras, India

Abstract

The behavior of reinforced concrete slab exposed to fire is presented. Two stages of analysis is carried out using Finite Element package ABAQUS to find thermal response of structural members namely thermal analysis and structural analysis. In the first step, the distribution of the temperature over the depth during fire is determined. In the next step, the mechanical analysis is made in which these distributions are used as the temperature loads. The responses of structure depend on the type of concrete and the interactions of structural members. The RCC slab were modeled to show the role of slab thickness, percentage of reinforcement, width of slab and different boundary condition when expose to fire loading. Effects for both materials in RCC slab at elevated temperatures are also evaluated.

Keywords: ABAQUS, Concrete, Fire, Floor slabs, Modeling, Structural response, Thermal response.

1. Introduction

Fire is considered one of the most serious potential risks for buildings and structures. But concrete is generally considered to have an acceptable resistance to fire in comparison with other construction materials such as wood or steel. When concrete remains exposed for long time to high temperatures, mechanical losses of its properties take place. Laboratory experiences show that in case of concrete not protected the mechanical properties decrease drastically for temperatures above 300ºC. They are attributed to the microstructure transformations occurring in cement paste and aggregates, and the volume changes induced by thermal stresses. After fire the assessment of deterioration of the structure is needed in order to identify the level of damage induced by the chemical transformation and the cracking, both contributing to losses in mechanical strength.The behaviour of structures exposed to fire is usually described in terms of the concept of fire resistance, which is the period of time under exposure to a standard fire time-temperature curve at which some prescribed form of limiting behaviour occurs. In real buildings structural elements form part of a continuous assembly, and building fires often remain localized, with the fire-affected region of the structure receiving significant restraint from cooler areas surrounding it. The real behaviour of these structural elements can therefore be very different from that indicated by standard furnace tests.
When concrete is under fire, it usually causes a build-up of pressure within the concrete after exceeding 100^0C.When the temperature reaches about 400 °C, the calcium hydroxide in the cement will begin to dehydrate, generating more water vapour and also bringing about a significant reduction in the physical strength of the material [1]. The material behavior during heating is nonlinear itself according to its deterioration with temperature [2]. Most real fires heat the floor and beams from below, leading to a regime in which temperature differentials develop between the upper and lower surfaces. These differentials lead to thermally induced bending or thermal bowing, which can increase deflections. High temperatures will result in loss of strength (both yield and ultimate strengths) and stiffness (moduli of elasticity) [3]. Whilst material degradation is the key phenomenon in determinate structures under fire, for highly redundant structures the single most important factor is the effect of thermal expansion [3].

2. Mechanical Behaviour of The Constituent Materials

2.1 General

Constitutive laws are used to define the stress–strain characteristics of a material. The accuracy of the analysis is dependent on the constitutive laws used to define the mechanical behaviour. In materials such as concrete, structural steel and reinforcing steel, profiled steel sheeting and shear connectors, the constitutive laws are represented by the stress–strain relationships of the materials. In this paper, the mechanical behaviour at ambient and elevated temperatures is considered. When elevated temperature is involved, the main properties required to carry out an accurate calculation of the temperature distribution in a composite cross-section are the specific heat, thermal expansion and thermal conductivity.

2.2 Thermal properties of concrete: An important design consideration for concrete includes the effects of fire. The behaviour of concrete slabs subjected to fire conditions is complex. In a fully developed fire, to prevent fire spread to the upper floors, the slab has to carry and withstand the applied loads and prevent collapse during and after the fire. The effect of fire, which is not generally considered in typical structural design practice, involves the thermal conductivity, specific heat

and high thermal expansion of the concrete. This will cause the surrounding structure to respond against these effects and generate compressive forces in the heated concrete slab.

2.2.1 Thermal conductivity. Thermal conductivity is the capability of a material to conduct heat, and is defined as the ratio of heat flux to the temperature gradient. It represents the uniform flow of heat through concrete of unit thickness over a unit area subjected to a unit temperature difference between the two opposite faces [6]. The thermal conductivity of siliceous aggregate concrete as represented in Eurocode 2, British Standards Institution in section 3.3.3 is shown in Fig 1.

2.2.2 Specific heat. The specific heat of a material is the amount of heat per unit mass which is required to change the temperature of the material by a degree. The specific heat of concrete with siliceous aggregates as a function of temperature according to Eurocode2, British Standards Institution in section 3.3.2 is shown in Fig. 2.

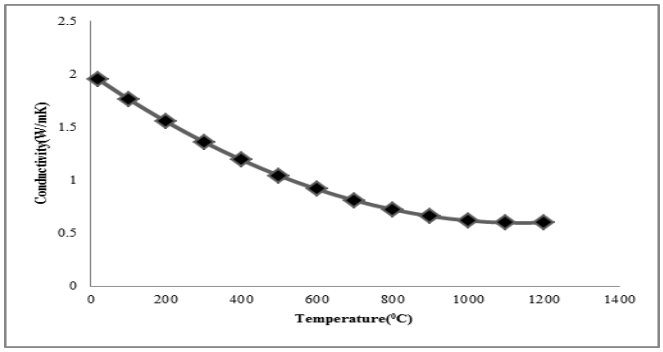

Fig. 1 Thermal conductivity of concrete, EC2 [4]

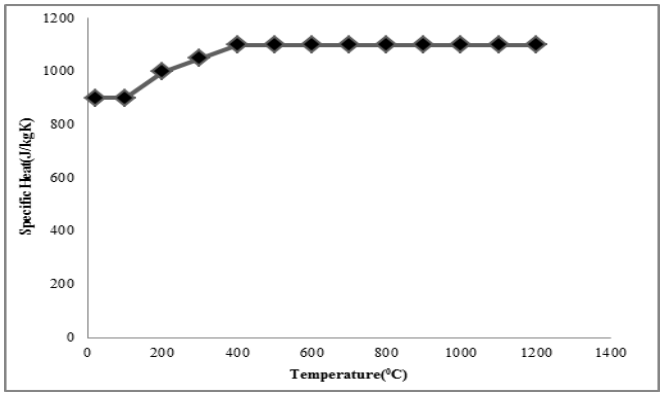

Fig. 2 Specific heat of concrete, EC2 [4]

2.2.3 Thermal expansion. Due to its isotropic nature, concrete exhibits thermal expansion when it is subjected to a temperature change. Cracking occurs when stresses develop in concrete structures due to non-uniform thermal expansion. The thermal expansion of concrete with siliceous aggregates expressed as a function of temperature according to Eurocode 2, British Standards Institution in section 3.3.1 is shown in Fig. 3

2.2.4 Stress–strain relationship of concrete at elevated temperatures. The most substantial consequence of fire on a concrete slab is the stiffness and strength degradation which may lead to eventually collapse. It is important to study the concrete property changes according to temperature. The stress–strain relationship of concrete with siliceous aggregates expressed as a function of temperature according to Eurocode 2, British Standards Institution and the distributions given in Figs. 5 and 6 represent the compressive and tensile stress–strain behaviour of the concrete, respectively. Fig. 4 illustrates that the compressive strength of the concrete decreases when temperature increases but the ultimate strain of the concrete increases with temperature. The tensile strength of the concrete also decreases with an increase in temperature, as depicted in Fig. 5. A tensile stress can also be obtained for temperatures up to 500^0C. The modulus of elasticity of the concrete in Fig. 6 decreases with an increment in temperature. The reduction of the modulus of elasticity is due to the rupture of bonds in the microstructure of the cement paste when the temperature increases and is the result of the onset of rapid short-term creep.

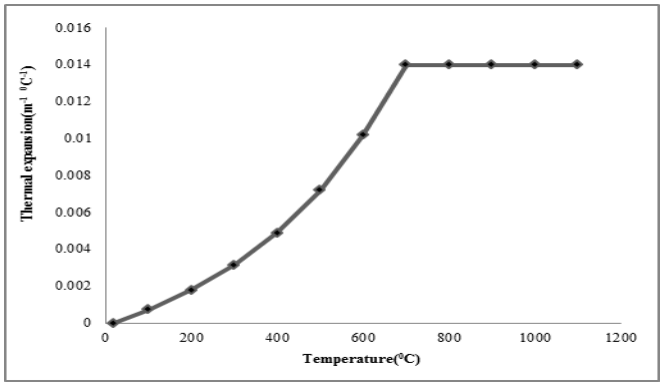

Fig. 3 Concrete thermal expansion, EC2 [4]

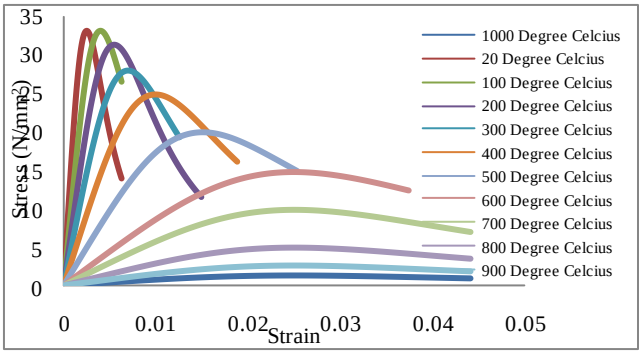

Fig. 4 Compressive stress–strain relationship at elevated temperature for concrete, EC2

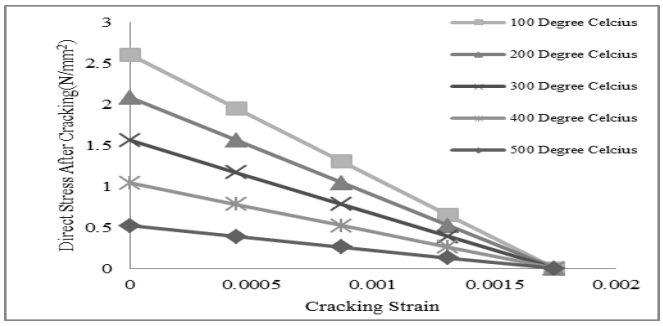

Fig. 5 Tensile stress–strain relationship at elevated temperature for concrete, EC2

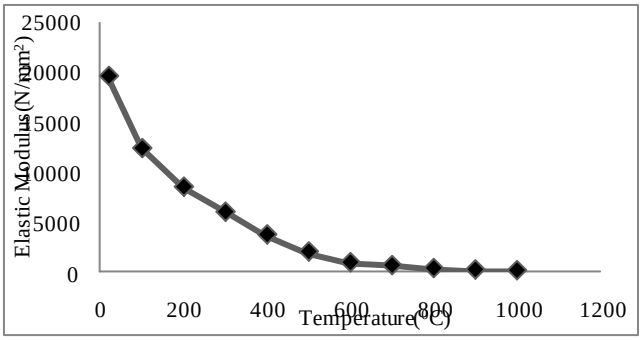

Fig. 6 Modulus of elasticity of structural concrete at elevated temperatures, EC2.

2.3 Thermal properties of steel

The stress–strain characteristics of reinforcing steel are essentially similar to structural steel. Their behaviour is initially elastic after which yielding and strain hardening develops. A piecewise linear approach was found to be sufficiently accurate to represent the stress–strain relationship. Moreover, these curves are utilized in the model when the stress–strain data is not available. The stress–strain relationship for structural steel is represented as a simple elastic–plastic model with strain hardening. The mechanical behaviour for both compression and tension is assumed to be similar. Fig. 10 represents the stress–strain relationship for steel. The effects of thermal conductivity, specific heat and high thermal expansion of the reinforcing steel are considered when the temperature changes.

2.3.1 Thermal conductivity. The thermal conductivity of steel depends mainly on the amount of alloying elements and on the heat treatment. The thermal conductivity of steel according to Eurocode 3, British Standards Institution in section 3.4.1 .3 is presented in Fig. 7

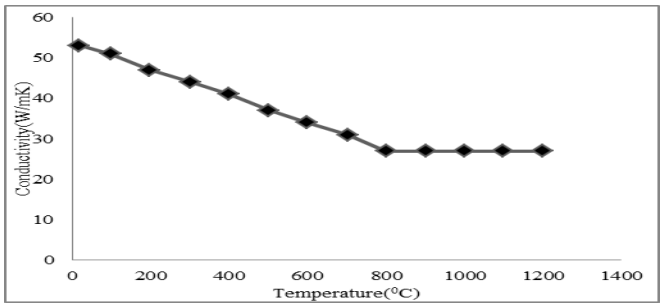

Fig. 7 Thermal conductivity for structural steel, EC3.

2.3.2 Specific heat. The specific heat of the steel is expressed in Eurocode 3, British Standards Institution in section 3.4.1.2 and is shown in Fig. 8

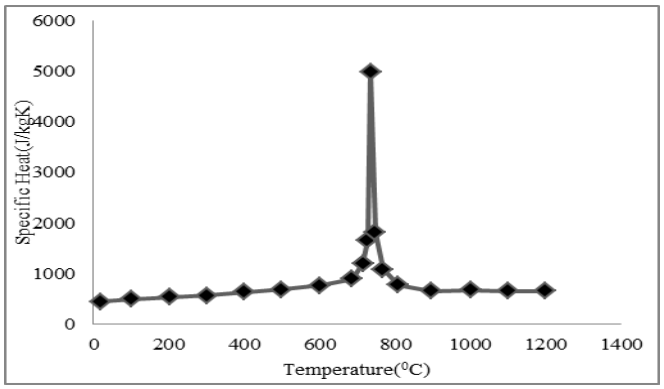

Fig. 8 Specific heat of structural steel, EC3.

2.3.3 Thermal expansion. The thermal expansion of steels depends mainly on the heat treatment used. The coefficient of thermal expansion of steel at room temperatures is expected to be $11{:}4x10^{-6}$ m^{-1} C^{-1}. Furthermore, the thermal elongation of structural and reinforcing steel according to Eurocode 3, British Standards Institution is evaluated in section 3.4.1.1 and is illustrated in Fig. 9

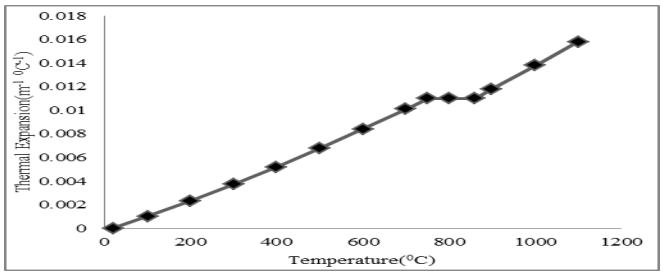

Fig. 9 Specific heat of structural steel, EC3.

2.3.4 Stress–strain relationship of reinforcing steel at elevated temperatures. Most normal constructional steels have well-defined yield strengths at normal temperatures. Upon further temperature increase, the ultimate strength of the steel declines steadily. The stress–strain relationships may be applied to steel in both tension and compression. The effects of high temperature on creep have also been taken into account. The stress–strain relationships of structural steel as a function of temperature according to Eurocode 3, British Standards Institution are shown in Fig. 10.The ultimate strength of the structural steel decreases when the temperature increases, as illustrated. Furthermore, the modulus of elasticity decreases with an increase in temperature. The relationship of the modulus of elasticity of the structural steel according to temperatures is illustrated in Fig. 11.

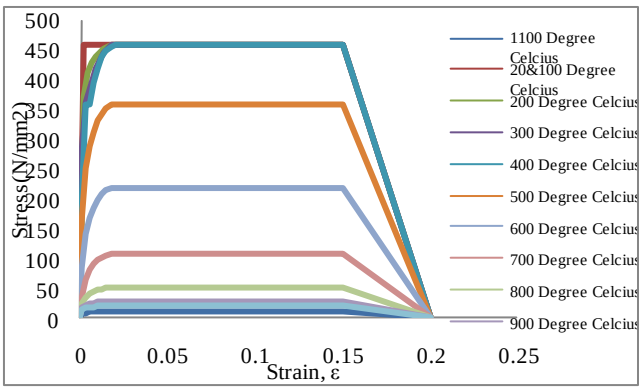

Fig. 10 Stress–strain relationship at elevated temperature for structural steel, EC3.

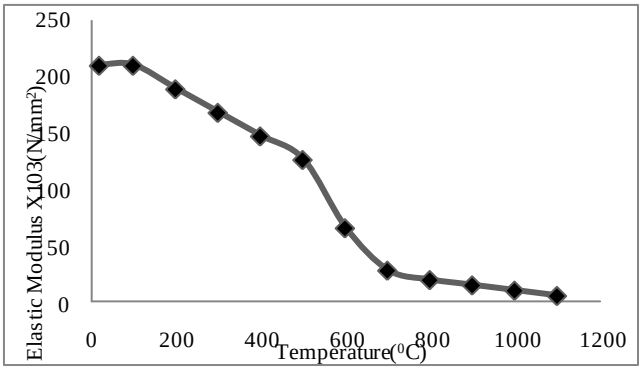

Fig. 11 Modulus of elasticity of structural steel at elevated temperatures, EC3.

3. Finite Element Analysis at Elevated Temperatures

Finite element package ABAQUS was used to model and analyze the RCC slabs. Dynamic temperature displacement explicit analysis was performed to input the temperature distribution obtained from thermal analysis to the structure analysis so as to obtain the required stress, strain and displacement.

3.1 Experimental Tests

Experimental results were taken from the test conducted by BRE (Building Research Establishment) slab test on RCC in Cardington, Bedford. The tests were made in the fire resistance floor furnace at the Warrington Fire Research Centre [6] heated under ISO-834 curve shown in Fig 1. The slab is design to resist up to 90 minutes. The ends of each slab were simply supported

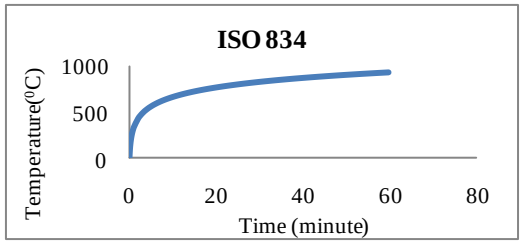

Fig. 12 ISO-834 Fire standard curve (BS 456 part 20) [6]

3.2 Finite Element Type and Mesh

Three-dimensional solid element and surface element were used to model the test specimen in order to achieve an accurate result from the finite element analysis. For concrete, C3D8RT- An 8-node thermally coupled brick, tri-linear displacement and temperature was used and for steel, SFM3D4R- A 4-node quadrilateral surface element, reduced integration was used.

3.3 Model Validation

For validating the existing experimental test result by using ABAQUS, the modeling of slab is shown Fig. 12. RCC slab are heated from below by ISO-834 fire. In ABAQUS, the RCC slab model is heated up to 90 minutes as the slab is design to resist up to 90 minutes .Two stage analysis is carried out that is thermal and structural analysis. The analysis results are compared with experimental results.

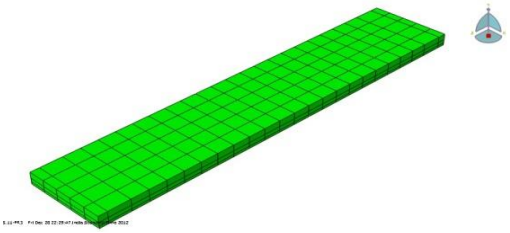

Fig 13 Slab Modeling of RCC by ABAQUS

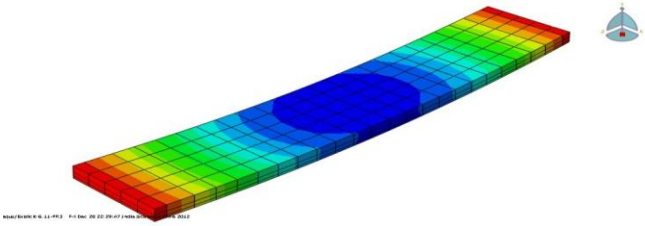

Fig 14 RCC slab model showing displacement contour by ABAQUS after temperature loading.

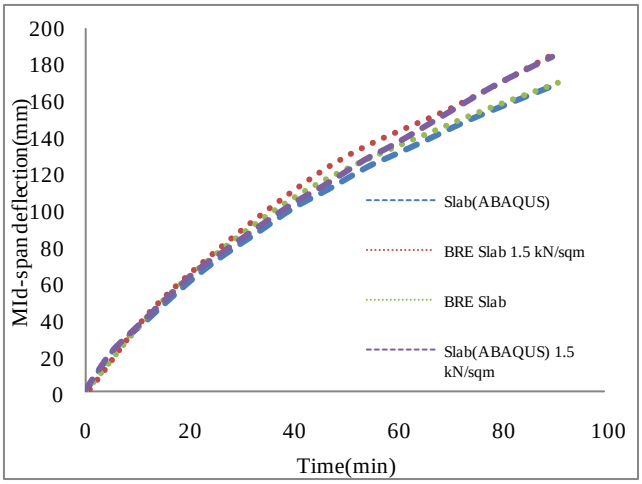

Fig. 15 Comparison of 150mm BRE slab with ABAQUS model, Mid-span deflection with Time

4. Result and Discussion

4.1 General

RCC models are taken to study the thermal response of building subjected to fire. Non-linear analysis is carried out with full temperature on different boundary condition. Similarly non-linear analysis is carried out on different bars and different thickness. It is modeled in three dimensional for temperature-time curve ISO-834. ABAQUS/CAE 6.11 has been used for the analysis of thermal and structural behaviour of concrete structures for different temperature. Thermal analysis is done based on steady state condition in three dimensional members.

4.2 Temperature Analysis

Table 1 Specification of slab for studying temperature distribution

Span	4.5 m
Width × Depth	925 mm × 150 mm
Temperature	ISO-834 Curve
Concrete grade	M30

The temperature analysis is performed independently of the structural analysis. To perform the temperature analysis, the geometry of the cross-section is similar to the structural analysis specimen. Conversely, its material properties are defined in chapter 3 for concrete and structural steel, respectively. The materials in the section can vary from element to element, and their properties are temperature dependent. The mechanical behaviour is much more complicated when the temperature changes because there are two materials involved, which are mainly concrete and steel. The test specimen model is similar to the structural analysis model in order to compare the results. Fire is usually represented by a temperature–time curve ISO-834 fire (BS 456 part 20) [8] in Fig 12. This gives the average temperature reached during a fire in a small sized compartment or in the furnaces used for fire resistance tests

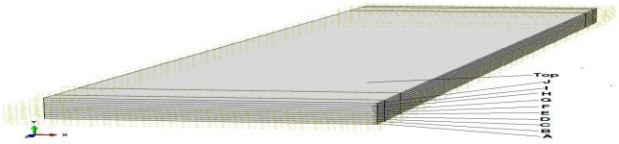

Fig. 16 Different layers of the slab

The resulting temperature distributions have been adopted here for the application of the finite element ABAQUS analysis. Fig. 16 show that the concrete & reinforcing steel are divided into layers which is necessary to differentiate the temperature distributions according to time. Fig 17 provides the temperature distribution of the layers with respect to time

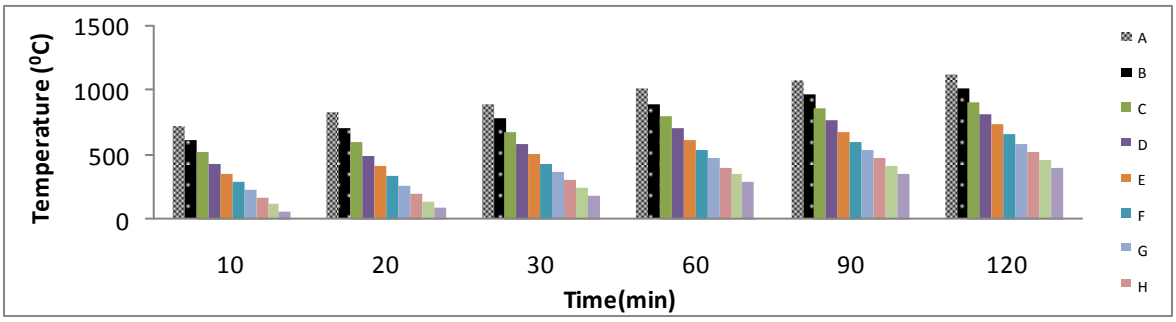

Fig. 17 Temperature changes according to time

4.3 Analysis

ABAQUS/CAE 6.11 has been used for the analysis of thermal and structural behaviour of concrete structures for different temperature. Thermal analysis is done based on steady state condition in three dimensional members. Temperature distribution is found in thermal analysis and by using the thermal result in structural static analysis.

4.3.1 Role of width of slab

For studying the role of width in slab two thickness of slab are studied (i.e. 150mm and 180mm

Table 2 Specification of slabs for studying role of width of slab

Span	4.5 m
Live Load	1.5 kN/m^2
Width	9m, 4.5m, 3m & 2.25m
Slab thickness	150 mm & 180 mm
Rebar	8mm dia
Temperature	ISO-834 fire
Support condition	Simply supported on two side Free on the other two side

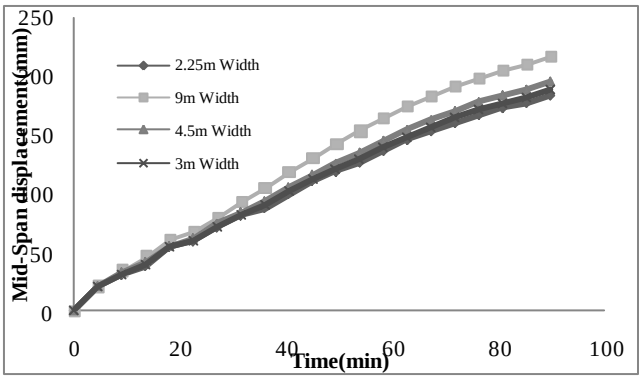

Fig. 18 Effect of 150mm thick slab, 4.5m span c/c with LL

For studying the role of width of slab, RCC slab model are analyzed by using thickness as 150mm thick slab with load of 1.5kN/m^2 with different width i.e. 9m, 4.5m, 3m, 2.25m. The mid-span deflection vs. time are given in Fig. 18 in which after 90minutes of fire exposure, slab with 9m, 4.5m, 3m, 2.25m thickness have mid-span deflection of 217mm,196mm,188mm & 183mm. The allowable temperature is then calculated from the allowable deflection as 518^{0}C, 520^{0}C, 523^{0}C & 527^{0}Cfor 9m, 4.5m, 3m, 2.25m width slab.Another RCC slab model are analyzed by using thickness as 180mm thick slab with load of 1.5kN/m^2 with different width i.e. 9m, 4.5m, 3m, 2.25m. The mid-span deflection vs. time are given in Fig. 19 in which after 90minutes of fire exposure, slab with 9m, 4.5m, 3m, 2.25m thickness have mid-span deflection of 173mm,163mm, 158mm & 153mm. The allowable temperature is then calculated as 550^{0}C, 560^{0}C, 580^{0}C & 614^{0}C for 9m, 4.5m, 3m, 2.25m width slab

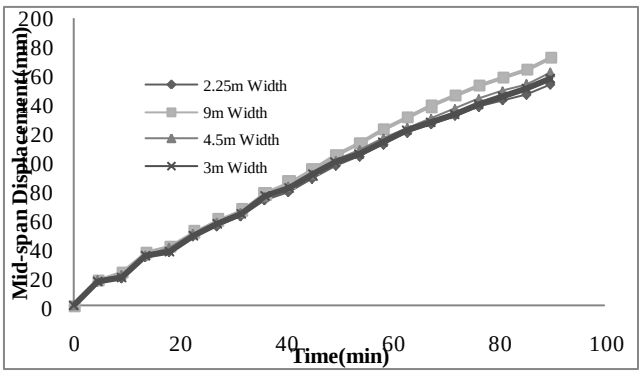

Fig. 19 Effect of 180mm thick slab, 4.5m span c/c with LL

Fig. 18 & Fig 19 shows the effect of 150mm and 180mm slabs with different width 9m, 4.5m, 3m, 2.25m for normal weight concrete slabs, when exposed to ISO 834.the deflection is highest in 9m width and followed by 4.5m & 3m and lowest in 2.25m width. This shows that the larger width of the slab deflects less, which shows that thermal bowing is inversely proportional to the width for simply supported slab.

4.3.2 Role of rebar in slab

Table 3 Specification of slabs for studying role of rebar in slab

Span	4.5 m
Live Load	1.5 kN/m^2
Width	4.5m
Slab thickness	150 mm
Rebar	6mm, 8mm, 10mm dia
Temperature	ISO-834 fire
Support condition	Simply supported on two side Free on the other two side

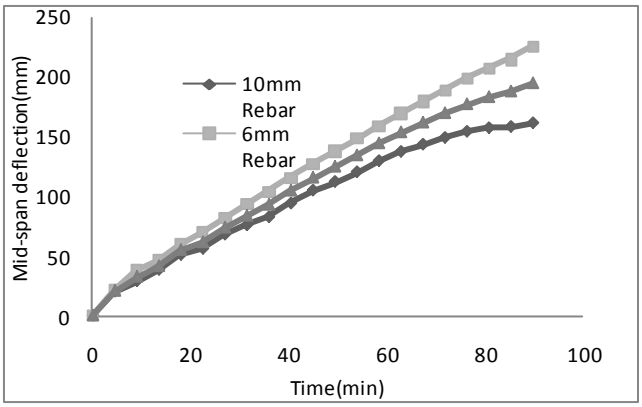

Fig. 20 Effect of 150mm thick slab, 4.5m span c/c, 4.5m width with LL

For studying the role of rebar, first 3 RCC slab model are analyzed by giving load 1.5 kN/m^2 with different rebar i.e. 6mm, 8mm & 10mm rebar. The mid-span deflection vs. time are given in Fig. 20 in which after 90minutes of fire exposure, slab with 10mm,8mm & 6mm rebar have mid-span deflection of 162mm,195mm &225mm. The allowable temperature is then calculated from the allowable deflection as 524^{0}C, 520^{0}C, 516^{0}C for 10mm, 8mm, 6mm rebar.

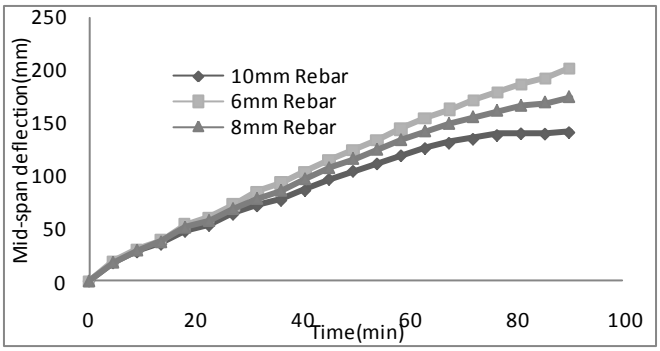

Fig. 21 Effect of 150mm thick slab, 4.5m span c/c, 4.5m width without LL

For studying the role of rebar, another 3 RCC slab model are analyzed without giving load (.i.e. with only self-weight load) with different rebar i.e. 6mm, 8mm & 10mm rebar. The mid-span deflection vs. time are given in Fig. 20 in which after 90minutes of fire exposure, slab with 10mm,8mm & 6mm rebar have mid-span deflection of 141mm,174mm &202mm. The allowable temperature is then calculated from the allowable deflection as 546.7^{0}C, 540^{0}C, 536^{0}C for 10mm, 8mm, 6mm rebar. Fig. 20 & Fig 21 shows the effect of 6mm, 8mm and 10mm rebar 150mm slabs with live load and without live load with 4.5m width for normal weight concrete slabs, when exposed to ISO 834.The deflection is highest in 6mm diameter bar and followed by 8mm & 10mm diameter bar. Therefore, Fig. 19 & Fig. 20 clearly shows that increase in percentage of steel in RCC slab decreases the deflection when subjected under fire.

4.3.3 Role of slab thickness

Table 4 Specification of slabs for studying role of slab thickness

Span	4.5 m
Live Load	1.5 kN/m^2
Width	4.5m
Slab thickness	150mm, 180mm & 250mm
Rebar	8mm dia
Temperature	ISO-834 fire
Support condition	Simply supported on two side Free on the other two side

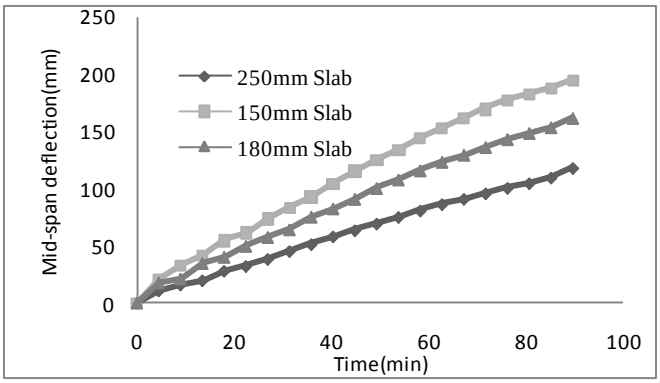

Fig. 22 Effect of slab, 4.5m span c/c, 4.5m width with rebar & LL

For studying the role of slab thickness by ABAQUS, RCC slab model are analyzed by giving load 1.5kN/m^2 with different thickness i.e. 150mm, 180mm & 250mm. The mid-span deflection vs. time are given in Fig. 22 in which after 90minutes of fire exposure, slab with 150mm, 180mm & 250mm thickness have mid-span deflection of 196mm,163mm &119mm. The allowable temperature is then calculated as 520^{0}C, 560^{0}C, 660^{0}C for 150mm, 180mm & 250mm thick slab.

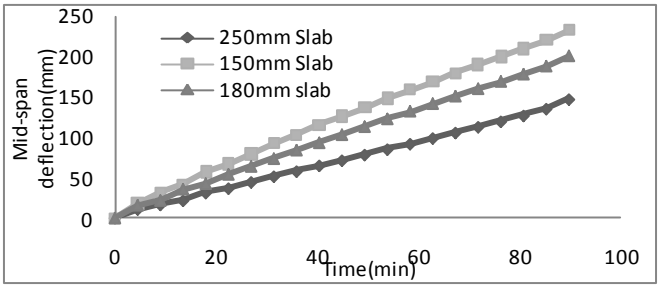

Fig. 23 Effect of slab, 4.5m span c/c, 4.5m width without rebar & LL

Here, RCC slab model are analyzed without giving load and without rebar in slab and with different thickness i.e. 150mm, 180mm & 250mm. The mid-span deflection vs. time are given in Fig. 22 in which after 90minutes of fire exposure, slab with 150mm, 180mm & 250mm thickness have mid-span deflection of 234mm,201mm &147mm. The allowable temperature is then calculated as 541^{0}C, 585^{0}C, 664^{0}C for 150mm, 180mm & 250mm thick slab without rebar.Fig. 22 & Fig. 23 show the effect of slab thickness with rebar and live load & without rebar and live load, when exposed to ISO 834. The thicker slab deflects less which is what one might expect intuitively and agrees with the theory of thermal bowing which shows that thermal bowing is inversely proportional to the slab thickness. The defection curve for the non-loaded 180mm thick slab suggests that the relative magnitudes of deflection agree with the theory of thermal bowing up to 90 min the curve for 180mm thickness lies between those for 150 and 250 mm.

4.3.4 Role of boundary condition

Table 5 Specification of slabs for studying role of boundary condition

Span	4.5 m
Live Load	1.5 kN/m^2
Width	4.5m
Slab thickness	150 mm
Rebar	8mm dia
Temperature	ISO-834 fire
Support condition	Pinned-pinned, Pinned-roller, fixed-fixed, fixed roller on two side & Free on the other two side

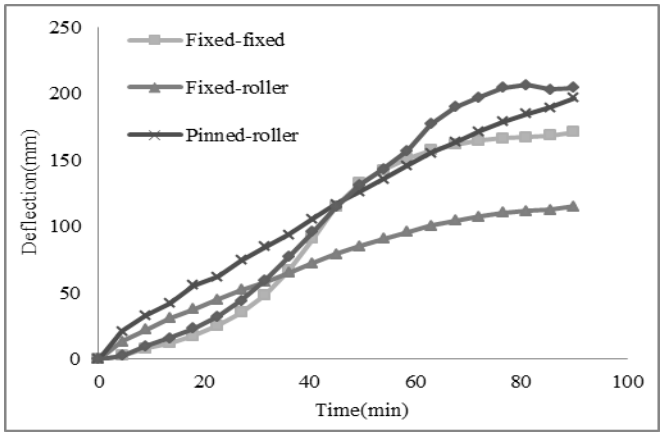

Fig. 24 Effect of slab on different boundary condition, 4.5m span c/c, 4.5m width with LL

Fig. 24 shows the effect of slab on different boundary condition with 1.5 kN/m^2 live load when exposed to ISO 834. Fixed-fixed and pinned-pinned have less deflection till 20 minutes and then suddenly increases. After exposure for 90 minutes, fixed-fixed, fixed-roller, pinned-roller, pinned-pinned have deflection of 171mm, 115mm, 196mm, 204mm. The safe temperatures are calculated from allowable deflection. Safe temperature for fixed-fixed, fixed-roller, pinned-roller, pinned-pinned are 748 ^{0}C, 604 ^{0}C, 541 ^{0}C, 717 ^{0}C.

5. Conclusions

- An accurate finite element model has been developed by using ABAQUS to study the behavior of reinforced concrete slab when subjected to fire. Based on the comparisons between the results obtained from the finite element models and available BRE slab experimental results, it was observed that they are in good agreement. The mid-span deflection with duration of heating is accurately predicted by the finite element model and a maximum discrepancy of 6% was observed when comparing the finite element model with experimental studies.
- Temperature distribution was studied for different layers of the slab along the depth of the slab when temperature changes according to time and it was found that temperature decreases along the depth of the slab
- Role of width of slab, role of rebar and role of slab thickness were also observed in this paper and it was found that
  - For simply supported slab , displacement increases when width of slab increases
  - Displacement decreases when percentage of steel in RCC slab increases
  - Displacement decreases when thickness increases
- Role of boundary condition were also observed and it was found that fixed-fixed have the highest safe temperature and followed by pinned-pinned, fixed-roller, pinned-roller.

References

[1]. Ian A. Fletcher, Stephen Welch, José L. Torero. Behaviour of Concrete Structures in Fire. BIBLID, 112: 37-52, 2007
[2]. Khoury, G. A. . Effect of Fire on Concrete and Concrete Structures. *Progress in Structural Engineering and Materials*, 2, 4: 429-447.2000
[3]. Rotter J.M, Sanad A.M.,Usmani A.S. and Gillie .M. Structural Performance Of Redundant Structures Under Local Fires In Proceedings of Interflam. Edinburgh, Scotland, 1999.
[4]. British Standards Institution. Design of concrete structures, Part 1.1 General rules and rules for buildings. London: British Standard Institute 2004. ENV 1992-1-1.
[5]. British Standards Institution. Design of the steel structures, Part 1.1 General rules and rules for buildings. London: British Standard Institute 2002. ENV 1993-1-1.
[6]. ISO Fire Resistance Tests. Elements of Building Construction, ISO 834, International Organization for Standardization. Geneva, 1975
[7]. ASTM Standards. Standard Test Methods for Fire Tests of Building Construction and Materials, in Annual Book of ASTM Standards. Vol. 04, Designation: E 119-88, ASTM, 922–942, 1988
[8]. Bailey C.. Holistic Behaviour of Concrete Buildings in Fire. Structures & Buildings, 152 : 199-212, 2002
[9]. Dhaval Vora, Umesh Kumar Sharma , Pradeep Bhargava. Finite Element Analysis Of Composite Columns Subjected To Fire. Journal of Structural Engineering, 37: 322 – 328, 2010.
[10]. Gordon M.E. Cooke. Behaviour of precast concrete floor slabs exposed to standardized fires. Fire Safety Journal, 36: 459-475. 2001.

[11]. Kang S.W. and Hong, S.G.. Material Model and Thermal Response Analysis of Concrete at Elevated Temperatures. Journal of the Korea Concrete Institute, 13: 268–276, 2001.
[12]. Kang, Suk Won, Hong, Sung-Gul . Behavior of Concrete Members at Elevated Temperatures Considering Inelastic Deformation. Fire Technology, 39:9–22, 2003
[13]. Kuldeep Prasad, Howard R. Baum . Coupled Thermal-Elastic Response of Structures to Fires Building and Fire Research Laboratory. National Institute of Standards and Technology Gaithersburg, MD 20899, 2006.
[14]. Li L, Purkiss J. Stress-Strain Constitutive Equations of Concrete Material at Elevated Temperatures. Fire Safety Journal, 40: 669-686, 2005.
[15]. Mirza O, B. Uy . Behaviour of headed stud shear connectors for composite steel–concrete beams at elevated temperatures. Journal of Constructional Steel Research, 65: 662–674, 2009.
[16]. Schneider U. Concrete at High Temperatures – A General Review. Fire Safety Journal, 13: 55-68, 1988.
[17]. Sebastjan Bratina, Bojan Cas, Miran Saje, Igor Planinc. Numerical modelling of behaviour of reinforced concrete columns in fire and comparison with Euro code 2. International Journal of Solids and Structures, 42: 5715–5733, 2005.
[18]. Terro, M. J. . Numerical Mod el ling of the Behaviour of Concrete Structures. ACI Struct Journal, 95: 183-93, 1998.
[19]. Usmani, A. S., Rotter, J. M., Lamont, S., Sanad, A. M., Gillie M. Fundamental Principles of Structural Behaviour under Thermal Effects. Fire Safety Journal, 36: 721-744, 2001.

Strength, Economic and Sustainability Characteristics of Coal Ash –GGBS Based Geopolymer Concrete.

Mr. Bennet Jose Mathew[1], Mr. M Sudhakar[2], Dr. C Natarajan[3]

[1]M Tech Scholar, National Institute of Technology, Thiruchirappalli, India
[2]PhD Scholar, National Institute of Technology, Thiruchirappalli, India,
[3]Professor, National Institute of Technology, Thiruchirappalli, India ,

Abstract
The need to reduce the global anthropogenic carbon dioxide has encouraged researchers to search for sustainable building materials. Cement, the second most consumed product in the world, contributes nearly 7% of the global carbon dioxide emission. Geopolymer concrete (GPC) is manufactured using industrial waste like fly ash, GGBS is considered as a more eco-friendly alternative to Ordinary Portland Cement (OPC) based concrete. The feasibility of production of geopolymer concrete using coarser bottom ash is evaluated in this study. Additionally, the effect of replacement of fly ash with bottom ash at varying percentage on strength of Geopolymer concrete is also studied. The effect of curing methodology on strength of fly ash-GGBS based geopolymer concrete has also been evaluated. Economic impact and sustainability studies were conducted on both OPC based concrete and geopolymer concrete. Comparison studies shows that geopolymer concrete can be prepared at comparable cost with that of OPC concrete while they offer huge reduction in carbon dioxide emissions.

Keywords: Geopolymer concrete, Sustainability, Green concrete, coal ash concrete, sustainability, waste materials, Cost analysis

1. Introduction

Concrete is the second most used material in the world after water. Ordinary Portland cement has been used traditionally as a binding material for preparation of concrete. Theworld-wide consumption of concrete is believed to rise exponentially primarily driven by theinfrastructural development taking place in China and India. 1 tone of carbon dioxide isestimated to be released to the atmosphere when 1 ton of ordinary Portland cement ismanufactured. Also the emission by cement manufacturing process contributes 7% to theglobal carbon dioxide emission [1]. It is important to find an alternate binder which has less carbon footprint than cement.

Geopolymer is an excellent alternative which transform industrial waste products like GGBS and fly ash into binder for concrete.The amorphous to semi-crystalline three dimensional silico-aluminate structures of the Poly(sialate) type (-Si-O-Al-O-) or of the Poly(sialate-siloxo) type (-Si-O-AI-O-Si-O-) were christened "geopolymers" by Davidovits[2].Al- Si materials which are used as source materials undergoes dissolutions, gel formation, setting and hardening stages to formgeopolymers[3]. The alumino silicate material used in this study is a combination of coal ash and ground granulated blast furnace slag (GGBS).

The final properties of geopolymer concrete is influenced by large number of factors like curing temperature, water content, alkali concentration, initial solids content, silicate and aluminate ratio, pH and others [4].Research into fly ash based geopolymer concrete have found that it has higher high compressive strength, low drying shrinkage, low creep and good resistance against acid and sulphate attacks [5-8]. Geopolymer concrete cured at ambient temperature can be developed using a combination of coal ash and GGBS. Alkali activation of GGBS results in precipitation of Calcium-Silicate-Hydrate(CSH) gel for geopolymer concrete at 27^{o}C while if cured at 60^{o}C a combination of calcium-silicate-hydrate(CSH) and alumino–silicate–hydrate (ASH) gel is formed[9].This study aims to synthesize geopolymer concrete using combination of coarser bottom ash and GGBS. Fly ash was replaced in varying percentages by bottom ash to understand the effect on compressive strength. Cost and environmental impact using embodied energy is also discussed.

2. Properties Of Materials Used

The physical properties and chemical composition of materials as obtained by X-ray fluorescence (XRF) is shown in Table 1 and Table 2. Fly ash and bottom ash are having specific gravity of 2.05.The sieve analysis result for bottom ash is given in Figure 1. Locally available sand of specific gravity 2.63 was used for the study. Coarse aggregate (12mm) is of specific gravity 2.88. OPC 53 grade cement used is of specific gravity 3.13.

Table 1.Chemical composition of bottom ash and fly ash. (By mass percentage).

Oxide	SiO_2	Al_2O_3	Fe_2O_3	CaO	SO_3
Fly Ash	53.30	29.50	10.70	7.60	1.80
Bottom Ash	56.76	21.34	5.98	2.88	0.72

Table 2.Chemical composition of GGBS.

Oxide	SiO_2	Al_2O_3	FeO	CaO	MgO	Others
Mass Percentage (%)	35.47	19.36	0.8	33.25	8.69	3.25

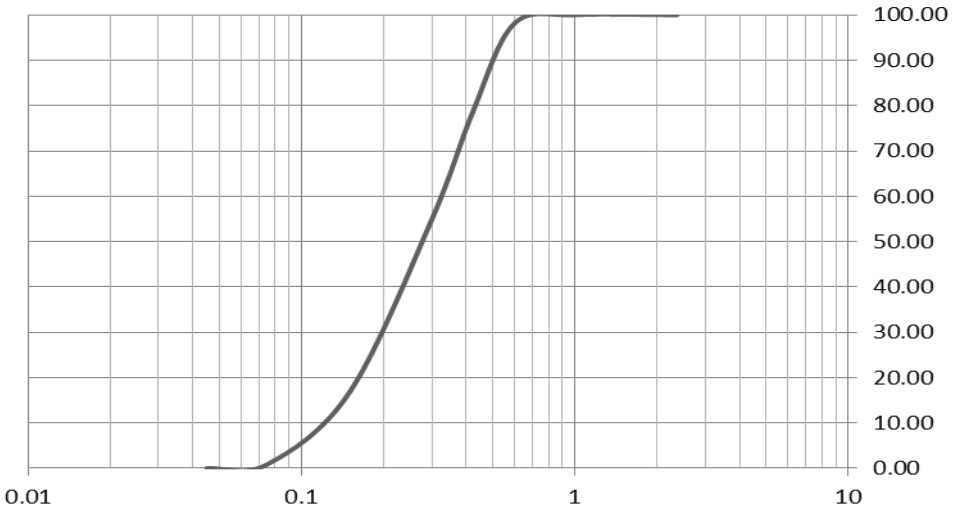

Figure 1.Particle size distribution of bottom ash.

A combination of 15 molar sodium hydroxide and sodium silicate in the ratio of 2.33 was used as solution for activation. Sodium hydroxide is of laboratory grade with purity of 97% and had a specific density of 2.13 g/cm^3. Sodium meta silicate also known as sodium silicate is of industrial grade with SiO_2 as 37.67% by mass and Na_2O as 35.67%. Water used for the mix is of potable quality.

3. Mix Proportions And Experimental Program

The proportions used in the mix were obtained after series of trial mixes. Various proportions used in the mix are given in Table 3. The term geopolymer solid mentioned in the table denotes all the solid particles in the binder like solids in activator solution, coal ash and GGBS.

Table 3. Various proportions by weight used in the mix.

Coal Ash: GGBS	Molarity of NaOH Solution	Na_2SiO_3 : NaOH	Activator: (Coal Ash + GGBS)	Water : Geopolymer Solid
75:25	15M	2.33	0.42	0.29

A total of five geopolymer mix was considered along with a standard OPC based M55 grade concrete (CM). Fly ash - GGBS and bottom ash - GGBS based geopolymer concrete mixes are manufactured separately. Additionally mixes were prepared by replacing fly ash with bottom ash in 10%, 20% and 30% replacement levels (by weight). OPC based concrete mix was designed as per IS 10262:2009[10]. Bottom ash-GGBS based geopolymer was casted assuming particles finer than 300 microns (58% by weight) takes part in the reaction and remaining replaces fine aggregate. Naphthalene sulphonate based superplasticizer was added to each mix (2% of (FA+GGBS) to improve workability.100mm cube specimens of each geopolymer concrete mix are cured at elevated temperature at 60^{o}C for 6 hours and then at 100^{o}C for 3 hours. Another set of specimens of each mixes are cured by air curing for 28 days. OPC based concrete is cured in both elevated and ambient temperature by respective standard practices. All specimens were casted in accordance with IS 516.

4. Experimental Results And Discussions

The strength of geopolymer concrete using fly ash is studied and effect of replacement on the strength of fly ash–GGBS based geopolymer concrete is discussed along with cost and environmental impact analysis.

4.1. compressive Strength

Fly ash based geopolymer concrete attained compressive strength of 68MPa while bottom ash based concrete attained only 32MPa. The low compressive strength is due to larger particle size in bottom ash. Larger particle size reduces the dissolution of bottom ash in activator solution and hence does not take part in the reaction.

Concrete cured at ambient temperature attained comparable strength with that of specimens cured at elevated temperatures. Thus curing at elevated temperature doesn't add much to the final strength of coal ash-GGBS based concrete. The experimental results are summarized in Figure 2.

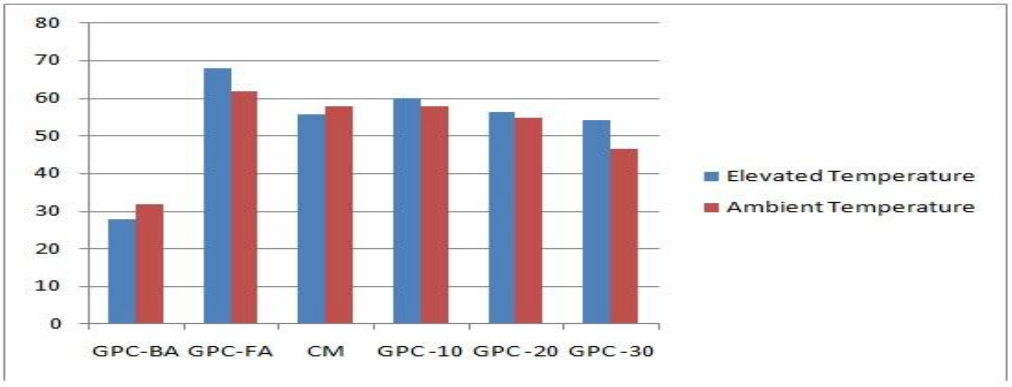

Figure 2. Average compressive strength of samples

4.2. Cost Analysis

Cement has a very effective hauling and transportation system in our country which makes its transportation cost less. GGBS and coal ash currently doesn't have such a system. To normalize this effect, the transportation of these materials are assumed to be in the same manner as cement. Standard freight charge from Indian Railway website is considered for this analysis. Local market price for NaOH and aggregates were considered in this study. The cost per quantity and total cost is mentioned in Table 4. Only fly ash-GGBS based concrete and OPC based concrete are used for this study.

Table 4. Cost and Energy per unit weight of materials.

Material	COST(Rs/kg)	Energy (MJ/kg)
GGBS	1.50	0.31
Fly Ash	1.00	0
Coarse Aggregate	0.43	0.10
Fine Aggregate	2.20	0.02
Water	0	0
NaOH	80.00	20.50
Sodium Silicate	10.00	5.37
Cement	7.00	4.53

The total cost of geopolymer concrete (Rs 5611.54) is 7% more than OPC based concrete (Rs 5207.65). This reduced cost is mainly due to the assumptions made for the transportation of coal ash, GGBS and sodium silicate. Without normalizing the fly ash and GGBS transportation cost, price of geopolymer based concrete will be more than twice that of OPC based concrete.

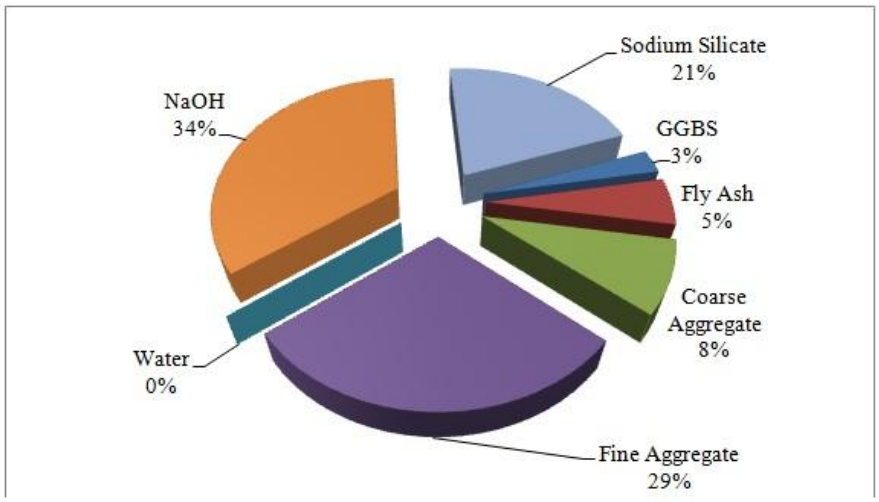

Figure 3. Cost contribution of each material to fly ash-GGBS based geopolymer concrete.

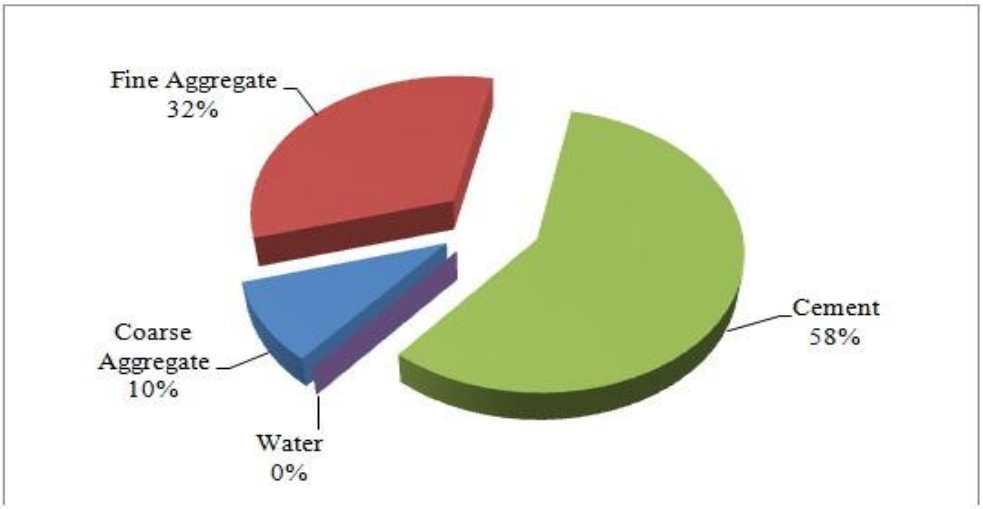

Figure 4. Cost contribution of each material to of OPC based concrete

Studies have to be made in the area of manufacturing process of sodium hydroxide so as to make its cost less. The fine aggregate cost can be minimized by using alternate materials like crusher dust. However, the impact of using such materials on the strength of concrete has to be studied.

4.3. Sustainability

This study considers only the embodied energy consumed in the production of basic building materials. In India 90% of the cement is manufactured by dry processes (4.2MJ/kg) and remaining by more energy intensive wet Process (7.5MJ/kg).(TERI 2004 and Venkatarama Reddy &Jagadish,2001[11]).Therefore, for cement embodied energy is taken as 4.53MJ/kg by weighted average. Fly ash and GGBS are waste products from industry. The embodied energy of fly ash is zero as collection of fly ash from flue gas is mandatory in India. GGBS will have to be grinded after quenching. Therefore am embodied energy of 0.31MJ/kg (6-7% that of cement) have been considered.The embodied energy of sodium hydroxide is 20.5MJ/kg as per SPLINE LCI datasheet. The embodied energy of sodium silicate shall be taken as 5.37 MJ/kg. (Fawer et al 1999)[12].Embodied energy of fly- ash GGBS based geopolymer concrete is found to be 1265.73 MJ and that of OPC based concrete is calculated as 2083.33 MJ.

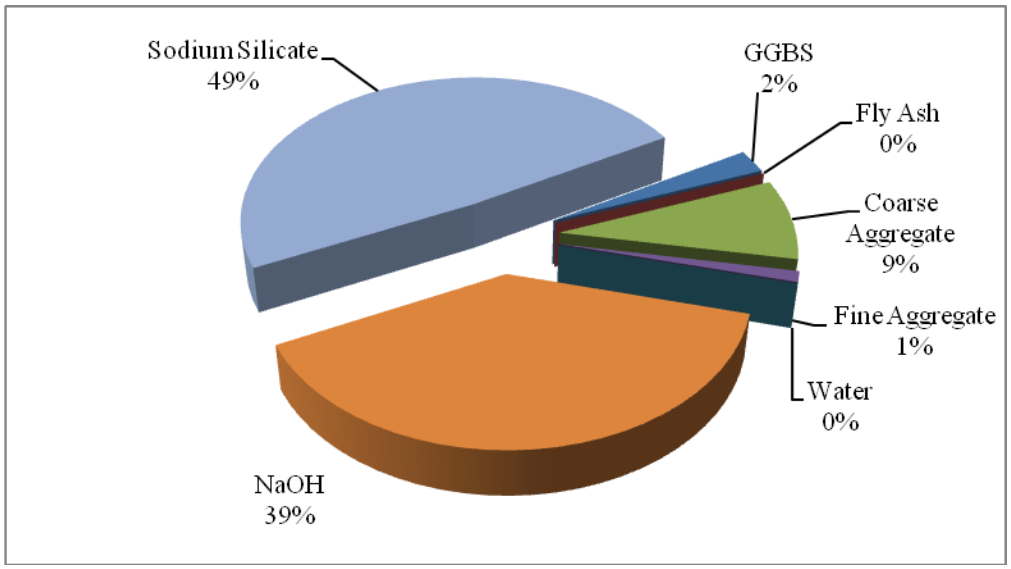

Figure 5. Embodied energy contribution of each material on fly ash-GGBS based geopolymer concrete.

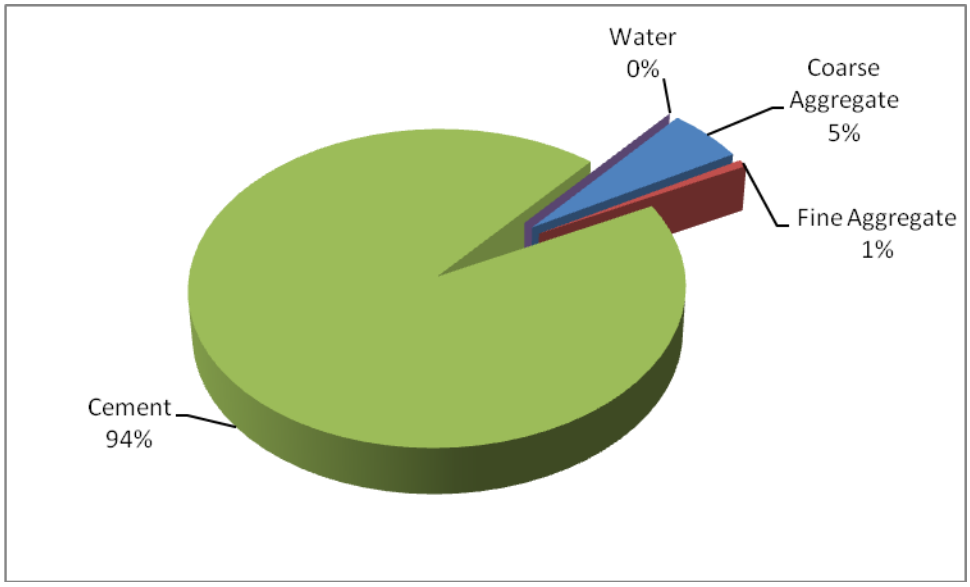

Figure 6. Embodied energy contribution of each material on OPC concrete.

The contribution of sodium silicate and sodium hydroxide to the embodied energy of geopolymer concrete is very high. Manufacturing processes of these materials for large scale production must be redesigned so as to reduce the embodied energy. High energy in sodium silicate is due to melting and drying process involved during its manufacturing.

5. Conclusion

The following are the conclusions obtained after the study

- Curing at elevated and ambient temperature will form fly ash-GGBS based concrete of comparable strengths.
- Bottom ash –GGBS based geopolymer concrete gives very low strength probably due to large particle size.
- Geopolymer concrete can be prepared at comparable cost with OPC based concrete provided transportation system for raw materials is well established.
- The embodied energy of fly ash- GGBS based geopolymer concrete is 40 % less than that of OPC based concrete.

- Sodium hydroxide (39%) and sodium silicate (49%) together contributes a lion's share to embodied energy of geopolymer concrete while in OPC cement contributes nearly 94% of the total embodied energy.

References

[1] Mehta, P. Kumar. "Reducing the environmental impact of concrete." *Concrete international* 23.10 (2001): 61-66.
[2] J. Davidovits, SPE PACTEC '79, Society of Plastic Engineers, Brookfield Center, USA, (1979) 151.
[3] Xu, Hua, and J. S. J. Van Deventer. "The geopolymerisation of alumino-silicate minerals." International Journal of Mineral Processing 59.3 (2000): 247-266.
[4] Khale, Divya, and RubinaChaudhary. "Mechanism of geopolymerization and factors influencing its development: a review." Journal of Materials Science 42.3 (2007): 729-746.
[5] Hardjito, Djwantoro, et al. "On the development of fly ash-based geopolymer concrete." ACI Materials Journal-American Concrete Institute 101.6 (2004): 467-472.
[6] Hardjito, Djwantoro, et al. "Fly ash-based geopolymer concrete." Australian Journal of Structural Engineering 6.1 (2005): 77-84.
[7] Hardjito, Djwantoro, and B. VijayaRangan. "Development and properties of low-calcium fly ash-based geopolymer concrete." Perth, Australia: Curtin University of Technology (2005).
[8] Fernandez-Jimenez, Ana M., Angel Palomo, and Cecilio Lopez-Hombrados. "Engineering properties of alkali-activated fly ash concrete." ACI Materials Journal 103.2 (2006).
[9] Kumar, Sanjay, Rakesh Kumar, and S. P. Mehrotra. "Influence of granulated blast furnace slag on the reaction, structure and properties of fly ash based geopolymer." Journal of materials science 45.3 (2010): 607-615.
[10] Recommended guidelines for concrete mix design, IS 10262:2009, Bureau of Indian Standards.
[11] B. V. Venkatarama Reddy, and K. S. Jagadish. "Embodied energy of common and alternative building materials and technologies." Energy and buildings 35.2 (2003): 129-137.
[12] Fawer, Matthias, Martin Concannon, and Wolfram Rieber. "Life cycle inventories for the production of sodium silicates." The International Journal of Life Cycle Assessment 4.4 (1999): 207-212.

Prediction and Control of Weld Bead Geometry in Gas Metal Arc Welding Process Using Simulated Annealing Algorithm

[1,]P, Sreeraj, [2,]T, Kannan , [3,]Subhasis Maji

[1,]Department of Mechanical Engineering, Valia Koonambaikulathamma College of Engineering Technology, Kerala, 692574 India

[2,]Principal, SVS College of Engineering,Coimbatore,Tamilnadu,642109 India.

[3,]Professor, Department of Mechanical Engineering IGNOU, Delhi, 110068, India.

Abstract

In order to automate a welding process, which is a present trend in fabrication industry, it is necessary to have a mathematical model that is to relate the process parameters. Because of high reliability, easiness in operation, high penetration good surface finish and high productivity gas metal arc welding (GMAW) became a natural choice for fabrication industries. This paper presents five level factorial techniques to predict four critical dimensions of bead geometry. The developed models have been checked for adequacy and significance. The bead geometry is predicted again using Simulated annealing Algorithm (SA).

Key Words: GMAW, Weld bead geometry, Multiple Regression, Mathematical models,

1. Introduction

Quality is a vital factor in today's manufacturing world. Quality can be defined as the degree of customer satisfaction. Quality of a product depends on how it performs in desired circumstances. Quality is a very vital factor in the field of welding. The quality of a weld depends on mechanical properties of the weld metal which in turn depends on metallurgical characteristics and chemical composition of the weld [1]. The mechanical and metallurgical feature of weld depends on bead geometry which is directly related to welding process parameters. In other words quality of weld depends on in process parameters.GMA welding is a multi objective and multifactor metal fabrication technique. The process parameters have a direct influence on bead geometry [2]. Fig 1 shows the clad bead geometry. Mechanical strength of clad metal is highly influenced by the composition of metal but also by clad bead shape. This is an indication of bead geometry. It mainly depends on wire feed rate, welding speed, arc voltage etc. Therefore it is necessary to study the relationship between in process parameters and bead parameters to study clad bead geometry. This paper highlights the study carried out to develop mathematical and GA models to predict clad bead geometry, in stainless steel cladding deposited by GMAW [3].

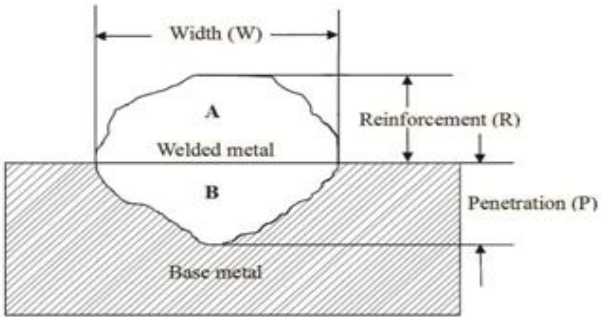

Percentage dilution (D) = [B/ (A+B)] X 100

Figure 1: Clad bead geometry

2. Experimentation

The following machines and consumables were used for the purpose of conducting experiment.

1) A constant current gas metal arc welding machine (Invrtee V 350 – PRO advanced processor with 5 – 425 amps output range)
2) Welding manipulator
3) Wire feeder (LF – 74 Model)
4) Filler material Stainless Steel wire of 1.2mm diameter (ER – 308 L).
5) Gas cylinder containing a mixture of 98% argon and 2% of oxygen.
6) Mild steel plate (grade IS – 2062)

Test plates of size 300 x 200 x 20mm were cut from mild steel plate of grade IS – 2062 and one of the surfaces is cleaned to remove oxide and dirt before cladding. ER-308 L stainless steel wire of 1.2mm diameter was used for depositing the clad beads through the feeder. Argon gas at a constant flow rate of 16 litres per minute was used for shielding. The properties of base metal and filler wire are shown in Table 1. The important and most difficult parameter found from trial run is wire feed

rate. The wire feed rate is proportional to current. Wire feed rate must be greater than critical wire feed rate to achieve pulsed metal transfer. The relationship found from trial run is shown in equation (1). The formula derived is shown in Fig 2.

Wire feed rate = 0.96742857 *current + 79.1 ---------- (1)

The selection of the welding electrode wire based on the matching the mechanical properties and physical characteristics of the base metal, weld size and existing electrode inventory [4]. A candidate material for cladding which has excellent corrosion resistance and weld ability is stainless steel. These have chloride stress corrosion cracking resistance and strength significantly greater than other materials. These have good surface appearance, good radiographic standard quality and minimum electrode wastage. Experimental design used for this study is shown in Fig 3 and importance steps are briefly explained.

Table 1: Chemical Composition of Base Metal and Filler Wire

	Elements, Weight %								
Materials	C	SI	Mn	P	S	Al	Cr	Mo	Ni
IS 2062	0.150	0.160	0.870	0.015	0.016	0.031	-	-	-
ER308L	0.03	0.57	1.76	0.021	1.008	-	19.52	0.75	10.02

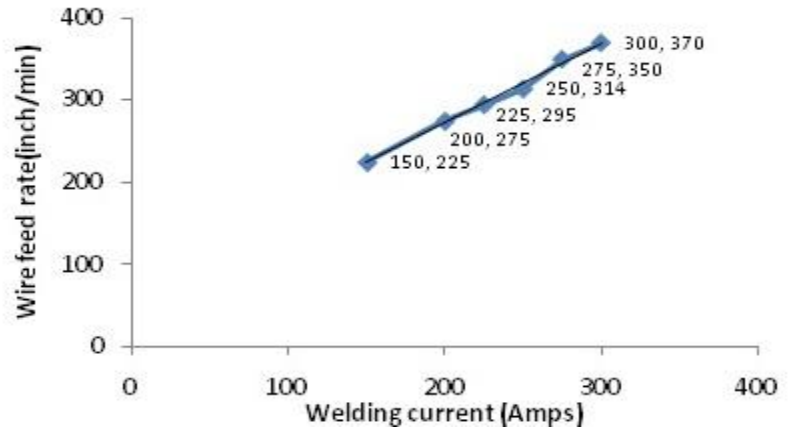

Figure 2: Relationship between Current and Wire Feed Rate

3. Plan of Investigation

The research work is carried out in the following steps [5] .Identification of factors, finding the limit of process variables, development of design matrix, conducting experiments as per design matrix, recording responses, development of mathematical models, checking adequacy of developed models, and predicting the parameters.

3.1 Identification of Factors and Responses

The basic difference between welding and cladding is the percentage of dilution. The properties of the cladding is the significantly influenced by dilution obtained. Hence control of dilution is important in cladding where a low dilution is highly desirable. When dilution is quite low, the final deposit composition will be closer to that of filler material and hence corrosion resistant properties of cladding will be greatly improved. The chosen factors have been selected on the basis to get minimal dilution and optimal clad bead geometry [1]. These are wire feed rate (W), welding speed (S), welding gun angle (T), contact tip to work to The following independently controllable process parameters were found to be affecting output parameters distance (N) and pinch (Ac), The responses chosen were clad bead width (W), height of reinforcement (R), Depth of Penetration. (P) and percentage of dilution (D). The responses were chosen based on the impact of parameters on final composite model.

3.2 Finding the limits of process variables

Working ranges of all selected factors are fixed by conducting trial run. This was carried out by varying one of factors while keeping the rest of them as constant values. Working range of each process parameters was decided upon by inspecting the bead for smooth appearance without any visible defects. The upper limit of given factor was coded as -2. The coded value of intermediate values were calculated using the equation (2)

$$X_i = \frac{2[2X-(X_{max}+X_{min})]}{(X_{max}-X_{min})]} \quad \text{---------- (2)}$$

Where X_i is the required coded value of parameter X is any value of parameter from $X_{min} - X_{max}$. X_{min} is the lower limit of parameters and X_{max} is the upper limit parameters [4].
The chosen level of the parameters with their units and notation are given in Table 2.

Table 2: Welding Parameters and their Levels

Parameters	Factor Levels						
	Unit	Notation	-2	-1	0	1	2
Welding Current	A	1	200	225	250	275	300
Welding Speed	mm/min	S	150	158	166	174	182
Contact tip to work distance	mm	N	10	14	18	22	26
Welding gun Angle	Degree	T	70	80	90	100	110
Pinch	-	Ac	-10	-5	0	5	10

3.3 Development of design matrix

Design matrix chosen to conduct the experiments was central composite rotatable design. The design matrix comprises of full replication of 2^5(= 32), Factorial designs. All welding parameters in the intermediate levels (o) Constitute the central points and combination of each welding parameters at either is highest value (+2) or lowest (-2) with other parameters of intermediate levels (0) constitute star points. 32 experimental trails were conducted that make the estimation of linear quadratic and two way interactive effects of process parameters on clad geometry [5].

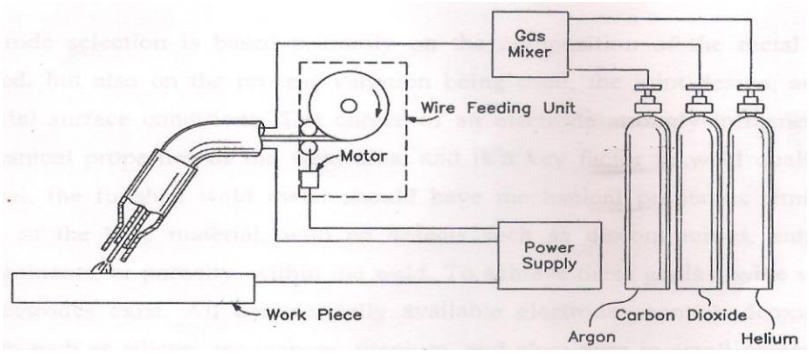

Figure 3: GMAW Circuit Diagram

Table 3: Design Matrix

Trial Number	Design Matrix				
	I	S	N	T	Ac
1	-1	-1	-1	-1	1
2	1	-1	-1	-1	-1
3	-1	1	-1	-1	-1
4	1	1	-1	-1	1
5	-1	-1	1	-1	-1
6	1	-1	1	-1	1
7	-1	1	1	-1	1
8	1	1	1	-1	-1
9	-1	-1	-1	1	-1
10	1	-1	-1	1	1

11	-1	1	-1	1	1
12	1	1	-1	1	-1
13	-1	-1	1	1	1
14	1	-1	1	1	-1
15	-1	1	1	1	-1
16	1	1	1	1	1
17	-2	0	0	0	0
18	2	0	0	0	0
19	0	-2	0	0	0
20	0	2	0	0	0
21	0	0	-2	0	0
22	0	0	2	0	0
23	0	0	0	-2	0
24	0	0	0	2	0
25	0	0	0	0	-2
26	0	0	0	0	2
27	0	0	0	0	0
28	0	0	0	0	0
29	0	0	0	0	0
30	0	0	0	0	0
31	0	0	0	0	0
32	0	0	0	0	0

I - Welding current; S - Welding speed; N - Contact tip to work distance; T - Welding gun angle; Ac – Pinch

3.4 Conducting experiments as per design matrix

In this work Thirty two experimental run were allowed for the estimation of linear quadratic and two-way interactive effects of correspond each treatment combination of parameters on bead geometry as shown Table 3 at random. At each run settings for all parameters were disturbed and reset for next deposit. This is very essential to introduce variability caused by errors in experimental set up. The experiments were conducted at SVS College of Engineering, Coimbatore, 642109, India.

3.5 Recording of Responses

For measuring the clad bead geometry, the transverse section of each weld overlays was cut using band saw from mid length. Position of the weld and end faces were machined and grinded. The specimen and faces were polished and etched using a 5% nital solution to display bead dimensions. The clad bead profiles were traced using a reflective type optical profile projector at a magnification of X10, in M/s Roots Industries Ltd. Coimbatore. Then the bead dimension such as depth of penetration height of reinforcement and clad bead width were measured [6]. The profiles traced using AUTO CAD software. This is shown in Fig 4. This represents profile of the specimen (front side).The cladded specimen is shown in Fig. 5. The measured clad bead dimensions and percentage of dilution is shown in Table 4.

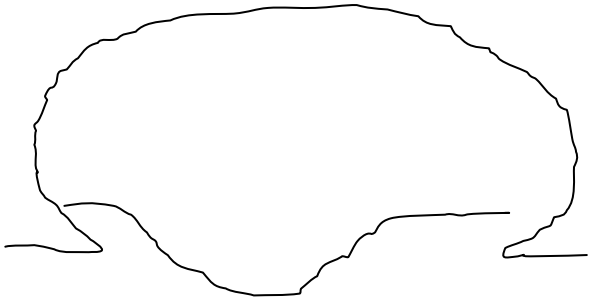

Figure 4: Traced Profile of bead geometry

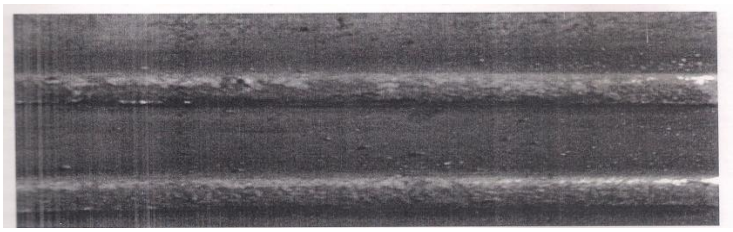

Figure 5: cladded specimen

Table 4: Design Matrix and Observed Values of Clad Bead Geometry

W-

Trial No.	Design Matrix					Bead Parameters			
	I	S	N	T	Ac	W (mm)	P (mm)	R (mm)	D (%)
1	-1	-1	-1	-1	1	6.9743	1.67345	6.0262	10.72091
2	1	-1	-1	-1	-1	7.6549	1.9715	5.88735	12.16746
3	-1	1	-1	-1	-1	6.3456	1.6986	5.4519	12.74552
4	1	1	-1	-1	1	7.7635	1.739615	6.0684	10.61078
5	-1	-1	1	-1	-1	7.2683	2.443	5.72055	16.67303
6	1	-1	1	-1	1	9.4383	2.4905	5.9169	15.96692
7	-1	1	1	-1	-1	6.0823	2.4672	5.49205	16.5894
8	1	1	1	-1	-1	8.4666	2.07365	5.9467	14.98494
9	-1	-1	-1	1	-1	6.3029	1.5809	5.9059	10.2749
10	1	-1	-1	1	1	7.0136	1.5662	5.9833	9.707297
11	-1	1	-1	1	1	6.2956	1.58605	5.5105	11.11693
12	1	1	-1	1	-1	7.741	1.8466	5.8752	11.4273
13	-1	-1	1	1	1	7.3231	2.16475	5.72095	15.29097
14	1	-1	1	1	-1	9.6171	2.69495	6.37445	18.54077
15	-1	1	1	1	-1	6.6335	2.3089	5.554	17.23138
16	1	1	1	1	1	10.514	2.7298	5.4645	20.8755
17	-2	0	0	0	0	6.5557	1.99045	5.80585	13.65762
18	2	0	0	0	0	7.4772	2.5737	6.65505	15.74121
19	0	-2	0	0	0	7.5886	2.50455	6.4069	15.77816
20	0	2	0	0	0	7.5014	2.1842	5.6782	16.82349
21	0	0	-2	0	0	6.1421	1.3752	6.0976	8.941799
22	0	0	2	0	0	8.5647	3.18536	5.63655	22.94721
23	0	0	0	-2	0	7.9575	2.2018	5.8281	15.74941
24	0	0	0	2	0	7.7085	1.85885	6.07515	13.27285
25	0	0	0	0	-2	7.8365	2.3577	5.74915	16.63287
26	0	0	0	0	2	8.2082	2.3658	5.99005	16.38043
27	0	0	0	0	0	7.9371	2.1362	6.0153	15.18374
28	0	0	0	0	0	8.4371	2.17145	5.69895	14.82758
29	0	0	0	0	0	9.323	3.1425	5.57595	22.8432
30	0	0	0	0	0	9.2205	3.2872	5.61485	23.6334
31	0	0	0	0	0	10.059	2.86605	5.62095	21.55264
32	0	0	0	0	0	8.9953	2.72068	5.7052	19.60811

Width; R - Reinforcement W - Width; P - Penetration; D - Dilution %

3.6 Development of Mathematical Models

The response function representing any of the clad bead geometry can be expressed as [7, 8, and 9],

$$Y = f(A, B, C, D, E) \quad \text{---------- (3)}$$

Where, Y = Response variable

A = Welding current (I) in amps

B = Welding speed (S) in mm/min

C = Contact tip to Work distance (N) in mm
D = Welding gun angle (T) in degrees
E = Pinch (Ac)

The second order surface response model equals can be expressed as below

$$Y = \beta_0 + \sum_{i=0}^{5} \beta_i X_i + \sum_{i=0}^{5} \beta_{ii} X_i^2 + \sum_{i=0}^{5} \beta_{ij} X_i X_j$$

$Y = \beta_0 + \beta_1 A + \beta_2 B + \beta_3 C + \beta_4 D + \beta_5 E + \beta_{11} A^2 + \beta_{22} B^2 + \beta_{33} C^2 + \beta_{44} D^2 + \beta_{55} E^2 + \beta_{12} AB + \beta_{13} AC + \beta_{14} AD + \beta_{15} AE + \beta_{23} BC + \beta_{24} BD + \beta_{25} BE + \beta_{34} CD + \beta_{35} CE + \beta_{45} DE$ --------- (4)

Where, β_0 is the free term of the regression equation, the coefficient $\beta_1, \beta_2, \beta_3, \beta_4$ and β_5 is are linear terms, the coefficients β_{11}, $\beta_{22}, \beta_{33}, \beta_{44}$ and ß$_{55}$ quadratic terms, and the coefficients $\beta_{12}, \beta_{13}, \beta_{14}, \beta_{15}$, etc are the interaction terms. The coefficients were calculated by using Quality America six sigma software (DOE – PC IV). After determining the coefficients, the mathematical models were developed. The developed mathematical models are given as follows.

$\beta_o = 0.166338((\sum X_0 Y) + 0.05679(\sum\sum X_{ii} Y))$ ---------- (5)

$\beta_i = 0.166338 (\sum X_i Y)$ ---------- (6)

$\beta_{ii} = 0.0625 ((\sum X_{ii} Y) + 0.06889 (\sum\sum X_{ii} Y) - 0.056791 (\sum\sum X_0 Y))$ ---------- (7)

$\beta_{ij} = 0.125 (\sum X_{ij} Y)$ ---------- (8)

Clad Bead Width (W), mm = 8.923 + 0.701A + 0.388B + 0.587C + 0.040D + 0.088E – 0.423A^2 – 0.291B^2 – 0.338C^2 – 0.219D^2 – 0.171E^2 + 0.205AB + 0.405AC + 0.105AD + 0.070AE– 0.134BC+0.225BD+0.098BE+0.26CD+0.086CE+0.012DE ---------- (9)

Depth of Penetration (P), mm = 2.735 + 0.098A – 0.032B + 0.389C – 0.032D – 0.008E – 0.124A^2– 0.109B^2 – 0.125C^2 – 0.187D^2 – 0.104E^2 – 0.33AB + 0.001 AC + 0.075AD + 0.005 AE–0.018BC+0.066BD+0.087BE+0.058CD+0.054CE–0.036DE ---------- (10)

Height of Reinforcement (R), mm = 5.752 + 0.160A – 0.151B – 0.060C + 0.016D – 0.002E + 0.084A^2 + 0.037B^2 – 0.0006C^2 + 0.015D^2 – 0.006E^2 + 0.035AB + 0.018AC – 0.008AD – 0.048AE–0.024BC–0.062BD–0.003BE+0.012CD–0.092CE–0.095DE.----------(11) **Percentage Dilution (D), %** = 19.705 + 0.325A + 0.347B + 3.141C – 0.039D – 0.153E – 1.324A^2 – 0.923B^2 – 1.012C^2 – 1.371D^2 – 0.872E^2 – 0.200AB + 0.346 AC + 0.602 AD + 0.203AE+0.011BC+0.465BD+0.548BE+0.715CD+0.360CE+0.137DE ---------- (12)

Co-efficient of the above polynomial equation where calculated by regression as given by equations (5) to (8)

3.7 Checking the adequacy of the developed models

Analysis of variance (ANOVA) technique was used to test the adequacy of the model. As per this technique, if the F – ratio values of the developed models do not exceed the standard tabulated values for a desired level of confidence (95%) and the calculated R – ratio values of the developed model exceed the standard values for a desired level of confidence (95%) then the models are said to be adequate within the confidence limit [10]. These conditions were satisfied for the developed models. The values are shown in Table 5.

Table 5: Analysis of variance for Testing Adequacy of the Model

Parameter	1st Order terms		2nd order terms		Lack of fit		Error terms		F-ratio	R-ratio	Whether model is adequate
	SS	DF	SS	DF	SS	DF	SS	DF			
W	36.889	20	6.233	11	3.51 3	6	2.721	5	1.076	3.390	Adequate
P	7.810	20	0.404	11	0.142	6	0.261	5	0.454	7.472	Adequate
R	1.921	20	0.572	11	0.444	6	0.128	5	2.885	3.747	Adequate
D	506.07 4	20	21.73 9	11	6.289	6	15.45	5	0.339	8.189	Adequate

SS - Sum of squares; DF - Degree of freedom; F Ratio (6, 5, 0.5) = 3.40451; R Ratio (20, 5, 0.05) = 3.20665

4. The Prediction Function

The mathematical models furnished above provide one to one relationships between process parameters and weld bead geometry. They can be used in two ways;

1) Predicting weld bead geometry based on input parameters and
2) Predicting process parameters for a desired weld bead specification.

The later one is more practical since the welding parameters are usually set based on desired bead geometry. For this purpose, the set of non-linear equations must be solved simultaneously for all the process parameters. Evolutionary algorithms are powerful optimization techniques widely used for solving combinatorial problems. Nevertheless, other capabilities of these techniques have rarely been explored. As a new and promising approach, one of these algorithms, called SA, is implemented for prediction purposes in this research.

To predict the process parameters based on a desired bead quality, we first define the prediction function as follow(13):

$$E=\propto_1 \frac{(P_t-P_{Equ})^2}{P_t}+\propto_2 \frac{(R_t-R_{Equ})^2}{R_t}+\propto_3 \frac{(W_t-W_{Equ})^2}{W_t}+\propto_4 \frac{(D_t-Dp_{Equ})^2}{Ap_t}+ \qquad (13)$$

Where:

$P_{Equ}, R_{Equ}, W_{Equ} D_{Equ}$ are bead specifications namely penetration, reinforcement, width of weld bead and percentage of dilution respectively which are given by Equations 9 to 12. In the same manner, we define $P_t, R_t, W_t D_t,$ as the target values for the desired weld bead geometry.

The coefficients $\propto_i$ represent weighing importance of different parameters in the objective function. In the prediction process, the purpose is to minimize this objective function. By doing so, the process parameters are calculated in such way that the bead geometry parameters approach their desired values. A SA method is employed to find the best welding variables with respect to process specifications.

5. Simulated Annealing Algorithm

Simulated annealing was originally inspired by formation of a crystal in solids during cooling. As discovered by long ago by Iron Age black smiths the slower cooling, the most perfect crystal is formed. By cooling complex physical systems naturally converge towards state of minimal energy. The systems move randomly, but probability to stay in a particular configuration depends directly on the energy of the system and on its temperature. Gibbs law stated as equation (14).

$$P = e^{\frac{E}{kT}} \quad \text{----------} \ (14)$$

Where E stands for energy k is the Boltzmann constant and T is the temperature. The iteration of the simulated annealing consists of randomly choosing a new solution in the neighbourhood of actual solution. If the fitness function of the new solution is better than the fitness function of the current one the new solution is accepted as the new current solution. If the fitness function is not improved the new solution will be retained with probability shown in equation (15).

$$P = e^{\frac{-(f(y)-f(x))}{kT}} \quad \text{--------} \ (15)$$

Where f(y)-f(x), being the difference between new and old solutions.

In this study Simulated Annealing (SA) which utilizes stochastic optimization is used for the optimization of clad bead geometry deposited by GMAW. The main advantage of using this stochastic algorithm is that global optimization point can be reached regardless of the initial starting point. Since the algorithm incorporates. The major advantage of SA is an ability to avoid being trapped at a local optimum point during optimization. The algorithm employs a random search accepting not only the changes that improve the objective function but also the changes that deteriorate it.Fig.6 shows simulated annealing algorithm. [11]

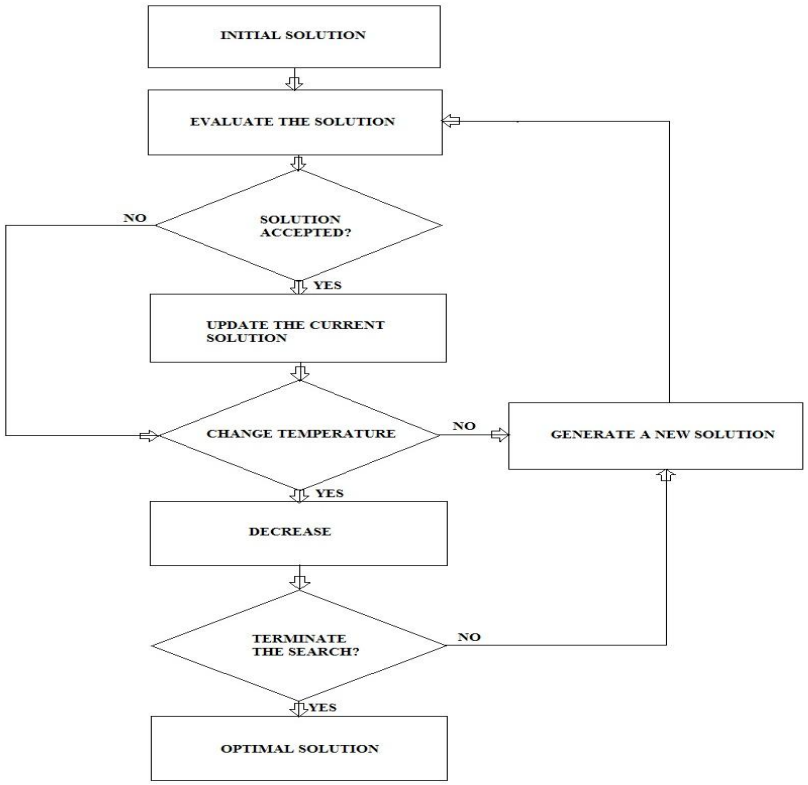

Figure. 6 Traditional Simulated Annealing Algorithms

6 An Illustrative Example

In this section a numerical example is presented to illustrate the performance of proposed procedure and solution technique [12]. The target values for desired weld bead geometry are given in Table 6.

Table 6 Target values for weld bead geometry.

Weld Bead Geometry	Target Value
P_t , *(mm)*	2.49
R_t (mm)	5.83
W_t (mm)	7.99
D_t (%)	12.59

Without lose of generality, all elements of the bead geometry are assumed to be of the same importance and therefore constants a_1 to a_7 are set to unity [13].

The prediction function given in Equation 13 along with weld bead modeling equations 9 to 12 are embedded into SA algorithm. The parameters for the algorithm are set as follows and shown in Table 7:

Table 7. SA process parameters

Annealing Function	Boltzmann Annealing
Population size	30
Re annealing temperature	100
Initial Temperature	100
Data Type	Double

The objective is to minimize the perdition function which is used as the fitness criterion in evaluation each generation of solutions. The best values found by proposed SA for process parameters are presented in Table 8. By setting these parameters in GMAW, the target weld bead geometry specifications may be achieved.

Table 8 Predicted values for process parameters.

Process parameters	Predicted value by SA
Welding current (I)	242
Welding Speed (S) (mm/min)	161
Contact tip to work distance (N) mm (m/min)	16
Welding Gun Angle (T) Degree	88
Pinch(Ac)	-10

The performance of the solution procedure was tested by substituting parameters values obtained by GA into the weld bead models and comparing the results with the desired values of bead geometry. The comparison of the calculated and desired values is shown in Table 9. The largest error is around 0.3 while most parameters deviate much less than 1% from their desired values. The computational results show that GA can be used efficiently and with good accuracy as a prediction technique.

Table 9 Comparison between desired and predicted weld bead geometry values

Weld Bead Geometry	Targets	SAResults	Error
Penetration	2.29	2.493	.203
Reinforcement	5.83	6.213	.383
Clad Bead Width	7.9	8.35	.45
Clad Bead Width	7.9	8.35	.45

7. Results and Discussions

1. A five level five factor full factorial design matrix based on central composite rotatable design technique was used for the mathematical development of model to predict clad bead geometry of austenitic stainless steel deposited by GMAW.
2. SA tool available in MATLAB 7 software was efficiently employed for prediction of clad bead geometry.
3. In cladding by a welding process clad bead geometry is very important for economising the material. This study effectively used SA models to predict weld bead geometry.
4. In this study two models regression and SA system for prediction of bead geometry in GMAW welding process. In this study it is proved that SA model prediction is efficient and error is approximately equal to five percent.

8. Conclusions

Based on the above study it can be observed that the developed model can be used to predict clad bead geometry within the applied limits of process parameters. This method of predicting process parameters can be used to get minimum percentage of dilution. In this study regression and SA was used for achieving optimal clad bead dimensions. In the case of any cladding process bead geometry plays an important role in determining the properties of the surface exposed to hostile environments and reducing cost of manufacturing. In this approach the objective function aimed for predicting weld bead geometry within the constrained limits.

Acknowledgement

The authors sincerely acknowledge the help and facilities extended to them by the department of mechanical engineering SVS college of Engineering, Coimbatore, India.

References

[1] Kannan,T.;Murugan,N.(2006).Effect Of Flux Cored Arc Welding Process Parameters On Duplex Stainless Steel Clad Quality ,Journal Of Material Processing Technology Vol.176 Pp 230-239.
[2] Kannan,T.; Murugn,N.(2006).Prediction Of Ferrite Number Of Duplex Stainless Steel Clad Metals Using RSM, *Welding Journal.* Pp. 91 - 99.
[3] Gunaraj,V.; Murugan, N. (2005). Prediction And Control Of Weld Bead Geometry And Shape Relationships In Submerged Arc Welding Of Pipes, *Journal Of Material Processing Technology.* Vol. 168, Pp. 478 – 487.
[4] Kim, I,S.; Son, K,J.; Yang, Y, S.; Yaragada, P, K, D,V. (2003). Sensitivity Analysis For Process Parameters In GMA Welding Process Using Factorial Design Method, *International Journal Of Machine Tools And Manufacture.* Vol.43, Pp. 763 - 769.
[5] Cochran, W,G.; Coxz, G,M. (1987). *Experimental Design.* Pp.370, New York, John Wiley & Sons.

[6] Serdar Karaoglu.; Abdullah Secgin. (2008). Sensitivity Analysis Of Submerged Arc Welding Process Parameters,*Journal Of Material Processing Technology.* Vol-202, Pp 500-507.
[7] Ghosh, P,K.; Gupta, P,C.; Goyal, V,K. (1998) . Stainless Steel Cladding Of Structural Steel Plate Using The Pulsed Current GMAW Process, *Welding* -314.
[8] Gunaraj, V.; Murugan, N. (1999) . Prediction And Comparison Of The Area Of The Heat Effected Zone For The Bead On Plate And Bead On Joint In SAW Of Pipes, *Journal Of Material Processing Technology.* Vol. 95, Pp. 246 - 261.
[9] Montgomery, D,C.; (2003). Design *And Analysis Of Experiments*, John Wiley & Sons (ASIA) Pvt. Ltd.
[10] Kannan,T.; Yoganath. (2010). Effect Of Process Parameters On Clad Bead Geometry And Shape Relationships Of Stainless Steel Cladding Deposited By GMAW, *Int. Journal Of Manufacturing Technology.* Vol-47, Pp 1083-1095.
[11] Deepa,S,N;Sivanandam,S,N.;Introduction To Genetic Algorithms;Springer ;Spin 12053230.
[12] Farhad Kolahan.; Mehdi Heidari; (2010). A New Approach For Predicting And Optimising Weld Bead Geometry In GMAW, *International Journal Of Mechanical System Science And Engineering, 2:2*: Pp.138 -142.
[13] Mostafa, N,B.;Khajavi, M,N.(2006).Optimization Of Welding Parameters For Weld Penetration In FCAW, *Journal Of Achievements In Materials And Manufacturing Engineering*, Vol-16 Issue 1-2 May June.

Image Authentication Using Distributed Source Coding

[1,]Dr. Krishna Mohanta, [2,]Dr.V.Khanaa
[1,]Sri Sai Ram Engineering College, Chennai 600 044.
[2,]Dean – Pg Studies Bharath University., Chennai-600 073

Abstract:
We Present A Novel Approach Using Distributed Source Coding For Image Authentication. The Key Idea Is To Provide A Slepian-Wolf Encoded Quantized Image Projection As Authentication Data. This Version Can Be Correctly Decoded With The Help Of An Authentic Image As Side Information. Distributed Source Coding Provides The Desired Robustness Against Legitimate Variations While Detecting Illegitimate Modification. The Decoder Incorporating Expectation Maximization Algorithms Can Authenticate Images Which Have Undergone Contrast, Brightness, And Affine Warping Adjustments. Our Authentication System Also Offers Tampering Localization By Using The Sum-Product Algorithm.

Index Terms- Distributed Source Coding, EM Algorithm, Image Authentication, Sum-Product Algorithm.

1. Introduction

Media content can be efficiently delivered through intermediaries such as peer-to-peer sharing. In these system each user not only receives the requested content but also act as a rely forwarding the received portion to the other user .since the same content can be re- encoded several times, media content in those p2p file sharing system is available in various digital format such as JPEG and JPEG2000.On the other hand, the untrusted intermediaries might tamper with the media for a variety of reason such as interfering with the distribution of particular files as piggy backing unauthentication content orgenerally discrediting a particular distribution system .In 2005 survey indicates that more than fifty percentage of popular songs in KaZaA are corrupted and replaced with noise of different songs. The problem is more challenging if some legitimate adjustment such as crop [ping and resizing an image .We applied distributed source coding and statistical methods to solve image authentication problem.

2. Background

Previous Work in Image Authentication Past approaches for image authentication fall into three groups: forensics, watermarking, and robust hashing. Fixed projection has the weakness that an attacker who knows the null space of the projection can alter the image without affecting the authentication data. Using pseudo-random projections or tilings, such as in [28], keeps the null space a secret. Secure Biometrics Our approach has similarities to slepian-wolf coding for secure storage of biometric data The secure biometric problem and the image authentication problem have important differences, For secure biometric data from two different peoples are assumed to be independent. In image authentication the tampered target images are usually correlated to the original but with static different to those of the authentic target image.

3. Image Authentication System

The authentication data provides information about the original image to the user. The user makes the authentication decision based on the target image and the authentication data. (a).x original image (b).y at the output of the legitimate channel (c).y at the output of the tampered channel It demonstrates a sample input and two outputs of this channel. The source image x is a Kodak test image at 512 x 512 resolution. In the legitimate state, the channel is JPEG2000 compression and reconstruction at (the worst permissible) 30dB PSNR. In the tampered state, a further malicious attack is applied: a 19x163 pixel text banner is overlaid on the reconstructed image and some objects are removed. Proposed Image Authentication System In our authentication system shown in Fig.4, a pseudorandom projection (based on a randomly drawn seed Ks) is applied to the original image x and the projection coefficients X are quantized to yield Xq. The authentication data are comprised of two parts, both derived from Xq. The Slepian-Wolf bitstream S(Xq) is the output of a Slepian-Wolf encoder based on LDPC codes [45] and the much smaller digital signature D (Xq, Ks) consists of the seed Ks and a cryptographic hash value of Xq signed with a private key. The authentication data are generated by a server upon request. Each response uses a different random seed Ks, which is provided to the decoder as part of the authentication data. This prevents an attack which simply confines the tampering to the null space of the projection. Based on the random seed, for each 16 x 16 non overlapping block Bi, we generate a 16 x 16 pseudorandom matrix Pi by

drawing its elements independently from a Gaussian distribution N(1,) and normalizing so that =1. We choose=0.2 empirically. In this way, we maintain the properties of the mean projection while gaining sensitivity to high-frequency attacks. The inner product is uniformly quantized into an element of Xq. The rate of the Slepian-Wolf bitstream S(Xq) determines how statistically similar the target image must be to the original to be declared authentic. If the conditional entropy H(Xq/Y) exceeds the bitrate R in bits per pixel, Xq cannot be decoded correctly [2]. Therefore, the rate of S(Xq) should be chosen to be just sufficient to authenticate the legitimate image at its worst permissible quality. In our system, we select a Slepian-Wolf bitrate just sufficient to authenticate both legitimate 30 dB JPEG2000 and JPEG reconstructed versions of the original image. Practically, the Slepian- Wolf bitrate is determined by finding the minimum decodable rate for the training images with the worst permissible quality. This worst permissible quality is external parameter that depends on the particular

application. Generally, if a smaller quality degradation is permissible, fewer bits are required for authentication. If a worse quality is permissible, more bits are needed.At the receiver, the user seeks to authenticate the image y with authentication data S(Xq) and D(Xq,Ks). It first projects y to Y in the same way as during thentication data generation using the same random seed Ks. A Slepian- Wolf decoder reconstructs Xq‘ from the Slepian-Wolf bitstream S(Xq) using Y as side information. Decoding is via LDPC belief propagation [45] initialized according to the statistics of the legitimate channel state at the worst permissible quality for the given original Finally, the image digest of Xq‘ is computed and compared to the image digest, decrypted from the digital signature D(Xq,Ks) using a public key. If these two image digests do not match, the receiver recognizes that image y is tampered. Otherwise the receiver makes a decision based on the likelihood ratio test:P(Xq‘,Y)/Q(Xq‘,Y)> T, Where P and Q are probability models derived from (1) for legitimate and tampered states, respectively, and T is a fixed decision threshold.The authentication system presented in this section can address various types of lossy compression. The next section discusses an adaptive distributed source coding decoder to broaden the robustness of the system for some common adjustments, such as contrast and brightness adjustment, and affine warping.

(a).The original imag
(b).Legitimate image
(c).Realigned target image color overlaid

It shows a target image which has simultaneously undergone contrast brightness and affine wrapping adjustment .The blue area associated with the 16x16 blocks indicate the cropped -out regions the other block from the cropped-in region.

4. Tampering Localization

Decoder Factor Group There are two classes of nodes :the variable nodes represent the random variables of interest the factor nodes represent the probabilistic relationship among the adjacent image. variable nodes based on the factor graph representation the sum product algorithm is used.

5. Conclusions

This paper presents and investigates a novel image authentication scheme that distinguishes legitimate ncoding variations of an image from tampered versions based on distributed source coding and statistical methods. A two-state lossy channel model represents the statistical dependency between the original and the target images. Tampering degradations are captured by using a statistical image model, and legitimate compression noise is assumed to be additive white Gaussian noise. Slepian-Wolf coding that exploits the correlation between the riginal and the target image projections achieves significant rate savings.

References

[1]. R.B.Wolfgang and E.J.Delp,‖A Watermark for Digital Images,‖.
[2]. J.Fridrich,‖Robust Bit Extraction From images‖.
[3]. S.Roy and Q.Son,‖Robust Hash For Detecting And Locallizing Image Tampering,‖.
[4]. A. Liveris Z.Xiong, and C.Georghiades,‖compression of Binary Sources with side information at the decoder
[5]. using LPDC Codes,‖.Y.C.Lin,‖Image Authentication Using Distributed Source Codind,‖.

On The Enestrom –Kakeya Theorem and Its Generalisations

[1,]M. H. Gulzar
[1,]Department of Mathematics University of Kashmir, Srinagar 190006

Abstract

Many extensions of the Enestrom –Kakeya Theorem are available in the literature. In this paper we prove some results which generalize some known results .

Mathematics Subject Classification: 30C10,30C15

Key-Words and Phrases: Complex number, Polynomial , Zero, Enestrom – Kakeya Theorem

1. Introduction And Statement Of Results

The Enestrom –Kakeya Theorem (see[7]) is well known in the theory of the distribution of zeros of polynomials and is often stated as follows:

Theorem A: Let $P(z)=\sum_{j=0}^{n}a_j z^j$ be a polynomial of degree n whose coefficients satisfy

$$a_n \geq a_{n-1} \geq \ldots\ldots \geq a_1 \geq a_0 > 0.$$

Then P(z) has all its zeros in the closed unit disk $|z| \leq 1.$

In the literature there exist several generalizations and extensions of this result. Joyal et al [6] extended it to polynomials with general monotonic coefficients and proved the following result:

Theorem B: Let $P(z)=\sum_{j=0}^{n}a_j z^j$ be a polynomial of degree n whose coefficients satisfy

$$a_n \geq a_{n-1} \geq \ldots\ldots \geq a_1 \geq a_0.$$

Then P(z) has all its zeros in

$$|z| \leq \frac{a_n - a_0 + |a_0|}{|a_n|}.$$

Aziz and zargar [1] generalized the result of Joyal et al [6] as follows:

Theorem C: Let $P(z)=\sum_{j=0}^{n}a_j z^j$ be a polynomial of degree n such that for some $k \geq 1$

$$ka_n \geq a_{n-1} \geq \ldots\ldots \geq a_1 \geq a_0.$$

Then P(z) has all its zeros in

$$|z+k-1| \leq \frac{ka_n - a_0 + |a_0|}{|a_n|}.$$

For polynomials ,whose coefficients are not necessarily real, Govil and Rahman [2] proved the following generalization of Theorem A :

Theorem C: If $P(z)=\sum_{j=0}^{n}a_j z^j$ is a polynomial of degree n with $\mathrm{Re}(a_j)=\alpha_j$ and $\mathrm{Im}(a_j)=\beta_j$, j=0,1,2,……,n, such that

$$\alpha_n \geq \alpha_{n-1} \geq \ldots\ldots \geq \alpha_1 \geq \alpha_0 \geq 0,$$

where $\alpha_n > 0$, then P(z) has all its zeros in

$$|z| \le 1 + (\frac{2}{\alpha_n})(\sum_{j=0}^{n} |\beta_j|) .$$

Govil and Mc-tume [3] proved the following generalisations of Theorems B and C:

Theorem D: Let $P(z) = \sum_{j=0}^{n} a_j z^j$ be a polynomial of degree n with $\mathrm{Re}(a_j) = \alpha_j$ and $\mathrm{Im}(a_j) = \beta_j$, j=0,1,2,……,n.

If for some $k \ge 1$,

$$k\alpha_n \ge \alpha_{n-1} \ge ..... \ge \alpha_1 \ge \alpha_0 ,$$

then P(z) has all its zeros in

$$|z + k - 1| \le \frac{k\alpha_n - \alpha_0 + |\alpha_0| + 2\sum_{j=0}^{n} |\beta_j|}{|\alpha_n|} .$$

Theorem E: Let $P(z) = \sum_{j=0}^{n} a_j z^j$ be a polynomial of degree n with $\mathrm{Re}(a_j) = \alpha_j$ and $\mathrm{Im}(a_j) = \beta_j$, j=0,1,2,……,n.

If for some $k \ge 1$,

$$k\beta_n \ge \beta_{n-1} \ge ..... \ge \beta_1 \ge \beta_0 ,$$

then P(z) has all its zeros in

$$|z + k - 1| \le \frac{k\beta_n - \beta_0 + |\beta_0| + 2\sum_{j=0}^{n} |\alpha_j|}{|\beta_n|} .$$

M. H. Gulzar [4] proved the following generalizations of Theorems D and E:

Theorem F: Let $P(z) = \sum_{j=0}^{n} a_j z^j$ be a polynomial of degree n with $\mathrm{Re}(a_j) = \alpha_j$ and $\mathrm{Im}(a_j) = \beta_j$, j=0,1,2,……,n.

If for some real number $\rho \ge 0$,

$$\rho + \alpha_n \ge \alpha_{n-1} \ge ..... \ge \alpha_1 \ge \alpha_0 ,$$

then P(z) has all its zeros in the disk

$$\left| z + \frac{\rho}{\alpha_n} \right| \le \frac{\rho + \alpha_n + |\alpha_0| - \alpha_0 + 2\sum_{j=0}^{n} |\beta_j|}{|\alpha_n|} .$$

Theorem G: Let $P(z) = \sum_{j=0}^{n} a_j z^j$ be a polynomial of degree n with $\mathrm{Re}(a_j) = \alpha_j$ and $\mathrm{Im}(a_j) = \beta_j$, j=0,1,2,……,n.

If for some real number $\rho \ge 0$,

$$\rho + \beta_n \ge \beta_{n-1} \ge ..... \ge \beta_1 \ge \beta_0 ,$$

then P(z) has all its zeros in the disk

$$\left| z + \frac{\rho}{\beta_n} \right| \le \frac{\rho + \beta_n + |\beta_0| - \beta_0 + 2\sum_{j=0}^{n} |\alpha_j|}{|\beta_n|} .$$

In this paper we give generalization of Theorems F and G. In fact, we prove the following:

Theorem 1: Let $P(z) = \sum_{j=0}^{n} a_j z^j$ be a polynomial of degree n with $\mathrm{Re}(a_j) = \alpha_j$ and $\mathrm{Im}(a_j) = \beta_j$, j=0,1,2,……,n. If for some real numbers λ, $\rho \ge 0$, $1 \le k \le n, a_{n-k} \ne 0,$

$$\rho+\alpha_n \geq \alpha_{n-1} \geq \ldots \alpha_{n-k+1} \geq \lambda\alpha_{n-k} \geq \alpha_{n-k-1} \geq \ldots \geq \alpha_1 \geq \alpha_0,$$

and $\alpha_{n-k-1} > \alpha_{n-k}$, then P(z) has all its zeros in the disk

$$\left|z+\frac{\rho}{a_n}\right| \leq \frac{\rho+\alpha_n+(\lambda-1)\alpha_{n-k}+|\lambda-1||\alpha_{n-k}|+|\alpha_0|-\alpha_0+2\sum_{j=0}^{n}|\beta_j|}{|a_n|},$$

and if $\alpha_{n-k} > \alpha_{n-k+1}$, then P(z) has all its zeros in the disk

$$\left|z+\frac{\rho}{a_n}\right| \leq \frac{\rho+\alpha_n+(1-\lambda)\alpha_{n-k}+|1-\lambda||\alpha_{n-k}|+|\alpha_0|-\alpha_0+2\sum_{j=0}^{n}|\beta_j|}{|a_n|}$$

Remark 1: Taking $\lambda=1$, Theorem 1 reduces to Theorem F.
Taking k=n ,and $\lambda \leq 1$ in Theorem 1, we get a result due to M.H. Gulzar [5, Theorem 1] .
If a_j are real i.e. $\beta_j = 0$ for all j, we get the following result:

Corollary 1: Let $P(z)=\sum_{j=0}^{n} a_j z^j$ be a polynomial of degree n. If for some real numbers $\lambda, \rho \geq 0$, $1 \leq k \leq n, a_{n-k} \neq 0,$

$$\rho+a_n \geq a_{n-1} \geq \ldots \geq a_{n-k+1} \geq \lambda a_{n-k} \geq a_{n-k-1} \geq \ldots \geq a_1 \geq a_0,$$

and $a_{n-k-1} > a_{n-k}$, then P(z) has all its zeros in the disk

$$\left|z+\frac{\rho}{a_n}\right| \leq \frac{\rho+a_n+(\lambda-1)a_{n-k}+|\lambda-1||a_{n-k}|+|a_0|-a_0}{|a_n|},$$

and if $a_{n-k} > a_{n-k+1}$, then P(z) has all its zeros in the disk

$$\left|z+\frac{\rho}{a_n}\right| \leq \frac{\rho+a_n+(1-\lambda)a_{n-k}+|1-\lambda||a_{n-k}|+|a_0|-a_0}{|a_n|}$$

If we apply Theorem 1 to the polynomial –iP(z) , we easily get the following result:

Theorem 2: Let $P(z)=\sum_{j=0}^{n} a_j z^j$ be a polynomial of degree n with $\mathrm{Re}(a_j)=\alpha_j$ and $\mathrm{Im}(a_j)=\beta_j$, j=0,1, 2,……,n.
If for some real numbers $\lambda, \rho \geq 0, 1 \leq k \leq n, a_{n-k} \neq 0,$

$$\rho+\beta_n \geq \beta_{n-1} \geq \ldots. \geq \beta_{n-k+1} \geq \lambda\beta_{n-k} \geq \beta_{n-k-1} \geq .. \geq \beta_1 \geq \beta_0,$$

and $\beta_{n-k-1} > \beta_{n-k}$, then P(z) has all its zeros in the disk

$$\left|z+\frac{\rho}{a_n}\right| \leq \frac{\rho+\beta_n+(\lambda-1)\beta_{n-k}+|\lambda-1||\beta_{n-k}|+|\beta_0|-\beta_0+2\sum_{j=0}^{n}|\alpha_j|}{|a_n|},$$

and if $\beta_{n-k} > \beta_{n-k+1}$, then P(z) has all its zeros in the disk

$$\left|z+\frac{\rho}{a_n}\right| \leq \frac{\rho+\beta_n+(1-\lambda)\beta_{n-k}+|1-\lambda||\beta_{n-k}|+|\beta_0|-\beta_0+2\sum_{j=0}^{n}|\alpha_j|}{|a_n|}$$

Remark 2: Taking $\lambda=1$, Theorem 2 reduces to Theorem G.

Theorem 3: Let $P(z)=\sum_{j=0}^{n}a_j z^j$ be a polynomial of degree n such that for some real numbers $\lambda,\rho\geq 0$, $1\leq k\leq n, a_{n-k}\neq 0, and \beta$,

$$|\rho+a_n|\geq|a_{n-1}|\geq\ldots\geq|a_{n-k+1}|\geq\lambda|a_{n-k}|\geq|a_{n-k-1}|\geq\ldots\geq|a_1|\geq|a_0|$$

and

$$|\arg a_j-\beta|\leq\alpha\leq\frac{\pi}{2},\ j=0,1,\ldots\ldots,n.$$

If $|a_{n-k-1}|>|a_{n-k}|$ (i.e. $\lambda>1$), then P(z) has all its zeros in the disk

$$\left|z+\frac{\rho}{a_n}\right|\leq\frac{[|\rho+a_n|(\cos\alpha+\sin\alpha)-|a_{n-k}|(\cos\alpha-\sin\alpha-\lambda\cos\alpha-\lambda\sin\alpha-\lambda+1)}{-|a_0|(\cos\alpha-\sin\alpha-1)+2\sin\alpha\sum_{j=1,\,j\neq n-k}^{n-1}|a_j|]}{|a_n|}$$

If $|a_{n-k}|>|a_{n-k+1}|$ (i.e. $\lambda<1$), then P(z) has all its zeros in the disk

$$\left|z+\frac{\rho}{a_n}\right|\leq\frac{[|\rho+a_n|(\cos\alpha+\sin\alpha)+|a_{n-k}|(\cos\alpha+\sin\alpha-\lambda\cos\alpha+\lambda\sin\alpha+1-\lambda)}{+|a_0|(\sin\alpha-\cos\alpha+1)+2\sin\alpha\sum_{j=1,\,j\neq n-k}^{n-1}|a_j|]}{|a_n|}$$

Remark 3: Taking $\lambda=1$ in Theorem 3, we get the following result:

Corollary 2: Let $P(z)=\sum_{j=0}^{n}a_j z^j$ be a polynomial of degree n. If for some real number $\rho\geq 0$,

$$|\rho+a_n|\geq|a_{n-1}|\geq\ldots\ldots\geq|a_1|\geq|a_0|,$$

then P(z) has all its zeros in the disk

$$\left|z+\frac{\rho}{a_n}\right|\leq\frac{[|\rho+a_n|(\cos\alpha+\sin\alpha)-|a_0|(\cos\alpha-\sin\alpha-1)+2\sin\alpha\sum_{j=1,}^{n-1}|a_j|]}{|a_n|}.$$

Remark 4: Taking $\rho=(k-1)a_n, k\geq 1$, we get a result of Shah and Liman [8,Theorem 1].

2. Lemmas

For the proofs of the above results , we need the following results:

Lemma 1: . Let P(z)= $\sum_{j=0}^{n}a_j z^j$ be a polynomial of degree n with complex coefficients such that $|\arg a_j-\beta|\leq\alpha\leq\frac{\pi}{2}, j=0,1,\ldots n,$ *for* some real β. Then for some t>0,

$$|ta_j-a_{j-1}|\leq\left[t|a_j|-|a_{j-1}|\right]\cos\alpha+\left[t|a_j|+|a_{j-1}|\right]\sin\alpha.$$

The proof of lemma 1 follows from a lemma due to Govil and Rahman [2]. **Lemma 2.**If p(z) is regular ,$p(0)\neq 0$ and $|p(z)|\leq M$ in $|z|\leq 1,$ then the number of zeros of p(z)in $|z|\leq\delta, 0<\delta<1,$ does not exceed $\frac{1}{\log\frac{1}{\delta}}\log\frac{M}{|p(0)|}$ (see[9],p 171).

3. Proofs Of Theorems

Proof of Theorem 1: Consider the polynomial

$$\begin{aligned}F(z) &= (1-z)P(z)\\ &= (1-z)(a_n z^n + a_{n-1}z^{n-1} + \ldots\ldots + a_1 z + a_0)\\ &= -a_n z^{n+1} + (a_n - a_{n-1})z^n + \ldots\ldots + (a_{n-k+1} - a_{n-k})z^{n-k+1} + (a_{n-k} - a_{n-k-1})z^{n-k}\\ &\quad + (a_{n-k-1} - a_{n-k-2})z^{n-k-1} + \ldots\ldots + (a_1 - a_0)z + a_0\\ &= -(\alpha_n + i\beta_n)z^{n+1} + (\alpha_n - \alpha_{n-1})z^n + \ldots\ldots + (\alpha_{n-k+1} - \alpha_{n-k})z^{n-k+1}\\ &\quad + (\alpha_{n-k} - \alpha_{n-k-1})z^{n-k} + (\alpha_{n-k-1} - \alpha_{n-k-2})z^{n-k-1} + \ldots\ldots + (\alpha_1 - \alpha_0)z + \alpha_0\\ &\quad + i\sum_{j=1}^{n}(\beta_j - \beta_{j-1})z^j + i\beta_0\end{aligned}$$

If $\alpha_{n-k-1} > \alpha_{n-k}$, then $\alpha_{n-k-1} > \alpha_{n-k}$, and we have

$$\begin{aligned}F(z) &= -(\alpha_n + i\beta_n)z^{n+1} - \rho z^n + (\rho + \alpha_n - \alpha_{n-1})z^n + \ldots\ldots + (\alpha_{n-k+1} - \alpha_{n-k})z^{n-k+1}\\ &\quad + (\lambda\alpha_{n-k} - \alpha_{n-k-1})z^{n-k} - (\lambda - 1)a_{n-k}z^{n-k} + (\alpha_{n-k-1} - \alpha_{n-k-2})z^{n-k-1} + \ldots\ldots\\ &\quad + (\alpha_1 - \alpha_0)z + \alpha_0 + i\sum_{j=1}^{n}(\beta_j - \beta_{j-1})z^j + i\beta_0.\end{aligned}$$

For $|z| > 1$,

$$\begin{aligned}|F(z)| &\geq \left|a_n z^{n+1} + \rho z^n\right| - \left|(\rho + \alpha_n - \alpha_{n-1})z^n + (\alpha_{n-1} - \alpha_{n-2})z^{n-1} + \ldots\ldots + (\alpha_{n-k+1} - \alpha_{n-k})z^{n-k+1}\right.\\ &\quad + (\lambda\alpha_{n-k} - \alpha_{n-k-1})z^{n-k} + (\lambda - 1)a_{n-k}z^{n-k} + (\alpha_{n-k-1} - \alpha_{n-k-2})z^{n-k-1} + \ldots\ldots\\ &\quad \left. + (\alpha_1 - \alpha_0)z + \alpha_0 + i\sum_{j=1}^{n}(\beta_j - \beta_{j-1})z^j + i\beta_0\ \right|\\ &= |z|^n\left[\left|a_n z + \rho\right| - \left|(\rho + \alpha_n - \alpha_{n-1}) + (\alpha_{n-1} - \alpha_{n-2})\frac{1}{z} + \ldots\ldots + (\alpha_{n-k+1} - \alpha_{n-k})\frac{1}{z^{k-1}}\right.\right.\\ &\quad + (\lambda\alpha_{n-k} - \alpha_{n-k-1})\frac{1}{z^k} - (\lambda - 1)\alpha_{n-k}\frac{1}{z^k} + (\alpha_{n-k-1} - \alpha_{n-k-2})\frac{1}{k+1} + \ldots.\\ &\quad \left.\left. + (\alpha_1 - \alpha_0)\frac{1}{z^{n-1}} + \frac{\alpha_0}{z^n} + i\sum_{j=1}^{n}(\beta_j - \beta_{j-1})\frac{1}{z^{n-j}} + i\frac{\beta_0}{z^n}\ \right|\ \right]\\ &> |z|^n\left[\left|a_n z + \rho\right| - \left\{\ \left|\rho + \alpha_n - \alpha_{n-1}\right| + \left|\alpha_{n-1} - \alpha_{n-2}\right| + \ldots\ldots + \left|\alpha_{n-k+1} - \alpha_{n-k}\right|\right.\right.\\ &\quad + \left|\lambda\alpha_{n-k} - \alpha_{n-k-1}\right| + \left|\lambda - 1\right|\left|\alpha_{n-k}\right| + \left|\alpha_{n-k-1} - \alpha_{n-k-2}\right| + \ldots\ldots + \left|\alpha_1 - \alpha_0\right|\\ &\quad \left.\left. + \left|\alpha_0\right| + \sum_{j=1}^{n}\left|\beta_j - \beta_{j-1}\right| + \left|\beta_0\right|\ \right\}\ \right]\\ &\geq |z|^n\left[\left|a_n z + \rho\right| - \left\{\rho + \alpha_n - \alpha_{n-1} + \alpha_{n-1} - \alpha_{n-2} + \ldots\ldots + \alpha_{n-k+1} - \alpha_{n-k} + \lambda\alpha_{n_{n-k}} - \alpha_{n-k-1}\right.\right.\\ &\quad \left.\left. + \left|\lambda - 1\right|\left|\alpha_{n-k}\right| + \alpha_{n-k-1} - \alpha_{n-k-2} + \ldots\ldots + \alpha_1 - \alpha_0 + \left|\alpha_0\right| + 2\sum_{j=0}^{n}\left|\beta_j\right|\ \right\}\ \right]\\ &= |z|^n\left[\left|a_n z + \rho\right| - \left\{\rho + \alpha_n + (\lambda - 1)\alpha_{n-k} + \left|\lambda - 1\right|\left|\alpha_{n-k}\right| - \alpha_0 + \left|\alpha_0\right| + 2\sum_{j=0}^{n}\left|\beta_j\right|\ \right\}\ \right]\\ &> 0\end{aligned}$$

if

$$|a_n z+\rho| > \rho+\alpha_n+(\lambda-1)\alpha_{n-k}+|\lambda-1||\alpha_{n-k}|-\alpha_0+|\alpha_0|+2\sum_{j=0}^{n}|\beta_j|$$

This shows that the zeros of F(z) whose modulus is greater than 1 lie in

$$\left|z+\frac{\rho}{a_n}\right| \le \frac{\rho+\alpha_n+(\lambda-1)\alpha_{n-k}+|\lambda-1||\alpha_{n-k}|+|\alpha_0|-\alpha_0+2\sum_{j=0}^{n}|\beta_j|}{|a_n|}.$$

But the zeros of F(z) whose modulus is less than or equal to 1 already satisfy the above inequality. Hence all the zeros of F(z) lie in

$$\left|z+\frac{\rho}{a_n}\right| \le \frac{\rho+\alpha_n+(\lambda-1)\alpha_{n-k}+|\lambda-1||\alpha_{n-k}|+|\alpha_0|-\alpha_0+2\sum_{j=0}^{n}|\beta_j|}{|a_n|}.$$

Since the zeros of P(z) are also the zeros of F(z), it follows that all the zeros of P(z) lie in

$$\left|z+\frac{\rho}{a_n}\right| \le \frac{\rho+\alpha_n+(\lambda-1)\alpha_{n-k}+|\lambda-1||\alpha_{n-k}|+|\alpha_0|-\alpha_0+2\sum_{j=0}^{n}|\beta_j|}{|a_n|}.$$

If $\alpha_{n-k} > \alpha_{n-k+1}$, then $\alpha_{n-k} > \alpha_{n-k-1}$, and we have

$$\begin{aligned}F(z) = &-(\alpha_n+i\beta_n)z^{n+1}-\rho z^n+(\rho+\alpha_n-\alpha_{n-1})z^n+.....+(\alpha_{n-k+1}-\lambda\alpha_{n-k})z^{n-k+1}\\ &+(\alpha_{n-k}-\alpha_{n-k-1})z^{n-k}-(1-\lambda)\alpha_{n-k}z^{n-k+1}+(\alpha_{n-k-1}-\alpha_{n-k-2})z^{n-k-1}+.....\\ &+(\alpha_1-\alpha_0)z+\alpha_0+i\sum_{j=1}^{n}(\beta_j-\beta_{j-1})z^j+i\beta_0.\end{aligned}$$

For $|z|>1$,

$$\begin{aligned}|F(z)| \ge &|a_n z^{n+1}+\rho z^n|-|(\rho+\alpha_n-\alpha_{n-1})z^n+(\alpha_{n-1}-\alpha_{n-2})z^{n-1}+.....+(\alpha_{n-k+1}-\lambda\alpha_{n-k})z^{n-k+1}\\ &+(\alpha_{n-k}-\alpha_{n-k-1})z^{n-k}-(1-\lambda)\alpha_{n-k}z^{n-k+1}+(\alpha_{n-k-1}-\alpha_{n-k-2})z^{n-k-1}+.....\\ &+(\alpha_1-\alpha_0)z+\alpha_0+i\sum_{j=1}^{n}(\beta_j-\beta_{j-1})z^j+i\beta_0\ |\\ =|z|^n\Big[&|a_n z+\rho|-\Big|(\rho+\alpha_n-\alpha_{n-1})+(\alpha_{n-1}-\alpha_{n-2})\frac{1}{z}+.....+(\alpha_{n-k+1}-\lambda\alpha_{n-k})\frac{1}{z^{k-1}}\\ &+(\alpha_{n-k}-\alpha_{n-k-1})\frac{1}{z^k}-(1-\lambda)\alpha_{n-k}\frac{1}{z^{k-1}}+(\alpha_{n-k-1}-\alpha_{n-k-2})\frac{1}{z^{k+1}}+....\\ &+(\alpha_1-\alpha_0)\frac{1}{z^{n-1}}+\frac{\alpha_0}{z^n}+i\sum_{j=1}^{n}(\beta_j-\beta_{j-1})\frac{1}{z^{n-j}}+i\frac{\beta_0}{z^n}\ |\ \Big]\\ >|z|^n\Big[&|a_n z+\rho|-\{\ |\rho+\alpha_n-\alpha_{n-1}|+|\alpha_{n-1}-\alpha_{n-2}|+.....+|\alpha_{n-k+1}-\lambda\alpha_{n-k}|\\ &+|\alpha_{n-k}-\alpha_{n-k-1}|+|1-\lambda||\alpha_{n-k}|+|\alpha_{n-k-1}-\alpha_{n-k-2}|+.....+|\alpha_1-\alpha_0|\\ &+|\alpha_0|+\sum_{j=1}^{n}|\beta_j-\beta_{j-1}|+|\beta_0|\ \}\ \Big]\\ \ge|z|^n\Big[&|a_n z+\rho|-\{\rho+\alpha_n-\alpha_{n-1}+\alpha_{n-1}-\alpha_{n-2}+.....+\alpha_{n-k+1}-\lambda\alpha_{n-k}+\alpha_{n_{n-k}}-\alpha_{n-k-1}\end{aligned}$$

$$+|1-\lambda||\alpha_{n-k}|+\alpha_{n-k-1}-\alpha_{n-k-2}+.....+\alpha_1-\alpha_0+|\alpha_0|+2\sum_{j=0}^{n}|\beta_j|\ \}\ ]$$

$$=|z|^n\left[|a_nz+\rho|-\left\{\rho+\alpha_n+(1-\lambda)\alpha_{n-k}+|1-\lambda||\alpha_{n-k}|-\alpha_0+|\alpha_0|+2\sum_{j=0}^{n}|\beta_j|\ \}\ \right]\right.$$

>0

if

$$|a_nz+\rho|>\rho+\alpha_n+(1-\lambda)\alpha_{n-k}+|1-\lambda||\alpha_{n-k}|-\alpha_0+|\alpha_0|+2\sum_{j=0}^{n}|\beta_j|$$

This shows that the zeros of F(z) whose modulus is greater than 1 lie in

$$\left|z+\frac{\rho}{a_n}\right|\le\frac{\rho+\alpha_n+(1-\lambda)\alpha_{n-k}+|1-\lambda||\alpha_{n-k}|+|\alpha_0|-\alpha_0+2\sum_{j=0}^{n}|\beta_j|}{|a_n|}.$$

But the zeros of F(z) whose modulus is less than or equal to 1 already satisfy the above inequality. Hence all the zeros of F(z) lie in

$$\left|z+\frac{\rho}{a_n}\right|\le\frac{\rho+\alpha_n+(1-\lambda)\alpha_{n-k}+|1-\lambda||\alpha_{n-k}|+|\alpha_0|-\alpha_0+2\sum_{j=0}^{n}|\beta_j|}{|a_n|}.$$

Since the zeros of P(z) are also the zeros of F(z), it follows that all the zeros of P(z) lie in

$$\left|z+\frac{\rho}{a_n}\right|\le\frac{\rho+\alpha_n+(1-\lambda)\alpha_{n-k}+|1-\lambda||\alpha_{n-k}|+|\alpha_0|-\alpha_0+2\sum_{j=0}^{n}|\beta_j|}{|a_n|}.$$

That proves Theorem 1.

Proof of Theorem 3: Consider the polynomial

$$F(z)=(1-z)P(z)$$

$$=(1-z)(a_nz^n+a_{n-1}z^{n-1}+.....+a_1z+a_0)$$

$$=-a_nz^{n+1}+(a_n-a_{n-1})z^n+.....+(a_{n-k+1}-a_{n-k})z^{n-k+1}+(a_{n-k}-a_{n-k-1})z^{n-k}$$

$$+(a_{n-k-1}-a_{n-k-2})z^{n-k-1}+.....+(a_1-a_0)z+a_0.$$

If $|a_{n-k-1}|>|a_{n-k}|$, then $|a_{n-k+1}|>|a_{n-k}|$, $\lambda>1$ and we have, for $|z|>1$, by using Lemma1,

$$|F(z)|\ge|a_nz^{n+1}+\rho z^n|-|(\rho+a_n-a_{n-1})z^n+(a_{n-1}-a_{n-2})z^{n-1}+.....+(a_{n-k+1}-a_{n-k})z^{n-k+1}$$

$$+(\lambda a_{n-k}-a_{n-k-1})z^{n-k}+(\lambda-1)a_{n-k}z^{n-k}+(a_{n-k-1}-a_{n-k-2})z^{n-k-1}+.....$$

$$+(a_1-a_0)z+a_0\ |$$

$$=|z|^n\left[|a_nz+\rho|-\left|(\rho+a_n-a_{n-1})+(a_{n-1}-a_{n-2})\frac{1}{z}+.....+(a_{n-k+1}-a_{n-k})\frac{1}{z^{k-1}}\right.\right.$$

$$+(\lambda a_{n-k}-a_{n-k-1})\frac{1}{z^k}+(\lambda-1)a_{n-k}\frac{1}{z^k}+(a_{n-k-1}-a_{n-k-2})\frac{1}{z^{k+1}}+....$$

$$\left.\left.+(a_1-a_0)\frac{1}{z^{n-1}}+\frac{a_0}{z^n}\ |\ \right]\right.$$

$$
\begin{aligned}
&> |z|^n \Big[|a_n z + \rho| - \{\, |\rho + a_n - a_{n-1}| + |a_{n-1} - a_{n-2}| + \ldots\ldots + |a_{n-k+1} - a_{n-k}| \\
&\quad + |\lambda a_{n-k} - a_{n-k-1}| + |\lambda - 1||a_{n-k}| + |a_{n-k-1} - a_{n-k-2}| + \ldots\ldots + |a_1 - a_0| \\
&\quad + |a_0| \,\} \Big] \\
&\geq |z|^n \Big[|a_n z + \rho| - \{ (|\rho + a_n| - |a_{n-1}|)\cos\alpha + (|\rho + a_n| + |a_{n-1}|)\sin\alpha \\
&\quad + (|a_{n-1}| - |a_{n-2}|)\cos\alpha + (|a_{n-1}| + |a_{n-2}|)\sin\alpha + \ldots\ldots + (|a_{n-k+1}| - |a_{n-k}|)\cos\alpha \\
&\quad + (|a_{n-k+1}| + |a_{n-k}|)\sin\alpha + (\lambda|a_{n-k}| - |a_{n-k-1}|)\cos\alpha + (\lambda|a_{n-k}| + |a_{n-k-1}|)\sin\alpha \\
&\quad + |\lambda - 1||a_{n-k}| + (|a_{n-k-1}| - |a_{n-k-2}|)\cos\alpha + (|a_{n-k-1}| + |a_{n-k-2}|)\sin\alpha \\
&\quad + \ldots\ldots + (|a_1| - |a_0|)\cos\alpha + (|a_1| + |a_0|)\sin\alpha + |a_0| \} \Big] \\
&= |z|^n \Big[|a_n z + \rho| - \{ |\rho + a_n|(\cos\alpha + \sin\alpha) - |a_{n-k}|(\cos\alpha - \sin\alpha - \lambda\cos\alpha - \lambda\sin\alpha \\
&\quad - \lambda + 1) + |a_0|(\sin\alpha - \cos\alpha + 1) + 2\sin\alpha \sum_{j=1, j\neq n-k}^{n-1} |a_j| \} \Big] \\
&> 0
\end{aligned}
$$

if

$$
\begin{aligned}
\Big[|a_n z + \rho| &> |\rho + a_n|(\cos\alpha + \sin\alpha) - |a_{n-k}|(\cos\alpha - \sin\alpha - \lambda\cos\alpha - \lambda\sin\alpha \\
&\quad - \lambda + 1) + |a_0|(\sin\alpha - \cos\alpha + 1) + 2\sin\alpha \sum_{j=1, j\neq n-k}^{n-1} |a_j|
\end{aligned}
$$

This shows that the zeros of F(z) whose modulus is greater than 1 lie in

$$
\left| z + \frac{\rho}{a_n} \right| \leq \frac{[|\rho + a_n|(\cos\alpha + \sin\alpha) - |a_{n-k}|(\cos\alpha - \sin\alpha - \lambda\cos\alpha - \lambda\sin\alpha - \lambda + 1) - |a_0|(\cos\alpha - \sin\alpha - 1) + 2\sin\alpha \sum_{j=1, j\neq n-k}^{n-1} |a_j|]}{|a_n|} \ldots
$$

But the zeros of F(z) whose modulus is less than or equal to 1 already satisfy the above inequality. Hence all the zeros of F(z) lie in

$$
\left| z + \frac{\rho}{a_n} \right| \leq \frac{[|\rho + a_n|(\cos\alpha + \sin\alpha) - |a_{n-k}|(\cos\alpha - \sin\alpha - \lambda\cos\alpha - \lambda\sin\alpha - \lambda + 1) - |a_0|(\cos\alpha - \sin\alpha - 1) + 2\sin\alpha \sum_{j=1, j\neq n-k}^{n-1} |a_j|]}{|a_n|} .
$$

Since the zeros of P(z) are also the zeros of F(z), it follows that all the zeros of P(z) lie in

$$
\left| z + \frac{\rho}{a_n} \right| \leq \frac{[|\rho + a_n|(\cos\alpha + \sin\alpha) - |a_{n-k}|(\cos\alpha - \sin\alpha - \lambda\cos\alpha - \lambda\sin\alpha - \lambda + 1) - |a_0|(\cos\alpha - \sin\alpha - 1) + 2\sin\alpha \sum_{j=1, j\neq n-k}^{n-1} |a_j|]}{|a_n|}
$$

If $|a_{n-k}| > |a_{n-k+1}|$, then $|a_{n-k}| > |a_{n-k-1}|$, $\lambda < 1$ and we have, for $|z| > 1$, by using Lemma 1,

$$
\begin{aligned}
|F(z)| \geq \Big| a_n z^{n+1} + \rho z^n \Big| &- \Big| (\rho + a_n - a_{n-1}) z^n + (a_{n-1} - a_{n-2}) z^{n-1} + \ldots\ldots + (a_{n-k+1} - \lambda a_{n-k}) z^{n-k+1} \\
&+ (a_{n-k} - a_{n-k-1}) z^{n-k} - (1-\lambda) a_{n-k} z^{n-k+1} + (a_{n-k-1} - a_{n-k-2}) z^{n-k-1} + \ldots\ldots \\
&+ (a_1 - a_0) z + a_0 \Big|
\end{aligned}
$$

$$= |z|^n \Big[|a_n z + \rho| - \Big| (\rho + a_n - a_{n-1}) + (a_{n-1} - a_{n-2})\frac{1}{z} + \ldots\ldots + (a_{n-k+1} - \lambda a_{n-k})\frac{1}{z^{k-1}}$$
$$+ (a_{n-k} - a_{n-k-1})\frac{1}{z^k} - (1-\lambda)a_{n-k}\frac{1}{z^{k-1}} + (a_{n-k-1} - a_{n-k-2})\frac{1}{z^{k+1}} + \ldots.$$
$$+ (a_1 - a_0)\frac{1}{z^{n-1}} + \frac{a_0}{z^n} \Big| \Big]$$
$$> |z|^n \Big[|a_n z + \rho| - \{ |\rho + a_n - a_{n-1}| + |a_{n-1} - a_{n-2}| + \ldots\ldots + |a_{n-k+1} - \lambda a_{n-k}|$$
$$+ |a_{n-k} - a_{n-k-1}| + |1-\lambda||a_{n-k}| + |a_{n-k-1} - a_{n-k-2}| + \ldots\ldots + |a_1 - a_0|$$
$$+ |a_0| \} \Big]$$
$$\geq |z|^n \Big[|a_n z + \rho| - \{ (|\rho + a_n| - |a_{n-1}|)\cos\alpha + (|\rho + a_n| + |a_{n-1}|)\sin\alpha$$
$$+ (|a_{n-1}| - |a_{n-2}|)\cos\alpha + (|a_{n-1}| + |a_{n-2}|)\sin\alpha + \ldots\ldots + (|a_{n-k+1}| - |\lambda a_{n-k}|)\cos\alpha$$
$$+ (|a_{n-k+1}| + |\lambda a_{n-k}|)\sin\alpha + (|a_{n-k}| - |a_{n-k-1}|)\cos\alpha + (|a_{n-k}| + |a_{n-k-1}|)\sin\alpha$$
$$+ |1-\lambda||a_{n-k}| + (|a_{n-k-1}| - |a_{n-k-2}|)\cos\alpha + (|a_{n-k-1}| + |a_{n-k-2}|)\sin\alpha$$
$$+ \ldots\ldots + (|a_1| - |a_0|)\cos\alpha + (|a_1| + |a_0|)\sin\alpha + |a_0| \} \Big]$$
$$= |z|^n \Big[|a_n z + \rho| - \{ |\rho + a_n|(\cos\alpha + \sin\alpha) + |a_{n-k}|(\cos\alpha + \sin\alpha - \lambda\cos\alpha + \lambda\sin\alpha$$
$$+ 1 - \lambda) + |a_0|(\sin\alpha - \cos\alpha + 1) + 2\sin\alpha \sum_{j=1, j\neq n-k}^{n-1} |a_j| \} \Big]$$
$$> 0$$

if

$$\Big[|a_n z + \rho| > |\rho + a_n|(\cos\alpha + \sin\alpha) + |a_{n-k}|(\cos\alpha + \sin\alpha - \lambda\cos\alpha + \lambda\sin\alpha$$
$$+ 1 - \lambda) + |a_0|(\sin\alpha - \cos\alpha + 1) + 2\sin\alpha \sum_{j=1, j\neq n-k}^{n-1} |a_j|$$

This shows that the zeros of F(z) whose modulus is greater than 1 lie in

$$\Big| z + \frac{\rho}{a_n} \Big| \leq \frac{[|\rho + a_n|(\cos\alpha + \sin\alpha) + |a_{n-k}|(\cos\alpha + \sin\alpha - \lambda\cos\alpha + \lambda\sin\alpha + 1 - \lambda) + |a_0|(\sin\alpha - \cos\alpha + 1) + 2\sin\alpha \sum_{j=1, j\neq n-k}^{n-1} |a_j|]}{|a_n|}.$$

But the zeros of F(z) whose modulus is less than or equal to 1 already satisfy the above inequality. Hence all the zeros of F(z) and therefore P(z) lie in

$$\Big| z + \frac{\rho}{a_n} \Big| \leq \frac{[|\rho + a_n|(\cos\alpha + \sin\alpha) + |a_{n-k}|(\cos\alpha + \sin\alpha - \lambda\cos\alpha + \lambda\sin\alpha + 1 - \lambda) + |a_0|(\sin\alpha - \cos\alpha + 1) + 2\sin\alpha \sum_{j=1, j\neq n-k}^{n-1} |a_j|]}{|a_n|}$$

That proves Theorem 3.

References

[1] A.Aziz And B.A.Zargar, Some Extensions Of The Enestrom-Kakeya Theorem, Glasnik Mathematiki, 31(1996), 239-244.

[2] N.K.Govil And Q.I.Rehman, On The Enestrom-Kakeya Theorem, Tohoku Math. J.,20(1968), 126-136.

[3] N.K.Govil And G.N.Mc-Tume, Some Extensions Of The Enestrom- Kakeya Theorem, Int.J.Appl.Math. Vol.11,No.3,2002, 246-253.

[4] M.H.Gulzar, On The Location Of Zeros Of A Polynomial, Anal. Theory. Appl., Vol 28, No.3(2012), 242-247.

[5] M. H. Gulzar, On The Zeros Of Polynomials, International Journal Of Modern Engineering Research, Vol.2,Issue 6, Nov-Dec. 2012, 4318- 4322.

[6] A. Joyal, G. Labelle, Q.I. Rahman, On The Location Of Zeros Of Polynomials, Canadian Math. Bull.,10(1967), 55-63.

[7] M. Marden , Geometry Of Polynomials, Iind Ed.Math. Surveys, No. 3, Amer. Math. Soc. Providence,R. I,1996.

[8] W. M. Shah And A.Liman, On Enestrom-Kakeya Theorem And Related Analytic Functions, Proc. Indian Acad. Sci. (Math. Sci.), 117(2007), 359-370.

[9] E C. Titchmarsh,The Theory Of Functions,2nd Edition,Oxford University Press,London,1939.

Effect Of Mode Of Training On Product Quality The Case Study Of Arc Welding In Small Scale Metalworking Enterprises In Kenya

[1]Dr. Charles M.M. Ondieki, [2]Prof.Elifas T. Bisanda, [3]Prof. Wilson O.Ogola

[1,]Multimedia University college of Kenya;
[2,]Open University of Tanzania;
[3,]Kenya Polytechnic University College

Abstract

The quality of products from the micro and small enterprise sector is affected by both the entrepreneur's and enterprise's attributes. This paper presents and discusses findings of a study that was designed to investigate experimentally the relationship between the quality of arc welding in the Small Scale Metalwork sub-sector and the artisan's mode of training. Four pairs of groups with a total of 36 with secondary education and 36 with primary education consisting of formally and informally trained artisans from urban and rural areas participated in the evaluation. A mild steel product was fabricated by each participating artisan, assessed and scores awarded based on the quality of arc welding. The analysis of variance (ANOVA) was used to show any variation in the quality of arc welding; comparisons of means using the Least Significant Difference (LSD) at the alpha level of 5% were done to determine which pairs of artisans affected quality significantly. The study found out that informally trained artisans with secondary education working in urban areas exhibited the highest quality of arc welding. The informally trained artisans with primary education working in rural areas exhibited the lowest quality of arc welding. Generally formal training does not have a significant effect on urban artisans, but it does improve product quality of arc welding from artisans in rural areas. The findings of the study provide evidence that formal training can improve product quality from artisans working in rural areas, and therefore more resources should be channelled to training of rural artisans.

Key Words: Modes of Training, Product Quality, MSE, Metalworking sub-sector, Arc welding

1. Introduction

The quality of products from the MSE sector is affected by both the entrepreneur's and enterprise's attributes. Many school leavers, retirees and retrenchees as well as those dissatisfied with formal wage employment resort to entrepreneurial activities within this sector as a means of earning a living. However, the MSE sector entrepreneurs suffer various deficiencies in business management. These deficiencies are attributable to their low education levels and training, which in turn adversely affect their ability to produce high quality products among others. The influence of the entrepreneur's attributes such as age, gender, educational level, mode of training, work experienceand membership to business support groups on the productivity and performance of enterprises has been reported. Similarly, enterprise attributes such as its age, location, ownership structure, and formal status and business activity determine production outcomes (Kimuyu, 2001). This paper discusses the findings of a study that was designed to investigate experimentally the relationship between the quality of arc welding in the Small Scale Metalwork sub-sector and the artisan's mode of training. The understanding and validation of this relationship is important for the effective marketing of the MSE products. While it is accepted that higher education and training is necessary for faster individual development, the same may not necessarily be true for product quality. Many people argue that education levels do not affect the quality of products; what matters is the working experience and training and so far there are no experimental data to support this. It is also believed that the MSE/*Jua Kali* products are of poor quality and thus cannot get regional and international markets. There is, therefore, a need to find out how the artisan's mode of training and other attributes influence the quality of products. In their studies Fluitman (1989), K'Aol (1995) and Ferej (1994) found out that training for skills or management for entrepreneurs in the metalworking sub-sector is provided in an uncoordinated manner through on-the-job training or apprenticeships. Apprenticeship has been identified by many studies as appropriate for the informal sector (Fluitman, 1989; K'Aol, 1995; Ferej, 1994).

According to McGrath *etal*., (1994) enterprise-based training provides a package of technical and other skills that the worker will require in the world of work. Kinyanjui (1997) found out that most of the technical training in the MSE sector (particularly in manufacturing and services) was carried out through the traditional apprenticeship system; according to the study 71% of MSE artisans obtain their skills on-the-job training, 19% in formal training, and 7% from friends; formal training are not deemed to be very important by the small producers - most MSE owners indicated that there was no need for formal training for their workers. Haan (2001) reported that a tracer study of theWorld Bank Training Voucher Scheme (MSETTP)hadfound out the mean sales of MSEs who did not participate in the training decreased by 2% while the mean sales of the MSEs who participated in the training voucher scheme more than doubled: from KSh.8,342 to KSh.18,235 per month. The beneficiaries of the scheme performed better than the control group on almost all variables studied such as assets, volume of sales, and diversification of products, business creation, and

employment creation. This is an indication that organized training significantly improves the performance of the MSEs. More survey results suggest a relationship between the possession of vocational training certificates and income, but weaker than in the case of education(Haan, 2001).However, no experimental study has been carried out in Kenya (both in urban and rural areas) to find out whether the enterprise-based training is superior to formal training conducted by technical institutions or other similar organized programs. Most of the previous studies obtained their data through the use of one or more of the following instruments: questionnaires, desk reviews, observations, interviews, focus group discussions, and content analysis. These studies were either qualitative or survey researches, while the present study was mainly experimental research (with a bit of qualitative using observation as far as the use of welding equipment and welding techniques are concerned to find out which groups – secondary/primary or urban/rural - were proficient or understood the welding process).In arc welding processes the most common defects are either surface defects (cracks, distortion, overlaps and rolls, undercuts, excessive spatter, and bad weld surface appearance) or subsurface (hidden) weld defects. These defects come as a result of:

a) Improper selection of process, for example, using a very deep penetrating heat source on a narrow Vee angle so causing cracking in the root run due to large depth-to-width ratio;
b) Applying the welding process incorrectly for the particular application, such as incorrect current setting or excess weld metal deposition;
c) The interaction of the weld metal with prior defects in the base metal, e.g. laminations and impurities like phosphorous, sulphur, and silicate, etc. that cause brittle and weak zones resulting in lamellar tearing;
d) Undesirable metallurgical structure with respect to grain size and hardness as well as undesirable inclusions such as tungsten oxide and slag. Hydrogen is a most undesirable inclusion as it is often the main cause of cold cracking in steels;
e) Undesirable shape and size of weld bead due to overfill and/or poor profile;
f) Incorrect joint preparations and poor fit-up leading to inaccessibility and lack of fusion, cracking, etc.;
g) Stray arcing, tool marks, undercuts, inclusions, poor finish, lack of fusion and penetration, and incorrect weld shape causing a reduction in fatigue life and joint strength;

All these are consequences of the level of training, experience and equipment used. For one to produce a quality product the sequence of welding techniques commonly used (Parmar, 1997), are:

a) The preliminary operations like cleaning, edge preparation, and the fixing of tab-in and tab-out plates are accomplished;
b) Parts are assembled by tack welding or by employing jigs and fixtures;
c) The assembled work piece is presented to the machine or vice versa;
d) Welding is initiated by striking the arc for fusion welding or by bringing electrodes in contact with the work and switching on the current for resistance welding;
e) Relative movement between the welding head and the work to attain the desired welding speed is created;
f) The welding variables like arc voltage, welding current, and wire feed rate is controlled - controlling the welding variables like arc voltage controls the arc length, welding current, and wire feed rate;
g) Welding process is stopped by stopping the relative movement between the welding head and the work;
h) The welding head is shifted to the position the next welding cycle is to be initiated;
i) The completed work is removed.

1.1 Objectives of the Study

The objectives of this study were to compare the product quality in terms of mean scores from formally trained artisans with the artisans that are trained-on-the-job, both with the following attributes:

i) Secondary education working in urban and rural areas;
ii) Primary education working in urban and rural areas.

2 .Material And Methods

2.1 Sampling

The target population of the study consisted of experienced artisans who had completed class eight of the Kenyan primary education and experienced artisans who had completed form four of the Kenyan secondary education. The artisans were selected both from rural and urban areas with two modes of training (on-the-job training and formal technical training). The Kenyan MSE sector engages about 8.33 million operators (Government of Kenya, 2010). Out of this the *Jua Kali* sector (the MSEs that are engaged in technical work) is about 18% according to the National MSE baseline Survey conducted in 1999. The most widely used welding method is arc welding for mild steel products, and according to the survey the number of artisans engaged in welding and fabrication is about 37,485 (Government of Kenya, 1999). About 60% and 40% of this number comprise primary education class eight graduates and secondary education form four graduates respectively (Government of Kenya, 2004). Based on these figures the total population for primary class eight artisans was taken to be 22,491 and for secondary form four was taken to be 14,994. A total of

36 artisans with primary education class eight and a total of 36 artisans with secondary education form four were selected for assessment. The sample size determination was based on the relation:

$n = \frac{Nc^2}{c^2 + (N-1)e^2}$; where n = sample size, N = population size,

c = coefficient of variation (≤ 30%), and e = error margin (≤ 5%).

This formula enabled the researchers to minimize the error and enhance stability of the estimates (Nassiuma, 2000). In this study *c* was taken to be 30% and *e* to be 5% (using the maximum percentage in each case). Table 1 show the number and category of artisans who participated in this study.

Table 1: Number and category of artisans who participated

Education Level	Attributes	Urban Area	Rural Area	Total
Secondary Education	Formally trained	5	14	**19**
	Informally trained	10	7	**17**
	Total	***15***	***21***	***36***
Primary Education	Formally trained	6	10	**16**
	Informally trained	8	12	**20**
	Total	***14***	***22***	***36***
Total		**29**	**43**	**72**

The Directorate of Industrial Training (DIT) testing centers were used for this research. This was meant to minimize the effect on the quality of the fabricated products due to the condition of the welding equipment; (the welding equipments used in all DIT testing centers are more else of the same working condition).

Table 2: DIT Testing centres and number of participating artisans

DIT Centre (Province)	Education Level	Urban		Rural		Total
		F	**I**	**F**	**I**	
1. NIVTC (Nairobi)	Primary	2	2	0	0	4
	Secondary	2	3	0	1	6
2. Ruaraka (Nairobi)	Primary	1	0	0	0	1
	Secondary	1	2	0	0	3
3. Kakamega (Western)	Primary	0	0	1	1	2
	Secondary	0	0	1	0	1
4. Turbo (Western)	Primary	0	0	4	0	4
	Secondary	0	0	11	1	12
5. Kiambu (Central)	Primary	0	0	2	2	4
	Secondary	0	0	0	1	1
6. Machakos (Eastern)	Primary	0	0	3	7	10
	Secondary	0	0	0	2	2
7.Mombasa (Coast)	Primary	0	5	0	0	5
	Secondary	1	2	0	1	4
8. Eldoret (Rift Valley)	Primary	0	0	0	0	0
	Secondary	0	1	0	0	1
9. Nakuru (Rift Valley)	Primary	0	0	0	1	1
	Secondary	1	0	1	0	2
10.Kisumu (Nyanza)	Primary	3	1	0	1	5
	Secondary	0	2	1	1	4
Total		**11**	**18**	**24**	**19**	**72**

F – Formally Trained; I – Informally Trained (i.e. trained-on-the-job)

The selected DIT testing centers were those with high concentrations of welders, and easily accessible by the researchers. A total of ten (10) DIT testing centers were used as shown in Table 2. Work started at the same time in all testing centers. Research assistants (who had been selected from among the DIT trained examiners) were used to supervise the participating artisans. The independent variable of the study was the mode of training, while the dependent variable was the scores awarded to indicate the quality of the product fabricated by the artisan-using arc welding processes. The effect of mode of training was evaluated by comparing the mean scores of the following groups:

a) Formally and informally trained artisans with secondaryeducation in urban areas.
b) Formally and informally trained artisans with secondaryeducation in rural areas.
c) Formally and informally trained artisans with primary education in urban areas.
d) Formally and informally trained artisans with primary education in rural areas.

Besides the above primary groups, the effect of mode of training was also evaluated by comparing the mean scores of the following combined groups of artisans with different other attributes:

e) All formally and informally trained artisans with secondaryeducation.
f) All formally and informally trained artisans with primaryeducation.
g) All formally and informally trained artisans working in urban areas.
h) All formally and informally trained artisans working in rural areas.
i) All formally and informally trained artisans.

2.2 Data Generation Tools

Two instruments were used to collect the required data. These were:
i) Structured questionnaires, and
ii) Assessment of fabricated product.

The questionnaire was used mainly to get information regarding the artisan's attributes and business characteristics. The participating artisans were generally observed to find out how proficient they were in using the welding equipment and methods/techniques as outlined in the introduction.

2.3 Assessment of Product Design

Drawing a mild steel product shown in figures 1 was used in the research. The welding project was marked out 100%. The product was designed in such a way that most of the welding techniques were to be used in fabricating it.

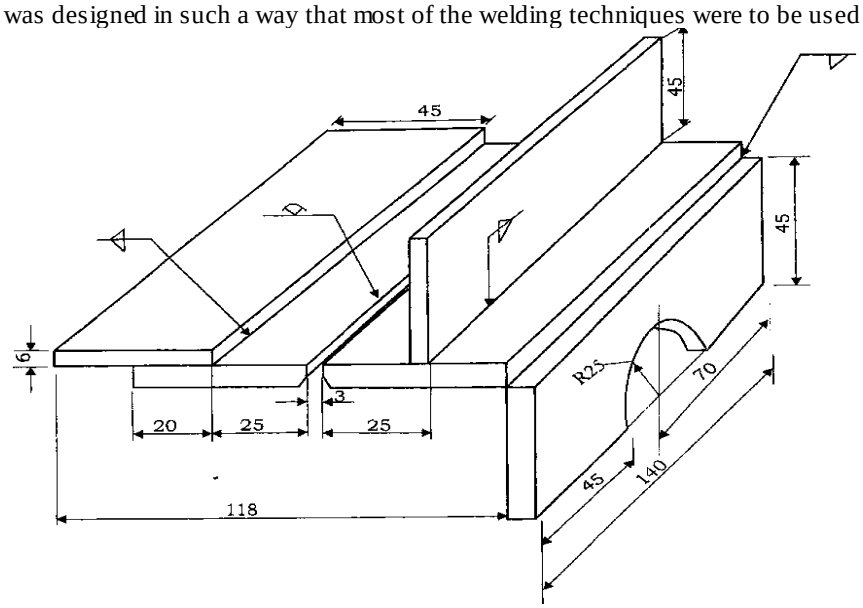

Figure 1: Mild Steel Welding Project

In this study, manual welding was employed; the artisans were given materials in the form of sheets and they were supposed to measure and cut the parts to the sizes shown. The parts were joined together using arc welding processes. The assessment was carried out by checking for the correct part sizes (by using vernier calipers), and examining for the correct part alignment, correct welding and product finish; visual inspection was used to detect surface defects. Careful visual inspection of welds can detect about 80% to 90% of the defects and flaws (Parmar, 1997). The quality of welded joints depends upon the design of the product, the performance of welding equipment, the welding procedures followed, and the skill of the operator. In this study any deficiency in the design and equipment affected all artisans equally. Therefore, the skill of the welder was to determine the scores obtained.

3.Results And Discussion

The data scores collected were analyzed using the Statistical Analysis System (SAS) and excel spreadsheet. The means and standard deviations were generated to describe the quality of arc welding with regard to mode of training. The scores were matched with the artisans' attributes to find their relationships. The analysis of variance (ANOVA) was used to show any variation in the quality of arc welding in each of the eight groups of artisans due to the different treatments, that is, modes of training. Comparisons of all possible pairs of means using the Least Significant

Difference (LSD) method with alpha set at 5% were done to determine which pairs of artisans with quality performances that was significantly different.The eight primary groups could broadly be divided into two: those artisans who were formally trained and those artisans who were trained-on-the-job. A total of 35 participants/artisans who had been formally trained were selected, while a total of 37 participants/artisans who had been trained-on-the-job were selected for this study. The artisans' marks awarded for quality of arc welding provided the data for determining the effects or impact of training on product quality. The objective of the study sought to determine whether there were differences in product quality when using arc welding processes by formally trained artisans and those artisans trained-on-the-job. The specific objective was to find out whether there is any relationship between product quality (quality of arc welding) and mode of training.The analysis of variance was carried out and the results are presented in Tables 3 and 4. Table 3 shows mean scores of product quality for modes of training for primary groups of artisans with the same attributes, and Table 4 showsmean scores of product quality for modes of training from combined groups of artisans with different other attributes.

Table 3: Mean scores of product quality for modes of training for primary groups of artisans with same attributes

Mode of Training	Secondary		Primary		Cumulative Mean Scores
	Urban	Rural	Urban	Rural	
Formal	68.700[a]	69.857[a]	66.583[a]	60.350[b]	**66.41[b]**
Informal	73.450[a]	65.071[a]	70.250[a]	50.875[c]	**63.85[b]**

The means followed by the same letter in the same column are not significantly different at α = 5% using LSD.

Table 3 shows that there are no significant differences in the mean scores of the first three columns. Both formally and informally trained artisans with secondary education perform equally irrespective of their business locations. The same also applies to those artisans with primary education but located in urban areas. However, there is a significant difference in mean scores of the formally trained and informally trained artisans located in the rural areas, with the mean score of product quality from artisans formally trained being higher. The implication from this analysis is that the combined effect of business location and training has very little effect on the performance of artisans with secondary education irrespective of their business locations. In the case of artisans with primary education the combined effect of business location and training has very little effect on the performance of those in urban areas while having a significant effect on those artisans in the rural areas; those informally trained artisans in the rural areas performed poorly. Although the analysis of variance (ANOVA) showed that the combination of education level, mode of training and business location does not have a significant impact on the quality of arc welding, it does affect the informally trained artisans in the rural areas significantly.

Table 4: Mean scores of product quality for modes of training from combined groups of artisans with different other attributes

Modes of Training	Secondary	Primary	Urban	Rural	Overall Mean
Formal	69.55[a]	62.69[b]	67.55[a]	65.90[b]	**66.41[a]**
Informal	70.00[a]	58.63[b]	72.03[a]	56.11[c]	**63.85[a]**

The means followed by the same letter in the same column are not significantly different at α = 5% using LSD.

Table 4 shows that there are no significant differences in the mean scores in all columns except for the rural column. This means that the performance of both formally and informally trained artisans with secondary and primary education, or working in urban areas does not significantly differ. This implies that the mode of training does not have a significant impact on product quality of products from artisans with secondary and primary education, or working in urban areas. However, there is a significant difference in the mean scores in the rural column. This implies that the mode of training has significant impact on product quality of products from artisans working in rural areas. Overall there is no significant difference in mean scores between the formal training and the informal training; however, the formally trained artisans mean score is slightly better than that from artisans with informal training.These results are consistent with the findings of Mullei (2003). In his study on small manufacturing firms Mullei (2003) sought to identify factors that determine firm growth and transformation among small firms in Kenya. The study covered food processing, woodworking, textile and garments, and metal working sub-sectors. The study found out that for an enterprise to graduate from, say micro to small enterprise, the education of the manager/owner and the sector to which the enterprise belonged to, had a significant influence on enterprise graduation. Education was found to have a marginal effect on graduation, probably indicating the importance of vocational training skills (formal training), which are lacking among many small producers. Mullei (2003) also found out that more than half of small producers were

primary school graduates whose ability to assimilate new technologies, innovate and imitate perfectly is limited. The study, therefore, recommends the raising of managerial, vocational and technical skills of small entrepreneurs for long-term industrial development. This shows the importance of higher level of education and formal training.In overall there is no significant difference in mean scores from formally and informally trained artisans, as the last column shows. This further confirms the ANOVA results using SAS which showed that the mode of training has very little impact on product quality from artisans. This also confirms that the combined effect of training and education does not have a significant impact on product quality.

From these analyses it can be concluded that formal training has very little impact on artisans with secondary education or those working in urban areas, but it has a significant impact on artisans with primary education working in rural areas. The formal training improves product quality from artisans with primary education working in the rural areas. Those artisans with secondary education are able to follow the recommended welding techniques better than those artisans with primary education; this was observed during the evaluation exercise. The urban artisans perform better than the rural artisans because they have more exposure and more information, have more work and therefore more experience, more competition, use standard tools similar to those used at DIT centres, better methods of working, more contact with more experienced artisans etc.

Generally artisans formally trained performed better than artisans that trained-on-the-job (or informally trained) in all cases except for those artisans working in urban areas. Artisans that trained-on-the-job working in urban areas performed better than those artisans formally trained irrespective of their education levels. This confirms what Ferej (1994) found out in his study on the entrepreneurial knowledge and skills of apprentices in formal and informal training systems in Kenya, to determine the efficacy of apprenticeships in preparing skilled workers for self employment. He found out that informal sector apprentices were perceived to have acquired significantly higher competency levels than the formally trained apprentices in marketing and technical and operational skills. This study, however, was carried out in Nairobi (urban) through interviews and observations. This could be the reason why it is widely believed in Kenya that enterprise-based training (that is, informal training) is superior to formal training. Most studies on MSEs in Kenya have been carried out in urban areas, where, as this study's results also confirm, the product quality from informally trained artisans is superior to that from formally trained artisans. This study was carried out both in urban and rural areas and went further by categorizing the artisans into eight (8) distinct groups, thus making it more unique in approach.

The study found out that both informally trained artisans with secondary education as well as those with primary education whose businesses are located in urban areas performed better than their counterparts located in the same areas even though they are formally trained. However, it was expected that the formally trained could perform better than those informally trained since they are all working in the same urban areas. From the questionnaires it was found out that more than 60% of the formally trained artisans working in urban areas planned to look for formal employment, while less than 20% of those artisans trained-on-the-job working in urban areas planned to look for formal employment. In the case of those in rural areas the result was different; less than 25% of the formally trained artisans and less than 10% those trained-on-the-job planned to look for formal employment. This means that the formally trained artisans in urban areas are not contented with their self-employment and therefore do not concentrate on their work as much as those without formal training do. This could probably explain why the informally trained artisans in urban areas perform better than the formally trained artisans. The formally trained artisans can easily get formal employment because they hold certificates, while those trained-on-the-jobs find it difficult to be employed in the formal sector without certificates. On the other hand those in the rural areas have very little opportunity for formal employment, which is mostly found in urban areas; hence even those formally trained artisans concentrate on their jobs as much as those without formal training do.

Overall, there is no significant difference in product quality between formally trained artisans and informally trained artisansas evidenced from the last columns of the two tables of mean scores. This implies that training alone does not have a significant impact on product quality.

4.Conclusions And Recommendations

The following are the conclusions of this study:

a) Training alone has very little impact on product quality; however, when combined with business location the impact on product quality is very significant.
b) Formal training can improve the product quality from artisans with lower education working in rural areas.
c) The product quality from informally trained artisans with low education can be improved by either giving them formal training or raising their education level.
d) While formal training improves performance of artisans working in the rural areas, it, however, contributes very little to those artisans working in urban areas.

The following **recommendations** are suggested:

a. More formal training should be given to primary school leavers working in the rural areas so as to raise their product quality to the level of those artisans with secondary education level.
b. Since formal training does not make any significant difference to those working in urban areas, more resources should be channelled to those artisans working in rural areas rather than to those artisans working in urban areas.
c. To further augment the present achievements of this study:

- Research studies should be designed to investigate how other attributes (such as the entrepreneur's age, gender, educational attainment, work experienceand membership in business support groups, and enterprise attributes such as its age, location, ownership structure, and formality status and business activity) affect product quality and/or the performance of the MSE sector;
- Research should be conducted to investigate how the mode of training affect the quality of product quality in other disciplines especially those that are mostly dominated by women, for example tailoring, tie and dye, embroidery, and basketry;
- The study found out that both informally trained artisans with secondary education as well as those with primary education whose businesses are located in urban areas performed better than their counterparts located in the same areas even though they are formally trained. However, it was expected that the formally trained could perform better than those informally trained since they are all working in the same urban areas. It is recommended that further research be conducted to investigate this phenomenon.

References

[1] A. Ferej. The efficacy of apprenticeship training as preparation for self-employment in Kenya. Unpublished Doctoral Thesis. Illinois; University of Illinois at Urbana-Champaign, 1994.
[2] F. Fluitman. Training for work in the informal sector: An agenda item for the 1990s. Discussion Paper (16). Geneva: ILO, 1989.
[3] Government of Kenya. Economic Survey 2010. Nairobi, Government Printer, 2010.
[4] Government of Kenya. Directorate of Industrial Training Records on Trade Tests. Nairobi; DIT records, 2004.
[5] Government of Kenya. National Micro and Small Enterprise Baseline Survey 1999. Nairobi: Government Printer, 1999.
[6] Government of Kenya. Industrial transformation to the year 2020.Sessional Paper No. 2. Nairobi, Government Printers, 1996.
[7] H. C. Haan. Training for Work in the Informal Sector: Evidence from Kenya, Tanzania and Uganda. Turin; UNDP/ILO Turin Centre paper, p. 26-27, 2001.
[8] G. O. K'Aol. Perceptions of craftsmen and apprentices regarding self-employment skill acquisition in the Kenyan informal sector. Doctoral Thesis: Illinois; University of Illinois at Urbana-Champaign, 1995.
[9] P. Kimuyu. Micro-Level Institutions & Enterprise Productivity: Insights From Kenya's Small Business Sector, 2001.
[10] M. Kinyanjui. A study of training needs and aspects of training in informal workshop clusters in Nairobi. Nairobi; Institute for Development Studies, University of Nairobi, 1997.
[11] S. McGrath andK. King with F. Leach andC. Roy,in association with O. Boeh-Ocansey, K. D'Souza, G. Messina andH. Oketch. Education and training for the informal sector. Education Research Paper No. 11. London; ODA, 1994.
[12] A. Mullei. Growth and Transformation of Small Manufacturing Firms in Africa: Insights from Ghana, Kenya, and Zimbabwe, Nairobi: African Centre for Economic Growth, 2003.
[13] D. K. Nassiuma. Survey sampling: Theory and methods. Nairobi, University of Nairobi press, 2000.
[14] R. S. Parmar. Welding Engineering and Technology, First edition; Khana publishers, New Delhi, India, 1997.

Strong Triple Connected Domination Number of a Graph

[1,]G. Mahadevan, [2,]V. G. Bhagavathi Ammal, [3,] Selvam Avadayappan, [4,]T. Subramanian

[1,4]Dept. of Mathematics, Anna University : Tirunelveli Region, Tirunelveli.
[2]PG. Dept. of Mathematics, Sree Ayyappa College for Women, Chunkankadai, Nagercoil.
[3]Dept.of Mathematics, VHNSN College, Virudhunagar.

Abstract: The concept of triple connected graphs with real life application was introduced in [14] by considering the existence of a path containing any three vertices of a graph G. In [3], G. Mahadevan et. al., introduced Smarandachely triple connected domination number of a graph. In this paper, we introduce a new domination parameter, called strong triple connected domination number of a graph. A subset S of V of a nontrivial graph G is said to be smarandachely triple connected dominating set, if S is a dominating set and the induced sub graph $<S>$ is triple connected. The minimum cardinality taken over all triple connected dominating sets is called the triple connected domination number and is denoted by γ_{tc}. A set $D \subseteq V(G)$ is a strong dominating set of G, if for every vertex $x \in V(G) - D$ there is a vertex $y \in D$ with $xy \in E(G)$ and $d(x,G) \leq d(y,G)$. The strong domination number $\gamma_{st}(G)$ is defined as the minimum cardinality of a strong domination set. A subset S of V of a nontrivial graph G is said to be strong triple connected dominating set, if S is a strong dominating set and the induced sub graph $<S>$ is triple connected. The minimum cardinality taken over all strong triple connected dominating sets is called the strong triple connected domination number and is denoted by γ_{stc}. We determine this number for some standard graphs and obtain bounds for general graph. Its relationship with other graph theoretical parameters are also investigated.

Key Words: Domination Number, Triple connected graph, Strong Triple connected domination number

AMS Subject Classification: *05C 69*

1 Introduction

By a graph we mean a finite, simple, connected and undirected graph G(V, E), where V denotes its vertex set and E its edge set. Unless otherwise stated, the graph G has p vertices and q edges. Degree of a vertex v is denoted by d(v), the maximum degree of a graph G is denoted by Δ(G). We denote a cycle on p vertices by C_p, a path on p vertices by P_p, and a complete graph on p vertices by K_p. A graph G is connected if any two vertices of G are connected by a path. A maximal connected subgraph of a graph G is called a component of G. The number of components of G is denoted by ω(G). The complement $\overline{G}$ of G is the graph with vertex set V in which two vertices are adjacent if and only if they are not adjacent in G. A tree is a connected acyclic graph. A bipartite graph (or bigraph) is a graph whose vertex set can be divided into two disjoint sets V_1 and V_2 such that every edge has one end in V_1 and another end in V_2. A complete bipartite graph is a bipartite graph where every vertex of V_1 is adjacent to every vertex in V_2. The complete bipartite graph with partitions of order $|V_1|=m$ and $|V_2|=n$, is denoted by $K_{m,n}$. A star, denoted by $K_{1,p-1}$ is a tree with one root vertex and p – 1 pendant vertices. A bistar, denoted by B(m, n) is the graph obtained by joining the root vertices of the stars $K_{1,m}$ and $K_{1,n}$. The friendship graph, denoted by F_n can be constructed by identifying n copies of the cycle C_3 at a common vertex. A wheel graph, denoted by W_p is a graph with p vertices, formed by connecting a single vertex to all vertices of C_{p-1}. A helm graph, denoted by H_n is a graph obtained from the wheel W_n by attaching a pendant vertex to each vertex in the outer cycle of W_n. Corona of two graphs G_1 and G_2, denoted by $G_1 \circ G_2$ is the graph obtained by taking one copy of G_1 and $|V_1|$ copies of G_2 ($|V_1|$ is the number of vertices in G_1) in which i^{th} vertex of G_1 is joined to every vertex in the i^{th} copy of G_2. If S is a subset of V, then <S> denotes the vertex induced subgraph of G induced by S. The open neighbourhood of a set S of vertices of a graph G, denoted by N(S) is the set of all vertices adjacent to some vertex in S and N(S) ∪ S is called the closed neighbourhood of S, denoted by N[S]. The diameter of a connected graph is the maximum distance between two vertices in G and is denoted by diam(G). A cut – vertex (cut edge) of a graph G is a vertex (edge) whose removal increases the number of components. A vertex cut, or separating set of a connected graph G is a set of vertices whose removal results in a disconnected. The connectivity or vertex connectivity of a graph G, denoted by κ(G) (where G is not complete) is the size of a smallest vertex cut. A connected subgraph H of a connected graph G is called a H -cut if ω(G – H) ≥ 2. The chromatic number of a graph G, denoted by χ(G) is the smallest number of colors needed to colour all the vertices of a graph G in which adjacent vertices receive different colour. For any real number x, ⌊x⌋ denotes the largest integer less than or equal to x. A Nordhaus -Gaddum-type result is a (tight) lower or upper bound on the sum or product of a parameter of a graph and its complement. Terms not defined here are used in the sense of [2]. A subset S of V is called a dominating set of G if every vertex in V − S is adjacent to at least one vertex in S. The domination number γ(G) of G is the minimum cardinality

taken over all dominating sets in G. A dominating set S of a connected graph G is said to be a *connected dominating set* of G if the induced sub graph <S> is connected. The minimum cardinality taken over all connected dominating sets is the **connected domination number** and is denoted by γ_c. A subset *S* of *V* is called a **strong dominating set** of G, if for every vertex $x \in V(G) - D$ there is a vertex $y \in D$ with $xy \in E(G)$ and $d(x,G) \leq d(y,G)$. The **strong domination number** $\gamma_{st}(G)$ is defined as the minimum cardinality of a strong domination set. One can get a comprehensive survey of results on various types of domination number of a graph in [17, 18, 19].Many authors have introduced different types of domination parameters by imposing conditions on the dominating set [15, 16]. Recently, the concept of triple connected graphs has been introduced by Paulraj Joseph J. et. al.,[14] by considering the existence of a path containing any three vertices of G. They have studied the properties of triple connected graphs and established many results on them. A graph G is said to be **triple connected** if any three vertices lie on a path in G. All paths, cycles, complete graphs and wheels are some standard examples of triple connected graphs. In [3] Mahadevan G. et. al., introduced triple connected domination number of a graph and found many results on them.

A subset S of V of a nontrivial connected graph G is said to be **triple connected dominating set**, if S is a dominating set and the induced sub graph <S> is triple connected. The minimum cardinality taken over all triple connected dominating sets is called the **triple connected domination number** of G and is denoted by γ_{tc}(G). In [4, 5, 6, 7, 8, 9] Mahadevan G. et. al., introduced complementary triple connected domination number, paried triple connected domination number, complementary perfect triple connected domination number, triple connected two domination number, restrained triple connected domination number, dom strong triple connected domination number of a graph. In [10], the authors also introduced weak triple connected domination of a graph and established many results.In this paper, we use this idea to develop the concept of strong triple connected dominating set and strong triple connected domination number of a graph.

Theorem 1.1 [14] A tree *T* is triple connected if and only if $T \cong P_p$; $p \geq 3$.

Theorem 1.2 [14] A connected graph *G* is not triple connected if and only if there exists a*H* -cut with $\omega(G - H) \geq 3$ such that $|V(H) \cap N(C_i)| = 1$ for at least three components C_1, C_2, and C_3 of $G - H$.

Theorem 1.3 Let G be any graph and D be any dominating set of G. then $|V - D| \leq \sum_{u \in V(D)} \deg(u)$ and equality hold in this relation if and only if D has the following properties.

i. D is independent
ii. For every $u \in V - D$, there exists a unique vertex $v \in D$ such that $N(u) \cap D = \{v\}$

Notation 1.4 Let *G* be a connected graph with *m* vertices $v_1, v_2, \ldots, v_m$. The graph obtained from *G* by attaching n_1 times a pendant vertex of P_{l_1} on the vertex v_1, n_2 times a pendant vertex of P_{l_2} on the vertex v_2 and so on, is denoted by $G(n_1P_{l_1}, n_2P_{l_2}, n_3P_{l_3}, \ldots, n_mP_{l_m})$ *where* $n_i, l_i \geq 0$ and $1 \leq i \leq m$.

Example 1.5 Let v_1, v_2, v_3, v_4, be the vertices of K_5. The graph $K_5(P_2, 3P_2, P_3, 2P_4, P_2)$ is obtained from K_5 by attaching 1 time a pendant vertex of P_2 on v_1, 3 time a pendant vertex of P_2 on v_2, 1 time a pendant vertex of P_3 on v_3 and 2 times a pendant vertex of P_4 on v_4, 1 time a pendant vertex of P_2 and is shown in Figure 1.1.

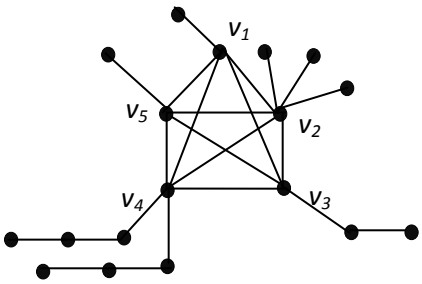

Figure 1.1 : $K_5(P_2, 3P_2, P_3, 2P_4)$

2 Strong Triple connected domination number

Definition 2.1

A subset *S* of *V* of a nontrivial graph *G* is said to be a *strong triple connected dominating set*, if *S* is a strong dominating set and the induced subgraph <*S*> is triple connected. The minimum cardinality taken over all strong triple connected dominating sets is called the *strong triple connected domination number* of *G* and is denoted by $\gamma_{stc}(G)$. Any strong triple connected dominating set with γ_{stc} vertices is called a γ_{stc} -set of *G*.

Example 2.2 For the graph H_1 in Figure 2.1, $S = \{v_2, v_3, v_5\}$ forms a γ_{stc} -set of H_1. Hence $\gamma_{stc}(H_1) = 3$

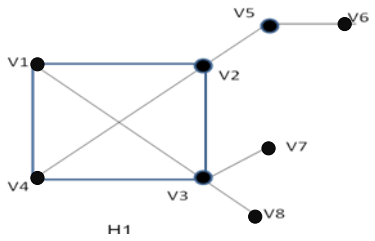

Figure 2.1 : Graph with $\gamma_{stc} = 3$.

Observation 2.3 Strong triple connected dominating set (stcd set) does not exists for all graphs and if exists, then $\gamma_{stc}(G) \geq 3$.

Example 2.4 For the graph G_1 in Figure 2.2, any minimum dominating set must contain the supports and any connected subgraph containing these supports is not triple connected, which is a contradiction and hence γ_{stc} does not exists.

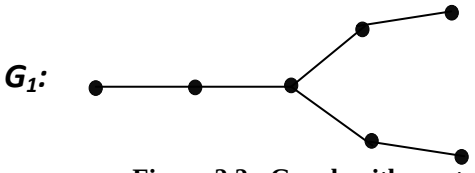

Figure 2.2 : Graph with no stcd set

Throughout this paper we consider only connected graphs for which strong triple connected dominating set exists.

Preposition 2.5 Let D be any strong triple connected dominating set. Then $|V - D| < \sum_{u \in V(D)} d(u), \quad \forall\ u \in D.$

Proof The proof follows directly from Theorem 1.3.

Observation 2.6 Every strong triple connected dominating set is a dominating set but not conversely.

Observation 2.7 Every strong triple connected dominating set is a triple connected dominating set but not conversely.

Observation 2.8 The complement of the strong triple connected dominating set need not be a strong triple connected dominating set.

Example 2.9 For the graph H_1 in Figure 2.3, $S = \{v_1, v_2, v_3\}$ forms a Strong triple connected dominating set of H_1. But the complement $V - S = \{v_4, v_5, v_6\}$ is not a strong triple connected dominating set.

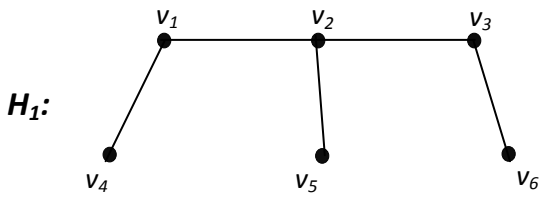

Figure 2.3 : Graph in which V – S is not a stcd set

Observation 2.10 For any connected graph G, $\gamma(G) \leq \gamma_c(G) \leq \gamma_{tc}(G) \leq \gamma_{stc}(G)$ and the bounds are sharp for the graph H_1 in Figure 2.3.

Theorem 2.11 If the induced subgraph of each connected dominating set of G has more than two pendant vertices, then G does not contain a strong triple connected dominating set.

Proof The proof follows from *Theorem 1.2*.

Exact value for some standard graphs:

1) For any path of order $p \geq 3$, $\gamma_{stc}(P_p) = \begin{cases} 3 & if\ p < 5 \\ p-2 & if\ p \geq 5. \end{cases}$

2) For any cycle of order $p \geq 3$, $\gamma_{stc}(C_p) = \begin{cases} 3 & if\ p < 5 \\ p-2 & if\ p \geq 5. \end{cases}$

3) For any complete bipartite graph of order $p \geq 4$, $\gamma_{stc}(K_{m,n}) = \begin{cases} 3 & if\ m = n \\ 2m-1 & if\ m < n. \end{cases}$

(where $m, n \geq 2$ and $m + n = p$).

4) For any star of order $p \geq 3$, $\gamma_{stc}(K_{1, p-1}) = 3$.

5) For any complete graph of order $p \geq 3$, $\gamma_{stc}(K_p) = 3$.

6) For any wheel of order $p \geq 4$, $\gamma_{stc}(W_p) = 3$.

7) For any helm graph of order $p \geq 7$, $\gamma_{stc}(H_n) = \frac{p+1}{2}$ (where $2n - 1 = p$).

8) For any bistar of order $p \geq 4$, $\gamma_{stc}(B(m, n)) = 3$ *(where* $m, n \geq 1$ and $m + n + 2 = p$).

9) For the friendship graph, , $\gamma_{stc}(F_n) = 3$.

Observation 2.12 For any connected graph G with p vertices, $\gamma_{stc}(G) = p$ if and only if $G \cong P_3$ or C_3.

Theorem 2.13 For any connected graph G with $p > 3$, we have $3 \leq \gamma_{stc}(G) \leq p - 1$ and the bounds are sharp.

Proof The lower bound follows from *Definition 2.1* and the upper bound follows from *Observation 2.12*. The lower bound is attained for C_5 and the upper bound is attained for $K_{1,3}$.

Theorem 2.14 For a connected graph G with 5 vertices, $\gamma_{stc}(G) = p - 2$ if and only if G is isomorphic to P_5, C_5, W_5, K_5, $K_{2,3}$, F_2, $K_5 - \{e\}$, $K_4(P_2)$, $C_4(P_2)$, $C_3(P_3)$, $C_3(2P_2)$, $C_3(P_2, P_2, 0)$, $P_4(0, P_2, 0, 0)$ or any one of the graphs shown in Figure 2.4.

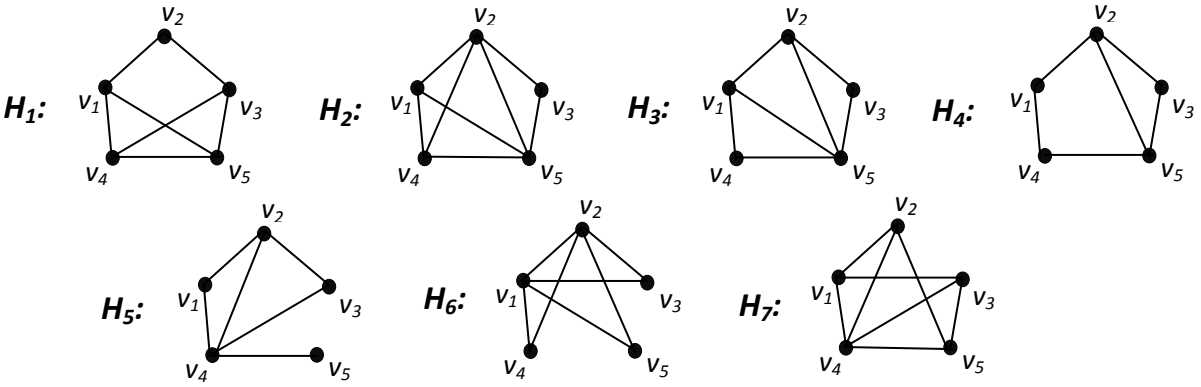

Figure 2.4 : Graphs with $\gamma_{stc} = p - 2$.

Proof Suppose G is isomorphic to P_5, C_5, W_5, K_5, $K_{2,3}$, F_2, $K_5 - \{e\}$, $K_4(P_2)$, $C_4(P_2)$, $C_3(P_3)$, $C_3(2P_2)$, $C_3(P_2, P_2, 0)$, $P_4(0, P_2, 0, 0)$ or any one of the graphs H_1 to H_7 given in Figure 2.4., then clearly $\gamma_{stc}(G) = p - 2$. Conversely, let G be a connected graph with 5 vertices and $\gamma_{stc}(G) = 3$. Let $S = \{v_1, v_2, v_3\}$ be a γ_{stc} -set, then clearly $\langle S \rangle = P_3$ or C_3. Let $V - S = V(G) - V(S) = \{v_4, v_5\}$, then $\langle V - S \rangle = K_2$ or $\overline{K}_2$.

Case (i) $\langle S \rangle = P_3 = v_1v_2v_3$.

Subcase (i) $\langle V - S \rangle = K_2 = v_4v_5$.

Since G is connected, there exists a vertex say v_1 (or v_3) in P_3 which is adjacent to v_4 (or v_5) in K_2. Then $S = \{v_1, v_2, v_4\}$ forms a γ_{stc} -set of G so that $\gamma_{stc}(G) = p - 2$. If v_4 is adjacent to v_1, if $d(v_1) = d(V_2) = 2$, $d(v_3) = 1$, then $G \cong P_5$. Since G is connected, there exists a vertex say v_2 in P_3 is adjacent to v_4 (or v_5) in K_2. Then $S = \{v_2, v_4, v_5\}$ forms a γ_{stc} -set of G so that $\gamma_{stc}(G) = p - 2$. If $d(v_1) = d(v_3) = 1$, $d(v_2) = 3$, then $G \cong P_4(0, P_2, 0, 0)$. Now by increasing the degrees of the vertices, by the above arguments, we have $G \cong C_5$, W_5, K_5, $K_{2,3}$, $K_5 - \{e\}$, $K_4(P_2)$, $C_4(P_2)$, $C_3(P_3)$, $C_3(2P_2)$, $C_3(P_2, P_2, 0)$ and H_1 to H_5 and H_7 in Figure 2.4. In all the other cases, no new graph exists.

Subcase (ii) $\langle V - S \rangle = \overline{K}_2$.

Since G is connected, there exists a vertex say v_1 (or v_3) in P_3 is adjacent to v_4 and v_5 in $\bar{K}_2$. Then $S = \{v_1, v_2, v_3\}$ forms a γ_{stc} -set of G so that $\gamma_{stc}(G) = p - 2$. Since G is connected, there exists a vertex say v_2 in P_3 which is adjacent to v_4 and v_5 in $\bar{K}_2$. Then $S = \{v_1, v_2, v_3\}$ forms a γ_{stc} -set of G so that $\gamma_{stc}(G) = p - 2$. Since G is connected, there exists a vertex say v_1 in P_3 which is adjacent to v_4 in $\bar{K}_2$ and v_2 in P_3 is adjacent to v_5 in $\bar{K}_2$. Then $S = \{v_1, v_2, v_3\}$ forms a γ_{stc} -set of G so that $\gamma_{stc}(G) = p - 2$. Since G is connected, there exists a vertex say v_1 in P_3 which is adjacent to v_4 in $\bar{K}_2$ and v_3 in P_3 which is adjacent to v_5 in $\bar{K}_2$. Then $S = \{v_1, v_2, v_3\}$ forms a γ_{stc} -set of G so that $\gamma_{stc}(G) = p - 2$. In all the above cases, no new graph exists.

Case (ii) $\langle S \rangle = C_3 = v_1v_2v_3v_1$.

Subcase (i) $\langle V - S \rangle = K_2 = v_4v_5$.

Since G is connected, there exists a vertex say v_1 (or v_2, v_3) in C_3 is adjacent to v_4 (or v_5) in K_2. Then $S = \{v_1, v_2, v_4\}$ forms a γ_{stc} -set of G so that $\gamma_{stc}(G) = p - 2$. If $d(v_1) = 4$, $d(v_2) = d(v_3) = 2$, then $G \cong F_2$. In all the other cases, no new graph exists.

Subcase (ii) $\langle V - S \rangle = \bar{K}_2$.

Since G is connected, there exists a vertex say v_1 (or v_2, v_3) in C_3 is adjacent to v_4 and v_5 in $\bar{K}_2$. Then $S = \{v_1, v_2, v_3\}$ forms a γ_{stc} -set of G so that $\gamma_{stc}(G) = p - 2$. If $d(v_1) = d(v_2) = 4$, $d(v_3) = 2$, then $G \cong H_6$. In all the other cases, no new graph exists. Since G is connected, there exists a vertex say v_1(or v_2, v_3) in C_3 is adjacent to v_4 in $\bar{K}_2$ and v_2 (or v_3) in C_3 is adjacent to v_5 in $\bar{K}_2$. Then $S = \{v_1, v_2, v_3\}$ forms a γ_{stc} -set of G so that $\gamma_{stc}(G) = p - 2$. In this case, no new graph exists.

Theorem 2.15 Let G be a connected graph with $p \geq 3$ vertices and has exactly one full vertex. Then $\gamma_{stc} = 3$.

For, let v be the full vertex in G. Then $S = \{v, v_i, v_j\}$ is a minimum strong triple connected dominating set of G, where v_i and v_j are in $N(v)$. Hence $\gamma_{stc}(G) = 3$.

Theorem 2.16 For any connected graph G with $p \geq 3$ vertices and exactly one vertex has $\Delta(G) = p - 2$, $\gamma_{stc}(G) = 3$.

Proof Let G be a connected graph with $p \geq 3$ vertices and exactly one vertex has maximum degree $\Delta(G) = p - 2$. Let v be the vertex of maximum degree $\Delta(G) = p - 2$. Let $v_1, v_2, \ldots$ and v_{p-2} be the vertices which are adjacent to v, and let v_{p-1} be the vertex which is not adjacent to v. Since G is connected, v_{p-1} is adjacent to a vertex v_i for some i. Then $S = \{v, v_i, v_{p-1}\}$ forms a minimum strong triple connected dominating set of G. Hence $\gamma_{stc}(G) = 3$.

The Nordhaus – Gaddum type result is given below:

Theorem 2.18 Let G be a graph such that G and $\bar{G}$ have no isolates of order $p > 3$. Then $\gamma_{stc}(G) + \gamma_{stc}(\bar{G}) \leq 2(p - 1)$ and $\gamma_{stc}(G).\ \gamma_{stc}(\bar{G}) \leq (p - 1)^2$ and the bound is sharp.

Proof The bounds directly follows from *Theorem 2.13*. For the path P_4, the bounds are sharp.

3 Relation With Other Graph Theoretical Parameters

Theorem 3.1 For any connected graph G with $p > 3$ vertices, $\gamma_{stc}(G) + \kappa(G) \leq 2p - 2$ and the bound is sharp if and only if $G \cong K_4$.

Proof Let G be a connected graph with $p > 3$ vertices. We know that $\kappa(G) \leq p - 1$ and by *Theorem 2.13*, $\gamma_{stc}(G) \leq p - 1$. Hence $\gamma_{stc}(G) + \kappa(G) \leq 2p - 2$. Suppose G is isomorphic to K_4. Then clearly $\gamma_{stc}(G) + \kappa(G) = 2p - 2$. Conversely, Let $\gamma_{stc}(G) + \kappa(G) = 2p - 2$. This is possible only if $\gamma_{stc}(G) = p - 1$ and $\kappa(G) = p - 1$. But $\kappa(G) = p - 1$, and so $G \cong K_p$ for which $\gamma_{stc}(G) = 3 = p - 1$ so that $p = 4$. Hence $G \cong K_4$.

Theorem 3.2 For any connected graph G with $p > 3$ vertices, $\gamma_{stc}(G) + \chi(G) \leq 2p - 1$ and the bound is sharp if and only if $G \cong K_4$.

Proof Let G be a connected graph with $p > 3$ vertices. We know that $\chi(G) \leq p$ and by *Theorem 2.13*, $\gamma_{stc}(G) \leq p - 1$. Hence $\gamma_{stc}(G) + \chi(G) \leq 2p - 1$. Suppose G is isomorphic to K_4. Then clearly $\gamma_{stc}(G) + \chi(G) = 2p - 1$. Conversely, let $\gamma_{stc}(G) + \chi(G) = 2p - 1$. This is possible only if $\gamma_{stc}(G) = p - 1$ and $\chi(G) = p$. Since $\chi(G) = p$, G is isomorphic to K_p for which $\gamma_{stc}(G) = 3 = p - 1$ so that $p = 4$. Hence $G \cong K_4$.

Theorem 3.3 For any connected graph G with $p > 3$ vertices, $\gamma_{stc}(G) + \Delta(G) \leq 2p - 2$ and the bound is sharp.

Proof Let G be a connected graph with $p > 3$ vertices. We know that $\Delta(G) \leq p - 1$ and by *Theorem 2.13*, $\gamma_{stc}(G) \leq p - 1$. Hence $\gamma_{stc}(G) + \Delta(G) \leq 2p - 2$. The bound is sharp for K_4.

References

[1] Acharya.B.D, (1980): The strong domination number of a graph and related concepts, J.Math.Phys.Sci,14 pp 471-475.

[2] John Adrian Bondy, Murty U.S.R. (2009): Graph Theory, Springer, 2008.

[3] Mahadevan G., Selvam A., Paulraj Joseph J., and Subramanian T. (2012):Triple connected domination number of a graph , International J.Math. Combin., Vol.3, 93-104.

[4] Mahadevan G., Selvam A., Paulraj Joseph J., Ayisha B., and Subramanian T. (2012): Complementary triple connected domination number of a graph , Accepted for publication in Advances and Applications in Discrete Mathematics, ISSN 0974-1658.

[5] Mahadevan G, Selvam Avadayappan, Mydeen bibi A., Subramanian T. (2012): Complementary perfect triple connected domination number of a graph, International Journal of Engineering Research and Application, ISSN 2248- 9622, Vol.2, Issue 5,Sep – Oct, pp 260-265.

[6] Mahadevan. G, Selvam Avadayappan, Nagarajan. A, Rajeswari. A, Subramanian. T.(2012): Paired Triple connected domination number of a graph, International Journal of Computational Engineering Research, Vol. 2, Issue 5, Sep. 2012, pp. 1333-1338

.[7] Mahadevan G., Selvam A., Ayisha B., and Subramanian T. (2012): Triple connected two domination number of a graph, International Journal of Computational Engineering Research Vol. 2, Issue 6, Oct. 2012, pp.101-104.

[8] Mahadevan G., Selvam A., Bhagavathi Ammal V. G, and Subramanian T. (2012): Restrained triple connected domination number of a graph, International Journal of Engineering Research and Application, ISSN 2248-9622, Vol. 2, Issue 6, Nov – dec. 2012, pp.225-229.

[9] Mahadevan G., Selvam Avadayappan., Hajmeeral . M., and Subramanian T. (2012): Dom strong triple connected domination number of a graph, American Journal of Mathematics and Mathematical Sciences, ISSN 2278-0874, Vol. 1, Issue No. 2, July – dec. 2012, pp.29-37.

[10] Mahadevan G., Selvam A., Bhagavathi Ammal V. G, and Subramanian T. (2012): weak triple connected domination number of a graph - Preprint.Mahadevan G., Selvam A., Bhagavathi Ammal V. G, and Subramanian T. (2012): weak triple connected domination number of a graph - Preprint.

[11] Nordhaus E. A. and Gaddum J. W. (1956): On complementary graphs, Amer. Math. Monthly, 63: 175–177.

[12] Paulraj Joseph J. and Arumugam. S. (1992): Domination and connectivity in graphs, International Journal of Management Systems, 8 (3): 233–236.Paulraj Joseph J. and Arumugam. S. (1992): Domination and connectivity in graphs, International Journal of Management Systems, 8 (3): 233–236.

[13] Paulraj Joseph J. and Arumugam. S. (1997): Domination and coloring in graphs, International Journal of Management Systems, 8 (1): 37–44.Paulraj Joseph J. and Arumugam. S. (1997): Domination and coloring in graphs, International Journal of Management Systems, 8 (1): 37–44.

[14] Paulraj Joseph J., Angel Jebitha M.K., Chithra Devi P. and Sudhana G. (2012): Triple connected graphs, Indian Journal of Mathematics and Mathematical Sciences, ISSN 0973-3329,Vol. 8, No.1, pp 61-75.

[15] Paulraj Joseph J. and Mahadevan G. (2006): On complementary perfect domination number of a graph, Acta Ciencia Indica, Vol. XXXI M, No. 2.: 847–853.

[16] Sampathkumar, E.; Walikar, HB (1979): The connected domination number of a graph, J.Math. Phys. Sci 13 (6): 607–613.

[17] Sampathkumar E and Puspalatha.L (1996): Strong weak domination and domination balance in a graph, Discrete math. 161, pp 235-242.

[18] Teresa W. Haynes, Stephen T. Hedetniemi and Peter J. Slater (1998): Domination in graphs, Advanced Topics, Marcel Dekker, New York.

[19] Teresa W. Haynes, Stephen T. Hedetniemi and Peter J. Slater (1998): Fundamentals of domination in graphs, Marcel Dekker, New York.